`

Evaluating the role of invadopodia in glioma invasion and response to therapeutics

Clarissa Anne Whitehead

Thesis submitted to The University of Melbourne in total fulfilment of the requirements for the degree of

Doctor of Philosophy

The Royal Melbourne Hospital

The Department of Surgery

The University of Melbourne

March 2021

ORCID ID: https://orcid.org/0000-0003-1584-8138

Abstract

Glioblastoma (GBM) is the most prevalent and aggressive form of glioma. Due to the highly infiltrative nature of this disease, median GBM patient survival remains low at just 15 months with the standard treatment protocol involving surgery followed by radiotherapy (RT) and adjuvant chemotherapy with temozolomide (TMZ) [2]. Evidence to date suggests that the efficacy of this therapeutic approach may be compromised by an enhanced invasive phenotype in surviving GBM cells [3-7]. Uncovering the mechanisms behind such treatment-induced invasion may identify potential anti-invasive targets and assist in the development of urgently needed novel treatments for GBM.

Tumour cell invasion may be facilitated by actin-rich membrane protrusions known as invadopodia that actively degrade the surrounding extracellular matrix via highly localised proteolytic activity. Here, we have demonstrated that the enhanced invasive capabilities of GBM cells post-RT/TMZ treatment may be gained through an increase in invadopodia formation and activity. Furthermore, commercially available gene and miRNA arrays revealed an upregulation of invasion-related genes, including thrombospondin-1, and a downregulation of miRNAs with invadopodia-related targets in GBM cells post-treatment. Importantly, augmented invadopodia activity was maintained in long-term (LT) treated (exposed to RT/TMZ once a week for 10 consecutive weeks) GBM cell lines. However, the LN229 cell line was found to instead adopt a highly proliferative but minimally invasive phenotype following LT treatment, highlighting the different responses to prolonged RT/TMZ treatment that may contribute to tumour heterogeneity and the complexity of patient responses to treatment.

As research has highlighted the importance of GBM cell secreted extracellular vesicles (EVs) in promoting invasion [8-11], the role of EVs in facilitating a treatment-induced invasive phenotype was also investigated. Small EVs (sEVs) from a high invadopodia activity donor GBM cell line were found to transfer a pro-invadopodia phenotype to recipient GBM cells. Enhanced sEV secretion was also observed from GBM cells following RT/TMZ treatment, correlating with increased invadopodia formation and activity. Demonstrating the potential to dualistically target invadopodia activity and sEV secretion to overcome RT/TMZ-induced GBM invasion, the addition of the microtubule-targeting agent

Vinorelbine Tartrate (VT) alongside RT/TMZ reduced the enhanced secretion of sEVs, in accordance with previous data from our laboratory showing VT also reduces invadopodia activity in GBM cells surviving RT/TMZ [12].

Lastly, to elucidate the specific proteins that may drive invadopodia formation and activity in GBM cells, a comprehensive proteomic analysis of GBM cell lines and corresponding sEVs was performed. A total of 61 established invadopodia-related proteins were identified in the GBM cell and vesicle proteomes. sEVs were specifically enriched in adhesion-, GTPase-, and kinase- related proteins indicative of a potential role in the sEV-mediated promotion of a pro-invadopodia phenotype in recipient GBM cells. Furthermore, the impact of both single and LT RT/TMZ treatment on the proteome of GBM cells and sEVs was also examined. The findings presented here provide insight into the dysregulated proteomic landscape of GBM cells and sEVs following exposure to RT/TMZ treatment that may contribute to enhanced invasive capacity, which may ultimately assist in the development of novel adjuvant therapeutic strategies to improve the clinical efficacy of RT and TMZ treatment.

Declaration

This declaration is to certify that:

I. This thesis comprises only the candidate's original work towards the Ph.D. except where indicated in the preface.

II. Due acknowledgement has been made in the text to all other material used.

III. The thesis is fewer than 100,000 words in length, exclusive of tables, maps, figure legends, bibliographies and appendices.

Clarissa Anne Whitehead

COVID-19 Impact Statement

Due to the global COVID-19 pandemic and restrictions implemented by the Victorian government and adopted by The University of Melbourne, laboratory access was heavily restricted. These restrictions prevented the completion of further experiments that would have generated additional data and have been included in the future directions section of the thesis.

Preface

The experimental data described in this thesis comprises only the candidate's original work, except for the following results, obtained in collaboration:

I. Original ImageJ scripts for determining the number of total and active invadopodia in GBM cells were developed by Cameron Nowell from the Monash Institute of Pharmaceutical Sciences.

II. The FITC-gelatin-coated coverslips utilized in the invadopodia FITC-gelatin degradation assays were prepared by Dr. Stanley Stylli, who also assisted with the confocal imaging of these experiments.

III. Dr. Martin Tymms, from the Department of Microbiology and Immunology at The University of Melbourne, assisted in the plasmid preparation of THBS1.

IV. The LC/MS-MS proteomic generation of data from GBM cell and EV lysates in Chapters 5 and 6 was performed by Dr. David Greening, Head of Molecular Proteomics at the Baker Heart and Diabetes Institute.

V. The cryogenic electron microscopy images in ***Figure 4-2D*** were captured by A/Prof Eric Hanssen from the Bio21 Institute.

Author Attribution Statement

The information and figures in section 1.6 of this thesis has been published as part of two review articles that were authored by Clarissa Whitehead during her PhD candidature. Clarissa's contributions to each review article are listed as follows:

Whitehead, C. A., Luwor, R. B., Morokoff, A. P., Kaye, A. H., & Stylli, S. S. (2017). Cancer exosomes in cerebrospinal fluid. *Translational Cancer Research*, ***6***(8), s1352-s1370.

Clarissa Whitehead is first author for this article. Clarissa wrote the manuscript and composed all figures and tables, contributing approximately 90% of the total work involved.

Whitehead, C. A., Kaye, A. H., Drummond, K. J., Widodo, S. S., Mantamadiotis, T., Vella, L. J., & Stylli, S. S. (2020). Extracellular vesicles and their role in glioblastoma. *Critical Reviews in Clinical Laboratory Sciences*, **57**:4, 227-252

Clarissa Whitehead is first author for this article. Clarissa wrote the manuscript and composed all figures and tables, contributing approximately 90% of the total work involved.

Acknowledgements

A PhD journey is by no means a solo mission, and the completion of this doctoral thesis would not have been possible without the support of many individuals over the years. Whilst I cannot list everyone in this section for whom I am grateful, it is my pleasure to acknowledge a few individuals whose input, guidance and support have been immeasurable over the course of this PhD.

I would first like to express my sincerest gratitude to my primary supervisor Dr. Stanley Stylli for the opportunity to work on this incredible project, as well as for your continual guidance and unwavering support. From our first meeting in 2015, throughout my honours project, and all the way through to the completion of this doctorate, you have been a wonderful mentor and have dedicated so much of your time towards supporting both myself and this project. Your passion and excitement for research continues to be inspiring, and I truly appreciate your endless encouragement and valuable feedback over the years which has shaped me into a more confident researcher. I struck gold when I chose your honours project all those years ago, and I cannot thank you enough for your positive influence in my life.

I would also like to thank my co-supervisors, Dr. Rodney Luwor and Professor Chris Hovens, and committee members, Dr. Laura Vella and Dr. Hongjian Zhu, for your advice and input throughout my candidature. I would especially like to thank Dr. Laura Vella for your support, encouragement and willingness to share your expertise in extracellular vesicle research which has been pivotal to this project. Thank you also to Cameron Nowell from the MIPs faculty for your assistance in imaging, especially during COVID-19 restrictions, and for writing the scripts that enabled the quantification of invadopodia. Additionally, thank you to all my lab members, both current and in the past, for all of your help and for your friendship.

A huge thank you goes to my partner, Joshua, for your encouragement, reassurance, and patience during my PhD candidature. You have brought so much love and happiness into my life. Your ceaseless support over the last few years has underpinned my determination and allowed me to overcome every obstacle I have faced. Thank you for listening to me ramble on about science, for sharing my joy when

I am excited about the outcome of an experiment, and for comforting me when the journey has been tough.

Lastly, I would like to dedicate this project to my mother, Anne Soden-Whitehead, who passed away in 2016 after battling with GBM. My mother always supported my life ambitions and taught me to constantly do my best. She was a source of great inspiration in life, and her strength whilst fighting GBM motivated and compelled me to make a difference in this field of research. I owe this doctorate to her, as I would not be where I am today without her.

Contents

Abbreviations

ADAM: A Disintegrin And Metalloproteinase

ATP: Adenosine Triphosphate

BBB: Blood-Brain Barrier

CNS: Central Nervous System

CSF: Cerebrospinal Fluid

CUSA: Cavitron Ultrasonic Surgical Aspirate

Da: Dalton

DE: Differentially Expressed

DMSO: Dimethyl Sulphoxide

DNA: Deoxyribonucleic Acid

ECM: Extracellular Matrix

EGF: Epidermal Growth Factor

EGFR: Epidermal Growth Factor Receptor

EMT: Epithelial to Mesenchymal Transition

EV: Extracellular Vesicle

FC: Fold Change

GBM: Glioblastoma

GSC: Glioblastoma Stem Cell

h: Hour

HPLC: High-Performance Liquid

IDH: Isocitrate Dehydrogenase

ILV: Intraluminal Vesicle

kDa: Kilodalton

LC-MS/MS: Liquid Chromatography-Tandem

LT: Long-Term

M: Molar

MGMT: O-6-Methylguanine-DNAmethyltransferase

Min: Minute

miRNA: MicroRNA

mL: Millilitre

MMP: Matrix Metalloproteinase

MRI: Magnetic Resonance Imaging

mRNA: Messenger RNA

MS: Mass Spectrometry

Mths: Months

MT1-MMP: Membrane Type 1-Matrix Metalloproteinase

MV: Microvesicle

MVB: Multivesicular Body

NF1: Neurofibromatosis Type-1

nm: Nanometre

NTA: Nanosight Tracking Analysis

PBS: Phosphate-Buffered Saline

PTEN: Phosphatase and Tensin Homolog

RB: Retinoblastoma

RNA: Ribonucleic Acid

RT: Radiotherapy

RTK: Receptor Tyrosine Kinase

SD: Standard Deviation

SNARE: SNAP Receptor

TCGA: The Cancer Genome Atlas

THBS1: Thrombospondin-1

TMZ: Temozolomide

TP53: Tumour Protein P53

VEGF: Vascular Endothelial Growth Factor

VT: Vinorelbine Tartrate

WHO: World Health Organisation

List of Figures

List of Tables

CHAPTER 1: Introduction

1.1 Introduction to Glioma

1.1.1 Burden of disease and prevalence

Malignant brain tumours are amongst the most aggressive types of cancer, reducing the cognitive ability of patients and leading to disproportionate levels of morbidity and mortality. This in turn creates a high social burden not only upon patients, but also their carers. Gliomas are cancerous tumours that derive from glial cells in the brain; including astrocytic tumours, oligodendrogliomas, ependymomas and mixed gliomas. They are characterised by their high proliferative potential, infiltrative growth patterns, intratumoural heterogeneity and high incidence of recurrence.

Gliomas account for approximately 80% of brain malignancies, of which 18,000 new cases arise annually in the US [13]. In Victoria (Australia) brain malignancies are the eighth leading causing of cancer-related deaths [14]. Survival time is related to a patient's age at diagnosis as well as the histologic type of tumour within the glioma classification, as poorer prognosis is associated with increasing tumour grade and older age. Interestingly, epidemiological studies have observed that malignant gliomas are more common in males than females [13]. However, such studies are not able to make greatly accurate comparisons of glioma incidence geographically, as international differences in diagnostic methods and reporting make such comparisons problematic [15].

1.1.2 Grades and Histological Subtypes

Traditionally, the World Health Organisation (WHO) has categorised diffuse gliomas based on the morphology as either astrocytomas, oligodendrogliomas or oligoastrocytomas, depending on whether the tumour exhibits histologic features similar to astrocytes (diffusely proliferating of cells with elongated cytoplasmic processes), oligodendrocytes (cells with round nuclei surrounded by a clear cytoplasmic halo), or a mixture of both, respectively [16]. Under the current WHO 2016 classification for integrated diffuse glioma diagnostics, these histopathological categories are further assigned a grade

(ranging from I to IV) based on further histological features such as proliferative (mitotic) activity, pleomorphism, necrosis, and vascular proliferation (neoangiogenesis) [16]. These classifications assist in predicting clinical outcome and range from lower grade tumours, such as grade I (non-invasive astrocytoma) and II (diffuse astrocytoma), to more aggressive higher-grade tumours, such as grade III (anaplastic astrocytoma) and IV (Glioblastoma or 'GBM'). Tumours listed under grades II to IV have the potential to infiltrate into the surrounding brain tissue and therefore may recur after surgical resection [17]. Histological criteria has been refined over time, and now with the ability to examine DNA, RNA and methylation, biomarkers have also been established which allow for more accurate classification of tumour biopsies [18]. A number of common genetic alterations in glioma have been identified, including amplification of the EGFR (Epidermal Growth factor) locus, as well as deletions in loci encoding for MGMT, PTEN and CDKN2 [19]. Notably, the discovery of mutations in the Krebs cycle enzymes, isocitrate dehydrogenase 1 and 2 (IDH1/IDH2), has led to a further refinement of the classical diagnostic scheme for diffuse gliomas, whereby IDH1 and IDH2 mutations are indicative of lower grade (II-III) gliomas or secondary GBMs (grade IV astrocytomas that have progressed from lower-grade tumours) [16, 20]. As gliomas that harbour IDH mutations are generally less aggressive than IDH-wildtype lesions and correlated with favourable patient prognosis, including an earlier age of onset and longer overall survival, glioma diagnoses are now based on both tumour histology and IDH1 and IDH2 genetic status.

1.2 Glioblastoma

1.2.1 Glioblastoma - Incidence and Mortality

The most common malignant central nervous system (CNS) tumour is glioblastoma, also known as glioblastoma multiforme (GBM), accounting for 46.6% of all malignant primary CNS tumours, 56% of all gliomas and 14.9% of all primary brain and CNS tumours (***Figure 1-1A***) [21]. Listed as a grade IV astrocytoma, GBM is the most aggressive and malignant form of primary brain tumour in adults. The

histopathological features of GBM include diffusely infiltrative tumour cells, microvascular proliferation, necrosis, and the presence of palisading of tumour cells around necrotic foci. Although considered a relatively rare disease due to an annual incidence of 5.26 per 100,000 individuals, GBM carries an extremely poor prognosis and is currently incurable, with less than 5% of GBM patients survive 5 years post-diagnosis (***Figure 1-1B***) [18, 22]. Owing to the highly infiltrative nature of GBM, tumour recurrence is inevitable and patient survival remains at just 12-15 months with the current therapeutic approach of maximal safe surgical resection, followed by radiotherapy (RT) and chemotherapy with the drug temozolomide (TMZ) [2, 18]. In Victoria (Australia), population studies examining 542 GBM patients over 12 years have indicated worse patient survival times, with a median survival of just 7 months obtained from a large respective study [14]. GBMs may arise as either primary (*de novo*) or secondary lesions. Primary GBMs account for over 90% of cases and are most common in older patients, whereas secondary GBMs progress from lower grade astrocytomas and are more common in younger patients [23]. This disease is 1.57 times more common in males than females and, with an average age of diagnosis at 64 years, the incidence of GBM is expected to increase as the world's aging population continues to grow [13].

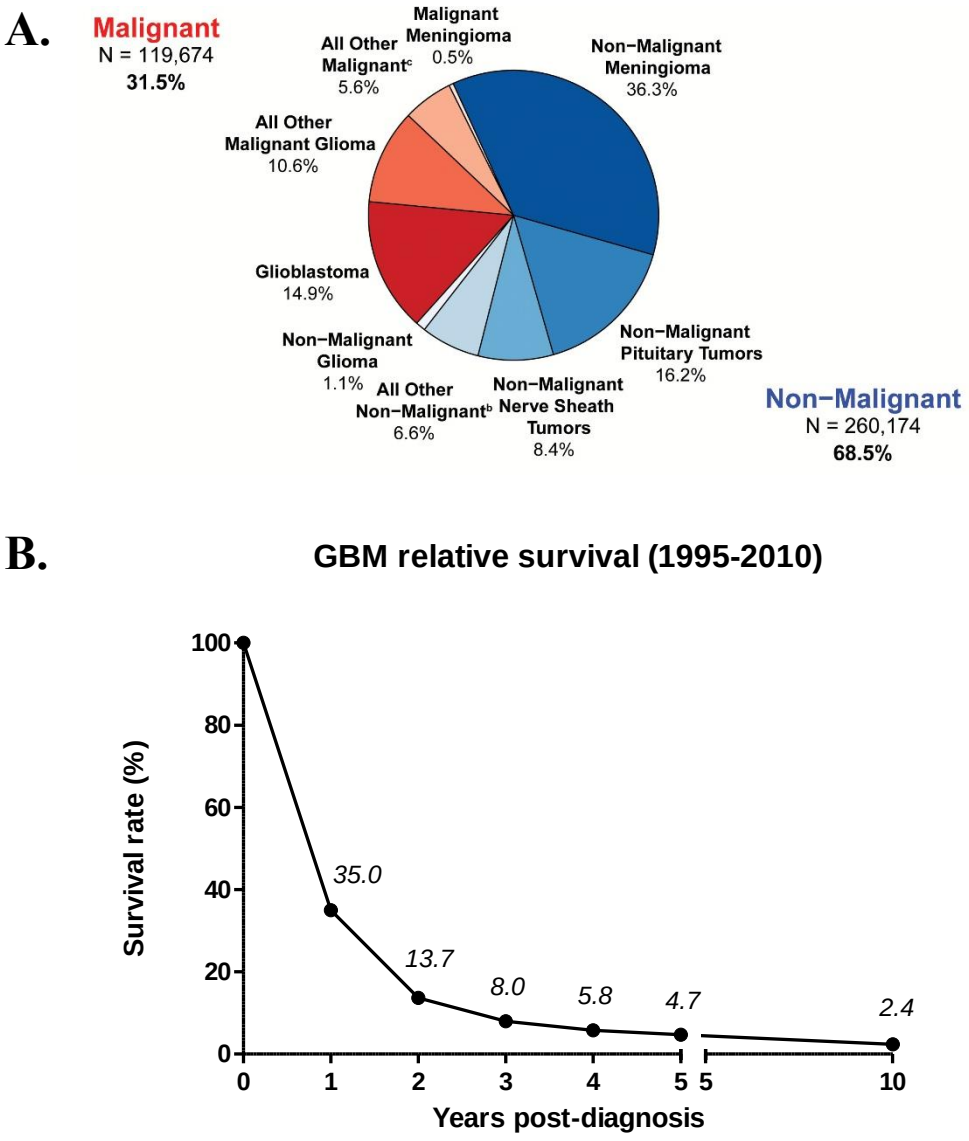

Figure 1-1: GBM incidence and survival

Distribution of Primary Brain and Other CNS Tumors in the United States of America (2010-2014). (**A.**) GBM constitutes the greatest proportion of malignant CNS tumours (Malignant tumours shown in red. Non-malignant tumours are shown in blue *(n=379,848; percentages may not add up to 100 due to rounding) (Image source: CBTRUS, 2017).* (**B**.) Relative survival estimates for GBM patients in the United States of America obtained from the SEER 18 registries (1995 to 2010), showing the low survival rate of less than 5% at 5 years post-diagnosis.

1.2.2 Glioblastoma – Molecular Subtypes

GBM exhibits a great degree of heterogeneity, with the one tumour mass harbouring an abundance of genetic and epigenetic alterations. In order to classify GBMs based on molecular profiles, The Cancer Genome Atlas (TCGA) has divided GBMs into four subtypes each with distinct molecular modifications: classical, mesenchymal, proneural and neural (***Figure 1-2***) [24].

1.2.2.1 Classical Subtype

The classical subtype is typified by amplification of chromosome 7, loss of chromosome 10, EGFR amplification, and the upregulation of stem cell markers such as Nestin and Notch.

1.2.2.2 Mesenchymal Subtype

The mesenchymal subtype contains mutations to tumour suppressors TP53 (tumour protein p53) and PTEN (Phosphatase and Tensin Homolog), and deletions in a region encoding the neurofibromatosis type-1 tumour suppressor gene (NF1). Mesenchymal tumours also exhibit high expression of nuclear factor kappa-light-chain-enhancer of activated B cells (NF-κβ).

1.2.2.3 Proneural Subtype

The proneural subtype also expresses alterations in TP53, as well as platelet derived growth factor receptor A (PDGFRA) and isocitrate dehydrogenase 1 (IDH1) and is most common in younger patients and secondary GBMs.

1.2.2.4 Neural Subtype

The neural subtype is characterised by the expression of certain neuronal markers (including *NEFL*, *GABRA1*, *SYT1*, and *SLC12A5)* and shares a similar molecular profile to normal brain tissue [24].

1.2.2.5 The prognostic value of TCGA molecular subtypes

These molecular biomarkers can be predictive, thereby estimating response to treatment, or prognostic, signifying a likely outcome of disease regardless of treatments. Notably, the greatest clinical benefit to current therapy with the chemotherapeutic agent temozolomide (TMZ) is seen in the classical subtype, whereas minimal benefit is seen in the proneural subtype [24]. As the classical subtype is characterised by loss of chromosome 10, which contains the MGMT (*O-6-methylguanine-DNA methyltransferase*) locus known to be involved in treatment resistance, this may be thought to contribute to the benefit seen in the classical subtype. However, research has shown that differential responses to treatment between subtypes appears largely independent of MGMT methylation status [24]. This benefit is more likely associated with the upregulation of stem cell markers seen in the classical subtype. As disease progresses, a shift to the mesenchymal subtype is commonly seen, similar to cancer cells undergoing EMT (epithelial to mesenchymal transition) to become more invasive [25, 26]. This suggests that factors that would induce EMT in epithelial cancers may also activate mesenchymal features in GBM. Unfortunately, whilst the molecular features of GBM may serve as diagnostic or prognostic biomarkers that can contribute towards the development of individualised treatments, the current molecular subtypes have shown little clinical utility in the management of GBM to date.

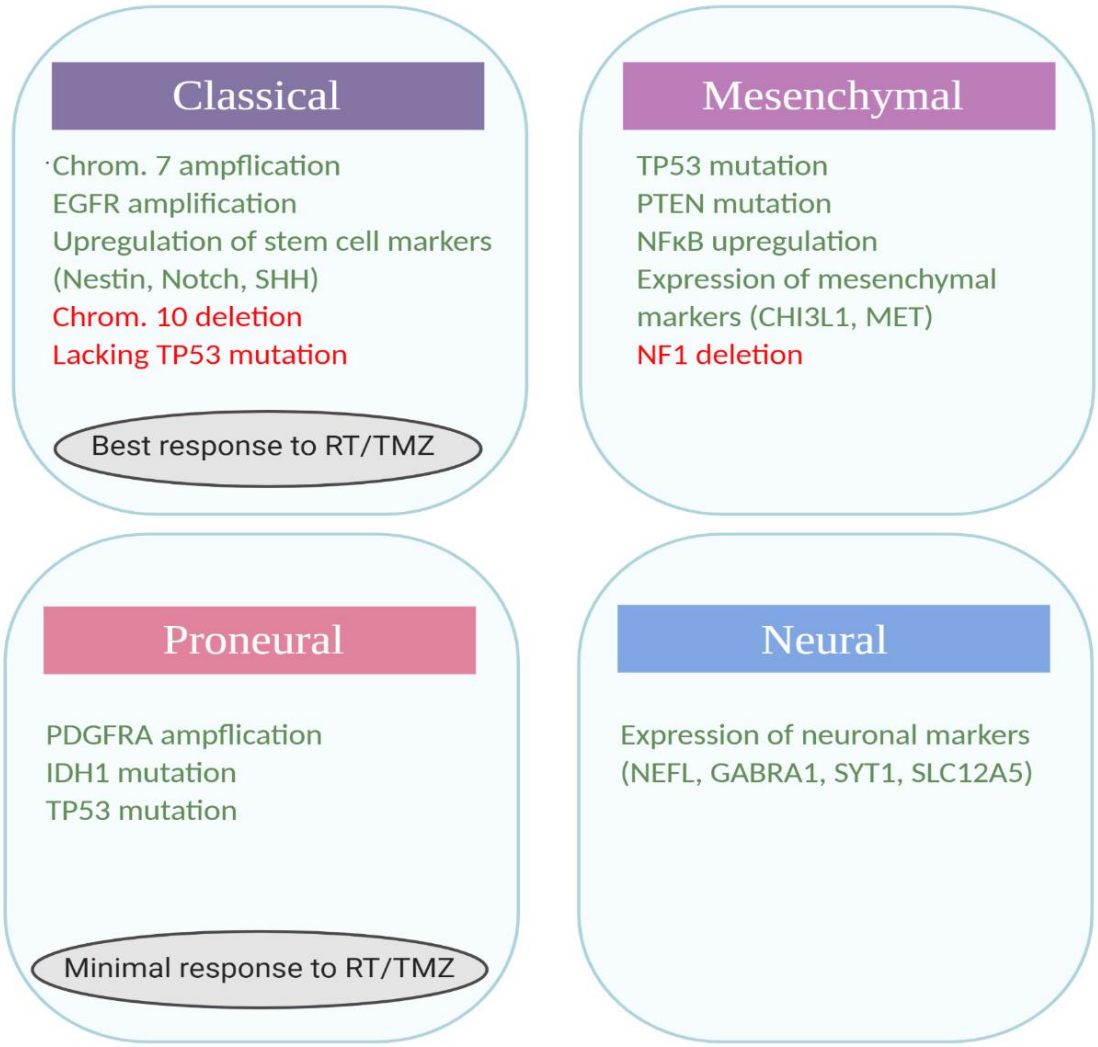

Figure 1-2: The molecular subtypes of GBM

The four GBM molecular subtypes as initially identified via The Cancer Genome Atlas network: Classical, Mesenchymal, Proneural and Neural. Distinct genetic signatures as proposed by Verhaak et al (2010) exist for the four clinically relevant subtypes. Treatment with radiotherapy (RT) and temozolomide (TMZ) shows the most benefit for the Classical subtype, whereas minimal response is observed in the Proneural subtype.

1.2.3 The Hallmarks of Cancer in GBM

The commonalities across all types of cancer have been investigated and described in detail as six hallmarks of cancer and two emerging hallmarks by Hanahan and Weinberg [1]. These hallmarks include self-sufficient proliferative signalling, evasion of growth suppressors, resisting cell death, replicative immortality, induced angiogenesis, activated invasion and metastasis, and two emerging hallmarks; evasion of the immune response and differing cellular metabolism (***Figure 1-3***). Focus surrounding these hallmarks has shifted from the cancerous cells alone, as it is becoming increasingly recognized that the tumour microenvironment plays an fundamental role in tumourigenesis [27]. During cancer progression, the surrounding microenvironment enters an activated state whereby sustained paracrine signalling maintains malignant cell growth. In this way the hallmarks are generated not just by cellular genomic instability, but also may be reinforced by inflammation and other various stromal factors. These were described by Hanahan and Weinberg as the two 'enabling characteristics' of neoplasia that facilitate acquisition of the aforementioned hallmarks: 'genomic instability and mutation' and 'tumour-promoting inflammation' [1].

The following briefly discusses each of the hallmarks and their relevance in GBM.

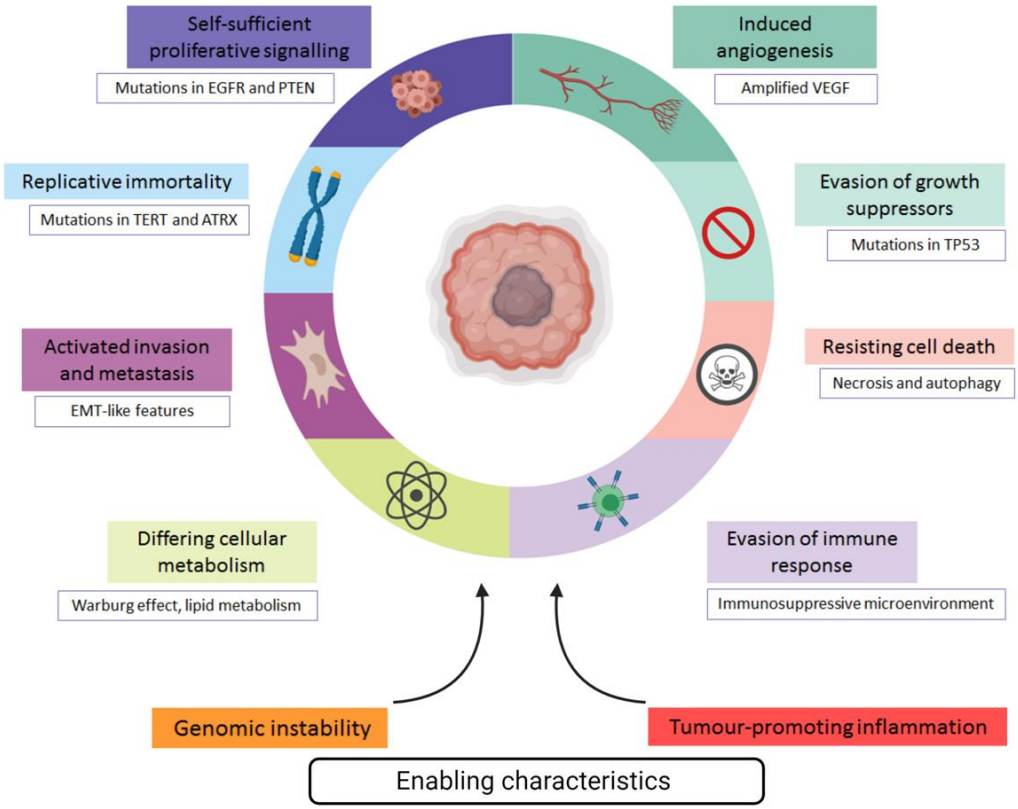

Figure 1-3: The hallmarks of cancer and GBM

The hallmarks of cancer represent biological capabilities acquired by cancer cells during the multistep development of human tumours. These hallmarks, consisting of six established hallmarks and two emerging hallmarks ('differing cellular metabolism' and 'evasion of the immune response') are facilitated by two enabling characteristics: 'genomic instability and mutation' and 'tumour-promoting inflammation'. Examples of molecules and mechanisms associated with each hallmark in relation to GBM are summarized in the above illustration and are discussed in the following sections. The figure has been adapted from Hanahan and Weinberg, 2011 [1].

1.2.3.1 Self-sufficient proliferative signalling

Cancerous cells exhibit deregulation of various signalling pathways, allowing these cells to proliferate and grow beyond the confines of normal homoeostasis. These proliferative signalling pathways generally involve growth factors that bind to receptors on the surface of a cell, thereby activating the receptor's intracellular tyrosine kinase domains that govern downstream signalling within the cell, and ultimately promoting various processes such as cell growth, proliferation, and metabolism. Two major mutations in GBM can be seen under this hallmark, with 45% of TCGA GBM specimens displaying EGFR gene mutations and 36% of specimens displaying inactivating mutations in the PTEN gene, both of which result in increased proliferation [28].

Additionally, GBMs are known to harbour a subpopulation of tumour cells known as glioma stem cells (GSCs) that are capable of self-renewal and differentiation. Accumulating evidence indicates that GSCs are largely implicated in both GBM invasion and treatment resistance, and therefore are contribute to tumour recurrence. Although this population of GBM cells remains challenging to treat, novel strategies to target GSC are currently under investigation [29].

1.2.3.2 Evasion of growth suppressors

In order to continue proliferating, malignant cells must also avoid the actions of tumour suppressors that function to negatively regulate and limit cellular growth and proliferation. Generally, these tumour suppressor genes are seen to be inactivated in many forms of cancer and include genes such as retinoblastoma protein (RB) and TP53, the latter of which is mutated in approximately 27-33.8% of GBM cases [30]. These mutations in TP53 may vary and are not specific to tumour type, with many isoforms present in GBM also found in other cancers. Interestingly, TP53 has no prognostic significance in GBMs treated with RT , and it has been suggested that mutations in other genes are superior predictors for GBM patient survival [31, 32].

1.2.3.3 Resisting Cell Death

Cell death can occur via three separate processes: apoptosis, autophagy and necrosis. Normal cells may undergo apoptosis through either the extrinsic (death receptor) or intrinsic (cellular stress) apoptotic pathway, with both pathways resulting in the activation of either caspase -8 or -9 respectively [33]. Under normal conditions, a cell may undergo apoptosis when its cell cycle is interrupted by oncogenic mutation, whereas cancer cells exhibit impaired apoptosis allowing these mutated cells to circumvent usual checkpoints. The most common methods of evading apoptosis in GBM include loss of TP53 and RB, causing the cell to loses its ability to identify DNA damage [30]. Other means include increased expression of anti-apoptotic factors or down-regulation of pro-apoptotic factors [1].

Autophagy allows cells to digest organelles and re-use the recycled catabolites in times of nutrient starvation/energy deprivation or when such organelles are damaged. During this process, intracellular vesicles called autophagosomes take up the organelles destined for degradation, before fusing with lysosomes. It has been found that tumorigenesis is promoted when the autophagic gene *beclin1* is haploinsufficent, causing a reduction in autophagic vacuole formation, although further research needs to be carried out to better understand this mechanism [34]. Indeed, the expression level of beclin-1 mRNA is significantly lower in GBM tumours compared to lower grades [35].

Unlike the other forms of cell death, necrosis begins with cellular swelling and membrane blebbing, before the membrane ruptures and the contents of the cell is leaked into the microenvironment. Necrotic cells induce an inflammatory response by releasing lysosomal enzymes and pro-inflammatory signals, which can promote tumorigenesis as inflammatory cells can aid the processes of angiogenesis, proliferation and invasion [36]. In GBM, cells are more prone to necrosis and autophagy than apoptosis [30].

1.2.3.4 Replicative Immortality

Normal cells typically exhibit a limited number of growth and division cycles, whereas cancerous cells generally display indefinite replicative potential. The shift from contained to infinite replicative abilities is known as 'immortalisation' and is seen in most cultured cell lines that are able to proliferate *in vitro* without entering a state of senescence [1]. The immortalisation of human cell lines has been attributed to the action of telomerase, a ribonucleic enzyme that adds repeat DNA sequences onto the ends of telomeres in order to compensate for their shortening [1]. The TCGA found mutations in the telomerase gene TERT were present in 21/25 of the GBM cases assessed in a 2013 study, with the remaining four cases displaying mutations in a different gene called 'the transcriptional regulator gene alpha thalassemia mental retardation' (*ATRX*) [37]. These ATRX mutations were seen together with TP53 and IDH1 mutations, signifying a potential role in secondary GBM.

1.2.3.5 Induced Angiogenesis

Vasculature development involves two processes; vasculogenesis, involving the growth of new endothelial cells that can form tubes, and angiogenesis, involving the sprouting of new blood vessels from those currently present. Angiogenesis generally remains constitutively active in cancerous tissue, allowing for the growth of new vessels around a neoplasm and thus sustaining the tumour mass via the provision of oxygen and various other nutrients [1]. In the brain, the proliferation and migration of endothelial cells to produce new vessels causes disruption of the tight junctions in the blood-brain barrier (BBB) and is responsible for the BBB-associated leakage seen in brain cancer patients [38]. Angiogenesis is largely regulated by Vascular Endothelial Growth Factor (VEGF), with VEGF gene expression seen to be amplified in the presence of hypoxia as well as oncogenic signalling [39].

1.2.3.6 Activated Invasion and Metastasis

Migration is a normal cellular process exhibited during strictly regulated processes, such as during development, injury or the immune response. However, in cancerous cells this process becomes deregulated, allowing these malignant cells to invade outside of the local tumour mass. The steps of invasion and metastatic spread to distant regions of the body has been named 'the metastatic cascade [40]. However, extracranial metastases are extremely rare in GBM which instead is characterised by extensive local infiltration. As invasion has usually already occurred by the time of diagnosis, it presents to be an important clinical challenge.

There are three main types of invasion/migration; amoeboid, collective and mesenchymal [41]. Amoeboid migration consists of cells adjusting their shape to squeeze through spaces in the extracellular matrix (ECM). Changes in cell shape and motility are generated by the actin cytoskeleton, and amoeboid cells do not require degradation of the matrix to migrate, as their low adhesion to ECM substrates allows for relatively rapid translocation. Collective migration involves the migration of nodules of cancer cells that are connected via cadherins and intercellular junctions. The group of cells generally has a 'leading edge' or 'invasive front' that employs the use of integrins and proteases to form a pathway that can allow the cluster of cells to move together into the surrounding tissue [41]. Generally, the cells at the leading edge are similar to mesenchymal cells, whilst the trailing cells are packed more tightly together. Collective migration is typically seen in cancers with cells that are not completely de-differentiated and is not usually metastatic, with a common example seen in oral squamous cell carcinoma [42].

Mesenchymal migration generally involves the process of epithelial-to-mesenchymal transition (EMT). EMT can be seen during migratory processes in embryonic development, but also occurs in malignant cancer cells, allowing them to become motile. In the process of EMT, malignant cells detach from the tumour mass and invade into the surrounding tissue. They achieve this by abolishing cell-cell contacts, remodelling the surrounding ECM, and following the resulting pathway formed by secreted proteases [43]. EMT is able to be induced by intrinsic signals, such as mutations in Snail/Slug and Twist, or extrinsic signals, including growth factor signalling via the transforming growth factor β (TGFβ),

hepatocyte growth factor (HGF), and epidermal growth factor (EGF) pathways [44, 45]. Although unable to undergo EMT, due to the cancerous cells in the brain deriving from glial and not epithelial cells, invading GBM cells exhibit mesenchymal features and EMT-like processes have been observed [25].

1.2.3.7 Differing Cellular Metabolism

The ability for tumour cells to alter their metabolic phenotype in response to changing environmental conditions is essential for survival, allowing cells to continue proliferation under different metabolic demands. Metabolic reprogramming is seen in multiple cancer types, and involves increased ATP generation, as well as the availability of macromolecules (such as lipids and amino acids) and reducing equivalents (such as NADH, NADPH, $FADH_2$) to fuel continued tumour growth. The most common example of metabolic reprogramming in cancer is known as the Warburg effect, also known as 'aerobic glycolysis' as it involves a switch to using glucose to generate ATP, even in the presence of oxygen and fully functioning mitochondria [46]. However, other relevant metabolic pathways that contribute to altered behaviour in cancer cells exist including oxidative phosphorylation and lipid/fatty acid metabolism, with recent studies revealing a previously overlooked relevance in cancer [47]. A study using MCF-7 breast cancer cells demonstrated that oxidation and aerobic glycolysis can co-exist, as 80% of cells were oxidative and 20% glycolytic [48]. When examined, GBM cells were found to be highly oxidative and were not significantly affected by inhibition of glycolysis, suggesting a reliance on fatty acid metabolism [49]. As the Warburg effect is also widely observed in GBM [50], this suggests the ability of GBM cells to utilise both metabolic pathways in order to sustain growth and promote tumour progression.

1.2.3.8 Evasion of Immune Response

Tumour cells exploit several mechanisms to suppress the immune system, ultimately producing a local immunosuppressive microenvironment that enables cancer cells to evade immune detection. GBM cells can secrete immunosuppressive cytokines such as TGFβ-2, prostaglandin E (PGE), IL-1, IL-10 and colony stimulating factor 1 (CSF-1) that suppress the activation of T effector cells [51]. Furthermore, these secreted factors were shown to polarise tumour associated macrophage (TAMs) toward an anti-inflammatory M2 phenotype, characterised by suppressed phagocytic ability and increased inhibition of cytotoxic T-cell proliferation [52]. GBM cells are also able to modulate and escape immune checkpoints via surface expression of programmed death ligand 1 (PD-L1), which engages with programmed cell death-1 (PD-1) on the surface of T cells to suppress effector activity, as well as inducing immunosuppressive microglia and TAMs which also express PD-L1 on their surface [53]. Following stimulation by GBM cells, these recruited immune cells also secrete tumorigenic factors such as EGF, CSF-1, TGF-β1, IL-6, and MMPs to further promote GBM cell invasion and migration [54, 55]. In these ways, GBM cells not only escape immune surveillance through the creation of an immunosuppressive microenvironment, but also influence nearby immune cells to support tumour growth.

1.2.3.9 Enabling Characteristics: 'Tumour-promoting Inflammation' and 'Genomic Instability and Mutation'

Underpinning the acquisition of these eight hallmarks of neoplasia are two enabling characteristics, 'tumour-promoting inflammation' and 'genomic instability and mutation', as defined by Hanahan and Weinberg [1]. Accumulating evidence indicates an important role for inflammation in GBM progression, involving the aberrant activation and infiltration of immune cells that promote tumour growth and survival. The contributions of this pro-inflammatory microenvironment to GBM progression is becoming increasingly recognized, and studies have shown intracellular communication

between GBM and immune cells can influence a variety of processes, such as tumour cell proliferation, invasion, and chemoresistance [56, 57]. The specific roles of immune cells in GBM are discussed in more depth in the previous section ***1.2.3.8***.

Genomic instability is prominent in GBM tumours that are known to harbour high levels of gene mutations and alterations, as well as chromosomal instability that frequently generates an abnormal number of chromosomes in GBM cells (termed 'aneuploidy'). Indeed, GBMs are characterised by common genetic alterations such as loss of heterozygosity 10q (70% of cases), EGFR amplification (36% of cases) and PTEN mutations (25% of cases) [23]. Such genomic instability drives tumour heterogeneity, promoting progression and resistance to treatment, however, debate remains over the clinical impact of the high levels of genomic instability in GBM. On the one hand, heterogeneity may drive clonal variation and treatment resistance [58], however excessive DNA disruption may also compromise cell viability and could therefore sensitise tumours to conventional therapy [21].

1.3 Glioblastoma – Therapeutic Management

1.3.1 Current therapeutic management for GBM

Prior to 2005, radiation therapy (RT) was the only strategy used to treat GBM patients that showed any significant increase in survival. RT was shown to improve median survival by 8 months compared to untreated controls, however difficulties arose as 90% of GBMs relapsed close to the vicinity of the irradiated area [59, 60]. A study by Stupp et al. [2] in 2005 identified TMZ adjuvant to RT increased median survival by approximately 2.5 months, with an improvement in 2 year survival from 12% to 20%. After this pioneering study, surgical resection followed by both RT and TMZ has become the standard protocol for the treatment of GBM patients. However, even with the introduction of TMZ, median overall survival time remains low for GBM patients at only 14.6 months, and follow-up studies reveal that 88.8% of patients still die within two years due to tumour recurrence [61]. As GBM tumours are poorly demarcated, owing to their invasive capacity, increasing the scope of surgical resection has

been shown to increase patient survival, but carries a greater risk of damage to vital brain tissue. Despite ongoing research efforts, there has been no further improvement in GBM treatment. Thus, improved chemotherapeutic strategies that offer further improvements in survival are urgently needed.

It is possible that the low efficacy of current chemotherapy for GBM may be due to a variety of different factors such as resistance to therapy, limited ability of the chemotherapeutic to cross the BBB and restricted tolerability of the drug in the brain itself [62]. Ongoing efforts have been underway to develop novel therapeutics that are able to target pathways associated with gliomagenesis (discussed in the following sections), however, many of the same difficulties are generally seen for these novel therapies. Challenges associated with GBM protocols include limited surgical resection (due to the potential to impact quality of life via intrusion and removal of brain matter), the infiltrative nature of GBM cells into the surrounding brain (which is a major contributor to tumour relapse and treatment failure), and the relative impermeability of the BBB that allows only small (<500 Da) lipid-soluble molecules to penetrate into the central nervous system, thus impeding effective drug delivery.

1.3.2 Understanding the mechanisms driving treatment resistance

As mentioned previously, drug resistance remains a pivotal clinical challenge in improving the survival of GBM patients. A number of mechanisms may play a role in resistance to treatment, including mutations in the target, reactivation of the target pathway, up regulation and activation of alternative pathways, and interactions with the microenvironment [63]. On top of this, pharmacokinetic factors such as drug absorption, metabolism and elimination, may also limit the concentration of drug that reaches the tumour mass. Despite the introduction of new compounds and advances in treatment, still only small numbers of GBM patients survive to 5 years, and no drugs that have reached phase III trials have shown a significant improvement in survival within the last 10 years [64]. Clinical translation of most targeted therapies for GBM has been poor as many therapies prove ineffective either in the short-term, with almost immediate lack of treatment response, or long-term, with the emergence of acquired

resistance to the treatment [64]. Several strategies targeting different pathways in GBM have been employed in clinical trials with varying success, as listed in ***Table 1-1***. A brief summary of the major targeted pathways in GBM is provided in the following sections, highlighting the urgent need for advancements in GBM chemotherapeutic strategies to improve patient survival.

1.3.2.1 Targeting MGMT to improve response to TMZ

Cytotoxicity from the current therapeutic agent used for GBM, TMZ, results from the methylation of DNA at either the O6 or N7 positions of guanine, which blocks DNA replication and results in apoptosis. Resistance to TMZ has been linked to MGMT methylation status, as epigenetic methylation of the promoter region of MGMT is linked to improved patient survival, with a median overall survival of 18.2 months for patients with methylation and 12.2 months for patients without [65]. As the MGMT gene encodes a DNA repair protein, methylation of the promoter region inhibits its transcription, thereby sensitizing patients to DNA-damaging alkylating agents such as TMZ. In the same way, high levels of MGMT protein can create a resistant phenotype and could determine failure to current treatment. As unmethylated MGMT is more common in GBM than other grades of glioma and is associated with IDH wildtype tumours, comprising approximately 90% of GBMs, TMZ may have little impact for many GBM patients [66, 67].

Clinical trials attempting to address this by selecting GBM patients with an unmethylated MGMT promoter for treatment with a range of agents have been largely inefficacious [68-70]. Targeting MGMT has also been investigated using a small-molecule inhibitor, methoxyamine, that works by covalently binding to damaged DNA sites and inhibiting base excision repair, and has shown promise in potentiating the cytotoxic effects of TMZ in colon cancer cells both *in vitro* and in human xenograft models [71]. Further studies would be beneficial to investigate its effects on TMZ-treated GBM cells as well as assessing BBB penetration. In addition to methoxyamine to target MGMT resistance, a combination of alkylating chemotherapy using TMZ paired with lomustine was investigated in a phase II trial, in the hopes that the combination of nitrosoureas (alkylating agents able to cross the BBB)

would deplete MGMT and improve GBM patient survival [69]. However, the combination therapy demonstrated an improved median overall survival of 23 months for MGMT-methylated patients only [69].

1.3.2.2 Targeting VEGF-induced angiogenesis with Bevacizumab

Another avenue for GBM treatment that has had considerable interest is targeting tumour vascularisation via the vascular endothelial growth factor (VEGF) pathway, which promotes angiogenesis. By blocking the VEGF pathway, it is hoped that abnormal tumour vasculature will be amended and vascular permeability along with the volume of cerebral blood around the tumour will be reduced [72]. Bevacizumab, a recombinant humanized monoclonal antibody to VEGF, has been investigated for this purpose. Bevacizumab is able to bind to VEGF ligand and inhibits its ability to couple with its cell membrane receptor. A number of trials have shown that bevacizumab provides a modest improvement in progression-free survival (PFS) but does not impact overall survival (OS). A phase III trial showed a PFS benefit of 10.6 vs 6.2 months with bevacizumab treatment (10 mg/kg every 2 weeks) compared to untreated control [73]. This outcome was also reflected in a greater PFS, but not OS, in a phase II trial of bevacizumab at the same dose with 125 mg of irinotecan every 2 weeks alongside RT and TMZ [74]. A study by Sandmann et al. [75] has suggested that the greatest overall survival advantage with bevacizumab may be seen in the proneural subtype that respond the poorest to TMZ treatment. Additionally, studies have shown that mesenchymal-like tumours may be more resistant to, and derive little to no benefit from, anti-VEGF therapy [76, 77]. Prolonged anti-VEGF treatment has been associated with a shift towards an invasive phenotype, with infiltrating tumours that develop post-treatment displaying higher expression levels of insulin-like growth factor binding protein-2 (IGFBP-2) and matrix metalloprotease-2 (MMP-2) [78]. The pro-invasive tumours that progress during bevacizumab treatment are also highly resistant to successive therapies [79]. In 2013, an Australian study known as CABARET determined bevacizumab was less effective in GBM compared to previous studies and advised that it should not be used in conjunction with TMZ for

recurrent GBM [80]. Despite these outcomes, bevacizumab is approved in the US and Japan for treatment of recurrent GBM, and is mostly used because of improvements in patient quality of life, a possible delay in tumour progression, and the reduced use of corticosteroids [64].

1.3.2.3 Targeting EGFR

Targeting common mutations in GBM, such as the truncated and constitutively active form of EGFR (EGFR-vIII) or IDH mutations, has also been investigated with limited success. EGFR-vIII is a driver mutation that promotes tumour proliferation, that is present in approximately 25-30% of GBMs and is linked to poor long-term survival [81]. Trials of small-molecule receptor tyrosine kinase (RTK) inhibitors specific to EGFR have shown minimal effect in tumours expressing EGFR-vIII, with gefitinib and erlotinib both failing to suppress EGFR-vIII phosphorylation and downstream signalling [82, 83]. A vaccine known as 'rindopepimut' has been developed to generate an immune response specifically against EGFR-vIII-positive tumour cells, and a number of trials have been carried out following a promising reduction in tumour size and a 26% increase in survival time in treated mice harbouring intracerebral EGFR-vIII mutant cells [84]. However, a phase III clinical trial of rindopepimut alongside TMZ was unsuccessful in improving OS compared to TMZ treatment alone in EGFR-vIII harbouring patients, with an average OS of 20.4 vs 21.1 months respectively [85]. One reason for this failure seen in RTK monotherapy is due to the presence and activation of other various RTKs that can maintain downstream signalling and thus continue to promote tumour growth: a phenomenon known as 'RTK-switching'. Profiling of individual cells from primary GBMs identified that cells from the same tumour mass can harbour different splice variants and expression levels of RTKs, as well as other signalling molecules, which results in redundant signalling pathways contributing to resistance [86]. Studies have shown that heterogeneous amplification of common receptors such as EGFR, PDGFRA and MET is present in GBM, and thus targeting these receptors, and pathways, individually may prove to be ineffective, ultimately contributing to the lack of clinical efficacy seen for molecular based therapies [87, 88].

1.3.2.4 Targeting IDH mutations in secondary GBM

Mutations in genes such as EGFR, PTEN and CDKN2A-CDKN2B are common in primary GBM, whereas IDH mutations are mostly seen in secondary GBMs and are lacking in primary tumours. For this reason, it is believed that IDH-mutant tumours arise from a distinctly different molecular pathway to primary GBMs [89]. IDH mutation results in a loss of alpha-ketoglutarate (a-KG) and an excess of D-2-hydroxyglutarate (2-HG), leading to DNA hypermethylation and chromatin alteration. Consequently, inhibitors aimed at lowering 2-HG levels have been investigated to treat IDH mutant tumours. A study by Tatesishi *et al.* found that 2-HG depletion alone was unable to inhibit tumour growth, however depletion of NAD+ was discovered to be a promising pathway, with studies in NAD+ depleted IDH-mutated mice showing a reduction in progression and improvements in survival [90].

Table 1-1: Clinical Trials in GBM

Treatment	Phase	Target	Response (median OS)	Response (median PFS)	Interpretation/ Predicted reason for failure	Ref.
Rindopepimut (vaccine) combined with TMZ	III	EGFRvIII	Rindopepimut= 20.1 mths vs. Ctl=20.0 mths)	Rindopepimut= 8.0 mths vs. Ctl=7.4 mths)	Potential elevated immune response in both groups due to keyhole limpet haemocyanin as a control injection	Weller, et al. [91]
Afatanib (alone or combined with TMZ)	II	EGFRvIII in recurrent GBM	Afatanib alone= 9.8 mths, Afatanib+TMZ = 8.0 mths, TMZ alone = 10.6 mths	Afatanib alone = 0.9 mths, Afatanib+TMZ =1.53 mths, TMZ alone = 1.87 mths	No improvement from TMZ treatment response with addition of Afatanib	Reardon, et al. [92]
Dacomitinib	II	EGFRvIII in recurrent GBM	7.4 mths (Patients without EGFRvIII= 7.8 mths, Patients with EGFRvIII= 6.7 mths)	2.7 mths (Patients without EGFRvIII= 2.7 mths, Patients with EGFRvIII= 2.6 mths)	-	Sepúlveda-Sánchez, et al. [93]
Cetuximab	II	EGFRvIII in recurrent GBM	5 mths	1.9 mths	No significant correlation was found between response, survival and EGFR amplification	Neyns, et al. [94]
Cediranib	II	VEGF in recurrent GBM	8 mths	4 mths	-	Batchelor, et al. [95]
Erlotinib + Bevacizumab (with RT/TTMZ)	II	EGFR and VEGF in recurrent GBM with unmethylated MGMT	13.2 mths	9.2 mths	-	Raizer, et al. [96]
Cilengitide (with RT/TMZ)	II	αvβ3 and αvβ5 integrins in primary GBM with unmethylated MGMT	RT/TMZ alone= 13.4 mths, RT/TMZ + cilengitide= 16.3 mths, RT/TMZ + high dose cilengitide= 14.5 mths	RT/TMZ alone=4.1 mths, RT/TMZ + cilengitide= 5.6 mths, RT/TMZ + high dose cilengitide= 5.9 mths	Inconsistent OS/PFS outcomes and small sample size likely impacted results	Nabors, et al. [70]

Bevacizumab + Irinotecan (with RT/TMZ)	II	VEGF/DNA in GBM with unmethylated MGMT	RT/TMZ alone= 14.8 mths, RT/TMZ + bevacizumab + irinotecan= 16.6 mths	RT/TMZ alone= 5.99 mths, RT/TMZ + bevacizumab + irinotecan= 9.74 mths	Significant differences were reported between treatment and control arms	Herrlinger, et al. [97]
Bevacizumab (with RT/TMZ)	II	VEGF in primary GBM with unmethylated MGMT	RT/TMZ alone= 14.6 mths, RT/TMZ + bevacizumab=15.1 mths	RT/TMZ alone= 5.8 mths, RT/TMZ + bevacizumab=10.0 mths	-	Chinot, et al. [68]
Carboplatin + Bevacizumab	II	VEGF/DNA in recurrent GBM	bevacizumab alone= 6.4 mths, bevacizumab + carboplatin=6.9 mths	-	Determined that clinical outcomes for recurrent GBM patient treated with BEV were inferior to previously reported studies	Field, et al. [98]
Anti-EGFR antibody with radioactive isotype conjugated (125I-mAb 425)	II	EGFR in primary GBM	15.7 mths	-	-	Li, et al. [99]
Gefitinib	II	EGFR in recurrent GBM	8.9 mths	1.9 mths	EGFR expression did not correlate with survival	Rich, et al. [100]
Lenvatinib	II	Angiogenic cytokines in recurrent GBM	4.1 mths	1.9 mths	-	Reardon, et al. [101]
Sunitinib	II	VEGF in recurrent GBM	9.4 mths	-	No improvement in survival was seen for either for BEV-resistant and BEV-naïve recurrent GBM	Kreisl, et al. [102]
Pazopanib	II	VEGF in recurrent GBM	8.1 mths	2.8 mths	No improvement to survival but showed in situ biological activity as demonstrated by radiographic responses	Iwamoto, et al. [103]

1.4 Glioblastoma Invasion

1.4.1 Mechanisms of invasion in GBM cells

GBM cells, like all tumour cells, utilise a variety of signalling pathways and processes to interact with the ECM. The brain ECM is mostly composed of collagens, laminins, proteoglycans and fibronectin with many ECM components contributing to a pro-invasive environment [104]. Cell-matrix interactions are important in regulating invasion, requiring a balance between adhesion and detachment to the ECM, as well as ECM remodelling via proteolysis. In the latter circumstance, the cell may secrete proteases to degrade or modify components of the local ECM. GBM cells are known to secrete a variety of MMPs for this purpose and studies have observed higher expression of MMP-2 and MMP-9 (also known as gelatinase-A and gelatinase-B) in GBM tissue compared to the surrounding brain [105]. Primarily regulated by growth factors, the upregulation of MMP-2 and MMP-9 has been found to be influenced by EGF, TGF-ß and VEGF in tissue biopsies from glioma patients [105]. It has been observed that MMP-9 is more often strongly expressed along proliferating margins and close to blood vessels, whereas MMP-2 has a less restrictive pattern of expression, localising to both normal and malignant glial cells [106]. Consequently, it has been suggested that MMP-9 is predominantly involved in neovasculature remodeling, while MMP-2 is involved in both invasive and angiogenic events. Both MMP-2 and MMP-9 are activated by membrane type 1-matrix metalloproteinase (MT1-MMP) at the cell surface. MT1-MMP expression has been shown to correlate with tumour stage, and displays a strong association with ECM-degrading structures protruding from the membrane of cancer cells known as invadopodia [107]. In addition to MMPs, several other proteases are known to be upregulated in GBM, including serine proteases such as urokinase-type plasminogen activator (uPA) and its receptor (uPAR), cysteine proteases such as cathepsin B, and ADAMs (a disintegrin and metalloproteinase). Many upregulated signalling pathways in GBM converge on protease expression, particularly MMPs [104].

As mentioned briefly prior, GBM cells do not typically metastasize outside of the brain, and as such GBM is characterised by extensive local infiltration into the surrounding brain with recurrence predominantly seen within 1-3cm of the cavity remaining after surgical removal of the initial tumour mass [108]. It has been proposed that GBM cells invade along existing structures within the brain, including myelinated fibre tracts and vasculature. An example of this was reported in a murine model whereby navigation of HuN human glioma cells was seen along blood vessels in the perivascular space, comparable to the routes of migration travelled by neural progenitor cells and stem cells [109]. Invading cells undergo a number of changes during an EMT-like shift, such as increased motility and degrading capacity, and consequentially recurrent GBM cells commonly exhibit a mesenchymal-like subtype and display increased levels of proteases, such as MMPs [25]. Comparative analysis has shown that invading residual glioma cells following surgical resection are markedly different to the primary tumour mass from which they initially derived, and can be considered as distinct sub-entities [110]. Residual cells can vary not only in their invasive and proliferative abilities, but also their molecular profiles and sensitivity to various treatment modalities. It has been proposed that this population of cells may arrest from the cell cycle, potentially altering sensitivity to local irradiation and therapeutics [111, 112]. This may be significant for the treatment of GBM patients, as it is the residual cells that are exposed to treatment following the de-bulking of the original tumour mass. Consequently, these residual cells may have the potential to evade the effects of current adjuvant therapeutic protocols such TMZ and RT, ultimately contributing to disease recurrence.

1.4.2 The link between RT/TMZ treatment and enhanced GBM invasion

A number of studies have revealed a link between ionising radiation and enhanced cell invasion. One such study by Jung *et al*. observed that irradiated A549 lung epithelial cells changed in morphology to look more alike to fibroblasts, indicating these cells had undergone EMT to develop a mesenchymal phenotype, and also displayed an increased rate of migration [113]. In addition, an *in vivo* study examining the effects of ionizing radiation on rats with primary Lewis lung carcinoma (LLC-LM)

demonstrated the presence of an increased number of surface metastases in treated (46-62 metastases) versus untreated (2-8 metastases) rats [114]. The average number of surface metastases observed on the lung surface of treated rats was also found to rise from 5 to 53 per lung with an increase in irradiation dose (20-40Gy). It has also been established that radiation can induce an enhancement of MMP-2 secretion in a wide range of cancer cell types, including lung [115], pancreas [116], kidney [117], and brain [118-120]. An increase in MMP-2 secretion may assist tumour survival by decreasing apoptosis, inducing proliferation and angiogenesis, and promoting invasion. In one study, the intracellular expression of MMP-2 was seen to increase in just one out of three glioma cell lines following exposure to radiation, however, the extracellular secretion and activation of MMP-2 was observed across all the treated cell lines [7]. This correlated with an enhanced invasive capacity, with irradiated glioma cells which were subsequently implanted into rat brains resulting in more invasive tumours determined by an increase in the number of tumour microsatellites [7]. Additional studies have also reported that GBM cells surviving radiotherapy can exhibit enhanced migratory and invasive potential, indicating that the long-term inadequacy of treatment observed for most patients may be related to surviving cells exhibiting an increased invasive capacity [3, 4]. Studies by Trog *et al*. investigated the effect of radiotherapy (2Gy) and TMZ (30μM) on U87MG GBM cells in vitro, and observed that the treated cells exhibited activation of pro-invasive proteins via western blot analysis indicative of the greater malignancy grade also seen in the clinical observations of post-treatment aggressive recurrent tumours, as well as enhanced extracellular degrading activity of MMP-2 via zymography [5, 6]. Altogether, these findings demonstrate that cells surviving current therapy may display increased invasive potential, thereby negatively impacting patient survival.

As outlined by Hanahan and Weinberg, tumour growth and invasion to distant sites is influenced by more than just genetic abnormalities, as a wide variety of cellular features and interactions with the tumour microenvironment also play a role in tumour progression and resistance to therapies, contributing to a proliferative and invasive phenotype [1]. When examining the outcomes of targeted therapies to specific cancers, it is imperative to consider the multitude of ways tumour cells are able to adapt to a specific treatment, and in the future, it may be most beneficial to implement a combination of therapies to combat tumour progression and invasion more effectively.

1.5 Invadopodia

1.5.1 Invadopodia: An Introduction

To aid the process of invasion, tumour cells may form dynamic F-actin-rich membrane protrusions known as invadopodia. These 'finger-like' structures may reach lengths greater than 2μm, with diameters typically ranging from 0.1 to 1μm, and are known for their ability to overcome physical barriers presented in the microenvironment by adhering to the ECM and mediating its degradation through the action of transmembrane proteases, such as MT1-MMP, and secreted proteases, such as MMP-2 and MMP-9 [121, 122]. Invadopodia also act as mechanosensors, as changes in ECM rigidity can stimulate the formation of these dynamic structures. The invasive capacity of cancer cells has been correlated with their invadopodia-forming ability, and these structures have been detected in many cancer cell types [123-133] including GBM [121].

Owing to their ability to degrade the ECM in order to facilitate invasion, 'invadopodia' were first named by Chen in 1989, who described them as adhesive ventral protrusions that arose in v-src transformed fibroblasts [134]. They belong to a family of structures known as invadosomes, referring to both podosomes in normal cell types and invadopodia in malignant cells. All invadosomes adhere to and remodel the ECM, which is necessary for normal physiological conditions, such as embryogenesis and wound healing, but is hijacked in dysregulated tumour cells to allow for invasion and metastasis. Whilst both podosomes and invadopodia share the same basic molecular network, ubiquitous isoforms of specific regulatory proteins are often substituted in invadopodia that form in malignant cells. For example, the Wiskott-Aldrich Syndrome protein WASp is substituted for its ubiquitous counterpart N-WASp in invadopodia [135]. Invadopodia also have a longer turnover time than podosomes (capable of existing for a few hours), are able to extend further from the cell membrane, and are known to degrade the ECM more aggressively than podosomes [136, 137]. It is this highly localised proteolytic activity that is the defining feature of invadopodia, suggesting that these membrane structures represent a key mechanism of protease-dependent tumour cell invasion. Although non-proteolytic modes of invasion

are also known, these methods of invasion are generally seen in less dense areas of ECM such as loose stroma, whereas invadopodia are required in more rigid matrices such as basement membranes or tightly cross-linked ECM that require ECM remodelling for cell migration [138]. MMP activity is also involved in the cleavage of other non-matrix targets such as latent cytokines or integrins, which may also enhance tumour progression via the activation of specific signalling pathways. As invadopodia serve as sites of activation (whereby proteases are cleaved from a pro-state to their active form) and secretion of MMPs, they can influence invasion in a variety of ways, and therefore represent promising candidates for cancer therapies.

1.5.2 Stages of Invadopodia Formation

The formation and proteolytic activity of invadopodia involves various signalling pathways and can be separated into three distinct stages as proposed by Artym *et al.*: initiation, assembly and maturation [139]. A variety of invadopodia regulator proteins are involved with each stage, as outlined in ***Figure 1-4***.

1.5.2.1 Initiation

The first stage, known as initiation, involves the dissolution of focal adhesions and the formation of non-degradative precursors of invadopodia in response to a variety of stimuli, including growth factors, oncogenic transformation, hypoxia, induction of EMT, and MMP activity producing degraded fragments of the ECM [135, 139, 140]. Epidermal growth factor (EGF) stands to be the best characterised growth factor stimulus in the induction of invadopodia formation [123, 135], however other growth factors such as transforming growth factor-β (TGF-β) [141, 142], hepatocyte growth factor (HGF, also known as MET) [143] and heparin-binding EGF (HB-EGF) [127, 144] have also been shown to play a role in invadopodia initiation. These growth factor pathways require the action of integrins and phosphorylated focal adhesion kinase (FAK) at sites where the cell membrane contacts the ECM [137]. Ultimately, this results in the phosphorylation and subsequent activation of

invadopodia-regulating proteins predominantly through Src serine kinase-related pathways [137]. Protein kinase C (PKC) activation is also able to induce invadopodia formation by phosphorylating many of the same substrates as Src, thereby reinforcing the invadopodia initiation cascade [145].

1.5.2.2 Assembly

Once activated, Src is able to recruit a variety of proteins that form the core structure of the invadopodium, such as actin, cortactin, cofilin, N-WASP and Tks5 [146]. These proteins form the regulatory machinery that promotes the formation of an actin network required for invadopodia function via the severing and polymerisation of actin filaments. This process is highly coordinated, with Tks5 last to join the invadopodia-core protein complex to allow anchoring to PI(3,4)P2 (a phosphoinositide on the cell membrane) via its PX domain; with this step of the assembly process taking approximately 2-3 minutes [147]. Furthermore, elongation and stabilisation of the invadopodium structure is also driven by actin polymerisation, requiring interactions between regulators such as NWASP and Arp2/3 as well as the phosphorylation of cortactin and Tks5, and actin stabilisation by regulators such as Fascin [121, 137, 148].

1.5.2.3 Maturation

When their structure is stabilised, invadopodia reach the maturation stage of their lifecycle, involving the localisation of MT1-MMP to the tip of the protrusion and the subsequent extracellular secretion and activation of proteases [149]. This process involves the activities of key proteins such as Tks4, cortactin and β-integrin, which act to localise as well as stabilise MT1-MMP in the structure, and is also dependent on microtubules for the delivery of components to the tip of the invadopodium where they may be secreted, including proteases such as the matrix metalloproteinases MMP-2 and MMP-9 [137, 150], ADAMs such as ADAM12 [151], cathepsin cysteine proteases [137], and the serine proteases such as seprase [152]. Additionally, the exocyst complex has been shown to interact with proteins

NWASP and WASH to promote MT1-MMP delivery to the maturing invadopodium [153], accompanied by the v-SNARE/VAMP7 which enables the anchoring and fusion of vesicles containing MT1-MMP for insertion into the invadopodial membrane [154]. Subsequently secreted proteases are then able to modify and degrade the surrounding ECM, enabling the creation of pathways for cell motility which is ultimately crucial for invasion.

Figure 1-4: Stages of Invadopodia formation and function:

Initiation: Invadopodium initiation occurs at focal adhesions allowing for the adhesion and interaction of cancer cells with the surrounding ECM and involving interactions between integrins, Src and FAK signaling. β1 integrin activation leads to the recruitment of the tyrosine kinase FAK, which then recruits Src via phosphorylation on tyrosine 397. Src activity is also reinforced by the serine/threonine kinase PKC. Growth factors such as EGF, PDGF and TGF- β also activate Src via ligand binding to receptor tyrosine kinases (RTKs). Phosphorylation of Src leads to the activation of several proteins, including Tks5, phosphoinositide 3-kinase (PI3K) and PKC. Tks5, when phosphorylated by Src, localises to PI(3,4)P2 on the cell membrane.

Assembly: The assembly stage involves recruitment of actin regulatory machinery to the site of the developing invadopodium. Rho GTPase signalling (e.g. RhoA cooperation with Cdc42) converges on N-WASP, which subsequently activates the Arp2/3 complex to promote actin assembly. Phosphorylation of the key regulator, cortactin by kinases such as Src, PKC and Arg allows for the formation of the N-WASP–Arp2/3–cortactin–dynamin complex and the commencement of actin nucleation and polymerization. In addition, the phosphorylation of cortactin releases cofilin from the complex, leading to the severing of actin filaments and creation of barbed ends. Tks5 is subsequently recruited to the invadopodium-core allowing for anchoring to PI(3,4)P2 on the cell membrane.

Maturation: Dephosphorylation of cortactin blocks the severing ability of cofilin and enables the stabilization of the invadopodium actin core. Delivery of the exocyst complex, containing MT1-MMP, to the tip of the invadopodium is facilitated by microtubules. The V-SNARE protein, VAMP7 is involved in fusing the vesicle to the cell membrane, allowing delivery of MT1-MMP to sites of invadopodium-mediated ECM degradation. Cortactin and Tks4 regulate the delivery and secretion of proteases, such as MMP-2 and MMP-9 to the invadopodium tip, which digest the surrounding ECM.

Initiation

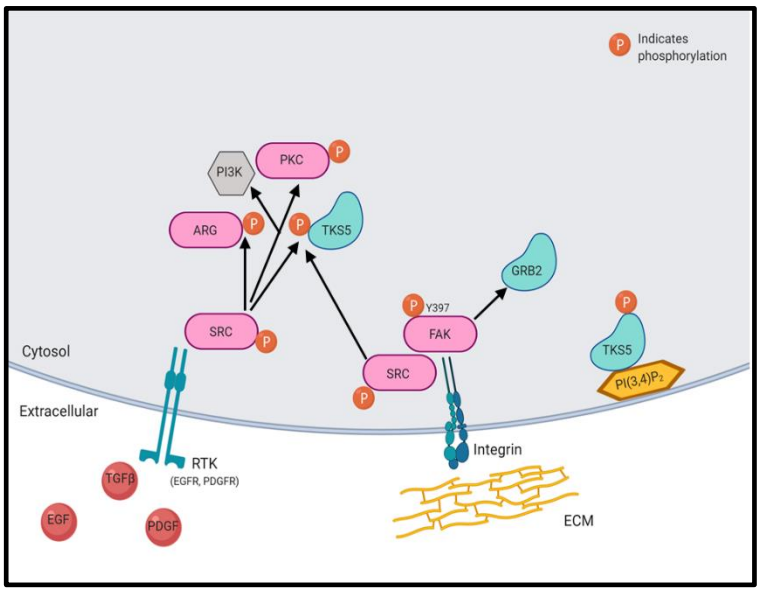

Assembly

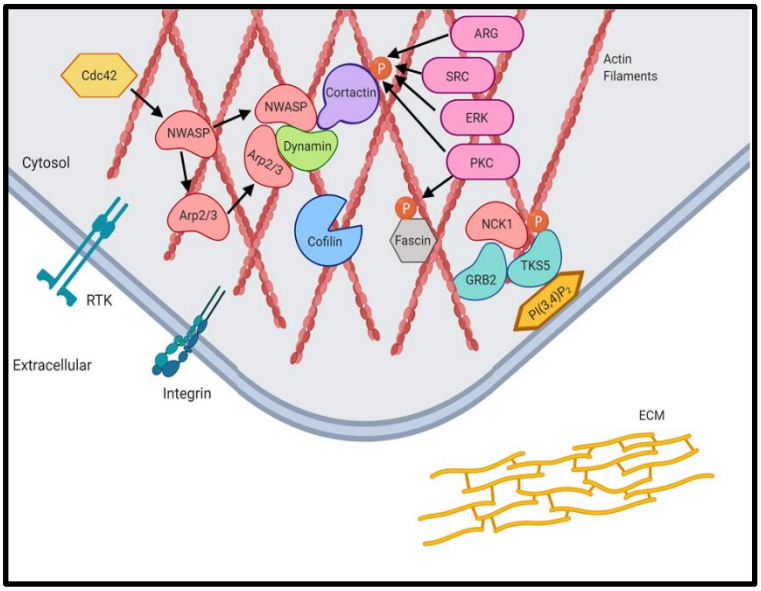

Maturation

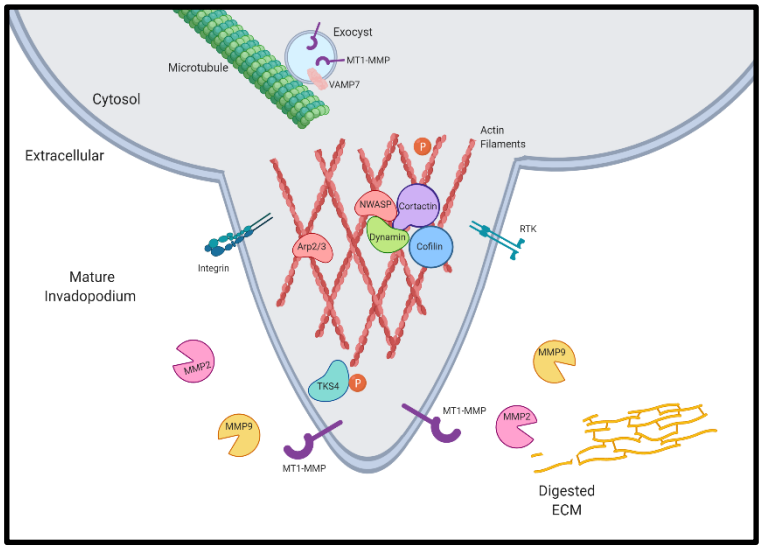

1.5.3 Invadopodia as a Target in Human Cancer

Proteins involved in the regulation of invadopodia have been shown to influence the invasive potential of a number of different cancers, including breast [123, 124], colorectal [128, 129], head and neck [155], bladder [131, 132] and brain [156, 157]. Invadopodia have also been observed in primary tumour cells from these cancers, indicating that invadopodia formation could serve as a diagnostic marker for malignant cancers [124, 129, 158]. Invadopodia regulators are expressed in glioma cell lines and cells derived from glioma patient-derived biopsies, with Tks5-positive glioma patients displaying a significant reduction in survival compared to Tks5-negative patients [158]. Additionally, Tks5 overexpression has also been reported in a number of other cancers, including lung, breast, colon and prostate, and is correlated with an increase in the invasive and metastatic potential of tumour cells [159]. Immunohistochemical and quantitative real-time PCR analyses have revealed that overexpression of the crucial invadopodia regulator, cortactin, promotes colorectal cancer progression and invasion [160]. In addition, siRNA knockdown or pharmacological inhibition of structural or functional invadopodia proteins, including cortactin, Tks5, Tks4 and MT1-MMP, has been shown to hinder cancer cell extravasation and metastatic colony formation in experiments utilising an *in vivo* mouse lung model [156]. These reports highlight the fundamental role of invadopodia in tumour cell invasion, thereby signifying their potential as a target for anti-invasive therapy. Currently the standard protocol for GBM therapy does not include therapeutics to block metastatic dissemination, including invadopodia-mediated invasion.

1.5.3.1 Targeting growth factor receptors

Targeting the various mediators and regulators, and associated pathways, contributing to invadopodia formation / activity may lead to the development of new therapeutics that could improve patient survival. The first potential target for novel anti-invasive therapies could include growth factor receptor pathways such as EGFR [161] and PDGFR [162]. EGFR inhibitors such as Gefitinib have been reported

to block invadopodia formation, whereas EGF stimulation of serum-starved breast cancer cells induced invadopodia formation via the N-WASP/Arp2/3 pathway [135]. Head and neck squamous cell carcinoma (HNSCC) cells co-cultured with inhibitors of EGFR (AG1478 and PD152035) also showed a reduction in invadopodia formation and ECM degradation [161]. However, clinical trials of anti-EGFR therapies in GBM have failed to show significant clinical effects, falling short of significantly inhibiting tumour growth (***Table 1-1***) [91-93, 95, 99, 100, 163-166]. Further studies may be required on biopsies from GBM patients who have been recruited to these studies compared to non-study GBM patients, in assessing whether these agents showed any effects on cell invasiveness at the tumour edge and the local expression levels of invadopodia regulators.

1.5.3.2 Targeting matrix metalloproteinases

As invadopodia are reliant on the activity of proteases to degrade the ECM, as well as their important role in metastasis and angiogenesis [167], MMPs are a family of proteases that represent another therapeutic target against tumour cell invasion. MMP inhibitors (MMPIs) have been investigated for this purpose. Some inhibitors can mimic the structure of collagen and block the activity of MMPs by occupying the substrate-binding site [168]. Promising developments have been seen in *in vitro* studies of MMP antagonists Batimastat and Marimastat, indicating that these inhibitors may impede GBM invasion, as well as possessing cytostatic effects at high concentrations [169]. However, problems have arisen in clinical trials of MMPIs due to non-specificity and adverse effects at high doses, thus limiting efficacy of these drugs due to the associated toxicities [167]. Pre-clinical studies have shown that these treatments are better applied in the case of early tumour onset, instead of patients with advanced, metastatic cancer where the treatments may be largely ineffective [170]. It is reasonable to conclude that other means of targeting MMP activity should be considered in this case, such as inhibiting their delivery to the membrane for example.

1.5.3.3 Targeting Src Kinase

Src also poses as a potential therapeutic target due to its role in many processes including migration, angiogenesis, resistance to therapy, and invadopodia activity [171-173]. Since Src is known to phosphorylate a number of invadopodia regulators, inhibitors of Src have been shown to suppress the invasive ability of colon, prostate and ovarian cancer cells *in vitro* [174, 175]. Interestingly, in the case of EGF-induced actin polymerisation via the phosphorylation of cortactin, loss of Src activity can be rescued by Arg (another tyrosine kinase) overexpression, but not vice versa [123]. This indicates that Arg may act downstream of Src, and thus Arg should also be considered as a candidate target for the inhibition of invadopodia activity. Src inhibition monotherapy has showed little success in early clinical trials [175-178], however more recent trials indicate potential when inhibitors of Src are combined with other inhibitors, such as dasatinib and erlotinib that target EGFR in the treatment of non-small cell lung cancer patients [179].

Continued investigation into therapies that target invadopodia may be promising, as these agents could potentially be used as novel adjuvant treatments that prevent the metastatic spread of cells that survive, or are resistant to, current clinical therapies such as radiation and temozolomide treatment. As previously mentioned, GBM cells that survive the current treatment regime have been shown to exhibit a more invasive phenotype. Therefore, by abrogating invadopodia formation and/or function, additional therapeutics that target specific invadopodia-pathways may have an anti-invasive effect and thus could improve patient outcome.

1.6 Extracellular Vesicles (EVs)

1.6.1. EV Subtypes and Biogenesis

Since their discovery 30 years ago, extracellular vesicles (EVs) have emerged as a diverse group of secreted membrane-bound vesicles that are released by most cell types [180]. Ranging from 30-2,000nm in diameter, EVs play an important role in mediating intercellular communication in a wide variety of normal biological processes, such as tissue repair [181, 182], and pathological processes, such cancer progression [183, 184]. The importance of EVs lies within their ability to shuttle bioactive molecules contained within their lipid bilayer or aqueous core -including proteins, lipids, DNA and RNA- from donor cells to nearby or distant recipient cells. Release of donor-cell specific EV cargo, particularly mRNA and miRNA, can modulate gene expression and signalling pathways in recipient cells, ultimately altering the phenotype of these cells [185]. Indeed, this EV-mediated communication is known to aid tumour progression by influencing processes such as proliferation, invasion, drug resistance and establishment of a tumour-permissive microenvironment [186-191].

EVs have previously been categorised based on their mode of biogenesis and size: exosomes (30-150nm in diameter), microvesicles (MVs) (100-1500nm in diameter) and apoptotic bodies (1000-5000 nm in diameter) [192]. Considerable focus has been given to the biogenesis of MVs (EVs shed from the plasma membrane) and exosomes (EVs of endosomal origin) and has resulted in a basic understanding of the mechanisms regulating the production of these vesicles. Less focus has been given to apoptotic bodies, which are formed via fragmentation of the cell during apoptosis, and are generally engulfed by surrounding cells in order to evade immune response, although they have been shown to be involved in intracellular communication [193].

Although these subtypes of EVs are commonly referred to throughout the literature, their overlapping size distribution in the 100-200nm range means that microvesicles and exosomes cannot be experimentally distinguished based on size alone [194]. It is also now apparent that additional classes or subtypes of EVs are likely to exist. A recent study, employing asymmetric-flow field-flow

fractionation to precisely separate small vesicles of different sizes, demonstrated that cancer cells produce large quantities of small (35nm in diameter) EVs termed ‘exomeres’ that are distinct from exosomes and MVs [195]. Unlike exosomes derived from the same cells, these smaller exomeres were absent in components of ESCRT complexes, and displayed unique cargo and biophysical properties, suggesting that these smaller vesicles may exert distinct -but currently unknown- biological functions.
Given the overlap in size and density of most small EVs, current isolation methods are unable to efficiently separate EV subtypes and are likely to produce mixtures of EVs of different origin. As it is not possible to verify the subcellular origin of most experimentally obtained EVs, current guidelines suggest researchers adopt operational terminology such as referring to size (< 200 nm are generally refers to small EVs, while > 200 nm are large EVs), density (low/high density EVs with defined ranges) or composition (CD63+/CD81+ EVs) in place of ‘exosome’ and ‘microvesicle’ to describe EVs of unconfirmed subcellular origin [196].
The following sections briefly cover the origin and biogenesis of MVs and exosomes, which is also summarised in ***figure 1-5***.

1.6.1.1 Microvesicle Biogenesis

MVs are generated by the outward budding and fission of the plasma membrane and are thus often referred to as ‘shed microvesicles’. The generation of MVs may be influenced by the redistribution of phospholipids within the plasma membrane during lipid-raft restructuration, requiring that phosphatidylserine is first translocated from the inner to the outer leaflet of the membrane, followed by actin-myosin cytoskeletal contractions that trigger MV release [197, 198]. In melanoma cells, contraction of actin-myosin cytoskeleton at the neck of developing MVs has been shown to be mediated by a small GTPase known as Arf6 [199]. In this study, activation of Arf6, along with the recruitment of proteins such as arrestin domain-containing protein-1 (ARRDC1) and the endosomal protein Tumour Susceptibility Gene 101 (TSG101), was suggested to contribute to MV budding and release. The EGFR pathway has also been implicated in MV biogenesis via activation of another small GTPase known as RhoA [200]. In this pathway, downstream activation of Rho-associated protein kinase (ROCK) and

LIM kinase (LIMK) allows for the phosphorylation of cofilin, in turn promoting the actin-cytoskeletal rearrangements necessary for MV budding. Supporting the role of the actin cytoskeleton in MV formation, F-actin has been found within MVs from aggressive cancer cells [200, 201]. Inhibition of myosin II activity (with blebbistatin) or actin polymerisation (with latrunculin A) prevents MV release from the plasma membrane [199].

1.6.1.2 Exosome Biogenesis

Exosomes are produced via an endocytic pathway, whereby invaginations of the membrane of late endosomes result in the formation of multivesicular bodies (MVBs) containing tiny vesicles known as intraluminal vesicles (ILVs). Once these MVBs fuse with the plasma membrane, the ILVs are released into the extracellular space as exosomes. The generation of ILVs can occur through the Endosomal Sorting Complex Required for Transport (ESCRT)-dependent or –independent pathways.

The ESCRT machinery aids selective packaging of ubiquitinated cargo into ILVs and consists of four protein complexes (ESCRT-0, -I, -II, -III), comprising of a total of 20 proteins [235, 236]. shRNA depletion of ESCRT components, such as TSG101 or hepatocyte growth factor-regulated tyrosine kinase substrate (HRS), has been shown to inhibit ILV formation and exosome release in cervical cancer cells [202]. Whilst the presence of ESCRT-associated proteins, such as TSG101 or ALIX, has often been used as evidence of endosomal origin in purified EVs, ESCRT components may also be involved in budding and EV release from the plasma membrane and are therefore not specific to exosomes [203, 204]. In the case of plasma membrane-shed vesicles, RNA interference (RNAi) targeting the ESCRT-0 and ESCRT-I subunits was found to partially suppress shedding, whilst targeting ESCRT-II and ESCRT-III had no effect on the release of these vesicles [205].

Exosome generation can also occur in an ESCRT-independent manner, as cells are still able to form MVBs despite depletion of all four ESRCT subunits [206]. The proposed mechanisms driving ESCRT-independent biogenesis suggest the involvement of lipids (such as ceramide), tetraspanins (such as CD9,

CD63, CD37, CD81) and heat shock proteins (such as Hsp70, Hsp90). Ceramide and ceramide-producing enzymes known as sphingomyelinases have also been implicated in glial cell exosome release, whilst the ESRCT-associated proteins TSG101 and ALIX were found to not be involved [207, 208]. Importantly, these ESCRT-independent mechanisms may not be exclusive to exosome generation, as ceramide activity has also been implicated in MV shedding from ATP-stimulated glial cells [209].

Figure 1-5: EV biogenesis and uptake

A schematic representation of the biogenesis of exosomes and microvesicles and their uptake in recipient cells. Whilst MVs form via budding of the plasma membrane, exosomes develop via an endosomal pathway, whereby endocytosis at the cell membrane results in the formation of early endosomes. Early endosomes undergo a second invagination event whilst maturing into late endosomes (also termed multivesicular bodies (MVBs)), which can result in cytosolic proteins, DNA, RNA being captured within the newly formed intraluminal vesicles (ILVs). Late MVBs can be transported to lysosomes for degradation or may be transported to the plasma membrane for exosomal release. These processes can be mediated through the action of Rab GTPases, such as Rab27a/b or Rab7/11/35. Fusion of the MVB and cellular plasma membranes is assisted by SNAREs present on both membranes, thereby allowing ILVs to be released into the extracellular space as exosomes. Uptake of EVs by recipient cells may occur via endocytosis, fusion of the exosomal membrane with the cell membrane, or ligand-binding between transmembrane proteins on the exosomal surface or cleaved fragments from the exosomal surface with the recipient cell that can initiate signaling cascades in the recipient cell.

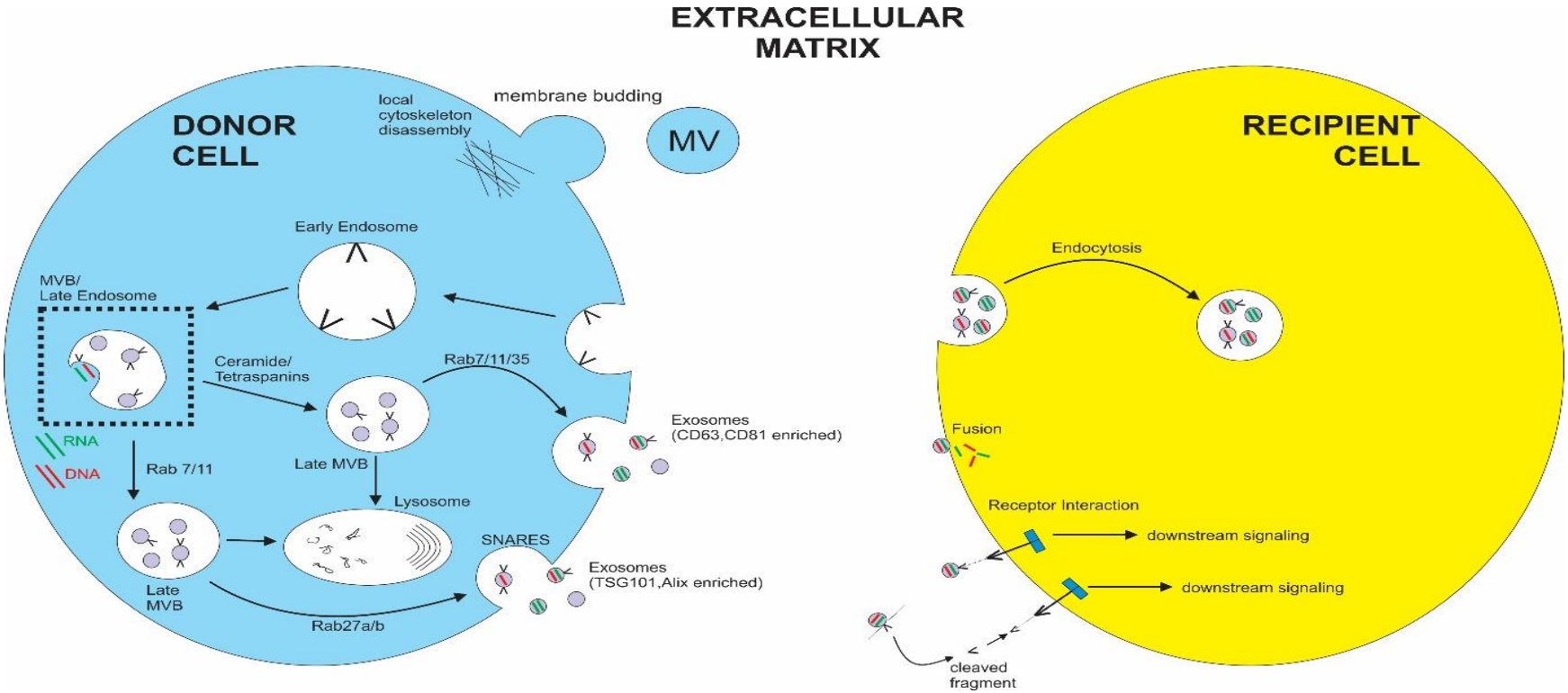
EXTRACELLULAR MATRIX
DONOR CELL
local cytoskeleton disassembly
membrane budding
MV
Early Endosome
MVB/ Late Endosome
Ceramide/ Tetraspanins
Rab7/11/35
Exosomes (CD63,CD81 enriched)
RNA
DNA
Rab 7/11
Late MVB
Lysosome
SNARES
Exosomes (TSG101,Alix enriched)
Late MVB
Rab27a/b
RECIPIENT CELL
Endocytosis
Fusion
Receptor Interaction
downstream signaling
downstream signaling
cleaved fragment

1.6.2. EV Trafficking and Release

Whilst microvesicles form at the cell plasma membrane, exosomes require the transport of MVBs to the cell periphery for release into the extracellular space. Although there is a clear distinction in secretory pathways for each EV subtype, several common mechanisms exist.

1.6.2.1 Rab GTPases

Although not fully elucidated, one pathway involved in EV release is known to be mediated through the involvement of Rab GTPases, such as Rab27a or Rab27b, that are involved in the trafficking of MVBs to the plasma membrane [210]. Importantly, Rab27a/b are not exclusive to exosome trafficking, and are also involved in the secretion of Golgi-derived granules [211] and lysosome-related organelles [212]. Other Rab GTPases, such as Rab11 [213, 214] and Rab35 [215], have also been implicated in MVB transport, and knockdown of both Rab GTPases together has been shown to result in accumulation of endosomal cargo using a *C. Elegans* model [216]. Rab3a has been implicated in vesicle trafficking [217], and specific isoforms of the Rab3 family proteins have been identified in glial cells [218].

1.6.2.2 SNAREs

Soluble N-ethylmaleimide-sensitive factor attachment protein receptors (SNAREs) assist in the fusion of the MVB and plasma membranes, with vesicular SNARES (v-SNAREs) interacting with target SNAREs (t-SNAREs) on the cell membrane. Studies have demonstrated their involvement in Ca2+ regulated exocytosis [219], and exosome secretion [220, 221]. SNARE-proteins, synaptosome associated protein 25 (SNAP25), vesicle associated membrane protein 2 (VAMP2) and Syntaxin-1 (Stx1), are required for neurotransmitter release in CNS cells [222]. Stx1 plays a role in exosome

secretion [223] and early studies have shown that knockdown of Stx1 inhibits GBM tumour growth *in vivo* and GBM invasion *in vitro* [224], however further investigation into its mode of action is required.

1.6.2.3 Cytoskeletal Regulation

Microtubules and the actin cytoskeleton are known to be involved in MV shedding [225], but may also facilitate the transport of MVBs to the site of release at the cell periphery [226]. Endosomal trafficking via microtubules is well documented in neurons and cultured cells [227], and EVs have also been associated with protrusive cytoskeletal structures at the cell membrane [228, 229]. Overexpression of cortactin, a critical actin cytoskeletal regulatory protein, has been correlated with an increase the number of small EVs released from cancer cells without altering their cargo, suggesting that targeting cytoskeletal remodelling may impact upon vesicle secretion [230]. Nevertheless, further investigation into the mechanisms controlling EV secretion is required to gain a better understanding of the various processes at play.

1.6.3 EV Uptake

In order to facilitate intercellular communication, donor EVs may interact with recipient cells in a variety of ways. These include interactions between the recipient cell surface and EV-membrane (whereby EV surface proteins bind to recipient cell surface receptors), the fusion of the EV- and recipient cell- membranes (thereby releasing the contents of the EV into the cytoplasm), or EV internalization via endocytosis (first requiring receptor binding followed by internalization). Proteases may also cleave EV surface proteins to produce free ligands that may bind to membrane receptors on the recipient cell [231]. Interestingly, EVs show tropism towards specific cell types, with such recipient cells also capable of mediating the mechanism of uptake [232]. It is also likely that multiple modes of EV uptake may also operate within the same cell type. This is supported in a study that identified GBM-EVs were internalized by human umbilical vein endothelial cells (HUVECs) via heparan sulfate

proteoglycan (HSPG)-mediated endocytosis [233]. However, targeting EV internalization with inhibitors such as heparin only partially disrupted uptake, suggesting that different mechanisms of EV uptake may operate within the same cell type [234].

1.6.4 EV Cargo

EV cargo is donor-cell specific, thus reflecting the cell of origin, localisation and biogenesis pathway, and can consist of an assortment of cellular metabolites, DNA, RNA, protein, and lipids. Currently there are no markers specific to MVs compared to exosomes [235], however molecules required for the generation of exosomes are generally enriched in these vesicles, and include tetraspanins (CD63, CD9, and CD81), endosome-associated proteins (TSG101 and ALIX – although these proteins are likely to be absent in exosomes generated via an ESCRT-independent pathway) and heat-shock proteins (HSP90) [236-238], which are widely accepted as exosomal markers [239]. Importantly, these enriched proteins are not exclusive to exosomes and, depending on the approach used to isolate EVs, may be detected in other vesicle subtypes such as microvesicles [240, 241]. EVs are also able to incorporate transmembrane proteins into their membrane and can display receptors on their surface, as well as soluble mediators in their aqueous core, such as cytokines and growth factors [242]. Additionally, it is now recognised that the coronal layer of EVs, consisting of surface-conjugated macromolecules, can influence the biophysical properties of EVs such as their hydrodynamic diameter and mobility, and is therefore an important component of EVs [243]. Nevertheless, the proteins found in EVs are generally divided into several broad categories, as represented in ***figure 1-6***. Although there is not yet a consensus on markers that confirm the subcellular origin of isolated vesicles and thus distinguish between each type of EV [196], online databases such as EVpedia [244], Vesiclepedia [245] and Exocarta [246] have been able to record the range of molecules and markers identified in various EVs from multiple cell types.

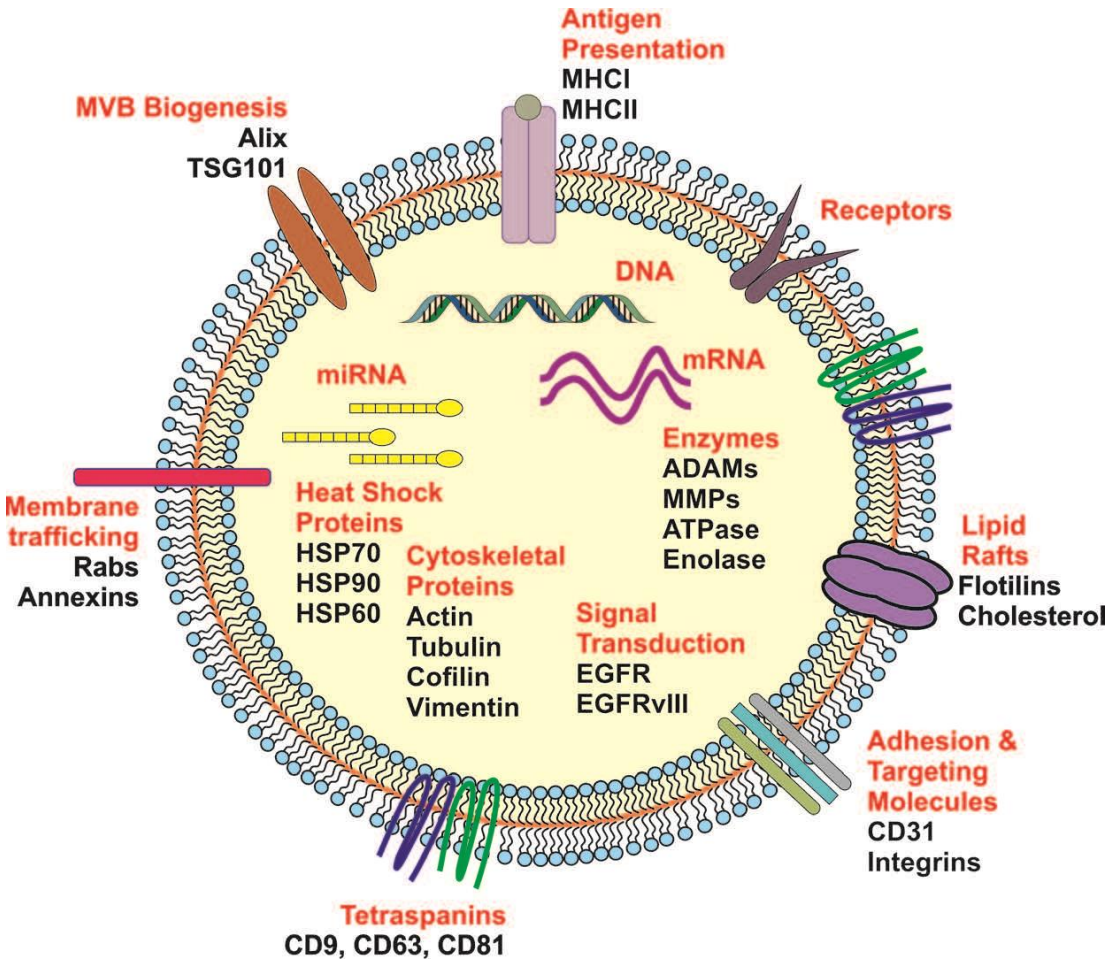

Figure 1-6: The molecular components of small EVs/exosomes

An illustrative representation of the protein composition of small EVs (exosomes). These vesicles are enclosed by a phospholipid bilayer (colored blue) and contain various proteins on the membrane surface as well internally within their cargo. This internal cargo is also comprised of nucleic acids such as miRNA, mRNA and DNA. This figure has been published as part of the review 'Cancer Exosomes in Cerebrospinal Fluid' [247].

Growing evidence suggests that EV cargo is selectively incorporated, with specific mRNAs and miRNAs found to be enriched in EVs relative to their cell of origin [10, 248]. Although the mechanisms of cargo selection are not yet fully understood, post-transcriptional modifications of proteins and transcripts may influence the process. For example, the ubiquitination of proteins has been found to influence ESCRT-mediated packaging into MVBs [249]. Furthermore, a study by Batagov et al. [250] has revealed that most mRNA found in GBM-EVs is likely fragmented and is less than 700nt in length (compared to 400-12,000nt RNA present in donor GBM cells). The EV-contained mRNA showed a bias towards the 3'-UTR region which is rich in miRNA binding sites and elements dictating localisation, however the authors did not report on the size of these vesicles, making it difficult to determine the subpopulation of EVs examined. Similarly, miRNAs with uradine at their 3' end have been found to be enriched in B cell- derived exosomes, suggesting a possible mechanism of miRNA sorting into these vesicles [251]. Similarly, mRNA in GBM cell-derived exosomes shows a bias towards the 3'-UTR region, known to be rich in miRNA-binding sites and elements dictating mRNA localisation [250]. The enrichment of specific cargo in EVs compared to their donor cell of origin suggests that selection of cargo may occur during EV formation, and implicates that the release of this cargo could impact on gene expression levels or initiate signalling cascades in recipient cells [185, 252].

1.6.5 EVs in Cancer

The role of EVs in cancer lies within their ability to mediate intracellular communication through the transfer of their lipid-bilayer enclosed cargo, with oncogenic genes, proteins, receptors, and miRNAs able to be delivered to nearby or distant recipient cells [253]. EVs have been found to influence a variety processes in cancer progression, such as proliferation and invasion [186, 187], modifying the tumour microenvironment to support tumour growth response [191]., and transferring acquired drug resistance [188-190]. Although the findings to date highlight a role for EVs in cancer progression, the extent of this influence is still not definitive. Like many other cancer types, studies have demonstrated that brain

tumour cells secrete EVs containing cargo selectively enriched for oncogenic related functions (***Table 1-2***), with an estimated 10,000 EVs released from a single GBM cell over 48 hours [11]. The following sections briefly cover current knowledge of the influence of EVs on important cancer-related processes.

Table 1-2: Laboratory studies investigating the impact of brain tumour cell derived-EV cargo on recipient cells

Publication	Donor Cell	Recipient Cell	EV Subtype	Cargo Marker	Biological Effect
D'Agostino, S., et al., 2006 [254]	G26/24 oligodendroglioma cells	Rat Fetal Cortical Neurons	MVs (100-500 nm)	Fas-ligand (Fas-L)	Induction of neuronal apoptosis
Al-Nedawi, K., et al., 2008 [255]	U373vIII GBM Cells	U373 GBM Cells	MVs (100-500 nm)	EGFRvIII	Transfer and expression of EGFRvIII and activation of tumour promoting pathways associated with EGFRvIII (MAPK/ERK and Akt)
Skog, J., et al, 2008 [11]	GBM Patient-Derived Cells	U87MG GBM Cells	MVs (50-500 nm)	VEGF, angiogenin, IL-6, IL-8	Stimulated angiogenesis and proliferation
Skog, J., et al, 2008 [11]	GBM Patient-Derived Cells	HMVECs	MVs (50-500 nm)	Gluc mRNA	Transfer of Gluc mRNA and expression of Gluc protein in endothelial cells. GBM-derived EVs stimulated tubule formation in endothelial cells, and proliferation in GBM cells.
Svensson, K.J., et al., 2011 [256]	U87MG GBM Cells	HUVECs	Small EVs (60-100 nm)	TF (Tissue Factor)	Induction of pERK1/2 and HB-EGF, elicited a proangiogenic phenotype
Arscott, W.T., et al., 2013 [257]	Irradiated U87MG Cells	U87MG GBM Cells	Small EVs (140 nm)	CTGF-mRNA, IGFBP2	Enhanced cell migration
Kucharzewska, P., et al., 2013 [258]	Hypoxic U87MG GBM Cells	HUVECs	Small EVs (50-200 nm)	CAV1, IL8, PDGFs, MMP-9	Enhanced proliferation and survival in hypoxic conditions, and increased tube forming capacity

Sharghi-Namini, S., et al., 2014 [259]	U87MG GBM Cells-overexpressing DLL4	HMVECs	Small EVs (191 nm)	DLL4	Activation of Notch target genes Hey1 and Hes1, increased cell motility, suppression of angiogenic sprouting
van der Vos, K.E., et al., 2015 [260]	GBM Patient-Derived Cells	Microglia	Small EVs (100-200 nm)	miR-451, miR-21	Reduced c-Myc mRNA, increased proliferation
Zhang, L., et al., 2015 [261]	Astrocytes	Metastatic HCC1954 breast cancer cells	Small EVs (30-100 nm)	miR-19a	Downregulation of PTEN, and increased cranial metastatic outgrowth
Setti, M., et al., 2015 [262]	U87MG GBM Cells overexpressing CLIC1	U87MG GBM Cells	Small EVs (146 nm)	Chloride Intracellular Channel-1 (CLIC1)	Enhanced tumour growth *in vivo* in a CLIC1 dose-dependent manner
Ricklefs, F., et al., 2016 [263]	Proneural GSCs	Mesenchymal GSCs	Small EVs (majority <200 nm)	p-ERK, p-SRC, p-P65, EGFR	Phosphorylation of these kinases, and EGFR expression, increased in proneural GSCs treated with mesenchymal-derived EVs
Pinet, S., et al., 2016 [264]	U87MG GBM Cells	YKL-40-silenced U87MG GBM Cells	Small EVs (90 nm)	TrkB	Increase in proliferation and endothelial cell migration
Lang, H., et al., 2017 [265]	A172 GBM Cells	HBMECs	Small EVs (50-100 nm)	linc-POU3F3	Increase in migration, proliferation, tubular-like structure formation *in vitro* and arteriole formation *in vivo*
Lang, H.-L., et al., 2017 [266]	A172, U87MG, U251, and T98G GBM Cells	HUVECs	Small EVs (50-100 nm)	linc-CCAT2	Increase in migration, proliferation, tubular-like structure formation *in vitro*, and arteriole formation *in*

					vivo, through upregulated VEGFA and TGFβ
Sun, X., et al., 2017 [267]	GSCs overexpressing miR-21	HBMECs	Small EVs (20-120 nm)	miR-21 and VEGF	Increase in tube formation and migration, and VEGF secretion
Figueroa, J., et al., 2017 [268]	Glioma-associated human mesenchymal stem cells (GA-hMSCs)	GSCs	Small EVs (40-100 nm)	miR-1587	Increase in proliferation and clonogenicity, through the downregulation of NCOR1
Kore, R.A., et al., 2018 [269]	Hypoxic U87MG GBM Cells	EPCs	Small EVs (61 nm)	LOX, TSP1, VEGF, ADAMTS1	Increase in tube formation, length and branching
Hallal, S., et al., 2018 [270]	U87MG, stem and differentiated GBM cells	Human Astrocytes	Small EVs (<150 nm)	No specific cargo marker detected	Activation of Myc and inhibition of p53, and induction of invadopodia activity in GBM-EV treated astrocytes
Taheri, B., et al., 2018 [271]	Rat-derived C6 Glioma Cells	Rat astrocytes	MVs (200-300 nm)	Unknown	Increase in proliferation and upregulated mRNA expression of GFAP, MMP2, MMP14 and downregulation of TIMP2
Dai, X., et al., 2019 [8]	GBM Cells - overexpressing AHIF	U251MG and U87MG GBM Cells	Small EVs	AHIF	Increase in viability, invasion and radio-resistance through inhibition of HIF-1A
Zhao, M., et al., 2019 [272]	Radio-resistant U251 GBM Cells	U251 GBM Cells	Small and larger EVs (50-500 nm)	Circular RNA: CircATP8B4	CircATP8B4 acts as a miR-766 sponge in normal U251 cells and promoted radio-resistance

1.6.5.1 EVs in Proliferation

As a tumour progresses, it accumulates genetic and epigenetic changes that may promote the expression or activity of oncogenes, resulting in unregulated neoplastic growth. Malignant progression may be driven, at least in part, by EVs. For example, U373 glioma cells produce a greater number of EVs when expressing the constitutively active form of the epidermal growth factor receptor (EGFRvIII), which enhances the horizontal propagation of oncogenes and the resulting transformed phenotype [255]. Indeed, aggressive cancer cells have been observed to secrete greater quantities of vesicles compared to their lower-grade or untransformed counterparts, suggesting that malignant cells are capable of producing large quantities of EVs which may be, in part, influenced by established cancer-promoting proteins such as EGF [11, 201, 255, 273]. The autocrine function of tumour EVs in enhancing the growth and survival of cancer cells has been extensively studied in recent years [11, 255, 274, 275]. One study found that exosomes from a highly malignant pancreatic cell line can enhance the proliferation rate of a less malignant pancreatic cell line via the transfer of a zinc transporter, ZIP4, that was upregulated in these vesicles [276]. Similarly, prostate cancer cell-derived exosomes significantly increase proliferation and migration in recipient prostate cancer cells *in vitro*, as well as enhancing tumour volume *in vivo* when administered intravenously in xenograft bearing mice [277]. EVs may also act upon other surrounding cells in a paracrine manner, as is seen for EVs derived from senescent cells that exert an pro-proliferative on other cancer cells [278]. Oncogenic EVs may also serve to modify the tumour microenvironment to favour malignant growth, having been shown to reprogram surrounding fibroblasts to secrete growth factors and cytokines that promote tumour growth and survival [279, 280].

1.6.5.2 EVs in Migration and Invasion

Tumour EVs are well documented to promote invasion and migration in recipient cells and are emerging as important mediators in cancer metastasis. EVs secreted from highly metastatic cells may function at the primary tumour site to transfer metastatic activity to poorly metastatic cells [281, 282], or may be released into the bloodstream where they can facilitate metastatic spread by preparing secondary sites, known as premetastatic niches, for the arrival of tumour cells [283]. A number of EMT-related proteins have been associated with tumour-derived EVs, such as TGF-β [284], Wnt [285, 286], annexin A2, casein kinase II α [287] and caveolin-1 [288], and functional studies have shown the EV-mediated delivery of these EMT inducers promotes a metastatic phenotype in recipient cells [286, 289, 290]. In addition to proteins, EV-associated miRNAs, such as miR499a, miR-10b and miR-221, have also been shown to promote the invasive potential of recipient cells [291-294].

Lending to their pro-invasive role, tumour EVs are often rich in proteases (such as MMPs and ADAMs), their regulators (such as EMMPRIN) and their inhibitors (such as TIMPs) [295-297]. It is possible that the delivery of these proteases may facilitate invasion in recipient cells. Indeed, there exists a positive correlation between the number of shed microvesicles, the proteases they contain, and the *in vitro* invasive capacity of breast cancer cell lines [298]. Furthermore, it was recently shown that MMP-1 - carrying exosomes are able to facilitate peritoneal dissemination, and thus metastasis, in ovarian cancer [299]. In addition to proteases, transfer of their regulators can also exert a pro-invasive effect, as human uterine epithelial cells secrete EMMPRIN (also known as basigin or CD147) in EVs that stimulates the production of MMPs in recipient cells [297]. Likewise, the horizontal transfer of exosomal CXC chemokinerecepter-4 (CXCR4) promotes hepatocarcinoma cell migration and invasion through the enhanced secretion of MMP-2 and MMP-9 in recipient cells [300, 301]. Evidence also suggests that proteases contained within EVs may be functionally active, possibly providing another mechanism of directed matrix degradation to aid cancer cell invasion [199, 295, 302].

1.6.5.3 EVs in Angiogenesis

As the uncontrolled growth of a tumour mass causes a reduction in nutrient and oxygen supply in the surrounding microenvironment, the process of angiogenesis becomes essential for tumour survival. Hypoxic conditions are known to stimulate the formation of new vessels that can supply oxygen to the developing tumour mass [39], and more recently, hypoxia has also been shown to stimulate the release of EVs with pro-angiogenic cargo [258, 303-306]. Many studies have investigated the pro-angiogenic content of tumour-cell EVs. Taraboletti and colleagues [307] discovered that endothelial cell-derived EVs contain β1 integrin and active MMP-2, MMP-9 and MT1-MMP that may promote endothelial cell invasion as well as the formation of new vessels. Interestingly, this study also demonstrated that VEGF and FGF-2 (fibroblast growth factor-2) stimulation led to an increase in the amount of MMP present in EV cargo. Studies have also shown that tumour cell-derived EVs can stimulate the growth and migration of endothelial cells in order to promote angiogenesis during tumour development [258, 303, 308]. This effect was highlighted in a study by Skog et al., [11] which demonstrated a doubling of tubule length in endothelial cells treated with GBM-cell MVs enriched with pro-angiogenic proteins (such as angiogenin, IL-6, IL-8, TIMP-1, VEGF and TIMP-2), compared to endothelial cells treated with angiogenic growth factors.

1.6.5.4 EVs in Immune Suppression

It is well established that the local tumour microenvironment is often immunosuppressed, allowing cancer cells to evade immune detection and continue their unregulated growth [309]. This often occurs through T cell mediated immune suppression [310]. It has now also emerged that cancer cells release immunosuppressive EVs that can assist immune evasion and promote a pro-tumorigenic phenotype in immune cells. One way in which tumour cells may suppress T cell activity is through the upregulated expression of program cell death ligand 1 (PD-L1) on their surface that inactivates T cells via interaction with their PD-1 receptor [311]. Tumour cells can release EVs containing PD-L1, suggesting a vesicle-

driven mechanism of immune suppression in the tumour microenvironment, and levels of circulating PD-L1-postive EVs have been associated with tumour progression in a variety of cancers [312-314]. EV-transferred miRNAs may also possess an immunosuppressive role via the promotion of apoptosis in CD8+ T cells [294, 315] or an inflammatory response in recipient immune cells that ultimately facilitates tumour growth and metastasis [316].

1.6.5.5 EVs in Therapeutic Resistance

As EVs can transfer various aspects of the donor cell phenotype to recipient cells, the emerging role of EV cargo in conveying drug resistance has been the focus of a number of studies [188-190]. Importantly, EVs have now been recognized for their ability to confer drug resistance in cancer cells through a variety of possible mechanisms. The first of these involves direct binding of the EV to the drug, thereby acting as a decoy and interfering with its ability to bind to and inhibit tumour cell activity, as is seen in small EVs secreted by HER2-positive breast cancer cells that bind directly to Trastuzumab [317]. Vesicles may also transport bioactive cargo that confers drug resistance, including the exchange of drug transporters. A well-known drug transporter, P-glycoprotein, has been shown to correlate with cancer treatment failure [318] and recent evidence has highlighted this multidrug resistance transporter may be shuttled between cells via EVs [319]. Another mechanism that may operate to protect cells from the cytotoxic effects of chemotherapeutic agents involves the expulsion of drug from the cytoplasm via vesicle secretion, as demonstrated in the exosome-mediated removal of cisplatin from ovarian cancer cells [320]. A reduction in cisplatin resistance was observed upon treatment with proton pump inhibitors that inhibit exosome secretion using an *in vivo* subcutaneous melanoma mouse model [321]. A study also confirmed this mechanism of drug removal using fluorescent microscopy to capture vesicle-encapsulated doxorubicin expelled from breast cancer cells [322].

1.6.6 Brain-Tumour Derived EVs as Biomarkers

An ideal molecular biomarker predicts changes prior to observable macroscopic malignant change. EVs have been successfully isolated from a variety of human biofluids, including saliva, breast milk, blood, serum and CSF [323-325]. Circulating EVs represent a non-invasive source of biomarkers for the longitudinal monitoring of cancer progression in patients, without the need for repeated and invasive tumour biopsies or expensive imaging. This is particularly important for brain tumour patients, as histological analysis requires an invasive intracranial surgical biopsy. Less-invasive monitoring using MRI scans also has limitations, both of resolution and specificity, thus no imaging can unequivocally distinguish tumours from other lesions or treatment-induced changes [326]. Additionally, MRI scans are an expensive and limited resource, and are thus not performed repeatedly over short periods (e.g., weekly) as may be possible with a more convenient method of tumour monitoring, such as a blood examination. Major changes in tumour size or characteristics can occur in the period between MRI scans (typically a few months), thus "missing the boat" for treatment changes. Circulating biomarkers could bypass many of these limitations, allowing non-invasive, repeated monitoring of disease progression over time. As studies have shown that GBM patients have elevated levels of circulating EVs compared to healthy controls [327, 328], longitudinal monitoring of circulating GBM EV quantities may identify GBM relapse. Furthermore, small EVs, labelled with iodine-125, have a short half-life in peripheral blood circulation, and could be used to monitor rapidly progressing changes within the tumour [329].

Investigation of the cargo of GBM patient EVs from blood, CSF, and Cavitron ultrasonic surgical aspirator (CUSA) fluid (a specimen obtained during surgical removal of the tumour), has revealed several potential diagnostic or prognostic biomarkers, including protein/mRNA transcripts and miRNAs [330-332]. In GBM patient plasma-derived EVs, expression of syndecan-1 (SDC1) can discriminate between low- and high-grade gliomas [331]. CCT6A, found in in CUSA-derived GBM-EVs, correlates with EGFR amplification, further highlighting how EVs may assist in identifying underlying molecular alterations in tumours [330]. By comparison, the isolation of CSF-based EVs is

ideal compared to serum as the BBB is not a concentration-limiting factor as it would be with serum-derived EVs and CSF would provide a 'cleaner' source of GBM EVs compared to serum which would contain EVs from normal (non-tumour) based processes (for example—maturation of reticulocytes and platelet activation). However, the highly invasive method of obtaining CSF-EVs, relying on the use of lumbar punctures that is also not able to be performed routinely, presents to be a major limitation compared to obtaining EVs from the peripheral circulation. Furthermore, there is also a risk of blood contamination with CSF samples, meaning that the possibility of obtaining circulating EVs cannot be completely excluded. Neverthless, a study by Chen *et al*. [332] involving the analysis of human CSF and serum EV samples using BEAMing RT-PCR, reliably detected and quantified mutant and wild-type IDH1 RNA transcripts in CSF-based EV from glioma patients, whereas the mutant IDH1 transcript was not detected in EVs isolated from the sera of patients that possessed tumours positive for this IDH1 mutation. Significantly, the levels of mutant IDH1 transcript showed a strong correlation with tumour volume, signifying the strong possibility of CSF-based EVs predicting glioma disease burden.

There has also been a focus on investigating the miRNA signatures of isolated EVs for discovering potential biomarkers, given that a differential expression has been detected between healthy control and GBM patients [10]. Akers et al. [333] demonstrated that nine CSF-derived EV miRNAs correlated with changes in GBM tumour volume, which may be useful in monitoring disease progression in GBM patients. Additionally, miR-151a levels in CSF-derived EVs have been proposed to reflect the underlying chemoresistant status of GBMs, with lower levels indicating poorer response to TMZ [334]. However, endeavors to identify relevant EV-biomarkers of GBM are still in their infancy and whilst these studies have identified a myriad of putative biomarkers, the clinical robustness of these potential prognostic biomarkers for patients remains to be validated.

1.7 Rationale and Significance of Project

Glioblastoma (GBM) is the most prevalent and aggressive form of glioma, and is associated with an extremely poor prognosis, with a low median patient survival time of just 15 months post-diagnosis with the current therapeutic approach consisting of surgical resection, followed by radiotherapy (RT) and concomitant chemotherapy with temozolomide (TMZ). Recent evidence suggests that effectiveness of this treatment regime may be compromised by surviving GBM cells that exhibit an enhanced invasive phenotype, although the exact mechanisms behind such treatment-induced invasion requires further research. As GBM cells have been shown to form invadopodia to facilitate invasion, it is possible that the enhanced invasive capabilities of GBM cells post-RT/TMZ treatment may be mediated by invadopodia.

In order to facilitate intracellular communication, tumour cells are known to secrete extracellular vesicles (EVs) which can contribute to an altered phenotype in recipient tumour cells. As current research has highlighted the emerging importance of EV-mediated communication in promoting oncogenic processes, including GBM cell invasion, we propose that EVs may serve to assist the invasion process through the mediation of invadopodia activity in recipient GBM cells. Elucidating the potential role of EVs in facilitating a treatment-induced invasive phenotype, potentially linked to the action of invadopodia, may highlight novel pathways and therapeutic targets to impede GBM invasion and improve patient survival.

1.8 Project Aims

1. To investigate the role of invadopodia in GBM cells and response to RT/TMZ treatment
2. To examine the role of GBM cell derived-EVs in invadopodia-mediated invasion and response to RT/TMZ treatment
3. To examine the proteome of GBM cells and GBM cell derived EVs that may contribute to invadopodia formation and activity via mass spectrometric analysis
4. To investigate alterations in the proteome of GBM cells and GBM cell derived EVs in response to RT/TMZ treatment and how this may contribute to an enhanced invasive phenotype

CHAPTER 2: Materials and Methods

2.1 Materials

2.1.1 Materials and Reagents

The following materials and reagents were used for experimental work presented in this thesis:

Table 2-1: Materials and Reagents

Materials/Reagents	Catalogue Number	Source
2-Mercaptoethanol (1000x)	21985023	Gibco (Life Technologies)
5% Bovine Serum Albumin	BSAS-AU	Bovogen Biologicals
Rhodamine conjugated Phalloidin	P2141	Sigma Aldrich
CellTiter 96® Non-Radioactive Cell Proliferation Assay	G4000	Promega
DAPI	D1306	Invitrogen (Life Technologies)
Dimethyl Sulphoxide (DSMO) Hybri-max®	D2650	Sigma Aldrich
Dulbecco's Modified Eagle's Medium (DMEM)	12430047	Gibco (Life Technologies)
Dulbecco's phosphate-buffered saline (PBS)	14190250	Gibco (Life Technologies)
ECL Western Blotting Detection Reagents	RPN2134	Amersham – GE Healthcare bioscience
Ethanol	-	Chem-supply
FITC (Fluorescin Isothiocyanate Isomer I)	0855167	MP Biomedical
Foetal Bovine/Calf Serum (FBS/FCS)	092910154	MP Biomedical
LDS Sample Buffer (4X)	NP0007	Novex (Life Technologies)
Lysis Buffer	-	Dept. Surgery, Royal Melbourne Hospital
Methanol	-	Grale HDS
MOPS SDS Running Buffer (20x)	NP0001	Invitrogen (Life Technologies)
Nitrocellulose Transfer Membrane	10600006	GE Healthsciences
Novex™ 10% Zymogram Plus (Gelatin) Protein Gels	EC6175	Novex (Life Technologies)
NuPAGE4-12% Bis-tris Gel (SDS PAGE)	NP0321BOX	Novex (Life Technologies)
Opti-MEM®	31985070	Gibco (Life Technologies)
Paraformaldehyde	C007	Proscitech
Penicillin/Streptomycin	15140122	Invitrogen (Life Technologies)
Pierce™BCA Protein Assay Kit	23225	Thermo Scientific
Precision Plus Protein™ All Blue Standards	1610373	Bio-Rad
Sample Reducing Agent (10x)	NP0004	Novex (Life Technologies)

Simply Blue™Safestain	LC6065	Novex (Life Technologies)
Sodium Azide (10%)	08591	Sigma Aldrich
TBS-Tween Tablets	09-7510-100	Medicago
Transfer Buffer (10x)	35040	Invitrogen (Life Technologies)
Tris Glycine SDS Running Buffer (10x)	LC26754	Invitrogen (Life Technologies)
Tris Glycine SDS Sample Buffer (2x)	LC2676	Novex (Life Technologies)
Triton-X-100	108643	Merck
Trypan Blue Stain (0.4%)	15250061	Gibco (Life Technologies)
TrypLE™Express	12604039	Gibco (Life Technologies)
Tween-20	93773	Sigma-Aldrich
Vector Shield	H-1000	Vector Laboratories
Western Stripping Buffer	-	Dept. Surgery, Royal Melbourne Hospital
X-ray medical film		Fujifilm
Zymogram Developing Buffer (10x)	LC2671	Novex (Life Technologies)
Zymogram Renaturing Buffer (10x)	LC2670	Novex (Life Technologies)
Thrombospondin-1/TSP1 cDNA ORF Clone, Human, N-DDK (Flag®) tag	HG10508-NF	Sino Biological
SpeI RESTRICTION ENDONUCLEASE	R0133S	New England Biolabs
DiI stain	D282	Invitrogen (Life Technologies)
Muse® Cell Cycle Kit	MCH100106	Merck
Muse® Annexin V & Dead Cell Kit	MCH100105	Merck
Proteome Profiler Human Protease Array Kit	ARY021B	R&D Systems
Proteome Profiler Human Protease Inhibitor Array Kit	ARY023	R&D Systems
Ultracentrifuge polycarbonate tube assembly	355618	Beckman Coulter

2.1.2 Antibodies

The following primary and secondary antibodies were used for experimental work presented in this thesis:

Table 2-2: Antibodies

Antibodies	Catalogue Number	Dilution	Source
PRIMARY ANTIBODIES			
Anti-Alix Mouse Monoclonal	ab117600	1:1000	Abcam
Anti-Calnexin Rabbit Polyclonal	ab22595	1:10000	Abcam
Anti-Cortactin Mouse Polyclonal	SC-55588	1:1000	Santa Cruz Biotechnology
Anti-P-Cortactin Rabbit Polyclonal	Y421	1:1000	Cell Signalling Technologies
Anti-GAPDH Rabbit Polyclonal	14C10	1:1000	Cell Signalling Technologies
Anti-HSP27 Mouse Monoclonal	SC-13132	1:1000	Santa Cruz Biotechnology
Anti-P-HSP27 Mouse Monoclonal	SC-166693	1:1000	Santa Cruz Biotechnology
Anti-NWASP Rabbit Polyclonal	30D10	1:1000	Cell Signalling Technologies
Anti-MMP-2 Rabbit Polyclonal	SC-10736	1:1000	Santa Cruz Biotechnology
Anti-c-Src Mouse Polyclonal	SC-8056	1:1000	Santa Cruz Biotechnology
Anti-TKS5/SC-FISH Rabbit Polyclonal /Mouse Monoclonal	SC-30122 (Rabbit) SC-376211 (Mouse)	1:1000	Santa Cruz Biotechnology
Anti-THBS1- Mouse Polyclonal	SC-59886	1:50	Santa Cruz Biotechnology
Anti-β-tubulin Rabbit Polyclonal	2146S	1:1000	Cell Signalling Technologies
SECONDARY ANTIBODIES			
Rabbit anti-goat IgG HRP conjugate	#170-6515	1:5000	Bio-Rad
Mouse anti-goat IgG HRP conjugate	#170-6516	1:5000	Bio-Rad

2.1.3 Cell Lines

Human GBM cell lines used are listed in **Table 2-3**. U87MG and LN229 were obtained from the ATCC Biological Material Repository. Primary GBM cell lines MU4 and MU41 were derived from glioma patient biopsy specimens from The Royal Melbourne Hospital (courtesy of the Morokoff laboratory; Ethics Approval Number: HREC 2009.016).

Table 2-3: Details of GBM cell lines utilised in this project

Cell line	Age	Gender	WHO Grade	Known mutations	IDH1 status	Primary or Recurrent
U87MG	44	Male	IV	PTEN, NF1	WT	Primary
LN229	60	Female	IV	TP53	WT	Primary
MU4	48	Male	IV	TP53, MET	ND	Primary
MU41	82	Male	IV	PTEN, ERB2, EGFRvIII	ND	Primary

Information listed for each cell line was sourced as follows: MU4/MU41- information obtained from Morokoff Laboratory (personal communication), U87MG/LN229- information obtained from the Cancer Cell Line Encyclopedia [335] and published whole exome and RNA sequencing data [336]. *IDH1 status: WT (wildtype), Mut (mutant).* ND: unknown (IDH1 was not examined during exome sequencing of MU4 and MU41 cell lines).

2.2 Methods

2.2.1 Cell Culture

All cells were grown in adherent flasks (75cm^2; catalogue no. CLS430641U, and 175cm^2; catalogue no. CLS431080, Sigma-Aldrich, Corning) and maintained in Dulbecco's Modified Eagle's Medium (DMEM) with heat-inactivated foetal calf serum (FCS) (10%), 1X Antibiotic-Antimycotic (Amphotericin B (0.25mg/ml), penicillin (100 units/ml) and streptomycin (10mg/ml). All cell lines were cultured in a humidified atmosphere with 5% CO_2 at 37^{0}C.

2.2.1.1 Cell Passaging

Cells were regularly passaged when 70-80% confluent by aspirating culture media and subsequently allowing cells to dissociate from the flask surface using 1X TrypLE™ Express (Gibco, Life technologies). Once detached, cells were resuspended at a 1:10 dilution in culture medium and reseeded into adherent flasks for further use. Cells underwent a maximum of 10-15 passages.

2.2.1.2 Freezing Cells

Cells were handled as described in 2.2.2 and resuspended in 10mL of culture media. Cells were then counted, centrifuged at 300xg for 5 min at RT and resuspended at 10^6 cells/1mL in FCS supplemented with 10% dimethyl sulfoxide (DMSO). Cells were then aliquoted into cryovials and cryopreserved at -80^{0}C for long-term storage.

2.2.1.3 Thawing Cells

Cells were thawed in a 37^{0}C water bath for 1 min and transferred to a 10mL tube containing pre-warmed culture medium. To remove DMSO, cells were centrifuged at 300xg for 5 min at RT, the supernatant was aspirated, and the cell pellet was resuspended in 10mL of culture medium.

2.2.1.4 Cell Counting

A 10µl volume of cell suspension was pipetted on a Neubauer Chamber Haemocytometer and visualised using an inverted light microscope. Cells were counted for each corner quadrant (four quadrants scored in total), and the cell density was calculated as:

$$(\text{Cells/mL}) = \frac{(\text{Total number of cells counted}) \times 10^4}{\text{Number of quadrants}}$$

2.2.1.5 RT and TMZ Treatment

For experiments investigating the effects of RT/TMZ treatment, GBM cells were seeded into 6-well plates at 2.5 x 10^4 cells per well and allowed to adhere overnight in a humidified environment at 37^{o}C. Cells were then subjected to 2Gy of irradiation and left to incubate for 4h prior to addition of 50µM of TMZ for a further 24h.

2.2.1.6 Generation of Long-Term (LT) Treated Cell Lines

To simulate a 'multiple treatment' regime, the four GBM cell lines U87MG, LN229, MU4 and MU41 were repeatedly treated with 2Gy RT and 50µM TMZ once a week for a period of 10 weeks, and subsequently referred to as Long-Term (LT) treated cell lines (***Figure 2-1***).

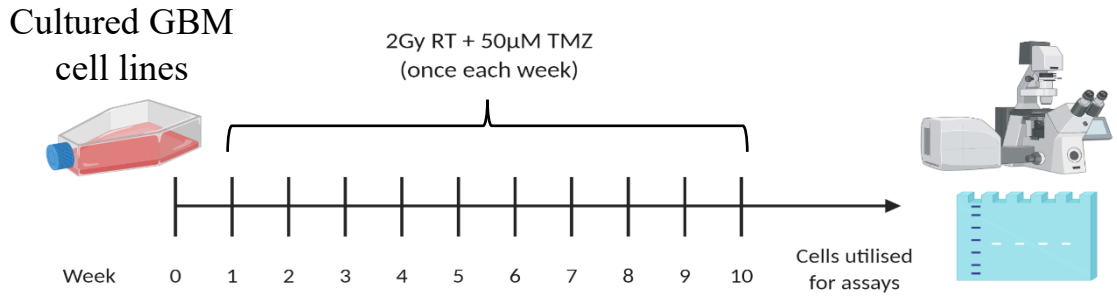

Figure 2-1: Schematic of the Generation of LT Treated Cell Lines

2.2.2 Online Databases/Datamining

2.2.2.1 Oncomine

OncomineTM v4.5 (www.oncomine.org. Compendia Bioscience™, Ann Arbor, MI, USA, part of Life Technologies) was utilised to perform differential expression analyses on the mRNA expression levels of invadopodia regulators and EV-markers in glioma tissue compared to normal brain tissue. This online database contains 729 cancer microarray datasets (91,866 samples) from numerous studies. Where clinical information was available, these expression levels were compared to patient survival. The data available on Oncomine is log transformed and the standard deviation normalized to one per array studied. Additionally, threshold criteria of a p-value <0.05 for the inclusion of data for analysis was applied.

2.2.2.2 SurvExpress

SurvExpress (http://bioinformatica.mty.itesm.mx:8080/Biomatec/SurvivaX.jsp) is a cancer-wide gene expression database with information on clinical outcome and survival data, comprising 26 tissue types, 225 datasets and 39,325 samples (as of February 20th, 2018). SurvExpress was used to examine datasets for significant (log rank p-value <0.05) survival differences between low and high expression (lowest and highest 25th percentile) of invadopodia-related genes (Cortactin, Tks4, Tks5, MMP2, MMP9, and Src) and EV-related genes (Alix, TSG101, CD9, CD63, CD81 and CD151), as well as experimentally shortlisted proteases (CTSD, CTSV, MMP-12, MMP-2) and genes (THBS1). As SurvExpress lost access to many databases in October 2019, SurvExpress was only used for survival analyses in *Chapters 3 and 4*.

2.2.2.3 GlioVis

GlioVis (http://gliovis.bioinfo.cnio.es/) is a brain tumour specific database, containing mRNA expression data on 6500 tumour samples from approximately 50 expression datasets. This data was processed using R programming and combined with phenotypic information to be displayed in a homogenous way that is easy to visualise. Through the GlioVis portal, mRNA expression differences of invadopodia regulators (Cortactin, Tks5, MMP2, MMP9, and Src) in different brain tumour grades, histology, and GBM subtypes was examined.

2.2.2.4 Glioblastoma Bio Discovery Portal

The Glioblastoma Bio Discovery Portal (http://gbm-biodp.nci.nih.gov) is a web resource that utilises GBM data from three TCGA microarray platforms (Affymetrix HGU133A, Agilent G4502A, and HuEx-1_0-st-v2) as well as one dataset generated by aggregating all three platforms (3-Platform Aggregates). This web resource allows GBM patient survival analyses to be conducted with multiple genes using a Cox proportional hazards model, whereby a prognostic index is computed for each sample by averaging individual gene expression by its Cox regression coefficient. Using the prognostic index, samples were stratified into highest and lowest expression quartiles for each cohort. As SurvExpress database access was lost in 2019, the Glioblastoma Bio Discovery Portal was used for multi-gene survival analyses in *Chapter 6*.

2.2.2.5 Vesiclepedia

The Vesiclepedia database (http://www.microvesicles.org/) is an online compendium of identified extracellular vesicle (EV) cargo including RNA, proteins, lipids and metabolites from 1254 published and unpublished studies. Proteins identified in GBM-EVs were compared to 22750 mRNA/proteins

from the 35 glioma/GBM datasets listed on Vesiclepedia. These proteins and transcripts were also separated into microvesicle (MV)-, exosome- and EV- specific datasets for further analysis.

2.2.3 Cell Viability Assay

$1x10^4$ cells were seeded per well in 96-well plates in triplicate and allowed to adhere overnight in a humidified incubator ($37^oC/5\%$ CO_2). The cells were subsequently treated with 2Gy of irradiation and 50µM of TMZ and left to incubate for one week before a CellTiter 96® Non-Radioactive Cell Proliferation Assay ('MTT assay', Promega) was used as per the manufacturer's instructions to assess the viability of the cells. Absorbance was read on a Thermo electron Multiskan EX spectrophotometer at 570nm, indicating the quantity of metabolically active (alive) cells.

2.2.4 Western Blotting and Immunodetection

2.2.3.1 Preparation of Cell Lysates

2×10^5 cells were grown under mentioned conditions and lysed using 100µl of lysis buffer (50 mM Tris (pH 7.4), 150 mM NaCl, 1% Triton X-100, 50 mM NaF, 2 mM $MgCl_2$, 1 mM Na_3VO_4 and protease inhibitor cocktail (Roche)) on ice for 15 min. Cell lysates were subsequently centrifuged at 13,000xg for 15min at 4^0C and the supernatant was collected.

2.2.3.2 BCA Assay for determination of protein concentration

Protein quantitation of lysates was performed using a Pierce ™ BCA Protein Assay Kit (Thermo Fisher Scientific) as per the manufacturer's instructions. This assay allows for the colorimetric detection and quantification of proteins based on the reduction of Cu^{2+} to Cu^{1+} by protein in an alkaline solution

containing bicinchoninic acid (BCA). BCA reacts with the Cu^{1+} to produce a water-soluble complex with a strong linear absorbance at 562nm with increasing protein concentrations. Standards provided in the kit were serially diluted as per the manufacturer's instructions. After incubation for 30min, protein the concentration was read using a Thermo electron Multiskan EX spectrophotometer at 570nm. Concentrations of unknown samples were then calculated from the equation obtained by regression to the standard curve.

2.2.3.3 Gel Electrophoresis and Blotting/Transfer

Whole cell lysates were prepared at a concentration of 1μg/μl in sample reducing agents and sample buffer (Invitrogen). The samples were loaded and separated by SDS-PAGE on NuPAGE 4-12% Bis-Tris pre-cast gels (Invitrogen) at 120V for 120min, transferred onto nitro-cellulose membrane at 30V for 100 min, and then blocked with 1.5% BSA/TBST for 1h at room temperature.

2.2.3.4 Antibody Incubation and ECL Detection

Membranes were probed with the relevant primary antibodies overnight at 4^0C (**Table 2-1**) and then washed in Tris-Buffered Saline and Tween 20 (TBST) (Aniara, OH, U.S.A) for 3 x 5 min washes. Secondary antibodies (Goat Anti-Rabbit / Mouse Antibody Conjugated to Horseradish Peroxidase (Bio-Rad, CA, U.S.A)) were diluted to 1:5000 with 1.5% Bovine Serum Albumin were added for 1h at room temperature on a rocker platform. After incubation, membranes were again washed, and an ECL chemiluminescence detection kit (GE Healthcare) was used to allow for visualisation of the signal. All western blotting experiments were repeated three times and representative images are shown. All results were quantified by densitometry (Image J software, Version 1.53a, MD, USA).

2.2.5 Zymogram Analysis of Cell Culture Medium

2.2.5.1 Preparation of Conditioned Medium

2×10^5 cells were grown in 6-well plates under mentioned conditions, before being washed with sterile PBS (pH 7.4) and incubated in serum-free OptiMEM® (Thermofisher Scientific) for 24h. 100µl aliquots of supernatant were isolated and frozen until required for zymographic analysis.

2.2.5.2 Sample Preparation and Gel Electrophoresis

To determine the levels of gelatinase (pro- and active-MMP) secreted from the GBM cell lines, samples of conditioned media were separated by gel electrophoresis on Novex™ 10% Zymogram Plus (Gelatin) Protein Gels (Novex, Life Technologies) at 125V for 1.5h in 1X Novex tris-glycine sodium dodecyl sulfate running buffer. Sample loading was normalised against the concentration of the corresponding cell protein lysates, determined with a BCA protein assay (Pierce, Thermofisher Scientific).

2.2.5.3 Gel Staining/Detection of Zymographic Activity

Following electrophoresis, gels were transferred to a container and incubated in 1X Novex zymogram renaturing buffer for 30min (Thermofisher Scientific) at room temperature. Gels were then placed in 1X Novex zymogram developing buffer for 30 min (room temperature), which was replaced with new developing buffer for overnight incubation at 37 ^{o}C. The gels were then washed in distilled water and stained blue using Simply-Blue Stain (Life Technologies). Once clear bands of enzymatic activity became visible against the stained blue background, the dye was rinsed off in distilled water and gels were placed in plastic sleeves. Gels were then scanned on a flatbed scanner for densitometric analysis using ImageJ (Version 1.53a). The results were analysed and graphed in GraphPad Prism 8 (GraphPad

Software, CA, U.S.A). The molecular weight of the bands was identified against the loaded Precision Blue (BioRad) protein markers.

2.2.6 In-Vitro Wound Healing Migration Assay

$3x10^5$ cells were seeded per well in 6-well plates and were cultured under mentioned conditions until approximately 100% confluent. 5µg/ml of Mitomycin C was added to arrest proliferation, and cells were incubated for 2h before a p1000 pipette tip was used to introduce a cross scratch (wound) in the confluent layer of cells. Cells were washed three times in sterile PBS before new media was added. Images were acquired near the centre of the cross at time points 0, 6 and 24h using a 4X objective. Images were analysed using ImageJ (Version 1.53a) in order to quantify the area of the wound.

2.2.7 Invadopodia-mediated FITC-gelatin Degradation Assay

2.2.7.1 Seeding Cells onto FITC-gelatin Coverslips

Autoclaved coverslips were coated in fluorescein isothiocyanate (FITC)-conjugated gelatin and placed into a 6-well plate for 2h at 37^0C in serum-free DMEM. The serum-free DMEM was removed and 1 x 10^5 GBM cells were seeded onto the coverslips with DMEM supplemented with 5% FCS and incubated overnight at 37ºC (5% CO2) to allow for degradation of the gelatin.

2.2.7.2 Fixing/Staining of Cells on FITC-gelatin Coverslips

Adherent cells on the coverslips were washed with PBS and fixed in 4% paraformaldehyde in PBS, before being permeabilized using a 0.2% solution of Triton-X-100 in PBS and stained for F-actin, to detect the actin puncta of the invadopodium core, for 1h at room temperature using Rhodamine-

conjugated Phalloidin (dilution 1:75, Sigma-Aldrich). For experiments investigating the co-localisation of thrombospondin-1 (THBS1) with F-actin puncta, cells were also probed with anti-THBS1 antibody (dilution: 1:50, Santa Cruz) and Alexa Fluor405 conjugated goat anti-mouse IgG (H+L) secondary antibody (dilution: 1:500). Cell nuclei were stained with DAPI for 5 min, to allow the total number of cells per image to be determined, and coverslips were then again washed with PBS and mounted onto glass slides with a droplet of Vectashield anti-fade mounting medium (Vector Laboratories).

2.2.7.3 Confocal Microscopy/Imaging of Coverslips

Images were acquired with a Nikon A1+ Confocal microscope system utilizing a Plan Apo VC 60X Oil DIC N2 immersion objective at a resolution of 1024 x 1024 and a 1x zoom factor, and analysed using ImageJ (Version 1.53a) to calculate the total area of FITC-conjugated gelatin degradation, defined as the black areas depleted of fluorescent gelatin, relative to the number of DAPI-positive cells. Threshold and region tools were used to define the total region of matrix degradation in each image field, and the area of degradation was calculated using the particle counter function and normalised against the number of DAPI-stained cells (***Figure 2-2***).

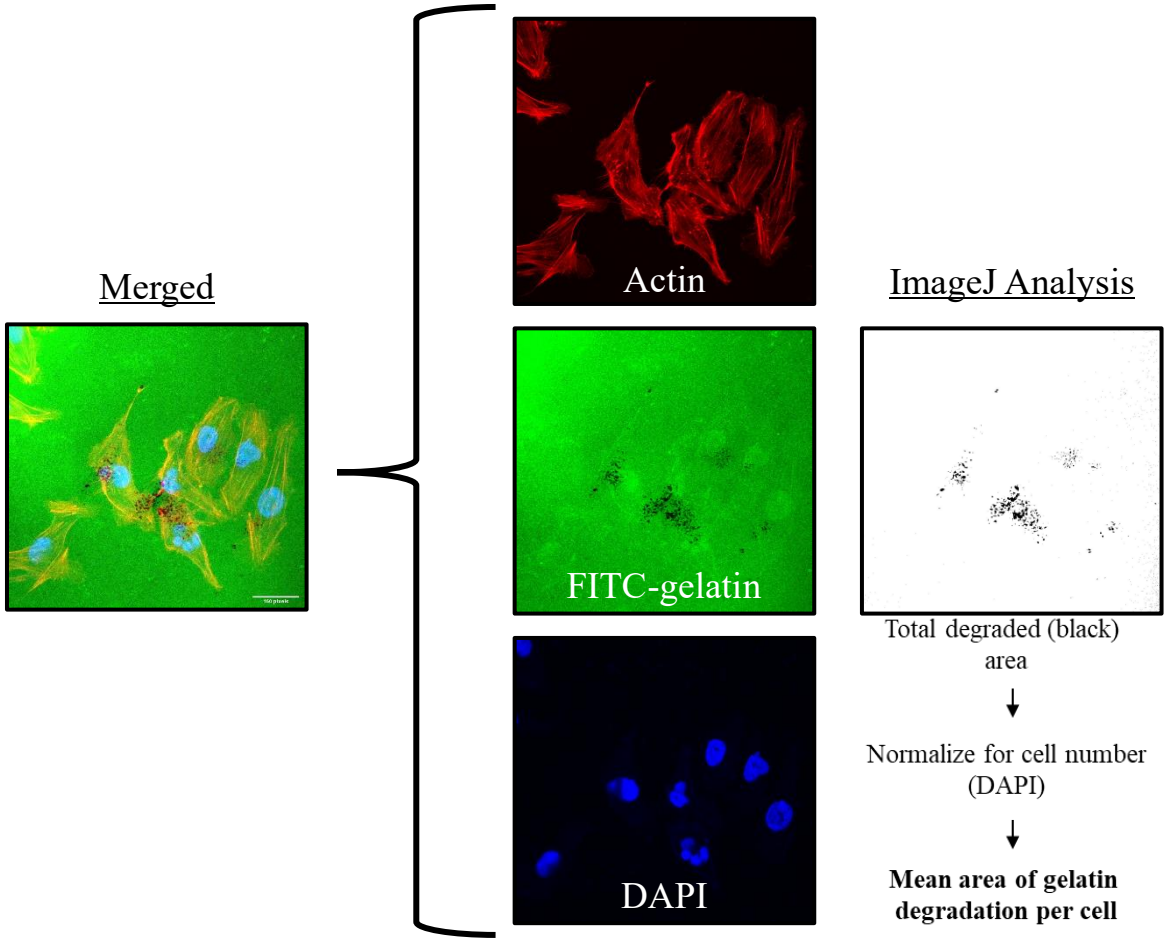

Figure 2-2: Schematic of FITC-gelatin Degradation Analysis

Confocal image of GBM cells seeded on a FITC-gelatin coated coverslip. The image was acquired using three laser lines: 532nm - rhodamine phalloidin (red) for actin staining, 405 nm - DAPI (blue) for cell nucleus staining and 488nm - FITC-gelatin (green). Image J (Version 1.53a) threshold and region tools were used to define areas of degraded FITC-gelatin (black), which was subsequently normalised to the number of cells as determined by DAPI staining.

2.2.7.4 Identification and Quantification of Invadopodia by Actin Puncta

For further analysis, Cameron Nowell (MIPS) wrote a customised script for Fiji (ImageJ) to analyse the number of total actin puncta and puncta that overlapped with areas of degraded FITC-gelatin. The overlay of actin puncta with gelatin degradation was used to quantify invadopodia formation and activity. Actin thresholds were manually set for each image to include individual puncta whilst excluding cytoskeletal actin and background as much as possible. Regions of interest were manually outlined to eliminate areas of actin not specific to puncta, and areas of actin that were not likely representative of invadopodia based on their shape and size, with a maximum diameter threshold of 1µM per puncta applied, were excluded to further ensure specificity (***Figure 2-3***).

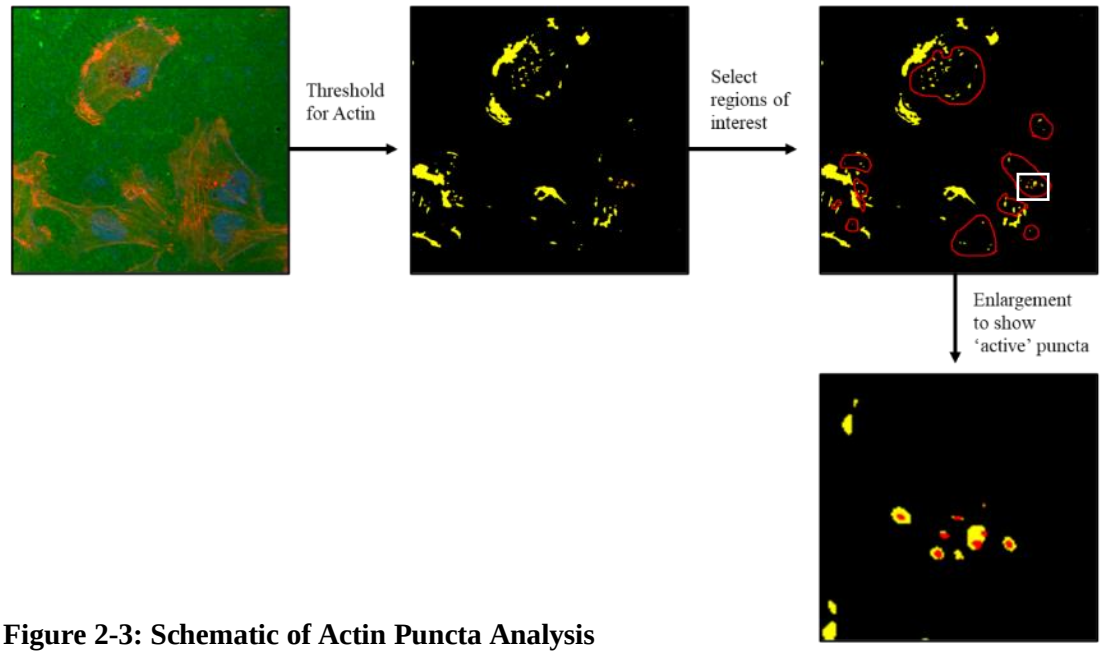

Figure 2-3: Schematic of Actin Puncta Analysis

Actin puncta (highlighted in yellow) were quantified in ImageJ (Version 1.53a) using a customized script written by Cameron Nowell (MIPS). To ensure specificity, defined regions of interest were placed around clusters of actin puncta that were selected for analysis (indicated by red circles). This allowed for the quantification of (i) total actin puncta and (ii) actin puncta that overlap with degraded FITC-gelatin (indicated by the red area over the top of the yellow regions of actin). A white square indicates the region that was magnified for the final 'enlarged' image.

2.2.8 Cultrex® 24 Well BME Cell Invasion Assay

A commercially available Cultrex® BME Cell Invasion Assay (R&D Systems) was used to assess invasive capacity of cells according to the manufacturer's instructions.

2.2.8.1 Preparation of Cells and Coating of Insert Membranes

Cells were seeded in triplicate in 6-well plates at 2.5 x 10^4 cells per well and allowed to adhere overnight. Cells were then serum-starved in OptiMEM® for 24h prior to the assay. During this time, membrane inserts were coated with 100µl of 0.5X BME stock solution and were left to incubate at 37^{o}C overnight.

2.2.8.2 Addition of Cells and Assembly of Chambers

After 24h of serum-starvation, cells were harvested and centrifuged at 250 x g for 10 min, the supernatant removed, and washed once with wash buffer (included in kit). Cells were resuspended at 1x10^6 cells/ml in OptiMEM® and 100µl was added to the top chamber of each well. 500µl of DMEM was added to the bottom chamber, and the plates were incubated at 37^{o}C overnight.

2.2.8.3 Quantification of Invasion

The wells were then aspirated and washed once before 500µl of Calcein-AM solution was added to the bottom chamber. After a further 1h incubation at 37^{o}C, the dissolved Calcein-AM was read at 485nm excitation and 520nm emission to quantify the cells that had invaded through the membrane.

2.2.9 Human protease and inhibitor antibody arrays

Commercially available Human Protease and Inhibitor Antibody Arrays (Proteome Profiler™ Array, R&D Systems) were used to assess the secreted levels of proteases/protease inhibitors in conditioned medium.

2.2.9.1 Preparation of Conditioned Medium

Cells were seeded at $2x10^6$ in 10cm dishes and were incubated overnight at 37°C. Cells were then either left untreated or treated with 2Gy RT and 50μM of TMZ before a further 24h incubation period in serum-free OptiMEM®. Conditioned media was then collected and stored at 4°C, and cell lysates were collected.

2.2.9.2 Normalisation of Sample Loading

The protein concentrations of cell lysates were determined as per section 2.2.3.2. Loading volumes of conditioned media were normalised to 350μg of cell lysate per sample, whereby 500μL of cell culture conditioned media corresponded to 350μg of total cell protein, using the $C_1V_1 = C_2V_2$ formula as follows:

V_2 (volume of conditioned media in μL) = (350 x 500) / (μg total protein)

Total loading volumes were then adjusted as necessary to a final volume of 1.5mL with the supplied array buffer and added to array membranes.

2.2.9.3 Array Incubation and Analysis

Briefly, membranes were incubated at 4ºC overnight on a rocking platform before incubation with secondary antibodies (included in kit) for 1h at room temperature on a rocking platform. Chemiluminescent reagents included in the kit were then used to detect array spots developed on X-ray film (Fujifilm). Densitometric analysis of array spots was performed using ImageJ and graphed on GraphPad Prism 8 (GraphPad Software, CA, U.S.A).

2.2.10 MUSE™ Annexin V and Dead Cell Assay and Cell Cycle Assay

2.2.10.1 Preparation of Cells

Cells were seeded in triplicate in 6-well plates at 2.5 x 10^4 cells per well and allowed to adhere overnight in a humidified environment at 37ºC. Cells were then treated with 2Gy of RT and 50μM of TMZ and left to incubate for a further 24h. The cells were then trypsinised and resuspended in culture medium.

2.2.10.2 Processing of Cells

For the Muse™ Annexin V & Dead Cell Assay, 100μl of cell suspension was added to 100μl of Muse™ Annexin V & Dead Cell Reagent and left to incubate for 20min in the dark at room temperature. Samples were then processed via fluorescence activated cell sorting using the Muse™ Annexin V & Dead Cell Software Module. This software then calculates the percentage of viable cells (Annexin V-negative/dead cell marker-negative), early apoptotic cells (Annexin V-positive/dead cell marker-negative), late apoptotic cells (Annexin V-positive/dead cell marker-positive) or dead cells that have died via necrosis (Annexin V-negative/dead cell marker-positive).

For the Muse™ Cell Cycle Assay, 200µl of cell suspension was then centrifuged at 300xg for 5 min, washed with sterile PBS, and centrifuged again at 300xg for 5min. 200µl of ice-cold ethanol was then slowly added per sample whilst vortexing at a medium speed and samples were stored at -20 ^{o}C for a minimum of 3h. Cells were then centrifuged at 300xg for 5 min, washed with sterile PBS, and centrifuged again at 300xg for 5min. The cell pellet was resuspended in 200µl of Muse™ Cell Cycle Reagent and incubated in the dark for 20min at room temperature. Samples were then processed via fluorescence activated cell sorting using the Muse™ Cell Cycle Software Module.

2.2.11 Nanostring® analysis of gene and miRNA expression in GBM cells

2.2.11.1 Nanostring® Arrays

Gene expression was investigated using the nCounter Human Pan Cancer Progression Panel Array. miRNA expression was investigated using the nCounter Human V3 miRNA Array.

2.2.11.2 Preparation of cells

Cells were seeded into 4 x 10cm^2 dishes per cell line at 70% confluency and incubated at 37^{o}C overnight. Cells were then either left untreated or exposed to 2Gy RT and 50µM of TMZ before a further 24h incubation. Cells were scraped in sterile PBS, transferred to 1ml tubes and centrifuged at 2000xg for 10min (4^{o}C). Supernatant was aspirated and cell pellets were resuspended in 1ml of sterile PBS. A further centrifugation at 10,000xg at 4^{o}C for 10min was carried out, supernatant was then aspirated, and cell pellets stored at -80^{o}C.

2.2.11.3 Preparation of RNA

RNA was extracted from cell pellets by Dr Koldej (Ritchie Laboratory) using a Qiagen RNeasy plus mini kit according to the manufacturer's protocol. The RNA amounts required for the various Nanostring analyses were as follows - 100ng in 3µl (nCounter Human V3 miRNA Array) and 50ng in 5µl (nCounter Human Pan Cancer Panel Array).

2.2.11.4 Analysis of gene and miRNA expression data

The arrays were processed in an nCounter FLEX analysis system by Dr Koldej (Ritchie Laboratory) to generate the RCC data files required for analysis. Probes for housekeeping genes are incorporated into the Nanostring analysis for normalisation, as well as positive and negative controls. A minimum threshold of 100 transcript counts was applied for subsequent analysis.

2.2.12 Transient Transfections

2.2.12.1 Preparation of cells

U87MG, LN229, MU4 and MU41 cell lines were seeded at 3 x 10^5 cells per well in 6 well plates and incubated overnight at 37^{o}C.

2.2.12.2 Transfection protocol

Each well of cells was transfected with 2.5µg of human THBS1 plasmid DNA (Sino Biological) and 7.5µg Lipofectamine™ 3000 Reagent (Invitrogen) and left to incubate for 48h at 37^{o}C. For controls, cells were exposed to 7.5µg Lipofectamine™ 3000 Reagent (Invitrogen) and the rest of the volume

was made up with OptiMEM serum-free media. For siRNA transfections, the same protocol was followed, however plasmid DNA was substituted for non-specific or THBS1 -targeting siRNA diluted to 25nM, 50nM and 100nM in the same total volume.

2.2.12.3 Processing of cells

Following a 48h incubation, cells were washed with sterile PBS and media was replaced with serum-free OptiMEM for a further 24h. Conditioned media was then harvested for zymographic analysis, and cell lysates were prepared for western blotting as per section 2.2.4.

2.2.13 Enrichment of Extracellular Vesicles (EVs) from Cultured Cells

2.2.13.1 Preparation of conditioned media

Cells were grown at 37°C and 5% CO_2 in 15cm-diameter dishes until approximately 60% confluent. Cells were washed with sterile PBS before serum-free OptiMEM® was added for a further 24h. Conditioned media was then collected and centrifuged at 300xg for 10min at room temperature to remove cells. Supernatant was collected and centrifuged at 2000xg for 15min, followed by a further 15min centrifugation at 3166xg to remove cell debris.

2.2.13.2 Differential ultracentrifugation to pellet EVs

Prepared conditioned media was placed into 45Ti Beckman tubes (topped up to capacity with filtered calcium- and magnesium-free PBS if required) and centrifuged at 10,000xg (4^0C, 30min) to pellet larger vesicles (MVs; >200nm). The supernatant was then transferred to clean 45Ti Beckman tubes and small EVs (<200nm) were pelleted at 100,000xg (4^0C, 2h) before a wash with sterile filtered PBS at

100,000xg (4^0C, 2h). EV pellets were resuspended in 50µl of filtered PBS. A schematic of the EV enrichment protocol is shown in ***Figure 2-4***.

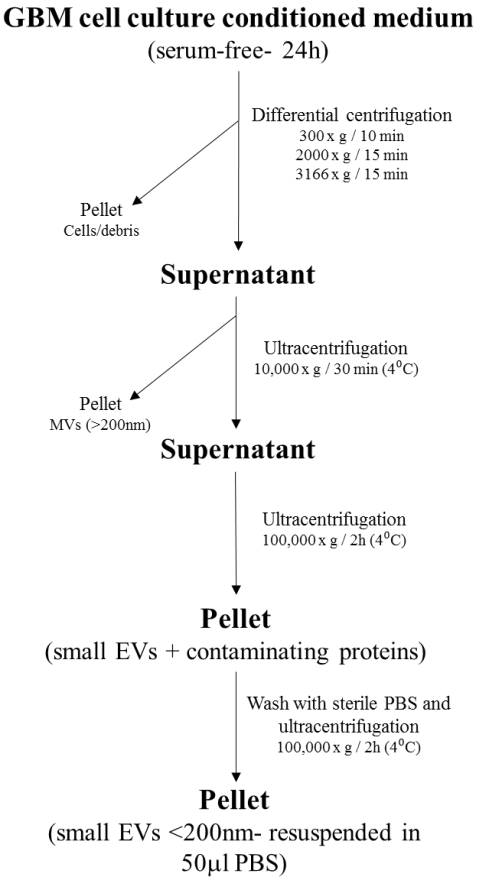

Figure 2-4: EV enrichment protocol

2.2.13.3 Protein quantification of EV pellets

Protein content was estimated using a Pierce ™ BCA Protein Assay Kit as previously described in section 2.2.3.2. For protein estimation, a 5µl aliquot of EVs resuspended in PBS was lysed with 5µl of lysis buffer (50mM Tris (pH 7.4), 150mM NaCl, 1% Triton X-100, 50mM NaF, 2 mM $MgCl_2$, 1mM Na_3VO_4 and protease inhibitor cocktail (Roche)).

2.2.14 Nanoparticle Tracking Analysis (NTA)

2.2.14.1 Preparation of conditioned media

For experiments utilising the Nanosight, EVs were either harvested as stated in 2.2.8 or, for crude EV mixes, the following method was used. Cells were seeded in triplicate in 6-well plates at 2.5 x 10^4 cells per well and allowed to adhere overnight in a humidified environment at 37^{o}C. Cells were then treated as described in each experiment. 24h prior to NTA, cells were washed with sterile PBS and subsequently incubated in serum-free OptiMEM®, before cultured medium was collected and the cells were trypsinised and counted. Media was centrifuged at 300xg for 5min to remove cell debris. The supernatant was then centrifuged at 10,000xg for 1.5h (4^{0}C) to remove larger vesicles (>200nm). The remaining supernatant was then utilised for Nanosight analysis.

2.2.14.2 NTA analysis of harvested EVs

The size distribution and concentration of EVs were measured by NTA software (version 3.0) using the Nanosight LM10-HS (NanoSight Ltd, Amesbury, UK), configured with a 532nm laser for light scattering and an optical element for detection. Where necessary, EVs were diluted in sterile PBS to ensure that less than 100 particles were in the field of view of the microscope camera, and images were acquired at a rate of 30 frames per second for a total of 5 x 1 min videos per sample. NTA software is then able to identify and track individual EVs and uses Brownian motion and light scattering to determine size distribution and concentration [337]. Videos were analysed at a detection threshold of 5 and particle concentration was normalised against the corresponding cell count for each sample.

2.2.15 Imaging Techniques for EVs

2.2.15.1 Cryogenic Electron Microscopy (Cryo-EM) of EVs

Cryo-EM was carried out by Eric Hanssen (Bio21 – Advanced Microscopy Facility). A 3µl sample aliquot (enriched EVs resuspended in filtered PBS) was pipetted onto holey carbon grids (ProSciTech), and excess liquid was blotted off before grids were plunge-frozen in liquid ethane. The grids were then mounted in a Gatan cryoholder (Gatan, Inc., Warrendale, PA, USA) which was pre-cooled in liquid nitrogen. Images were acquired at 200 kV using a Tecnai F30 (FEI) Transmission Electron Microscope. The electron dose was below 6000 electrons/nm for each dataset. Images were recorded using a FEI CETA 4kx4k CMOS camera.

2.2.15.2 DiI-labelled EV uptake

To visualise EV uptake by GBM cells, 500µg/ml of enriched LN229-EVs in PBS were labelled with 1µM of DiI (Invitrogen) and incubated at 37°C for 10min. Excess dye was removed by washing with PBS and ultracentrifugation at 100000xg for 2 x 90min, before labelled-EVs were resuspended in PBS at a final concentration of 1µg/µl. Control samples of DiI dye background were prepared following the same procedures without the EV pellet. 5µg/ml of labelled-EVs, or equivalent amounts of a DiI background control, were added to cells in serum-free OptiMEM (seeded at $1x10^4$ cells in 8-well plates 24h prior). Following a 4h incubation, cells were washed with PBS and fixed in 4% paraformaldehyde in PBS. Cell nuclei were stained with Hoechst for 10min before images were acquired using a Leica Sp8 Lightning confocal microscope and analysed using ImageJ (Version 1.53a).

2.2.16 Proteomic Analysis of GBM Cell Lines and EVs

2.2.16.1 Proteomics: sample preparation

Cell lysates and EVs were solubilised in sodium dodecyl sulphate (SDS) 1% (v/v), 50mM triethylammonium bicarbonate (TEAB), pH 8.0, and centrifuged at 16,000x*g* for 20min at 4°C, and quantified by microBCA (Life Technologies). For mass spectrometry-based proteomics, samples (5 µg) were normalized and reduced with 10 mM dithiothreitol (DTT) for 45 min at 50 °C followed by alkylation with 20 mM iodoacetamide for 30min at 25 °C in the dark. The reaction was quenched to a final concentration of 20 mM DTT. Lysates were precipitated with six volumes of acetone overnight at -20 °C. Protein pellets were centrifuged at 16,000x*g*, 10min at 4°C resuspended in 50mM TEAB, pH 8.0. Samples digested with trypsin (Promega, V5111) at a 1:50 enzyme-to-substrate ratio for 16h at 37°C. The peptide mixture was acidified to a final concentration of 2% formic acid and centrifuged at 16,000x*g* for 5 min, frozen at -20°C for 30min, and dried by vacuum centrifugation. For proteomic analysis, peptides were resuspended in 0.07% trifluoroacetic acid (TFA) TFA in MS-grade water, quantified by Fluorometric Peptide Assay and normalized to 1µg per 3µl.

2.2.16.2 Proteomic liquid chromatography–tandem mass spectrometry

Peptides were analysed on a Dionex 3000 nanoUHPLC coupled to a Q-Exactive HF-X hybrid quadrupole-Orbitrap mass spectrometer equipped with a nanospray ion source in positive mode. Peptides were loaded (Acclaim PepMap100 C18 3µm beads with 100 Å pore-size, Thermo Fisher Scientific) and separated (3-µm particle size C18, 0.075 × 200mm, Nikkyo Technos Co. Ltd) with a gradient of 2–28% acetonitrile containing 0.1% formic acid over 55min at 300nl min-1 at 55°C. An MS1 scan was acquired from 350–1,650 m/z (60,000 resolution, 3 × 106 automatic gain control (AGC), 128ms injection time) followed by MS/MS data-dependent acquisition (top 30) with collision-induced dissociation and detection in the ion trap (15,000 resolution, 1 ×105 AGC, 60ms injection time, 28%

normalized collision energy, 1.3 m/z quadrupole isolation width). Unassigned precursor ions charge states and slightly charged species were rejected and peptide match disabled. Selected sequenced ions were dynamically excluded for 30sec.

2.2.16.3 Data Processing and Bioinformatics Pipeline

Peptide identification and quantification were performed using MaxQuant (v1.6.6.0) with its built-in search engine Andromeda [338]. Tandem mass spectra were searched against Homo sapien (human) reference proteome (74,788 entries, downloaded 11-2019) supplemented with common contaminants. Search parameters included carbamidomethylated cysteine as fixed modification and oxidation of methionine and N-terminal protein acetylation as variable modifications. Data was processed using trypsin/P as the proteolytic enzyme with up to 2 missed cleavage sites allowed. The search tolerance and fragment ion mass tolerance were set to 7ppm and 0.5Da, respectively, at less than 1% false discovery rate on peptide spectrum match (PSM) level employing a target-decoy approach at peptide and protein levels. Label free quantification (LFQ) algorithm in MaxQuant was used to obtain quantification intensity values. Perseus was used to quantify proteins whose expression was identified in at least 50% in at least one group [339]. LFQ intensities were log2 transformed after removing contaminants and reverse identifications. Proteins were subjected to a two-tail student's t-test with p-value adjusted at 5% permutation-based FDR. Functional enrichment analysis and annotation of proteins was performed using FunRich software (FunRich; v3.1.3) [340], and protein classes were determined using the Protein ANalysis THrough Evolutionary Relationships (PANTHER) Classification System (version 10.0, released 2015-05-15, available from http://pantherdb.org) [341]. Pathway enrichment map analysis was performed using STRING (https://string-db.org/) [342]. P-values were calculated by a two-sided hypergeometric test. Invadopodia-related proteins were identified by filtering proteins based on key words within the Uniprot identifier description generated in Andromeda: invasion/ invasive/ invade/ migration/ migratory/ remodelling/ degradation/ proteolytic/

adhesion/ metastasis/ invadopodia/ podosome. Proteins were then further shortlisted based on PubMed searches for ‘protein name’ and ‘invadopodia’.

2.2.17 Statistical Analysis

Statistical analyses were performed using an unpaired, two-tail Student’s *t* test. Datasets were generated using the program GraphPad Prism 8 (GraphPad Software, CA, U.S.A), and represent mean ± SD. A probability value (*p*-value) of less than 0.05 was considered statistically significant and indicated using the following asterisks: *p<0.05, **p<0.01, ***p<0.001.

CHAPTER 3:
Investigating the role of invadopodia in GBM and response to treatment (radiotherapy and temozolomide)

3.1 Introduction

3.1.1 Glioblastoma and current therapeutic management

Glioblastoma (GBM) is the most common primary central nervous system tumour in adults and is highly proliferative, invasive and infiltrative [343]. Patient prognosis is extremely poor with a median survival of just 12-15 months, utilizing the current gold standard therapeutic approach consisting of surgical resection, followed by concomitant radiotherapy (RT) and chemotherapy with the DNA-alkylating drug temozolomide (TMZ) [2, 18]. Despite the high degree of molecular heterogeneity in GBM, all patients generally receive the same treatment, and the vast majority (88.8%) die within two years due to tumour recurrence [13, 61, 344]. A contributing factor to the poor patient prognosis is resistance to the current therapy and continued invasion of tumour cells into the surrounding brain, ultimately leading to tumour recurrence. This may be further aided by the therapeutic approach involving RT and TMZ, which is capable of introducing new driver mutations during the course of treatment, leading to more aggressive recurrent tumours [345, 346]. Ongoing efforts to develop and evaluate novel therapeutics have thus far failed to significantly improve GBM patient survival [64]. Many of the trialled drugs are known to target cell viability, mostly via inhibition of cell division or promotion of apoptotic pathways [347, 348]. However, GBM cells which survive these therapies inevitably lead to tumour recurrence. Therefore, there is a need for new therapeutic strategies to improve GBM patient outcome.

3.1.2 GBM invasion

A critical feature contributing to the poor prognosis of GBM patients is the ability of the tumour cells to infiltrate into the surrounding normal brain parenchyma. Metastatic spread of tumour cells from the primary tumour mass and the subsequent development of secondary tumours at distant sites is the leading cause of cancer patient mortality [40]. Whilst most other cancers can metastasize to distant organs, GBM cells do not typically metastasize outside of the brain, but extensively invade throughout

the surrounding local brain tissue [30]. The widespread dissemination of tumour cells prevents complete surgical resection of the tumour mass and also limits the capacity of chemotherapy or radiation based treatments to effectively reach all tumour cells [349]. As a result, GBMs inevitably relapse, with 90% of secondary tumours occurring within 2-3cm of the original tumour border [60, 108]. Importantly, a number of studies have revealed a link between RT and TMZ treatment and an enhanced migratory/invasive potential of GBM cells [3-7], indicating that the long-term inadequacy of GBM treatment may be related to surviving cells displaying an increased invasive capacity. Suppression of the enhanced invasive phenotype exhibited by these GBM cells could be an attractive target for improving patient outcome, however the mechanisms utilised by invasive GBM cells following treatment are not well understood.

3.1.3 Invadopodia as facilitators of invasion

During the invasion process, a cancer cell must degrade or remodel the surrounding extracellular matrix (ECM) which acts as a physical barrier [350]. To facilitate this process, cancer cells may form specialised actin-rich membrane protrusions known as invadopodia. Invadopodia may reach lengths greater than 2μm [121] and are known to degrade the surrounding ECM through the action of transmembrane proteases, such as MT1-MMP, and secreted proteases, such as MMP-2 and MMP-9 [122]. It is this highly localised proteolytic activity that is a defining feature of invadopodia, suggesting that these membrane structures are key facilitators of protease-dependent tumour cell invasion. In addition to remodelling the ECM, MMP activity is also involved in the cleavage of other non-matrix targets such as latent cytokines or integrins, which may also enhance tumour progression via the activation of pro-invasive signalling pathways. As invadopodia serve as sites of activation (whereby proteases are cleaved from a pro-state to their active form) and secretion of MMPs, they can influence the invasion process in a variety of ways, and therefore represent promising targets for cancer therapies.

3.1.4 Rationale and Aims

The highly infiltrative nature of GBM cells is a critical feature that contributes to the resilience of GBM to current therapeutic strategies, ultimately resulting in the relapse of this disease. Invadopodia have been identified in a number of different cancers including breast, head and neck, bladder, lung and melanoma [123-125, 127, 131, 133], and only recently has there been a focus on investigating these structures in GBM [121, 351, 352]. Studies have reported that GBM cells surviving RT/TMZ treatment display an enhanced invasive phenotype [3-7], and recent studies by our laboratory indicate that there may be a potential role for invadopodia in mediating this treatment-induced invasiveness, although this has not been extensively studied to date [12, 352].

The aim of this chapter is to investigate the role invadopodia in GBM invasion and response to RT/TMZ treatment. Further elucidation of the role of invadopodia in GBM, especially post- RT/TMZ treatment, may highlight novel pathways and therapeutic targets to impede invadopodia activity and GBM cell invasion, potentially leading to an improved patient outcome through modified treatment protocols in the future. Importantly, as a study investigating TMZ penetration in GBM demonstrated that the concentration of TMZ detected in cerebrospinal fluid (CSF) was within a range of 1-10μg/ml (equivalent to 5.15-51.5μM of TMZ [353]), experiments were conducted at the 'clinically relevant' doses of 2Gy of RT (the daily dose received by GBM patients) and 50μM of TMZ.

3.2 Results

3.2.1 Invadopodia regulator expression in GBM tissue- gene expression datamining analysis

To investigate the potential significance of invadopodia in GBM, mRNA expression levels of a number of genes that are involved in the regulation of invadopodia, including Tks5, Tks4, cortactin, Nck1, NWASP, Src, and MMP-2 were evaluated using the online cancer microarray database, Oncomine™ (version 4.5, www.oncomine.org, Compendia Bioscience, Ann Arbor, MI, USA, Thermo Fisher) [354]. Gene expression datasets were examined from five independent GBM studies, which showed that there is a significant increase in the mRNA expression levels of a number of invadopodia regulators in GBM tissue samples compared to normal brain samples (***Figure 3-1***). Higher gene expression levels of these regulators, either alone or in combination, also associated with a significantly ($p<0.05$) reduced GBM patient overall survival, as determined with GBM datasets deposited with the online database, SurvExpress (***Supplementary Table 1***). Amongst the 42 significant gene combinations across the different datasets that significantly correlated with poorer GBM patient survival, cortactin appeared most frequently (20/42), followed by Tks5 (18/42), and Tks4 (13/42). These findings indicate that there is a potential clinical relevance for invadopodia in GBM patients.

Figure 3-1: Invadopodia regulators are overexpressed in GBM relative to normal brain tissue

mRNA expression levels of invadopodia regulators (Tks5, Tks4, Nck1, NWASP, MMP-2, Src and Cortactin) was examined in GBM datasets deposited within the Oncomine database. Only datasets that reached a significance threshold of $p<0.05$ are displayed, demonstrating the mean fold changes in expression between GBM and normal brain in each study. Gene expression data are log transformed and normalized as previously described [355].

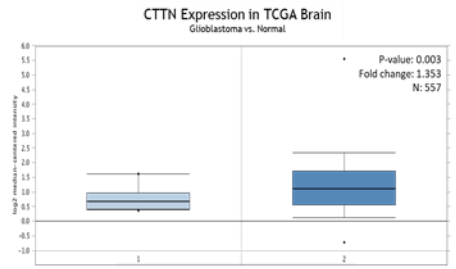
CTTN Expression in TCGA Brain
Glioblastoma vs. Normal
P-value: 0.003
Fold change: 1.353
N: 557

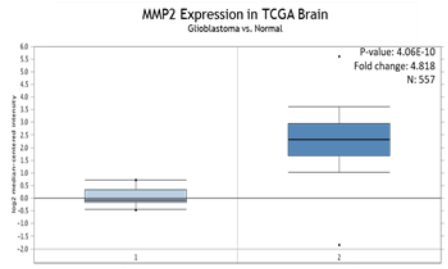
MMP2 Expression in TCGA Brain
Glioblastoma vs. Normal
P-value: 4.06E-10
Fold change: 4.818
N: 557

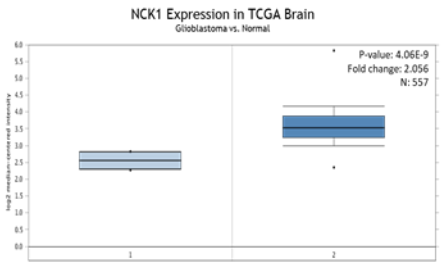
NCK1 Expression in TCGA Brain
Glioblastoma vs. Normal
P-value: 4.06E-9
Fold change: 2.056
N: 557

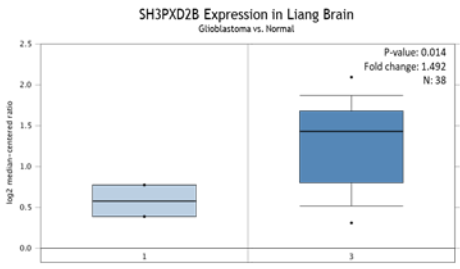
SH3PXD2B Expression in Liang Brain
Glioblastoma vs. Normal
P-value: 0.014
Fold change: 1.492
N: 38

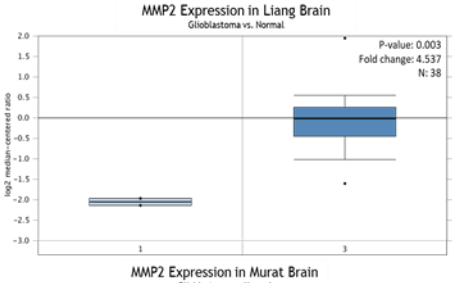
MMP2 Expression in Liang Brain
Glioblastoma vs. Normal
P-value: 0.003
Fold change: 4.537
N: 38

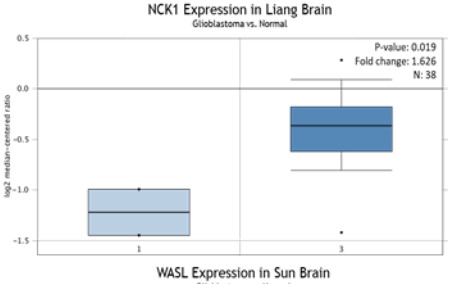
NCK1 Expression in Liang Brain
Glioblastoma vs. Normal
P-value: 0.019
Fold change: 1.626
N: 38

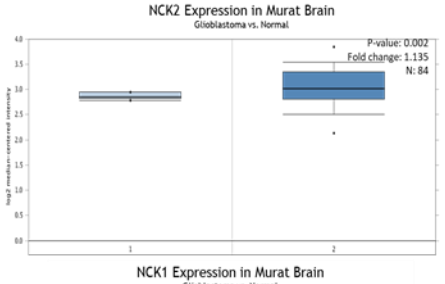
NCK2 Expression in Murat Brain
Glioblastoma vs. Normal
P-value: 0.002
Fold change: 1.135
N: 84

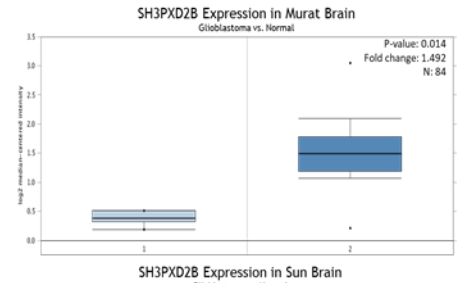
SH3PXD2B Expression in Murat Brain
Glioblastoma vs. Normal
P-value: 0.014
Fold change: 1.492
N: 84

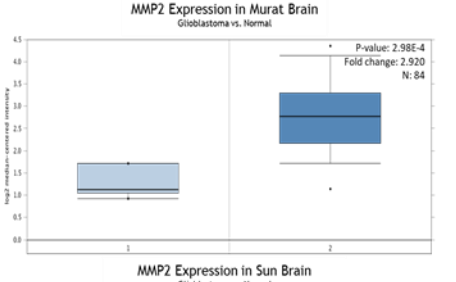
MMP2 Expression in Murat Brain
Glioblastoma vs. Normal
P-value: 2.98E-4
Fold change: 2.920
N: 84

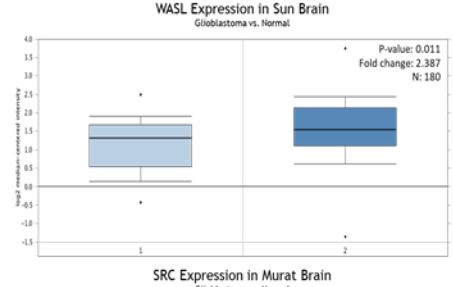
WASL Expression in Sun Brain
Glioblastoma vs. Normal
P-value: 0.011
Fold change: 2.387
N: 180

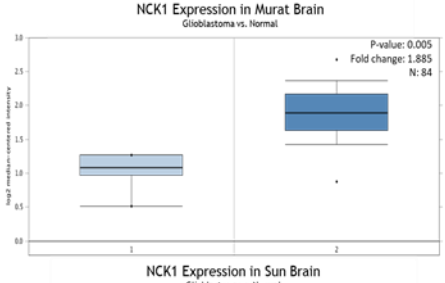
NCK1 Expression in Murat Brain
Glioblastoma vs. Normal
P-value: 0.005
Fold change: 1.885
N: 84

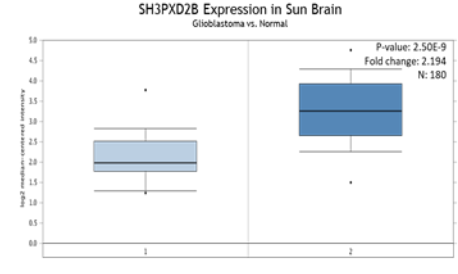
SH3PXD2B Expression in Sun Brain
Glioblastoma vs. Normal
P-value: 2.50E-9
Fold change: 2.194
N: 180

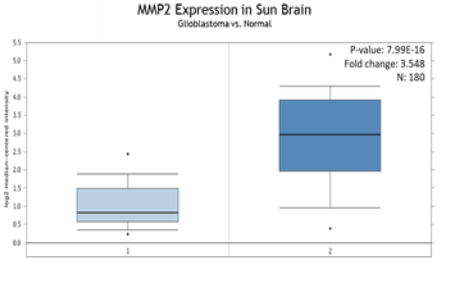
MMP2 Expression in Sun Brain
Glioblastoma vs. Normal
P-value: 7.99E-16
Fold change: 3.548
N: 180

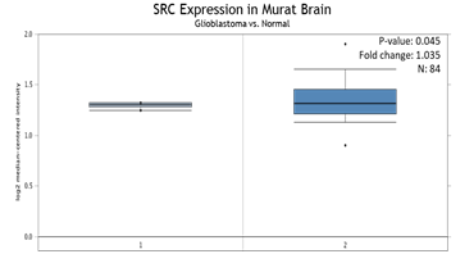
SRC Expression in Murat Brain
Glioblastoma vs. Normal
P-value: 0.045
Fold change: 1.035
N: 84

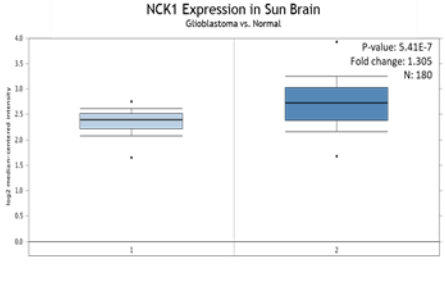
NCK1 Expression in Sun Brain
Glioblastoma vs. Normal
P-value: 5.41E-7
Fold change: 1.305
N: 180

3.2.2 GBM cell lines form functional matrix-degrading invadopodia

The following four GBM cell lines were utilized: two commercially available GBM cell lines (U87MG, LN229) and two in-house GBM cell lines (MU4, MU41). In order to assemble an 'invadopodia-related profile' for these GBM cell lines, the expression levels of a variety of invadopodia-related proteins were initially determined via western blot analysis, including cortactin, p-cortactin, NWASP and Src (***Figure 3-2A***). The expression of these proteins was seen to vary across all cell lines, except for NWASP which was expressed at a similar level across the four GBM cell lines. Tks5 was highly expressed in the LN229 cell line, Src was highly expressed in the MU41 cell line, and cortactin expression was reduced in the MU4 cell line compared to the other three cell lines.

The MMP secretory profile of the four selected GBM cell lines was next examined by performing gelatin-based zymogram analyses. MMP-2 was the only gelatinase detected in the serum-free conditioned medium from the four GBM cell lines, and varying amounts of both the inactive (latent) pro-MMP-2 and active-MMP-2 forms were detected (***Figure 3-2B***). Invadopodia FITC-gelatin degradation assays conducted with the four GBM cell lines demonstrated the presence of functional FITC-gelatin degrading invadopodia in the GBM cell lines (***Figure 3-2C***). In accordance with the zymography results indicating high levels of secreted MMP-2, the LN229 GBM cells also displayed the greatest level of invadopodia-mediated FITC-gelatin degradation, whereas MU4 cells exhibited the least FITC-gelatin degrading capacity.

Whilst MMP secretion and FITC-gelatin degradation are indicative of the presence of functional matrix-degrading invadopodia and are therefore used as an overall measure of invadopodia activity, these two assays do not allow for exact quantification of invadopodia. To quantify numbers of individual invadopodia, a customised script for Fiji (ImageJ Version 1.51f) was utilized to analyse the confocal images acquired for FITC-gelatin degradation assays, as outlined in *section 2.2.7.4.* The LN229 cells were observed to produce the most actin puncta (invadopodia) per cell, as well as possessing the highest percentage of active/degrading actin puncta. Interestingly, MU4 cells had relatively high numbers of actin puncta, however these puncta were largely non-degradative (***Figure 3-2D***).

Figure 3-2: GBM cell lines express invadopodia regulators, secrete MMP-2 and form functional invadopodia.

(**A.**) Immunoblot analysis of invadopodia regulators in GBM cell lines U87MG, LN229, MU4 and MU41. *Data shown is representative 3 independent experiments*. (**B.**) Gelatin zymographic analysis of conditioned serum-free OptiMEM GBM cell culture medium showing MMP-2 gelatinolytic activity. A representative scanned image of a zymogram gel is shown, revealing the presence of both the inactive (latent) pro-MMP-2 and active-MMP-2 forms. Densitometric analysis on represented bands is shown below. *Data shown is representative of 3 independent experiments*. (**C.**) Representative confocal images of GBM cell lines plated onto a thin film of cross-linked FITC-gelatin for 24h to detect the presence of invadopodia-mediated FITC-gelatin degradation. Degraded areas of FITC-labeled gelatin are evident as black areas devoid of FITC-labeled gelatin (green). DAPI staining of the nucleus is shown in blue, and rhodamine phalloidin staining of actin filaments and actin puncta (invadopodia) is shown in red. A total of 8 random images were acquired per cell line in each experiment and analysed using Image J (1.53a) to determine the level of degradation for each cell line, normalised to the number of cells present (indicated by the DAPI staining) as depicted in the graph below *(n=3 separate experiments; mean +/- standard deviation). **(D.)*** The total number of actin puncta- (top graph) and the number of active actin puncta overlapping with degraded FITC-gelatin (bottom graph) were quantified using the customized macro with ImageJ (1.53a) and normalised to the number of cells present (indicated by the DAPI staining). *(n=3 separate experiments; mean +/- standard deviation).*

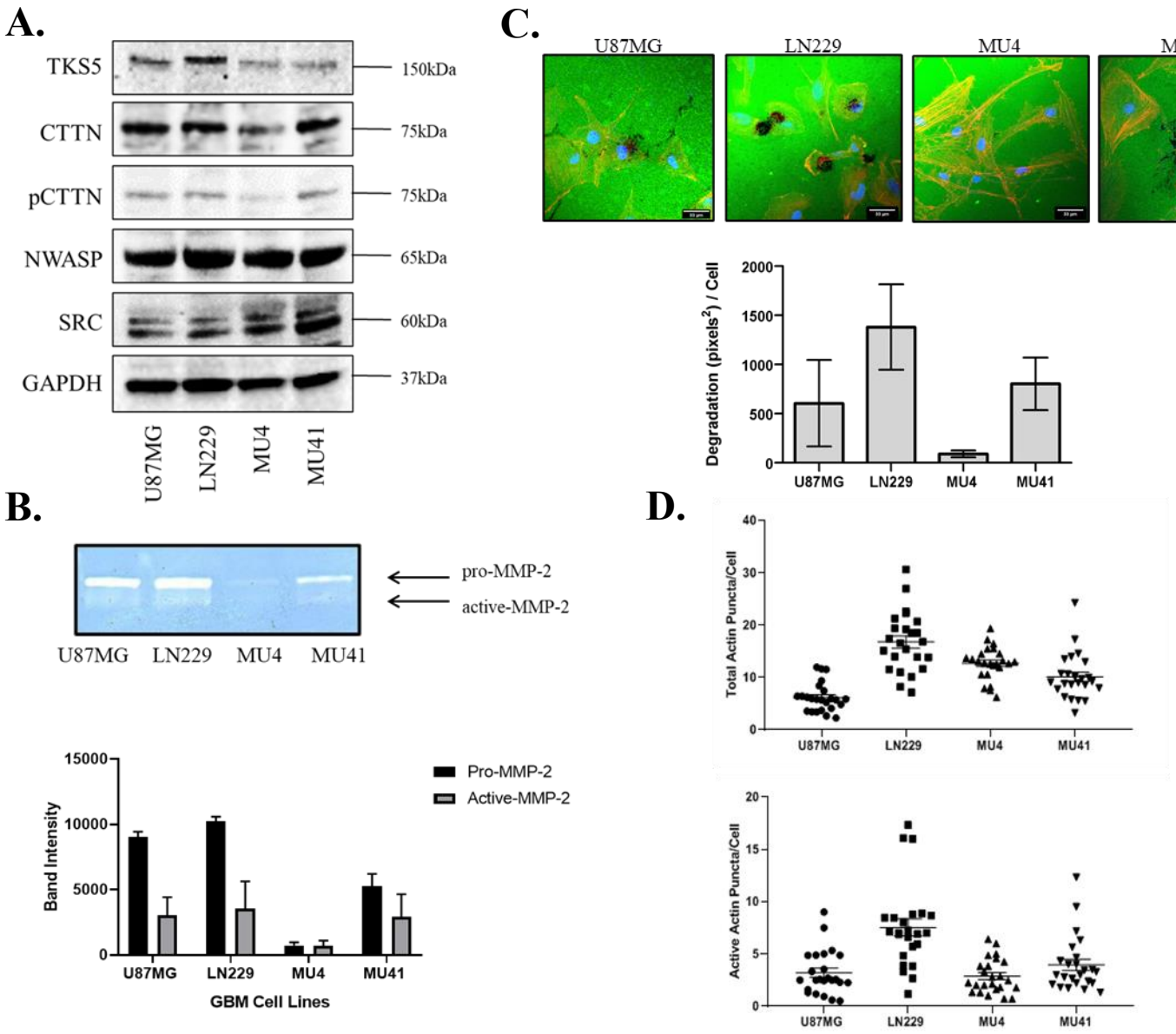
A.
TKS5
CTTN
pCTTN
NWASP
SRC
GAPDH
150kDa
75kDa
75kDa
65kDa
60kDa
37kDa
U87MG
LN229
MU4
MU41
B.
pro-MMP-2
active-MMP-2
U87MG LN229 MU4 MU41
Band Intensity
Pro-MMP-2
Active-MMP-2
GBM Cell Lines
C.
U87MG
LN229
MU4
MU41
Degradation (pixels²) / Cell
D.
Total Actin Puncta/Cell
Active Actin Puncta/Cell

3.2.3 RT/TMZ treated GBM cells exhibit augmented invadopodia mediated matrix-degrading activity

3.2.3.1 The effect of RT/TMZ on GBM cell viability

Cell viability assays were performed to examine the effect of RT (2Gy) and TMZ (50μM) on U87MG, LN229, MU4 and MU41 GBM cell lines, as these doses were utilized for experiments throughout the project. The assays conducted with an MTT protocol, involve the quantification of converted formazan which signifies the proportion of metabolically active cells that have survived treatment. For the current experiments, single and multiple daily doses, up to three consecutive days, were investigated (***Figure 3-3A***). The response to RT/TMZ treatment was observed to vary between the four GBM cell lines, with U87MG demonstrating the greatest reduction in cell viability with all treatment conditions. Additionally, the degree of apoptosis induced by RT/TMZ was also assessed using a Muse™ Annexin V & Dead Cell Assay that can quantitatively analyse and distinguish between live, early/late apoptotic, and dead cells. The degree of apoptosis was determined 24h after treatment to coincide with the planned zymogram and FITC-gelatin matrix degradation assays (***Figure 3-3B***) and was found to not significantly change following a single dose of RT/TMZ.

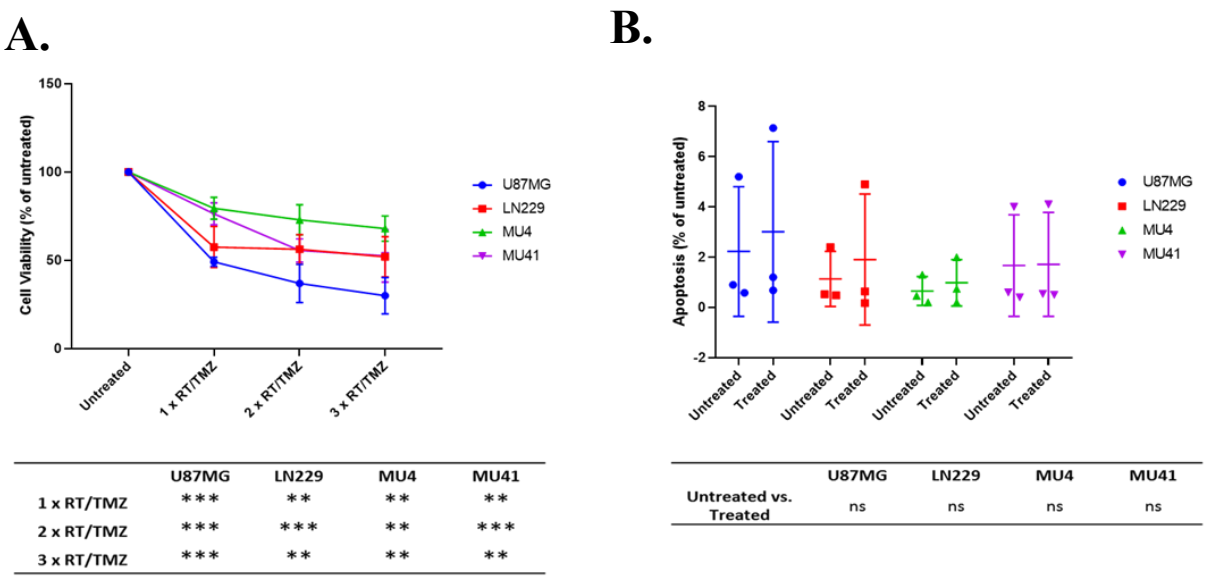

	U87MG	LN229	MU4	MU41
1 x RT/TMZ	***	**	**	**
2 x RT/TMZ	***	***	**	***
3 x RT/TMZ	***	**	**	**

Figure 3-3: Cell Viability of GBM cell lines in response to RT/ TMZ treatment

(**A**.) GBM cell lines U87MG, LN229, MU4 and MU41 (1×10^4 cells/100µl) were seeded into 96-well plates in triplicate and following an overnight incubation were subsequently treated with 2Gy RT and 50µM of TMZ, either singularly (1 x RT/TMZ), or on two (2 x RT/TMZ), or three (3 x RT/TMZ) consecutive days. The GBM cells were then incubated for a further 7 days before cell viability was determined using an MTT (3-(4,5-dimethylthiazol-2-yl)-2,5-diphenyltetrazolium bromide) cell-based assay. The data shown represents the mean of 3 independent experiments performed in triplicate (% viability compared to untreated cells). (**B.**) The proportion of apoptotic cells 24h after a singular treatment (1 x RT/TMZ) was also determined using a Muse™ Annexin V & Dead Cell Assay. The percentage of apoptotic (early and late apoptosis combined) cells in a population of untreated cells compared to single treated cells is shown, representing the mean of three triplicates for each experiment. *(n=3 experiments each performed in triplicates; mean ± SD, *p<0.05; **p<0.01; ***p<0.001, non-significant =ns, two-tailed student's t-test).*

3.2.3.2 The effect of RT/TMZ on invadopodia formation/activity in GBM cell lines

To investigate the impact of RT and TMZ treatment on invadopodia activity, zymographic analyses of serum-free OptiMEM® conditioned culture medium was initially performed to determine the impact of RT/TMZ treatment on the MMP secretory profiles of each GBM cell line (***Figure 3-4A***). A significant increase in MMP-2 secretion and activation was observed 24h after RT/TMZ treatment for U87MG, LN229 and MU4 cell lines. This trend was also observed for MU41 cells, although only the levels of active-MMP-2 were significantly increased post-treatment. These results were correlated with invadopodia FITC-conjugated gelatin degradation assays to determine the functional impact of RT/TMZ on invadopodia activity. In accordance with the increase in MMP-2 secretion, an increase in FITC-gelatin degradation was observed for the GBM cells post-RT/TMZ (***Figure 3-4B***).

To establish whether the changes in proteolytic activity following RT/TMZ treatment were due to an increase in invadopodia formation, the confocal images analysed in ***Figure 3-4B*** were further examined to quantitate the actin puncta as per section ***2.2.7.4.*** An increase in both the number of actin puncta and number of puncta overlapping with degraded FITC-gelatin was observed in GBM cells that had undergone RT/TMZ treatment (***Figure 3-4C***). Collectively, these findings indicate that GBM cells exposed to RT/TMZ treatment exhibit an increase in invadopodia formation and FITC-gelatin degrading activity.

The intracellular expression levels of various invadopodia regulators (MMP-2, Tks5, cortactin, p-cortactin) in untreated compared to RT/TMZ treated GBM cell lines was examined using western blot analysis of GBM cell lysates (***Figure 3-4D***). No significant changes in protein expression were observed, potentially suggesting that the mechanisms behind the observed functional changes (MMP secretion and matrix degrading ability), may involve different invadopodia regulators, or these changes may be due to a re-distribution and localisation of these proteins to the cell membrane, allowing the GBM cells to form more invadopodia in response to treatment.

Figure 3-4: Increased GBM cell invadopodia formation/activity is observed with a single RT/TMZ treatment

(**A**.) Gelatin-based zymographic analysis of serum-free OptiMEM conditioned medium showing (***i.***) the MMP-2 secretion profile of GBM cells post-RT/TMZ treatment and (***ii.***) densitometric analysis of pro-MMP-2 bands and active-MMP-2 bands represented as fold change relative to untreated cells. (**B**.) (i.) Representative confocal images of the GBM cell lines and (ii.) the corresponding analysis indicating an increase in FITC-conjugated gelatin degradation 24h post-RT/TMZ treatment. (Scale bar is equivalent to 20μm). (**C**.) An increase in (***i.***) the total number of actin puncta (invadopodia) per cell and (***ii.***) the number of actin puncta (invadopodia) overlapping with degraded FITC-gelatin is observed in RT/TMZ treated GBM cells. (**D.**) Western blot analysis of 20μg of whole cell lysates prepared from GBM cell lines that were either untreated (-) or treated (+) with 2Gy RT and 50μM TMZ. Various antibodies were used to probe for invadopodia regulator proteins - Tks5, MMP-2, Cortactin (CTTN) and p-Cortactin (p-CTTN). *Data shown is representative of at least 3 independent experiments*. All assays show GBM cell response 24h post-treatment with 2Gy RT and 50μM TMZ. *(n=3 experiments; mean ± SD, *p<0.05; **p<0.01; ***p<0.001, unpaired two-tailed student's t-test*.).

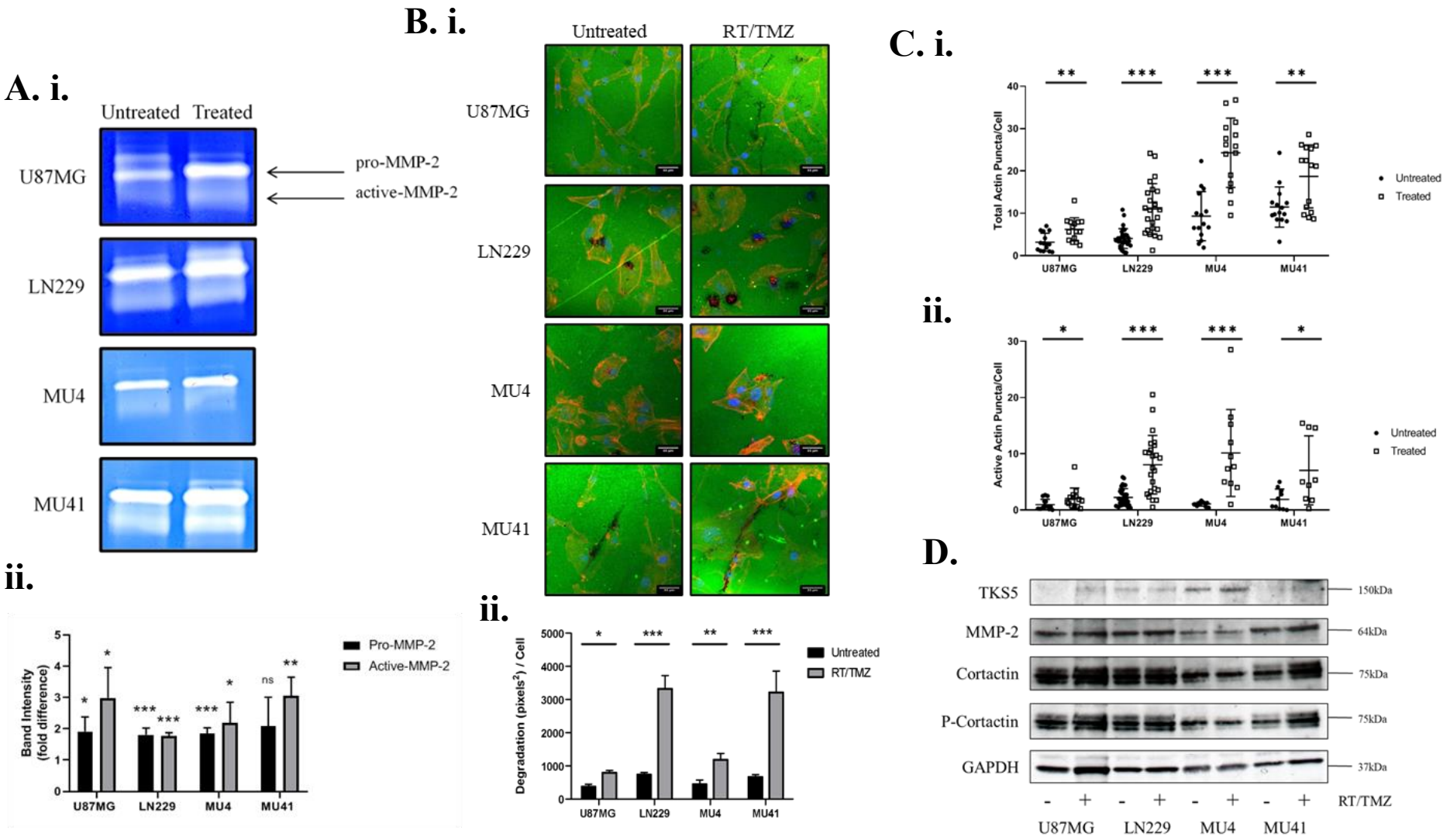
A. i.
Untreated
Treated
U87MG
LN229
MU4
MU41
pro-MMP-2
active-MMP-2
ii.
Band Intensity (fold difference)
Pro-MMP-2
Active-MMP-2
U87MG
LN229
MU4
MU41
B. i.
Untreated
RT/TMZ
U87MG
LN229
MU4
MU41
ii.
Degradation (pixels²) / Cell
Untreated
RT/TMZ
C. i.
Total Actin Puncta/Cell
Untreated
Treated
ii.
Active Actin Puncta/Cell
D.
TKS5
MMP-2
Cortactin
P-Cortactin
GAPDH
150kDa
64kDa
75kDa
75kDa
37kDa
RT/TMZ

A number of invadopodia regulators, such as cortactin, are also known to also play a role in cell motility through interactions with the actin cytoskeleton [356]. As such, the effect of RT and TMZ on the migratory abilities of the GBM cells was also examined (***Figure 3-5A***). LN229 and MU4 cell lines were chosen for their ability form uniform, confluent monolayers and were treated with RT (2Gy) /TMZ (50μM) 24h prior to the addition of Mitomycin C (5 μg/ml) for 2h (to prevent proliferation) and the subsequent introduction of a scratch (wound). The wound area of the treated cells relative to the untreated control suggests that GBM cells exhibit an increase in migration rate in response to RT/TMZ treatment. The observed increases in migration rate, MMP-2 secretion and invadopodia-mediated FITC-gelatin degradation activity indicate that GBM cells surviving RT/TMZ treatment display a pro-migratory / pro-invasive phenotype.

It is known that cancer cell invasion generally occurs during G1/G0 cell cycle arrest, co-occurring with the expression of EMT-inducers and rearrangement of the F-actin cytoskeleton [357]. Therefore, the cell cycle distribution of GBM cell lines in response to RT/TMZ treatment was also examined. It can be observed that in response to RT/TMZ treatment, there is an increase in the percentage of cells in the GO/G1 phase (***Figure 3-5B***). When coupled with the previous data showing an increase in matrix-degrading activity in the GBM cells treated with RT/TMZ, it is possible that the RT/TMZ treated cells favour cell cycle arrest in order to shift their energy demands away from a proliferative state and towards the process of invasion.

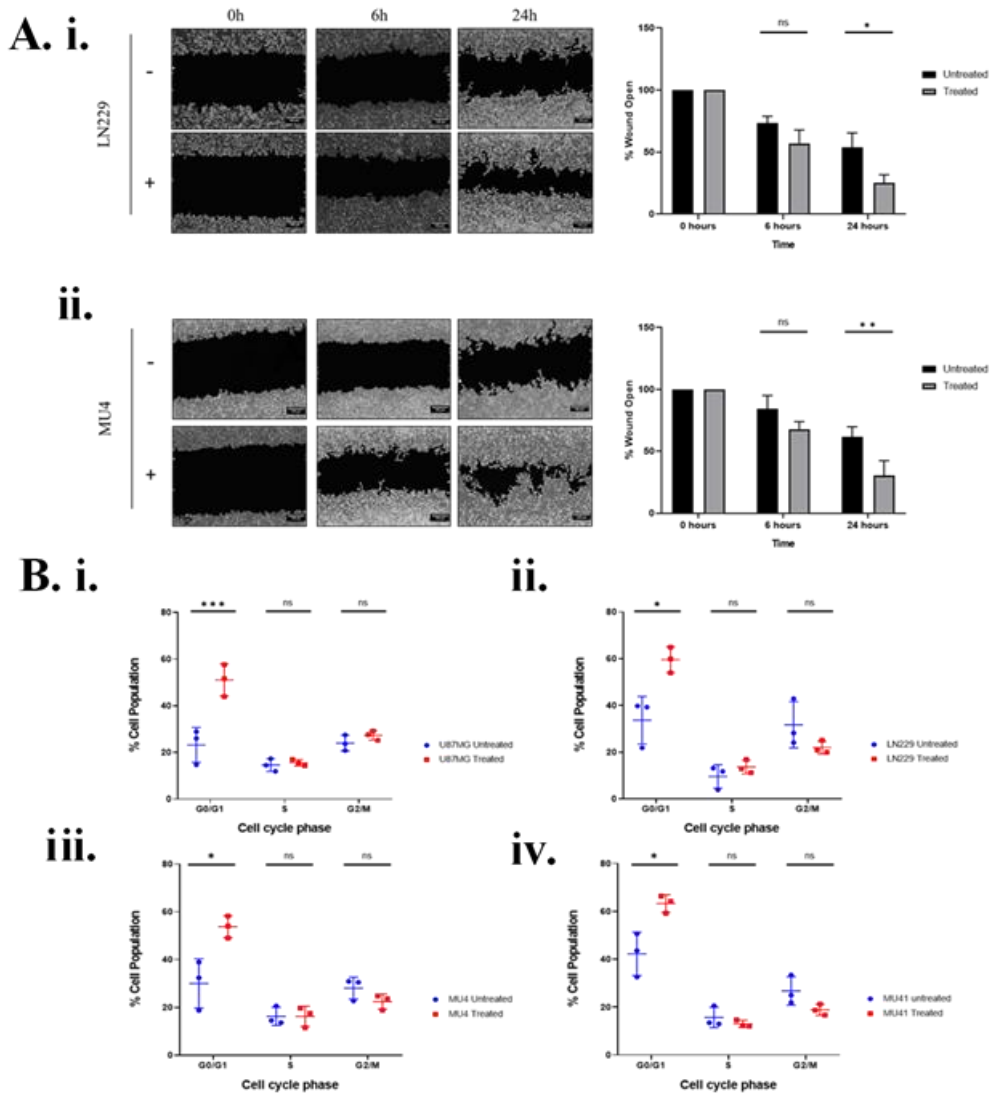

Figure 3-5: A single RT/TMZ treatment alters GBM cell migration and cell cycle distribution

(**A.**) The effect of 2Gy RT and 50μM TMZ on GBM cell migration was examined using a scratch (wound) healing assay in the (i.) LN229 and (ii.) MU4 cell lines. Results represent the percentage of wound remaining open relative to t = 0h. (Scale bar is equivalent to 100μm). (*n=3 experiments; 4 images per cell line per experiment; mean ± SD, *p<0.05; **p<0.01; non-significant =ns, unpaired two-tailed student's t-test*). (**B.**) The cell cycle phase distribution (G0/G1, S, G2/M) of GBM cell lines 24h after RT/TMZ treatment was determined using a Muse™ Cell Cycle Assay. Each point represents the percentage of cells in a sample that were within the specified cell cycle phase. *(n=3 experiments performed in triplicate; mean ± SD, *p<0.05; ***p<0.001, non-significant =ns, two-tailed student's t-test).*

3.2.4 The effect of long-term RT/TMZ treatment on the invadopodia-mediated matrix-degrading activity of GBM cell lines

3.2.4.1 Generation and characterisation of LT treated GBM cell lines

To simulate a 'multiple treatment' regime, the four GBM cell lines U87MG, LN229, MU4 and MU41 were repeatedly treated with RT and TMZ (2Gy and 50µM) once a week for a period of 10 weeks, to enable cultured cells time to recover after each dose of treatment, and termed 'long-term treated' (LT) cell lines (***Figure 3-6)***. The sensitivity of the LT cell lines to RT/TMZ treatment was examined using MTT cell viability assays, which were performed following treatment with RT (2Gy) / TMZ (50µM) over one, two and three consecutive days (***Figure 3-7A***). The LT cells exhibited a reduction in sensitivity to RT/TMZ treatment compared to untreated cells, which varied between cell lines. It is important to note that untreated and LT cell lines were maintained in culture for the same length of time, shortly after the long-term treatment protocol, prior to treatment in this set of experiments for comparison. The proliferation rate of LT cells was also assessed using MTT assays (***Figure 3-7B***). The observed trend displayed by all LT GBM cell lines was an increase in the proliferation rate compared to the untreated cells. Notably, the greatest increase in proliferation rate was seen in LN229 cells after LT treatment.

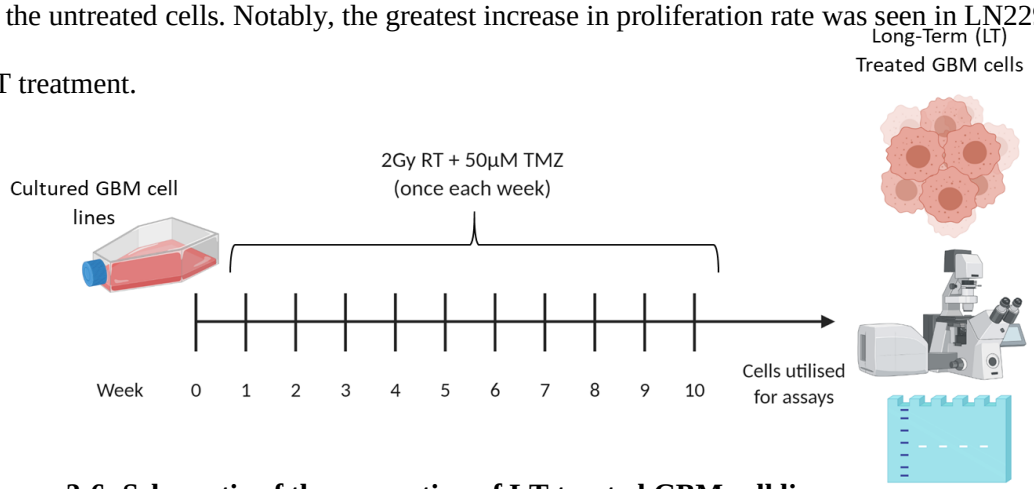

Figure 3-6: Schematic of the generation of LT treated GBM cell lines

GBM cell lines U87MG, LN229, MU4 and MU41 were treated with 2Gy RT and 50µM TMZ once a week for 10 consecutive weeks to generate long-term (LT) cells. Following the 10-week treatment regime, LT cells were frozen and thawed when required for various assays.

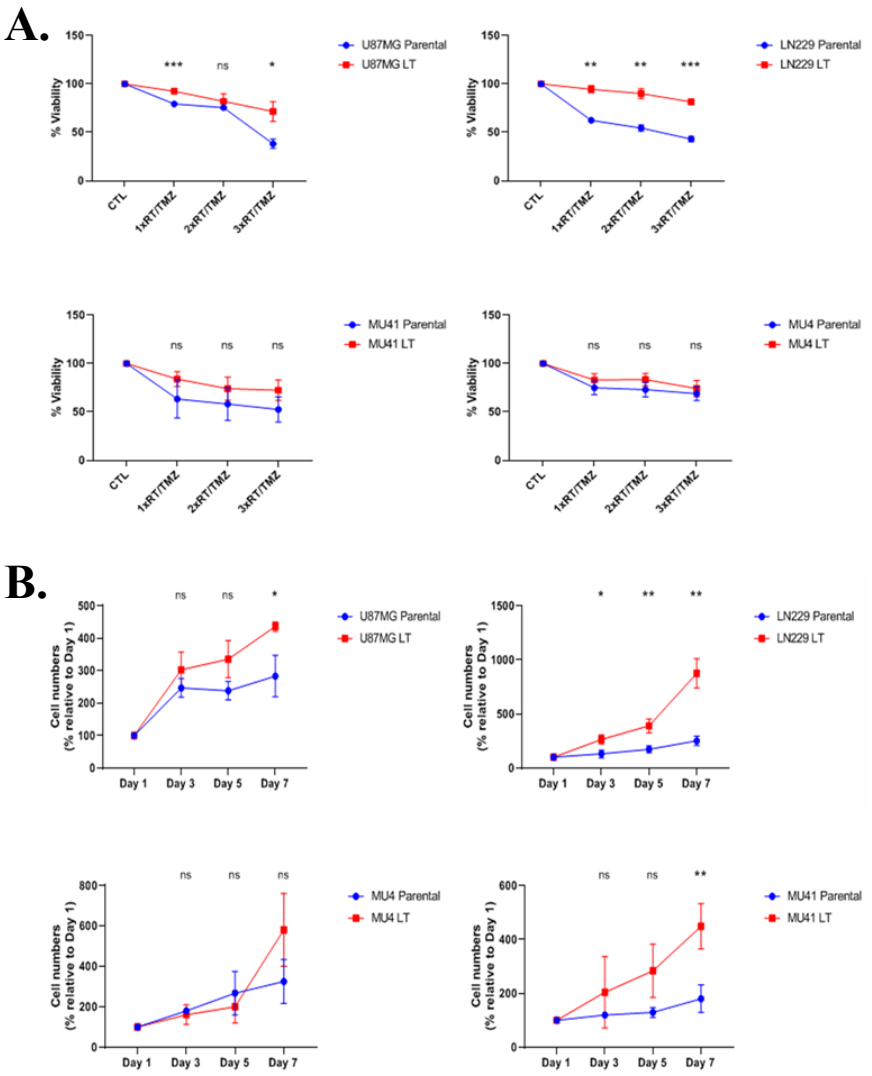

Figure 3-7: Long-term RT/TMZ treatment results in altered GBM cell sensitivity to RT/TMZ treatment and proliferation rate.

MTT analysis of parental (blue) and LT treated (red) GBM cell lines. (**A**.) GBM cells were treated with 2Gy RT and 50μM TMZ either singularly (1xRT/TMZ), or on two (2xRT/TMZ) or three (3xRT/TMZ) consecutive days, and incubated for 7 days before cell viability was determined, as represented as percentage survival relative to untreated control (CTL) cells. (**B**.) GBM cells were seeded into 96-well plates, and MTT assays were conducted on days 1, 3, 5 and 7 after seeding to determine the proportion of cells relative to day 1. (*n=3 experiments; each experiment performed in triplicate wells; mean ± SD, *p<0.05; **p<0.01; ***p<0.001, non-significant =ns, paired two-tailed student's t-test*).

3.2.4.2 The effect of LT treatment on invadopodia formation/activity in GBM cell lines

As a single treatment of RT/TMZ results in increase invadopodia-mediated FITC-gelatin degradation, the effect of LT treatment on invadopodia in GBM cells was next examined. Gelatin-based zymography was used to determine the impact of LT treatment on the MMP secretory profile of the GBM cells ***(Figure 3-8A)***. GBM cell lines U87MG, MU4 and MU41 exhibited an increase in MMP-2 secretion following LT treatment, however LN229 cells displayed a reduction in secreted MMP-2, with no detectable extracellular MMP-2 gelatinolytic activity present in the zymogram gels. In agreement with the MMP secretory profiles, an increase in FITC-gelatin degradation was observed for LT treated U87MG, MU4 and MU41 cells, whereas LN229 LT cells showed a loss of FITC-gelatin degrading activity (***Figure 3-8B)***.

To examine whether these differences in LT treated cells correlated with invadopodia formation and/or activity, confocal images of untreated and LT treated GBM cells seeded on FITC-gelatin were then utilised to quantify invadopodia formation and activity. An increase in the total number of actin puncta, representing the invadopodium core and actin puncta overlapping with degraded FITC-gelatin was observed for LT treated U87MG, MU4 and MU41 cells, whilst a decrease was observed for LN229 cells (***Figure 3-8C)***. Collectively, the results suggest that enhanced MMP-2 secretion and invadopodia formation/activity is maintained after LT treatment in U87MG, MU4 and MU41 cells, but is lost in the LT treated LN229 GBM cells.

To further validate the effect of LT treatment on the GBM cells, a commercially available Cultrex^{TM} BME invasion assay was utilized to determine if the LT treatment impacted the invasive capacity of the GBM cell lines ***(Figure 3-8D)***. The LT treated U87MG, MU4 and MU41 cells displayed an increase in invasion which was consistent with the enhanced invadopodia formation and levels of secreted MMP2. Importantly, the LT treated LN229 cells demonstrated a decrease in invasion, which is in agreement with the observed reduction in the secreted levels of MMP-2 and invadopodia-mediated FITC-gelatin degrading activity.

Figure 3-8: Altered invadopodia formation and activity is observed following long-term RT/TMZ treatment

(**A**.) Gelatin-based zymographic analysis of serum-free conditioned medium showing the MMP-2 secretion profile of untreated parental and long-term treated (LT) GBM cell lines, with densitometric analysis of (*ii*.) pro- and (*iii*.) active- MMP-2 bands shown. (**B**.) (*i*.) Representative confocal images of FITC-gelatin degradation assays comparing untreated parental and LT cell lines. A total of 10-25 random images were acquired. An increase in the (ii.) FITC-gelatin degradation activity and (*iii*.) the percentage of cells with FITC-gelatin degrading activity was observed for the LT treated U87MG, MU4 and MU41 GBM cells relative to the untreated cells, whereas there was an absence of FITC-gelatin degradation observed with the LT treated LN229 cells. *(Scale bar is equivalent to 20μm).* (**C**.) An increase in (*i***.**) the total number of actin puncta (invadopodia) and (*ii***.**) the number of actin puncta (invadopodia) overlapping with degraded FITC-gelatin is observed in the LT treated U87MG, MU4 and MU41 GBM cell lines compared to the parental (untreated) cells, whilst a reduction was observed with the LT treated LN229 GBM cell line. *(n=3 experiments for all results shown above; mean ± SD, *p<0.05; **p<0.01; ***p<0.001, non-significant =ns unpaired two-tailed student's t-test).* (**D**.) The invasion of parental/untreated (black) and LT treated (grey) GBM cell lines through an 8μm polycarbonate membrane coated with basement membrane extract was assessed according to the workflow in (*i*.). Invasion was measured as relative fluorescence units, to allow for comparison between untreated and LT cell lines and is displayed in (*ii*.) as fold change. (*Data shown is representative of 2 independent experiments, mean ± SD, **p<0.01, unpaired two-tailed student's t-test*).

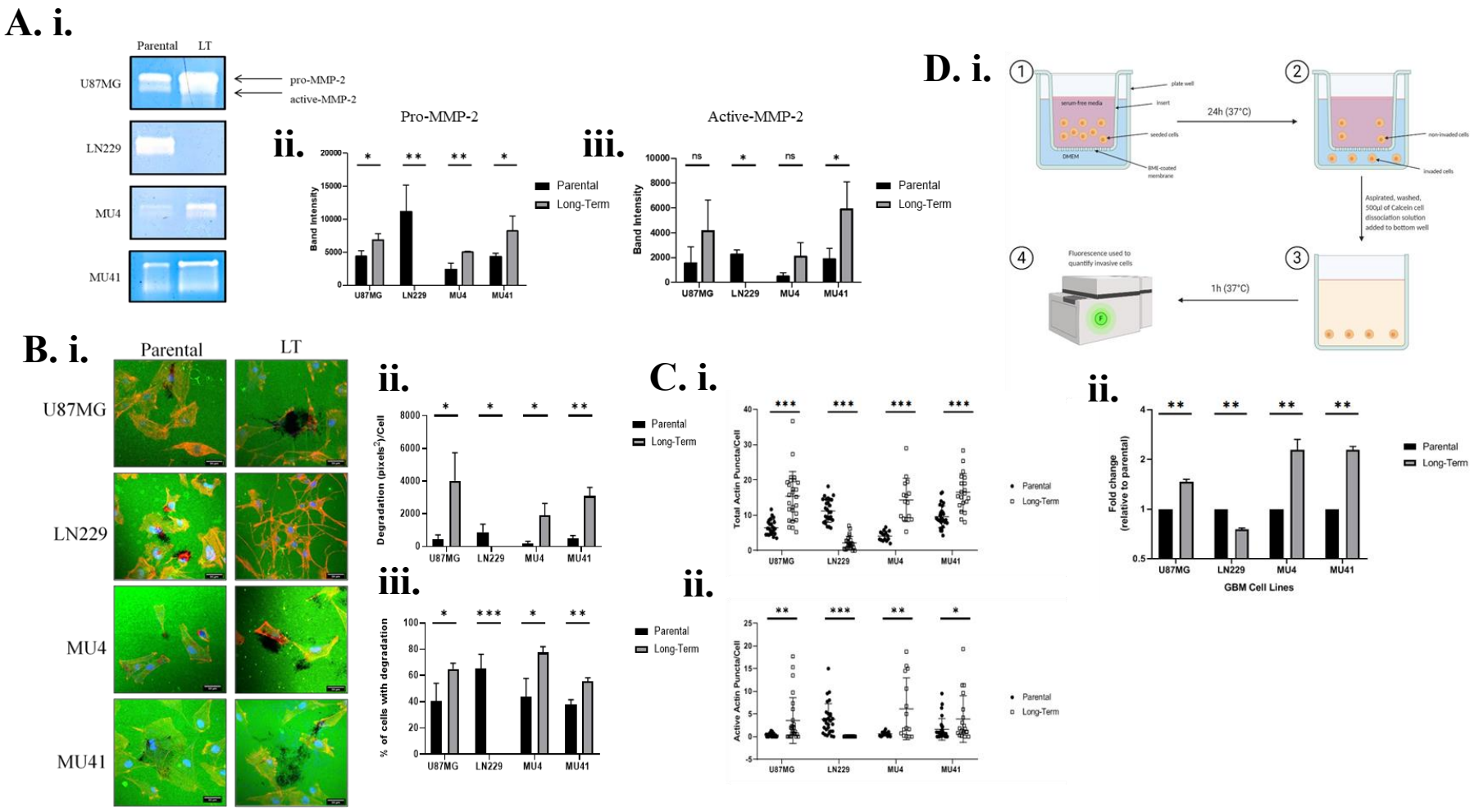
A. i.
Parental
LT
U87MG
LN229
MU4
MU41
pro-MMP-2
active-MMP-2
ii.
Pro-MMP-2
Band Intensity
Parental
Long-Term
iii.
Active-MMP-2
ns
B. i.
Parental
LT
ii.
Degradation (pixels²)/Cell
iii.
% of cells with degradation
C. i.
Total Actin Puncta/Cell
ii.
Active Actin Puncta/Cell
D. i.
plate well
insert
serum-free media
seeded cells
DMEM
BME-coated membrane
24h (37°C)
non-invaded cells
invaded cells
Aspirated, washed, 500µl of Calcein cell dissociation solution added to bottom well
Fluorescence used to quantify invasive cells
1h (37°C)
ii.
Fold change (relative to parental)
GBM Cell Lines

3.2.5 Profiling of proteases and inhibitors secreted by GBM cell lines

Although MMP-2 and MMP-9 are the main proteases that have been associated with invadopodia-mediated invasion, there exists an integrated network of proteases and inhibitors that have been implicated in the matrix remodelling abilities of malignant cells.

Therefore, the next aim was to profile the GBM cell line serum-free conditioned medium for the presence of additional secreted proteases that may contribute to their invasive capacity, and whether RT/TMZ treatment leads to changes in the secretion of these proteases and their inhibitors. This was undertaken with commercially available human protease and inhibitor antibody arrays (Proteome Profiler™ Array, R&D Systems) encompassing 35 proteases and 21 protease inhibitors (***Supplementary Figure 1***). Densitometric analysis of duplicate array spots, following incubation with conditioned serum-free media from untreated, single treated and LT treated U87MG, LN229, MU4 and MU41 cells was conducted to determine the levels of secreted proteases and inhibitors.

3.2.5.1 GBM cell lines predominantly secrete cathepsins and MMPs

Determination of the secreted levels of 35 proteases from untreated, single treated and LT treated U87MG, LN229, MU4 and MU41 cells is shown in ***Figure 3-9A***. Proteases detected above a pixel intensity threshold of 150 were compared in each cell line, highlighting the proteases commonly detected at higher levels across all three cell lines in each condition (***Figure 3-9B***). The proteases commonly secreted by all four GBM cell lines above the threshold, prior to treatment included Cathepsin D and V, as well as MMP -2 and -12. Following RT/TMZ treatment, secreted MMP -1, -7 and -8 were also detected above threshold for all GBM cell lines.

mRNA expression levels corresponding to the four common proteases secreted above threshold by untreated GBM cells (CTSD, CTSV, MMP2, MMP12) were examined using the TCGA dataset in the online Oncomine® database. The mRNA expression levels were significantly increased in GBM relative to normal brain tissue, with a 1.4 fold increase observed with MMP12, CTSD and CTSV , and a 4.8 fold increase in MMP2 mRNA expression (***Table 3-1.***). Furthermore, examination of gene expression with clinical data in datasets deposited within the SurvExpress database revealed a significant correlation between high expression of all four genes and poorer GBM patient survival in 8 independent datasets (***Table 3-2, Figure 3-10.***). This demonstrates the potential clinical relevance of these proteases, with the possibility of being involved in GBM cell invasion.

Changes in protease secretion following single or LT treatment were deemed significant if a protease was above the pixel intensity threshold of 150 in either of the untreated, single or LT treated groups corresponding to a cell line, and the fold change was greater than 2-fold (***Figure 3-11***). Significant changes in protease secretion following a single RT/TMZ treatment were observed for Kallikrein 13, MMP-10, Neprilysin and Proprotein Convertase 9 which increased greater than 2-fold in U87MG, as well as Cathepsin D in MU4 and Kallikrein 10 in MU41, both of which decreased 2-fold following RT/TMZ treatment. Proteases with increased secretion following LT treatment included ADAM8, Cathepsin S/V, Kallikrein 10/13 and MMP-8 in MU4, as well as Cathepsin A/B/D and MMP-2 in MU41. Additionally, the secreted levels of a variety of different proteases were also seen to decrease in

LT treated cells relative to the correpsonding untreated cell line, including a total of twenty proteases in U87MG, as well as Cathepsin D/V and MMP-1/-2/-9 in LN229, Cathepsin D in MU4, and ADAMTS1, MMP-1/-3/-7/-8, and Neprilysin/CD10 in MU41. The decrease in detected MMP-2 from LT treated LN229 cells is consistent with zymography results, showing a complete loss of detectable MMP-2 activity. However, the lack of significant pixel intensity changes for MMP-2 in the conditioned media of GBM cells following a single RT/TMZ treatment could suggest that the secreted levels of this protease may not greatly differ after treatment, despite the increase in MMP-2 activity detected via zymography. However, whilst the antibody array detects the protein levels of proteases including MMP-2, zymography measures the gelatinolytic activity of MMP-2 and can detect the activity of secreted MMP-2 in both its inactive/pro-- and active- forms. As such, the sensitivity of zymography is much greater than that of protein detection via antibody arrays or western blots, which depend on the affinity of an antibody to the protein of interest, and may explain these discrepencies in the detected levels of secreted MMP-2 [358].

Figure 3-9: Evaluation of secreted proteases in untreated, single RT/TMZ treated and long-term RT/TMZ treated GBM cells

(**A.**) A graphical representation of the densitometric analysis of the protease antibody arrays performed with GBM cell line conditioned medium. All data shown is represented as an average pixel density of duplicate antibody spots and normalized with the reference spots on each membrane. Densitometry was performed using ImageJ (1.53a). (**B.**) Venn diagrams represent the secreted proteases detected above threshold (>150-pixel intensity) in the conditioned media from untreated, single and long-term RT/TMZ treated cells. The proteases within each Venn diagram circle were above a normalised pixel intensity threshold set at 150. The proteases highlighted by a red box represent the 'common' proteases identified above threshold level across the cell lines.

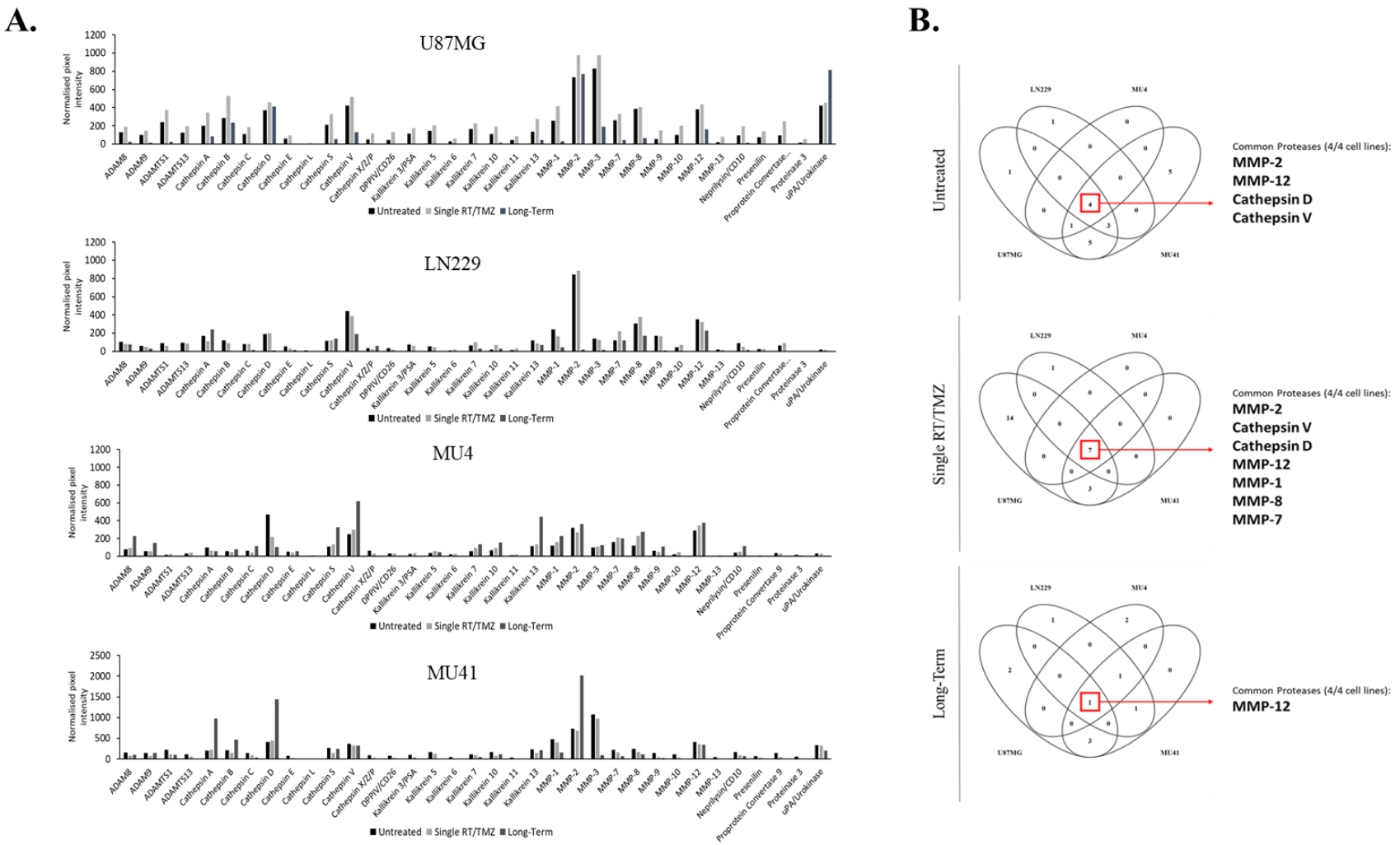
A.
U87MG
LN229
MU4
MU41
Normalised pixel intensity
Untreated
Single RT/TMZ
Long-Term
B.
Untreated
Single RT/TMZ
Long-Term
LN229
MU4
U87MG
MU41
Common Proteases (4/4 cell lines):
MMP-2
MMP-12
Cathepsin D
Cathepsin V
Common Proteases (4/4 cell lines):
MMP-2
Cathepsin V
Cathepsin D
MMP-12
MMP-1
MMP-8
MMP-7
Common Proteases (4/4 cell lines):
MMP-12

Table 3-1: mRNA expression levels of MMP-2, MMP-12, Cathepsin D (CTSD) and Cathepsin V (CTSV) are elevated in GBM tissue

mRNA	Mean Fold Change (Log-2)	p-value
MMP-2	4.818	4.06E-10
MMP-12	1.427	1.16E-06
CTSD	1.446	5.57E-05
CTSV	1.44	1.14E-04

The mRNA expression data analysis (GBM tissue vs. normal brain tissue) presented was obtained from the TCGA dataset within the Oncomine database (n=534).

Table 3-2: MMP-2, MMP-12, Cathepsin D (CTSD) and Cathepsin V (CTSL2) overexpression correlates with poorer GBM patient survival

Dataset	Gene 1	Gene 2	Gene 3	Gene 4	Concordance Index (CI)	p-value	Sample size
GRAVENDEED	MMP-2	MMP-12	CTSD	CTSL2	58.35	1.20E-04	270
TCGA	MMP-2	MMP-12	CTSD	CTSL2	55.16	3.76E-03	538
NUTT	MMP-2	MMP-12	CTSD	CTSL2	60.41	4.67E-03	50
LEE	MMP-2	MMP-12	CTSD	CTSL2	55.61	4.72E-03	218
MURAT	MMP-2	MMP-12	CTSD	CTSL2	58.75	1.05E-02	80
TCGA-2016	MMP-2	MMP-12	CTSD	CTSL2	60.82	1.57E-02	148
FREIJE	MMP-2	MMP-12	CTSD	CTSL2	62.46	2.20E-02	85
JOO KIM	MMP-2	MMP-12	CTSD	CTSL2	61.12	4.07E-02	55

The mRNA data analysis presented was obtained from GBM study datasets deposited within the SurvExpress database and is ordered by log-rank p-value.

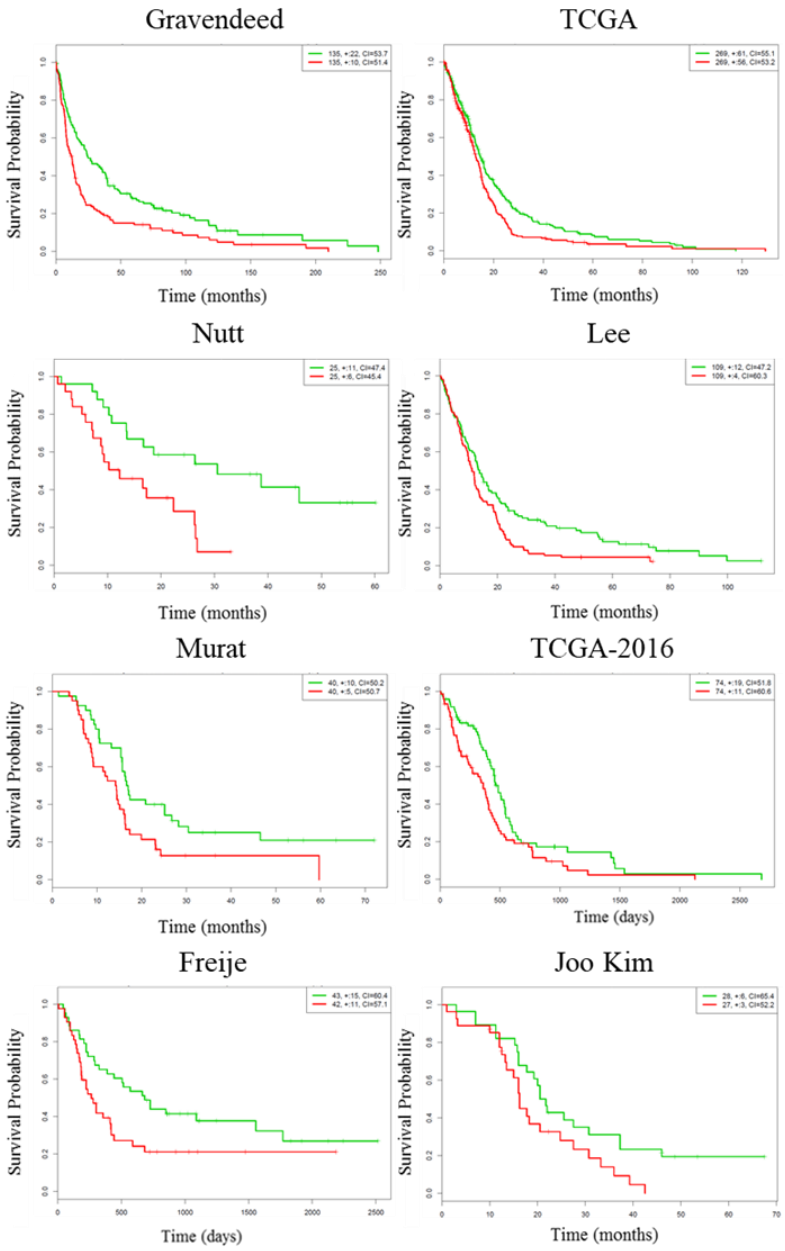

Figure 3-10: High expression of MMP-2, MMP-12, Cathepsin D and Cathepsin V correlates with poorer GBM patient survival

Kaplan Meier curves outlining the survival of GBM patients based on high- (red line) versus low- (green line) combined gene expression of MMP-2, MMP-12, CTSD and CTSV (CTSL2). This figure is derived from the SurvExpress datasets listed in ***Table 3-4*** and shows the prognostic potential of a 'protease signature' examining MMP-2, MMP-12, CTSD and CTSV mRNA levels in biopsy tissue from GBM patient**s.**

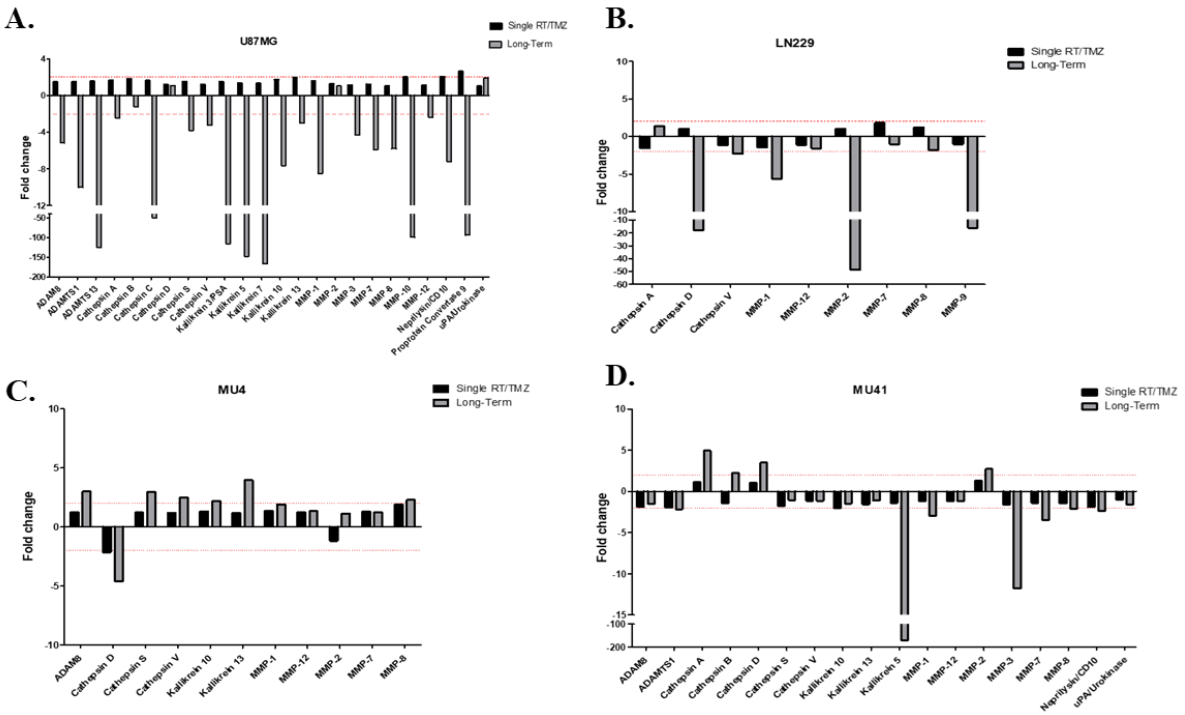

Figure 3-11: Changes in protease secretion following single and long-term RT/TMZ

Changes in the secreted levels of proteases following single and long-term RT/TMZ treatment were assessed for proteases that were above a threshold of >150-pixel intensity in either the conditioned media from untreated, single and long-term RT/TMZ treated cells. Secreted levels of these proteases were determined by densitometric analysis of antibody array spots and are displayed as fold change relative to untreated cells in the following GBM cell lines - (**A.**) U87MG, (**B.**) LN229, (**C.**) MU4 and (**D.**) MU41. A red line indicates a fold change of ± 2-fold. Densitometry was performed via ImageJ (1.53a).

3.2.5.2 GBM cells secrete protease inhibitors with pro-invasive functions

The proteolytic activities of secreted proteases, such as MMPs and Cathepsins, often serve multiple interconnected roles within regulatory circuits that involve the tight control of balance between proteases and their inhibitors. To further investigate these proteolytic networks in GBM cells, as well as the effect of RT/TMZ treatment on such networks, the secretion of 21 protease inhibitors from untreated, single treated and LT treated U87MG, LN229, MU4 and MU41 cells was also examined (***Figure 3-13A***). Using an antibody array, inhibitors detected above a pixel intensity threshold of 150 were compared in each cell line, to identify inhibitors which are commonly secreted by all three cell lines with each treatment (***Figure 3-13B***). No inhibitors were commonly secreted above threshold level by all four untreated GBM cell lines, however following a single RT/TMZ treatment, this increased to eight common inhibitors: PAI-1 (also known as Serpin E1), APP, Cystatin A, Cystatin C, Fetuin B, Latexin, Lipocalin-1 and Serpin B6. No inhibitors were commonly secreted above threshold level by all four LT treated GBM cell lines, however three inhibitors were commonly secreted above threshold level for the LT treated U87MG, MU4 and MU41 cell lines: TIMP-1, TFPI-2, and EMMPRIN/CD147.

Increasing evidence suggests that many protease inhibitors are multifunctional and can serve as either tumour suppressors or promotors in certain contexts via regulation (activation or inhibition) of their target ligands. Thus, as inhibitors regulate the balance between the production of active enzymes and their inhibition, their deregulation is often critical for cancer cell invasion [359]. Therefore, the detected secreted inhibitors with known pro-invasive functions were next examined. Seven of the inhibitors were identified as tumour promoting, with established roles in MMP activation and oncogenic signaling pathways (***Table 3-3***). These included APP, Fetuin B, EMMPRIN/CD147, Lipocalin-1, Serpin E1/PAI-1, as well as TIMP-1 and TIMP-2. Changes in the secreted levels of these inhibitors following single and LT treatment in each individual cell line is shown in ***Figure 3-14***. Notably, all single RT/TMZ treated GBM cell lines exhibited an increase in the secretion of inhibitors with pro-invasive roles, with the exception of Serpin E1/PAI-1 and EMMPRIN/CD147 in MU41, as well as APP in U87MG, although these still remained at relatively high secreted levels. The secretion of these inhibitors by single

treated GBM cells is in line with an enhanced invasive phenotype post-RT/TMZ treatment. However, the secreted levels of these inhibitors were observed to vary following LT treatment, indicating that there is a delicate balance of protease-inhibitor interactions which may differ between single and LT treatments. It is also important to note that membrane-bound inhibitors (such as TIMP-2 complexed with MT1-MMP) may not be present in conditioned media, and thus would not be detected via an antibody array.

Figure 3-13: Profiling of secreted protease inhibitors in untreated, single RT/TMZ treated and long-term RT/TMZ treated GBM cells

(**A.**) A graphical representation of the densitometric analysis performed with protease inhibitor array membranes using conditioned media from the following untreated, single RT/TMZ and LT treated GBM cell lines - (**i.**) U87MG, (**ii.**) LN229, (**iii.**) MU4 and (**iv.**) MU41. All data shown is represented as an average pixel density of duplicate antibody spots and normalized with the reference spots on each membrane. Densitometry was performed using ImageJ (1.53a). (**B.**) Venn diagrams represent the secreted inhibitors detected above threshold (>150-pixel intensity) in the conditioned media from untreated, single and long-term RT/TMZ treated cells. The inhibitors within each Venn diagram circle were above a normalised pixel intensity threshold set at 150. The inhibitors highlighted by a red box represent the 'common' inhibitors identified above threshold level across the three cell lines. As no inhibitors were commonly detected in the conditioned media from all three LT treated cells, a blue box represents secreted inhibitors that were common within the MU4 and MU41 cell lines.

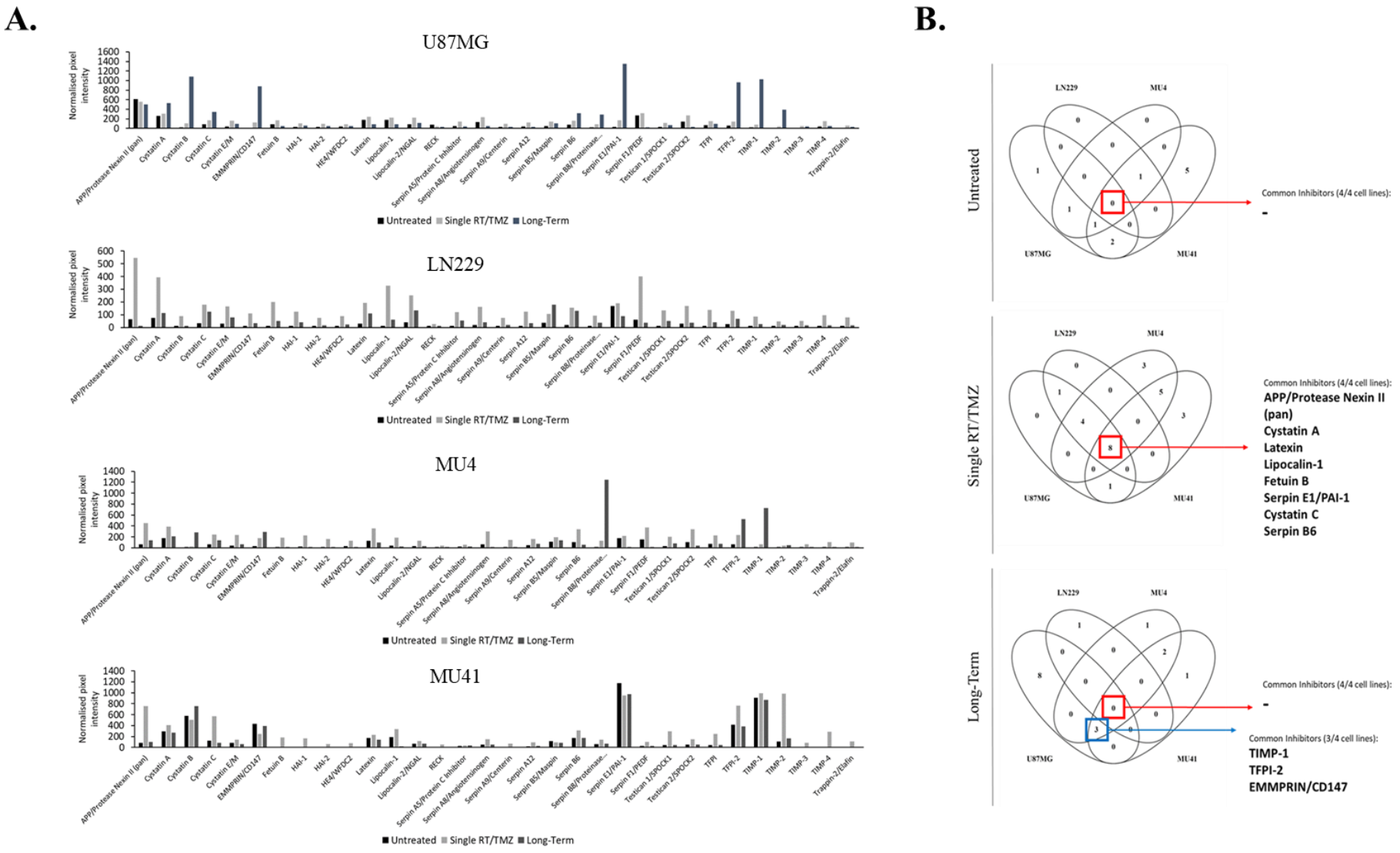
A.
U87MG
LN229
MU4
MU41
Normalised pixel intensity
APP/Protease Nexin II (pan)
Cystatin A
Cystatin B
Cystatin C
Cystatin E/M
EMMPRIN/CD147
Fetuin B
HAI-1
HAI-2
HE4/WFDC2
Latexin
Lipocalin-1
Lipocalin-2/NGAL
RECK
Serpin A5/Protein C Inhibitor
Serpin A8/Angiotensinogen
Serpin A9/Centerin
Serpin A12
Serpin B5/Maspin
Serpin B6
Serpin B8/Proteinase...
Serpin E1/PAI-1
Serpin F1/PEDF
Testican 1/SPOCK1
Testican 2/SPOCK2
TFPI
TFPI-2
TIMP-1
TIMP-2
TIMP-3
TIMP-4
Trappin-2/Elafin
Untreated
Single RT/TMZ
Long-Term
B.
Untreated
Single RT/TMZ
Long-Term
LN229
MU4
U87MG
MU41
Common Inhibitors (4/4 cell lines):
-
Common Inhibitors (4/4 cell lines):
APP/Protease Nexin II (pan)
Cystatin A
Latexin
Lipocalin-1
Fetuin B
Serpin E1/PAI-1
Cystatin C
Serpin B6
Common Inhibitors (4/4 cell lines):
-
Common Inhibitors (3/4 cell lines):
TIMP-1
TFPI-2
EMMPRIN/CD147

Table 3-3: Protease inhibitors with tumorigenic or pro-invasive functions

Protease Inhibitor	Inhibitory Target	Pro-invasive role/s	Studies in GBM
APP/Protease Nexin II (pan)	Serine proteases (including trypsin and coagulation factors)	Overexpression significantly increased the expression of MMP-9, MMP-2, MMP-3, N-cadherin and vimentin in breast cancer cells via regulation of the MAPK/ERK pathway [360]	APP mRNA and protein expression was reported to be elevated in GBM cells and tissue specimens compared to control neural cells and normal brain tissue [361]
EMMPRIN/CD147	ND	Upregulation induces MT1-MMP-expression and subsequent invadopodia activity in breast epithelial cells. Also promotes epidermal growth factor receptor (EGFR)-Ras-ERK signalling via interactions with CD44 [362, 363]	CD147 expression is elevated in GBM tissue, and increased CD147 expression is associated with poor overall survival in GBM patients [364]. Antisense RNA inhibition of CD147 expression reduces GBM cell invasion [365].
Fetuin B	Metallopeptidases of the astacin family	Enhances MMP-2 activation in monocytes and VSMCs [366]	NA
Lipocalin-1	Can bind various ligands, including hydrophobic ligands	Lipocalin-1 is overexpressed in breast cancer and associated with increasing tumour grade and poor survival in breast cancer patients [367]	NA
Serpin E1/PAI-1	Inhibits Kallikrein 5, uPa, activated protein C	PAI-1 promotes MMP-13 expression and secretion in osteosarcoma [368]. In GBM, has been implicated in the PI3K/AKT signaling pathway and enhanced VEGF expression [369, 370]	High PAI-1 expression correlates with poorer survival in GBM patients [371]
TIMP-1	MMP-7, MMP-9, MMP-1, MMP-3	TIMP-1 can promote invasion via induction of hepatocyte growth factor signaling or MET signaling, and is overexpressed along with MMP-2 in many cancers [372, 373]	Low TIMP-1 immunohistochemical expression correlates with longer overall survival in GBM patients [374]
TIMP-2	MMP-2	Cell surface bound TIMP-2 acts as a bridge between pro-MMP-2 and MT1-MMP and is required to for MMP-2 activation via this complex [375]	Increased levels of TIMP-2 can promote MMP-2 activation and invasion in GBM cell lines, however at concentrations in excess of 900 ng/ml, exogenous TIMP-2 was inhibitory to proMMP-2 activation [376]

Pubmed literature searches of the 21 protease inhibitors identified seven inhibitors have also been observed to demonstrate tumour promoting or pro-invasive functions. NA: not applicable- indicates no GBM-related studies were found.

A.

B.

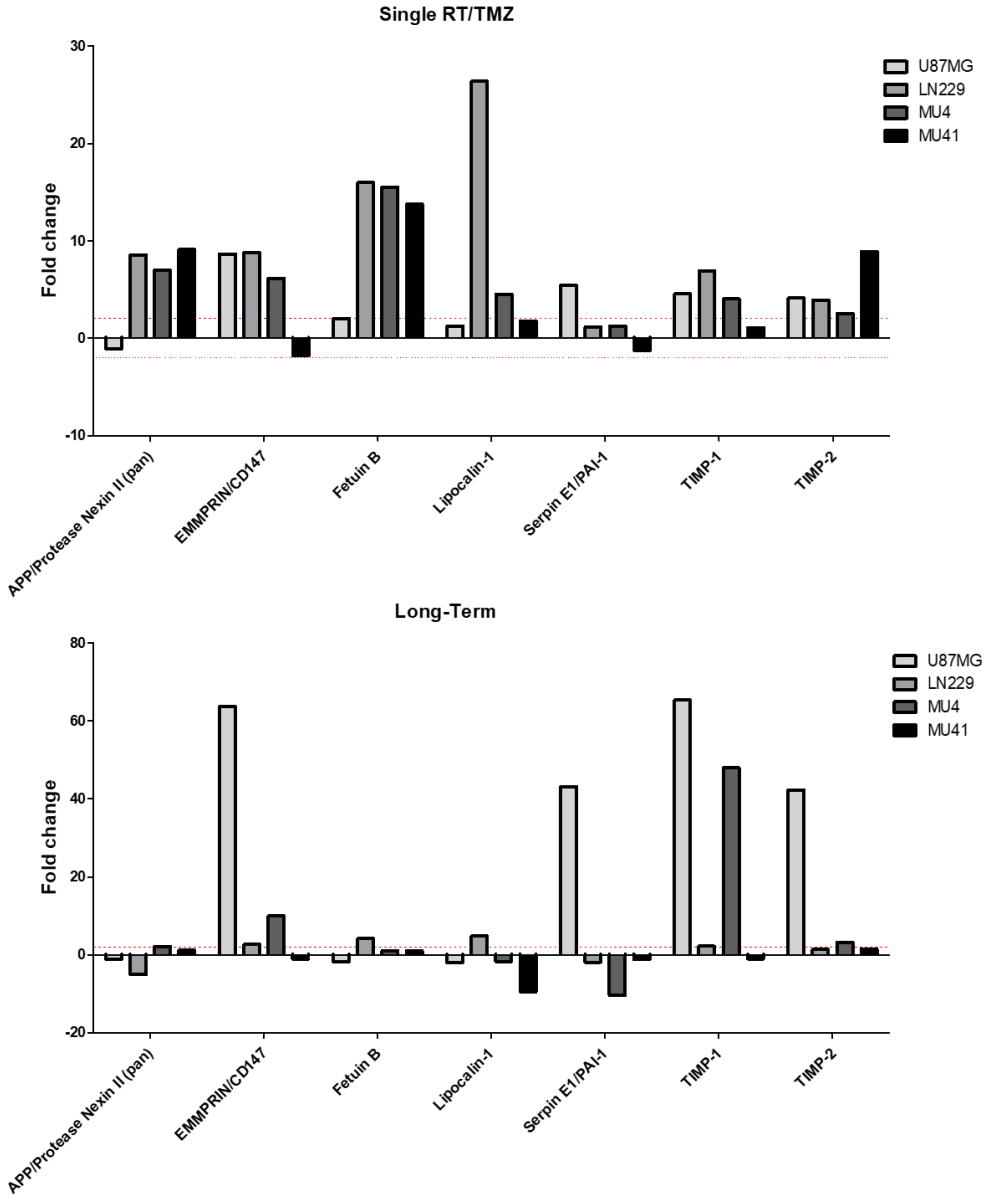

Figure 3-14: Single and long-term RT/TMZ treatment alters the secretion profile of protease inhibitors with pro-invasive functions

Seven secreted inhibitors were identified to potentially have pro-invasive roles as described in the published literature (***Table 3-5***). Secreted levels of these inhibitors were determined by densitometric analysis of antibody array spots and are displayed as fold change in (**A.**) single RT/TMZ treated cells and (**B.**) long-term treated cells, relative to untreated cells. Densitometry was performed via ImageJ (1.53a).

3.2.6 The Effect of RT/TMZ treatment on gene and miRNA expression in GBM cell lines

To identify potential molecular changes that may contribute to the enhanced invadopodia-mediated matrix degrading activity in GBM cells post-RT/TMZ treatment, Nanostring® technology was utilized to investigate changes in gene expression (nCounter Human Pan Cancer Progression Panel Array) in GBM cell lines (U87MG, LN229, MU4 and MU41) after a single RT/TMZ treatment, as well as changes in miRNA expression (nCounter Human V3 miRNA Array) after single and long-term RT/TMZ treatment.

3.2.6.1 GBM cell line gene expression analysis in response to RT/TMZ treatment

The nCounter Human Pan Cancer Progression Panel Array was used to examine the expression of 770 cancer-related genes. As shown in ***Figure 3-15A***, these genes can be divided into 4 main cancer progression groups (angiogenesis, ECM, EMT, metastasis), which can be further sub-divided into 10 categories based on a biological process (angiogenesis, cancer metabolism, ECM layers, ECM remodelling, EMT, hypoxia, metastasis, transcription factor, tumour growth, tumour invasion). A flow-chart highlighting the analysis of the gene panel is shown in ***Figure 3-15B***.

To examine changes in gene expression following RT/TMZ treatment, the log2-fold change (FC) difference in normalised gene expression was calculated for all 770 genes in each GBM cell line. Interestingly, whilst all GBM cell lines demonstrated upregulated gene expression related to each biological process following RT/TMZ treatment, the specific genes that were upregulated varied between the GBM cell lines (***Supplementary Figure 2A***). The top 100 most significantly changed genes identified following RT/TMZ treatment (above a threshold of 100 transcript counts) were also found to largely differ between each GBM cell line (***Supplementary Figure 2B***). Due to observing no clear clustering pattern of gene expression, genes showing a >1.5-fold increase in expression after RT/TMZ treatment were shortlisted and grouped according to the biological processes in which they were

involved in order to ascertain which biological processes were most upregulated following a single RT/TMZ treatment. The number of genes in each biological process with increased expression greater than 1.5-fold following RT/TMZ treatment was determined for each GBM cell line, and this was used to calculate the overall percentage of upregulated genes allocated to each biological process (***Figure 3-15C***). Despite the observation that different genes species are upregulated post-RT/TMZ treatment for each GBM cell line, the majority of these upregulated genes following treatment were present within the processes of ECM layers (22.54%), tumour invasion (15.03%) EMT (14.37%), tumour growth (14.70%) and angiogenesis (13.72%), indicating a pro-invasive phenotype that may potentially facilitate GBM cell invasion.

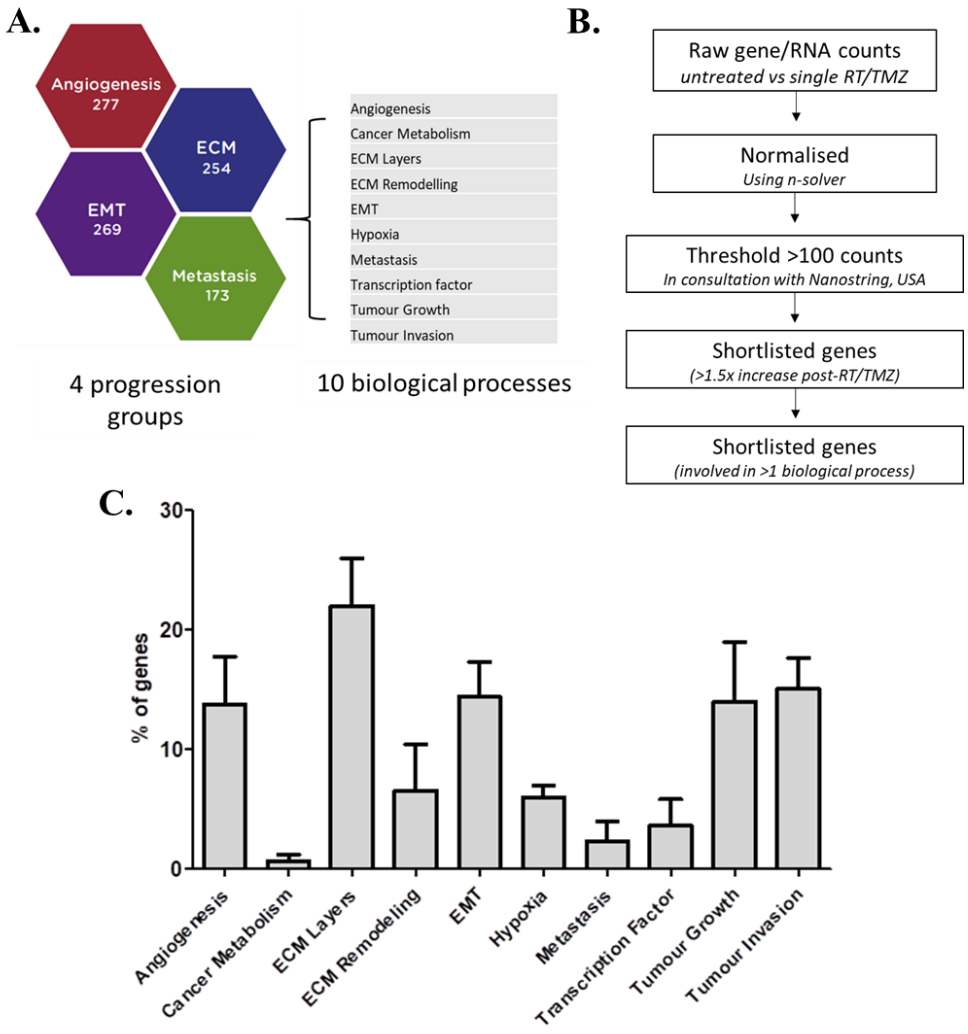

Figure 3-15: Invasion-related genes are upregulated following RT/TMZ treatment

(**A.**) The 770 cancer-related genes in the Nanostring® cancer gene panel can be classified into 10 biological processes (angiogenesis, cancer metabolism, ECM layers, ECM remodelling, EMT, hypoxia, metastasis, transcription factor, tumour growth, tumour invasion). (**B.**) A flow-chart representation of the analysis workflow. (**C.**) The percentage of genes showing a >1.5-fold increase in expression after RT/TMZ treatment within each biological process. Biological processes with the greatest percentage of upregulated genes included ECM layers (22.54%), tumour invasion (15.03%) and EMT (14.37%).

As these genes may possess a function contributing to more than one biological process, genes that were upregulated in at least one GBM cell line following treatment were further shortlisted based on the number of biological processes in which they have a functional role (***Table 3-4***). Twelve upregulated genes were identified to be involved in more than one biological process: VEGFB, ENPP2, COL7A1, GDF15 (2/5 biological processes); SRGN, SERPINE1, MFAP4, WNT5B, HMOX1 (3/5 biological processes); THBS1, VCAN, GPR56 (4/5 biological processes). The Oncomine database was used to assess the relative mRNA expression levels in GBM tissue corresponding to the twelve shortlisted genes (***Supplementary Table 2***). The mRNA expression levels in GBM tissue were compared to normal brain tissue in six independent studies. Three genes were observed to be significantly overexpressed in GBM tissue in all six independent studies: THBS1, VCAN and SERPINE1. mRNA expression levels of the three genes were within the top 25% of total detected genes in GBM tissue across all six studies (***Figure 3-16***).

To examine whether the overexpression of THBS1, VCAN and SERPINE1 was exclusive to GBM, the GlioVis database was used to assess mRNA expression levels across glioma grades (ranging from grade I to grade IV-GBM) in four independent datasets (***Figure 3-17***). SERPINE1 expression was significantly higher in GBM (grade IV) tissue compared to grade II and grade III glioma tissue in all four datasets (***Figure 3-17A***). THBS1 expression was also found to be significantly higher in GBM (grade IV) tissue compared to grade II and grade III glioma tissue in three datasets (***Figure 3-17C***), whilst VCAN expression was either lower or did not significantly differ in expression levels in GBM tissue compared to lower grades of glioma (***Figure 3-17B***). Therefore, these results suggest that SERPINE1 and THBS1 are overexpressed in GBM compared to lower grades of glioma, and therefore may play a significant role in GBM.

Table 3-4: Upregulated genes post RT/TMZ are associated with multiple biological processes

2/5 biological processes		3/5 biological processes		4/5 biological processes	
VEGFB	angiogenesis, tumour growth	**SRGN**	angiogenesis, ECM layers, EMT	**THBS1**	angiogenesis, ECM layers, tumour growth, tumour invasion
ENPP2	ECM layers, EMT	**SERPINE1**	angiogenesis, ECM layers, EMT	**VCAN**	ECM layers, EMT, tumour growth, tumour invasion
COL7A1	ECM layers, tumour invasion	**MFAP4**	ECM layers, EMT, tumour invasion	**GPR56**	angiogenesis, ECM layers, EMT, tumour invasion
GDF15	EMT, tumour growth	**WNT5B**	ECM layers, EMT, tumour growth		
		HMOX1	angiogenesis, tumour growth, tumour invasion		

Displayed are the 12 shortlisted upregulated genes classified according to the number of biological processes in which they have a functional role (2 out of 5, 3 out of 5, and 4 out of 5 biological processes).

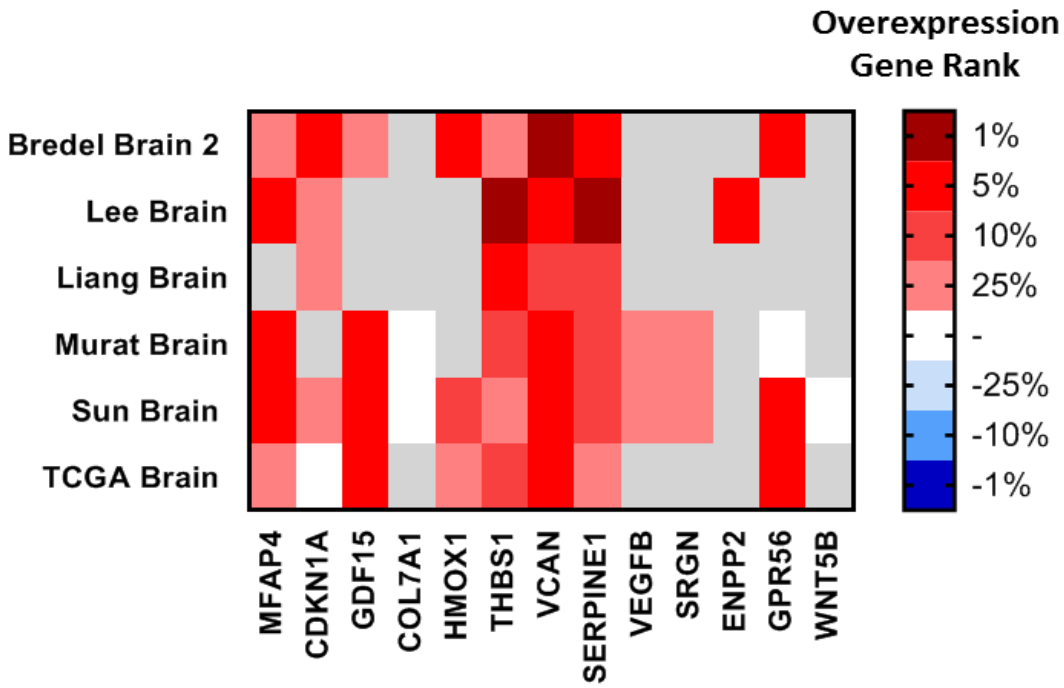

Figure 3-16: Comparison of mRNA levels of upregulated genes in GBM tissue

Comparison of shortlisted genes highlighting the overexpression gene rank in six separate studies (Bredel Brain 2, Lee Brain, Liang Brain, Murat Brain, Sun Brain, TCGA Brain). Genes in each study are listed from the most to the least enriched in GBM tissue compared to normal brain tissue, and the overexpression gene rank is calculated as a percentage. GBM datasets deposited within the Oncomine™ Platform (Thermo Fisher, Ann Arbor, MI) was used for the analysis. Oncomine comparisons listed below a p-value ≤ 0.05 were used in analyses. Grey boxes indicate excluded expression differences that were not significant ($p>0.05$). White boxes indicate that the gene was not measured.

Figure 3-17: SERPINE1, THBS1 and VCAN mRNA expression levels in glioma tissue

(**A.**) SERPINE1, (**B.**) VCAN and (**C.**) THBS1 mRNA levels were analysed across glioma grades in four independent glioma studies deposited within the GlioVis database: TCGA dataset [377], Gravendeel et al. [378], Rembrandt dataset [379] and Freije et al. [380]. The number of patient samples analysed within each tumour group in a dataset is as follows: TCGA: Grade II (n=226), Grade III (n=244), Grade IV (n=150); Gravendeel: Grade I (n=8), Grade II (n=24), Grade III (85), Grade IV (n=159); Rembrandt: Grade I (n=2), Grade II (n=98), Grade III (85), Grade IV (n=130); Freije: Grade III (n= 26), Grade IV (n=59). P values related to mRNA expression level comparisons between grade IV (GBM) and lower grades (I-III) are listed beneath each study (*unpaired two-tailed student's t-test with Bonferroni correction, ns= not significant*).

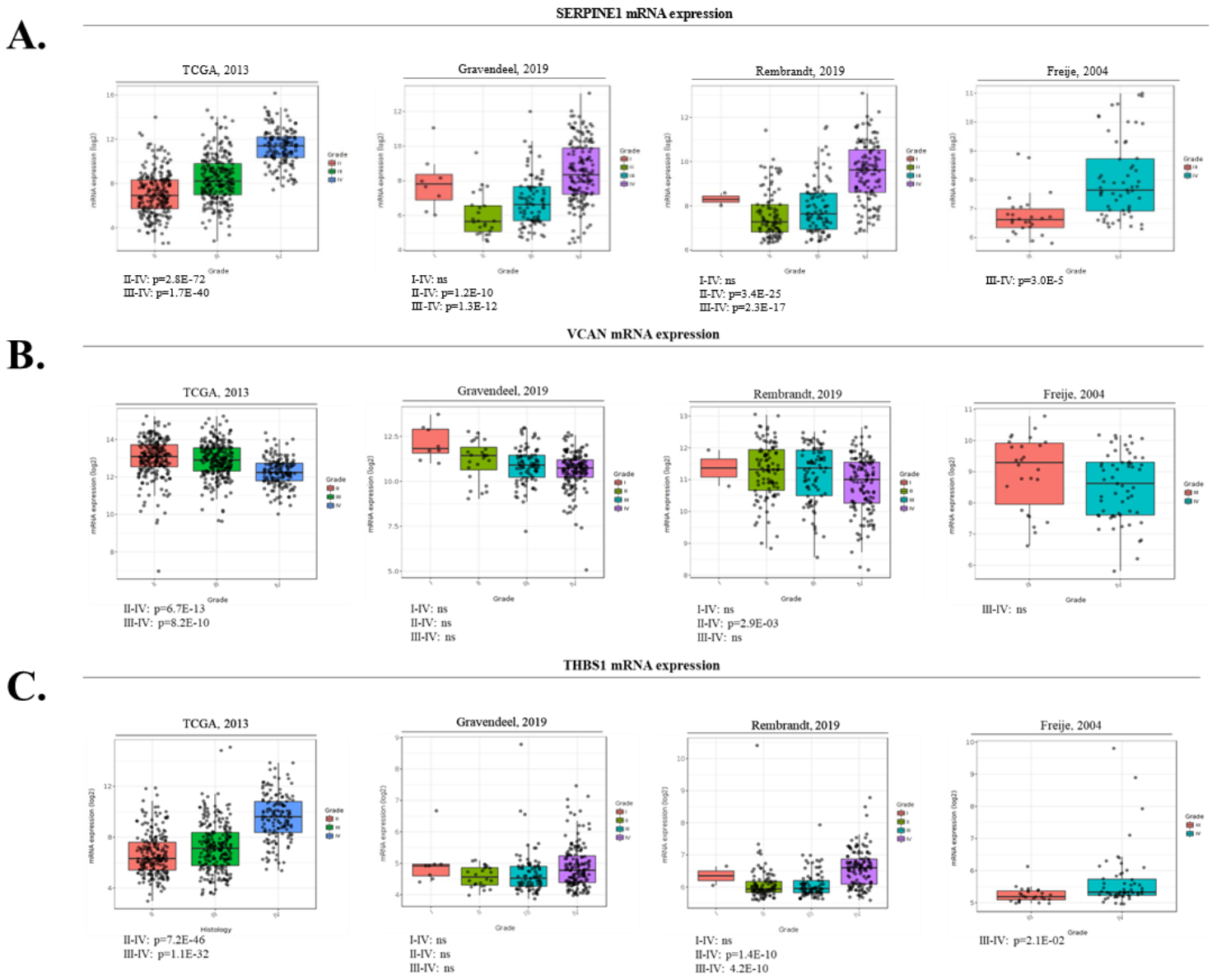
A.
SERPINE1 mRNA expression
TCGA, 2013
II-IV: p=2.8E-72
III-IV: p=1.7E-40
Gravendeel, 2019
I-IV: ns
II-IV: p=1.2E-10
III-IV: p=1.3E-12
Rembrandt, 2019
I-IV: ns
II-IV: p=3.4E-25
III-IV: p=2.3E-17
Freije, 2004
III-IV: p=3.0E-5
B.
VCAN mRNA expression
TCGA, 2013
II-IV: p=6.7E-13
III-IV: p=8.2E-10
Gravendeel, 2019
I-IV: ns
II-IV: ns
III-IV: ns
Rembrandt, 2019
I-IV: ns
II-IV: p=2.9E-03
III-IV: ns
Freije, 2004
III-IV: ns
C.
THBS1 mRNA expression
TCGA, 2013
II-IV: p=7.2E-46
III-IV: p=1.1E-32
Gravendeel, 2019
I-IV: ns
II-IV: ns
III-IV: ns
Rembrandt, 2019
I-IV: ns
II-IV: p=1.4E-10
III-IV: 4.2E-10
Freije, 2004
III-IV: p=2.1E-02

3.2.6.2 Investigating the role of THBS1 in GBM

THBS1 was identified as a potential candidate gene that was upregulated post-RT/TMZ treatment and is involved in four biological processes (angiogenesis, ECM layers, tumour growth and tumour invasion). The THBS1 gene encodes for the protein Thrombospondin-1 (TSP1), a multifunctional adhesive glycoprotein involved in cell-cell and cell-ECM interactions. THBS1 has been shown to mediate actin filament polymerisation [381], as well as promote invasion in breast cancer and oral squamous cell carcinoma [381, 382]. Therefore, the potential role of THBS1 as a driver of GBM invasion was next investigated.

The mesenchymal subtype of GBM is associated with enhanced tumour invasion, and consequently, the worst GBM patient prognoses [383]. Therefore, the mRNA expression levels of THBS1 in GBM from the mesenchymal, classical and proneural subtypes from datasets in the GlioVis database were compared. Examination of nine independent datasets in the GlioVis database revealed that THBS1 expression was significantly higher ($P<0.05$) in tissue from the mesenchymal subtype of GBM compared to the classical and proneural subtypes (***Figure 3-18A-I***). Invadopodia are known to associate with a mesenchymal phenotype in a number of cancers [384, 385]. To investigate whether THBS1 may interact with invadopodia-related proteins, the STRING database was utilised [386]. The protein interaction network shown by STRING analysis revealed several proteins with key regulatory roles in invadopodia formation and activity are associated with THBS1, including MMP-2, MMP-9, Src, Tks5 and the invadopodia-related integrins -α3 and -β1 (***Figure 3-18J***). Interestingly, MMP-2, MMP-9, integrin-α3 and integrin-β1 are directly co-expressed with THBS1 (designated by black lines), indicating that THBS1 may have a potential role in facilitating invadopodia activity. Multivariate survival analysis using GBM patient datasets within the SurvExpress database [387] revealed that high expression of THBS1 paired with these five invadopodia regulators (MMP-2, MMP-9, Src, Cortactin and Tks5) was significantly associated with poorer survival than high expression of invadopodia regulators alone (***Table 3-5*)**.

Figure 3-18: THBS1 is associated with a GBM mesenchymal subtype and invadopodia-related proteins

THBS1 mRNA levels were analysed in the classical (red), mesenchymal (green) and proneural (blue) GBM subtypes in nine independent studies deposited within the GlioVis database; (**A.**) TCGA dataset [377], (**B.**) Gravendeel et al. [378], (**C.**) Rembrandt dataset [379] (**D.**) Bao et. Al [388], (**E.**) Freije et al. [380], (**F.**) Joo et al. [389], (**G.**) Li et al. [390], (**H.**) Murat et al. [391], (**I.**) Nutt et al. [392]. The number of patient samples analysed within each tumour group in each dataset is as follows: TCGA: classical (n=199) mesenchymal (n=166), proneural (n=163); Gravendeel: classical (n=52) mesenchymal (n=54), proneural (n=53); Rembrandt: classical (n=79) mesenchymal (n=70), proneural (n=70); Bao: classical (n=24) mesenchymal (n=36), proneural (n=40); Freije: classical (n=18) mesenchymal (n=16), proneural (n=25); Joo: classical (n=20) mesenchymal (n=17), proneural (n=20); Li: classical (n=9) mesenchymal (n=7), proneural (n=7); Murat: classical (n=36) mesenchymal (n=23), proneural (n=21); Nutt: classical (n=10) mesenchymal (n=4) proneural (n=4). P values are listed beneath each study (*unpaired two-tailed student's t-test with Bonferroni correction*). (**J.**) Protein interaction network shown by STRING analysis reveals several invadopodia-related proteins (listed on the right) may associate with THBS1. The type of protein-protein interaction is indicated by line colour: black- co-expression; green- text mining evidence of interaction; pink- experimental evidence of interaction; blue- evidence of interaction in curated databases. (*PPI network enrichment p-value: 1.11e-16*)

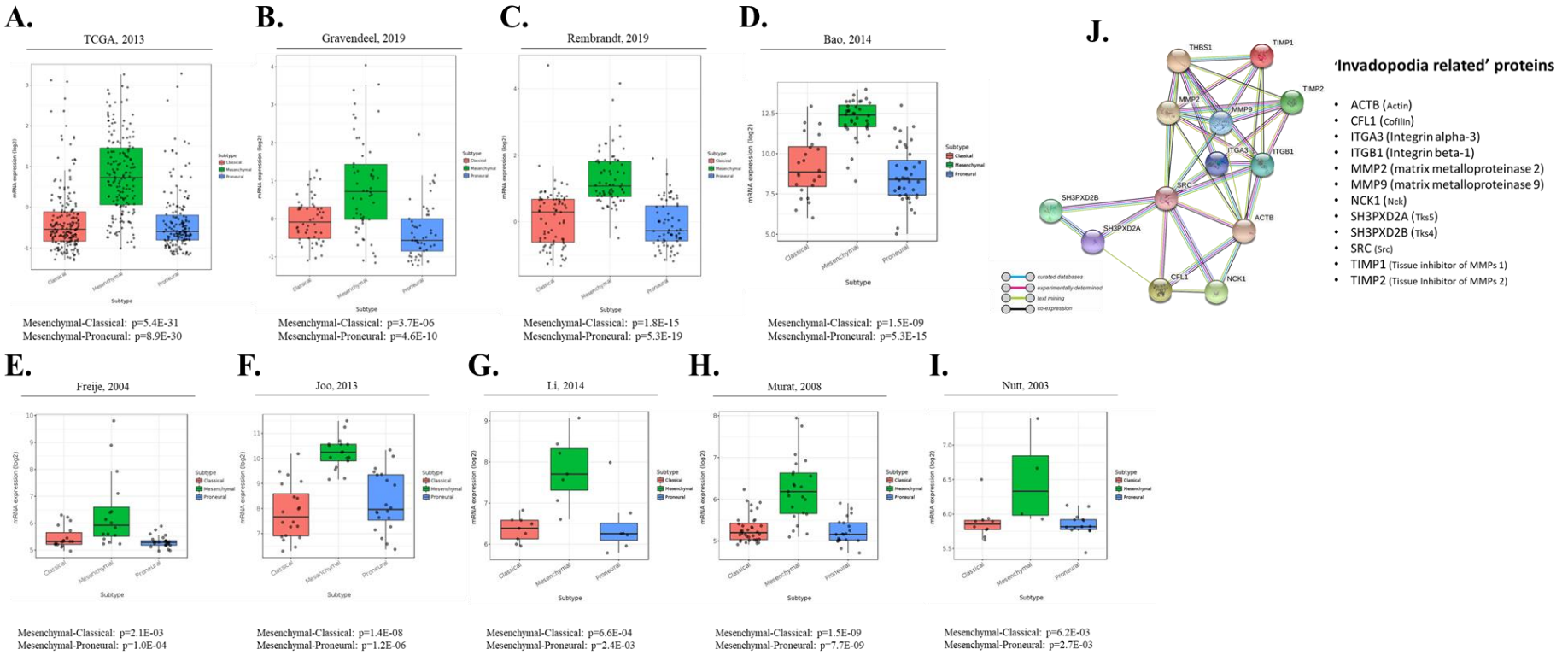
A.
TCGA, 2013
Mesenchymal-Classical: p=5.4E-31
Mesenchymal-Proneural: p=8.9E-30
B.
Gravendeel, 2019
Mesenchymal-Classical: p=3.7E-06
Mesenchymal-Proneural: p=4.6E-10
C.
Rembrandt, 2019
Mesenchymal-Classical: p=1.8E-15
Mesenchymal-Proneural: p=5.3E-19
D.
Bao, 2014
Mesenchymal-Classical: p=1.5E-09
Mesenchymal-Proneural: p=5.3E-15
J.
'Invadopodia related' proteins
ACTB (Actin)
CFL1 (Cofilin)
ITGA3 (Integrin alpha-3)
ITGB1 (Integrin beta-1)
MMP2 (matrix metalloproteinase 2)
MMP9 (matrix metalloproteinase 9)
NCK1 (Nck)
SH3PXD2A (Tks5)
SH3PXD2B (Tks4)
SRC (Src)
TIMP1 (Tissue inhibitor of MMPs 1)
TIMP2 (Tissue inhibitor of MMPs 2)
E.
Freije, 2004
Mesenchymal-Classical: p=2.1E-03
Mesenchymal-Proneural: p=1.0E-04
F.
Joo, 2013
Mesenchymal-Classical: p=1.4E-08
Mesenchymal-Proneural: p=1.2E-06
G.
Li, 2014
Mesenchymal-Classical: p=6.6E-04
Mesenchymal-Proneural: p=2.4E-03
H.
Murat, 2008
Mesenchymal-Classical: p=1.5E-09
Mesenchymal-Proneural: p=7.7E-09
I.
Nutt, 2003
Mesenchymal-Classical: p=6.2E-03
Mesenchymal-Proneural: p=2.7E-03

Table 3-5: Co-expression of THBS1 with invadopodia regulators correlates with poorer GBM patient survival

Gene/s	Study	Concordance Index (CI)	P-value	Sample size
CTTN	FREIJE	58.45	0.08533	85
THBS1/CTTN	FREIJE	59.45	0.009395	85
MMP9	FREIJE	59.38	0.002822	85
THBS1/MMP9	FREIJE	59.9	0.001454	85
TKS5	GRAVENDEED	55.43	0.055	270
THBS1/TKS5	GRAVENDEED	56.59	0.01836	270
CTTN	JOO KIM	58.33	0.3787	55
THBS1/CTTN	JOO KIM	58.93	0.04513	55
TKS5	JOO KIM	58.93	0.3717	55
THBS1/TKS5	JOO KIM	60.21	0.02179	55
SRC	LEE-2	62.36	0.04338	27
THBS1/SRC	LEE-2	64.37	0.02534	27
MMP2	NUTT	51.61	0.3603	50
THBS1/MMP2	NUTT	62.18	0.02531	50
MMP9	NUTT	55.44	0.3793	50
THBS1/MMP9	NUTT	62.8	0.04756	50
MMP2	TCGA-2016	54.78	0.03572	148
THBS1/MMP2	TCGA-2016	57.73	0.003203	148
TKS5	TCGA-2016	51.61	0.7874	148
THBS1/TKS5	TCGA-2016	54.65	0.04774	148
SRC	YAMANAKA	82.11	0.9985	29
THBS1/SRC	YAMANAKA	85.26	0.03641	29

Analysis of GBM gene expression datasets deposited within the SurvExpress database indicates that co-expression of THBS1 and invadopodia regulators (CTTN, MMP2, MMP9, SRC and TKS5) correlates with poorer patient outcome. Data presented is ordered by study and demonstrates that THBS1 co-expression with a single invadopodia regulator results in a more significant log-rank p-value and a poorer patient survival outcome. Only datasets with a significant P value (<0.05) were included in the analysis.

Collectively, the data linking THBS1 to invadopodia-related proteins, the mesenchymal subtype of GBM and poorer GBM patient survival suggests that this protein is associated with a pro-invasive phenotype in GBM. Considering this, THBS1 may therefore have a role in promoting invadopodia-activity in GBM cells. Immunostaining of LN229 cells seeded onto FITC-gelatin probed with a THBS1 antibody revealed that endogenous THBS1 was expressed near F-actin puncta, and furthermore, that THBS1 was also present within the punctate extending through the FITC-gelatin matrix, as seen in the representative Z-section image, indicating that THBS1 localises to invadopodia (***Figure 3-19A***). Moreover, THBS1 expression was less prominent in punctate surrounded by larger areas of degraded FITC-gelatin, indicating that THBS1 may be recruited to invadopodia prior maturation and the secretion of proteases. Supporting this, THBS1 expression appeared to be highly concentrated in regions of small actin puncta with no clear FITC-gelatin degradation, whereas THBS1 expression was less prominent and more dispersed near larger puncta with greater levels of FITC-gelatin degradation (***Figure 3-19B***). As invadopodia are known to develop into larger protrusions over time [393], this indicates that THBS1 may be associated with the early stages of the invadopodia lifecycle prior to proteolytic degradation of the surrounding ECM.

Examination of THBS1 protein expression in all four GBM cell lines revealed the highest expression levels in LN229 cells whilst MU4 cells exhibited the lowest expression levels (***Figure 3-20A***). As the LN229 and MU4 cell lines display the highest and lowest levels of invadopodia activity, respectively (***Figure 3-2***), this indicates that THBS1 protein expression levels may correlate with invadopodia activity. Therefore, to test the hypothesis that THBS1 may facilitate invadopodia activity in GBM cell lines, the impact of THBS1 overexpression or knockdown on MMP-2 secretion and migration rate was next assessed. GBM cell lines were transfected with THBS1 plasmid (Sino Biological), and western blot analysis was performed to validate successful transfection of the plasmid. Zymographic analyses of serum-free OptiMEM® conditioned culture media revealed a significant increase in pro-MMP-2 secretion in GBM cells overexpressing THBS1 (***Figure 3-20B***). The functional effect of siRNA-mediated knockdown of THBS1 was also investigated using the LN229 cell line, as these cells exhibit high expression of THBS1. Validation of THBS1 knockdown was performed using western blot

analysis, and zymographic analysis of serum-free OptiMEM® culture media revealed a significant decrease in MMP-2 secretion and activation following knockdown of THBS1 in LN229 cells (***Figure 3-20C***). Next, the effect of THBS1 overexpression or knockdown on GBM cell migration was assessed using the LN229 ***(Figure 3-21A***) and MU4 (***Figure 3-21B***) cell lines that form uniform, confluent monolayers suitable for the scratch wound assay. Knockdown or overexpression of THBS1 was confirmed via western blot analysis, however as basal THBS1 protein expression levels are low in the MU4 cell line, no difference in THBS1 expression could be detected in the MU4 cells transfected with siRNA against THBS1. Future experiments using qPCR (quantitative PCR) to verify the low level of THBS1 protein detected in the siRNA-mediated THBS1 knockdown of the LN229 GBM cell should therefore also be performed. Nevertheless, the migration rate of both the LN229 and MU4 cell lines was significantly reduced at 6 and 24 hours in both cell lines transfected with siRNA against THBS1 relative to the controls. Similarly, the overexpression of THBS1 resulted in a significant increase in migration rate at 6 and 24 hours for the MU4 cell line, whilst the LN229 cell line demonstrated a significant increase in migration rate at 24 hours compared to the controls. These findings indicate that THBS1 protein expression levels in GBM cells correlates with MMP-2 secretion and migration rate, and therefore suggests that THBS1 may facilitate GBM invasion, potentially mediated through invadopodia activity.

Figure 3-19: THBS1 localizes to invadopodia in the LN229 cell line

LN229 cells were seeded on coverslips coated with a thin film of cross-linked FITC-labelled gelatin. After 24h, the cells were fixed and stained for actin with rhodamine-phalloidin (red) and THBS1 (1:50) and an Alexa 405 secondary antibody (1:500) (pink). (**A.**) (***i.***) A representative confocal image demonstrating the presence of endogenous THBS1 (pink) near regions of actin puncta in a LN229 GBM cell. Scale bars = 10μm. (***ii.***) Z- section images were constructed of the LN229 GBM cell for the region represented by a line through the boxed region of the image. The resulting Z sections show overlapping expression of THBS1 and actin in the same region within the FITC-gelatin, as outlined by the yellow and blue boxes. Puncta with minimal THBS1 expression can also be seen to the left of these boxed regions which are surrounded by large areas of degraded FITC-gelatin. (**B.**) (***i.***) A representative confocal image demonstrating the presence of endogenous THBS1 (pink) near regions of actin puncta in LN229 GBM cells. (***ii.***) The LN229 cell on the left (labelled box 1) displays low expression of THBS1, larger invadopodial actin puncta and enhanced FITC-gelatin degradation compared to the LN229 cell on the right (labelled box 2), displaying smaller actin puncta and high THBS1 expression that is highly concentrated in a single region. Scale bars = 10μm.

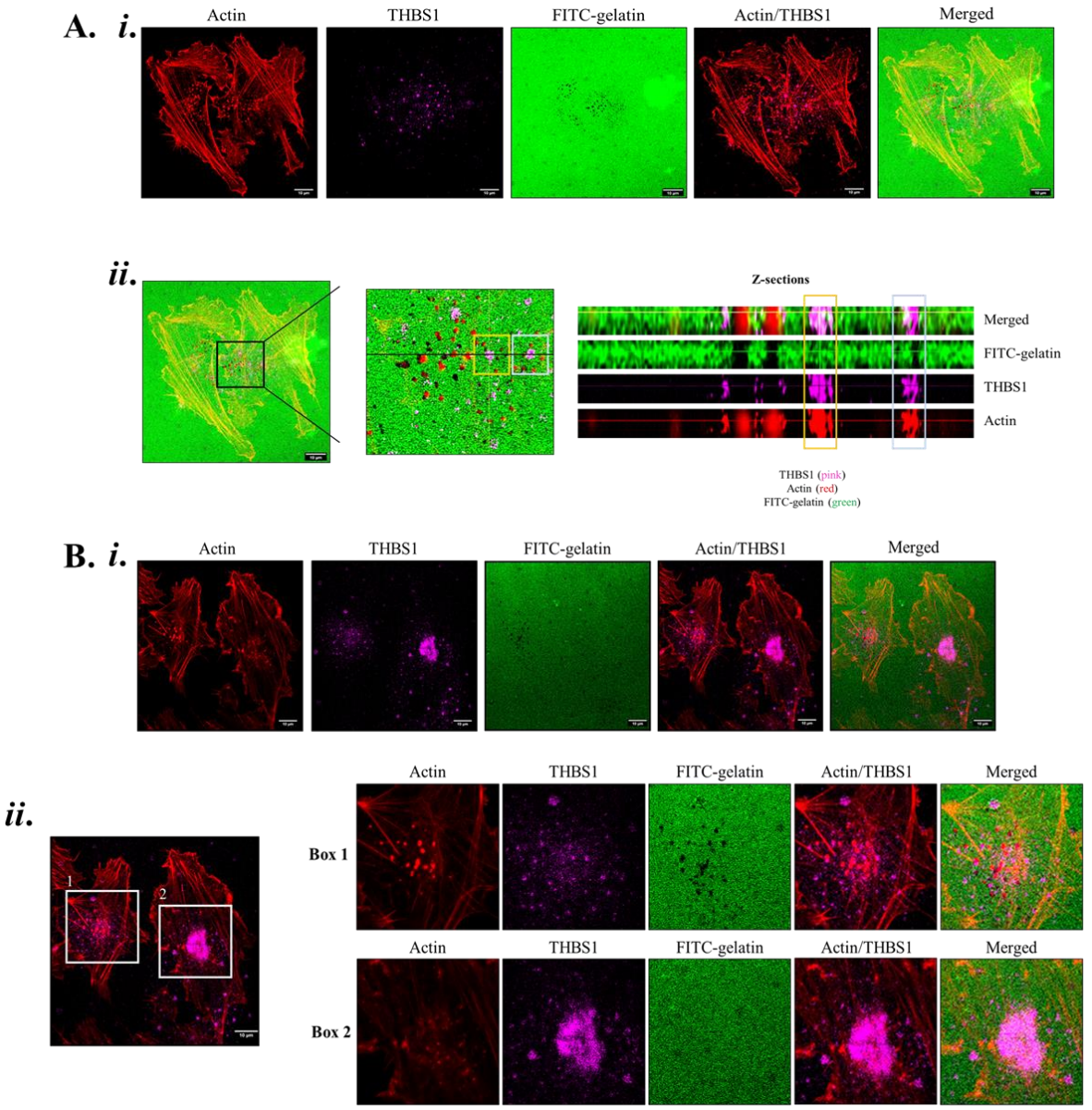
A. i.
Actin
THBS1
FITC-gelatin
Actin/THBS1
Merged
ii.
Z-sections
Merged
FITC-gelatin
THBS1
Actin
THBS1 (pink)
Actin (red)
FITC-gelatin (green)
B. i.
Actin
THBS1
FITC-gelatin
Actin/THBS1
Merged
ii.
1
2
Box 1
Box 2
Actin
THBS1
FITC-gelatin
Actin/THBS1
Merged

Figure 3-20: Increased THBS1 protein expression correlates with enhanced MMP-2 secretion in GBM cell lines

(**A.**) (***i.***) THBS1 basal protein expression levels in the GBM cell lines (U87MG, LN229, MU4 and MU41). (***ii.***) GBM cell lines were transfected with 2.5μg of human THBS1 plasmid (Sino Biological) with Lipofectamine™ 3000 Reagent (Invitrogen) using the manufacturer's protocol. A physical map of the plasmid from the manufacturer is shown. (**B.**) (***i.***) Western blots were performed to confirm increased THBS1 expression levels in the transfected (+) GBM cells. *Image representative of 3 independent experiments*. (***ii.***) Gelatin-based zymographic analysis following a 24h incubation period of the GBM cells (72h post transfection) in the serum-free OptiMEM® medium. (***iii.***) Densitometric analysis of pro- and active- MMP-2 bands is shown and represented as fold change relative to control cells. Sample loading volumes were standardised using the protein concentration from the corresponding cell lysates. *(n=3 experiments; mean ± SD, *p<0.05; **p<0.01; ***p<0.001; non-significant =ns, unpaired two-tailed student's t-test).* (**C.**) (***i.***) LN229 GBM cells (CTL) transfected with 50nM of non-specific/control siRNA (siRNA-MOCK) or transfected with 50nM of siRNA targeting THBS1 (siRNA-THBS1). Western blots were performed to confirm reduced THBS1 expression levels in siRNA-THBS1 transfected GBM cells prior to analysis of the conditioned medium for zymographic analysis. *Image representative of 3 independent experiments*. (***ii.***) Gelatin-based zymographic demonstrating a reduction in MMP-2 secretion in LN229 cells transfected with siRNA-THBS1. (***iii.***) Densitometric analysis of pro- and active- MMP-2 bands is shown and represented as fold change relative to control cells. Sample loading volumes were standardised using the protein concentration from the corresponding cell lysates. *(n=3 experiments; mean ± SD, ***p<0.001; non-significant =ns, 2-way ANOVA with Bonferroni correction).*

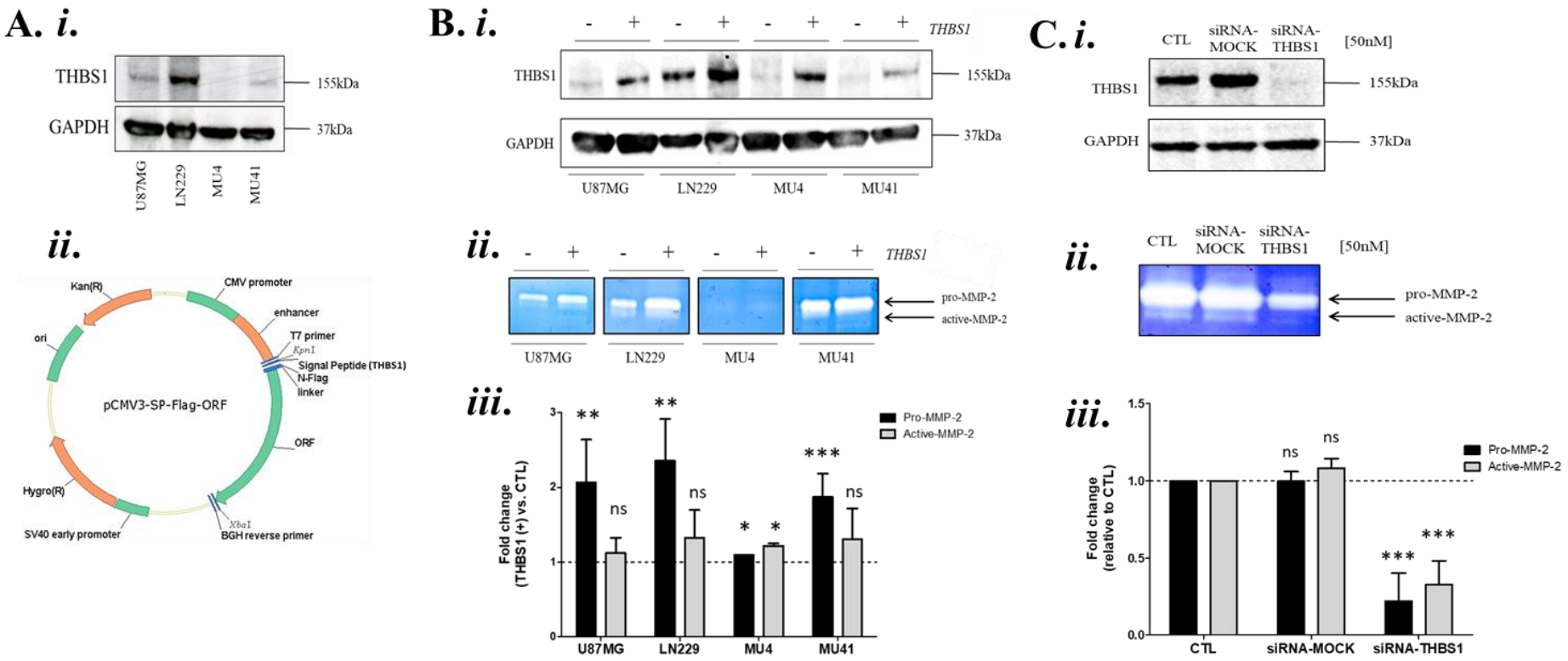
A. i.
THBS1
GAPDH
155kDa
37kDa
U87MG
LN229
MU4
MU41
ii.
Kan(R)
CMV promoter
enhancer
ori
T7 primer
KpnI
Signal Peptide (THBS1)
N-Flag
linker
pCMV3-SP-Flag-ORF
ORF
Hygro(R)
XbaI
SV40 early promoter
BGH reverse primer
B. i.
THBS1
- + - + - + - +
THBS1
GAPDH
155kDa
37kDa
U87MG
LN229
MU4
MU41
ii.
- + - + - + - +
THBS1
pro-MMP-2
active-MMP-2
U87MG
LN229
MU4
MU41
iii.
Pro-MMP-2
Active-MMP-2
Fold change (THBS1 (+) vs. CTL)
**
ns
**
ns
*
*
***
ns
U87MG
LN229
MU4
MU41
C. i.
CTL
siRNA-MOCK
siRNA-THBS1
[50nM]
THBS1
GAPDH
155kDa
37kDa
ii.
CTL
siRNA-MOCK
siRNA-THBS1
[50nM]
pro-MMP-2
active-MMP-2
iii.
Pro-MMP-2
Active-MMP-2
Fold change (relative to CTL)
ns
ns
***
***
CTL
siRNA-MOCK
siRNA-THBS1

Figure 3-21: THBS1 protein expression correlates with migration rate in GBM cell lines

The (**A.**) LN229 and (**B.**) MU4 GBM cell lines were either left untreated (CTL), transfected with 2.5µg of human THBS1 plasmid (THBS1-OE), transfected with 50nM of non-specific/control siRNA (siRNA-MOCK), or transfected with 50nM of siRNA targeting THBS1 (siRNA-THBS1). Western blots were performed to confirm increased or reduced expression levels of THBS1 in transfected cell lysates. At 72h post-transfection, GBM cell migration was examined at 0h, 6h, and 24h, via the introduction of a scratch (wound) (GBM cells were pre-treated with 5 µg/ml Mitomycin C, 2h prior to the wound to arrest cell proliferation). Results represent the percentage of wound remaining open relative to t = 0h. *(n=3 experiments each performed in triplicates; mean ± SD, *p<0.05; ***p<0.001; non-significant =ns, 2-way ANOVA with Bonferroni correction) (Scale bar is equivalent to 100µm).*

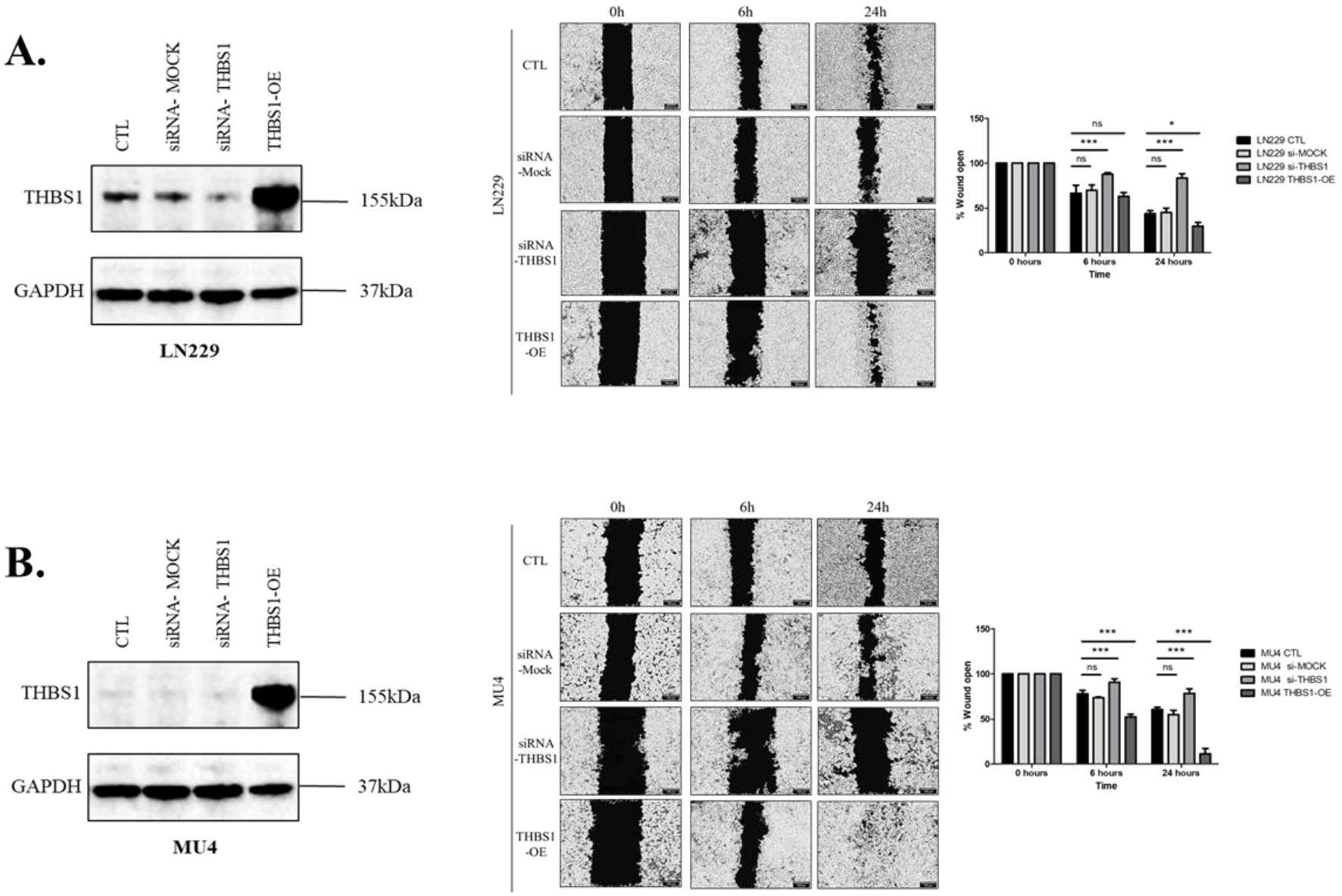
A.
CTL
siRNA- MOCK
siRNA- THBS1
THBS1-OE
THBS1
155kDa
GAPDH
37kDa
LN229
0h
6h
24h
CTL
siRNA -Mock
siRNA -THBS1
THBS1 -OE
LN229
% Wound open
0 hours
6 hours
24 hours
Time
ns
***
*
LN229 CTL
LN229 si-MOCK
LN229 si-THBS1
LN229 THBS1-OE
B.
CTL
siRNA- MOCK
siRNA- THBS1
THBS1-OE
THBS1
155kDa
GAPDH
37kDa
MU4
0h
6h
24h
CTL
siRNA -Mock
siRNA -THBS1
THBS1 -OE
MU4
% Wound open
0 hours
6 hours
24 hours
Time
MU4 CTL
MU4 si-MOCK
MU4 si-THBS1
MU4 THBS1-OE

3.2.6.3 GBM Cell line miRNA expression analysis in response to RT/TMZ treatment

To identify potential miRNAs that may be involved in altered invadopodia activity post-RT/TMZ treatment, the nCounter Human V3 miRNA Array was used to assess the expression levels of 798 miRNAs in GBM cell lines after single and long-term (LT) RT/TMZ treatment. miRNAs below a threshold of 100 transcript counts in all three GBM cell lines were removed from the analysis, and the log2-FC difference in normalised expression of the remaining miRNAs in GBM cell lines following single (***Figure 3-22A***) and LT RT/TMZ (***Figure 3-22B***) treatment were plotted as heatmaps. This revealed that the differential expression of these miRNAs post-single or LT RT/TMZ treatment varied between the GBM cell lines. However, as this analysis only considers fold change, many of these miRNAs were below the detection threshold in one or more GBM cell lines. Therefore, to determine which miRNAs may be relevant to all four GBM cells, common miRNAs above the detection threshold (set to 100 detected transcripts) for the four GBM cell lines were listed for single- (***Figure 3-22C***) and LT (***Figure 3-22D***) treated cells. Four miRNAs were commonly expressed in all GBM cell lines following both single and LT treatment: hsa-let-7a-5p, hsa-let-7b-5p, hsa-let-125b-5p, hsa-miR-4454+hsa-miR-7975 (***Figure 3-22E***).

Basal expression levels of these four miRNAs were highest in MU4 cells (low invadopodia activity) and lowest in LN229 cells (high invadopodia activity) (***Figure 3-22F***). Expression of these miRNAs was found to be lower in RT/TMZ treated U87MG, MU4 and MU41 cells relative to untreated cells, however LN229 cells demonstrated an increase in expression post-RT/TMZ treatment (***Figure 3-22G***). Furthermore, a greater decrease in the expression of these miRNAs was observed following LT treatment in all four GBM cell lines, with the exception of hsa-let-7a-5p in U87MG and LN229 LT treated cells that expressed 1.66- and 7.59- fold higher than untreated cells, respectively (***Figure 3-22H***).

Potential invasion and invadopodia-related targets of hsa-let-7a-5p, hsa-let-7b-5p, hsa-let-125b-5p, hsa-miR-4454+hsa-miR-7975 were explored using the online miRNA databases *MirTarBase* (for experimentally validated targets) and *miRDB* (for predicted targets based on sequencing). As shown in

Table 3-6, several invadopodia-related targets were identified for three of the miRNAs. Additionally, THBS1 was observed to be a predicted target for hsa-let-7b-5p and hsa-let-7a-5p, although this was below the target score threshold of 95.

Figure 3-22: Differential expression of common miRNAs following single RT/TMZ and LT treatment

Differential expression heatmaps for miRNAs, following (**A.**) single RT/TMZ treatment and (**B.**) LT RT/TMZ treatment. miRNA expression was first normalised, and the miRNAs below a minimum threshold of 100 transcript counts in all four GBM cell lines were removed from the analysis. The log2-FC differences in expression following single or LT RT/TMZ treatment were then calculated for these miRNAs, transformed to normalised Z-scores and unsupervised hierarchical clustering of miRNA expression fold changes was then performed using the Perseus Bioinformatics platform (version 1.5.5.0) [339]. Normalised Z-scores are indicated by colour, whereby red indicates upregulated gene expression and green indicates downregulated miRNA expression in RT/TMZ treated GBM cells relative to the corresponding untreated cells. miRNAs detected above a threshold of 100 transcript counts were then listed for each cell line following (**C.**) single RT/TMZ treatment and (**D.**) long-term (LT) treatment. The number of miRNAs detected above threshold in each GBM cell line is shown in the circles above the Venn diagram, and these were compared to determine the miRNAs that were commonly expressed in all four GBM cell lines. (**E.**) The detected miRNAs were then compared between treatment groups (single versus long term), resulting in a list of 4 commonly expressed miRNAs following single treatment and LT treatment of the four GBM cell lines. (**F.**) Basal expression levels of the four shortlisted miRNAs (hsa-let-7a-5p, hsa-let-7b-5p, hsa-let-125b-5p, and hsa-miR-4454+hsa-miR-7975) are shown for each GBM cell line. Expression levels are shown as normalised transcript counts for each miRNA. Differential expression of shortlisted miRNAs in GBM cell lines following (**G.**) single RT/TMZ treatment and (**H.**) LT treatment is represented as log2-fold change relative to untreated cells.

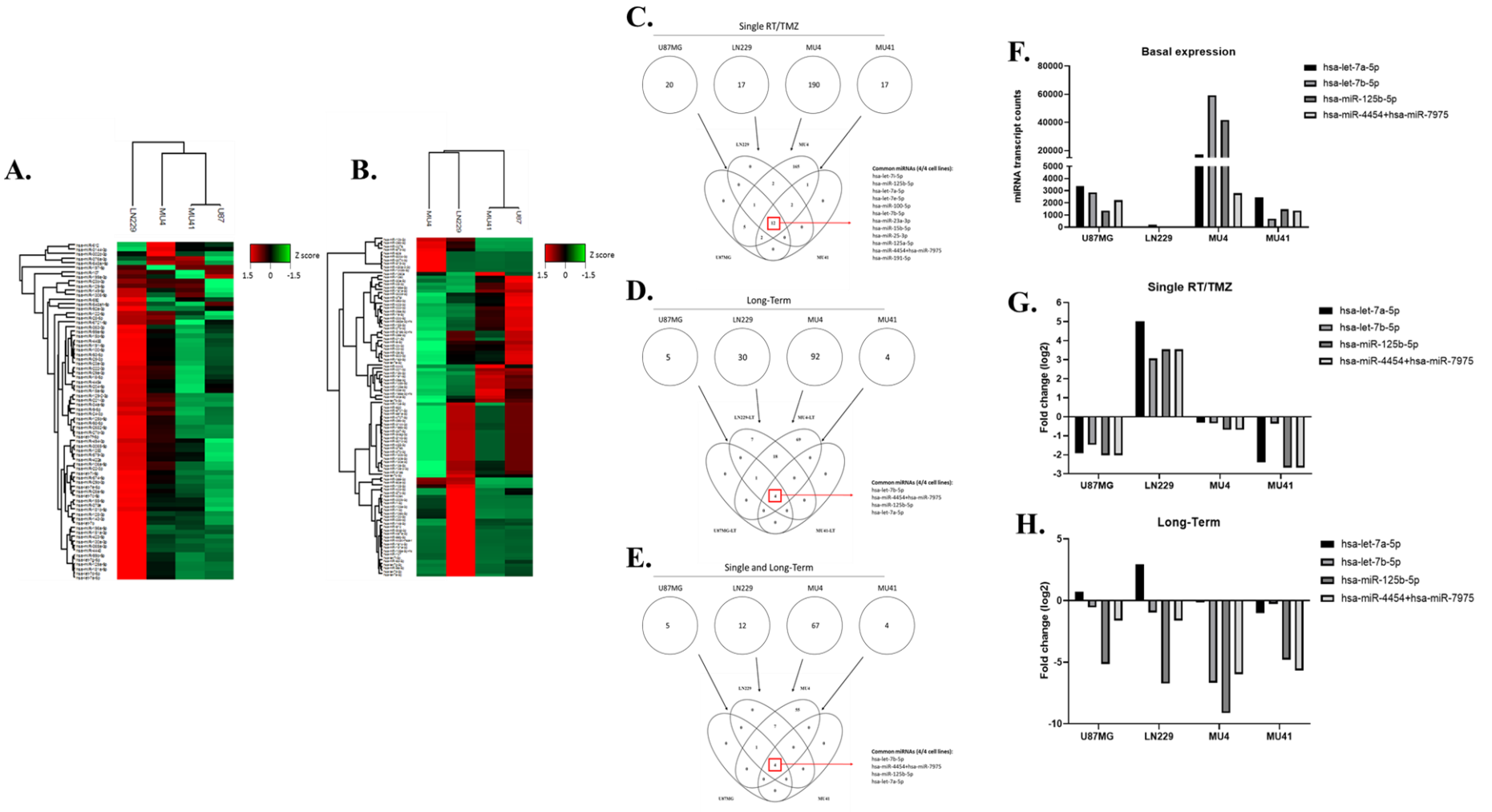
A.
LN229
MU4
MU41
U87
Z score
1.5
0
-1.5
B.
MU4
LN229
MU41
U87
Z score
1.5
0
-1.5
C.
Single RT/TMZ
U87MG
LN229
MU4
MU41
20
17
190
17
Common miRNAs (4/4 cell lines):
hsa-let-7i-5p
hsa-miR-125b-5p
hsa-let-7a-5p
hsa-let-7e-5p
hsa-miR-100-5p
hsa-let-7b-5p
hsa-miR-23a-3p
hsa-miR-150-5p
hsa-miR-25-3p
hsa-miR-125a-5p
hsa-miR-4454+hsa-miR-7975
hsa-miR-191-5p
D.
Long-Term
U87MG
LN229
MU4
MU41
5
30
92
4
Common miRNAs (4/4 cell lines):
hsa-let-7b-5p
hsa-miR-4454+hsa-miR-7975
hsa-miR-125b-5p
hsa-let-7a-5p
E.
Single and Long-Term
U87MG
LN229
MU4
MU41
5
12
67
4
Common miRNAs (4/4 cell lines):
hsa-let-7b-5p
hsa-miR-4454+hsa-miR-7975
hsa-miR-125b-5p
hsa-let-7a-5p
F.
Basal expression
miRNA transcript counts
80000
60000
40000
20000
5000
4000
3000
2000
1000
0
U87MG
LN229
MU4
MU41
hsa-let-7a-5p
hsa-let-7b-5p
hsa-miR-125b-5p
hsa-miR-4454+hsa-miR-7975
G.
Single RT/TMZ
Fold change (log2)
6
5
4
3
2
1
0
-1
-2
-3
U87MG
LN229
MU4
MU41
hsa-let-7a-5p
hsa-let-7b-5p
hsa-miR-125b-5p
hsa-miR-4454+hsa-miR-7975
H.
Long-Term
Fold change (log2)
5
0
-5
-10
U87MG
LN229
MU4
MU41
hsa-let-7a-5p
hsa-let-7b-5p
hsa-miR-125b-5p
hsa-miR-4454+hsa-miR-7975

Table 3-6: Potential invasion-related targets of shortlisted miRNAs

	Validated		Predicted
	Strongly Validated	**Weakly Validated**	**Predicted >95 target score**
hsa-let-7a-5p	**EGFR**, **ITGB3**, **KRAS**, LIN28A/B, MYC, **PAK1**, RAB40C, THBS1, TGFBR3	**ACTB**, COL8A1, FIGN, **WASL**	COL3A1, FIGN, FIGNL2, TGFBR1 *THBS1**
hsa-let-7b-5p	AKT2, LIN28B, TGFBR1	**ACTB**, DOCK5**, ITGA3, ITGB5, KRAS**, **PAK1**, **RHOB, RHOG**, RAB38, **SH3PXD2A**, TGFBR3, THBS1, VAMP3, **WASF1**, **WASL**	COL3A1, FIGN, FIGNL2, TGFBR1/3 *THBS1**
hsa-miR-4454+hsa-miR-7975	-	-	-
hsa-miR-125b-5p	**CD44, EGFR, MMP-2**, **MMP-13**, MMP-26, LIN28A/B, **TP53**	**ITGB3**, RAB4A	RAB3D, LIN28A

Experimentally validated (as listed on the MirTarBase database) and predicted (based on sequence information as listed on the miRDB database) invasion-related targets of the four shortlisted miRNAs expressed in the GBM cell lines. Targets linked to invadopodia activity are highlighted in bold. *Strongly validated methods include reporter assays, western blot and qPCR. Weakly validated methods include microarray, NGS, and pSILAC. All predicted targets are listed above a target score of 95, indicating that predicted targets are highly likely to bind to the listed miRNA. THBS1* (marked by an asterisk) was also a predicted target for hsa-let-7a-5p and hsa-let-7b-5p, although with a lower predicted target score of 71 and 64, respectively.*

As LN229 cells demonstrate a loss of MMP-2 secretion and invadopodia-mediated FITC-gelatin degradation following LT treatment, the miRNA expression data was next used to investigate whether altered miRNA expression levels may be associated with reduced invadopodia activity in LT-treated LN229 cells. 18 miRNAs with enhanced expression were identified in LT-treated LN229 cells that were below the threshold level of 100 transcript counts in untreated/parental LN229 cells (***Figure 3-23A***). 9 out of the 18 miRNAs detected in LT-treated LN229, but not untreated/parental, cells were also not detected above threshold level in the LT-treated U87MG, MU4 and MU41 cell lines (***Figure 3-23B***). Examination of validated and predicted targets of these 9 miRNAs identified numerous pro-invasive targets, including key invadopodia regulators involved in actin regulation such as WASL (N-WASP), Rac1, Grb2, ENAH (Mena), Cortactin, Tks5 and Paxillin (***Table 3-7***).

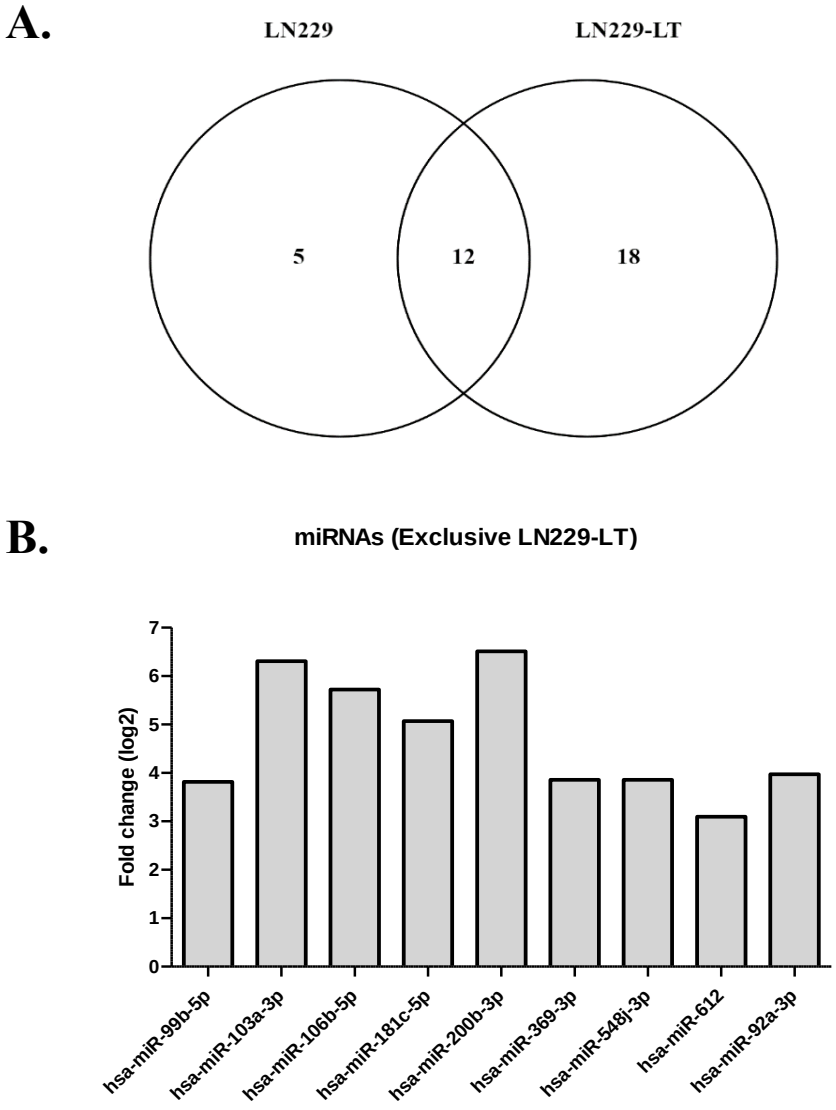

Figure 3-23: miRNAs displaying enhanced expression in LN229 LT treated cells

(**A.**) miRNAs above a detection threshold of 100 transcript counts were compared for untreated/parental and LT treated LN229 cells. 12 miRNAs were detected in both untreated and LT treated LN229 cells, 5 miRNAs in untreated alone, and 18 miRNAs in LT treated alone. (**B.**) 9 out of the 18 miRNAs detected in LT treated LN229, but not untreated, cells were not detected above threshold level in LT treated U87MG, MU4 and MU41 cell lines, and were therefore exclusively detected in LT treated LN229 cells. The log2-transformed fold change of these 9 miRNAs in LN229 cells after LT treatment is shown.

Table 3-7: Potential invasion-related targets of miRNAs with enhanced expression in LN229 LT treated cells

	Validated		Predicted
	Strongly Validated	**Weakly Validated**	**Predicted >95 target score**
hsa-miR-99b-5p	**MTOR**, IGF1R	–	–
hsa-miR-200b-3p	ADAM12, MYB, RAB21, RAB3B, RAB18, RAB23, **RHOA**, **ROCK2**, **VEGFA**, **WASF3**, **WNT1**	**ABI2**, **KRAS**, **PAK2**	ADAMTS3, RAB21, **RECK**, **VEGFA**
hsa-miR-103a-3p	**ADAM10, CAV1**, MYB, TIMP3	**ABL2**, **ACTR2**, BCL2, **CLIP1**, DOCK11, **ITGA2**, RECK, RAB1B, RAB10, RAB23, RAB42, TGFBR3, **TJP1**, WNT3A, **VCAN**	TGFBR3
hsa-miR-106b-5p	**APP**, **JAK1 MMP2**, MYC, TP53, **TWIST1**, **VEGFA**	**ABI2, ACTR2, CAV1, CDC42**, **CFL2**, CTSS, **ITGA2**, **ITGB1**, RAB10, RAB22A, RAB30, **RAB5B**, RACGAP1, **RHOC**, TGFBR2, **TSG101, WASL**	ADAM9, RAB8B
hsa-miR-181c-5p	**KRAS**, IL2, TGFBR1, TGFBR2	ADAM17, **ARF6**, RAB2B, **RHOG**, **TSG101**, VCAM1	ADAM11, AKT3, TGFBR1
hsa-miR-369-3p	–	**PAK2**, RAB32, RAB8B, **RAC1**, VEGFA	**RAB5B**
hsa-miR-548j-3p	–	ADAM17, **ARF1**, **ENAH**, **GRB2**, KRAS, **RHOB**, TGFBR3, VCAM1	**KRAS**, TGFBR1
hsa-miR-612	**AKT2**, TP53	**ACTR2**, ACTR3B, ADAM22, ADAMTS17, ADAMTS5, ARF3, CD81, DOCK7, FIGNL1, **GRB2**, **ITGB1**, RAB5B, RAB6B, **RAB7A**, **RAC1,** WNT3, **VAMP3**	–
hsa-miR-92a-3p	**ITGA5**, THBS1, TP53	**ABL2**, **ACTB**, ADAM10, ADAMTS1, **ARF1**, **BSG**, **CLIC1**, **CTTN**, **PXN, IQGAP1, RAB7B,** RAB8A, RAB8B, RAB36, **SH3PXD2A**, **WASL**	ADAM10, **ADAM19**, MMP10, RAB23

Targets with a link to invadopodia activity are highlighted in bold. *Strongly validated methods include reporter assays, western blot and qPCR. Weakly validated methods include microarray, NGS, and pSILAC. All predicted targets are listed above a target score of 95, meaning that predicted targets are highly likely to bind to the listed miRNA.*

3.3 Discussion

The current therapeutic approach for treatment of GBM, consisting of surgical resection followed by 2Gy RT for 5 days a week over 6 weeks and concomitant daily TMZ at 75 mg/m^2, provides a modest improvement in patient survival, however the majority of patients still succumb to the disease within two years due to tumour recurrence [61]. Research indicates that the efficacy of this therapeutic approach may be compromised by surviving tumour cells with enhanced invasive capabilities that contribute to more aggressive recurrent disease, however the mechanisms by which this enhanced treatment-induced invasion occurs are not well understood [3-5, 7]. Whilst enhanced MMP-2 secretion is often observed post-treatment in GBM cells, the intracellular protein expression levels of MMP-2 are not always seen to increase, suggesting that this enhanced extracellular degrading activity is not strictly due to upregulated MMP-2 protein expression [7]. As MMP-2 is known to be secreted by invadopodia on the cell surface, an upregulation of invadopodia activity may be responsible for these observations. In this chapter, evidence is provided to suggest that the enhanced invasive capabilities of RT/TMZ treated GBM cells may be gained through the action of invadopodia, highlighting the need to therapeutically target these structures in the context of GBM. Several candidate genes and miRNAs that may be involved in this pro-invadopodia phenotype following RT/TMZ are also identified and discussed.

3.3.1 Invadopodia are clinically relevant in GBM and detected in GBM cell lines

As the invasive potential of various cancers has been linked to their ability to form invadopodia, proteins involved in the regulation of invadopodia formation and activity have been proposed to possess diagnostic or prognostic potential [124, 156, 158]. To identify the clinical relevance of invadopodia in GBM, data was extracted from the Oncomine and SurvExpress databases and used to interrogate the mRNA expression levels of invadopodia regulators (including Tks5, Tks4, cortactin, Nck1, NWASP, Src, and MMP-2) in GBM tissue. These regulators were found to be significantly overexpressed in

GBM tissue samples when compared to normal tissue samples (***Figure 3-1***) and were correlated with poorer GBM patient survival (***Supplementary Table 1***), indicating that the expression of invadopodia regulators may also have prognostic significance in GBM.

Having highlighted the clinical relevance of invadopodia in GBM, initial experiments involved the application of several techniques to establish an 'invadopodia-related' profile for selected GBM cell line (U87MG, LN229, MU4 and MU41) (***Figure 3-2***). Zymographic analysis revealed that MMP-2 was the main protease secreted by the GBM cell lines, consistent with its prominent role in GBM invasion and progression [394]. The level of MMP-2 secretion reflected the amount of invadopodia-mediated FITC-gelatin degradation for each GBM cell line. Quantification of invadopodia as individual actin puncta revealed that LN229 cells formed the most invadopodia, with a large percentage of these puncta overlapping with degraded FITC-gelatin consistent with the high extracellular MMP-2 activity of this cell line. Surprisingly, MU4 cells also formed relatively high numbers of invadopodia per cell, however these puncta were largely non-degradative. Oser *et al.* has shown that not all invadopodia reach maturation, with a lack of stability in the F-actin core causing these 'invadopodia precursors' to disassemble prior to becoming proteolytically active [395]. Therefore, whilst MU4 cells form many actin-rich protrusions, they lack the proteolytic activity required for focal ECM degradation during the maturation phase of the invadopodia lifecycle. Oser *et al.* discovered that cortactin dephosphorylation is required to stabilise the invadopodium precursor for maturation [395], whilst Yamaguchi *et al*. demonstrated that knockdown of cofilin decreases both invadopodia lifetime and matrix degradation [135]. As MU4 cells exhibited lower expression levels of the actin-stabilising proteins Tks5 and Cortactin compared to the other cell lines, this could indicate that MU4 cells are inefficient at forming mature invadopodia. Alternatively, low MMP-2 protein expression or insufficient recruitment to the invadopodium tip could be responsible for the low proteolytic activity of this cell line.

3.3.2 Invadopodia matrix degrading-activity in GBM cells treated with RT/TMZ

3.3.2.1 Augmented invadopodia activity is seen in GBM cells post-RT/TMZ treatment

To investigate the impact of RT and TMZ treatment on invadopodia activity, GBM cell lines were treated with clinically relevant doses of RT (2Gy) and TMZ (50μM) 24h prior to each experimental analysis. These doses were determined based on pharmacokinetic studies showing TMZ levels in the cerebrospinal fluid (CSF) of GBM patients are within a concentration range of 1-10μg/ml, which is equivalent to 5.15 - 51.5μM of TMZ [353]. In line with previous studies, zymographic analyses of serum-free culture media revealed an increase in MMP-2 secretion and activation as well as FITC-gelatin degradation following RT/TMZ treatment in all four GBM cell lines (***Figure 3-2B-C***). This was correlated with an increase in the number of invadopodia per cell, (***Figure 3-2D***), indicating that RT/TMZ treatment enhances invadopodia formation in GBM cells. As invadopodia are known to influence both invasive and migratory behaviour in cancer cells [396], enhanced invadopodia formation may also underlie the observed increase in migration rate in LN229 and MU4 cells post-RT/TMZ treatment (***Figure 3-5A***). These findings support previous studies that reported enhanced migratory and invasive capacity in GBM cells exposed to either RT alone, or in combination with TMZ [3, 4, 7], and suggest that these observations may be due to the action of invadopodia.

Cancer cell invasion is known to be coordinated with the cell cycle, as invasion generally occurs during the G1/G0 (cell cycle arrest) phases, with expression of EMT-inducers and rearrangement of the F-actin cytoskeleton associated with this state [357, 397]. The ability to arrest from the cell cycle allows tumour cells to switch between a proliferative and invasive phenotype. As many chemotherapeutics target rapidly dividing cells, this phenotypic plasticity is an important aspect of treatment resistance and a potential target for therapy. Enhanced invadopodia-driven ECM degradation has been reported to occur in breast cancer cells synchronized in the G1 phase of the cell cycle, via upregulated expression of MT1-MMP and cortactin and subsequent increased localization of Tks5 to invadopodia [398].

Therefore, to explore whether cell cycle arrest could be a contributing factor to enhanced invadopodia activity in RT/TMZ treated cells, the cell cycle distribution of GBM cell lines in response to RT/TMZ treatment was next examined. A significantly larger proportion of GBM cells were in G0/G1 phase following RT/TMZ treatment (***Figure 3-5B***), indicating that increased invadopodia activity in GBM cells correlates with cell cycle arrest. Resistance to TMZ has previously been associated with G1/G0 arrest, along with increased migratory and invasive capabilities in these resistant cells [399]. Overall, these findings suggest that enhanced invadopodia activity in RT/TMZ treated GBM cells may coincide with cell cycle arrest and provides a rationale for exploring anti-invadopodia strategies in treatment resistant GBM.

3.3.2.2 The effect of LT treatment on invadopodia activity differs between GBM cell lines

To simulate a 'multiple treatment' regime, GBM cell lines were repeatedly treated with RT/TMZ once a week for a period of 10 weeks and termed 'Long-Term' (LT) treated cells. Enhanced invadopodia formation and activity was maintained in LT treated U87MG, MU4 and MU41 cells, however, surprisingly, LN229 cells exhibited a complete loss of detectable invadopodia-mediated matrix degradation activity, as well as reduced invadopodia formation after LT treatment (***Figure 3-8A-C***). These changes translated through to the invasive capacity of these LT treated cell lines, with a significant increase in the rate of invasion observed for LT treated U87MG, MU4 and MU41 cells whilst a significant decrease in invasion was seen for LT treated LN229 (***Figure 3-8D***). Notably, as LT RT/TMZ treated LN229 cells are still observed to pass through the BME-coated membrane, this could indicate that LN229 cells may adopt an amoeboid mode of invasion following LT RT/TMZ treatment that, unlike mesenchymal invasion, does not require the action of MMPs to degrade the surrounding ECM. Instead of adhering to and degrading the ECM, amoeboid cells instead de-adhere and adapt their shape to squeeze through the small spaces of the ECM. The loss of MMP-2 secretion and gelatinolytic activity in the LT RT/TMZ treated LN229 cells suggests that these cells are likely utilising amoeboid invasion to pass through the BME-coated membrane. As cancer cells have been observed to switch

between mesenchymal and amoeboid invasion in response to environmental pressures [400], this example highlights the phenotypic plasticity of GBM cells in response to selective pressures introduced by prolonged exposure to RT/TMZ treatment.

As the phenotypic plasticity of tumour cells allows them to switch between a proliferative or invasive phenotype, thereby conferring a survival advantage under different stress conditions, potential reasons for the lack of invadopodia activity in LT treated LN229 cells may be evidenced in the observed differences in proliferation rate. Whilst the U87MG, MU4 and MU41 cell lines did not show a consistently significant change in proliferation following LT treatment, LN229 cells demonstrated a significant increase in proliferation rate compared to parental cells (***Figure 3-7B***). Therefore, whilst LT treated LN229 cells possess reduced invadopodia activity and invasive potential, they instead rapidly divide and expand in population. This is in accordance with several studies reporting that highly invasive cancer cells display minimal or no proliferation, leading to the development of the 'go or grow' hypothesis [397, 401-406]. This hypothesis that suggests invasion and proliferation are spatiotemporally distinct and mutually exclusive phenotypes, as it is unlikely a single cell has the structural and energetic resources to actively engage in actin polymerisation required for invasion whilst simultaneously progressing through the cell cycle [407, 408]. The two distinct responses seen in GBM cell lines following LT treatment supports a previous study by Tiek *et al.* that discovered two independent TMZ-resistant GBM cell lines captured a different facet of the "go" or "grow" hypothesis, as one cell line was highly proliferative and the other highly invasive [409]. Although all LT treated GBM cell lines exhibited a reduction in sensitivity to RT/TMZ treatment, this was only significant for LT treated LN229 cells (***Figure 3-7A***). This may be due to either intrinsic resistance, allowing a subpopulation of LN229 cells to survive LT treatment, or acquired resistance induced by prolonged exposure to mutagenic agents. Additionally, this phenotypic switch observed following LT treatment may be essential for rapid tumour growth at secondary sites post-invasion, leading to recurrent tumours that are highly resistant to RT/TMZ. A better understanding of the mechanisms driving this response in LN229 LT treated cells may allow for the development of therapeutics that could be implemented for recurrent tumours of this type and will be addressed in ***Chapter 6***.

In conclusion, this data indicates that GBM cells respond to prolonged RT/TMZ treatment by promoting either a pro-proliferative phenotype (potentially able to withstand treatment) or a pro-invasive/pro-invadopodia phenotype (potentially able to evade treatment), both of which may contribute to tumour recurrence (***Figure 3-24***). Whilst these LT treated cell lines provide valuable insights into the differential mechanisms of RT/TMZ resistance, the heterogeneous nature of clinical GBM could indicate that such distinct phenotypes may instead exist in tumours as a spectrum. As the current treatment strategy is aimed at eradicating the most proliferative cells, this may not necessarily encompass all malignant cells, as demonstrated by the vast differences in these LT treated cells. Thus, understanding of GBM cell plasticity in response to treatment and its contributions to tumour heterogeneity is vital in developing new ways to prevent or treat recurrent GBM.

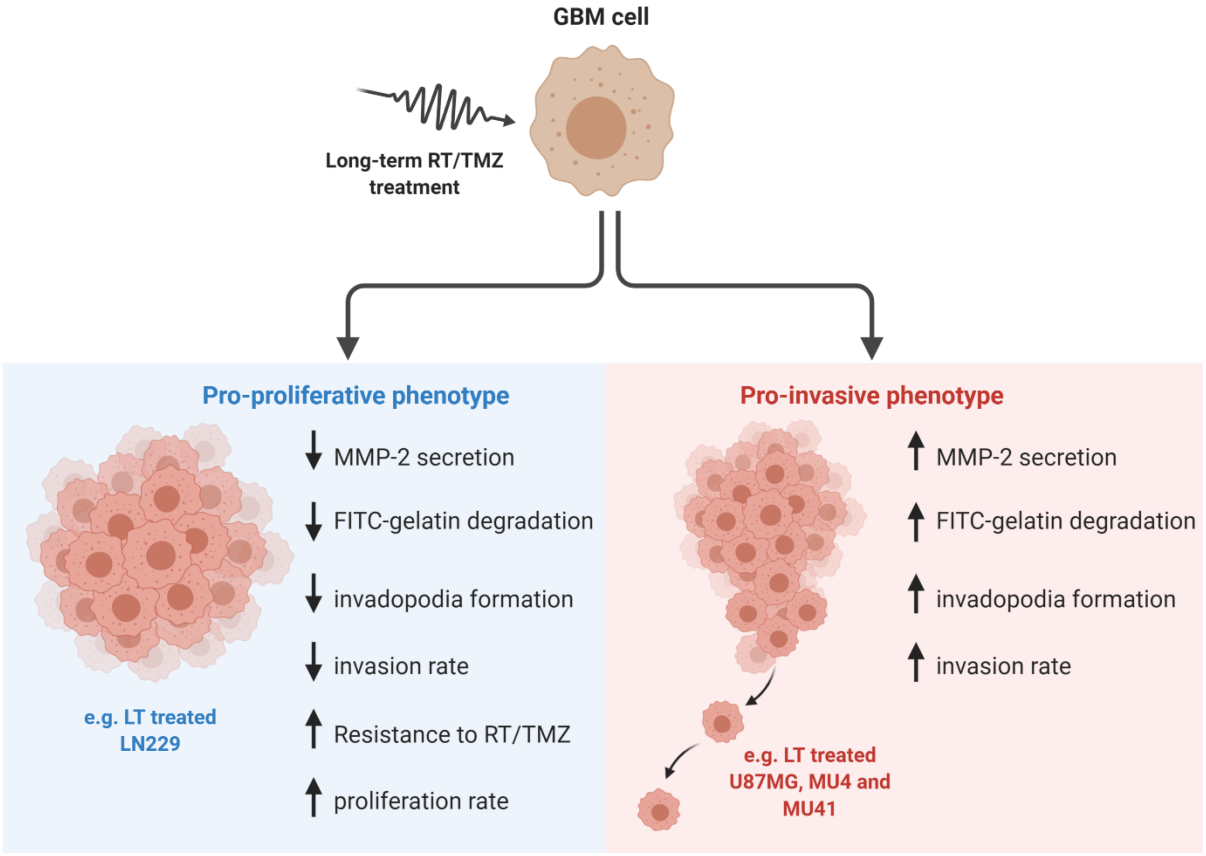

Figure 3-24: Functional changes in LT treated cells suggest two distinct phenotypes

Summary figure of different functional changes observed for the long-term (LT) treated GBM cell lines (exposed to RT/TMZ treatment once a week for 10 consecutive weeks), suggesting LN229 cells adopt a highly proliferative but minimally invasive phenotype following LT treatment, whilst U87MG, MU4 and MU41 cell lines maintain augmented invadopodia activity in order to facilitate invasion.

3.3.3 Secreted proteases and protease inhibitors that may contribute to GBM cell invasion post-RT/TMZ treatment

3.3.3.1 MMP-2, MMP-12, Cathepsin D and Cathepsin V may contribute to GBM invasion

Various proteases have been shown to be overexpressed in GBM tissue samples that are associated with poor patient outcome [410-412]. This so-called 'protease web' is becoming increasingly more diverse and complex, as proteases not only function to degrade proteins, but can also activate other proteases and signalling molecules via specialised cleavage of inactivated/pro-peptides. Protease arrays highlighted MMP-2, MMP-12, Cathepsin D and Cathepsin V to be the main proteases secreted by GBM cells, except for MMP-2 in LT treated LN229 cells, supporting previous results (***Figure 3-9***). These four proteases were determined to clinically relevant in GBM, as determined by overexpression in GBM relative to non-tumour tissue (***Table 3-1***), as well as being significantly correlated with poorer GBM patient survival (***Figure 3-10 and Table 3-2***). As these proteases have roles in degrading and modifying different components of the surrounding ECM, as well as cleaving proteins such as growth factors, precursor/inactive proteins to stimulate tumorigenic signalling cascades, they may be implicated in various aspects of GBM progression and invasion [413-416]. Both cathepsins and MMPs are shown to be part of a common proteolytic network in the GBM microenvironment, and whilst MMP-2 is one of the most significant proteases associated with GBM invasion, Cathepsin D has also been proposed to promote GBM invasion via lysosomal exocytosis [417]. Both of these proteases are upregulated in radioresistant GBM cells, suggesting that these proteases may be promising targets in treatment resistant GBM [418]. Aside from MMP-2, it is unclear whether these proteases may be directly involved in invadopodia activity in GBM cells, however some evidence exists in other cancers. Recently, Iizuka *et al*. found that the inhibition of MMPs (using a broad-spectrum MMP inhibitor) or Cathepsins (using CA074, an inhibitor of Cathepsin B) in breast cancer cells resulted in shorter invadopodia and reduced 3D invasion, suggesting a potential role for MMPs and cathepsins in invadopodia maturation [419].

This was also supported by Lee *et al*. that showed reduced expression of MMP-2, Cathepsin V and Cathepsin D upon inhibition of invadopodia formation in oral squamous cell [420].

3.3.3.2 The perturbation of proteolytic networks in GBM cells treated with RT/TMZ

Although protease arrays were useful in determining the proteases highly secreted by GBM cell lines, they may lack the sensitivity to detect low abundance proteins or minor changes in expression levels. Indeed, detection via array depends on the affinity of each antibody to the protein of interest [358], which may explain the lack of change in secreted protease expression observed following single and LT treatment, and thus the discrepancy between zymography results, indicating increased extracellular MMP-2, and protease array results. Kleiner *et al.* demonstrated that zymography bands indicative of MMP-2 activity can be detected at levels as low as 10ng, and the degree of gelatin digestion is directly proportional to the amount of enzyme present [421]. Therefore, whilst the antibody array gives an overview of the levels of secreted proteases, it is less sensitive to changes in secretion after treatment than zymography and, unlike zymography, does not infer the activity of these proteases outside of the cell. Moreover, as zymography indicated an increase in MMP-2 activity in the conditioned media of treated cells, however minimal changes in the detection of MMP-2 were observed with the protease arrays, this could also indicate a treatment-induced increase in the levels of proteins that drive extracellular MMP-2 activation after RT/TMZ treatment, such as MT1-MMP.

Due to their interconnectivity, certain proteases and protease inhibitors may exhibit diverse effects, functioning as tumour promoters or suppressors depending on context. Malignant progression is often associated with deregulation of this network, resulting in altered, most often upregulated, protease activity, however an in-depth understanding of the contextual interplay between these molecules that underlies GBM progression is lacking [422]. Interestingly, seven protease inhibitors that are also known to possess pro-invasive roles were identified in the conditioned media of GBM cells, including APP, Fetuin-B, EMMPRIN/CD147, Lipocalin-1, Serpin E1/PAI-1, TIMP-1 and TIMP-2 (***Table 3-3***). As

these seven inhibitors were detected at elevated levels in the conditioned media of single RT/TMZ treated GBM cell lines, this indicates a substantial treatment-induced increase in secretion that supports the enhanced invasive phenotype of GBM cells post-RT/TMZ treatment (***Figure 3-14***). Greater variation in secreted levels of these inhibitors was observed following LT treatment, suggesting a greater degree of proteolytic network dysregulation in LT treated GBM cell lines. Interestingly, TIMPs can regulate MMPs through a variety of mechanisms in which they can function as both an MMP inhibitor and an activator, the latter due to their ability to prevent active MMPs from undergoing autolytic inactivation [6]. Furthermore, the complex of MTI-MMP and TIMP-2 at the surface of cancer cells is required for the binding and activation of pro-MMP-2 [423]. Therefore, despite their known inhibitory roles, the increase in TIMP-1 and TIMP-2 secretion from RT/TMZ treated GBM cells may also potentially maintain MMP activity. Additionally, EMMPRIN (extracellular matrix metalloproteinase inducer, also known as basigin/CD147) was seen to increase in the conditioned media of RT/TMZ treated U87MG, LN229 and MU4 cells. This glycoprotein is known to stimulate adjacent cells to produce MMPs and has also been shown to complex with CD44 and EGFR to promote invadopodia assembly in breast cancer [362]. Importantly, inhibition of EMMPRIN expression in GBM cells via antisense RNA reduced invasion and MMP-2 secretion [365]. Whilst the remaining six pro-invasive inhibitors identified in this study have not been previously associated with invadopodia, they have been implicated in GBM cell invasion. Consequently, this raises the possibility for their potential role in the enhanced invadopodia formation and activity observed in RT/TMZ treated cells.

Ultimately, this data suggests that the deregulation of proteolytic networks in GBM cells treated with RT/TMZ may have the potential to either facilitate or suppress malignant progression. These results support the notion that proteolysis pathways do not function singularly, but rather they participate in a dynamic integrated network of protein-protein interactions that may contribute to the invasive abilities of GBM cells. As inhibition of protease activity with competitive inhibitors has proved disappointing in GBM clinical trials [104], future work should investigate targeting potential upstream mechanisms, such as inhibiting the secretion of proteases from invadopodia or blocking their proteolytic activation by other membrane-bound or secreted molecules, such as EMMPRIN/CD147.

3.3.4 Changes in gene and miRNA expression in GBM cells following RT/TMZ treatment may contribute to an enhanced invasive phenotype

Gene and miRNA expression profiles in GBM cell lines treated with RT/TMZ were assessed using Nanostring® technology. Analysis of 770 genes with a Cancer Gene Panel revealed the upregulation of pro-invasive genes in RT/TMZ treated GBM cells, classified as having oncogenic effects relating to the processes of tumour invasion, EMT, tumour growth, ECM layers/remodelling, and angiogenesis (***Figure 3-15***). mRNA expression levels corresponding to three upregulated genes were found to be significantly overexpressed in GBM compared non-tumour tissue in six independent datasets listed on the Oncomine database: THBS1, VCAN and SERPINE1 (***Figure 3-16***). Whilst VCAN can promote TGF-β2-mediated migration and invasion of U87MG and A172 GBM cells [424], VCAN mRNA expression was not found to significantly differ between WHO grades of glioma (***Figure 3-17B***) indicating that expression levels may not correlate with malignancy. On the other hand, both SERPINE1 and THBS1 mRNA expression levels were found to be significantly higher in GBM (grade IV) tissue compared to lower grade glioma tissue and thus may serve as indicators of glioma malignancy (***Figure 3-17A&C***). Indeed, both SERPINE1 and THBS1 have been associated with GBM invasion and a mesenchymal subtype, and therefore the upregulation of these genes in RT/TMZ treated GBM cells may contribute to enhanced invasive properties [425, 426].

Furthermore, analysis of a miRNA panel of 798 miRNAs, highlighted four miRNAs (let-7a-5p, hsa-let-7b-5p, hsa-let-125b-5p, hsa-miR-4454+hsa-miR-7975) that were significantly decreased in expression following a RT/TMZ treatment in U87MG, MU4 and MU41 cells (***Figure 3-22***). Several validated and predicted invadopodia-related targets were identified for three of these miRNAs (hsa-let-7a-5p, hsa-let-7b-5p, and hsa-let-125b-5p), including key invadopodia regulators such as EGFR, N-WASP, Tks5 and MMP-2, as shown in ***Table 3-6.*** As miRNAs negatively regulate gene expression by degrading their target mRNAs or inhibiting their translation, the reduced expression of hsa-let-7a-5p, hsa-let-7b-5p, and hsa-let-125b-5p following treatment may allow for greater expression levels of these invadopodia-related target genes, which could potentially contribute to the observed enhancement in invadopodia

formation and activity. Further supporting a potential role in invadopodia activity, the basal expression levels of these miRNAs in GBM cell lines inversely correlated with invadopodia activity, with highest expression in MU4 cells and lowest expression in LN229 cells (***Figure 3-22F***). Whilst functional studies have not been carried out to investigate the direct effect of these miRNA on invadopodia activity, evidence in the literature has shown that downregulation of these miRNAs promotes invasion and chemoresistance in a number of cancers [427-430], including GBM [430-432]. Supporting their tumour suppressive roles in GBM, the expression levels of let-7a, let-7b and miR-125b are seen to decrease with increasing glioma tumour grade, with deficiency of these miRNAs also associated with poor GBM patient prognosis [426, 428, 433]. It has been shown in GBM cells that the phosphatidylinositol-3 kinase/Akt and mitogen-activated protein kinase (MAPK, also known as ERK) pathways are inhibited by let-7a [428], and studies have also shown involvement of let-7b and miR-125b in these pathways [434, 435]. Both signalling pathways are known to mediate invadopodia formation, thereby providing a potential mechanism in which downregulated miRNAs following RT/TMZ treatment may promote invadopodia formation [436, 437]. Additionally, nine miRNAs were found to be elevated exclusively in LT treated LN229 cells which were found to target key invadopodia regulators involved in actin regulation (***Table 3-7***). miRNA-mediated downregulation of actin regulators such as cortactin and Tks5 has previously been reported to suppress invadopodia formation and activity [438, 439]. Therefore, the elevated expression of these miRNAs in LN229 LT cells could lead to downregulated expression of such targets, thereby potentially contributing to reduced invadopodia activity. Further investigation of these nine miRNAs in GBM cells in addition to hsa-let-7a-5p, hsa-let-7b-5p, and hsa-let-125b-5p is therefore warranted, as the activation of these miRNAs may be a useful strategy for combatting treatment induced invadopodia activity and subsequent GBM cell invasion.

3.3.5 The role of thrombospondin-1 in invasion and invadopodia in GBM cell lines

THBS1 was identified as a potential pro-invasive candidate gene from the Cancer Progression Gene Panel as it was upregulated in GBM cells that survive treatment with RT/TMZ. Therefore, we hypothesized that THBS1 may potentially be involved in the enhanced invasive abilities of GBM cells that survive therapy mediated through the action of invadopodia. THBS1 encodes for a protein known as Thrombospondin-1, a large multifunctional matrix protein known to be implicated in the modulation of cell-cell and cell-ECM attachment, migration, invasion, and inhibition of angiogenesis [440] (***Figure 3-25A***). Analysis of gene expression datasets revealed that high THBS1 expression correlated with an increase in glioma grade (***Figure 3-17C***) and this was predominantly associated with the mesenchymal subtype of GBM (***Figure 3-18***), suggesting a potential role in GBM invasion [383]. Exogenous THSB1 has previously been shown to promote invasion in a range of cancers, including glioma [441-444]. However, as most THBS1 interactions have been reported in the extracellular space, the intracellular role of THBS1 has not been fully elucidated. A study by Taraboletti *et al.* demonstrated that exogenous THBS1 added to endothelial cells in media promoted MMP-2 secretion and invasion, which was dependent on the heparin binding domain of THBS1, as heparin treatment inhibited THBS1-induced invasion [445]. As the high-affinity heparin-binding of THBS1 is required for endocytosis, via the endocytic receptor LRP-1 (low density lipoprotein-related protein), this suggests that internalised THBS1 may act within the cell to promote invasion [446]. Supporting a role for endogenously expressed THBS1 in GBM invasion, recently, Daubon *et al*. demonstrated that THBS1 expression levels positively correlated with U87MG cell invasion through a matrigel matrix using a THBS1 shRNA strategy [447]. Although the authors were able to demonstrate that interactions between THBS1 and the membrane receptor CD47 were implicated in this process, the mechanisms by which THBS1 may promote invasion in GBM cells remain poorly understood. Here, we propose that the involvement of THBS1 in GBM invasion may be linked to invadopodia activity. Supporting a potential involvement in GBM cell invadopodia activity, protein interactions between THBS1 and both MMP-2 and MMP-9 have been established, as highlighted in the STRING network in ***Figure 3-18J,*** which also included

invadopodia regulators such as Src, Tks5 and invadopodia-related integrins. Furthermore, THBS1 was also found to correlate with poorer GBM patient survival when over-expressed with these invadopodia regulators (***Table 3-5***). With the use of the FITC-gelatin invadopodia assay, we demonstrated that THBS1 localized within functional matrix-degrading invadopodia that form in the LN229 GBM cell line (***Figure 19***), indicating a potential role for THBS1 in the biogenesis of invadopodia in GBM cells. This hypothesis is further supported by functional experiments which demonstrated a significant increase in MMP-2 secretion and an enhanced migration rate upon overexpression of THBS1 in the GBM cell lines, whilst MMP-2 secretion and migration were decreased upon siRNA-mediated knockdown of THBS1 (***Figure 3-20 & Figure 3-21***). Furthermore, THBS1 localization was also more concentrated in areas near small actin puncta displaying less FITC-gelatin degradation than their larger counterparts (***Figure 19***), indicating that THBS1 expression may also be involved in the early stages of invadopodia biogenesis prior to proteolytic degradation of the surrounding ECM, such as the initiation of invadopodia assembly or the trafficking of invadopodia-related proteins, such as MMPs [393].

Reinforcing a potential role in the trafficking of proteins to invadopodia, the type 1 repeat regions of THBS1 and THBS2, which share close sequence homology, are known to directly bind to the catalytic domain of MMP-2 in the extracellular space, and this complex is reported to be internalised by LRP1 into endosomes [448, 449]. Additionally, THBS1 is reported to bind to several proteins associated with intracellular vesicles such as LIMPII [450] and STIM1 [451], as well as a variety of invadopodia-related proteins that are trafficked to invadopodia via the vesicular system such as MMP-2 [448], MMP-9 [452], and β1 integrins [453-455]. Therefore, it may be possible that THBS1 can form complexes with these proteins in GBM cells and in this way may participate in the vesicle-mediated transport of proteins to invadopodia (***Figure 3-25B***). Interestingly, THBS1 has been found to be highly expressed in extracellular vesicles secreted from breast cancer cells, which promoted migration when internalized by recipient breast cancer cells [456], whilst human corneal epithelial cells treated with media containing THBS1 have been shown to secrete THBS1-positive exosomes (secreted vesicles derived from the endosomal system) [457]. In addition to THBS1, these exosomes also contained invasion-related proteins, such as annexin A2, as well as proteins associated with MT1-MMP-positive vesicle

transport to invadopodia, such as IQGAP, further supporting the possibility that THBS1 may be implicated in the endosomal transport of proteins to invadopodia.

In addition, THBS1 may potentially play a role in the initiation of signalling cascades that drive actin polymerisation and subsequent assembly of invadopodia. It is known that the N-terminal domain of THBS1 binds to calreticulin and LRP1 to induce a signalling cascade that results in Src phosphorylation and the activation of ERK and PI3K, which are known to promote invadopodia initiation, independent of LRP1's role in the endocytosis of exogenous THBS1 [458, 459]. It has been demonstrated that knockdown of LRP1 impairs lamellipodia formation in mouse embryonic fibroblasts [460], and as both lamellipodia and invadopodia formation are dependent on branched actin assembly, this could indicate that THBS1 signalling through the calreticulin/LRP1 protein co-complex may also be important for invadopodia formation in GBM cells (***Figure 3-25C***). Further supporting a role in actin remodelling, the N-terminal domain of THBS1 has been shown to bind to integrin α3β1 in breast cancer cells, which was proposed to promote cytoskeletal organization and cell invasion in a PI3K-dependent manner [452]. This integrin, along with αvβ3 integrin and syndecan-1, are also suggested to act as cell-surface receptors for exogenous THBS1 in malignant glioma cells which may promote migration [442]. Collectively, these studies indicate that THBS1 may influence invadopodia formation or activity in GBM cell lines via either a potential involvement in the endosomal trafficking of invadopodia-related proteins, the promotion of invadopodia-related signalling cascades such as those involving ERK and PI3K, or potentially via another interaction that is yet to be determined. Future studies should therefore investigate the interactions between endogenous THBS1 and key proteins that are involved in the regulation of invadopodia in GBM cells (such as the activation of ERK, PI3K or Src), or proteins involved in endosomal trafficking (such as Rab11, a marker of recycling endosomes, or components of the exocyst complex that have both been shown to be required for invadopodia formation [461, 462]), in order to determine the role of THBS1 in invadopodia biogenesis.

Due to its complex multimeric structure, THBS1 contains numerous domains and binding sites for cellular receptors, cytokines and ECM molecules and is thus able to interact with a wide network of proteins (***Figure 3-25A***). Consequently, THBS1 is reported to exhibit diverse functions in tumours

depending on the expression of various interacting proteins [463]. THBS1 was first identified as an angiogenesis inhibitor, based on its procollagen homology (PCH) domain and type 1 repeats, whilst the pro-invasive properties of THBS1, involving the ability to bind integrins and syndecan-1 on the surface of glioma cells, have been attributed to either the N-terminal heparin-binding domain [445, 458, 459] or C-terminal domain when presented in trimeric form [442, 464-466]. Due to its multifunctional role, anti-tumour therapeutic strategies aimed at silencing THBS1 may induce adverse side effects, whilst targeting specific THBS1-protein interactions is also therapeutically challenging due to the association of THBS1 with a variety of ligands and receptors required for physiological processes [463]. Consequently, directly targeting THBS1 has been largely ineffective in clinical trials (reviewed in [467]). As the data presented in this chapter suggests that THBS1 may participate in processes that promote GBM invasion via invadopodia-mediated matrix-degrading activity, targeting invadopodia formation and activity downstream of THBS1 may represent a promising anti-invasive therapeutic approach. Future research should focus on elucidating the specific mechanisms by which THBS1 may drive invadopodia formation or activity in GBM cells through its interaction with other proteins, therefore identifying invadopodia-related targets.

Figure 3-25: The functional domains of Thrombospondin-1 and potential roles in invadopodia

(**A.**) The functional domains of Thrombospondin-1 (THBS1) comprise of three identical monomer chains linked together by disulfide bonds at the procollagen homology domain. The receptor binding partners identified for each domain are listed, with actin-cytoskeletal rearrangements associated with the C-terminal domain. The diverse functions of THBS1 depend on the presence of these cell surface binding partners as well as other ECM proteins, and therefore the actions of each domain may vary between different cell types and under different contexts. *Image adapted from Huang et al. [467]* (**B.**) THBS1 may play a role in the vesicle-mediated trafficking of proteins to invadopodia. The thrombospondin type 1 repeat region binds to the catalytic domain of MMP-2 in the extracellular space, and this complex may be internalised into endosomes via the endocytic receptor, LRP1 [448, 449]. As invadopodia rely upon the endosomal system for the delivery of proteins, such as MMP-2, and the recycling of surface receptors, such as MT1-MMP, these THBS1-positive endosomes may participate in this process of trafficking to invadopodia. (**C.**) THBS1 may promote invadopodia-related signalling cascades. Exogenous THBS1 is known to bind to calreticulin/LRP1 resulting in Src phosphorylation and activation of the ERK/PI3K signalling pathways which are known to promote actin polymerisation and subsequent invadopodia initiation [458, 459].

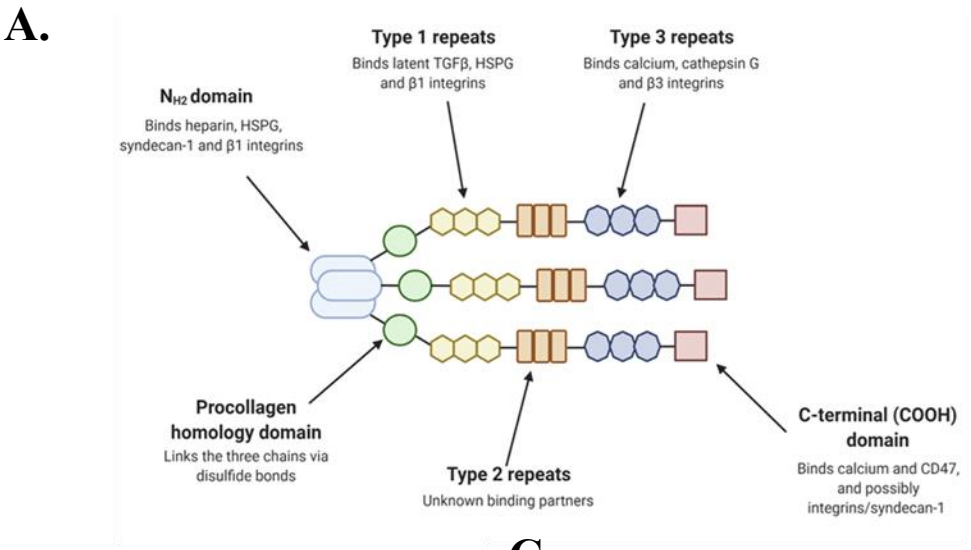
A.
Type 1 repeats
Binds latent TGFβ, HSPG and β1 integrins
Type 3 repeats
Binds calcium, cathepsin G and β3 integrins
NH2 domain
Binds heparin, HSPG, syndecan-1 and β1 integrins
Procollagen homology domain
Links the three chains via disulfide bonds
Type 2 repeats
Unknown binding partners
C-terminal (COOH) domain
Binds calcium and CD47, and possibly integrins/syndecan-1

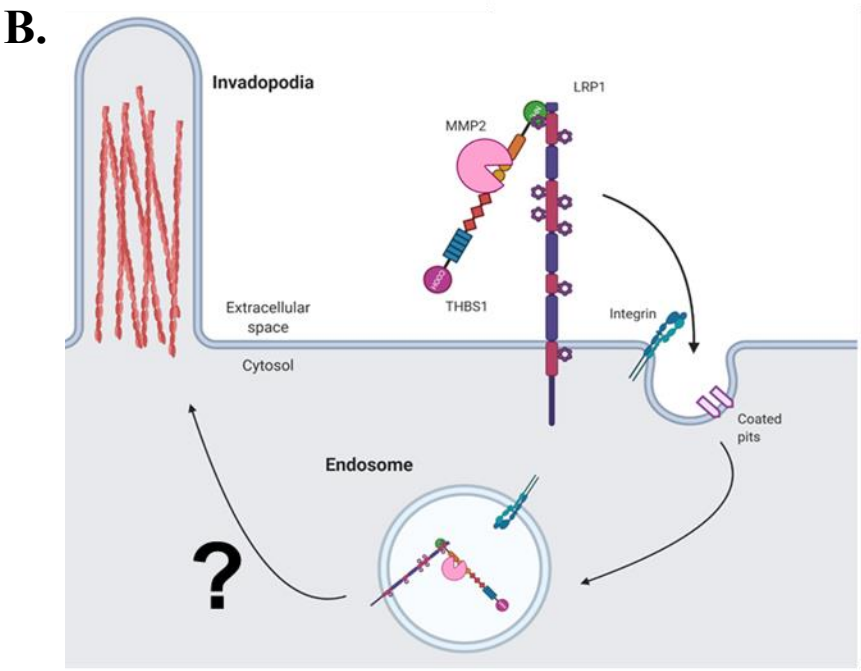
B.
Invadopodia
LRP1
MMP2
THBS1
Extracellular space
Cytosol
Integrin
Coated pits
Endosome
?

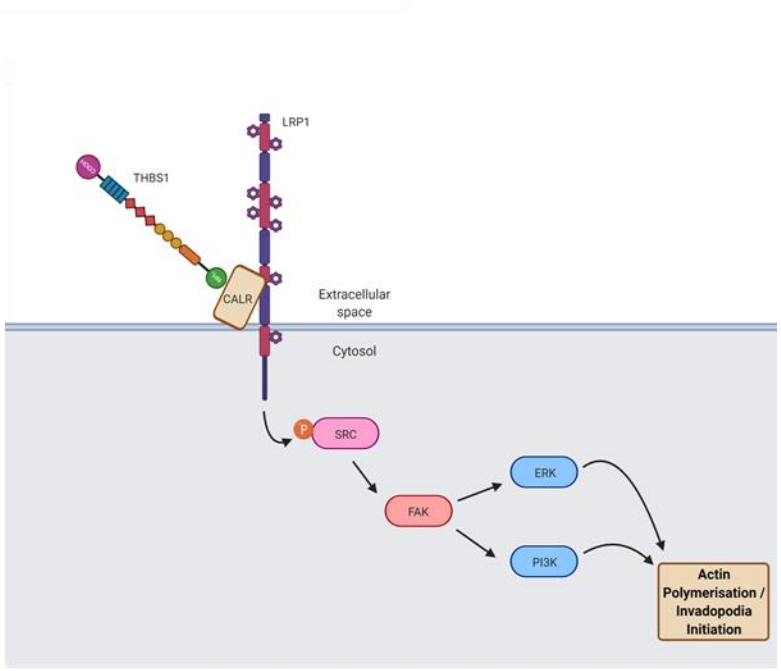
C.
LRP1
THBS1
CALR
Extracellular space
Cytosol
P
SRC
FAK
ERK
PI3K
Actin Polymerisation / Invadopodia Initiation

3.4 Conclusion

Collectively, the results in this chapter demonstrate that GBM cells that survive the current therapeutic approach of RT and TMZ exhibit a pro-invadopodia phenotype. This enhanced invadopodia formation and activity may contribute to the resilience of GBM, allowing surviving cells to rapidly invade throughout the surrounding normal brain parenchyma following treatment. The proteolytic activity of these cells may be facilitated by the secretion of cathepsins, MMPs and proteins such as EMMPRIN/CD147 that promote their activation, and accompanied by the upregulation of pro-invasive genes, such a THBS1, and the downregulation of miRNA with invasion-related targets. Whilst augmented invadopodia activity was maintained in three GBM cell lines following prolonged exposure to RT/TMZ, the phenotypic switch to a pro-proliferative phenotype observed in the LT treated LN229 cells may provide additional insight into GBM cell plasticity and treatment resistance observed during tumour recurrence post-treatment. Continued investigation will further elucidate the potential mechanisms involved and may identify novel therapeutic targets to combat GBM invasion in the future.

CHAPTER 4:
Examining the role of EVs as facilitators of invadopodia-mediated GBM invasion

4.1 Introduction

4.1.1 EV-mediated communication in GBM

Extracellular vesicles (EVs) are small lipid-bilayer enclosed particles that are released by most cell types into the extracellular environment [180]. Governed by their mode of biogenesis, EVs may be classified as either microvesicles (MVs) or exosomes. MVs (50-1000nm in diameter) are generated by the outward budding and fission of the plasma membrane whereas the smaller exosomes (30-150nm in diameter) are produced via an endosomal pathway. Where it is not possible to verify the subcellular origin of experimentally obtained EVs, the combined term 'EV' is used in place of 'MV or exosome' and operational terminology is used to describe EV subtypes, such as referring to size (small/large EVs with defined ranges) or composition (CD63+/CD81+ EVs) in place of 'exosome' and 'microvesicle' [196].

EV cargo is donor cell-specific and may consist of DNA, RNA, proteins, lipids and other metabolites [468]. Transfer of the EV cargo, particularly mRNA and miRNA, can modulate gene expression and alter signalling activity in the recipient cells, ultimately inducing phenotypic changes [185, 252]. For example, EVs can initiate signalling cascades in recipient cells via the binding of surface proteins expressed on EVs to the plasma membrane and, additionally, can also transfer cytoplasmic content via endocytosis or fusion of the EV membrane with the recipient cell membrane. Tumour cells are known to hijack this process in order to facilitate malignant progression via the transfer of oncogenic proteins, receptors, and small RNAs [468]. Moreover, aggressive cancer cells may also secrete greater quantities of EVs compared to lower-grade tumours, further supporting their role in facilitating tumour progression [11, 201, 255, 273].

Recently, studies have shown that GBM cells are able to secrete EVs containing enriched oncogenic material indicative of selective packaging, including DNA, mRNA and miRNA [9-11], with an estimated 10,000 EVs released from a single GBM cell over 48 hours [11]. Enriched mRNA transcripts reported by Skog *et al.* in GBM derived EVs were found to be pro-tumorigenic, examples of which

included paxillin (PXN) and tubulin-β-2C (TUBB2C) [11], whilst miR-451, which is known to play an important role in GBM cell proliferation and migration, was found to be highly enriched in EVs secreted by the U251 GBM cell line by Li *et al.* [10]. Although donor GBM cell derived EVs can be transferred to neighbouring GBM cells to promote oncogenic transformation and chemoresistance [255, 469], they can also be transferred to normal cells in the brain microenvironment such as astrocytes, microglia and macrophages to promote a tumour-supportive microenvironment [260, 270]. For example, Kucharzewska *et al.* has demonstrated that EVs released from hypoxic GBM cells contained greater levels of hypoxia-related mRNA and protein cargo, which were taken up by endothelial cells *in vitro* and subsequently promoted tumour growth and vascularisation in an *in vivo* subcutaneous mouse GBM xenograft model [258]. Indeed, EVs isolated from GBM donor cells can induce angiogenesis [11, 267], drive invasion [8], inhibit anti-tumour immune responses [313], and promote chemoresistance [8, 272] by facilitating intercellular communication with recipient GBM cells as well as with other cells in the tumour microenvironment. Although this identifies EVs as important mediators of communication within the GBM microenvironment, the full extent by which GBM derived EVs can cause functional changes in recipient cells to drive tumour progression or response to therapy has not been fully elucidated and is the subject of continued research.

4.1.2 The emerging role of EVs in Invadopodia-Mediated Invasion

Research has identified that EV-mediated communication can facilitate various processes of cancer progression, including invasion, and there has been a growing interest in investigating whether invadopodia-mediated invasion of cancer cells is also mediated by EVs. Indeed, proteomic-based studies of EVs enriched from GBM and breast cancer cell lines have identified of the presence of proteins that may be involved in invadopodia biogenesis [470-472]. One study comparing data of known EV cargo proteins in the ExoCarta database with invadopodia-associated proteins revealed that there were 43 overlapping proteins involved in cytoskeletal remodelling and vesicle-mediated transport present in the database [471]. Another study determined that mRNA transcripts corresponding to five

invasion related genes that are significantly higher in GBM compared to normal brain were detected in GBM cell line derived EVs, including actin-related protein 3 (ACTR3), insulin-like growth factor 2 receptor (IGFR2), integrin-b1 (ITGB1), annexin A1 (ANXA1) and programmed cell death 6-interacting protein (PDCD6IP, also known as ALIX) [472]. A common function of these proteins relates to actin polymerization which is central to invadopodia formation.

A complex synergistic relationship between invadopodia and EV-based communication has been highlighted in a recent study by Hoshino et al. [229]. Using an invasive SCC61 HNSCC cell line, the authors demonstrated that CD63- and Rab27a- positive MVBs were preferentially docked and secreted into the extracellular space at invadopodia. Knockdown of two key components of exosome biogenesis (Rab27a and Hrs) or inhibition of ceramide synthesis with GW4869 resulted in reduced invadopodia numbers and invadopodia-mediated matrix-degrading activity, supporting a role for EVs in invadopodia [229]. Indeed, the endosomal pathway is known to be implicated in invadopodia maturation as the transport of MT1-MMP to the tip of the invadopodium relies upon the exocyst complex and the late endosomal v-SNARE/VAMP7, leading to the presence of a system whereby cargo are transported to invadopodia via multi-vesicular endosomes (MVEs) [154, 462]. However, other studies have also shown a link between plasma membrane-shed MVs and invadopodia activity, via Arf1- and Arf6/ERK dependent mechanisms [199, 473]. MT1-MMP has been detected in plasma membrane shed MVs, the delivery of which was dependent on the v-SNARE/VAMP3 [302]. Therefore, both membrane-shed MVs and endosomal-derived exosomes may be involved in the regulation of invadopodia activity.

4.1.3 Rationale and Aims

In Chapter 3, the invasive potential of GBM cells was shown to be linked to their ability to form functional, matrix-degrading invadopodia, which was enhanced in cells that survived RT/TMZ treatment. As GBM cells have been known to secrete EVs to facilitate cell-to-cell communication, this chapter aims to identify whether GBM cell derived EVs may contribute to a pro-invadopodia phenotype in recipient GBM cells, as well as potentially contributing to enhanced invadopodia activity in response to RT/TMZ treatment. Further elucidation of the functional relationship between EVs and invadopodia in GBM, especially post-RT/TMZ, could highlight novel pathways utilised by GBM cells to promote invadopodia-mediated invasion in response to treatment. Overall, this would identify EV-mediated communication from GBM cells post-RT/TMZ as a potential target in the future, with a view to reducing GBM cell invasion and improving GBM patient survival.

4.2 Results

4.2.1 EV markers in GBM tissue- datamining analysis

The potential clinical relevance of EVs in GBM was examined by utilizing the online cancer microarray database, Oncomine™ (version 4.5, www.oncomine.org, Compendia Bioscience, Ann Arbor, MI, USA, Thermo Fisher) to analyse the differential mRNA expression levels of established EV markers (including CD9, CD63, CD81, CD151, TSG101 and Alix) in GBM tissue and normal brain tissue [354]. Analysis of gene expression datasets from seven independent studies indicated that the mRNA expression levels of these EV markers were significantly ($p<0.05$) higher in GBM tissue compared to normal brain tissue (***Figure 4-1***). Higher gene expression levels of the EV markers was also associated with a significantly ($p<0.05$) reduced GBM patient overall survival, as determined with GBM datasets deposited with the online database, SurvExpress (***Supplementary Table 3***). Amongst the 55 combinations of EV markers across the different datasets that significantly correlated with poorer GBM patient survival, CD9 appeared most frequently (28/55), followed by CD63 (27/55), CD81 (26/55) and CD151 (23/55). Therefore, a prognostic link between mRNA expression levels of EV markers and GBM patient survival may exist.

Figure 4-1: EV markers are overexpressed in GBM

mRNA expression levels of nominated EV markers (CD9, CD63, CD81, CD151, TSG101, and Alix) were examined in GBM and normal brain tissue within datasets deposited in the Oncomine database. Displayed in this table are the mean fold changes (GBM versus normal brain) in each study and statistical significance (p-value) of each dataset. Gene expression data are log transformed and normalized. Data is ordered from most to least significant ($p<0.05$).

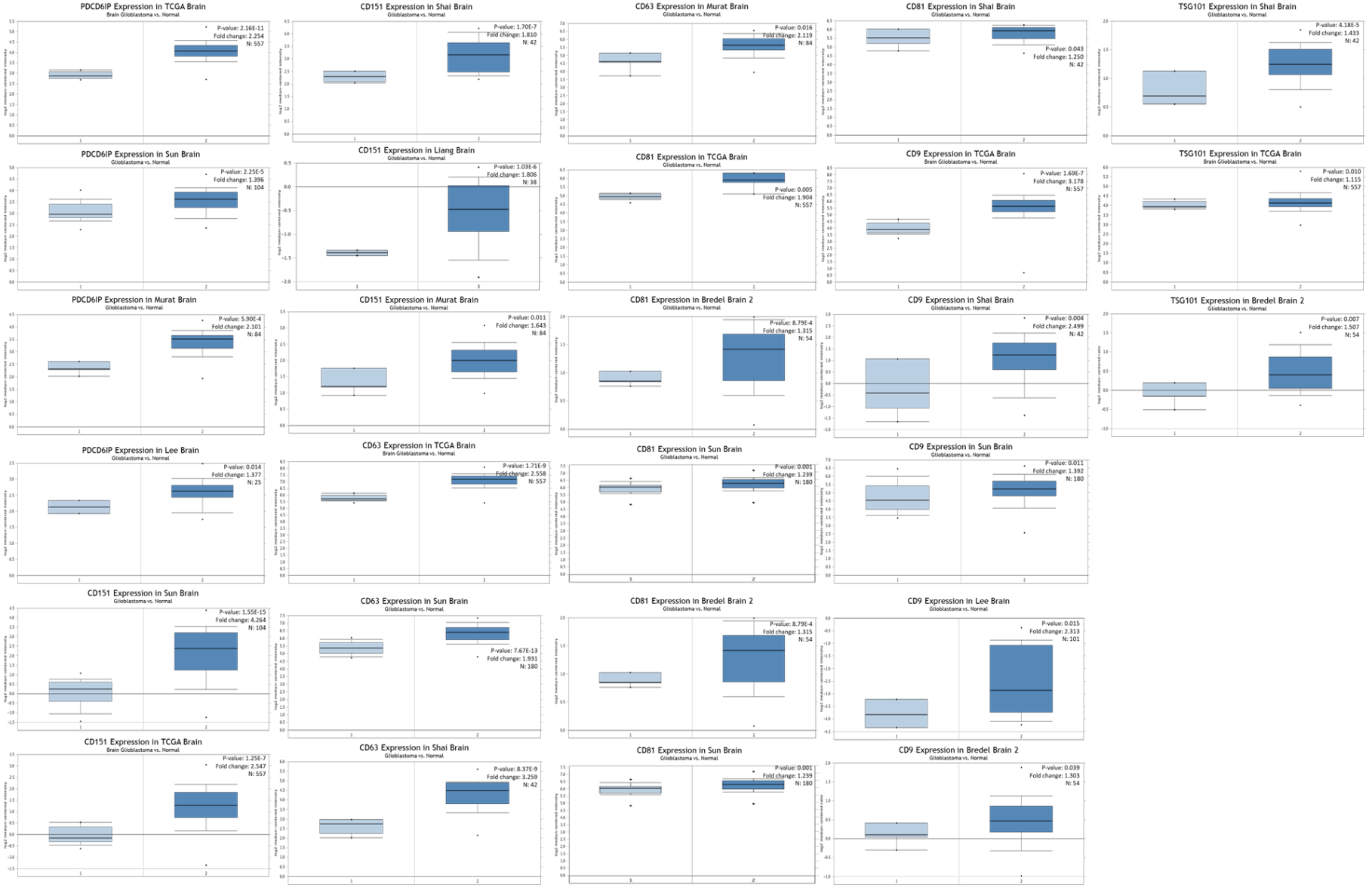
PDCD6IP Expression in TCGA Brain
Brain Glioblastoma vs. Normal
P-value: 2.16E-11
Fold change: 2.254
N: 557
CD151 Expression in Shai Brain
Glioblastoma vs. Normal
P-value: 1.70E-7
Fold change: 1.810
N: 42
CD63 Expression in Murat Brain
Glioblastoma vs. Normal
P-value: 0.016
Fold change: 2.119
N: 84
CD81 Expression in Shai Brain
Glioblastoma vs. Normal
P-value: 0.043
Fold change: 1.250
N: 42
TSG101 Expression in Shai Brain
Glioblastoma vs. Normal
P-value: 4.18E-5
Fold change: 1.433
N: 42
PDCD6IP Expression in Sun Brain
Glioblastoma vs. Normal
P-value: 2.25E-5
Fold change: 1.396
N: 104
CD151 Expression in Liang Brain
Glioblastoma vs. Normal
P-value: 1.03E-6
Fold change: 1.806
N: 38
CD81 Expression in TCGA Brain
Glioblastoma vs. Normal
P-value: 0.005
Fold change: 1.904
N: 557
CD9 Expression in TCGA Brain
Brain Glioblastoma vs. Normal
P-value: 1.69E-7
Fold change: 3.178
N: 557
TSG101 Expression in TCGA Brain
Brain Glioblastoma vs. Normal
P-value: 0.010
Fold change: 1.115
N: 557
PDCD6IP Expression in Murat Brain
Glioblastoma vs. Normal
P-value: 5.90E-4
Fold change: 2.101
N: 84
CD151 Expression in Murat Brain
Glioblastoma vs. Normal
P-value: 0.011
Fold change: 1.643
N: 84
CD81 Expression in Bredel Brain 2
Glioblastoma vs. Normal
P-value: 8.79E-4
Fold change: 1.315
N: 54
CD9 Expression in Shai Brain
Glioblastoma vs. Normal
P-value: 0.004
Fold change: 2.499
N: 42
TSG101 Expression in Bredel Brain 2
Glioblastoma vs. Normal
P-value: 0.007
Fold change: 1.507
N: 54
PDCD6IP Expression in Lee Brain
Glioblastoma vs. Normal
P-value: 0.014
Fold change: 1.377
N: 25
CD63 Expression in TCGA Brain
Brain Glioblastoma vs. Normal
P-value: 1.71E-9
Fold change: 2.558
N: 557
CD81 Expression in Sun Brain
Glioblastoma vs. Normal
P-value: 0.001
Fold change: 1.239
N: 180
CD9 Expression in Sun Brain
Glioblastoma vs. Normal
P-value: 0.011
Fold change: 1.392
N: 180
CD151 Expression in Sun Brain
Glioblastoma vs. Normal
P-value: 1.55E-15
Fold change: 4.264
N: 104
CD63 Expression in Sun Brain
Glioblastoma vs. Normal
P-value: 7.67E-13
Fold change: 1.931
N: 180
CD81 Expression in Bredel Brain 2
Glioblastoma vs. Normal
P-value: 8.79E-4
Fold change: 1.315
N: 54
CD9 Expression in Lee Brain
Glioblastoma vs. Normal
P-value: 0.015
Fold change: 2.313
N: 101
CD151 Expression in TCGA Brain
Brain Glioblastoma vs. Normal
P-value: 1.25E-7
Fold change: 2.547
N: 557
CD63 Expression in Shai Brain
Glioblastoma vs. Normal
P-value: 8.37E-9
Fold change: 3.259
N: 42
CD81 Expression in Sun Brain
Glioblastoma vs. Normal
P-value: 0.001
Fold change: 1.239
N: 180
CD9 Expression in Bredel Brain 2
Glioblastoma vs. Normal
P-value: 0.039
Fold change: 1.303
N: 54

4.2.2 Characterisation of GBM cell line derived EVs

EVs were enriched from all four GBM cell lines (U87MG, LN229, MU4 and MU41) via differential ultracentrifugation. Nanosight tracking analysis (NTA) was utilised to determine the particle size distribution of the enriched EVs (***Figure 4-2A***), as well as the approximate number of EVs released by each GBM cell line. NTA analysis revealed that the concentration range of secreted EVs was 0.6 – $1.5x10^8$ particles/ml (***Figure 4-2B***) and the majority were within a size range for small EVs (<200nm in diameter) (***Figure 4-2C***). This was further supported by the use of CryoEM of the enriched EVs (***Figure 4-2D***). Western blot analysis of GBM cell and EV lysates showed an enrichment of EV marker Alix in EV lysates from GBM cells, whilst expression of EV-negative marker Calnexin was not present in the EV lysates (***Figure 4-2E***). Internalisation of EVs was visualized using confocal microscopy which confirmed the uptake of DiI-labelled LN229 donor EVs by the recipient GBM cells (***Figure 4-2F***).

Figure 4-2: GBM cells predominantly secrete small EVs that can be internalised by recipient GBM cells

(**A**.) Representative NTA analysis graphs showing particle size distribution and concentration for EVs enriched from the serum-free conditioned medium of the following GBM cell lines: U87MG, LN229, MU4 and MU41. The EVs were enriched by differential ultracentrifugation and the resultant pellet resuspended in 60μl of PBS prior to NTA. (**B**.) The average concentration of EVs in the conditioned medium for each GBM cell line was determined using NTA and normalised to $1x10^5$ cells. (**C**.) The mode particle size, representing the diameter of the most prominent population of EVs revealed that the majority of enriched EVs are within the size range for small EVs/exosomes (30-150nm) *(n=6, each point represents the average of 5 NTA recordings; mean +/- standard deviation).* (**D**.) Cryogenic electron microscopy was utilized to analyse the morphology and size of the enriched EVs, confirming the presence of vesicles within a similar size range as determined via NTA (white arrows indicating the presence of vesicles in each image). (**E**.) Western blot analysis was undertaken on both cell (C) and EV (E) lysates from all four GBM cell lines. The presence of EV markers in the lysates were identified with positive EV marker antibody, Alix, and negative EV marker antibody, Calnexin. (**F.**) Representative confocal images of MU4 cells incubated with 5μg/ml of DiI-labelled LN229 EVs (DiI labelled EVs) or equivalent amounts of a DiI background control (DiI CTL). Following a 4h incubation, cells were washed, fixed in 4% PFA, and the nuclei stained with Hoechst. Internalised EVs within the can be observed as fluorescent red dots. (Scale bars represented as white lines in the bottom right of each image = 10μm).

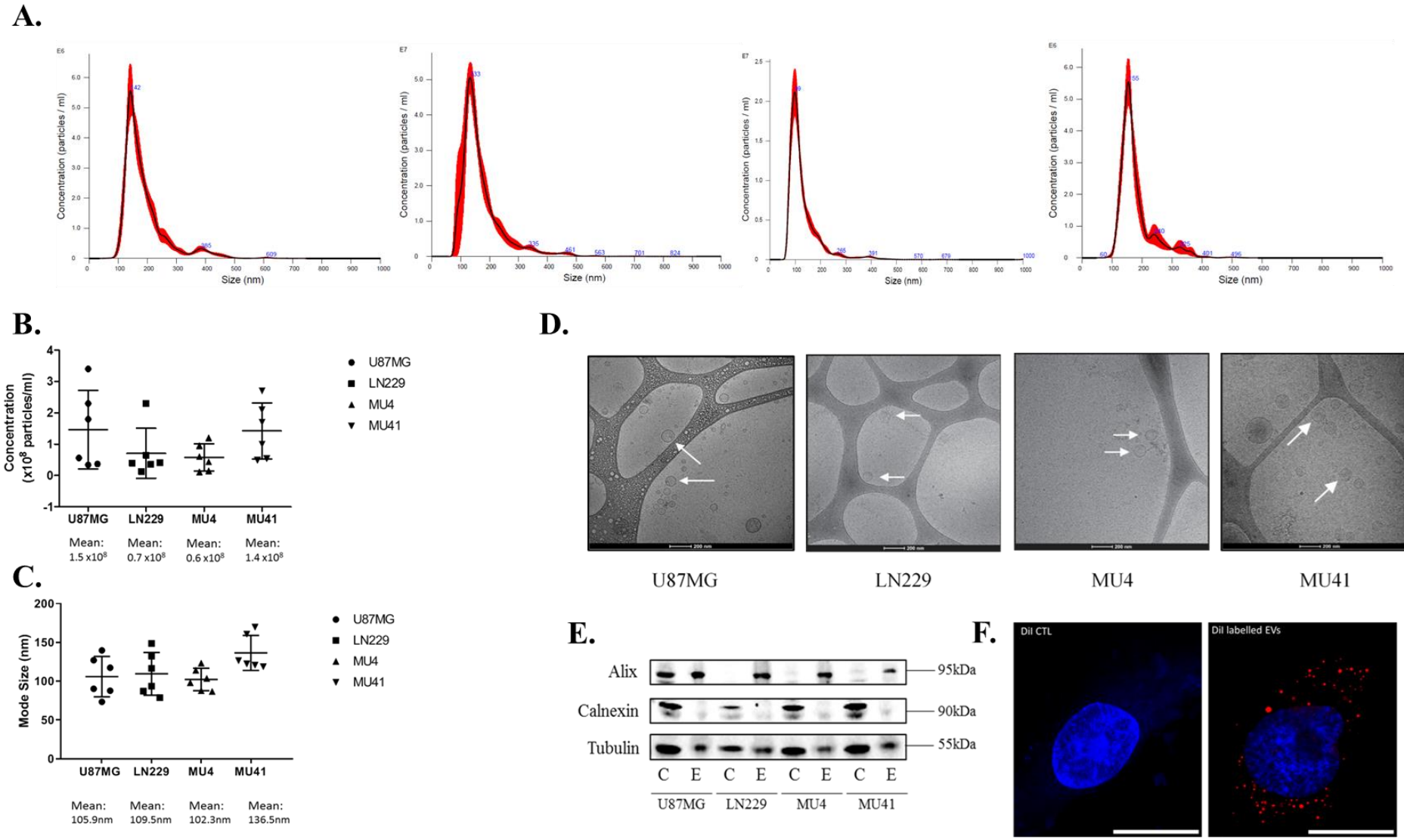
A.
Concentration (particles / ml)
Size (nm)
B.
Concentration (x10^8 particles/ml)
U87MG
LN229
MU4
MU41
Mean: 1.5 x10^8
Mean: 0.7 x10^8
Mean: 0.6 x10^8
Mean: 1.4 x10^8
C.
Mode Size (nm)
Mean: 105.9nm
Mean: 109.5nm
Mean: 102.3nm
Mean: 136.5nm
D.
U87MG
LN229
MU4
MU41
E.
Alix
Calnexin
Tubulin
95kDa
90kDa
55kDa
C E C E C E C E
U87MG LN229 MU4 MU41
F.
DiI CTL
DiI labelled EVs

4.2.3 Investigating the transfer of a pro-invadopodia phenotype via GBM-EVs

4.2.3.1 Donor LN229 GBM-EVs can promote a pro-invasive phenotype in recipient GBM cells

Zymographic analyses were utilized to investigate the presence and activity of gelatinolytic MMPs in GBM cell derived EVs. MMP-2 was detected in the EVs from all four GBM cell lines in both the pro- and cleaved (or active) form (***Figure 4-3A-B***). LN229-dervied EVs displayed the overall highest MMP-2 levels, whilst MU4-dervied EVs contained the least MMP-2, corresponding with the secreted MMP-2 levels of these cell lines (***refer to Figure 3-2***).

In addition to small EVs such as exosomes, MMP-2 may also be packaged into other EV subtypes, including microvesicles (MVs) [307]. Zymographic analysis was conducted with the two vesicle subtypes (EV and MV) derived from LN229 GBM cells, as well as the cell lysate and conditioned media (CM) (***Figure 4-3C-D***). MMP-2 levels were present at higher levels in small EVs compared to MVs. Furthermore, elevated levels of active-MMP-2 were detected in EVs compared to MVs and CM. It is possible that the enriched CM contains MMP-2 activity from two sources: freely secreted proteases from invadopodia and secreted EVs (with MMP-2 cargo) working in tandem in promoting a pro-invasive environment. The detection of MMP-2 in EVs and MVs could indicate that EVs may be capable of transferring this invadopodia-related ECM degrading protease from donor to GBM recipient cells in preparation for the recipient cells to form invadopodia.

Figure 4-3: MMP-2 is present in GBM cell line EV cargo

(**A.**) Zymographic analysis revealed the presence of MMP-2 in EVs enriched via differential ultracentrifugation (100,000xg) from U87MG, LN229, MU4 and MU41 cells. Loading volumes were normalised to particle count as determined using NTA and zymograms are representative of three experiments. (**B.**) Densitometry analysis on represented bands shown in ***A***. *(n=3 experiments; mean ± SD)* (**C.**) Zymographic analysis of LN229 cell lysate, conditioned media (CM), enriched small EVs (enriched at 100,000xg) and MVs (enriched at 10,000xg). Loading volumes were normalised to 20µg of protein for each sample and zymograms are representative of three experiments. (**D.**) Densitometry analysis on represented bands shown in ***C***. *(n=3 experiments; mean ± SD).*

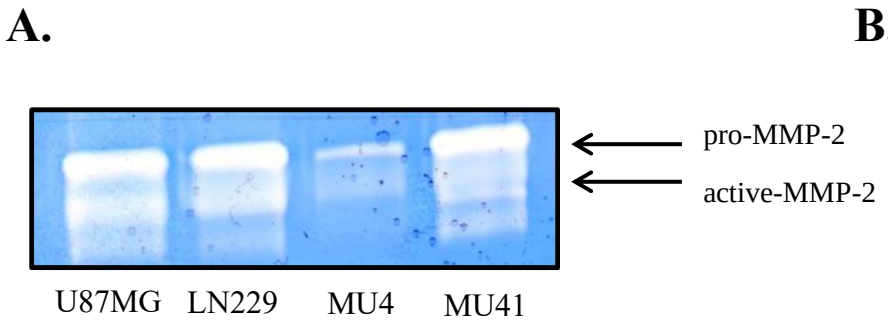
A.
pro-MMP-2
active-MMP-2
U87MG
LN229
MU4
MU41

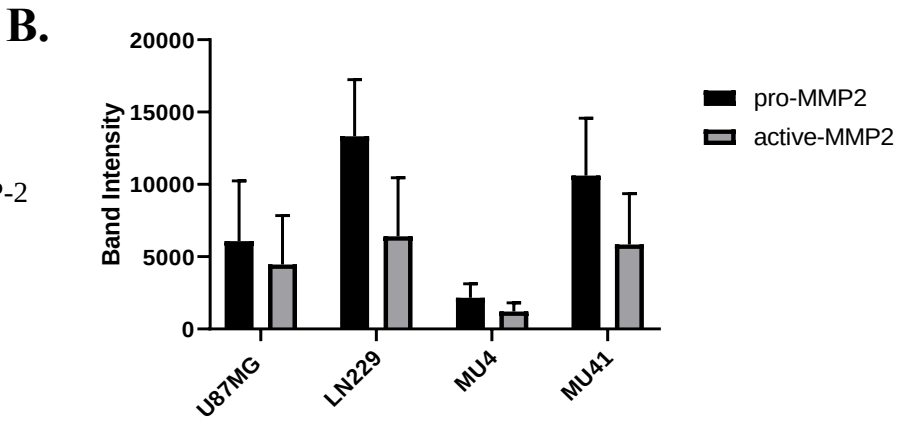
B.
Band Intensity
20000
15000
10000
5000
0
U87MG
LN229
MU4
MU41
pro-MMP2
active-MMP2

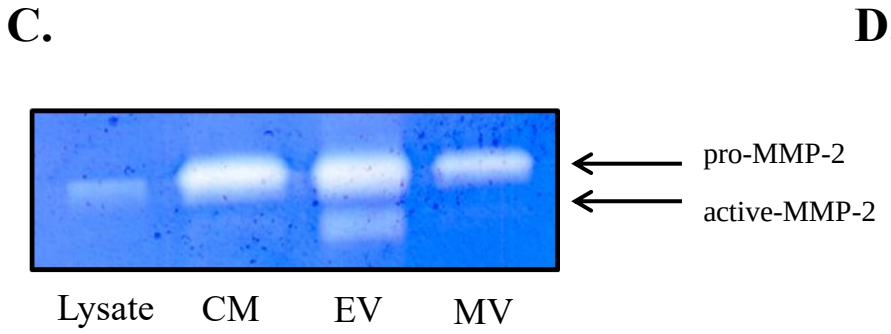
C.
pro-MMP-2
active-MMP-2
Lysate
CM
EV
MV

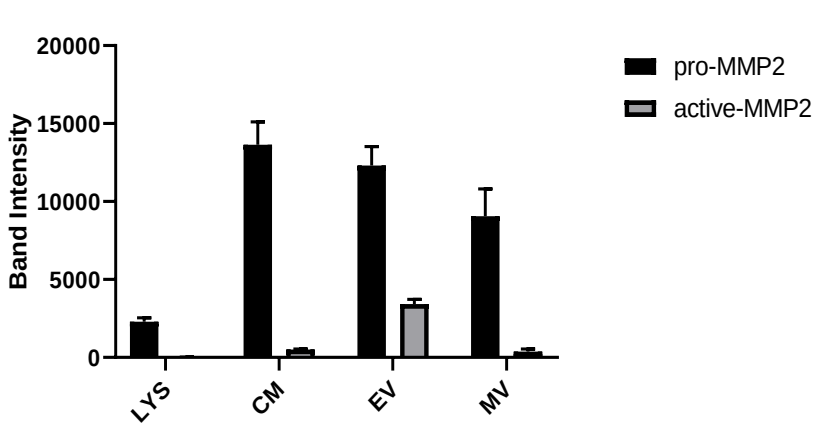
D.
Band Intensity
20000
15000
10000
5000
0
LYS
CM
EV
MV
pro-MMP2
active-MMP2

The ability for GBM cell-derived EVs to transfer a pro-invadopodia (matrix-degrading) phenotype to recipient GBM cells was next investigated. To determine the impact of EVs enriched from donor GBM cells on recipient GBM cell MMP-2 secretion, GBM cells were incubated with the enriched LN229 donor EVs (in serum free OptiMEM medium) for 24h before the media was replaced with fresh serum-free OptiMEM media to remove any remaining EVs not internalized by the recipient cells. The impact of the LN229 donor cell EVs (a cell line with high basal invadopodia-mediated FITC-gelatin degrading activity) was compared to EVs enriched from MU4 donor cells (low basal invadopodia-mediated FITC-gelatin degrading activity). Zymographic analysis of recipient GBM cells incubated with LN229-EVs revealed an increase in MMP-2 secretion and activation (***Figure 4-4A-C***), whilst MU4-EVs had no impact on MMP-2 secretion in the recipient cells (***Figure 4-4D-E***). Invadopodia-mediated FITC-gelatin degradation was also observed to increase across all four cell lines following incubation with LN229-EVs (***Figure 4-5***).

To establish whether the changes in MMP-2 secretion and FITC-gelatin degradation following the addition of enriched LN229-EVs were due to an increase in invadopodia formation, total- and active-actin puncta were quantified using the confocal images generated in ***Figure 4-5.*** A significant ($p<0.05$) increase in the total number of actin puncta and the number of actively degrading actin puncta was observed for recipient U87MG, MU4 and MU41 cell lines following incubation with LN229-EVs (***Figure 4-6***). These results indicate that EVs from donor cells with high invadopodia activity, such as LN229, may be able to transfer a pro-invadopodia phenotype to recipient GBM cells.

Figure 4-4: Donor LN229 GBM cell line EVs promote increased MMP-2 secretion in recipient GBM cells

EVs were incubated with the GBM cells (serum-free OptiMEM) in a 6-well plate at a final EV protein concentration of 25μg/ml. After a 24h incubation, cells were washed, and media was replaced with fresh serum-free OptiMEM and incubated for a further 24h before harvesting for analysis. (**A**.) NTA of LN229 EVs is shown, mode size of EVs was determined to be 79nm. (**B.**) Zymographic analysis of harvested serum-free conditioned medium showing the MMP-2 secretion profile of GBM cells with (+EVs) and without (-EVs) the addition of LN229 cell line EVs. Sample loading volumes were standardised using the protein concentration from the corresponding cell lysates. (**C.**) Densitometric analysis of pro- and active- MMP-2 bands is shown and represented as fold change relative to control cells. (*n=3 experiments; mean ± SD, *p<0.05; **p<0.01; unpaired two-tailed student's t-test*). (**D.**) NTA of EVs from MU4 cells is shown, mode size of EVs was determined to be 112nm. (**E.**) Zymographic analysis of harvested serum-free conditioned medium showing the MMP-2 secretion profile of GBM cells with (+EVs) and without (-EVs) the addition of MU4 cell line EVs. Sample loading volumes were standardised using the protein concentration from the corresponding cell lysates. (**F.**) Densitometric analysis of pro- and active- MMP-2 bands is shown and represented as fold change relative to control cells. (*n=3 experiments; mean ± SD, non-significant =ns, unpaired two-tailed student's t-test*).

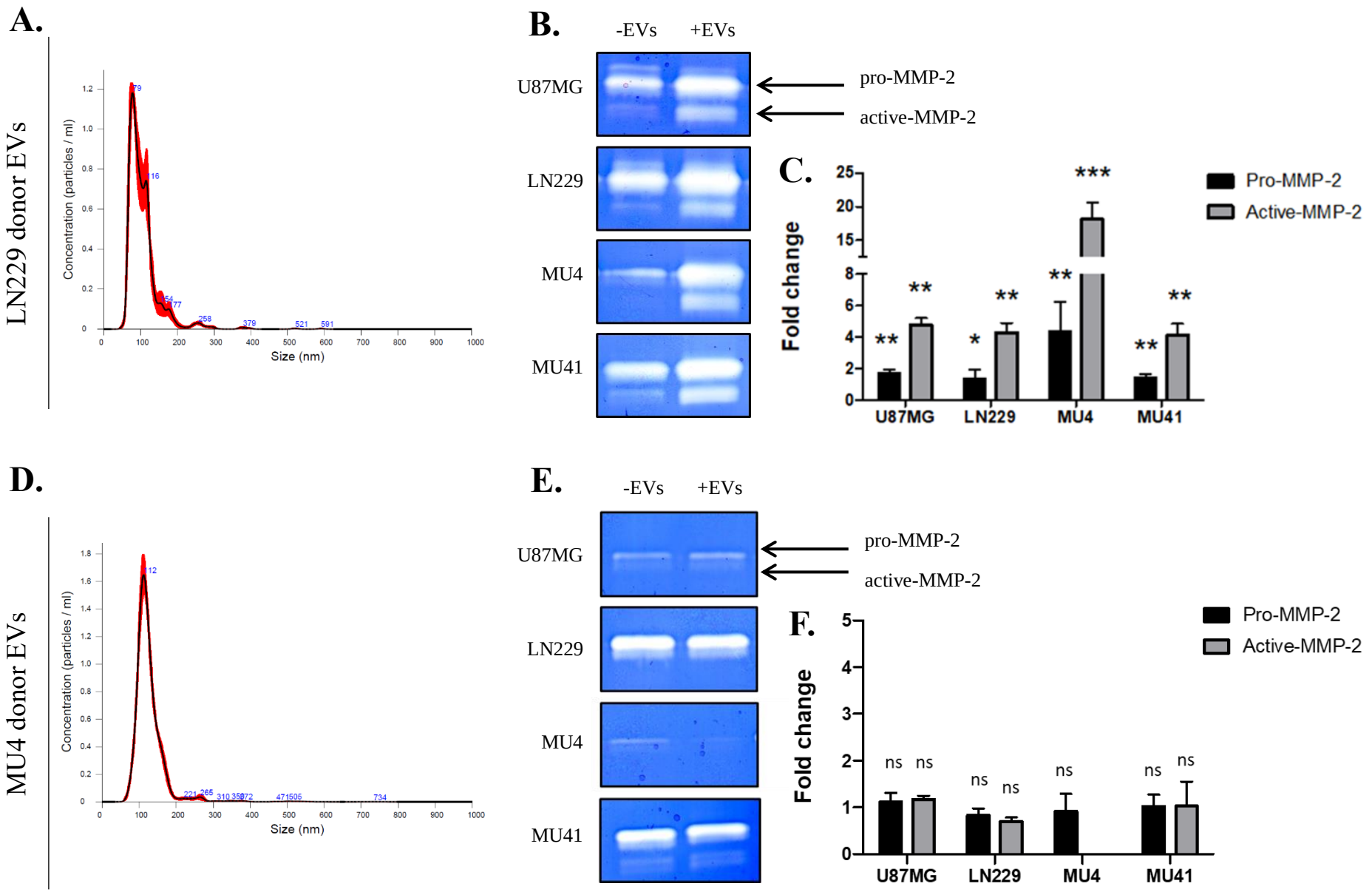
A.
LN229 donor EVs
Concentration (particles / ml)
Size (nm)
B.
-EVs
+EVs
U87MG
LN229
MU4
MU41
pro-MMP-2
active-MMP-2
C.
Fold change
Pro-MMP-2
Active-MMP-2
U87MG
LN229
MU4
MU41
D.
MU4 donor EVs
Concentration (particles / ml)
Size (nm)
E.
-EVs
+EVs
U87MG
LN229
MU4
MU41
pro-MMP-2
active-MMP-2
F.
Fold change
Pro-MMP-2
Active-MMP-2
ns
U87MG
LN229
MU4
MU41

Figure 4-5: Donor LN229 GBM cell line-EVs promote increased invadopodia mediated FITC-gelatin degradation in recipient GBM cells

(**A.**) NTA of EVs enriched from the conditioned medium of LN229 GBM cells indicate a mode size of 131nm. (**B**.) Representative confocal images of the GBM cell lines U87MG, LN229, MU4 and MU41 displaying significantly enhanced FITC-conjugated gelatin degradation when pre-incubated for 24h with 25μg/ml of LN229-cell line derived EVs in OptiMEM (+EVs) (prior to seeding on FITC-gelatin) compared to control GBM cells incubated in OptiMEM alone (-EVs). (**C**.) Images were analysed using Image J (1.51f) to determine the level of FITC-gelatin degradation. A total of 5-10 random images per experiment across 3 independent experiments were acquired for each cell line and the area of degradation was quantified to the number of cells present (indicated by the DAPI staining). (*n=3 experiments; mean ± SD, *p<0.05; **p<0.01, unpaired two-tailed student's t-test*). (Scale bar=20μm).

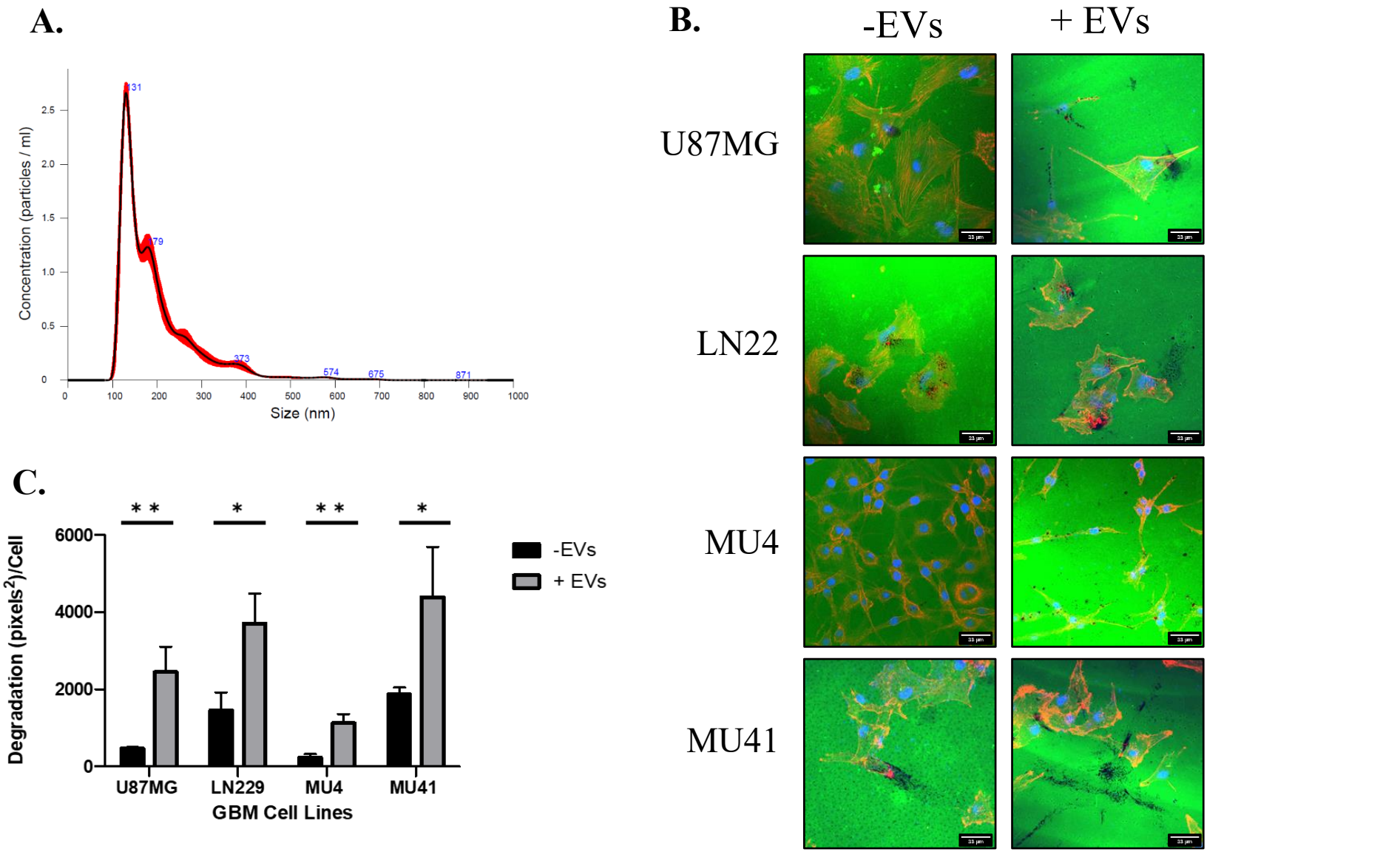
A.
Concentration (particles / ml)
Size (nm)
131
79
373
574
675
871
B.
-EVs
+ EVs
U87MG
LN22
MU4
MU41
C.
Degradation (pixels²)/Cell
-EVs
+ EVs
U87MG
LN229
MU4
MU41
GBM Cell Lines

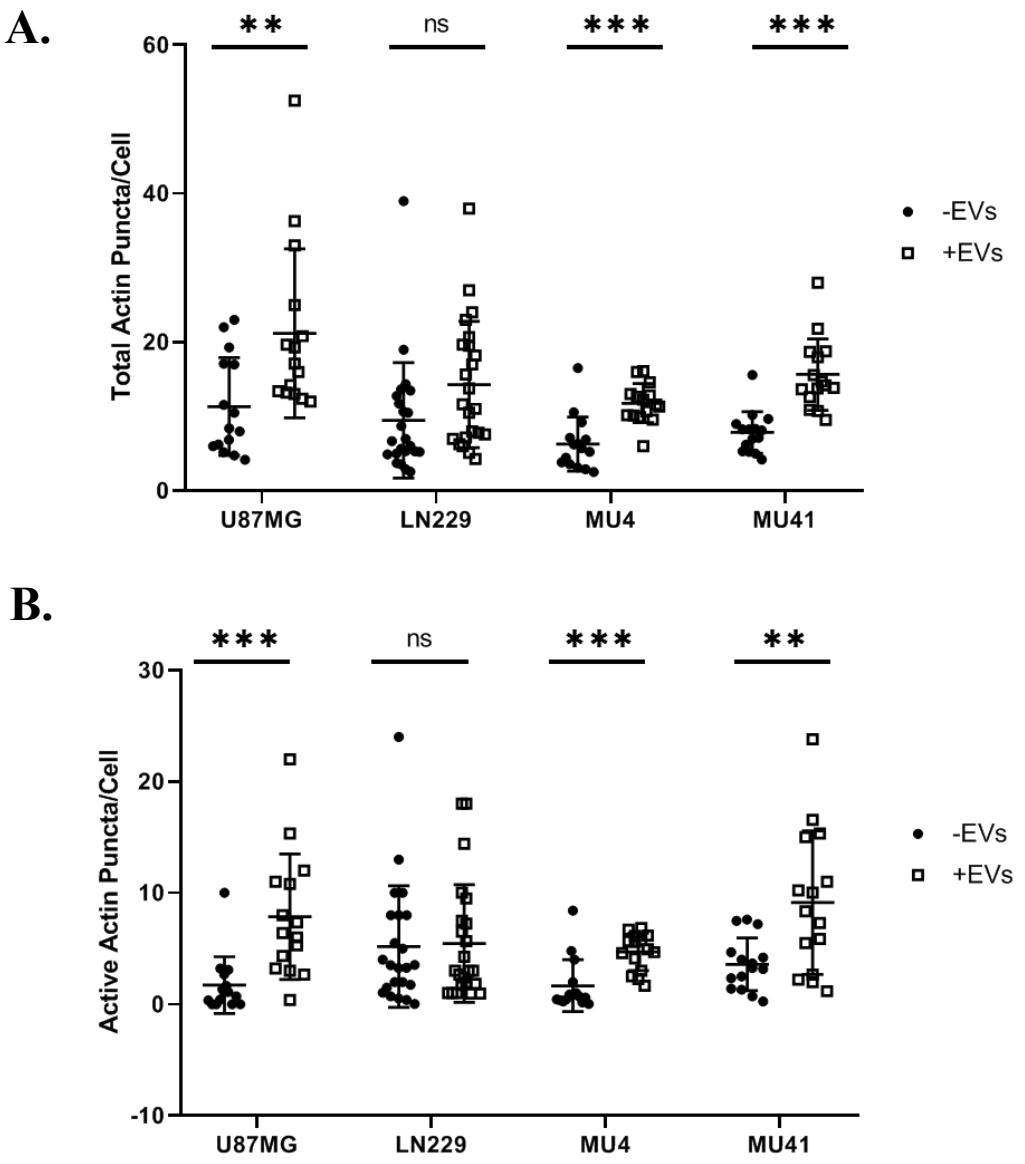

Figure 4-6: Donor LN229 GBM cell line-EVs alter invadopodia formation and activity in recipient GBM cells

Graphical representation of (**A**.) the total number of actin puncta per cell and (**B**.) the number of actin puncta overlapping with degraded FITC-gelatin in GBM cells following incubation with LN229 GBM cell line-EVs in OptiMEM (+EVs) (prior to seeding on FITC-gelatin) compared to control GBM cells incubated in OptiMEM alone (-EVs). A total of 5-10 random images per experiment across 3 independent experiments were acquired for each cell line and were analysed using a customised script written for Image J (1.53a), and actin puncta were normalised to the number of cells present (as indicated by DAPI staining). *(n=3 experiments; mean ± SD, *p<0.05; **p<0.01; ***p<0.001, ns= not significant, unpaired two-tailed student's t-test).*

4.2.3.2 LN229 GBM cell EVs alter miRNA expression in recipient GBM cells

Emerging focus on miRNAs as regulators of post-transcriptional gene expression has highlighted their important role in a number of oncogenic processes, including invasion and migration [474]. To identify changes in miRNA expression that may contribute to the enhanced invadopodia-mediated matrix degrading activity, Nanostring® technology (nCounter Human V3 miRNA Array) was utilized to investigate changes in miRNA expression in recipient MU4 cells (which demonstrate low basal invadopodia-mediated FITC-gelatin degrading activity) following the addition of donor LN229-EVs. Examination of only miRNAs above a detection threshold of 100 transcript counts revealed a decrease in the expression of 34 miRNAs in recipient MU4 cells following a 24h incubation with LN229-EVs (***Figure 4-7***). The online databases, MirTarBase (experimentally validated targets) and miRDB (predicted targets) were utilized to identify invasion related targets for the 34 miRNAs. Regulators of invadopodia formation and/or activity were identified including MMP-2, MMP-9, GRB2, SH3PXD2A (TKS5), WASL (N-wasp) and SRC (***Table 4-1***). A target score threshold of 95 was set for miRDB, meaning that there is a high degree of probability that there is an association between the miRNA and the predicted targets.

Figure 4-7: Donor LN229 GBM cell line-EVs reduce expression levels of miRNA with pro-invasive targets in recipient MU4 GBM cells

(**A.**) NTA of EVs enriched from the conditioned medium of LN229 GBM cells indicate a mode size of 121nm. (**B**.) MU4 cells were incubated with LN229 GBM cell line-EVs (25μg/mL) in OptiMEM for 24h. Media was then replaced with fresh serum-free OptiMEM for a further 24h prior to harvesting the recipient GBM cells. RNA was then extracted for Nanostring® analysis using the nCounter Human V3 miRNA Array. miRNAs above a normalized detection threshold of 100 transcript counts were included in the analysis. The expression levels of 34 miRNAs were observed to decrease by greater than 1.5-fold (***Table 4-1***) in MU4 cells incubated with LN229 GBM cell line EVs (+EVs) compared to the control cells in OptiMEM alone (-EVs), as indicated by the miRNA transcript counts.

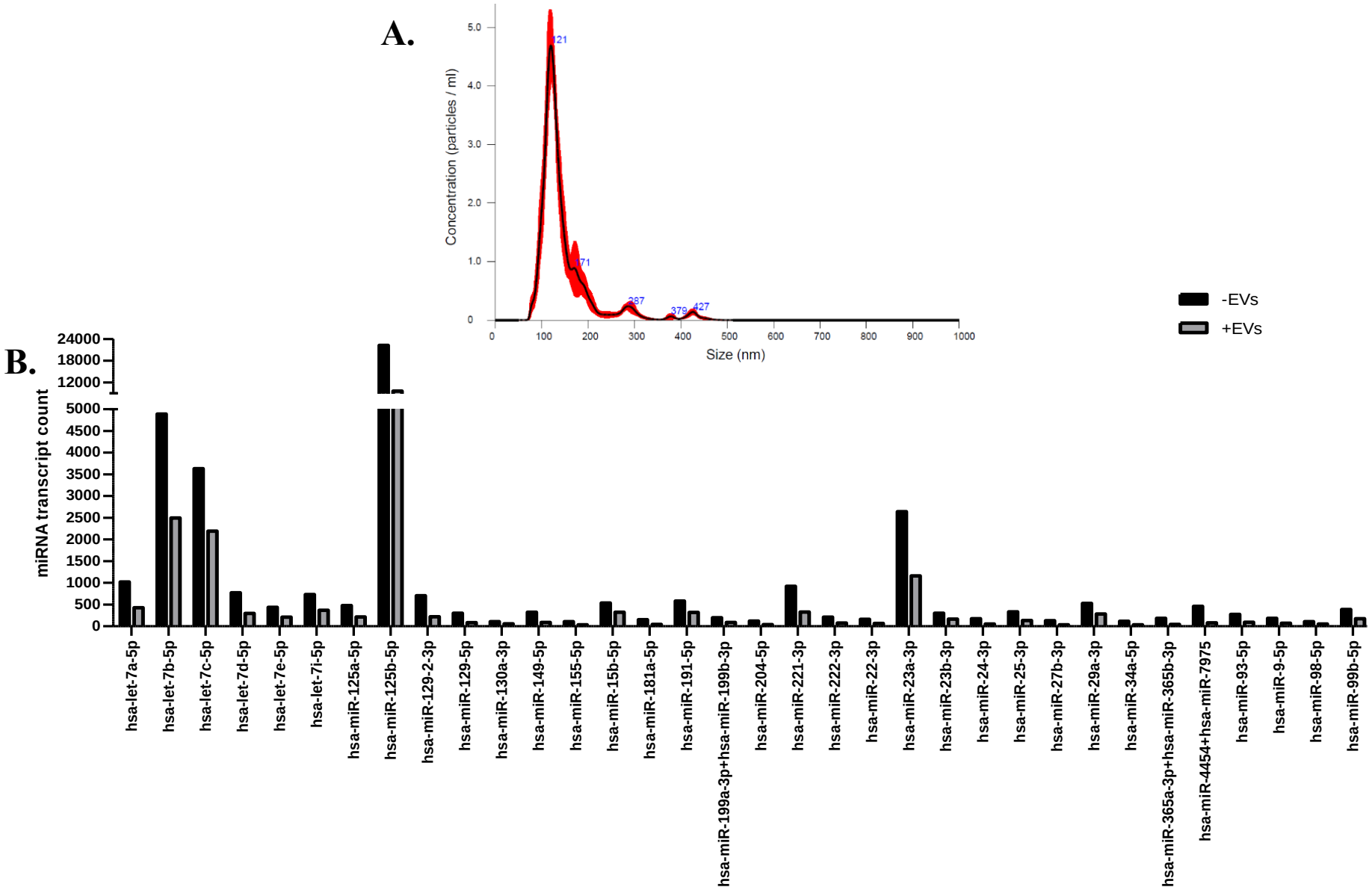
A.
Concentration (particles / ml)
Size (nm)
121
171
287
379
427
B.
miRNA transcript count
-EVs
+EVs
hsa-let-7a-5p
hsa-let-7b-5p
hsa-let-7c-5p
hsa-let-7d-5p
hsa-let-7e-5p
hsa-let-7i-5p
hsa-miR-125a-5p
hsa-miR-125b-5p
hsa-miR-129-2-3p
hsa-miR-129-5p
hsa-miR-130a-3p
hsa-miR-149-5p
hsa-miR-155-5p
hsa-miR-15b-5p
hsa-miR-181a-5p
hsa-miR-191-5p
hsa-miR-199a-3p+hsa-miR-199b-3p
hsa-miR-204-5p
hsa-miR-221-3p
hsa-miR-222-3p
hsa-miR-22-3p
hsa-miR-23a-3p
hsa-miR-23b-3p
hsa-miR-24-3p
hsa-miR-25-3p
hsa-miR-27b-3p
hsa-miR-29a-3p
hsa-miR-34a-5p
hsa-miR-365a-3p+hsa-miR-365b-3p
hsa-miR-4454+hsa-miR-7975
hsa-miR-93-5p
hsa-miR-9-5p
hsa-miR-98-5p
hsa-miR-99b-5p

Table 4-1: Invasion-related targets of miRNAs with reduced expression in MU4 cells following incubation with LN229 GBM cell line EVs

miRNA species	Strongly Validated	Weakly Validated	Predicted >95 target score	Fold change
hsa-miR-4454+hsa-miR-7975	–	–	–	-5.741
hsa-miR-365a-3p+hsa-miR-365b-3p	IL6, **KRAS**, RHOH	**AKT1**, THBS2	–	-4.107
hsa-miR-149-5p	IL6	ADAM17	–	-3.679
hsa-miR-129-5p	–	ADAMTS4, ADAM17, ADAM12, FIGN	–	-3.585
hsa-miR-27b-3p	**EGFR**, MET, MMP13, THBS1, THBS2	ADAMTS5**, WASL**	ADAMTS10	-3.555
hsa-miR-181a-5p	KRAS, PTEN, NRAS, STAT3	ADAM17, **RHOG**	ADAM11, FIGN, IL2,	-3.422
hsa-miR-24-3p	IL4, IL18, **MMP14**, MYC, **SH3PXD2A**, TP53	ADAM17	–	-3.330
hsa-miR-155-5p	MMP16, MYC, **RHOA**, **SH3PXD2A**, STAT1	ADAM10, ADAMTS4, STAT3	–	-3.294
hsa-miR-129-2-3p	MYC	THBS2	–	-3.183
hsa-miR-34a-5p	**CD44**, IL10, MET, MMP7, MYC, TP53, VEGFA	**CTTN,** STAT1	–	-3.137
hsa-miR-204-5p	IL11, JAK2, **MMP9**	MMP3	–	-3.011
hsa-miR-93-5p	PTEN, MMP3, MYC, **RHOC**	**GRB2, SH3PXD2A**, TSG101, STAT3, **WASL**	–	-2.946
hsa-miR-221-3p	ADAM1A**, MMP2, PAK1, PTEN**, STAT5A	**RHOA**		-2.800
hsa-miR-222-3p	ADAM1A, **GRB10**, MMP1, **PTEN**, P53, STAT5A,	–	–	-2.774
hsa-miR-9-5p	IL6, MMP13, **MMP2**, **MMP9**	–	–	-2.657
hsa-let-7d-5p	IL13	FIGN, THBS1, **WASL**	ADAMTS8, FIGNL2	-2.594
hsa-miR-25-3p	MYC, **PTEN**, TP53	**WASL**	ADAM19	-2.510
hsa-miR-22-3p	**BSG**, **CD151**, **PTEN**	–	–	-2.471
hsa-let-7a-5p	**EGFR**, IL2, **KRAS**, THBS1	COL8A1, FIGN, **WASL**	ADAMTS8, COL3A1, COL1A2, FIGN, TGFBR1	-2.375

hsa-miR-125b-5p	**CD44, EGFR,** MMP-13**, MMP-2,** MMP-26**,** TP53	ADAMTS1	RAB3D	-2.315
hsa-miR-23a-3p	SMAD3, STAT3	–	MET, STAT5B, TGFBR2	-2.279
hsa-miR-99b-5p	–	–	–	-2.232
hsa-miR-199a-3p+hsa-miR-199b-3p	MET	–	ADAM10, ADAMTS3, SERPINE2	-2.224
hsa-miR-125a-5p	ADAM9, **AKT1**, DOCK3, **EGFR**, JAK2, MMP11, MTOR, SMAD2, SMAD4, STAT3, VEGFA	–	–	-2.196
hsa-let-7e-5p	**MMP9**	FIGN, STAT3, THBS1, **WASL**	FIGNL2, NRAS	-2.099
hsa-miR-98-5p	IL10, IL6, MYC, NRAS, THBS1	FIGN, **WASL**	ADAMTS8	-2.027
hsa-let-7i-5p	IL13, IL2	FIGN, TGFBR3, THBS1, STAT2, **WASL**	ADAMTS8, FIGNL2, TGFBR1	-1.984
hsa-let-7b-5p	–	**KRAS**, RAB38**, RHOB, RHOG,** THBS1	ADAMTS8, COL1A2, COL3A1, FIGN, TGFBR1/3	-1.961
hsa-miR-130a-3p	MET, MYC, **PTEN**	**GRB10, WASL**	–	-1.882
hsa-miR-29a-3p	ADAM12, ADAMTS9, **CDC42, ITGA6, ITGB1, MMP2**, MYC, **PTEN,** VEGFA	TGFB3	ADAMTS17, ADAMTS7, **SH3PXD2A**	-1.856
hsa-miR-23b-3p	MET, **PTEN**, **SRC**, VCAN	ADAM17, ADAM28, DOCK4, VCAM1	ADAM23, STAT5B, TGFBR2	-1.836
hsa-miR-191-5p	–	–	–	-1.811
hsa-let-7c-5p	IL6, IL10, MTOR, MYC, STAT3, TGFBR1	STAT2, VCAM1, **WASL**	–	-1.655
hsa-miR-15b-5p	**MMP9**	**BSG**	–	-1.650

Experimentally validated (as listed in the MirTarBase database) and predicted (as listed in the miRDB database) invasion-related targets of the 34 downregulated miRNAs in MU4 cells incubated with LN229 cell line EVs. Targets linked to invadopodia activity are highlighted in bold. *Strongly validated methods: reporter assays, western blot and qPCR. Weakly validated methods: microarray, NGS, and pSILAC. All predicted targets are listed above a target score of 95, indicating that predicted targets are highly likely to bind to the listed miRNA. miRNAs are listed in order of greatest fold change.*

4.2.3.3 DMA treatment reduces EV secretion and FITC-gelatin degrading activity of invadopodia in GBM cells

Exosome secretion can be initiated by an intracellular increase of calcium (Ca^{2+}) [475]. Dimethyl amiloride (DMA) is an ion channel blocker capable of blocking H^+/Na^+ and Na^+/Ca^{2+} channels which serve to regulate intracellular Ca^{2+} concentrations, and is therefore understood to reduce exosome secretion triggered by an increase in intracellular Ca^{2+} [475-477] . To validate that DMA treatment can impact EV secretion, the GBM cell lines were pre-treated for 24h with increasing concentrations of DMA and subsequently the concentration of secreted EVs was analysed using NTA. It can be observed that DMA treatment impaired EV secretion in a concentration-dependent manner, without altering the size distribution of EVs released (***Figure 4-8***).

As we had earlier demonstrated that LN229 EVs caused an increase in the invadopodia-mediated FITC-gelatin degradation by the recipient GBM cells and as DMA treatment reduced GBM cell line EV secretion, the impact of DMA treatment on invadopodia-mediated FITC-gelatin degradation was subsequently examined. LN229 cells were chosen due to their high matrix-degrading ability and were incubated for 24h with increasing concentrations of DMA prior to seeding onto FITC-gelatin coated coverslips for a further 24h. Reduced FITC-gelatin degrading activity was observed with increasing concentrations of DMA (***Figure 4-9B***), as well as a reduction in the percentage of LN229 cells that exhibited FITC-gelatin degrading activity (***Figure 4-9C***).

Interestingly, there was no change in the total number of actin puncta that formed per cell across the DMA concentration range (***Figure 4-10A***), however there was an observed reduction in the number of actively degrading actin puncta (***Figure 4-10B***). This indicates that DMA inhibiting EV secretion may impact on an autocrine mechanism whereby the secreted EVs may contribute to the maintenance of invadopodia activity by the donor cell, especially as MMP recruitment and subsequent secretion and ECM degradation is observed during stage II and stage III of the invadopodia life cycle (Cmoch reference). In addition, this data is in agreement with the hypothesis that invadopodia may serve also as

additional sites of exosome release in GBM cells, as proposed in a study investigating exosome release in head and neck squamous cell carcinoma [229].

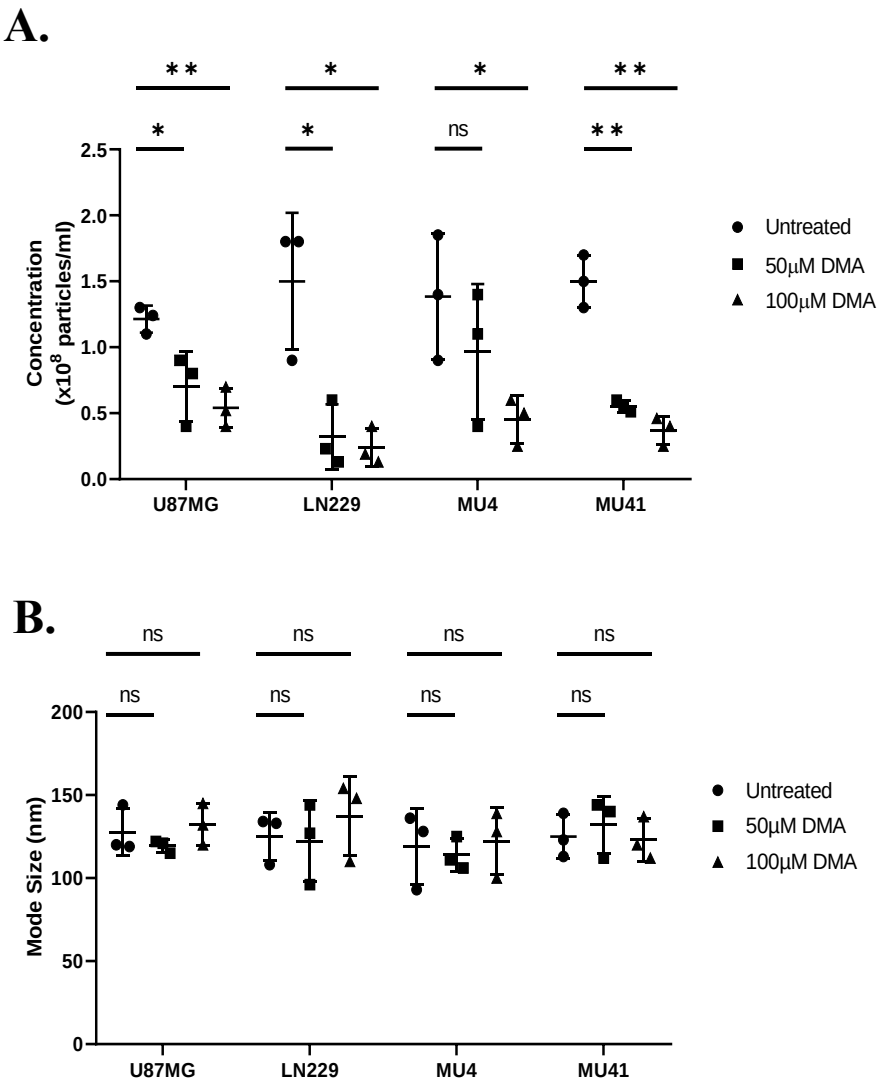

Figure 4-8: Increasing concentrations of DMA reduces GBM cell line EV secretion

GBM cells were pre-treated with varying DMA concentrations (0μM, 50μM or 100μM) in triplicate wells in serum-free media for 24h prior to NTA of the conditioned medium (A.) The concentration of EVs was observed to decrease with increasing concentrations of DMA (normalised to 1 x 10^5 cells). (B.) The mode size of EVs did not alter with the varying DMA concentrations. Cell debris was removed from conditioned media via centrifugation, and further centrifugation (2000xg -15 min, 3166xg -15 min, 10,000xg -1.5h) was carried out to obtain a concentrated sample of EVs. (*n=3 experiments each performed in triplicate; mean ± SD, *p<0.05, **p<0.01, non-significant =ns, unpaired two-tailed student's t-test).*

Figure 4-9: DMA treatment reduces invadopodia mediated FITC-gelatin degradation in LN229 GBM cells

(**A**.) Representative confocal images of FITC-gelatin degradation assays conducted with LN229 GBM cells and increasing concentrations of DMA (0μM, 25μM, 50μM, 100μM- 24h incubation prior to seeding on FITC-gelatin). A total of 5 random images were acquired for each condition in each experiment and the area of FITC-gelatin degradation was quantified to the number of cells present (indicated by the DAPI staining). (*Scale bars = 20μm*). (**B.**) The images were analysed using Image J (1.51f) indicating a reduction in FITC-gelatin degradation per cell with an increase in DMA concentration, as well as (**C**.) a reduction in the percentage of cells that overlapped with degraded gelatin. Graphs represent the average fold changes relative to untreated LN229 cells (0μM of DMA). *(n=3 experiments, *p<0.05; ***p<0.001, non-significant =ns, unpaired two-tailed student's t-test).*

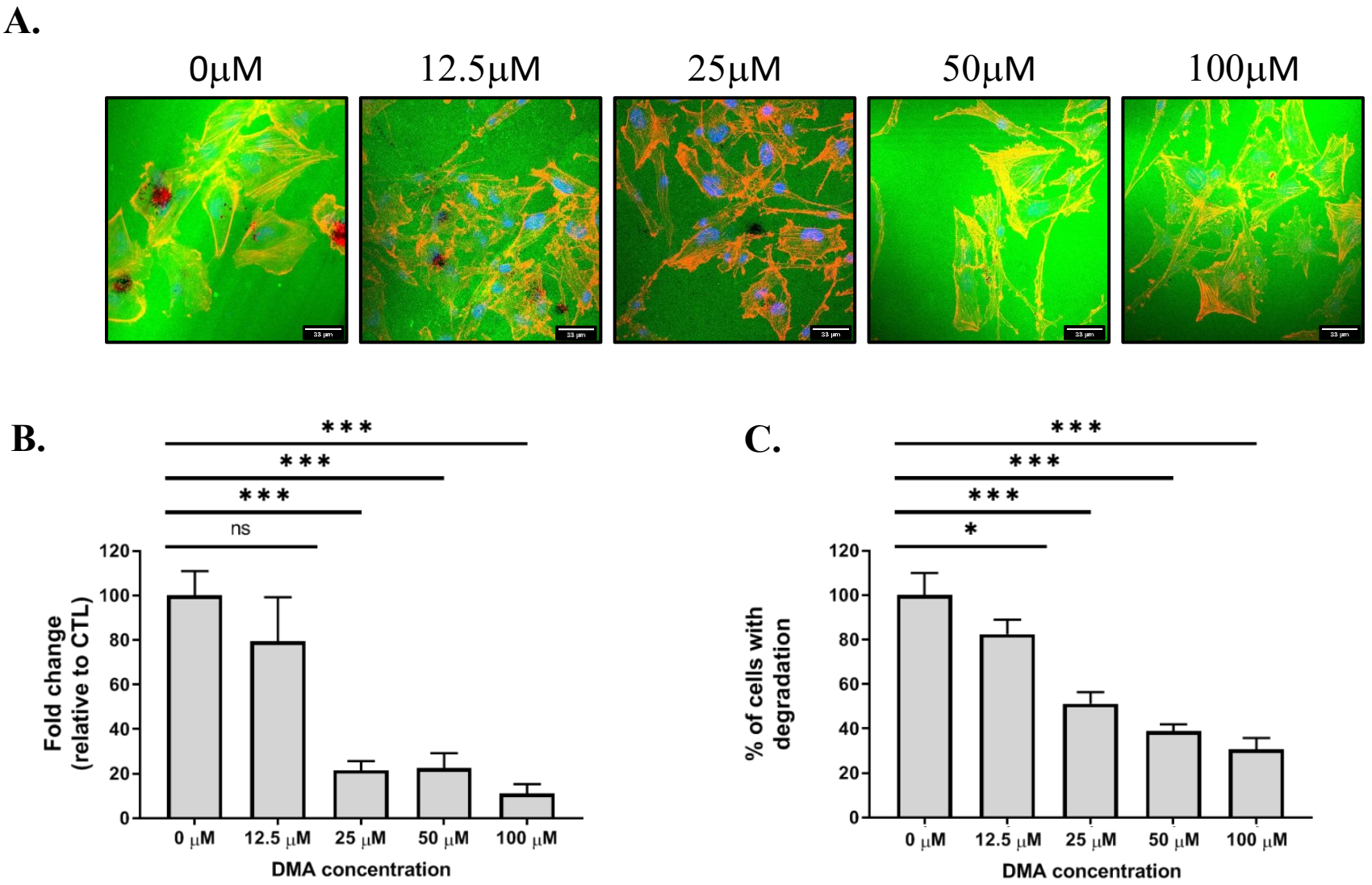
A.
0μM
12.5μM
25μM
50μM
100μM
B.
***
***
***
ns
Fold change (relative to CTL)
120
100
80
60
40
20
0
0 μM
12.5 μM
25 μM
50 μM
100 μM
DMA concentration
C.
***
***
***
*
% of cells with degradation
120
100
80
60
40
20
0
0 μM
12.5 μM
25 μM
50 μM
100 μM
DMA concentration

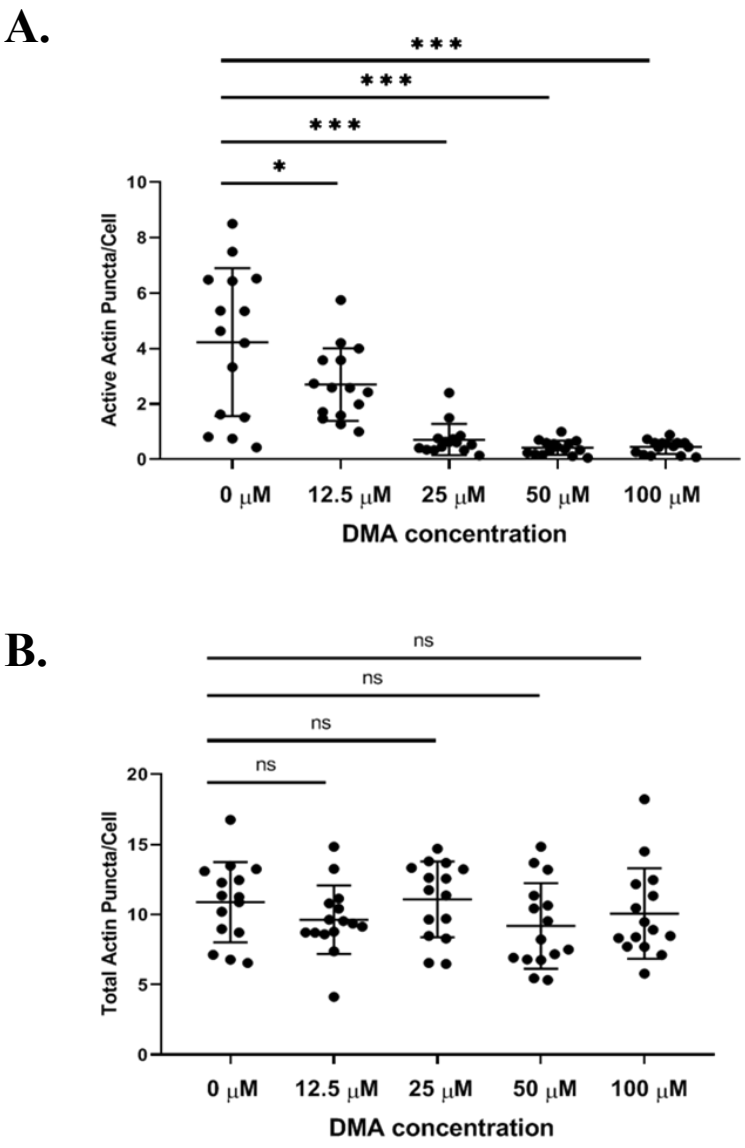

Figure 4-10: DMA impacts invadopodia activity and not total numbers

(**A.**) Further analysis of the sequence of images acquired for the analysis in ***Figure 4-8,*** revealed that DMA treatment did not significantly alter the total number of invadopodia irrespective of the DMA concentration (0μM, 12.5μM, 25μM, 50μM or 100μM). (**B.**) The number of actin puncta overlapping with degraded FITC-gelatin was observed to decrease with increasing concentrations of DMA treatment. Images were analysed using a customised script written for Image J (1.51f), and the number of actin puncta were normalised to the number of LN229 cells present (as indicated by DAPI staining). *(n=3 experiments; mean ± SD, * p<0.05; ***p<0.001, non-significant =ns, unpaired two-tailed student's t-test).*

4.2.4 Investigating the impact of RT/TMZ treatment on GBM cell line derived EVs

4.2.4.1 RT/TMZ treatment increases EV secretion from GBM cells

As the current therapeutic approach consisting of RT and TMZ may potentially enhance the invasive potential of surviving GBM cells through an increase in invadopodia activity, the impact of RT/TMZ treatment on the secretion of GBM cell derived EVs was next investigated. GBM cell lines were treated with 2Gy of RT and 50μM of TMZ and NTA was utilized to examine the concentration of EVs secreted into the serum-free medium at 24h post-treatment. All cell lines displayed an increase in EV secretion following single RT/TMZ treatment (***Figure 4-11A***), correlating with enhanced invadopodia activity. The modal size of EVs did not differ significantly between untreated and treated GBM cells and remained largely within a small-EV or 'exosome' size range (50-200nm), suggesting that a single RT/TMZ treatment does not alter the size of the EV subtype that is secreted (***Figure 4-11B***). This experiment was repeated with LT treated cell lines, which again revealed an increase in EV secretion from all GBM cell lines following LT treatment (***Figure 4-11C***), with no significant changes in size distribution of the untreated and LT treated GBM cell derived EV populations (***Figure 4-11D***).

Figure 4-11: GBM cell line EV secretion increases following RT/TMZ treatment

(**A.**) A graphical representation of EV concentration in the serum-free conditioned media of untreated and single RT/TMZ (2Gy/50μM) treated GBM cell lines, showing an increase in EV secretion following treatment. Cell debris was removed by centrifugation prior to NTA. Each experiment was performed in triplicate and the concentration of EVs per group was normalised to 1 x 10^5 cells. (**B.**) The corresponding modal size of EVs released post-single treatment remained unaltered (100-150nmn range). (**C.**) A graphical representation of EV concentration in the serum-free conditioned media of untreated and LT treated GBM cell lines, indicating that repeated (LT) RT/TMZ treatment of GBM cell lines results in enhanced EV secretion. Each experiment was performed in triplicate and the concentration of EVs per group was normalised to 1 x 10^5 cells. (**D**.) The corresponding modal size indicates that there is no significant change in EV size following a single or multiple RT/TMZ treatments of GBM cell lines.*(n=3 experiments each performed in triplicates; mean ± SD, *p<0.05; **p<0.01; ***p<0.001, non-significant =ns, unpaired two-tailed student's t-test).*

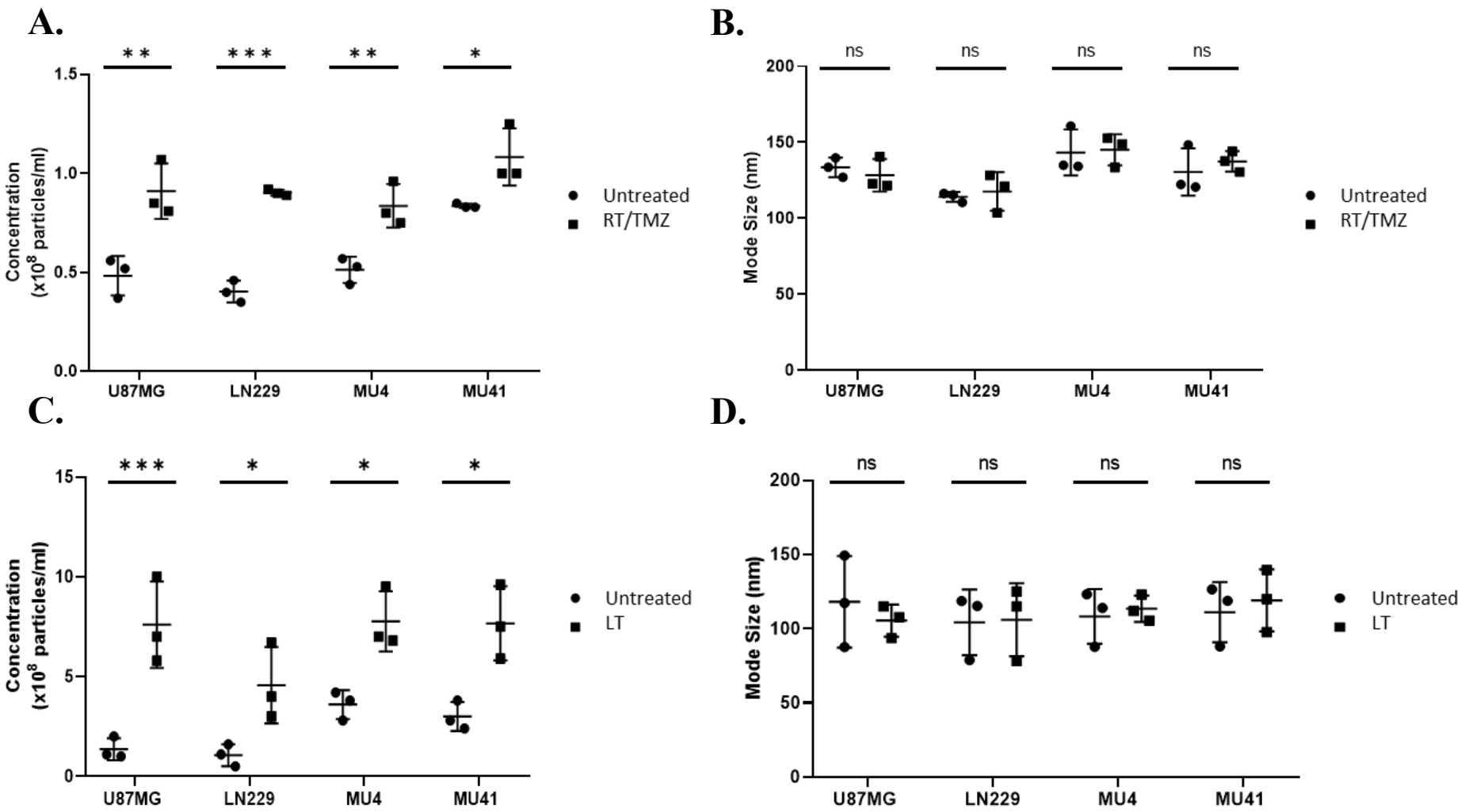
A.
B.
C.
D.
Concentration (x10^8 particles/ml)
Mode Size (nm)
U87MG
LN229
MU4
MU41
Untreated
RT/TMZ
LT
ns

To determine if the observed increase in EV secretion is impacted by RT or TMZ, or their combination, the GBM cell lines were treated with RT and TMZ either singularly or combined and the conditioned media was subjected to NTA. All treatment groups demonstrated an increasing trend in EV secretion which varied between cell lines, however the combination of RT/TMZ resulted in the greatest overall increase in EV secretion compared to untreated cells (***Figure 4-12A***). No significant differences were observed for EV size distribution, which remained primarily within a similar modal size (<200nm) encompassing small EVs (***Figure 4-12B***). This increase in EV secretion was also generally maintained up to 7 days post-RT/TMZ as displayed in U87MG, LN229 and MU41 cells, however MU4 cells showed a decline in EV secretion after 2 days, displaying similar levels to untreated MU4 cells by day 7 (***Figure 4-13)***. Further investigations could be carried out in future studies to determine if this increase in EV secretion is maintained for longer than 7 days post-RT/TMZ treatment.

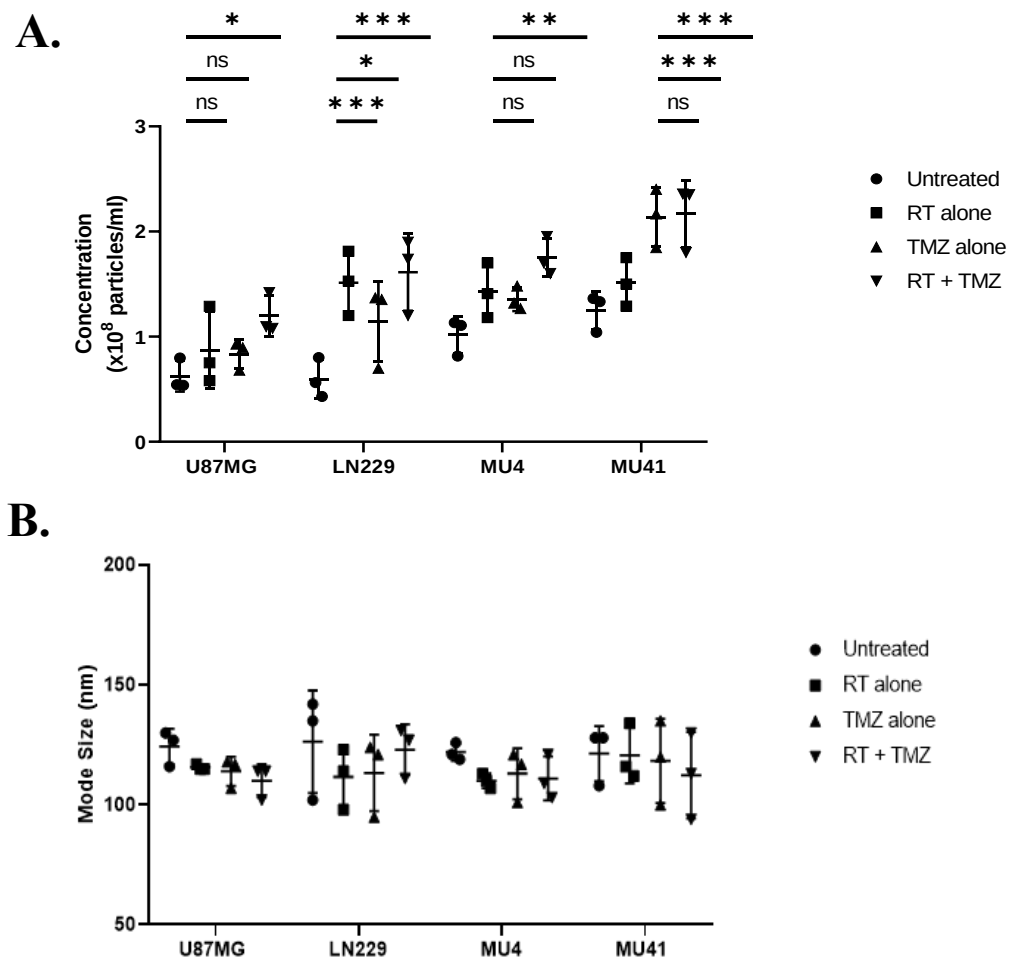

Figure 4-12: The combination of RT and TMZ can result in greater GBM cell EV secretion than either RT or TMZ treatment alone

GBM cell lines were seeded in triplicate (2.5 x 10^4 cells) into 6 well plates and designated as untreated or treated with 2Gy RT alone, 50μM TMZ alone, or both RT/TMZ combined. The culture medium was replaced with serum-free OptiMEM 24h post-treatment, and cells were incubated for a further 24h before media was harvested, cell debris removed and subsequently analysed via NTA. (**A.**) An increasing trend in EV secretion was observed in response to all treatments relative to the untreated cells. However, a significant increase in EV secretion was observed with a combined treatment of RT/TMZ relative to single agent treatment (**B.**) Modal size of EVs released post-treatment remained unaltered for both single and combination treatments. The concentration of EVs per group is normalised to 1 x 10^5 cells. *(n=3 experiments in triplicate; mean ± SD, *p<0.05; **p<0.01; ***p<0.001, non-significant =ns, unpaired two-tailed student's t-test).*

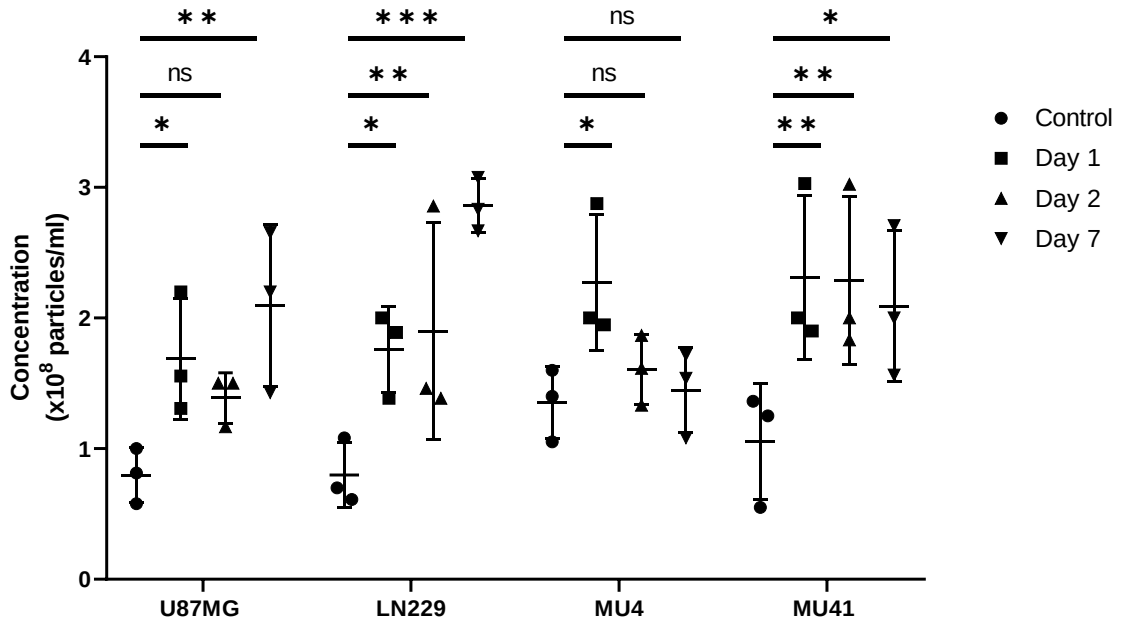

Figure 4-13: Enhanced GBM cell EV secretion is generally maintained up to 7 days following a single RT/TMZ treatment

GBM cell lines were seeded in triplicate (2.5 x 10^4 cells for control and day 1, 1.25 x 10^4 cells for day 2, and 0.1 x 10^4 cells for day 7) into 6 well plates and were either left untreated or treated with 2Gy RT and 50μM TMZ. 24h prior to NTA, at either 1, 2 or 7 days after treatment, the culture medium was replaced with serum-free OptiMEM. The NTA of serum-free conditioned medium shows a trend of increased EV secretion after treatment, which is generally maintained up to day 7 in U87MG, LN229 and MU41 cell lines. The concentration of EVs per group is normalised to 1 x 10^5 cells. *(n=3 experiments in triplicate; mean ± SD, *p<0.05; **p<0.01; ***p<0.001, non-significant =ns, unpaired two-tailed student's t-test)*

4.2.4.2 Investigating the functional impact of EVs enriched from untreated or RT/TMZ treated donor cells on recipient GBM cells

As we have demonstrated that invadopodia FITC-gelatin degrading activity (***Figure 3-5***) and EV secretion (***Figure 4-11***) increase following RT/TMZ treatment, experiments were then conducted to determine whether EVs from RT/TMZ treated donor GBM cells compared to EVs from untreated donor GBM cells resulted in functional differences in GBM recipient cells. The effect of EVs from untreated (*'untreated EVs'*) and treated ('*treated EVs'*) donor LN229 cells on the secretion of MMPs in GBM recipient cells was first assessed using zymography (***Figure 4-14***). An increase in MMP-2 secretion was observed following the addition of EVs to the recipient cells, however there was no significant difference between the EVs from untreated and treated donor cells. Additionally, an increase in migration rate was observed for LN229 and MU4 cells incubated with untreated and treated EVs, with a significantly ($p<0.05$) greater increase in migration rate following the addition of EVs from treated donor cells (***Figure 4-15***).

The ability of LN229-EVs to also promote EV secretion in recipient GBM cells, and whether this could be altered by RT/TMZ treatment was also investigated. EVs from untreated and treated donor LN229 cells were incubated with recipient GBM cells, and the EV secretion into serum-free medium was subsequently assessed using NTA. An increase in EV secretion was detected in all GBM cell lines following the addition of both untreated and treated EVs, with no significant differences between the two groups of EVs (***Figure 4-16***). This indicates that EVs secreted by LN229 cells can promote EV secretion in recipient GBM cells, however, there appears to be no significant RT/TMZ treatment-induced changes in EV cargo to further drive EV secretion in the recipient cells.

Figure 4-14: Incubation with EVs from untreated or RT/TMZ treated LN229 donor GBM cells can result in increased MMP-2 secretion from recipient GBM cells

EVs enriched from LN229 GBM cells were subjected to NTA (**A.**) untreated (NTA - mode size 120nm) and (**B.**) RT/TMZ treated (NTA - mode size 110nm). (**C**.) EVs from untreated and RT/TMZ treated LN229 cells were incubated with recipient GBM cells (25μg/ml protein concentration). After 24h, the conditioned serum-free medium was replaced and incubated with additional serum-free OptiMEM for a further 24h prior to zymographic analysis. Densitometric analysis of the zymograms revealed an increasing trend in the secreted levels of (**D**.) pro-MMP-2 and (**E.**) active-MMP-2 from the recipient GBM cells following incubation with EVs from both untreated and treated LN229 donor cells. *(n=3 experiments; mean ± SD, *p<0.05; **p<0.01; ***p<0.001, non-significant =ns, unpaired two-tailed student's t-test).*

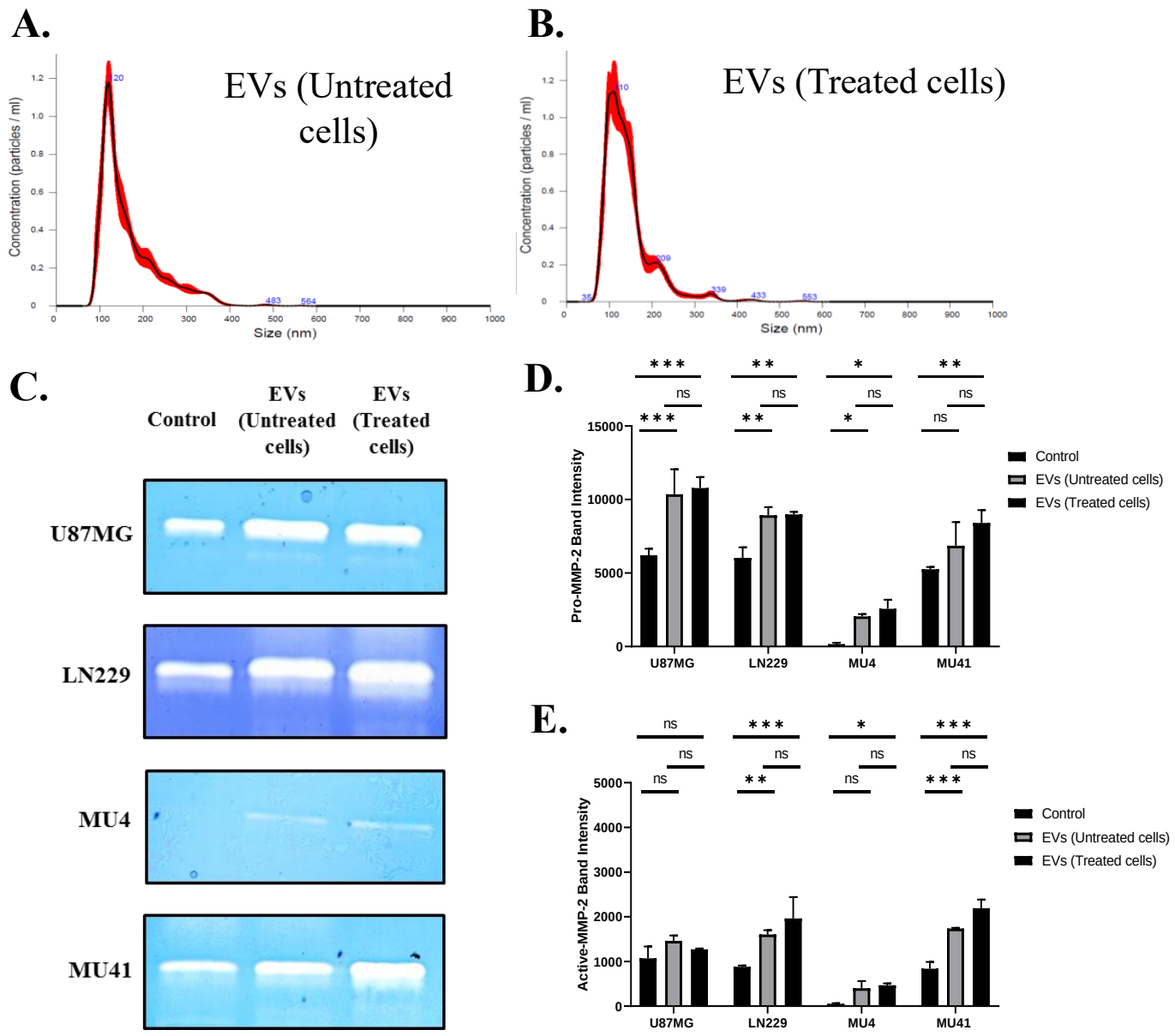
A.
EVs (Untreated cells)
Concentration (particles / ml)
Size (nm)
B.
EVs (Treated cells)
Concentration (particles / ml)
Size (nm)
C.
Control
EVs (Untreated cells)
EVs (Treated cells)
U87MG
LN229
MU4
MU41
D.
Pro-MMP-2 Band Intensity
Control
EVs (Untreated cells)
EVs (Treated cells)
U87MG
LN229
MU4
MU41
E.
Active-MMP-2 Band Intensity
Control
EVs (Untreated cells)
EVs (Treated cells)
U87MG
LN229
MU4
MU41

Figure 4-15: EVs from RT/TMZ treated LN229 donor GBM cells can enhance recipient GBM cell migration

EVs were enriched from LN229 GBM cells were subjected to NTA (**A.**) untreated (NTA mode size - 120nm) and (**B.**) RT/TMZ treated (NTA mode size - 124nm). (**C**.) LN229 and (**D.**) MU4 cells were then incubated for 24h with the enriched EVs (25μg/ml protein concentrations). Following EV incubation, the cells were treated with Mitomycin C (5 μg/ml; 2 h – to arrest cell proliferation) and a scratch (wound) was then introduced before cells were washed with PBS to remove floating cells. Image J (version 1.53a) analysis of images taken at 0, 6 and 24h after introduction of the wound/scratch revealed an increase in wound closer following addition of EVs relative to the control cells. *(n=3 experiments; 4 images per cell line per experiment; mean ± SD, *p<0.05; **p<0.01; ***p<0.001, non-significant =ns, unpaired two-tailed student's t-test)*

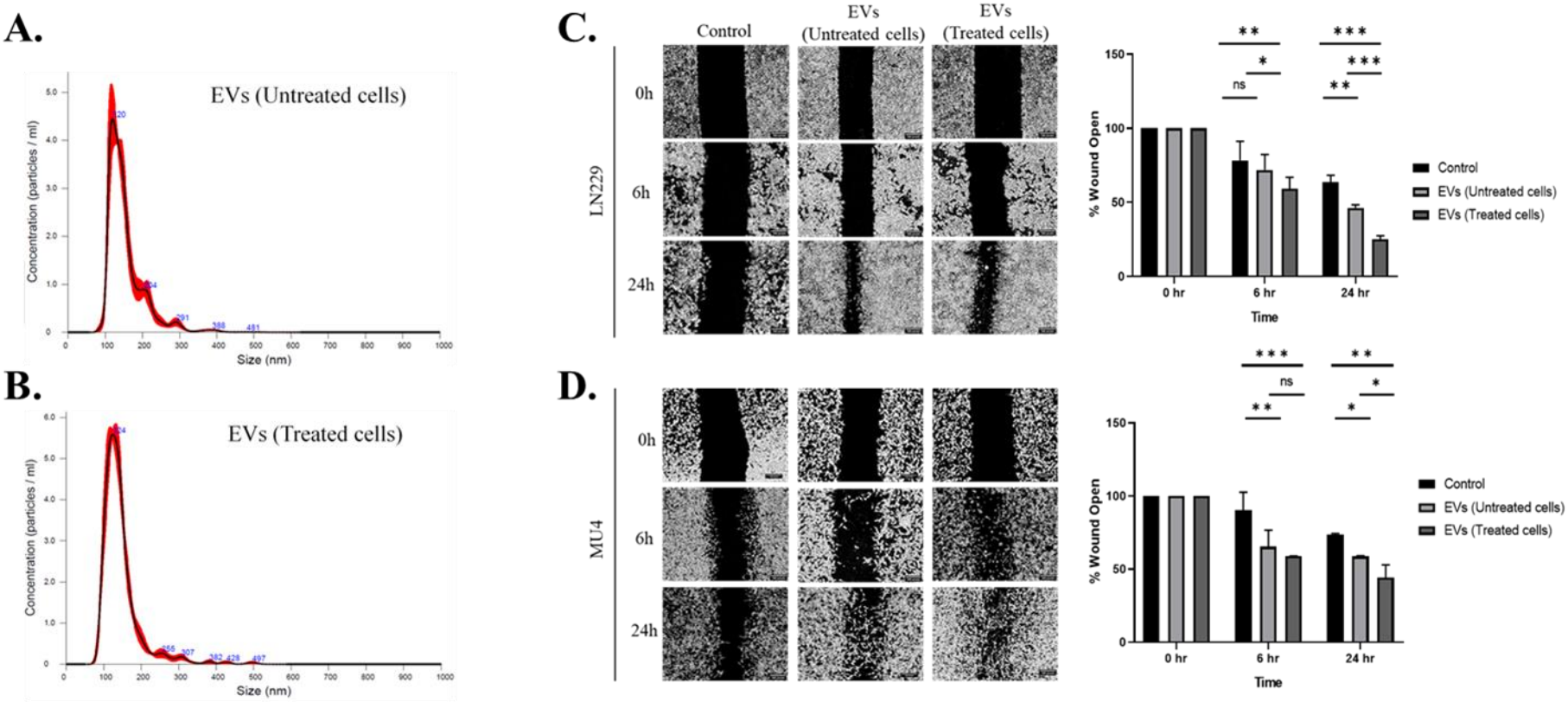
A.
EVs (Untreated cells)
Concentration (particles / ml)
Size (nm)
B.
EVs (Treated cells)
Concentration (particles / ml)
Size (nm)
C.
Control
EVs (Untreated cells)
EVs (Treated cells)
LN229
0h
6h
24h
% Wound Open
Time
0 hr
6 hr
24 hr
Control
EVs (Untreated cells)
EVs (Treated cells)
D.
MU4
0h
6h
24h
% Wound Open
Time
0 hr
6 hr
24 hr
Control
EVs (Untreated cells)
EVs (Treated cells)

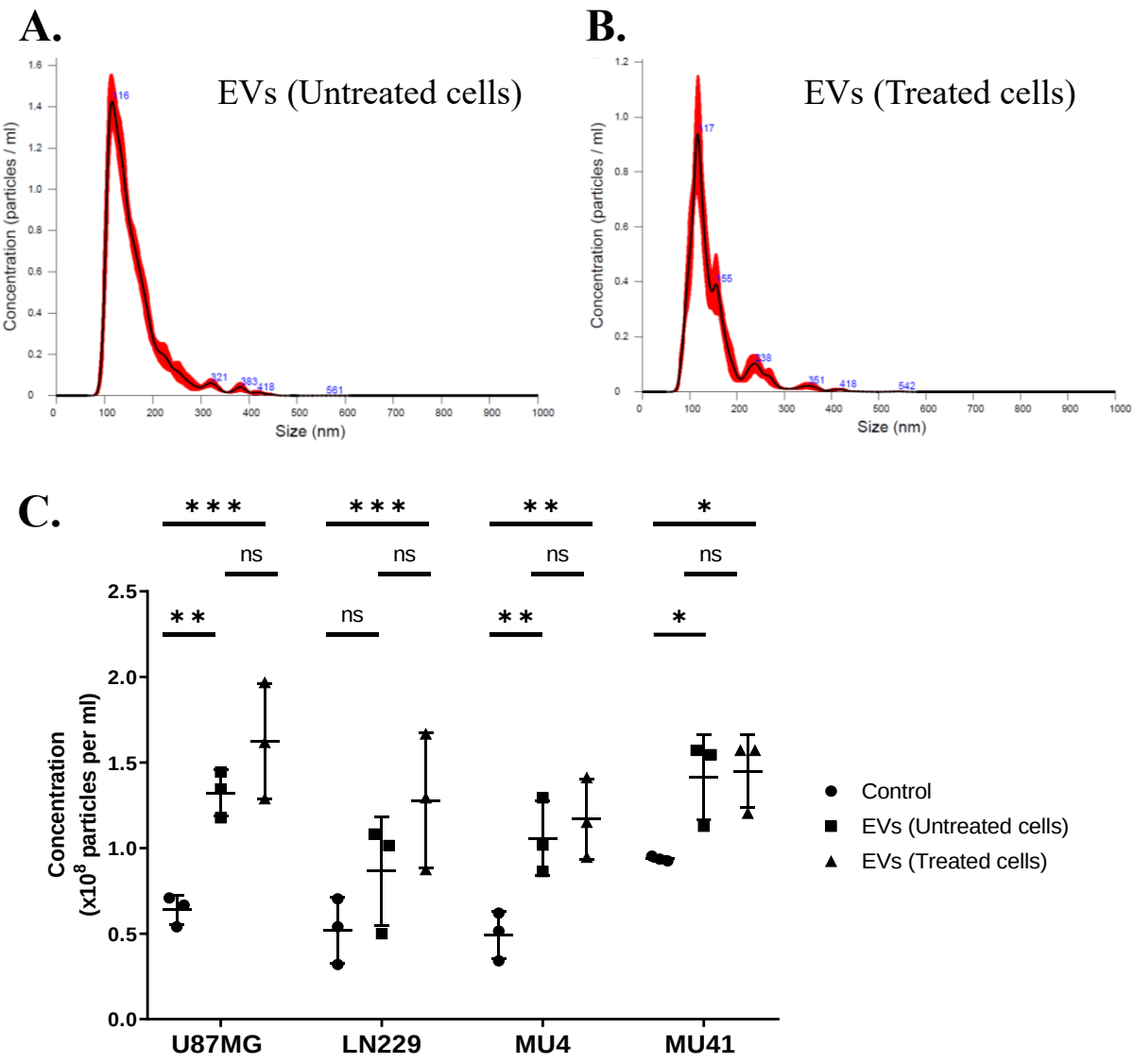

Figure 4-16: EVs enriched from untreated or RT/TMZ treated LN229 donor GBM cells can enhance recipient GBM cell EV secretion

EVs were enriched from LN229 GBM cells were subjected to NTA (**A.**) untreated (NTA mode size - 116nm) and (**B.**) RT/TMZ treated (NTA mode size - 111nm) LN229 cells were incubated with recipient GBM cells (25µg/ml protein concentration). After 24h, the culture medium was replaced with serum free OptiMEM and incubated for a further 24h. (**C.**) NTA of the conditioned medium revealed an increase in EV secretion (relative to control cells) in all four GBM cell lines following incubation with LN229-EVs. *(n=3 experiments; each point represents the mean of 5 NTA recordings; mean ± SD, *p<0.05; **p<0.01; ***p<0.001, non-significant =ns, unpaired two-tailed student's t-test).*

4.2.4.3 Vinorelbine tartrate reduces GBM cell EV secretion

Vinorelbine Tartrate (VT) is an FDA approved agent for non-small cell lung cancer that targets microtubules. In addition to their roles in cell structure and division, microtubules serve to form a network by which secretory vesicles may be trafficked to the cell surface, such as those containing MMPs to be transported to the tip of invadopodia. They also serve a structural role in invadopodia by stabilizing the invadopodium core. Our laboratory has previously shown that VT is able to reduce MMP-2 secretion, migration rate and invadopodia-mediated FITC-gelatin degradation in GBM cells surviving RT/TMZ [12]. As invadopodia may serve as sites for EV secretion, the impact of VT treatment on EV secretion was examined. GBM cells were treated with 1μM of VT and EV secretion was measured using NTA. A reduction in EV secretion was observed relative to the untreated control for all four GBM cell lines (***Figure 4-17A***). Similarly, VT treatment post- RT/TMZ resulted in a reduction of the enhanced levels of EV secretion observed post RT/TMZ treatment (***Figure 4-17B***).

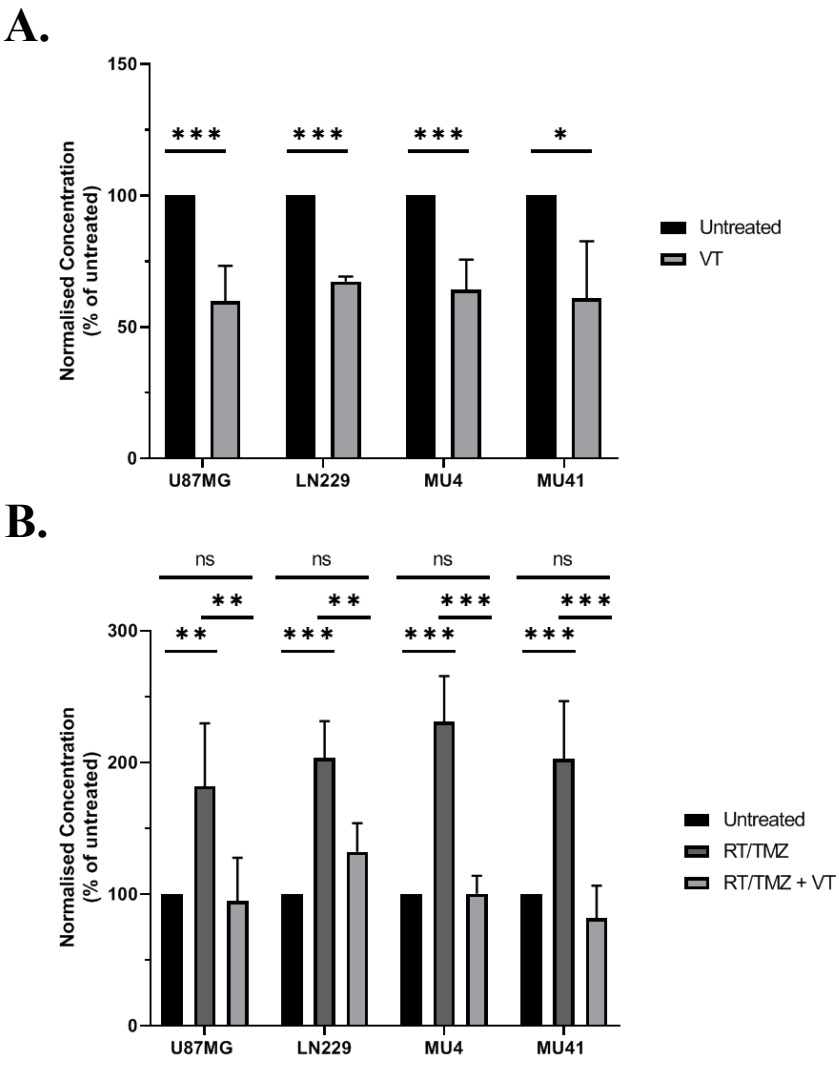

Figure 4-17: Vinorelbine Tartrate treatment reduces GBM cell EV secretion

(**A.**) GBM cells were seeded into 6 well plates in triplicate and treated with 1μM of VT. After a 24h incubation, the medium was replaced with serum-free OptiMEM and incubated for a further 24h. Analysis of conditioned media revealed a decrease in EV secretion in VT-treated cells relative to the untreated control of each experiment. (**B.**) GBM cells were examined under the following conditions: untreated, treated with RT/TMZ (2Gy/50μM), or a combination of RT/TMZ and 1μM of VT. An increase in EV secretion relative to each experimental untreated control was observed in RT/TMZ treated cells, which was reduced with the VT treatment. *(n=3 experiments performed in triplicate; mean ± SD, *p<0.05; **p<0.01; ***p<0.001, non-significant =ns, unpaired two-tailed student's t-test)*

4.3 Discussion

Increasing evidence suggests that EVs serve major roles in GBM tumour progression, whereby the transfer of oncogenic EV cargo to recipient cells promotes a range of malignant processes, including enhanced cellular invasion [478]. In the previous chapter, the invasive abilities of GBM cells were found to be facilitated by actin-rich membrane protrusions known as invadopodia. Here, the role of GBM cell-derived EVs in invadopodia-mediated invasion was examined. Specifically, this chapter demonstrates that EVs enriched from GBM cells with high invadopodia activity can induce a pro-invadopodia phenotype in recipient GBM cells, and additional evidence suggests that EVs may contribute to the enhanced invadopodia activity observed following RT/TMZ treatment.

Characterisation of GBM cell line derived EVs enriched by differential ultracentrifugation revealed that all four GBM cell lines secreted similar quantities of small (<200nm in diameter) EVs, which were enriched in the ESCRT-associated protein, ALIX (***Figure 4-2***). It is important to note that whilst these characteristics have been used as evidence of exosomes of endosomal origin in past studies, it is now recognised that such properties may be shared by EVs that bud from the plasma membrane, and therefore the small EVs enriched here may not strictly be defined as exosomes [196, 203, 204]. Importantly, small EVs secreted by the LN229 cell line that were subsequently fluorescently labelled were internalised by recipient GBM cell lines, indicating that these EVs may play a role in the horizontal transfer of oncogenic material from a donor GBM cell to a recipient GBM cell (***Figure 4-3***). Despite research into the biological effects of EV-mediated transfer in tumour progression, the exact mechanisms of uptake and unloading of EV cargo in recipient cells is not well defined, and may include endocytosis, membrane fusion or ligand-receptor binding [479]. Interestingly, Atai *et al*. observed that the inhibition of EV uptake by GBM cells using a well-known inhibitor of EV uptake, heparin, was at the level of cell-surface binding upstream of internalization [234]. Supporting this, Choi *et al*. demonstrated elevated uptake of EVs that were enriched with surface adhesion molecules by recipient GBM cells, including CD151 and basigin/CD147 that are also implicated in the regulation of invadopodia [228]. Whilst these studies demonstrate that EV uptake in GBM may heavily rely on

transmembrane proteins that allow vesicle binding to the recipient cell surface, further investigation is required to determine whether these, or other, mechanisms are responsible for the observed uptake of EVs by GBM cell lines.

4.3.1. GBM cell line EVs can facilitate invadopodia activity

Proteomic studies have identified both transmembrane and soluble MMPs in EVs isolated from both *in vitro* cell culture and the body fluids (serum or urine) of cancer patients [480]. Interestingly, in addition to the pro-form of MMP-2, functionally active MT1-MMP was also detected in EVs secreted from melanoma and breast cancer cells [302]. Whilst invadopodia secrete MMPs to aid invasion, these studies suggest that EVs may also facilitate this process by transporting invasion-related cargo. Zymographic analysis detected the presence of MMP-2 in the cargo of small EVs secreted from the GBM cell lines (***Figure 4-3***). As loading volumes were normalised to particle count, meaning equal numbers of EVs were examined, the amount of MMP-2 detected in the cargo of EVs was found to correlate with the invadopodia FITC-gelatin degrading activity of the corresponding donor cell line, with LN229-derived EVs containing the highest MMP-2 levels, whilst MU4-derived EVs contained the least MMP-2. Furthermore, both the pro- and cleaved/active- form of MMP-2 were detected in enriched EVs from the LN229 cell line, the latter of which was absent in LN229 cell lysates and vesicles enriched via a lower speed centrifugation (10,000xg) that is used to collect medium size EVs (potentially membrane-shed MVs), but was present to a lesser extent in the conditioned medium, which would contain both freely secreted proteases, as well as different subtypes of secreted vesicles. The presence of functionally active MMP-2 in GBM cell EVs suggests that these EVs may contain proteins capable of cleaving MMP-2. Supporting this hypothesis, Hoshino *et al*. has shown that exosomes secreted from SCC61 head and neck squamous cell carcinoma (HNSCC) cells contain both MT1-MMP and MMP-2, and further demonstrated that these exosomes were preferentially docked and secreted from invadopodia [229]. As invadopodia formation/activity occurs in stages, with ECM degradation occurring mainly during the maturation phase of their lifecycle, the low levels of MMP-2 in the cargo

of MU4-derived EVs in conjunction with their low invadopodia-mediated matrix degradation could indicate that small EVs play a substantial role in the delivery of proteases, such as MT1-MMP and MMP2, to mature invadopodia. These proteases may also be transferred to recipient cells, however it is possible that EVs themselves may also directly contribute to ECM remodelling [481]. Hakulinen *et* al. has shown that EVs containing MT1-MMP, derived from cultured fibrosarcoma and melanoma cells, degraded a fluorescently labelled gelatin matrix in the absence of cells, and this was impaired by the metalloproteinase inhibitor GM6001 [302]. As active MMP-2 was detected in GBM cell line derived EVs and was observed to correlate with the invadopodia activity of each donor cell line, this could suggest that EVs may work in conjunction with invadopodia in GBM to degrade the surrounding ECM. As the ECM also serves as a reservoir of bioactive fragments, EV-mediated proteolysis in the tumour microenvironment could also release ECM-bound factors, such as TGF-β, that further stimulate the formation of more invadopodia [482]. Supporting this, the observed inhibition of EV secretion with the calcium ion channel inhibitor dimethyl amiloride (DMA) resulted in reduced GBM cell line invadopodia-mediated matrix degradation but did not impact upon invadopodia formation (***Figure 4-8, 4-10 and 4-11***). As DMA is a known inhibitor of exosome secretion, this data also supports the hypothesis that invadopodia serve as additional sites of exosome release in GBM cells [229].

Whilst the transfer of MMP-2 in the cargo of EVs could potentially promote enhanced levels of MMP-2 secretion by invadopodia in GBM recipient cells, this does not account for the increase in the number of invadopodia observed in recipient GBM cells (***Figure 4-5***). Therefore, the donor GBM EVs must also be capable of transferring a pro-invadopodia phenotype by stimulating invadopodia formation in the recipient GBM cells. GBM-derived EVs can transfer cargo to recipient cells that promote a range of oncogenic processes. For example, Al-Nedawi *et al.* has shown that EGFRvIII can be transferred between GBM cells via an EV-mediated process, resulting in the activation of tumour-promoting signalling and subsequent transformation of previously indolent GBM cells [255]. Whilst the specific EV cargo that promotes invadopodia formation and activity in recipient GBM cells remain to be fully elucidated, as the effect of EV-mediated communication on invadopodia formation and activity between GBM cells has not been extensively examined to date, proteins known to induce invadopodia biogenesis

such as KRAS, EGFR, Src, and integrins have been reported to stimulate invasion via EV-mediated transfer in a number of other cancers such as colon and prostate cancer [483, 484]. The pro-invadopodia protein cargo in GBM cell derived EVs will be further addressed in the following chapters. It is important to note that as these experiments involve the use of a crude mix of ultracentrifugation-enriched small EVs, the observed changes in invadopodia formation/activity can be interpreted as 'activity present in EV-enriched preparations, rather than EV-specific activity'. Nevertheless, as fluorescently labelled LN229 EVs were observed to be internalised by recipient MU4 cells in ***Figure 4-2F***, this suggests a significant contribution from the EVs themselves. Alternatively, EV cargo may not need to be internalised to drive invadopodia formation, as EV membrane proteins can also bind to cell surface receptors on the recipient cells to stimulate intercellular signalling cascades. For example, tetraspanins present on EVs have been reported to induce integrin clustering on the recipient cell membrane, thereby activating downstream signalling pathways involved in cell motility, regulation of the actin cytoskeleton, and MMP production [485, 486]. Whilst integrins are traditionally known to stimulate invadopodia formation in response to ECM components [137], the same pathways may also be activated by EV-receptor binding.

In addition to the EV-mediated transfer of oncogenic proteins, emerging evidence has highlighted an important role for EV cargo in the miRNA-mediated regulation of post-transcriptional gene expression capable of promoting invasion in recipient cells [487]. Interestingly, MU4 cells incubated with LN229-dervied enriched EVs exhibited a reduction in the expression of 34 miRNAs (***Figure 4-7***), of which 25 were found to target transcripts involved in invadopodia formation and/or activity (***Table 4-1***). Moreover, included in this list of reduced miRNAs were the four miRNAs (let-7a-5p, let-7b-5p, miR-125b-5p, miR-4454+miR-7975) identified in ***Chapter 3*** that are potentially associated with invadopodia activity in GBM cell lines (refer to section ***3.3.4*** for more details on the involvement of these miRNAs in invasion and invadopodia-related activities). One explanation for the reduction of these miRNAs following incubation with LN229-dervied EVs involves the transfer of specific mRNAs in the EV cargo. Reinforcing this, a study by Batagov *et al.* observed that an enrichment of mRNA with a bias towards the 3'-UTR region, known to be rich in miRNA-binding sites and elements dictating mRNA

localisation, in the cargo of GBM cell-derived EVs [250]. Release of such cargo in recipient cells leads to interactions with recipient cell miRNA, which can outcompete recipient cell transcripts for preferential miRNA binding. Reduced miRNA binding to endogenous pro-invasive targets would thus allow for greater expression of pro-invasive proteins and could serve to promote an invasive phenotype in recipient cells that internalize EVs from donor GBM cells possessing high invadopodia activity, however further studies are necessitated to clarify these mechanisms.

4.3.2. Enhanced EV secretion by RT/TMZ treated GBM cells and the potential impact on GBM invasion

As we had previously demonstrated (in ***Chapter 3***) that the current therapeutic approach for GBM patients, consisting of RT/TMZ treatment, may promote a pro-invasive phenotype through the mediation of enhanced invadopodia activity, the effect of RT/TMZ treatment on EV secretion was next assessed. NTA of serum-free conditioned medium from the GBM cell lines following exposure to RT/TMZ treatment was conducted, revealing an increase in EV secretion from GBM cells following both single and LT treatment (***Figure 4-11***). Notably, the size of the EVs as determined by NTA remained unchanged, with modal EV diameters remaining within a small-EV or 'exosome' size range below 200nm, suggesting that RT/TMZ treatment does not significantly alter the size of the EV subtype being secreted. These results support previous studies that report an increase in EV secretion from irradiated U87MG GBM cells, however these studies did not investigate the impact of RT in combination with TMZ [257, 488]. Therefore, additional experiments were carried out to determine whether the changes observed in EV secretion were primarily due to RT, TMZ, or a combination of both. Whilst all treatment groups demonstrated an enhanced EV secretion compared to the untreated cells, the most significant increase in EV secretion was consistently observed with a combination of RT and TMZ treatment (***Figure 4-12***). As we have demonstrated that EVs can mediate the transfer of a pro-invadopodia phenotype to recipient GBM cells (***Figure 4-6***), the increased secretion of EVs post-RT/TMZ treatment may greatly enhance the invasive potential of GBM recipient cells. Indeed,

interrogation of the mRNA expression levels of EV markers (ALIX, CD9, CD63, CD81, CD151 and TSG101) using the SurvExpress database revealed that elevated expression of these markers correlates with poorer GBM patient survival, suggesting the observed increase in EV secretion following RT/TMZ may have critical prognostic importance (***Table 4-2***).

As invadopodia have been proposed as the sites of exosome release, it is possible that the increase in GBM cell EV secretion may be due to increased invadopodia formation following exposure to RT/TMZ (***Figure 3***-6). In addition, increased EV secretion by tumour cells exposed to chemotherapy may also be attributed to a cellular response to stress, and studies have shown that EVs from stressed cells often display alterations in composition and cargo that exert various functional effects within recipient cells [489]. It has been demonstrated that EVs from irradiated U87MG cells were found to contain an upregulation of oncogenic mRNAs, including Annexin A2 and Dynamin-2, which promoted radio-resistance in recipient U87MG cells [488]. Similarly, Arscott *et al*. observed that EVs from irradiated U87MG cells contained elevated levels of connective tissue growth factor (CTGF) mRNA and insulin-like growth factor binding protein 2 (IGFBP2) protein, which enhanced the migration of recipient cells compared to EVs from non-irradiated cells [257]. However, relatively little is known regarding the role of EVs from GBM cells treated with RT in combination with TMZ in promoting the invasive potential of GBM. Therefore, to investigate whether EVs secreted by GBM cells following RT/TMZ treatment may further contribute to enhanced invadopodia activity, the impact of EVs secreted from untreated and RT/TMZ treated LN229 cells on recipient GBM cells was compared. Whilst an increase in both MMP-2 and EV secretion was observed in recipient GBM cells incubated with LN229-dervied EVs, suggesting potential increased invadopodia activity, no further enhancement was seen with EVs from RT/TMZ treated LN229 cells (***Figure 4-14 and 4-17***).

In analysing these results, it is important to consider that equal amounts of EVs (based on a protein concentration of 25μg/ml protein concentration, approximately 5 $x10^{10}$ EVs in total) of EVs from untreated and treated LN229 cells were incubated with the recipient cells. Therefore, these results indicate that the cargo of EVs secreted by RT/TMZ treated LN229 cells may not enhance recipient cell MMP-2 secretion beyond that of EVs from untreated LN229 cells, although a significant increase in migration rate was observed in recipient GBM cells incubated with EVs from treated LN229 cells

compared to untreated cells, suggesting the presence of pro-migratory EV cargo following treatment (***Figure 4-15***). Importantly, as EV secretion is enhanced in RT/TMZ treated GBM cells (***Figure 4-11***), a greater quantity of EVs would likely be present in the tumour microenvironment following exposure to RT/TMZ. Although literature addressing the dose-dependent effects of EVs on recipient cells is limited so far, using a cell culture model for draining cells in the eye, Tabak *et al.* has shown that the biological effects of EVs are concentration-dependent, and incubation with a higher concentration of EVs resulted in significantly enhanced MMP-9 activity in recipient cells compared to lower EV concentrations [490]. Consequently, future work should investigate whether the higher number of EVs secreted by RT/TMZ treated GBM cells is able to promote augmented invadopodia activity in recipient cells to a greater extent compared to the corresponding lower number of EVs secreted by untreated GBM cells. Furthermore, it is important to note the current experiments were conducted with EVs from the LN229 GBM cell line that displays high basal invadopodia-mediated FITC-gelatin degrading activity. As LN229-derived EVs may already contain 'pro-invadopodia' cargo, evidenced by their ability to transfer invadopodia-mediated FITC-gelatin degrading activity to recipient GBM cells, it may be possible that alterations in EV cargo following RT/TMZ treatment may differ in EVs secreted from other GBM cell lines. Although the functional effects of EVs from the remaining GBM cell lines post-RT/TMZ treatment were not examined in this thesis, this should be further investigated in future studies. However, evidence of treatment-induced changes in the proteome of EVs from multiple GBM cell lines was investigated in ***chapter 6.***

4.3.3. EV secretion and invadopodia activity as potential targets for an anti-invasive treatment of GBM

The data presented in this chapter suggests that enhanced EV secretion following RT/TMZ treatment may facilitate the transfer of a pro-invadopodia phenotype and contribute to the enhanced invasive abilities of surviving GBM cells. As invadopodia have been suggested as the docking sites of MVBs, and subsequent sites of exosome release, this may result in a positive feedback loop, with both increased

invadopodia formation and EV secretion driving one another in response to RT/TMZ treatment, ultimately contributing to tumour recurrence and ultimately, treatment failure [229]. Therefore, novel therapeutic strategies that target both invadopodia activity and EV-mediated communication may impede GBM invasion and improve patient survival.

Recently, Keklikoglou *et* al. demonstrated that chemotherapy with taxanes enhances EV secretion from breast cancer cells, which was proposed to be dependent on the ability for taxanes to stabilise microtubules, thereby enforcing the trafficking of intracellular vesicles to plasma membrane [491]. Conversely, Vinorelbine Tartrate (VT) is an FDA approved agent for non-small cell lung cancer that belongs to the vinca alkaloid group of drugs that destabilise microtubules. VT hinders microtubule assembly by preventing a phenomenon known as 'treadmilling' that involves the addition of tubulin subunits at the positive end of lengthening microtubules [492]. This process assists in stabilizing the invadopodium core and is also involved in the transport of secretory vesicles, such as those containing MMPs, to the tip of the invadopodium for subsequent secretion and degradation of the surrounding ECM [137]. In accordance with previous data from our laboratory showing that VT reduces invadopodia-mediated FITC-gelatin degradation in GBM cells surviving RT/TMZ [12], VT treatment also reduced enhanced EV secretion from RT/TMZ treated GBM cells (***Figure 4-17***). These results therefore suggest that targeting microtubules may impede the ability of mature invadopodia to secrete EVs, which may also hinder the proteolytic modification of the ECM.

Although the impact of VT in GBM has not been thoroughly investigated in the literature, a single case study of a female GBM patient receiving intravenous VT reported an improved progression free survival period that extended beyond 24 months [493]. Studies have also shown significant clinical responses to VT treatment in paediatric diffuse pontine glioma and paediatric LGG [494-496]. Encouragingly, it has also been shown that VT is able to cross the blood-brain barrier in a preclinical mouse model of brain metastases of breast cancer, with concentrations of VT in brain metastases measured between 0.5µM and 7µM [497]. This supports our findings, as VT significantly reduced EV secretion from GBM cell lines at a low concentration of 1µM (***Figure 4-17***). Additionally, VT is reported to be less neurotoxic than other vinca alkaloids, thereby rendering it a promising candidate for

potential clinical use in GBM [498]. Therefore, whilst the efficacy of RT/TMZ treatment may be compromised by surviving GBM cells that exhibit an enhanced invasive phenotype, potentially linked to both augmented invadopodia activity and EV-mediated communication, this data highlights VT as a promising anti-invasive agent that can dualistically target invadopodia activity and EV secretion in RT/TMZ-treated GBM cells (***Figure 4-18***).

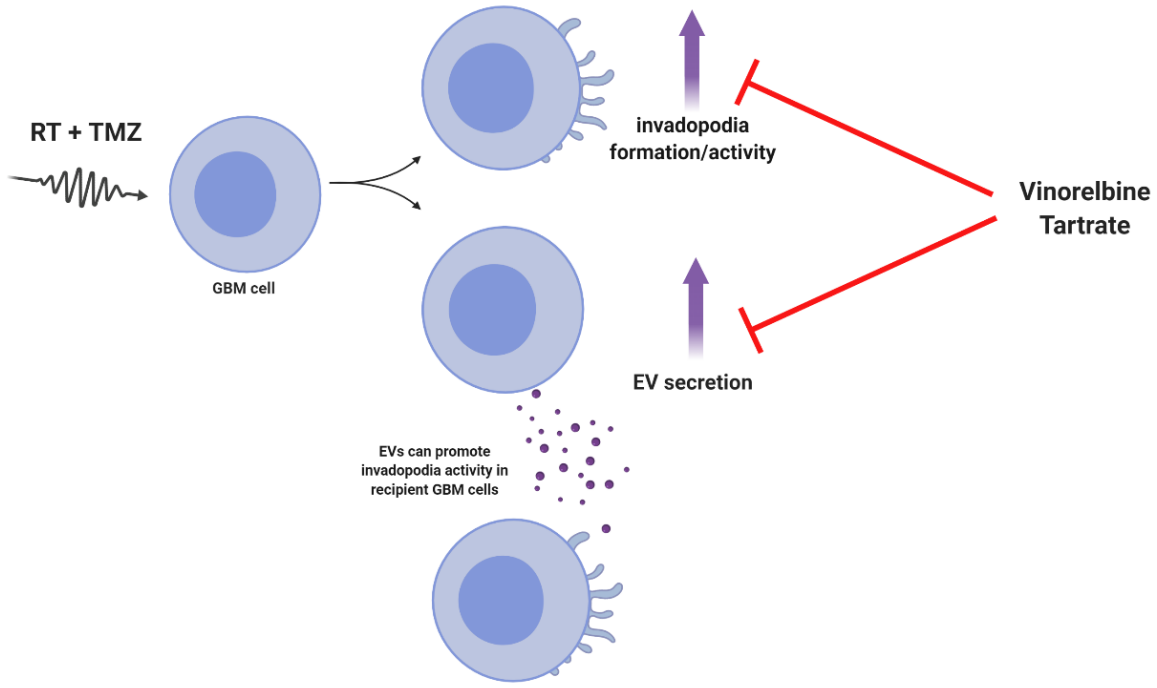

Figure 4-18: Vinorelbine Tartrate reduces EV secretion and invadopodia activity in RT/TMZ treated GBM cells

A schematic representation of the experimental findings indicating that VT treatment of GBM cell lines results in reduced invadopodia (FITC-gelatin degrading) activity and EV secretion. RT/TMZ treatment results in increased GBM cell invadopodia-mediated FITC-gelatin degrading activity and EV secretion, the latter of which may also promote invadopodia activity in recipient GBM cells via the potential EV-mediated transfer of pro-invadopodia cargo. VT treatment of GBM cells pre-treated with RT/TMZ resulted in a reduction of both augmented invadopodia activity (in our previously published study [12]) and EV secretion.

CHAPTER 5:
Proteomic characterisation of GBM cells, EVs and MVs

5.1 Introduction

5.1.1 Proteomic Analysis using Liquid Chromatography/Tandem Mass Spectrometry - An introduction

The proteome is the entire complement of proteins produced by the genome at any one time, and therefore reflects the dynamic state of a cell [499]. Cancer cells can respond to extracellular and intracellular changes by altering the expression levels of proteins that contribute to various functions within the cell. Whilst genetic abnormalities may underlie susceptibility to a disease, it is ultimately proteins that influence functional changes. Consequently, many therapeutic agents are designed to target proteins, and protein expression is often used as a reference point in diagnostic testing.

Proteomics is a large-scale, high-throughput approach to analysing protein expression, post-translational modifications (PTMs) and interactomes. Proteomics provides a global, integrated view of many cellular processes by simultaneously analysing total protein content. Protein-protein interactions have profound effects on numerous cellular functions including protein localisation, PTMs, and enzymatic activity. Furthermore, proteins may bind to other proteins to form larger protein complexes (such as the Arp2/3 complex required for F-actin polymerisation in the formation of invadopodia or the ESCRT complex required for EV biogenesis). Proteomic analysis can simultaneously identify the expression levels of numerous interacting proteins, and therefore offers potential insights into the various mechanisms of a disease. This is crucial for GBM as there exists an urgent need for novel drug targets, as well as identification of protein-based biomarker signatures that can assist in the diagnosis, prognosis, and assessment of response to treatment.

Mass spectrometry (MS) is a powerful tool that is utilised to identify proteins and calculate their relative abundance within a sample, and this technology has the ability to identify several thousand proteins in a single analysis [500]. Whilst a variety of MS methodologies have been established over time, many require the complex protein samples (containing multiple peptides) to be digested prior to MS analysis. The most common technique for quantitative analysis of multiple proteins is high-performance liquid

chromatography (HPLC) paired with tandem mass spectrometry (LC-MS/MS) [501] (***Figure 5-1***). An LC-MS/MS analysis results in a full spectrum of quantifiable proteins that is then matched to known sequences within databases, where protein identifications are constructed from the list of previously identified peptides. A standardised LC-MS/MS analysis platform delivers highly repeatable and reproducible protein identifications, however accurate chromatographic peak alignment is also required to ensure correct protein quantification [502]. Therefore, a careful and methodological LC-MS/MS workflow with high molecular specificity is required for the identification of a myriad of proteins which are present in complex biological samples.

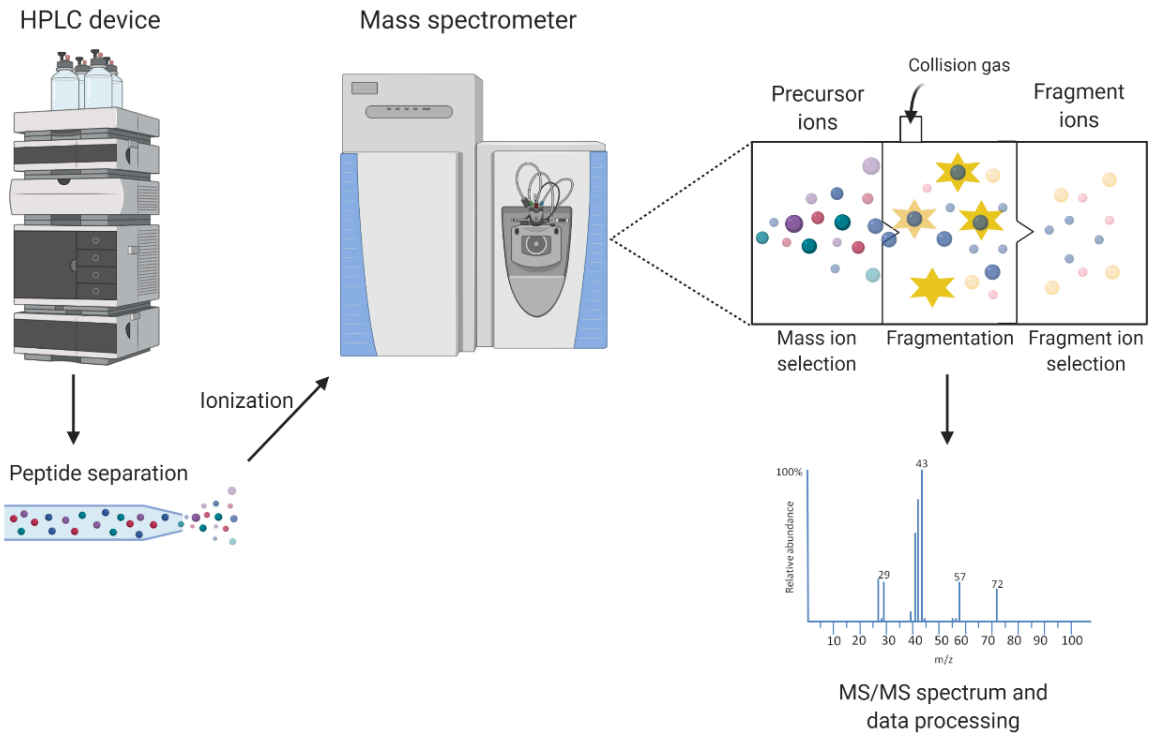

Figure 5-1: Schematic of a generalised LC-MS/MS workflow

As peptides are separated and elute from the HPLC column, they are converted from a solution into a gaseous phase by electron ionisation. An MS scan is carried out on all ions, with ions of a particular mass-to-charge ratio (m/z) being subsequently selected and fragmented via accelerated collision with neutral gaseous molecules such as helium or nitrogen. Fragmented ions are then analysed by MS/MS to generate a full MS/MS spectrum. Individual peptides are then identified by aligning peaks with the same m/z ratio and plotting peak intensities against the time taken for peptides to elute from the HPLC column ('retention time').

5.1.2 Molecular Regulation of Invadopodia Formation/Activity

Invadopodia are reliant on the cooperative interactions of a network of proteins that are implicated in the various processes and stages that govern the formation and activity of the invadopodium lifecycle. The full extent of this network of proteins is not yet fully elucidated, and studies continue to identify proteins involved in the formation and proteolytic activity of invadopodia. Based on their functional impact, invadopodia-affiliated proteins may be categorised into four main groups as follows [503].

5.1.2.1 ECM-interacting proteins

It is known that various signalling inputs facilitate invadopodium formation, however, cancer cell attachment to the ECM could be regarded the most critical input for regulating invadopodia formation, as invadopodia only develop in adherent cells [136]. Live cell imaging has shown that focal adhesions serve as precursors for invadopodia [504], and thus many adhesion related proteins are known to localise to invadopodia including vinculin, paxillin, filamin and integrins [505]. By binding to components of the ECM, integrins may initiate intracellular signalling cascades responsible for actin polymerisation, which is central to the structural integrity of the invadopodium. Adhesion to the ECM enables mechanosensing, allowing invading cancer cells to determine the rigidity of the microenvironment, which will subsequently influence the response of the cancer cell [107]. Extracellular signal inputs can lead to integrin clustering and the subsequent activation of intracellular signalling pathways or signals generated inside the cancer cell can influence their ligand binding ability outside the cell. Of particular interest is β1 integrin, a known activator of the tyrosine kinase, Arg, which is known to phosphorylate cortactin and induce actin polymerisation in invadopodia [140]. Loss of the β1 integrin subunit has been shown to inhibit invadopodia formation as it is necessary for stabilisation of the F-actin core [506].

5.1.2.2 Actin regulatory proteins

Assembly of branched actin is vital for the formation of the invadopodium core and trafficking to the membrane and is dependent on proteins such as the Arp2/3 complex, N-WASP and cortactin. These proteins are involved in actin polymerisation, with the Src Homology 3 (SH3) domain of cortactin able to bind to N-WASP when phosphorylated, consequently activating the Arp2/3 complex to bind to F-actin and initiate actin nucleation [507, 508]. It has been demonstrated that the siRNA knockdown of cortactin can reduce the number of invadopodia that are formed, as well as ECM degradation [126, 503]. In addition to these key actin regulators, the adaptor protein, Tks5 plays a critical role in the development of the actin core. Phosphorylation of Tks5 by Src recruits a number of actin regulatory proteins to the developing invadopodium, such as Nck and the WASP/WAVE family proteins [509, 510]. Tks5 is known to co-localise with cortactin during the formation of invadopodia, and as such it has been proposed that Tks5 acts as a scaffold by which cortactin may be recruited [395, 511].

5.1.2.3 Signalling proteins

Invadopodium initiation can be stimulated by growth factors, such as EGF and TGF-β, that bind to receptor tyrosine kinases (RTKs) on the cell surface. Most of these growth factor pathways converge on common signalling hubs involving Src, PI3Ks and Rho GTPases [136, 137]. Amongst the invadopodia-related proteins, Src kinase has the most connections to other signalling pathways through interactions with its numerous substrates involved in the various stages of invadopodia biogenesis, including Cortactin, Paxillin, Tks5, and Nck1, to name a few [149, 509, 512, 513], however other kinases have been implicated in the invadopodia lifecycle, including Abl-related gene kinase (Arg), p21-activated kinase (PAK) and ERK [123, 514]. Additionally, Rho GTPases, including Cdc42, RhoA and RhoC, are also required for invadopodia formation/activity. Of these, Cdc42 is essential for invadopodia precursor assembly, and influences actin dynamics via activation of the N-WASP/Arp2/3 signalling cascade [515, 516].

5.1.2.4 Proteases

Degradation of the surrounding ECM is achieved through the action of a variety of proteases, such as the MMPs, which are recruited to and secreted from the tip of mature invadopodia. MMPs are produced as pro-enzymes that require proteolytic cleavage for activation via release of their pro-peptide domain, and therefore can be regulated by endogenous activators and inhibitors. Invadopodia are known to secrete MMP-2 and MMP-9, which degrade gelatin and collagen type IV and are activated by transmembrane MT1-MMP (also known as MMP-14) at the protrusive tip, thereby establishing a localised zone of proteolytic activity of the ECM around these structures [453]. Emphasizing the dynamic nature of invadopodia, MT1-MMP is continually transported to the invadopodium membrane via recycling endosomal vesicles [504, 517]. Other proteases have also been implicated in invadopodia-mediated ECM-degradation, including seprase- a membrane-spanning serine protease that is co-expressed at the invasive front of malignant melanoma cells within invadopodia [125].

5.1.3 EV cargo proteins in GBM communication

Due to the ability of EVs to carry proteins and RNAs that are reflective of malignant donor cells, recently there has been considerable focus on the characterisation of tumour derived EVs. In examining the proteome of EVs, it is important to note that some proteins are enriched in EVs compared to their donor cell and therefore EV cargo composition may not exactly mirror the cell of origin [11, 250]. The mechanisms by which cargo is selectively packaged into EVs remain to be fully elucidated, although current evidence suggests a potential role for ubiquitination in MVB protein loading [237]. One of the first studies to extensively examine the cargo of GBM cell-derived EVs was performed by Skog et al. [11], which identified that some mRNAs could be enriched up to 380-fold in EVs compared to the cells of origin. Notably, many of the mRNAs were associated with regulation of angiogenesis, proliferation, migration and immune response [11]. Additionally, whilst EVs contain proteins that are dependent on donor cell composition, they are also known to contain proteins that are common to most EVs regardless

of the cell of origin. Online databases, such as 'Vesiclepedia' [245], serve as fundamental repositories of identified EV cargo (RNA, proteins, lipids and metabolites) from multiple studies involving cells and tissues. Importantly, it is critical to not only examine the cargo of the donor cell EVs, but also incorporate the functional effect of the donor cell EVs in recipient cells in order to gain a greater understanding of the role of EVs in GBM progression and response to treatment.

5.1.4 Rationale and Aims

Multiple proteins have been implicated in invadopodia formation and activity; however, this has not been extensively studied in GBM and therefore a better understanding of invadopodia-related proteins in GBM is required. Furthermore, the cargo of GBM cell derived secreted vesicles may be critical to invadopodia formation/activity, as the transfer of the GBM donor cell cargo may potentially be capable of inducing invadopodia formation/activity in recipient GBM cells. Proteomics enables the large-scale identification of multiple proteins simultaneously, providing a comprehensive profile of the proteins that are expressed. In this chapter, the proteomic profiles of GBM cells and their corresponding secreted vesicles, such as small EVs (sEVs) and microvesicles (MVs) will be examined to identify proteins that may facilitate an invasive phenotype through the formation/activity of invadopodia in GBM cells. Although differential ultracentrifugation is currently the gold standard method of EV isolation, it does not provide complete separation of different EV subtypes. Thus, for the purposes of this chapter, EVs enriched at 10,000xg will be referred to as 'MVs', and EVs enriched at 100,000xg will be referred to as 'small EVs (sEVs)', as the average size distribution of this vesicle population was previously confirmed to be <200nm in diameter (***Figure 4-2***). Proteomic characterisation of GBM cells, sEVs, and MVs in this context could ultimately identify novel pathways and therapeutic targets to impede GBM invasion.

5.2 Results

5.2.1 Proteomic characterisation of GBM cells, sEVs and MVs

5.2.1.1 Integrative analysis of GBM cell line proteome

Overall, a total of 2354 proteins were identified in the GBM cell line proteomes (***Figure 5-2A***) (individual cell line protein numbers identified: LN229–1882 proteins, MU4– 1714 proteins, MU41–1916 proteins). The U87MG cell line was omitted from the current study as the cell line and EV proteomes have been previously investigated [472, 518-521]. Functional enrichment analysis of the 1362 proteins commonly detected in all three GBM cell lines revealed that significantly ($p<0.05$) enriched proteins were associated with exosomes, mRNA translation processes and protein transport to the cellular membrane (***Figure 5-2B***). The identified proteins were further divided into invasion-related protein classes using the PANTHER Classification System (version 15.0), indicating that many of the proteins identified in GBM cells were linked with actin-, protease- and trafficking- related processes (***Figure 5-2C***).

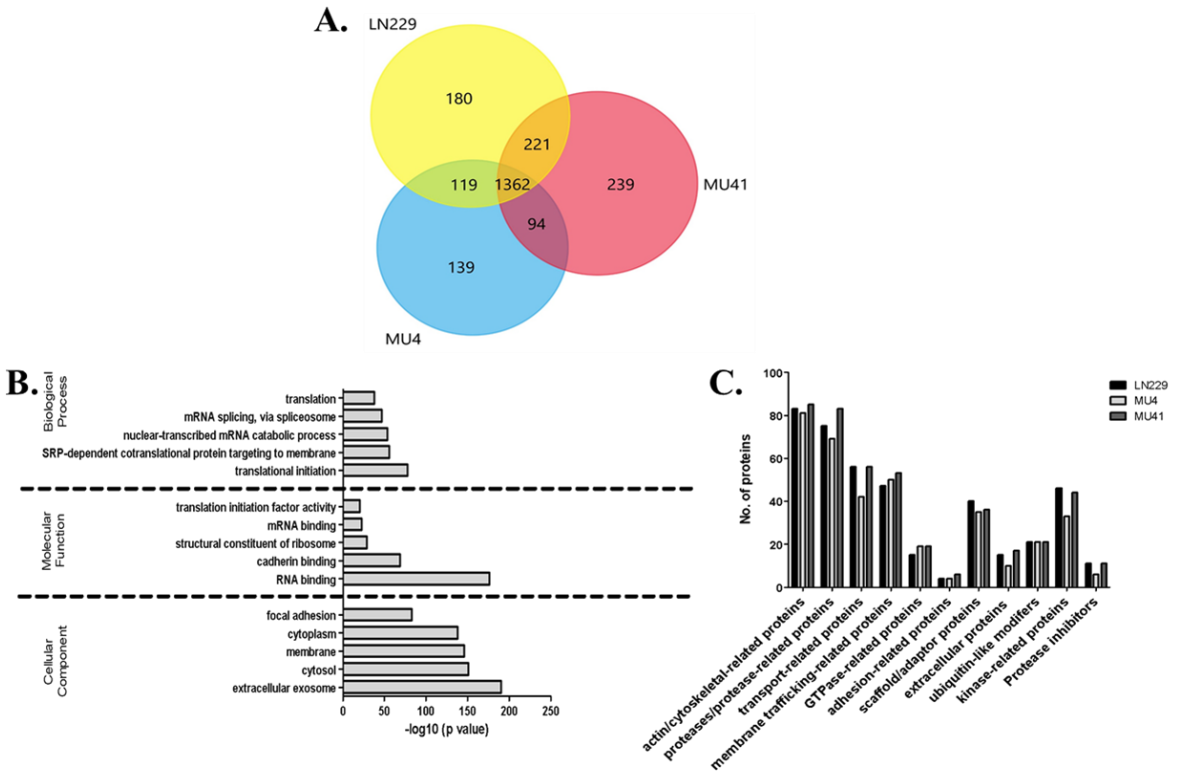

Figure 5-2: Integrative analysis of GBM cell line proteome using the FunRich and PANTHER bioinformatic platforms

(**A.**) Venn diagram of total proteins detected in the GBM cell lines - LN229, MU4 and MU41. 1362 proteins were common to all three cell lines. (**B.**) Functional enrichment analysis of the 1362 common proteins detected in GBM cells was conducted using FunRich (version 3.1.3), (P values were calculated by a two-sided hypergeometric test – the top significant 5 annotations are shown). (**C.**) Classification of proteins detected in each GBM cell line (according to the PANTHER Protein Classification system [341]) identified 11 potential invasion-related categories. The number of proteins within each invasion-related protein class is shown for each cell line.

5.2.1.2 Integrative analysis of GBM cell line sEV proteome

Overall, a total of 2086 proteins were identified in the secreted sEVs from the three different GBM cell lines (***Figure 5-3A***) (LN229–1213 proteins, MU4– 1023 proteins, MU41–1826 proteins). The U87MG cell line was omitted from the current study as the cell line and sEV proteomes have been previously investigated [472, 518-521]. Functional enrichment analysis of the 756 proteins commonly detected in sEVs from all three GBM cell lines revealed that significantly ($p<0.05$) enriched proteins in sEVs largely reflected the donor cell proteomes (***Figure 5-3B)*** and predominantly included actin/cytoskeletal and protease-related proteins which may be linked to invadopodia-related processes ***(Figure 5-3C***). Compared to GBM cells, sEVs exhibited higher relative expression levels of 'exosome' marker proteins (***Figure 5-3D***) that suggests these EVs may be of endosomal origin, although it is important to note that these markers have been detected in EVs of different subcellular origins [196]. Interestingly, CD9 was found to be the most enriched sEV marker, with a 15-fold higher expression in sEVs compared to cells. In addition, all top 100 EV cargo proteins recorded in Vesiclepedia (http://www.microvesicles.org) were detected in sEVs from at least one GBM cell line (***Figure 3-E***). At the time of writing, a total of 111 proteins identified in the GBM cell line derived sEV proteome were previously unreported as EV cargo in Vesiclepedia (***Figure 3-F***).

A total of 328 proteins were identified in the GBM cell line derived sEVs that were not previously listed within GBM/glioma EV studies recorded in Vesiclepedia. A list of the 111 proteins that were not listed within the proteins recorded in Vesiclepedia, as well as the 328 proteins that were not listed in GBM and glioma studies, is supplied in ***Supplementary Table 4.***

Figure 5-3: Integrative analysis of the GBM cell line sEV proteome using the FunRich and PANTHER bioinformatics platforms

(**A.**) A Venn diagram of total proteins detected in the proteome of the GBM cell line derived sEVs. 756 proteins were common to the sEVs enriched from all three GBM cell lines. (**B.**) Functional enrichment analysis of the 756 common proteins detected sEVs derived from the GBM cell lines was conducted using FunRich (version 3.1.3), (P values were calculated by a two-sided hypergeometric test – the top significant 5 annotations are shown). (**C.**) Classification of proteins detected in the GBM cell line-derived EVs (according to the PANTHER Protein Classification system [341]) identified 11 potential invasion-related categories. The number of proteins within each invasion-related protein class is shown for sEVs from each cell line. (**D.**) Proteins commonly used as exosomal markers: CD81, CD82, CD63, CD9, PDCD6IP (ALIX) and TSG101 were found to be elevated in sEVs compared to donor cells. (**E.**) Comparison of proteins identified in sEVs from each GBM cell line with the top 100 common proteins detected in EVs as compiled in Vesiclepedia. (**F.**) Venn diagram showing overlap between proteins identified in sEVs enriched from GBM cell lines (red-2086 proteins) and EV proteins compiled in Vesiclepedia (blue-13,267 proteins). *(Proteins matched by gene name; restricted to proteins annotated as originating from 'homo sapiens')*

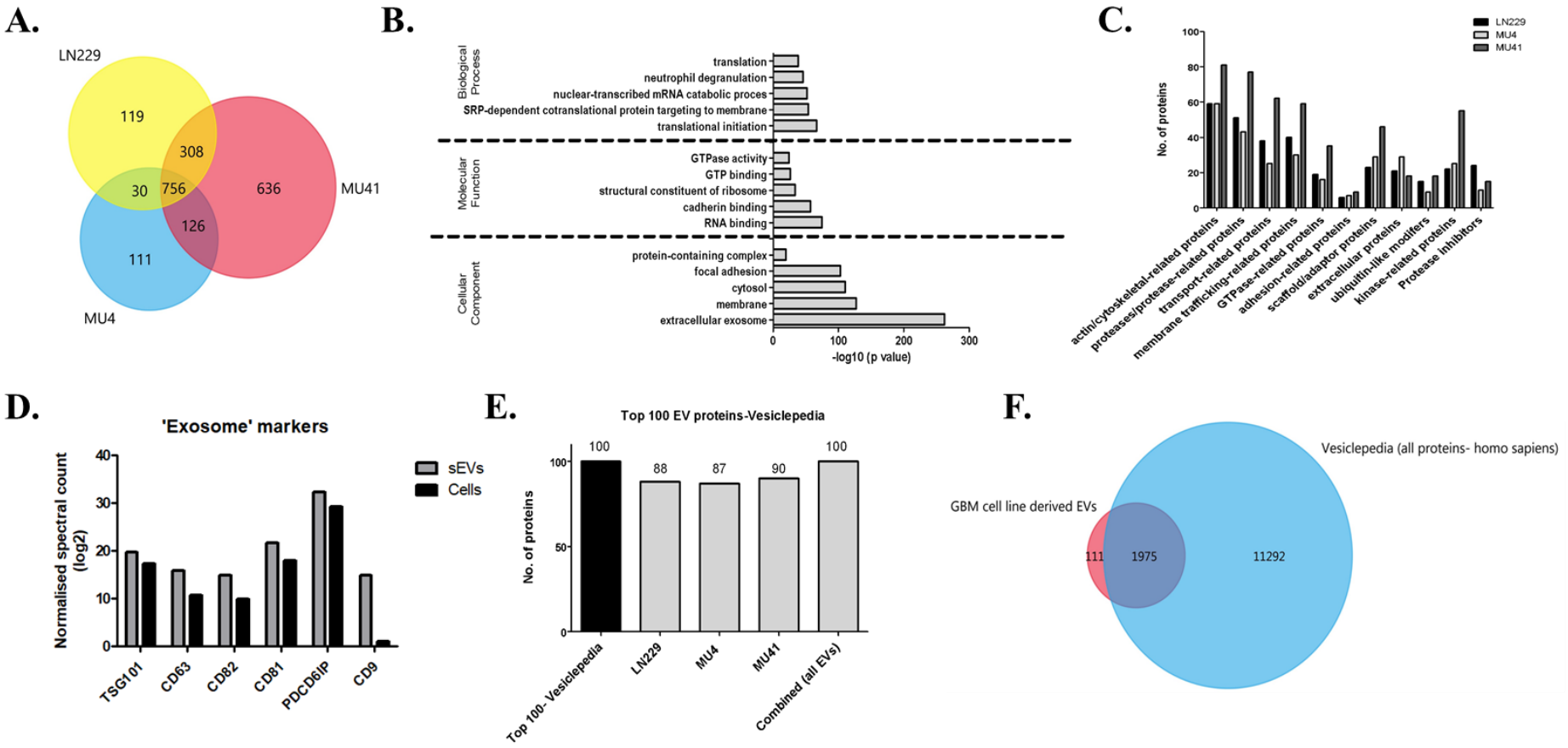
A.
LN229
119
308
30
756
636
MU41
126
111
MU4
B.
Biological Process
translation
neutrophil degranulation
nuclear-transcribed mRNA catabolic proces
SRP-dependent cotranslational protein targeting to membrane
translational initiation
Molecular Function
GTPase activity
GTP binding
structural constituent of ribosome
cadherin binding
RNA binding
Cellular Component
protein-containing complex
focal adhesion
cytosol
membrane
extracellular exosome
0
100
200
300
-log10 (p value)
C.
LN229
MU4
MU41
No. of proteins
actin/cytoskeletal-related proteins
proteases/protease-related proteins
transport-related proteins
membrane trafficking-related proteins
GTPase-related proteins
adhesion-related proteins
scaffold/adaptor proteins
extracellular proteins
ubiquitin-like modifers
kinase-related proteins
Protease inhibitors
D.
'Exosome' markers
Normalised spectral count (log2)
sEVs
Cells
TSG101
CD63
CD82
CD81
PDCD6IP
CD9
E.
Top 100 EV proteins-Vesiclepedia
No. of proteins
100
88
87
90
100
Top 100- Vesiclepedia
LN229
MU4
MU41
Combined (all EVs)
F.
Vesiclepedia (all proteins- homo sapiens)
GBM cell line derived EVs
111
1975
11292

5.2.1.3 Integrative analysis of GBM cell line MV proteome

Overall, a total of 1621 proteins were identified in the secreted MVs from the three different GBM cell lines (***Figure 5-4A***) (LN229–1283 proteins, MU4–790 proteins, MU41–1309 proteins). The U87MG cell line was omitted from the current study as the cell line and sEV proteomes have been previously investigated [472, 518-521]. Functional enrichment analysis of the 636 proteins commonly detected in sEVs from all three GBM cell lines revealed that significantly ($p<0.05$) enriched proteins in MVs largely reflected the donor cell and sEV proteomes (***Figure 5-4B***) and predominantly included actin/cytoskeletal and protease-related proteins, as observed in the corresponding proteomes for both GBM cells and sEVs (***Figure 5-4C***). Comparison of 'exosome' marker protein expression in sEVs, MVs and donor cells revealed that CD9 was the most enriched compared to donor cells, as seen in sEVs (***Figure 5-4D***). However, highlighting differences in vesicle composition, the MV proteome was lacking in TSG101 expression, unlike sEVs.

5.2.1.4 Comparison of protein cargo identified in GBM cell line sEVs and MVs

Comparison of the total proteins detected in GBM cell derived sEVs and MVs revealed 1470 proteins that were common in the cargo of both vesicle types, with 151 proteins unique to MVs and 616 unique to sEVs (***Figure 5-5A***). Functional annotations for proteins that were uniquely detected in MVs compared to sEVs was carried out using FunRich (version 3.1.3) (***Figure 5-5B-C***). Unlike MVs, the proteins uniquely detected in sEVs were assigned to annotations related to cell-ECM and cell-cell signalling ('integrin binding', 'signalling receptor binding', 'intracellular protein transport', 'cell adhesion'), whereas proteins uniquely detected in MVs were mainly assigned to annotations related to intercellular events ('RNA binding', 'ATP binding', 'cell proliferation' and 'protein transport').

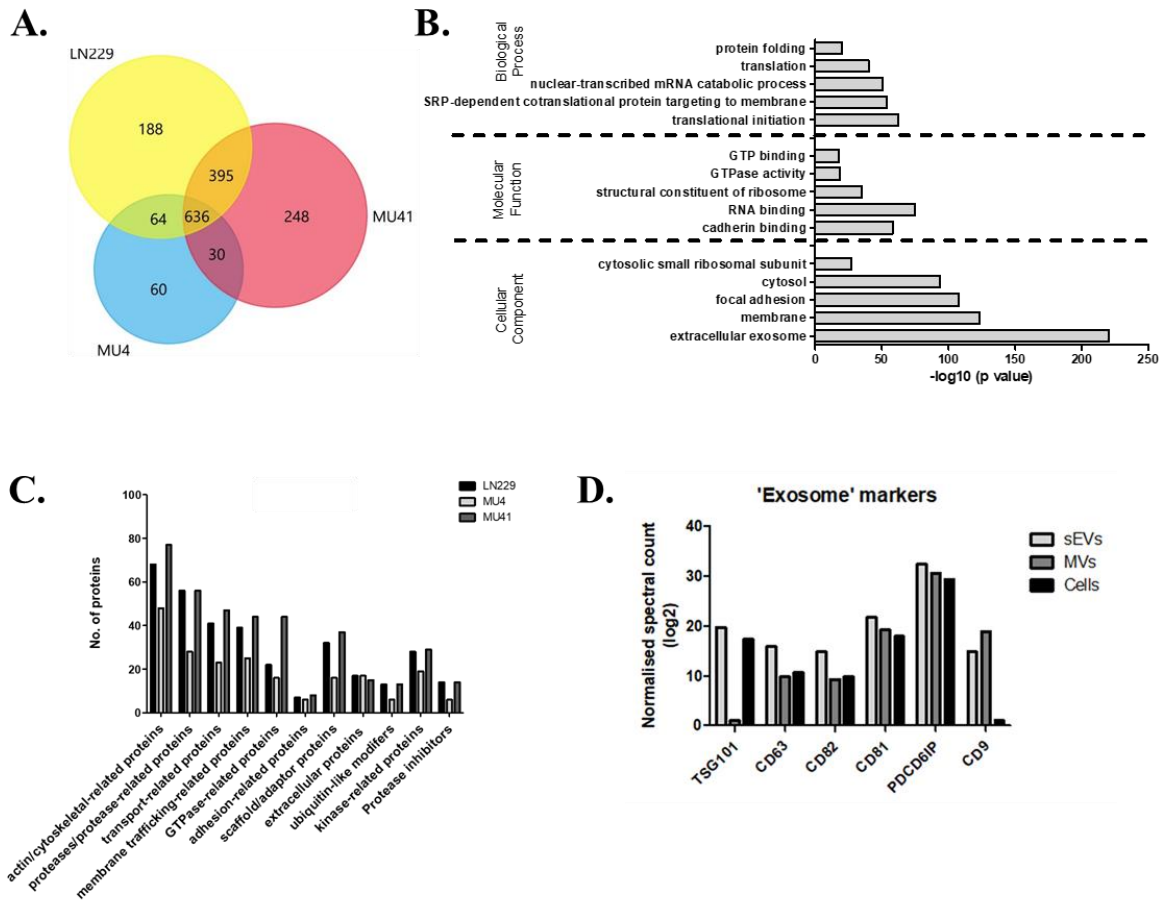

Figure 5-4: Integrative analysis of the GBM cell line MV proteome using the FunRich and PANTHER bioinformatics platforms

(**A.**) A Venn diagram of total proteins detected in GBM cell line derived MVs. 636 common proteins detected in the MVs enriched from the three GBM cell lines. (**B.**) Functional enrichment analysis of the 636 common proteins detected MVs derived from the GBM cell lines was conducted using FunRich (version 3.1.3), (P values were calculated by a two-sided hypergeometric test – the top significant 5 annotations are shown). (**C.**) Classification of proteins detected in the GBM cell line MVs (according to the PANTHER Protein Classification system [341]) identified 11 potential invasion-related categories. The number of proteins within each invasion-related protein class is shown for MVs from each cell line. (**D.**) Comparison of proteins commonly used as exosomal markers: CD81, CD82, CD63, CD9, PDCD6IP (ALIX) and TSG101 in sEVs, MVs and donor cells.

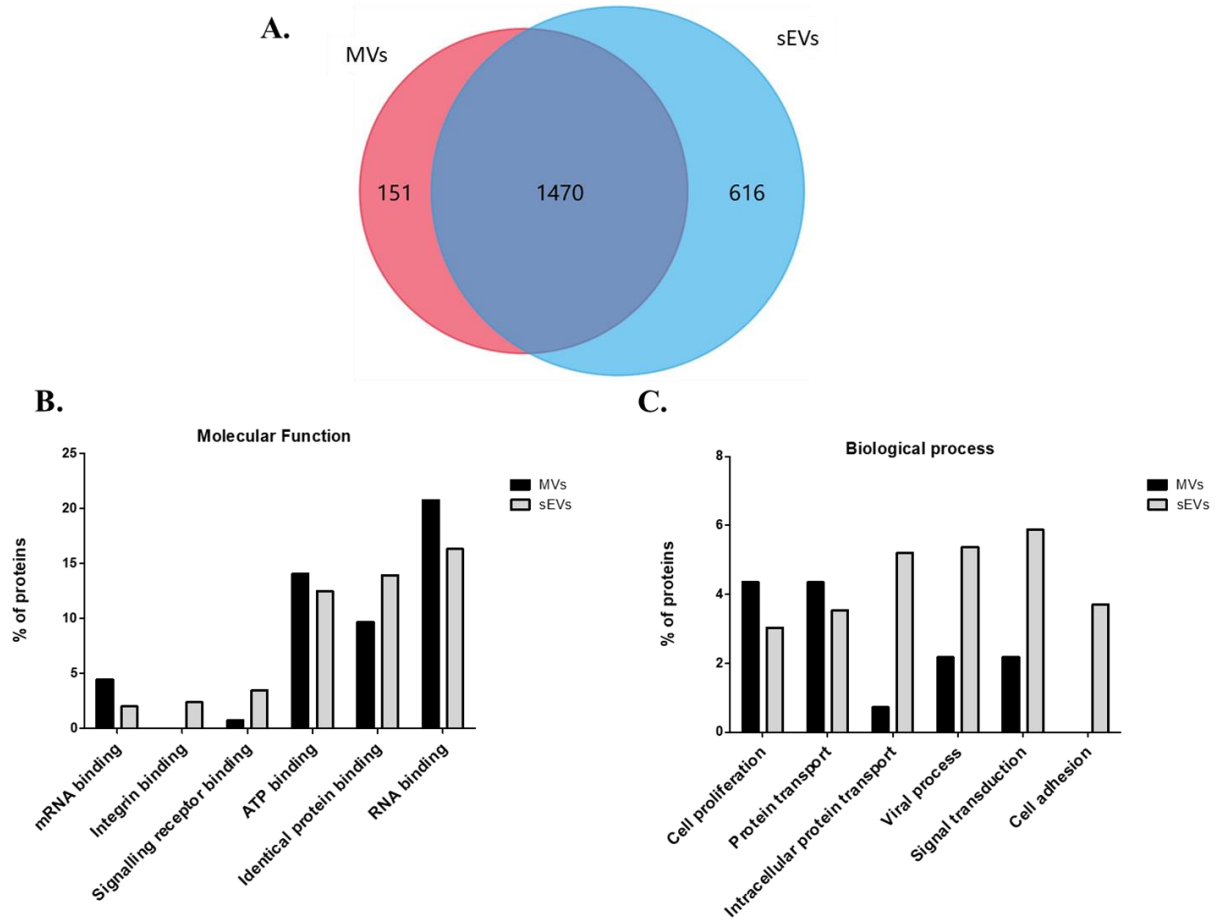

Figure 5-5: Comparison of GBM cell line derived sEV and MV proteomes

(**A.**) A Venn diagram representing the total proteins detected in the proteome of the GBM cell line derived MVs (red) and sEVs (blue), revealing 1470 proteins common in both vesicle populations (151 unique in MVs, and 616 unique in EVs). FunRich analysis of the proteins unique to each vesicle population (MV-151; EV-616) revealing the distribution of proteins within the top 6 annotations for (**B.**) molecular function and (**C.**) biological process comparing proteins uniquely detected in sEVs and MVs.

5.2.2 Invadopodia-related proteins in the GBM cell line, sEV and MV proteomes

5.2.2.1 Identification of invadopodia-related proteins in the GBM cell line proteome

Invadopodia-related proteins in each GBM cell line were identified according to the workflow represented in ***Figure 5-6A-B***. A total of 47 proteins known to facilitate invadopodia formation/activity were identified, of which 27 proteins were common to all 3 cell lines (***Table 5-1***). The relative expression levels of proteins identified in the GBM cell line proteomes were also examined and unsupervised hierarchical clustering revealed four distinct clusters of differentially expressed proteins, visualised as a heatmap, between the three GBM cell lines (***Figure 5-6C***). To gain further insight into these four distinct clusters, the invadopodia-related proteins within each cluster were listed (***Figure 5-6D***). This revealed that GBM cell lines with high FITC-gelatin degrading activity (LN229 and MU41) had high relative expression of key proteins involved in invadopodia maturation/proteolytic activity (such as BSG, CLIP1, MMP14, MMP2, RAB5A), whilst lower invadopodia activity MU4 cells were lacking in the expression of these proteins. Interestingly, further examination revealed that the pink cluster (representing proteins with high expression levels in LN229 and MU41 cells but low in MU4 cells) also contained three cathepsins (CTSA, CTSB and CTSD) which, although not directly linked with invadopodia activity, are known to promote an invasive phenotype [371, 522]. Lastly, proteins within the brown and dark blue clusters were highly expressed in MU4 cells (in conjunction with either MU41 in the brown cluster, or LN229 in the dark blue cluster). Examination of these two clusters revealed that MU4 cells have high expression of actin-related proteins and proteins that drive invadopodia assembly (ACTR2, ACTR3, ARF6, CFL1, CSNK2A1, ENAH, FHOD1, NCKAP1, WASF2), however these clusters lacked many of the proteins involved in invadopodia maturation/proteolytic activity (BSG, CLIP1, MMP14, MMP2, RAB5A). This is in accordance with previous findings that demonstrated MU4 cells form relatively high numbers of invadopodia but show minimal degradative ability (***Figure 3-2D***).

Figure 5-6: Invadopodia-related proteins detected in GBM cell line proteome

(**A.**) A schematic representing the workflow utilised to identify invadopodia-related proteins present in the proteome of each GBM cell line. (**B**.) The invasion-related proteins detected in the total proteome of each cell line were shortlisted based on PubMed searches ('protein name' and 'invasion'). The resultant invasion-related proteins were then subjected to literature searches to identify proteins in each cell line with published links to invadopodia (LN229- 35 proteins, MU4- 36 proteins, MU41- 39 proteins). (**C**.) Differential expression analysis of total proteins for each GBM cell line (normalised Z-scores generated using the Perseus Bioinformatics (version 1.5.5.0) platform [339]) displayed as a heatmap. Proteins were divided into four clusters based on hierarchical clustering, as shown to the left of the heatmap. (**D**.) Invadopodia-related proteins present within each cluster (indicated by the relevant cluster colour) are listed.

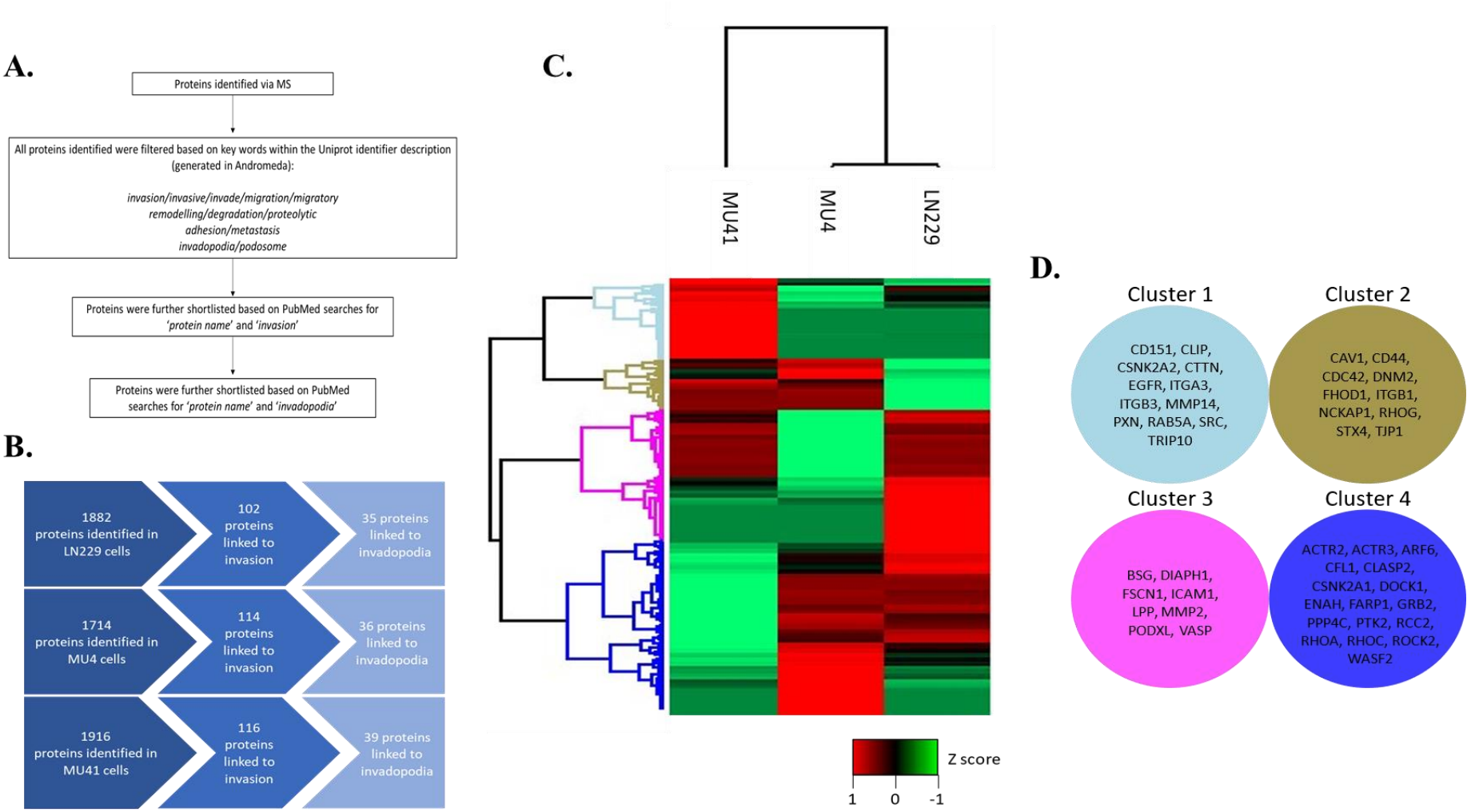
A.
Proteins identified via MS
All proteins identified were filtered based on key words within the Uniprot identifier description (generated in Andromeda):
invasion/invasive/invade/migration/migratory
remodelling/degradation/proteolytic
adhesion/metastasis
invadopodia/podosome
Proteins were further shortlisted based on PubMed searches for 'protein name' and 'invasion'
Proteins were further shortlisted based on PubMed searches for 'protein name' and 'invadopodia'
B.
1882 proteins identified in LN229 cells
102 proteins linked to invasion
35 proteins linked to invadopodia
1714 proteins identified in MU4 cells
114 proteins linked to invasion
36 proteins linked to invadopodia
1916 proteins identified in MU41 cells
116 proteins linked to invasion
39 proteins linked to invadopodia
C.
MU41
MU4
LN229
Z score
1
0
-1
D.
Cluster 1
CD151, CLIP, CSNK2A2, CTTN, EGFR, ITGA3, ITGB3, MMP14, PXN, RAB5A, SRC, TRIP10
Cluster 2
CAV1, CD44, CDC42, DNM2, FHOD1, ITGB1, NCKAP1, RHOG, STX4, TJP1
Cluster 3
BSG, DIAPH1, FSCN1, ICAM1, LPP, MMP2, PODXL, VASP
Cluster 4
ACTR2, ACTR3, ARF6, CFL1, CLASP2, CSNK2A1, DOCK1, ENAH, FARP1, GRB2, PPP4C, PTK2, RCC2, RHOA, RHOC, ROCK2, WASF2

Table 5-1: Invadopodia-related proteins detected in the GBM cell line proteome

Gene	Protein	Invadopodia related evidence	LFQ intensities[A]		
			LN229	**MU4**	**MU41**
ACTR2	Actin-related protein 2	Actin-related protein 2 is a major constituent of the ARP2/3 complex, an essential component involved in invadopodia precursor core formation. Arp2/3 promotes actin polymerization to form branched F-actin networks. [523, 524]	29.21	30.19	29.44
ACTR3	Actin-related protein 3	Actin-related protein 3 is a major constituent of the ARP2/3 complex, an essential component involved in invadopodia precursor core formation. Arp2/3 promotes actin polymerization to form branched F-actin networks. [523, 524]	30.26	30.97	29.94
ARF6	ADP-ribosylation factor 6	ARF6 has an established role in invadopodia. It promotes the formation of Rac1 and WAVE dependent ventral F-actin rosettes in breast cancer cells in response to epidermal growth factor. ARF6 also localizes to invadopodia in melanoma cells, where it regulates invadopodia activity through the activation of the MEK/ERK signalling pathway. [437, 525]	27.26	29.43	27.127
BSG	Basigin	Basigin/CD147: upregulation induced MT1-MMP-dependent invadopodia activity in breast epithelial cells. Also promotes epidermal growth factor receptor (EGFR)-Ras-ERK signalling via interactions with CD44. [362, 363]	28.86	24.37	29.80
CAV1	Caveolin-1	Mechanosensitive caveolin-1 activation-induced PI3K/Akt/mTOR signalling pathway promotes breast cancer motility, invadopodia formation and metastasis *in vivo*. [526]	26.70	29.56	29.42
CD151	CD151 antigen	CD151, together with integrin α3β1 located at invadopodia, was found to regulate expression and activity of MMPs. [527]	ND	ND	26.05
CD44	CD44 antigen	Splice isoform CD44s promotes cortactin phosphorylation and recruits MT1-MMP to invadopodia [528]	30.91	31.75	31.56
CDC42	Cell division control protein 42 homolog	N-WASP and Arp2/3 form an active complex through CDC42 which promotes invadopodia assembly [135]	28.27	29.08	29.168
CFL1	Cofilin-1	Cofilin is necessary for the stabilization and maturation of invadopodia [135]	33.45	32.81	32.52
CLASP2	CLIP-associating protein 2	Microtubule stabilising protein involved in the regulation of cell protrusions such as podosomes and invadopodia [529]	ND	25.46	ND
CLIP1	CAP-Gly domain-containing	Also known as CLIP-170. Microtubule binding protein that forms a complex with RAC1/Cdc42/IQGAP1 and is involved in the	ND	ND	23.95

	linker protein 2	regulation of invadopodia formation and invasion in human breast cancer cells [530, 531]			
CSNK2A1	Casein kinase II subunit alpha	Subunit of Casein Kinase 2. Casein Kinase 2 phosphorylates cortactin and regulates Arp2/3 activity and subsequent invadopodia function [532]	27.95	28.02	26.65
CSNK2A2	Casein kinase II subunit alpha	Subunit of Casein Kinase 2. Casein Kinase 2 phosphorylates cortactin and regulates Arp2/3 activity and subsequent invadopodia function [532]	24.47	24.57	25.16
CTTN	Src substrate cortactin	Cortactin is a critical regulator of actin nucleation in the development of invadopodia [533]	27.77	27.25	29.72
DIAPH1	Protein diaphanous homolog 1	Actin nucleation and elongation factor required for the assembly of F-actin structures. DIAPH1 was found to be critical for invadopodia formation in U87MG cells [534]	24.94	ND	24.33
DNM2	Dynamin-2	Dynamin2 GTPase is a microtubule-associated force-producing protein that contributes to invadopodia formation in invasive bladder cancer cells via its proline/arginine-rich domain (PRD) [535]	26.82	27.60	27.33
DOCK1	Dedicator of cytokinesis protein 1	Rac1 exchange factor that is localised to invadopodia, involved in modulating invadopodia dynamics in breast cancer cells [536].	ND	24.55	ND
EGFR	Epidermal growth factor receptor	Established receptor involved in invadopodia maturation, via an EGFR-Src-Arg-cortactin signalling pathway [123]	22.20	23.24	33.65
ENAH	Protein enabled homolog	Also known as 'Mena'. Involved in regulating the assembly of actin filaments. It is recruited to stabilise invadopodia via SHIP2 [537]	25.72	25.76	25.70
FARP1	FERM, ARHGEF and pleckstrin domain-containing protein 1	FARP1 overexpression promotes cell motility and filopodium formation via CDC42 activation [538]	ND	29.89	ND
FHOD1	FH1/FH2 domain-containing protein 1	Superresolution microscopy revealed the presence of formin FHOD1 and unbranched radial F-actin fibers emanating from invadopodia [539]	ND	24.41	26.27
FSCN1	Fascin	Actin bundling protein that stabilises actin filaments in invadopodia [470]	30.38	26.03	30.37
GRB2	Growth factor receptor-bound protein 2	Upstream activator of N-WASP in invadopodia formation [135]	25.67	25.88	ND

ICAM1	Intercellular adhesion molecule 1	A cell adhesion molecule in the ICAM superfamily, known for their ability to bind integrins to activate signalling. Often expressed at the cell surface where it may play a role in invadopodia maturation via interactions with integrins [540]	27.43	ND	24.33
ITGA3	Integrin alpha-3	Integrin alpha-3/beta-3 provides a docking site for FAP (seprase) at invadopodia plasma membranes in a collagen-dependent manner and hence may participate in the adhesion, formation of invadopodia and matrix degradation processes [541]	26.07	25.02	28.84
ITGB1	Integrin beta-1	β1 integrin regulates SNARE-dependent trafficking and is required for the activation and delivery of Src and EGFR to sites of invadopodia formation in order to support tumour cell invasion [542]	29.90	30.06	30.07
ITGB3	Integrin beta-3	Integrin alpha-3/beta-3 provides a docking site for FAP (seprase) at invadopodia plasma membranes in a collagen-dependent manner and hence may participate in the adhesion, formation of invadopodia and matrix degradation processes [541]	28.38	26.05	29.06
LPP	Lipoma-preferred partner	Src-mediated LPP phosphorylation at specific tyrosine residues (Y245/301/302) is critical for invadopodia formation in breast cancer cells [543]	25.89	ND	25.46
MMP14	Matrix metalloproteinase-14	MT1-MMP: transmembrane protease located within invadopodia [544]	27.13	27.27	27.48
MMP2	72 kDa type IV collagenase	Metalloprotease that is widely associated with invadopodia [136]	23.19	ND	26.32
NCKAP1	Nck-associated protein 1	A subunit of the Arp2/3-WAVE complex involved in actin organisation during invadopodia formation [545]	26.04	27.63	26.48
PODXL	Podocalyxin	Podocalyxin-like 1 promotes invadopodia formation and metastasis through activation of Rac1/Cdc42/cortactin signalling in breast cancer cells [546]	26.76	ND	ND
PPP4C	Serine/threonine-protein phosphatase 4 catalytic subunit	Protein phosphatase that upregulates MMP-2 and MMP-9 via pAKT [547]	ND	25.07	ND
PTK2	Focal adhesion kinase 1	PTK2 is a focal adhesion-associated protein kinase involved in focal adhesion-mediated motility and has been implicated in invadopodia regulation [548]	ND	23.54	ND
PXN	Paxillin	A cytoskeletal protein involved in actin-membrane attachment at sites of cell adhesion to the ECM. JNK-paxillin signalling can promote invadopodia activity [549]	25.26	26.29	28.12
RAB5A	Ras-related protein Rab-5A	Rab5a GTPase is a major regulator of MT1-MMP trafficking and invadopodia formation [550]. MT1-MMP vesicles that are positive for Rab5a localise to invadopodia [551]	ND	ND	25.99

RCC2	Protein RCC2	Acts as a regulator of Rac1 and Arf6, as well as binding to cortactin, linking RCC2 to number of key invadopodia proteins [552]	28.31	28.42	26.36
RHOA	Transforming protein RhoA	RhoA–ROCK signalling promotes invadopodia formation and activity [140]	ND	25.82	ND
RHOC	Rho-related GTP-binding protein RhoC	RhoC activation in areas surrounding invadopodia restricts cofilin activity to within the invadopodium core, resulting in a focused invadopodium [553]	30.08	30.73	29.93
RHOG	Rho-related GTP-binding protein RhoG	RhoG and SGEF modulate the phosphorylation of paxillin, which plays a key role during invadopodia disassembly [536]	25.89	27.63	27.62
ROCK2	Rho-associated protein kinase 2	Protein kinase which is a key regulator of actin cytoskeleton. Matrix rigidity can drive ROCK signaling to enhance invadopodia function [138]	26.69	27.30	24.36
SRC	Proto-oncogene tyrosine-protein kinase Src	Src tyrosine kinase activates numerous proteins in invadopodia-related signalling pathways, including adaptor proteins such as Tks5 [554]	ND	ND	28.22
STX4	Syntaxin-4	SNARE protein syntaxin4: mediates trafficking of MT1-MMP and EGFR for invadopodia activity [555]	25.98	26.79	26.96
TJP1	Tight junction protein ZO-1	Tight Junction Protein is a scaffolding protein that plays a role in the regulation of cell migration by targeting CDC42BPB to the leading edge of migrating cells. Plays a role as a partner for ADAM-12 in invadopodia [556, 557]	ND	26.04	23.76
TRIP10	Cdc42-interacting protein 4	CDC42-interacting protein 4: promotes metastasis of nasopharyngeal carcinoma by mediating invadopodia formation and activating EGFR signalling. Also promotes CDC42-induced actin polymerization by recruiting WASL/N-WASP which in turn activates the Arp2/3 complex [558]	ND	ND	24.82
VASP	Vasodilator-stimulated phosphoprotein	Actin-associated protein that stimulates actin filament elongation by promoting the transfer of profilin-bound actin monomers onto the barbed end of growing actin filaments. In colon cancer cells, VASP is found within invadopodia, where it colocalizes with cortactin and actin [559, 560]	25.75	ND	25.56
WASF2	Wiskott-Aldrich syndrome protein family member 2	Promotes formation of actin filaments. Part of the WAVE complex that activates actin nucleating machinery Arp2/3 to drive invadopodia formation [561, 562]	25.65	26.30	25.60

[A] indicates averaged MS/MS label-free quantitation intensity (*ND: not detected)*

5.2.2.2 Identification of invadopodia-related proteins in the GBM cell line sEV proteome

Invadopodia-related proteins in sEVs from each GBM cell line were identified according to the workflow represented in ***Figure 5-7A-B***. A total of 49 proteins known to promote invadopodia formation/activity were identified in the sEVs, of which 28 proteins were common in sEVs from all three cell lines (***Table 5-2***). The relative expression levels of proteins identified in the GBM sEV proteomes were also examined and unsupervised hierarchical clustering revealed four distinct clusters of differentially expressed proteins, visualised as a heatmap, between sEVs from the three GBM cell lines (***Figure 5-7C***). To gain further insight into these four distinct clusters, the invadopodia-related proteins within each cluster were listed (***Figure 5-7D***). This revealed that differences in the expression levels of invadopodia-related proteins in the donor GBM cell proteomes were also reflected in the sEV proteomes, with sEVs from high invadopodia activity donor cell lines, LN229 and MU41, found to be enriched in invadopodia-associated proteases (MMP2, MMP14) and proteins that promote protease production (BSG/CD147, ITGA3, ITGB3), as well as key proteins involved in the formation of the invadopodium actin core (CTTN, CFL1, SRC) compared to sEVs from the low invadopodia activity GBM cell line, MU4, corresponding with the low levels of FITC-gelatin degradation and MMP-2 secretion observed for the MU4 cell line (***Figure 3-2***).

Figure 5-7: Invadopodia-related proteins detected in GBM cell line sEV proteome

(**A.**) A schematic representing the workflow utilised to identify invadopodia-related proteins present in the proteome of each GBM cell line derived sEVs. (**B**.) The invasion-related proteins detected in the total proteome of sEVs were shortlisted based on PubMed searches ('protein name' and 'invasion'). The resultant invasion-related proteins were then subjected to literature searches to identify sEV proteins with published links to invadopodia (LN229- 35 proteins, MU4 – 33 proteins, MU41 -45 proteins). (**C**.) Differential expression analysis of total proteins for sEVs from each GBM cell line (normalised Z-scores generated using the Perseus Bioinformatics (version 1.5.5.0) platform [339]) displayed as a heatmap. Proteins were divided into four clusters based on hierarchical clustering, as shown to the left of the heatmap. (**D**.) Invadopodia-related proteins present within each cluster (indicated by the relevant cluster colour) are listed.

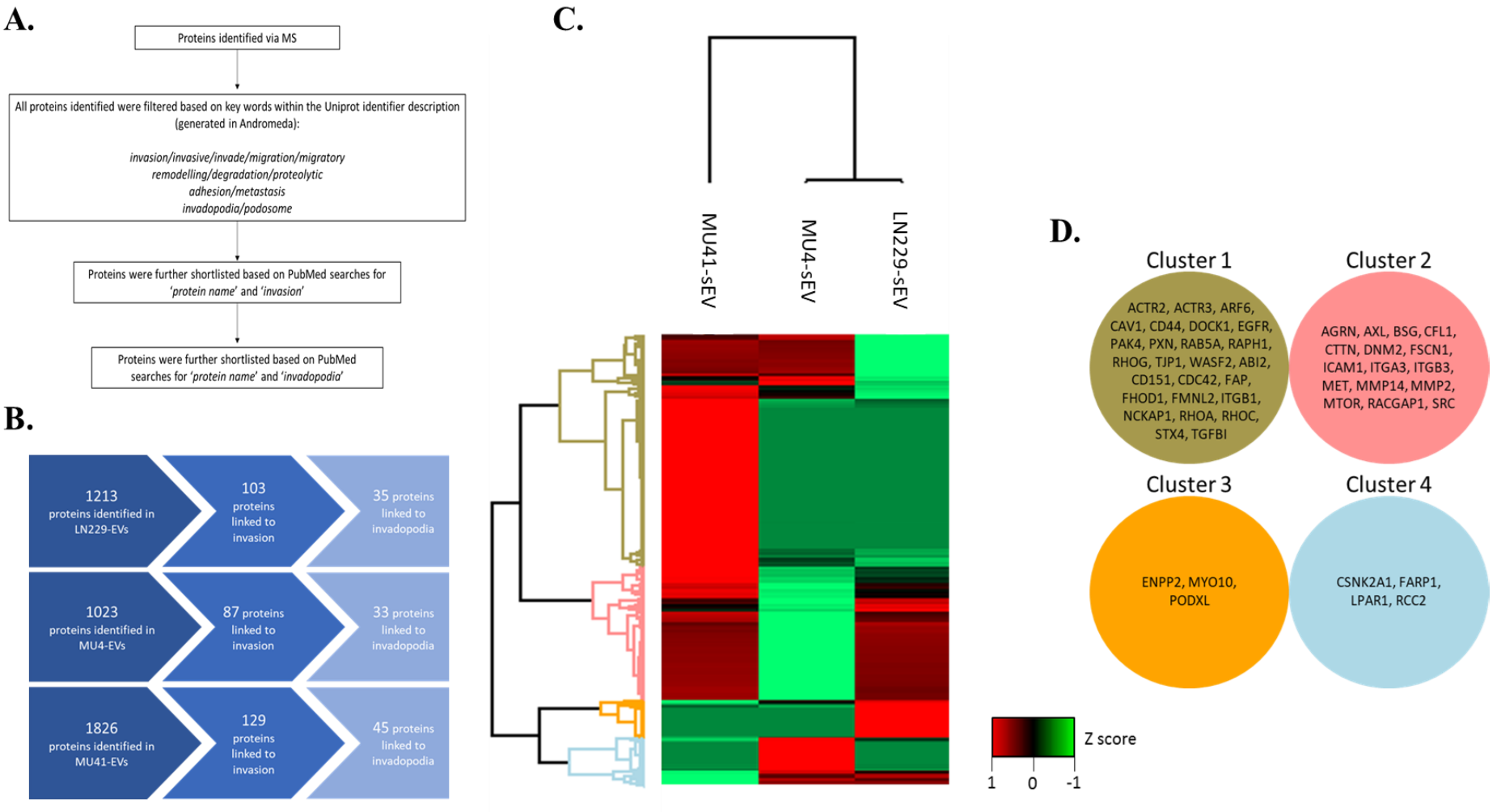
A.
Proteins identified via MS
All proteins identified were filtered based on key words within the Uniprot identifier description (generated in Andromeda):
invasion/invasive/invade/migration/migratory
remodelling/degradation/proteolytic
adhesion/metastasis
invadopodia/podosome
Proteins were further shortlisted based on PubMed searches for 'protein name' and 'invasion'
Proteins were further shortlisted based on PubMed searches for 'protein name' and 'invadopodia'
B.
1213 proteins identified in LN229-EVs
103 proteins linked to invasion
35 proteins linked to invadopodia
1023 proteins identified in MU4-EVs
87 proteins linked to invasion
33 proteins linked to invadopodia
1826 proteins identified in MU41-EVs
129 proteins linked to invasion
45 proteins linked to invadopodia
C.
MU41-sEV
MU4-sEV
LN229-sEV
Z score
1
0
-1
D.
Cluster 1
ACTR2, ACTR3, ARF6, CAV1, CD44, DOCK1, EGFR, PAK4, PXN, RAB5A, RAPH1, RHOG, TJP1, WASF2, ABI2, CD151, CDC42, FAP, FHOD1, FMNL2, ITGB1, NCKAP1, RHOA, RHOC, STX4, TGFBI
Cluster 2
AGRN, AXL, BSG, CFL1, CTTN, DNM2, FSCN1, ICAM1, ITGA3, ITGB3, MET, MMP14, MMP2, MTOR, RACGAP1, SRC
Cluster 3
ENPP2, MYO10, PODXL
Cluster 4
CSNK2A1, FARP1, LPAR1, RCC2

Table 5-2: Invadopodia-related proteins detected in the GBM cell line sEV proteome

Gene	Protein	Invadopodia related evidence	LFQ intensities[A]		
			LN229	**MU4**	**MU41**
ABI2	Abl interactor 2	Regulator of actin cytoskeleton dynamics underlying cell motility and adhesion. Functions as a component of the WAVE2 complex, which activates actin nucleating machinery Arp2/3 to drive invadopodia formation. [562, 563]	ND	ND	25.09
ACTR2	Actin-related protein 2	Actin-related protein 2 is a major constituent of the ARP2/3 complex, an essential component involved in invadopodia precursor core formation. Arp2/3 promotes actin polymerization to form branched F-actin networks. [523, 524]	27.97	27.76	29.63
ACTR3	Actin-related protein 3	Actin-related protein 3 is a major constituent of the ARP2/3 complex, an essential component involved in invadopodia precursor core formation. Arp2/3 promotes actin polymerization to form branched F-actin networks. [523, 524]	29.09	28.75	30.52
AGRN	Agrin	Secreted and cell surface Agrin binds the Lrp4 receptor and promotes the formation of a Agrin–Lrp4–MuSK signalling complex, which activates FAK and Arp2/3 associated invadopodia formation [564]	32.47	28.88	30.76
ARF6	ADP-ribosylation factor 6	ARF6 has an established role in invadopodia. It promotes the formation of Rac1 and WAVE dependent ventral F-actin rosettes in breast cancer cells in response to epidermal growth factor. ARF6 also localizes to invadopodia in melanoma cells, where it regulates invadopodia activity through the activation of the MEK/ERK signalling pathway [437, 525]	28.7	30.13	29.52
AXL	Tyrosine-protein kinase receptor UFO	Cross-talk between Receptor Tyrosine Kinases AXL and ERBB3 regulates invadopodia formation in melanoma cells [565]	26.28	24.99	25.71
BSG	Basigin	Basigin/CD147: upregulation induced MT1-MMP-dependent invadopodia activity in breast epithelial cells. Also promotes epidermal growth factor receptor (EGFR)-Ras-ERK signalling via interactions with CD44 [362, 363]	30.07	26.66	32.72
CAV1	Caveolin-1	Mechanosensitive caveolin-1 activation-induced PI3K/Akt/mTOR signaling pathway promotes breast cancer motility, invadopodia formation and metastasis *in vivo* [526]	ND	30.58	27.73
CD151	CD151 antigen	CD151, together with integrin α3β1 located at invadopodia, was found to regulate expression and activity of MMPs [527]	ND	ND	28.32
CD44	CD44 antigen	Splice isoform CD44s promotes cortactin phosphorylation and recruits MT1-MMP to invadopodia [528]	31.2	32.29	33.58

CDC42	Cell division control protein 42 homolog	N-WASP and Arp2/3 form an active complex through CDC42 which promotes invadopodia assembly [135]	28.62	28.68	29.79
CFL1	Cofilin-1	Cofilin is necessary for the stabilization and maturation of invadopodia [135]	34.36	30.03	33.04
CSNK2A1	Casein kinase II subunit alpha	Subunit of Casein Kinase 2. Casein Kinase 2 phosphorylates cortactin and regulates Arp2/3 activity and subsequent invadopodia function [532]	26.3	28.14	26.48
CTTN	Src substrate cortactin	Cortactin is a critical regulator of actin nucleation in the development of invadopodia [533]	25.84	ND	27.97
DNM2	Dynamin-2	Dynamin2 GTPase is a microtubule-associated force-producing protein that contributes to invadopodia formation in invasive bladder cancer cells via its proline/arginine-rich domain (PRD) [535]	26.32	25.49	27.6
DOCK1	Dedicator of cytokinesis protein 1	Rac1 exchange factor that is localised to invadopodia, involved in modulating invadopodia dynamics in breast cancer cells [536].	ND	27.47	25.47
EGFR	Epidermal growth factor receptor	Established receptor involved in invadopodia maturation, via an EGFR-Src-Arg-cortactin signalling pathway [123]	25.73	23.43	35.67
ENPP2	Ectonucleotide pyrophosphatase/phosphodiesterase family member 2	Can induce invadopodia formation in the fibrosarcoma cell line HT1080 through activation of the LPA4 receptor [566]	29.96	25.42	24.90
FAP	Prolyl endopeptidase FAP	Also known as Seprase, a gelatin-degrading membrane-protease complex that is expressed at the invasive front of malignant melanoma cells on invadopodia [125]	ND	ND	28.79
FARP1	FERM, ARHGEF and pleckstrin domain-containing protein 1	FARP1 overexpression promotes cell motility and filopodium formation via CDC42 activation [538]	27.51	31.32	26.42
FHOD1	FH1/FH2 domain-containing protein 1	Superresolution microscopy revealed the presence of formin FHOD1 and unbranched radial F-actin fibers emanating from invadopodia [539]	ND	ND	24.99
FMNL2	Formin-like protein 2	Cortactin directly binds to FMNL2 to promote actin polymerization and recycling endosome motility. FMNL2 was necessary for invadopodia formation and function in CRC cells [567]	26.32	26.51	26.39
FSCN1	Fascin	Actin bundling protein that stabilises actin filaments in invadopodia [470]	29.26	ND	29.36
ICAM1	Intercellular adhesion molecule 1	A cell adhesion molecule in the ICAM superfamily, known for their ability to bind integrins to activate signalling. Often expressed at the cell surface where it may play a role in invadopodia maturation via interactions with integrins [540]	30.86	ND	27.12

ITGA3	Integrin alpha-3	Integrin alpha-3/beta-3 provides a docking site for FAP (seprase) at invadopodia plasma membranes in a collagen-dependent manner and hence may participate in the adhesion, formation of invadopodia and matrix degradation processes [541]	30.64	25.61	33.4
ITGB1	Integrin beta-1	β1 integrin regulates SNARE-dependent trafficking and is required for the activation and delivery of Src and EGFR to sites of invadopodia formation in order to support tumour cell invasion [542]	33.04	33.23	34.57
ITGB3	Integrin beta-3	Integrin alpha-3/beta-3 provides a docking site for FAP (seprase) at invadopodia plasma membranes in a collagen-dependent manner and hence may participate in the adhesion, formation of invadopodia and matrix degradation processes [541]	31.09	28.21	32.09
LPAR1	Lysophosphatidic acid receptor 1	A common and major receptor used for hypoxia-induced invadopodia production [568]	ND	26.03	ND
MET	Hepatocyte growth factor receptor	Met receptor tyrosine kinase signals through a cortactin-Gab1 scaffold complex to mediate invadopodia activity [143]	26.27	ND	26.85
MMP14	Matrix metalloproteinase-14	MT1-MMP: transmembrane protease located within invadopodia [544]	28.05	ND	30.15
MMP2	72 kDa type IV collagenase	Metalloprotease that is widely associated with invadopodia [136]	32.69	23.73	27.89
MTOR	Serine/threonine-protein kinase mTOR	Cav-1 activation-induces PI3K/Akt/mTOR signaling to promote invadopodia formation in breast carcinoma MDA-MB-231 cells [526]	25.66	23.72	25.14
MYO10	Unconventional myosin-X	Myosin that is localised to invadopodia. Acts as an actin-based motor, with binding sites for phosphatidylinositol (3,4,5)-trisphosphate, microtubules and integrins [569]	22.89	ND	ND
NCKAP1	Nck-associated protein 1	A subunit of the Arp2/3-WAVE complex involved in actin organisation during invadopodia formation [545]	25.82	26.39	29.02
PAK4	Serine/threonine-protein kinase PAK 4	PAK4 is a key mediator of RhoA activity during invadopodia maturation [570]	ND	ND	25.06
PODXL	Podocalyxin	Podocalyxin-like 1 promotes invadopodia formation and metastasis through activation of Rac1/Cdc42/cortactin signalling in breast cancer cells [546]	25.94	ND	ND
PXN	Paxillin	A cytoskeletal protein involved in actin-membrane attachment at sites of cell adhesion to the ECM. JNK-paxillin signalling can promote invadopodia activity [549]	ND	ND	24.25
RAB5A	Ras-related protein Rab-5A	Rab5a GTPase is a major regulator of MT1-MMP trafficking and invadopodia formation [550]. MT1-MMP vesicles that are positive for Rab5a localise to invadopodia [551]	ND	ND	25.36

RACGAP1	Rac GTPase-activating protein 1	Binds to IQGAP1 to mediate Rac1 deactivation. Phosphorylation of RacGAP1 promotes its recruitment to IQGAP1 at the tips of invadopodia [571]	31.37	23.9	26.89
RAPH1	Ras-associated and pleckstrin homology domains-containing protein 1	Localised to invadopodia and regulates actin dynamics through interaction with Ena/Vasodilator proteins as well as direct binding to filamentous actin to regulate actin network assembly [559]	ND	ND	24.79
RCC2	Protein RCC2	Acts as a regulator of Rac1 and Arf6, as well as binding to cortactin, linking RCC2 to number of key invadopodia proteins [552]	ND	24.97	ND
RHOA	Transforming protein RhoA	RhoA–ROCK signalling promotes invadopodia formation and activity [140]	28.26	28.58	29.63
RHOC	Rho-related GTP-binding protein RhoC	RhoC activation in areas surrounding invadopodia restricts cofilin activity to within the invadopodium core, resulting in a focused invadopodium [553]	30.21	30.41	31.6
RHOG	Rho-related GTP-binding protein RhoG	RhoG and SGEF modulate the phosphorylation of paxillin, which plays a key role during invadopodia disassembly [536]	27.57	28.71	30.38
SRC	Proto-oncogene tyrosine-protein kinase Src	Src tyrosine kinase activates numerous proteins in invadopodia-related signalling pathways, including adaptor proteins such as Tks5 [554]	28.16	26.11	31.65
STX4	Syntaxin-4	SNARE protein syntaxin4: mediates trafficking of MT1-MMP and EGFR for invadopodia activity [555]	27.06	27.47	30.31
TGFBI	Transforming growth factor-beta-induced protein ig-h3	A transforming growth factor beta (TGFβ) inducible secreted extracellular matrix (ECM) protein. It has been shown to promote MMP secretion at invadopodia by interacting with integrin α2β1 and activating PI3K/AKT signalling. Processing of TGFBI by MMP-2 induces adhesion-related FAK/Src signalling in glioma cells and promotes invasion [572-574]	26.9	27.8	28.4
TJP1	Tight junction protein ZO-1	Tight Junction Protein is a scaffolding protein that plays a role in the regulation of cell migration by targeting CDC42BPB to the leading edge of migrating cells. Plays a role as a partner for ADAM-12 in invadopodia [556, 557]	ND	ND	25.17
WASF2	Wiskott-Aldrich syndrome protein family member 2	Promotes formation of actin filaments. Part of the WAVE complex that activates actin nucleating machinery Arp2/3 to drive invadopodia formation [561, 562]	ND	25.36	26.85

[A] indicates averaged MS/MS label-free quantitation intensity (*ND: not detected)*

5.2.2.3 Comparison of invadopodia-related proteins identified in the sEV and MV proteomes

A total of 45 invadopodia-related proteins were identified in the MV cargo from GBM cell lines, and 26 of these proteins were common in MVs from all three cell lines (***Table 5-3***). All 45 invadopodia-related proteins identified in the MV cargo were also detected in sEVs (***Figure 5-8)***. Furthermore, four invadopodia-related proteins that were identified solely in sEVs, were not detected in the MV cargo proteome: RCC2, PODXL, MYO10 and LPAR1. Examination of the mRNA expression levels of these four proteins in glioma and normal brain tissue using the Oncomine database revealed significant overexpression in ten independent datasets across all glioma grades, including grade IV GBM (***Table 5-4***). As approximately 70% of lower grade gliomas recur as GBMs within 5-10 years [575], this could implicate a role for these invadopodia-related proteins in the invasion of glioma cells of different histological grades.

Table 5-3: Invadopodia-related proteins detected in the GBM cell line MV proteome

Gene	Protein	Invadopodia related evidence	LFQ intensities[A]		
			LN229	**MU4**	**MU41**
ABI2	Abl interactor 2	Regulator of actin cytoskeleton dynamics underlying cell motility and adhesion. Functions as a component of the WAVE2 complex, which activates actin nucleating machinery Arp2/3 to drive invadopodia formation. [562, 563]	25.09	ND	ND
ACTR2	Actin-related protein 2	Actin-related protein 2 is a major constituent of the ARP2/3 complex, an essential component involved in invadopodia precursor core formation. Arp2/3 promotes actin polymerization to form branched F-actin networks. [523, 524]	28.23	28.28	30.55
ACTR3	Actin-related protein 3	Actin-related protein 3 is a major constituent of the ARP2/3 complex, an essential component involved in invadopodia precursor core formation. Arp2/3 promotes actin polymerization to form branched F-actin networks. [523, 524]	29.87	28.55	31.49
AGRN	Agrin	Secreted and cell surface Agrin binds the Lrp4 receptor and promotes the formation of a Agrin–Lrp4–MuSK signalling complex, which activates FAK and Arp2/3 associated invadopodia formation [564]	27.64	27.98	28.64
ARF6	ADP-ribosylation factor 6	ARF6 has an established role in invadopodia. It promotes the formation of Rac1 and WAVE dependent ventral F-actin rosettes in breast cancer cells in response to epidermal growth factor. ARF6 also localizes to invadopodia in melanoma cells, where it regulates invadopodia activity through the activation of the MEK/ERK signalling pathway [437, 525]	26.59	29.23	29.70
AXL	Tyrosine-protein kinase receptor UFO	Cross-talk between Receptor Tyrosine Kinases AXL and ERBB3 regulates invadopodia formation in melanoma cells [565]	24.85	24.89	24.88
BSG	Basigin	Basigin/CD147: upregulation induced MT1-MMP-dependent invadopodia activity in breast epithelial cells. Also promotes epidermal growth factor receptor (EGFR)-Ras-ERK signalling via interactions with CD44 [362, 363]	29.65	ND	32.39
CAV1	Caveolin-1	Mechanosensitive caveolin-1 activation-induced PI3K/Akt/mTOR signaling pathway promotes breast cancer motility, invadopodia formation and metastasis *in vivo* [526]	24.62	30.07	28.13
CD151	CD151 antigen	CD151, together with integrin α3β1 located at invadopodia, was found to regulate expression and activity of MMPs [527]	ND	ND	26.22
CD44	CD44 antigen	Splice isoform CD44s promotes cortactin phosphorylation and recruits MT1-MMP to invadopodia [528]	30.00	28.61	33.28
CDC42	Cell division control	N-WASP and Arp2/3 form an active complex through CDC42 which promotes invadopodia assembly [135]	30.08	28.67	29.21

	protein 42 homolog				
CFL1	Cofilin-1	Cofilin is necessary for the stabilization and maturation of invadopodia [135]	35.59	30.78	33.52
CSNK2A1	Casein kinase II subunit alpha	Subunit of Casein Kinase 2. Casein Kinase 2 phosphorylates cortactin and regulates Arp2/3 activity and subsequent invadopodia function [532]	26.06	27.36	ND
CTTN	Src substrate cortactin	Cortactin is a critical regulator of actin nucleation in the development of invadopodia [533]	25.07	ND	29.54
DNM2	Dynamin-2	Dynamin2 GTPase is a microtubule-associated force-producing protein that contributes to invadopodia formation in invasive bladder cancer cells via its proline/arginine-rich domain (PRD) [535]	26.41	25.88	27.77
DOCK1	Dedicator of cytokinesis protein 1	Rac1 exchange factor that is localised to invadopodia, involved in modulating invadopodia dynamics in breast cancer cells [536].	24.62	ND	24.46
EGFR	Epidermal growth factor receptor	Established receptor involved in invadopodia maturation, via an EGFR-Src-Arg-cortactin signalling pathway [123]	25.73	26.21	35.37
ENPP2	Ectonucleotide pyrophosphatase/phosphodiesterase family member 2	Can induce invadopodia formation in the fibrosarcoma cell line HT1080 through activation of the LPA4 receptor [566]	26.96	ND	25.19
FAP	Prolyl endopeptidase FAP	Also known as Seprase, a gelatin-degrading membrane-protease complex that is expressed at the invasive front of malignant melanoma cells on invadopodia [125]	25.46	ND	27.51
FARP1	FERM, ARHGEF and pleckstrin domain-containing protein 1	FARP1 overexpression promotes cell motility and filopodium formation via CDC42 activation [538]	25.92	30.39	25.52
FHOD1	FH1/FH2 domain-containing protein 1	Superresolution microscopy revealed the presence of formin FHOD1 and unbranched radial F-actin fibers emanating from invadopodia [539]	ND	ND	24.31
FMNL2	Formin-like protein 2	Cortactin directly binds to FMNL2 to promote actin polymerization and recycling endosome motility. FMNL2 was necessary for invadopodia formation and function in CRC cells [567]	26.77	27.29	27.61
FSCN1	Fascin	Actin bundling protein that stabilises actin filaments in invadopodia [470]	28.90	25.39	29.58
ICAM1	Intercellular adhesion molecule 1	A cell adhesion molecule in the ICAM superfamily, known for their ability to bind integrins to activate signalling. Often expressed at the cell surface where it may play a role in invadopodia maturation via interactions with integrins [540]	31.19	ND	27.48
ITGA3	Integrin alpha-3	Integrin alpha-3/beta-3 provides a docking site for FAP (seprase) at invadopodia plasma membranes in a	28.65	26.51	31.11

		collagen-dependent manner and hence may participate in the adhesion, formation of invadopodia and matrix degradation processes [541]			
ITGB1	Integrin beta-1	β1 integrin regulates SNARE-dependent trafficking and is required for the activation and delivery of Src and EGFR to sites of invadopodia formation in order to support tumour cell invasion [542]	31.73	32.64	33.59
ITGB3	Integrin beta-3	Integrin alpha-3/beta-3 provides a docking site for FAP (seprase) at invadopodia plasma membranes in a collagen-dependent manner and hence may participate in the adhesion, formation of invadopodia and matrix degradation processes [541]	31.07	25.67	31.55
MET	Hepatocyte growth factor receptor	Met receptor tyrosine kinase signals through a cortactin-Gab1 scaffold complex to mediate invadopodia activity [143]	ND	ND	26.16
MMP14	Matrix metalloproteinase-14	MT1-MMP: transmembrane protease located within invadopodia [544]	25.61	ND	28.96
MMP2	72 kDa type IV collagenase	Metalloprotease that is widely associated with invadopodia [136]	29.35	ND	24.35
MTOR	Serine/threonine-protein kinase mTOR	Cav-1 activation-induces PI3K/Akt/mTOR signaling to promote invadopodia formation in breast carcinoma MDA-MB-231 cells [526]	ND	ND	24.88
NCKAP1	Nck-associated protein 1	A subunit of the Arp2/3-WAVE complex involved in actin organisation during invadopodia formation [545]	25.86	25.09	28.65
PAK4	Serine/threonine-protein kinase PAK 4	PAK4 is a key mediator of RhoA activity during invadopodia maturation [570]	ND	ND	24.36
PXN	Paxillin	A cytoskeletal protein involved in actin-membrane attachment at sites of cell adhesion to the ECM. JNK-paxillin signalling can promote invadopodia activity [549]	ND	ND	25.41
RAB5A	Ras-related protein Rab-5A	Rab5a GTPase is a major regulator of MT1-MMP trafficking and invadopodia formation [550]. MT1-MMP vesicles that are positive for Rab5a localise to invadopodia [551]	ND	ND	25.42
RACGAP1	Rac GTPase-activating protein 1	Binds to IQGAP1 to mediate Rac1 deactivation. Phosphorylation of RacGAP1 promotes its recruitment to IQGAP1 at the tips of invadopodia [571]	32.17	25.87	30.10
RAPH1	Ras-associated and pleckstrin homology domains-containing protein 1	Localised to invadopodia and regulates actin dynamics through interaction with Ena/Vasodilator proteins as well as direct binding to filamentous actin to regulate actin network assembly [559]	ND	ND	26.57
RHOA	Transforming protein RhoA	RhoA–ROCK signalling promotes invadopodia formation and activity [140]	29.68	ND	29.88

RHOC	Rho-related GTP-binding protein RhoC	RhoC activation in areas surrounding invadopodia restricts cofilin activity to within the invadopodium core, resulting in a focused invadopodium [553]	31.50	29.44	31.21
RHOG	Rho-related GTP-binding protein RhoG	RhoG and SGEF modulate the phosphorylation of paxillin, which plays a key role during invadopodia disassembly [536]	28.15	27.70	30.06
SRC	Proto-oncogene tyrosine-protein kinase Src	Src tyrosine kinase activates numerous proteins in invadopodia-related signalling pathways, including adaptor proteins such as Tks5 [554]	26.06	26.40	30.92
STX4	Syntaxin-4	SNARE protein syntaxin4: mediates trafficking of MT1-MMP and EGFR for invadopodia activity [555]	26.53	26.81	30.06
TGFBI	Transforming growth factor-beta-induced protein ig-h3	A transforming growth factor beta (TGFβ) inducible secreted extracellular matrix (ECM) protein. It has been shown to promote MMP secretion at invadopodia by interacting with integrin α2β1 and activating PI3K/AKT signalling. Processing of TGFBI by MMP-2 induces adhesion-related FAK/Src signalling in glioma cells and promotes invasion [572-574]	25.61	24.39	25.50
TJP1	Tight junction protein ZO-1	Tight Junction Protein is a scaffolding protein that plays a role in the regulation of cell migration by targeting CDC42BPB to the leading edge of migrating cells. Plays a role as a partner for ADAM-12 in invadopodia [556, 557]	ND	ND	24.85
WASF2	Wiskott-Aldrich syndrome protein family member 2	Promotes formation of actin filaments. Part of the WAVE complex that activates actin nucleating machinery Arp2/3 to drive invadopodia formation [561, 562]	ND	26.39	26.86

[A] indicates averaged MS/MS label-free quantitation intensity. (*ND: not detected)*

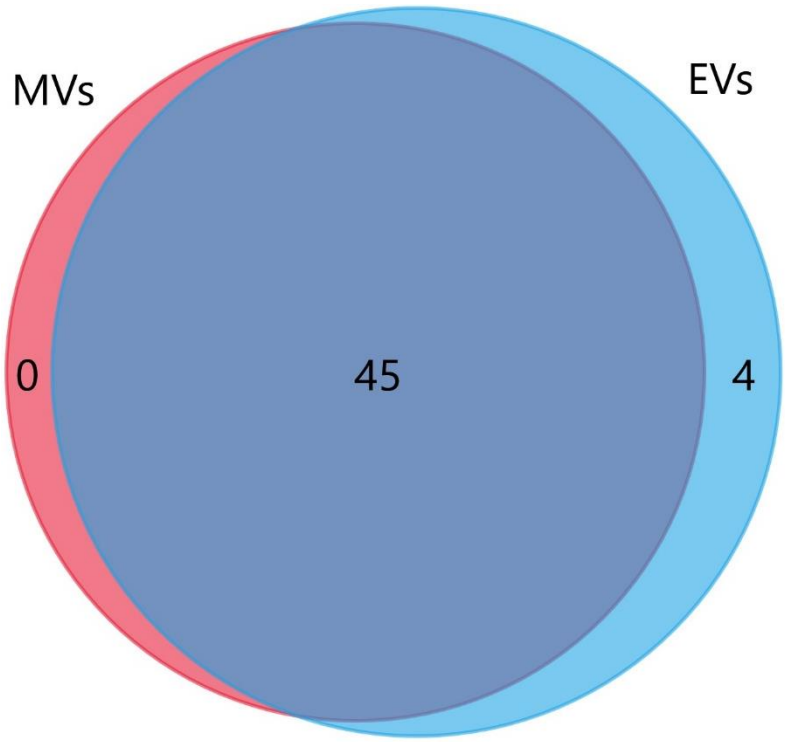

Figure 5-8: Common invadopodia-related protein cargos are present in GBM cell line derived sEVs and MVs

A Venn diagram comparing invadopodia-related proteins detected in the GBM cell line MV (red) and sEV (blue) proteomes. A total of 45 invadopodia-related proteins detected in the MV cargo proteome were also present in EVs, whilst 4 invadopodia-related proteins were identified exclusively in sEVs: RCC2, PODXL, MYO10 and LPAR1.

Table 5-4: mRNA expression levels of unique invadopodia-related proteins identified in GBM cell line sEVs (RCC2, PODXL, LPAR1, MYO10) are overexpressed in glioma tissue

Glioma grade	mRNA	Sample Number (normal/tumour)	Mean Fold Change (Log-2)	P-Value	Dataset
IV	PODXL	37/582	1.331	6.21E-183	TCGA 2
IV	PODXL	4/80	1.972	8.16E-12	Murat
IV	MYO10	37/582	1.027	2.44E-11	TCGA 2
II/III	PODXL	37/63	1.138	5.34E-10	TCGA 2
IV	PODXL	10/542	1.771	4.22E-08	TCGA
IV	MYO10	4/80	1.248	1.19E-07	Murat
IV	RCC2	23/81	1.583	2.32E-07	Sun
III	MYO10	23/19	2.388	2.92E-07	Sun
IV	MYO10	23/81	2.126	3.79E-07	Sun
III	RCC2	23/19	1.555	3.85E-06	Sun
IV	RCC2	4/27	1.556	9.82E-06	Bredel 2
IV	RCC2	37/582	1.023	1.69E-05	TCGA 2
IV	PODXL	4/27	2.208	8.07E-05	Bredel 2
IV	LPAR1	37/582	1.021	1.86E-04	TCGA 2
IV	RCC2	2/29	1.551	1.97E-04	Liang
IV	RCC2	4/80	2.052	2.18E-04	Murat
III	RCC2	6/4	2.908	2.52E-04	French

II	RCC2	23/7	1.587	6.04E-04	Sun
IV	MYO10	4/27	1.612	4.00E-03	Bredel 2
II/III	LPAR1	37/63	1.024	0.007	TCGA 2
III	PODXL	33/9	1.151	8.00E-03	Beroukhim
IV	MYO10	10/542	1.128	2.00E-02	TCGA
I	PODXL	3/8	2.29	0.031	Gutmann
III	MYO10	4/6	1.564	0.032	Bredel 2
III	RCC2	4/6	1.479	0.037	Bredel 2
III	MYO10	6/4	1.935	0.042	French
II/III	MYO10	7/5	1.466	0.064	Shai
II	RCC2	2/3	1.467	0.087	Liang

mRNA expression levels of the four invadopodia-related proteins detected uniquely in the GBM cell line sEV proteome, but absent in MVs, (RCC2, PODXL, MYO10 and LPAR1) were examined in glioma and normal brain tissue within the Oncomine database. Displayed in this table are the mRNA expression mean fold changes in glioma versus normal brain tissue in each study and the overall P value for this analysis within that dataset. Gene expression data are log transformed and normalized as previously described [355]. The data is ordered based on P value significance. Only datasets with significant P values were included.

5.2.2.4 Differential expression analysis of invadopodia-related proteins detected in the GBM cell, sEV and MV proteomes

A total of 61 invadopodia-related proteins were identified in either the GBM cell, sEV or MV proteomes (***Table 5-5***). Differences in the expression levels of these invadopodia-related proteins between GBM cells and secreted sEVs/MVs was first examined via unsupervised hierarchical clustering (***Figure 5-9A***). Interestingly, the sEVs and MVs from the same cell lines clustered together indicating that similar expression patterns of the invadopodia-related proteins exist within the cargo of the two vesicle subtypes secreted from the same GBM cell line. Next, the overall differential expression of the three different proteome populations (GBM cells, sEVs and MVs) was examined using the average spectral count (signifying protein abundance) of each invadopodia-related protein. This analysis revealed two clusters of proteins: a cluster representing invadopodia-related proteins with higher relative expression in GBM cells (blue), and a cluster representing invadopodia-related proteins with higher relative expression in the secreted sEVs/MVs (pink) (***Figure 5-9B***). Functional enrichment analysis of these two clusters demonstrated that GBM cells were enriched in actin and cytoskeletal related proteins, including MT1-MMP, CFL1 and CTTN that are required for dynamic cytoskeletal reorganisation and the transport of protease-containing vesicles which occurs during the invadopodia lifecycle. On the other hand, sEVs and MVs were enriched in proteins known to be involved in integrin-, GTPase- and kinase- related signalling pathways primarily required for invadopodia initiation, which is consistent with a role for EVs in intracellular signalling, potentially via the initiation of signalling cascades to drive invadopodia formation in recipient cells (***Figure 5-9C***).

Table 5-5: Comparison of the invadopodia-related proteins identified in the GBM cell, EV and MV proteomes

Gene name	GBM Cells	GBM sEVs	GBM MVs
ABI2	×	✓	✓
ACTR2	✓	✓	✓
ACTR3	✓	✓	✓
AGRN	×	✓	✓
ARF6	✓	✓	✓
AXL	×	✓	✓
BSG	✓	✓	✓
CAV1	✓	✓	✓
CD151	✓	✓	✓
CD44	✓	✓	✓
CDC42	✓	✓	✓
CFL1	✓	✓	✓
CLASP2	✓	×	×
CLIP1	✓	×	×
CSNK2A1	✓	✓	✓
CSNK2A2	✓	×	×
CTTN	✓	✓	✓
DIAPH1	✓	×	×
DNM2	✓	✓	✓
DOCK1	✓	✓	✓
EGFR	✓	✓	✓
ENAH	✓	×	×
ENPP2	×	✓	✓
FAP	×	✓	✓
FARP1	✓	✓	✓
FHOD1	✓	✓	✓
FMNL2	×	✓	✓
FSCN1	✓	✓	✓
GRB2	✓	×	×
ICAM1	✓	✓	✓
ITGA3	✓	✓	✓
ITGB1	✓	✓	✓
ITGB3	✓	✓	✓
LPAR1	×	✓	×
LPP	✓	×	×

MET	×	✓	✓
MMP14	✓	✓	✓
MMP2	✓	✓	✓
MTOR	×	✓	✓
MYO10	×	✓	×
NCKAP1	✓	✓	✓
PAK4	×	✓	✓
PODXL	✓	✓	×
PPP4C	✓	×	×
PTK2	✓	×	×
PXN	✓	✓	✓
RAB5A	✓	✓	✓
RACGAP1	×	✓	✓
RAPH1	×	✓	✓
RCC2	✓	✓	×
RHOA	✓	✓	✓
RHOC	✓	✓	✓
RHOG	✓	✓	✓
ROCK2	✓	×	×
SRC	✓	✓	✓
STX4	✓	✓	✓
TGFBI	×	✓	✓
TJP1	✓	✓	✓
TRIP10	✓	×	×
VASP	✓	×	×
WASF2	✓	✓	✓

Comparison of the 61 invadopodia-related proteins that were identified in either the GBM cell, sEV or MV proteomes. ✓ indicates the protein was detected in one or more GBM cell lines, × indicates that the protein was not detected in any of the GBM cell lines.

Figure 5-9: Differential expression analysis of invadopodia-related proteins present in the proteomes of the GBM cell lines, sEVs and MVs using the Perseus bioinformatics platform

(**A.**) Hierarchal clustering analysis of invadopodia-related protein expression in the GBM cell lines, sEVs and MVs. Red indicates a high relative expression and green indicates a low relative expression, as determined by the normalised Z scores for the 61 invadopodia-related proteins (listed left of the heatmap). Protein clustering is shown to the left and sample clustering is shown above the heatmap (**B.**) Hierarchal clustering analysis of the 61 invadopodia-related proteins was also conducted using the average protein abundance across all three GBM cell lines, identifying protein expression differences between cells, sEVs and MVs. Proteins were separated into two broad clusters: blue- high relative expression in cells and pink- high relative expression in MVs/sEVs. Proteins within each cluster are shown to the left and sample clusters are shown above the heatmap. (**C.**) GO annotations for each cluster were explored using functional enrichment analysis (FunRich, version 3.1.3), showing that different molecular functions are preferentially enriched within each cluster. Significant annotations for the pink cluster included 'integrin binding' (p= 5.97E-11), 'GTPase activity' (p= 2.11E-04), and 'protein tyrosine kinase activity'(p= 1.34E-05), whilst significant annotations for the blue cluster included 'actin binding' (p= 3.41E-10) and 'SH3 domain binding' (p=2.14E-06). *P values were calculated using a two-sided hypergeometric test.*

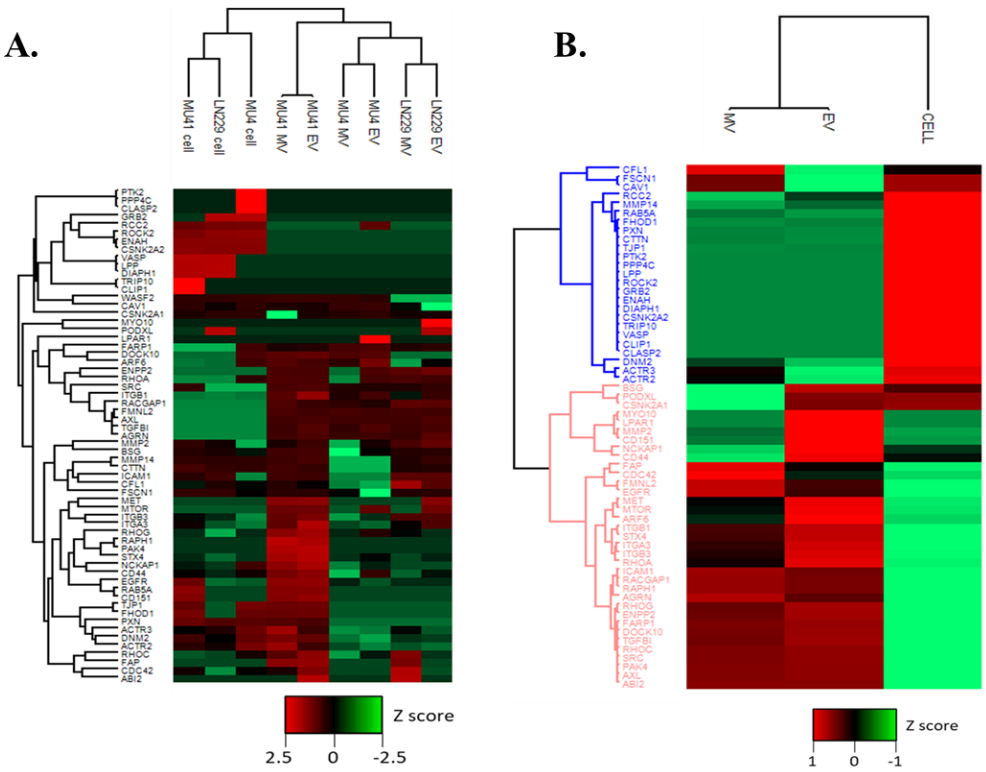
A.
MU41 cell
LN229 cell
MU4 cell
MU41 MV
MU41 EV
MU4 MV
MU4 EV
LN229 MV
LN229 EV
Z score
2.5
0
-2.5
B.
MV
EV
CELL
Z score
1
0
-1
C.
Molecular Function
integrin binding
GTPase activity
protein tyrosine kinase activity
SH3 domain binding
actin binding
0
5
10
15
20
25
30
35
% of proteins
Pink Cluster
Blue Cluster

5.2.3 GBM cell line derived sEVs are enriched in proteins involved in invasion and invadopodia

Additional comparison of the donor cell and corresponding sEV proteomes for each GBM cell line revealed a set of proteins that were uniquely detected in sEVs (LN229- 278 proteins, MU4- 188 proteins, MU41- 489 proteins) (***Supplementary Table 5***). These proteins are highly enriched in sEVs, as they were not detected in the proteomes from the corresponding donor cell lysates. In total, 36 proteins were found to be commonly enriched in sEVs from all three GBM cell lines (***Figure 5-10A***). Analysis of these common proteins using the STRING protein interaction network revealed that there is a significant interaction between several proteins (PPI enrichment p-value: 0.000797) and were annotated for terms associated with invadopodia ('positive regulation of cell projection organization' and 'regulation of plasma membrane bounded cell projection organization'), as well as 'vesicle mediated transport' (***Figure 5-10B***). Furthermore, sixteen of these proteins are known to promote cancer cell invasion and have been detected in GBM tissue or cultured GBM cells (***Table 5-6***). Additionally, ten of these proteins have been linked with roles in invadopodia formation or function, suggesting that the transfer of these enriched sEV cargo proteins may promote a pro-invadopodia phenotype in recipient GBM cells.

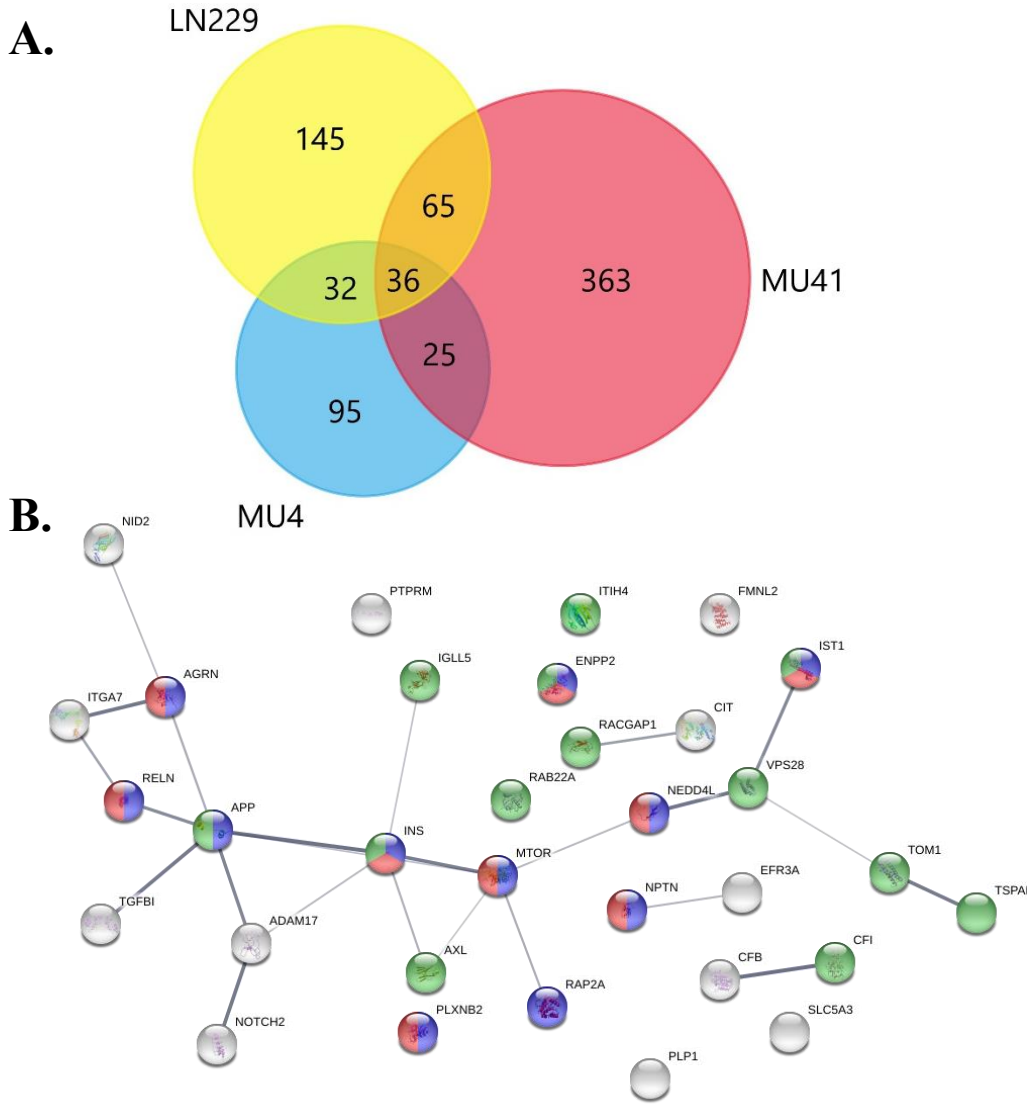

Figure 5-10: Examination of proteins enriched in GBM cell line sEVs

(**A**.) Venn diagram comparing proteins uniquely detected in the GBM cell line derived sEV proteomes compared to the matching donor GBM cell line proteomes. (**B**.) STRING protein interaction network of 36 proteins which are enriched in all three GBM cell line sEVs relative to GBM donor cell lines. Interactions between two proteins are indicated by the solid lines, whereby line thickness indicates the strength of data supporting the interaction. Node colour indicates proteins with the following GO annotations for a biological process: green nodes - vesicle-mediated transport; red nodes - regulation of plasma membrane bounded cell projection organization; purple nodes- positive regulation of cell projection organization.

Table 5-6: Invasion related proteins that are enriched in GBM cell line sEVs

Protein	Known role/s	**Reported role in GBM**
ADAM17	Involved in ligand/growth factor shedding from EGFR that promotes invasion [576]	ADAM17 promotes U87MG GBM cell proliferation, invasion, angiogenesis, *and in vivo* tumour growth [577]
AGRN*	Secreted and cell surface Agrin binds the Lrp4 receptor and promotes the formation of a Agrin–Lrp4–MuSK signalling complex, which activates FAK and Arp2/3 associated invadopodia formation [578]	Agrin is related to BBB dysfunction in GBM [579]
APP*	Linked to increased breast tumour cell proliferation, migration, and invasion [580].	APP demonstrates upregulated expression in GBM tissue [361]
CFI*	Complement Factor I was shown to promote the progression of cutaneous squamous cell carcinoma via ERK1/2 activation [581].	Complement Factor I was found to be secreted by glioma cell line CB193 [582]
ENPP2*	Can induce invadopodia formation in the fibrosarcoma cell line HT1080 through activation of the LPA4 receptor [566]	Oxidative stress stimulates U87MG cells to secrete ENPP2, and this correlates with increased invasive potential [583]
FMNL2*	Cortactin directly binds to FMNL2 to promote actin polymerization and recycling endosome motility. FMNL2 was necessary for invadopodia formation and function in CRC cells [567]	Understudied in GBM, however was shown to be expressed in rat C6 glioma cells [584]
ITGA7*	Required for GBM cell invasion on laminin via phosphorylated Src and focal adhesion kinase (FAK) [540]	High ITGA7 expression negatively correlated with both low- and high-grade glioma patient survival [585]
MTOR*	Cav-1 activation-induces PI3K/Akt/mTOR signalling to promote invadopodia formation in breast carcinoma MDA-MB-231 cells [526]	Elevated EGFR expression in GBM contributes to activation of the downstream mTOR signalling pathway [586]
NID2	A ubiquitous component in the basement membrane that plays an important role in the development of malignant tumours via protein digestion and absorption, PI3K-AKt-signaling pathway, focal adhesion and ECM-receptor interaction pathways [587]	NID2 was shown to be secreted by GBM-derived neural stem cells [588]
NOTCH2	Notch2 signalling promotes cell growth, invasion, and migration in salivary adenoid cystic carcinoma [589]	Notch2 expression levels in GBM tissue correlate with stemness genes (nestin, SOX2) and astrocyte fate genes (vimentin and GFAP) [590]

PLP1	Proteolipid protein 1 (PLP1) and Dynamin-1 (DNM1) are enriched in invasive GBM tumour areas [591]	Immunostaining of GBM patient-derived xenografts found that PLP1 was detected in the extracellular space and on the plasma membrane, and was more highly expressed in invasive tumour areas [591]
RAB22A	Colocalizes with MT1-MMP on vesicles and acts as a positive regulator of MT1-MMP surface exposure in MDA-M-231 breast carcinoma cells and macrophages [306]	miR-204-5p inhibits GBM cell growth, migration and invasion by directly targeting RAB22A [592]
RACGAP1*	Binds to IQGAP1 to mediate Rac1 deactivation. Phosphorylation of RacGAP1 promotes its recruitment to IQGAP1 at the tips of invadopodia [571]	RACGAP1 gene expression is upregulated in GBM tissue samples [593]
RAP2A	A member of the small GTPase superfamily that enhances invasive ability of cancer cells and increases activities of MMP-2 and MMP-9 by upregulating p-Akt [594]	Nedd4-1/Rap2a ubiquitination promoted the migration and invasion of U251 and U87MG GBM cells [595]
TGFBI*	Can promote MMP secretion and cell invasion by interacting with integrin α2β1 and activating PI3K/AKT signalling. Processing of TGFBI by MMP-2 induces adhesion-related FAK/Src signalling in glioma cells and promotes invasion [572-574]	TGFBI expression positively correlates with glioma grade and is a potential signature gene for the mesenchymal subtype of GBM [596]

* *indicates invasion-related proteins with published evidence identifying potential roles in invadopodia-related pathways*

5.3 Discussion

In the previous chapters, GBM cell invasion was shown to be mediated by the formation of functional matrix-degrading invadopodia. Although the FITC-gelatin degrading activity of invadopodia varied between the GBM cell lines examined, the cell lines were observed to secrete similar levels of sEVs. Interestingly, sEVs enriched from a high invadopodia mediated FITC-gelatin degrading cell line (LN229) could induce invadopodia formation and activity in recipient GBM cell lines. However, the specific proteins that may be involved in GBM cell invadopodia mediated FITC-gelatin degrading activity and in the sEV cargo facilitating an EV-mediated transfer of a pro-invadopodia phenotype to donor GBM cells remained elusive. Therefore, in this chapter, this was examined by undertaking a comprehensive proteomic analysis of the three GBM cell lines (LN229, MU4 and MU41) and the secreted vesicle populations - sEVs (enriched after centrifugation at 100,000xg) and microvesicles (MVs) (enriched after centrifugation at 10,000xg).

Overall, a total of 2354 proteins were identified in GBM cells, whilst 2086 proteins were identified in sEVs, and 1621 proteins were identified in MVs. A total of 328 proteins were identified in the sEV proteome that had not been previously recorded in glioma or GBM derived EVs in Vesiclepedia (***Figure 5-5***). However, as Vesiclepedia was last updated in 2018 (15th August), some of these proteins may have been identified in more recent studies that are not listed on this database and therefore may not be entirely novel in GBM. Nevertheless, the data presented here offers a substantial insight into the proteomic landscape of GBM cells and these two vesicles population, which may assist future research into EV-mediated communication in GBM. Furthermore, 61 invadopodia-related proteins were identified within the proteomic analyses of GBM cells, sEVs and MVs, providing a valuable insight into specifically enriched proteins in EVs that may be driving a pro-invadopodia phenotype in recipient GBM cells.

5.3.1 Comparison of the GBM cell, sEV, and MV proteomes

One of the largest obstacles currently faced by researchers is accurately defining EV subtypes, such as exosomes and membrane-shed microvesicles [192]. As the subcellular origin of secreted vesicles cannot be established in many studies, size is often used to define populations of EVs recovered in the different steps of the differential ultracentrifugation protocol [194]. Here, vesicles enriched at 10,000xg are referred to as MVs (typically 100-1500nm), whilst EVs enriched at 100,000xg are referred to as sEVs (typically 30-150nm). Investigation of the proteomic composition of GBM cell line derived sEVs and MVs revealed varying expression levels of several proteins often used as 'exosome markers' throughout the literature, including the ESCRT components TSG101 and Alix (PDCD6IP), and tetraspanins CD9, CD63, CD81, CD82. Whilst all six markers were detected in sEVs and were enriched compared to donor GBM cells, TSG101 expression which was present in sEVs was lacking in MVs (***Figure 5-4D***). Interestingly, CD9 was observed to be the most enriched marker in both EVs and MVs, with a 15-fold higher expression in sEVs and a 19-fold higher expression in MVs compared to donor cells. Interestingly, high expression of CD9 in small EVs has been previously correlated with a mesenchymal phenotype in donor GBM stem cells [597]. Furthermore, Li *et al.* has demonstrated that CD9 is capable of being transferred to GBM cells via endothelial cell derived EVs, whereby CD9 promoted tumorigenesis [598]. As there remains a lack of consensus on the most reliable EV markers, this data suggests that CD9 may potentially represent an additional highly enriched marker for EVs derived from GBM cells, however this marker alone cannot be used to distinguish between different EV subtypes.

Functional enrichment analysis of proteins commonly detected in all three GBM cell lines (1362 proteins- ***Figure 5-2B)***, sEVs (756 proteins- ***Figure 5-3B***), and MVs (636 proteins- ***Figure 5-4B***) was conducted to determine which processes and pathways were significantly enriched with each proteome. Interestingly, a large portion of significantly enriched proteins in GBM cells (41.1%), sEVs (62.8%) and MVs (62.9%) were associated with 'extracellular exosomes.' Although this would be expected for the vesicle proteome, the enrichment of exosomal proteins in GBM cells supports the hypothesis that GBM cells are primed for EV biogenesis and release, highlighting the potential significance of EV-

mediated communication in these cells. However, compared to the donor cell proteome, secreted vesicles were enriched in GTPases and GTP binding partners. As GTPases are key contributors in invadopodia signalling (including the Rho GTPases Cdc42, RhoA and RhoC) and have been implicated in GBM invasion, this demonstrates that both vesicle fractions may be involved in pro-invasive intracellular signalling, with the release of such vesicle cargo potentially contributing to pro-invadopodia signalling in recipient GBM cells [515, 516, 599]. Moreover, additional comparison of the sEV and MV proteomes revealed that sEVs were more enriched in signalling proteins, whilst MVs were more enriched in RNA/mRNA binding proteins (***Figure 5-5***). Therefore, it can be speculated that these two EV fractions (MVs enriched at 10,000xg and sEVs enriched at 100,000xg) may exert different functional roles in GBM recipient cells, although further characterisation of the MV fraction, such as vesicle morphology and functional impact on recipient GBM cells, should be addressed in future studies to help interpret these results further. Nevertheless, proteogenomic comparison of exosomes and MVs has previously reported an enrichment of receptors and kinases in exosomes compared to membrane shed vesicles, which were instead enriched in ribosomal and mitochondrial proteins [600]. As this is similar to the patterns of enrichment in the two enriched EV fractions presented here, the observed differences in enriched cargo may be indicative of the subcellular origin. In particular, the proteomic characterisation of sEVs indicates that the majority of these enriched sEVs may be of endosomal origin. This is also supported by the Nanosight analyses of the sEV populations which indicate particles predominantly within an exosomal size range.

5.3.2 Differential expression of invadopodia-related proteins in the GBM cell, sEV and MV proteomes

Examination of the proteome profiles of GBM cells, sEVs and MVs identified a total of 61 putative invadopodia-related proteins that play integral roles in the various stages of invadopodia formation and activity (***Table 5-5***). Hierarchal clustering of these 61 proteins amongst all three GBM cell lines, sEVs and MVs demonstrated that patterns of expression clustered similarly for cells, whilst MVs and sEVs

from the same cell line clustered closely, indicating that similar expression of invadopodia-related proteins exist in both vesicle fractions from a single GBM cell line (***Figure 5-9A***). Nevertheless, four invadopodia-related proteins were uniquely detected in sEVs compared to MVs; RCC2, PODXL, MYO10 and LPAR1 (***Figure 5-8***). Interestingly, these proteins converge on the regulation of invadopodia turnover via the activation and de-activation of various actin machinery components, involving Rac1, N-WASP, paxillin and cofilin [546, 552, 601, 602]. This process is essential for invadopodia dynamics, allowing for the continued endocytic recycling of key invadopodia proteins, such as MT1-MMP, that must be delivered back to the plasma membrane to form new invadopodia [453]. Indeed, endosomal recycling of LPAR1 back to the plasma membrane by N-WASP was shown to be essential for directional invasion in pancreatic cancer cells [602]. As these studies suggest a dual role for actin dynamics and endocytic recycling in invadopodia turnover, it is possible that the detection of these four proteins in sEVs, but not MVs supports that these sEVs may be of endosomal origin and targeted for secretion at invadopodia.

In addition, analysis of publicly available glioma patient datasets revealed that elevated mRNA levels of RCC2, PODXL and LPAR1 are detected in all grades of glioma patient tissue compared to normal brain tissue (***Table 5-4***). High expression of RCC2, PODXL, and LPAR1 are reported in GBM tissue within the literature, whereby elevated expression of these proteins was also an unfavourable predictor of GBM patient survival [603-605]. As these proteins were identified in GBM cell derived sEVs, future research could investigate their potential as circulating diagnostic and prognostic biomarkers for glioma/GBM patients. Additionally, silencing of RCC2 or PODXL via shRNA inhibition in GBM cells *in vitro* was found to reduce tumour cell proliferation and tumorigenicity [603, 604], whilst pharmacological inhibition of LPAR1 with the small molecule compound Ki16425 in a GBM mouse xenograft model was also found to suppress GBM progression *in vivo* [606]. As these proteins are linked to invadopodia activity, it is feasible that targeting the expression, or the sEV-mediated transport, of these proteins to recipient cells may also impede invadopodia activity in GBM. Indeed, targeting RCC2 or PODXL expression has been shown to attenuate invasion in hepatocellular carcinoma, breast

cancer, and colorectal cancer [607-609], therefore further studies are required to investigate the anti-invasive potential of targeting these proteins in GBM.

DE analysis using the average abundance of each invadopodia-related protein across all three GBM cell lines, sEVs, and MVs revealed that cells were enriched in actin binding proteins, whilst vesicles were enriched in invadopodia-related signalling proteins (***Figure 5-9B***). Specifically, enriched proteins within the EV cargo were associated with integrin binding, GTPase activity and tyrosine kinase functions and may therefore be relevant to the initiation of invadopodia-related signalling cascades in GBM recipient cells (***Figure 5-9C***). These molecular functions are consistent with the role of EVs in intercellular communication and suggest that donor GBM EVs may activate signalling cascades in recipient cells to drive invadopodia initiation, whilst the actin binding proteins enriched in cells regulate the dynamic cytoskeletal reorganisation and stabilisation required during the later stages of the invadopodium lifecycle.

Previously considered to be a barrier to exocytosis, the cortical cytoskeleton is now recognized to play a positive role in the trafficking of vesicles to the cell surface [610], and several of the actin-binding proteins enriched in GBM cells possess a dual role in endosomal vesicle trafficking and invadopodia formation. For example, cortactin (CTTN) and fascin-1 (FSCN1) regulate endosomal trafficking in breast cancer cells through their interactions with actin and microtubules, respectively, resulting in the release of EVs which were preferentially secreted from invadopodia [470]. Cortactin overexpression in head and neck squamous cell carcinoma (HNSCC) cells was also shown to positively regulate the secretion of the endocytically derived EVs [230]. Interestingly, no significant changes in EV protein cargo were observed in this study in response to cortactin overexpression, suggesting that cortactin regulates MVB trafficking and docking in HNSCC cells but is not involved in EV biogenesis. Likewise, dynamin-2 (DNM2), another protein that facilitates invadopodia formation and is enriched in our GBM cell line proteome, has established roles as a crucial regulator of both vesicle-mediated trafficking and endocytosis [611]. Collectively, these studies indicate that through dynamic cytoskeletal reorganisation, invadopodia may also serve as endosomal trafficking structures and the sites of EV release in GBM cells, supporting an enrichment of these proteins in cells compared to EVs. Experimental evidence

shows that the reduced expression of N-WASP with the drug Wikostatin or knockdown of Tks5, both key actin regulators in invadopodia formation, effectively reduces EV secretion from HNSCC cells [229]. Likewise, invadopodia may also represent a promising target to impair EV secretion and subsequent intercellular communication between GBM cells.

5.3.3 Invadopodia-related proteins that may contribute to the sEV-mediated transfer of a pro-invadopodia phenotype in GBM cells

Importantly, in ***Chapter 4***, sEVs secreted from the high invadopodia activity cell line LN229 were found to promote invadopodia formation and invadopodia-mediated matrix degradation in recipient GBM cell lines. We identified 49 proteins in the sEV proteome with established roles in invadopodia formation and activity, identifying that donor cell sEV cargo may confer a pro-invadopodia phenotype in the recipient cells. These proteins may be transported to recipient cells in the aqueous core of sEVs or may function as receptors on the sEV surface, and include proteins involved in key invadopodia-related signalling cascades, as well as actin regulators and proteases. The following section discusses the invadopodia-related proteins detected in GBM cell line derived sEVs and explores the potential of these proteins exhibiting a pro-invasive role in recipient cells as well as in the extracellular space (as summarised in ***Figure 5-11***).

5.3.3.1 Invadopodia-related receptors detected in the sEV proteome

A variety of signalling inputs are involved in the initiation of invadopodium formation at the cancer cell membrane, occurring through adhesion receptors, such as integrins, or growth factor receptors, such as EGFR. In order to transfer their cargo, EVs must first bind to the target cell membrane, which is often mediated by specific adhesion receptors on both the EV and cancer cell surface. As EGFR and integrins were identified in the GBM cell derived sEV proteome (***Table 5-2***), the presence of these receptors on

the sEV surface may be sufficient to induce pro-invasive signalling in recipient cells. This was evidenced in a study by Chanda *et al*. that demonstrated fibroblast-derived EVs induced an invasive phenotype in recipient fibroblasts through a direct interaction of EV surface fibronectin and its receptor, α5β1 integrin, on the membrane of recipient cells [612]. Additionally, the sEV-mediated horizontal transfer of these signalling receptors to recipient cells may also stimulate invadopodia formation. For example, αvβ6 and αvβ3 integrins are known to be horizontally transferred from tumour cells to recipient tumour cells via EVs resulting in increased adhesion-mediated signalling and cell migration [484, 613]. Interestingly, three integrin subunits (ITGA3, ITGA7, ITGB3) were found to be enriched in the sEV proteome compared to donor GBM cells, along with several invadopodia-related integrin binding partners, including CD151 (cluster of differentiation-151), Src, ICAM-1 (intercellular adhesion molecule-1) and TGFBI (transforming growth factor-beta induced protein ig-h3) (***Figure 5-9B***). The enrichment of these proteins in sEVs may indicate an important role for integrins in the horizontal communication between GBM cells mediated by sEVs.

5.3.3.1.1 EGFR

Demonstrating the critical role for EVs in GBM progression, Al-Nedawi *et al*. has shown that GBM cell line U373-derived EVs containing the mutant EGFR variant III (EGFRvIII) can transform GBM cells lacking EGFRvIII expression [255]. EGFR is a crucial receptor in invadopodia initiation, and EGFR signalling in breast cancer cell is known to stimulate CD44 and BSG (basigin, also known as EMMPRIN and CD147) to form invadopodia [362]. This signalling pathway may be activated by GBM cell line derived EVs, as all three of these proteins (EGFR, basigin and CD44) were enriched in the sEV proteome compared to the corresponding donor cells (***Figure 5-9B***) and has been previously detected in the cargo of GBM-cell line derived EVs [228]. Zhang *et* al. has shown that EVs secreted from gastric cancer cells can also deliver EGFR to liver stromal cells to promote a pro-metastatic microenvironment [614]. As this study demonstrated that EGFR was integrated into the plasma membrane of recipient cells, where it was shown to be functionally active, this could indicate that key invadopodia receptors

such as integrins and EGFR may also be transferred to recipient GBM cells via sEVs in order to promote pro-invadopodia signalling.

5.3.3.1.2 Basigin

Importantly, basigin also plays a central role in the progression of many cancers by stimulating the production and secretion of MMPs, including MMP-1, MMP-2, MMP-3 and MT1-MMP, and was consequently also given the name EMMPRIN (extracellular matrix metalloproteinase inducer) [615]. Expression of this membrane protein is sufficient to induce MT1-MMP expression and invadopodia formation in non-transformed breast epithelial cells, and it is capable of regulating invadopodia activity through the assembly of MT1-MMP-containing complexes within lipid-raft domains of the invadopodia [363]. Basigin has been reported to contribute to glioma invasion, whereby its expression on the surface of glioma cells was proposed to facilitate the production and activation of stromal MMP-2 [616]. Importantly, as basigin activity can be transferred via EVs, as demonstrated by Braundmeier *e al.* [297], the enrichment of basigin in sEVs secreted by high invadopodia FITC-gelatin degrading activity GBM cells suggests that the sEV-mediated transfer of basigin may also contribute to the induction of a pro-invadopodia phenotype in recipient GBM cells. Moreover, basigin is also capable of inducing its own gene expression [617]. Thus, its delivery via sEVs derived from high invadopodia activity cell lines may represent a positive feedback mechanism capable of sustaining high invadopodia activity in recipient cells.

5.3.3.1.3 Adhesion proteins for sEV uptake

Furthermore, the proteome of sEVs enriched from the low invadopodia FITC-gelatin degrading activity cell line, MU4, also exhibited lower expression levels of adhesion molecules compared to sEVs from the high invadopodia FITC-gelatin degrading activity cell lines, LN229 and MU41, including ICAM-1, ITGA3, ITGB3, CD151 and basigin (***Figure 5-7***). As Choi *et al.* demonstrated that that increased

expression of CD151 and basigin on the surface of GBM cell derived EVs enhanced EV uptake efficiency by recipient GBM cells [228], this could indicate that sEVs from high invadopodia activity cell lines may be more readily internalised by recipient cells. However, it is known that a variety of EV uptake mechanisms exist, such as the internalisation of EVs by recipient cells via clathrin-dependent and caveolin-dependent endocytosis, which involves proteins that were detected in sEVs from all three GBM cell lines (including Caveolae associated protein -1/-3 (CAVIN1/3), Clathrin (CLTC), and dynamin-2) [479]. Therefore, further investigation is warranted to determine whether the enrichment of specific sEV membrane proteins, such as basigin and CD151, may allow for the greater uptake of sEVs from high invadopodia FITC-gelatin degrading activity donor GBM cell lines.

Collectively, these findings provide evidence for the proposed role of sEVs in the biogenesis of invadopodia and suggest an important role for the vesicle-mediated delivery of receptors, such as integrins, EGFR and basigin, in the regulation of invadopodia in recipient cells.

5.3.3.2 Invadopodia-related signalling proteins in detected in the sEV proteome

5.3.3.2.1 Src and TGFBI

In addition to transmembrane receptors, a variety of key cytoplasmic proteins involved in invadopodia-related signalling pathways were also identified in the sEV proteome, including Src and several Rho GTPases. Amongst the invadopodia-related proteins, Src is central to many interactions amongst invadopodia regulators. It is a non-receptor tyrosine kinase that functions to phosphorylate, and thereby activate, a variety of downstream target substrates that are known to be involved in actin cytoskeletal assembly, including N-WASP, cortactin and Tks5 [149, 509, 512, 513]. Src was found to be highly expressed in the sEV proteome from all three GBM cell lines compared to the corresponding donor cell proteomes (***Figure 5-9***), which could signify that Src is selectively enriched for secretion in sEVs. In c-Src–transformed cells, Hikita *et* al. observed that Src localized to the endosomal membrane, whereby it promoted the secretion of Src-encapsulated exosomes [618]. This data further supports a link between

the endosomal pathway and invadopodia and suggests that Src may also be involved in both EV and invadopodia biogenesis.

Importantly, it has been demonstrated that the Src or TGF-β-induced transformation of epithelial cells is sufficient to induce *de novo* invadopodia formation [140, 142]. Interestingly, TGFBI was also highly expressed in sEVs from all three GBM cell lines compared to the corresponding donor cell proteomes (***Figure 5-9***). TGFBI is an ECM-interacting protein involved in the TGF-β signalling pathway, and is known to promote astrocytoma cellular adhesion and GBM invasion [572, 596]. Supporting its detection in GBM cell derived sEVs and potential pro-invasive role, TGFBI was recently also reported to be present in the proteome of small EVs derived from GBM cells displaying an aggressive mesenchymal subtype [619]. TGFBI is known to bind to integrins early in the TGF-β signalling pathway, which subsequently promotes invadopodia formation [142, 572]. Thus, the presence of both TGBFI and integrins in sEVs could also suggest these proteins may play important roles in the activation of invadopodia formation upon internalisation of sEVs by recipient GBM cells.

5.3.3.2.2 Rho GTPases

Additionally, Rho GTPases, including Cdc42, RhoA and RhoC, are also required for invadopodia formation/activity and these proteins were highly expressed in the sEV proteome compared to the GBM donor cells, suggesting an important role in intercellular EV-communication (***Figure 5-9***). Cdc42 is essential for invadopodia precursor assembly, and influences actin dynamics via activation of the N-WASP/Arp2/3 signalling cascade [515, 516]. RhoA, unlike Cdc42, is not vital for precursor formation but instead is involved in the delivery of exocyst-contained MT1-MMP to mature invadopodia together with Cdc42 [153]. Lastly, RhoC restricts cofilin activity to the invadopodium core to promote actin polymerisation and elongation. Consistent with its role within the invadopodium core, depletion of RhoC results in shorter protrusions that are unable to degrade the matrix efficiently for tumour invasion [620]. As studies have highlighted an important role for Rho GTPases in actin assembly and exocytosis required for the matrix degrading activity of invadopodia [153, 620], the high relative expression of

these proteins in sEVs could indicate a critical role in the stimulation of invadopodia formation and activity in recipient GBM cells. As siRNA-mediated reduction of Cdc42 expression in neuroendocrine cells has been shown to reduce the exocytosis of secretory granules [621], Rho GTPases may represent promising targets to reduce both invadopodia activity and the sEV-mediated transfer of a pro-invadopodia phenotype in GBM.

5.3.3.3 Invadopodia-related actin regulatory proteins in detected in the sEV proteome

Several proteins that form the core components of the invadopodia-associated actin machinery were identified in the proteome of the GBM cell line derived sEVs, including cortactin, cofilin, as well as key subunits of the WAVE and Arp2/3 complex (including WASF2, ACTR2, ACTR3) (***Table 5-2***). The detection of actin/cytoskeletal proteins in sEVs could reflect the pathways of biogenesis and secretion of these vesicles. For example, the trafficking of MVBs to the cell surface relies upon microtubule and actin structural components [226]. However, the actin cytoskeleton and microtubules are also implicated in MV formation, and actin has been detected in the cargo of membrane shed vesicles derived from the MDAMB231 breast cancer cell line and the U87MG GBM cell line [201]. Additionally, these proteins were also detected in the MV proteome (***Table 5-3***) and were not enriched in either vesicle proteome compared to donor cells (***Figure 5-9***).

Studies addressing the functional roles of actin-associated proteins in EVs are currently lacking, and it is not known whether the presence of actin-associated proteins in vesicles is a by-product of biogenesis, or whether they are involved in the regulatory functions of EVs in recipient cells. Recently, Holliday *et al*. suggested that actin-associated proteins, such as talin and filamin, in osteoclast-derived EVs may serve a functional role in maintaining integrins in a conformation that tightly binds the ECM [622]. However, this proposal was based on proteomic data, and such an association between these proteins in EVs is yet to be experimentally validated. Nevertheless, as actin polymerisation and microtubule dynamics are essential for the formation of invadopodia, the delivery of these proteins to recipient cells

via EV-mediated transfer may increase their availability in recipient GBM cells and thereby contribute towards invadopodia assembly and elongation. Ultimately, further research is required to confirm whether the actin-related proteins identified in sEVs serve a functional role in the transfer of a pro-invadopodia phenotype in recipient cells.

5.3.3.4 Invadopodia-related ECM-modifying proteins detected in the sEV proteome

5.3.3.4.1 Proteases

Several key invadopodia-related proteolytic proteins were identified in GBM cell line derived sEVs including MMP-2, as well as membrane-bound MT1-MMP and FAP (Fibroblast Activation Protein or Seprase) (***Table 5-2***). These three proteases are delivered to the cell surface during invadopodia maturation where they serve to facilitate ECM degradation [125, 149]. Although many studies have detected the presence of proteases in tumour derived EVs, such as MMPs and ADAMs, the EV-mediated exchange of proteases has not been directly demonstrated [623]. Nevertheless, it is possible that these proteases may be transferred to recipient GBM cells via EVs where they may contribute to increased cellular invasion.

Furthermore, GBM cell derived sEVs may be capable of interacting with and degrading ECM components. Indeed, MMPs contained in sEVs secreted by a variety of tumour cells are known to be proteolytically active and capable of ECM degradation [480, 623]. For example, both the pro- and active- forms of MT1-MMP have been detected in EVs secreted from fibrosarcoma and melanoma cells, which were able to recruit and activate pro-MMP-2 to degrade collagen and gelatin [302]. In a comprehensive analysis of the interactions between pancreatic adenocarcinoma EVs and the ECM, Mu *et al.* demonstrated that EVs carrying active proteases, including MMPs and ADAMs, also modify components of the ECM, which in turn promoted tumour growth [295]. The ability of these EVs to modify the ECM was dependent upon the presence of adhesion molecules on the EV membrane, such as integrins and CD44, which were also highly expressed in our GBM cell line derived sEV proteome

(***Figure 5-9***). As we demonstrated that reducing sEV secretion from GBM cells with DMA was shown to reduce invadopodia activity in a concentration-dependent manner (***Figure 4-9***), further research is required to verify the proteolytic activity of sEVs as a means of invadopodia-mediated matrix degradation in GBM.

Interestingly, differences in the proteolytic cargo of GBM cell line derived sEVs correlated with the level of invadopodia-mediated degradation observed for each cell line. sEVs secreted from the low invadopodia FITC-gelatin degrading activity cell line, MU4, were lacking in the expression of MT1-MMP, as well as exhibiting lower expression levels of MMP-2 and its inducer (BSG) compared to sEVs secreted by the high invadopodia FITC-gelatin degrading activity cell lines, LN229 and MU41 (***Figure 5-7***). As the level of MMP-2 secretion and activation is greater for LN229 and MU41 cells (***Figure 3-2***), one possibility is that MT1-MMP on the surface of sEVs may serve to activate MMP-2 secreted into the extracellular space, demonstrating that sEVs and invadopodia may work in unison to facilitate invadopodia-mediated ECM degradation. Indeed, a positive correlation has been shown to exist between the invasive capability of four breast cancer cell lines and one fibrosarcoma cell line, the quantity of EVs released, and the amount of proteolytic enzyme present in the EV cargo [624]. Therefore, sEVs secreted from high invadopodia FITC-gelatin degrading activity cell lines may be directly involved in ECM degradation and, in this way, may additionally serve to promote the proteolytic activity of invadopodia and subsequent GBM invasion. This data also supports the work of Hoshino *et al*. who proposed that exosome secretion is an integral part of invadopodia maturation and necessary for the invadopodia-mediated invasion of breast cancer cells through a matrigel matrix [229].

5.3.3.4.2 Adhesion proteins for sEV-ECM interactions

The modification of the ECM by sEVs enriched in proteases and adhesion proteins has also been demonstrated to facilitate cross-talk between the tumour microenvironment and malignant cells, with the EV-mediated degradation of collagens, laminins, and fibronectin shown to promote adhesion, motility, and invasiveness of nearby tumour cells [295, 625]. As signals from the tumour

microenvironment, including ECM rigidity, the release of growth factors, and changes in pH homeostasis are known to regulate invadopodia formation and function [482], this could represent another mechanism by which sEVs may promote invadopodia activity in recipient cells. Interestingly, by comparison, the MV proteomes possessed lower expression levels of many adhesion and integrin binding proteins that were detected in sEVs (***Figure 5-5***), and also exhibited lower expression levels of MMP-2, MT1-MMP and basigin compared to sEVs (***Figure 5-9B***), suggesting that sEVs may have a greater ability to interact with and degrade components of the ECM. Therefore, the presence of surface adhesion molecules (such as integrins and CD44) in the sEV proteome implies that sEV-induced signalling within the tumour microenvironment may represent another mechanism by which sEVs may promote invasion.

Figure 5-11: Potential mechanisms of the sEV-mediated transfer of pro-invadopodia cargo between GBM cells

A schematic representation of the proposed interactions between sEVs and invadopodia, whereby sEVs from high invadopodia activity GBM cell lines can promote invadopodia formation and activity in recipient GBM cell lines. ***A.*** In high invadopodia activity donor GBM cells, key proteins required for local proteolytic degradation of the ECM (e.g. MT1-MMP) are transported to mature invadopodia in MVBs, through interactions with the branched actin network in the invadopodium core. This process is dependent on actin regulators, such as cortactin, and Rho GTPases, such as Cdc42. Once docked at the plasma membrane, these MVBs may also be released as sEVs into the extracellular space that are enriched in invadopodia-related proteins, including surface proteins such as MT1-MMP that can activate extracellular MMP-2 to promote further ECM degradation. ***B.*** The sEVs secreted by high invadopodia activity cell lines are enriched in adhesion receptors and surface proteins (e.g. integrins, BSG, CD151) that may directly interact with proteins on the recipient GBM cell membrane, thereby activating signaling cascades to stimulate invadopodia formation. Additionally, these sEVs may be endocytosed by recipient GBM cells. As sEVs derived from high invadopodia activity donor cells are enriched in a variety of protein necessary for the multiple stages of the invadopodium lifecycle (e.g. signaling molecules, actin regulators and proteases), the sEV-mediated delivery of these proteins may subsequently stimulate *de novo* invadopodia formation, or enhance invadopodia initiation, assembly and maturation in recipient GBM cells.

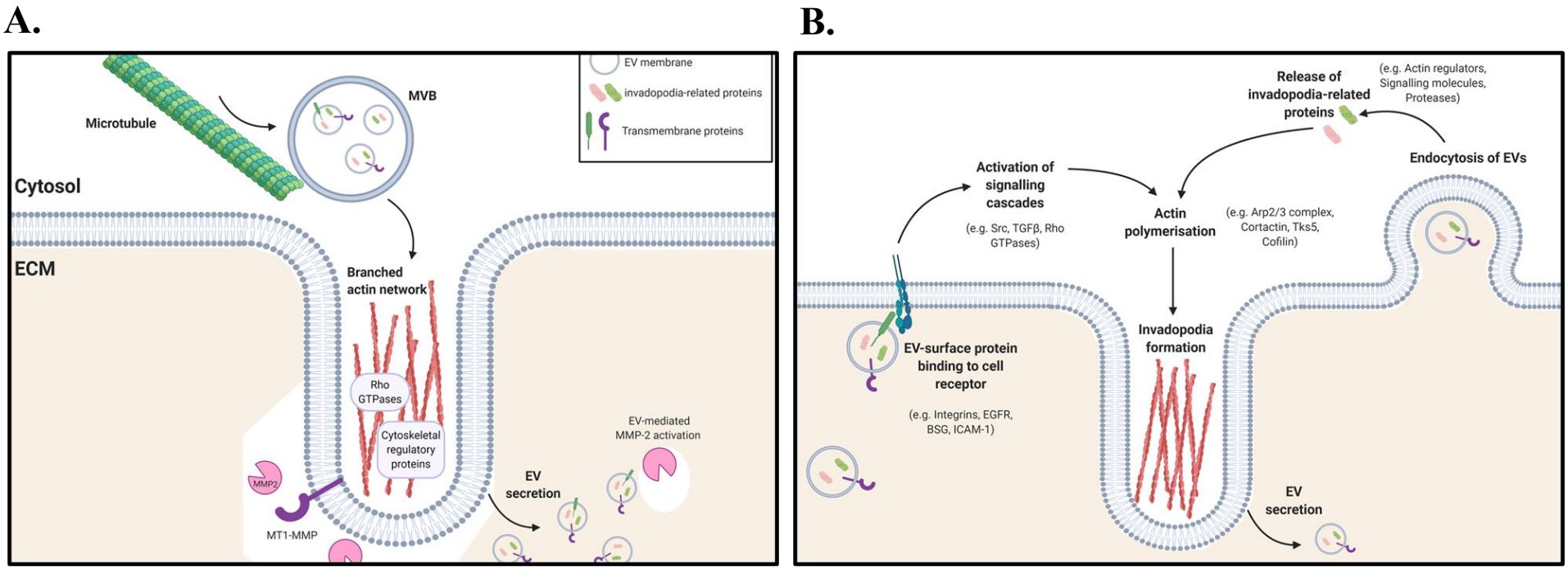
A.
B.
EV membrane
invadopodia-related proteins
Transmembrane proteins
Microtubule
MVB
Cytosol
ECM
Branched actin network
Rho GTPases
Cytoskeletal regulatory proteins
MMP2
MT1-MMP
EV secretion
EV-mediated MMP-2 activation
Release of invadopodia-related proteins
(e.g. Actin regulators, Signalling molecules, Proteases)
Endocytosis of EVs
Activation of signalling cascades
(e.g. Src, TGFβ, Rho GTPases)
Actin polymerisation
(e.g. Arp2/3 complex, Cortactin, Tks5, Cofilin)
Invadopodia formation
EV-surface protein binding to cell receptor
(e.g. Integrins, EGFR, BSG, ICAM-1)
EV secretion
Donor cell
(high basal level invadopodia activity)
Recipient cell
(low basal level invadopodia activity)

5.3.4 Conclusions

Increasing evidence suggests that oncogenic proteins carried by tumour derived EVs contribute to the horizontal transformation and phenotypic reprogramming of the recipient cells, including the ability to promote invasion through increased invadopodia activity. Therefore, the identification of EV-associated cargo proteins that possess potential invadopodia-related functions may highlight novel pathways in which to target tumour invasion.

Proteomic profiling revealed that GBM cell line derived sEVs carry invadopodia-related proteins, including proteases such as MMPs, components of the actin regulatory machinery such as subunits of the WAVE and Arp2/3 complex, and key signalling proteins such as Src and Rho GTPases, which may facilitate a pro-invadopodia phenotype in recipient GBM cells. Comparison of the GBM cell line and their corresponding sEV proteomes also revealed an enrichment of invadopodia-related trafficking proteins present in GBM cells, compared to invadopodia-related signalling proteins in the GBM cell derived sEVs, suggesting that signalling proteins may be selectively packaged and transported via sEVs and therefore may serve an important role in the sEV-mediated promotion of oncogenic processes in recipient cells. Moreover, it is feasible that many of the other proteins identified in the sEV proteome may also be essential, yet currently unidentified, regulators of invadopodia biogenesis. Indeed, several pro-invasive proteins were highly enriched in the GBM cell line derived sEV proteome (***Figure 5-10, Table 5-6)*** and therefore may warrant further investigation as invadopodia regulators, particularly in the context of GBM.

Ultimately, this data suggests that proteins carried by sEVs secreted from GBM cells may significantly enhance invadopodia-mediated matrix degradation and influence pro-invadopodia signalling pathways in recipient cells. Therefore, the proteins and functional pathways identified here may serve as targets for the development of novel inhibitors to combat invadopodia activity and limit the invasive potential of GBM tumours.

CHAPTER 6:
Proteomic analysis of RT/TMZ treated GBM cells and enriched EVs

6.1 Introduction

6.1.1 Therapeutic challenges in GBM

Despite advances in neurosurgical techniques and aggressive combinatorial treatment with RT and TMZ, the prognosis of GBM patients remains extremely poor, with a median survival time of approximately 12-15 months [2, 18]. Clinical studies have shown that 88.8% of GBM patients die within two years of their initial diagnosis due to tumour recurrence [61]. This can be attributed to both the highly infiltrative nature of GBM that renders curative surgery impossible and resistance to current therapeutics, meaning that GBM cells which survive treatment can invade the surrounding brain and form tumours at distant sites in the brain. Since the introduction of TMZ in 2005, there have been no significant improvements in GBM patient survival. Consequently, GBM remains incurable, with inevitable tumour relapse often seen within 2-3cm of the original lesion [60].

Chemoresistance is a hallmark of recurrent GBM and is defined by the ability of GBM cells to evade treatment, with the continued proliferation and invasion of these surviving cells leading to the emergence of a more aggressive disease [626]. Treatment resistance may result from existing genetic variations within the tumour, thereby allowing a population of cells to survive therapy, known as intrinsic resistance, or may be induced by the selective pressure of drug treatment on the surviving cells, known as acquired resistance [627]. The resulting resistant cells can often display genomic and proteomic alterations that drive aggressive tumour progression [626]. Genomic profiling has highlighted the degree of intra-tumour heterogeneity that is present in GBM tumours, which may contribute to the failure of targeted therapies as the response to treatment may not be consistent across the tumour [628].

A range of phenotypic changes that drive tumour progression have been reported in numerous cancers following chemotherapy, including a treatment-induced switch to either a pro-migratory or pro-proliferative phenotype (also known as the ‘Go or Grow’ mechanism) [629]. The phenotypical plasticity

of surviving tumour cells promotes therapeutic resistance by allowing cells to avoid or adapt to adverse microenvironment conditions imposed by anti-tumoral treatment, such as hypoxia or metabolic stress [630]. In the context of GBM, studies have revealed a link between the current therapeutic approach, consisting of RT and TMZ, and an augmented invasive capacity of the surviving cells [3, 4], potentially driven by enhanced MMP-2 activity [5, 6], leading to treatment failure and subsequent tumour recurrence. Although these findings highlight a key role for invasion in GBM treatment response, the underlying mechanisms are still not well understood. Therefore, a better understanding of the molecular changes that drive tumour progression in RT/TMZ treated GBM cells is imperative in uncovering potential novel treatment strategies.

6.1.2 The emerging role of EVs in tumour progression

Importantly, tumour growth and invasion are not only influenced by genetic abnormalities within a cell, but also interactions with the tumour microenvironment can contribute to tumour progression and resistance to therapies [1]. Due their ability to carry oncogenic cargo, EVs have emerged as facilitators of a pro-tumorigenic phenotype, as well as treatment resistance. Both the secretion and molecular composition of EVs can be affected by treatments such as irradiation and chemotherapy [489]. Several studies have shown that the horizontal transfer of EV-cargo from treated donor cells to recipient tumour cells can promote therapeutic resistance and tumour progression [188, 491]. EVs enriched from irradiated GBM cells have been reported to promote proliferation and radio-resistance in recipient GBM cells *in vitro*, as well as a larger tumour size and reduced survival *in vivo* [488]. Another study examining the molecular profile of EVs enriched from irradiated cultured GBM cells, observed elevated levels of connective tissue growth factor (CTGF) mRNA and insulin-like growth factor binding protein 2 (IGFBP2) protein, which are known to be involved in invasion [257]. These EVs enhanced migration in non-irradiated recipient tumour cells and promoted the activation of neurotrophic tyrosine kinase receptor type 1 (TrkA), focal adhesion kinase (FAK), paxillin, and proto-oncogene tyrosine-protein kinase Src (Src). These findings suggest a potential involvement of EV-mediated communication in

promoting invadopodia activity following exposure to RT/TMZ, since FAK, paxillin and Src are involved in the biogenesis of invadopodia [157].

6.1.3 Rationale and Aims

Whilst GBM cells surviving RT/TMZ treatment may possess genetic aberrations, ultimately, proteins are known to drive functional changes. Therefore, identifying changes in the proteome in response to RT/TMZ may reveal potential targets which can facilitate the development of new treatments. A proteomic approach has been undertaken to investigate the impact of both single and long-term (LT) RT/TMZ treatment (2Gy RT/50μM TMZ) on the proteome of GBM cells and sEVs. These analyses will highlight changes in the composition of cells and EVs in response to treatment, as well as providing a valuable insight into the specific sEV cargo proteins that may promote treatment induced invasion through the potential enhancement of a pro-invadopodia phenotype in recipient GBM cells.

6.2 Results

6.2.1 RT/TMZ treatment alters GBM cell and sEV protein expression

6.2.1.1 A distinct population of proteins is present in the proteome of RT/TMZ treated GBM cell lines

Overall, a total of 2586 proteins were detected in the proteomes of untreated and RT/TMZ treated GBM cell lines, of which 263 proteins were uniquely detected in the proteome of RT/TMZ treated cells (***Supplementary Figure 4***). Significantly enriched functional annotations as determined in FunRich, for these 263 proteins suggested an involvement in metabolism, exocytosis and GTPase activity, which encompassed proteins such as Rab GTPases (Rab5a, Rab3a, Rab27b) that are involved in membrane trafficking and fusion [631]. Increased abundance of these proteins could contribute to the enhancement of EV secretion post-RT/TMZ treatment in surviving GBM cells. Interestingly, proteins uniquely detected in the RT/TMZ treated GBM cells were also significantly associated with biological processes related to transcriptional regulation (including 'positive regulation of transcription elongation', 'histone H2B ubiquitination' and 'histone monoubiquitination') (***Supplementary Figure 4B***). Histone ubiquitination (particularly of H2A and H2B) is involved in the regulation of transcription initiation and elongation, as well as DNA repair, and therefore the upregulation of proteins as determined with these annotations may also enable surviving GBM cells to rapidly recover from RT/TMZ-induced DNA damage [632].

6.2.1.2 DE analysis of the GBM cell line proteome in response to RT/TMZ treatment

Differential expression (DE) analysis of the GBM cell proteomes was next performed to examine changes in protein abundance following RT/TMZ treatment that may facilitate the acquisition of a pro-invasive/pro-invadopodia phenotype. Significant DE proteins (log2-transformed LFQ ratio of >±2 and FDR ≤ 0.05) in RT/TMZ treated cells relative to untreated cells were determined for each GBM cell line (***Figure 6-1A***). To investigate whether these proteins may contribute to an increase in invasive capacity, the number of increased proteins corresponding to invasion-related protein classes using PANTHER was also investigated. Notably, the abundance levels of proteins associated with membrane trafficking/transport, kinase-activity, and the cytoskeleton were observed to increase in RT/TMZ treated GBM cells (***Figure 6-1B***). The top-50 DE proteins following RT/TMZ treatment were next identified, encompassing the top 25 proteins with increased and decreased abundance across all three GBM cell lines, and were visualised as a heatmap plotted using the Perseus bioinformatics platform [339] (***Figure 6-1C***). To determine which proteins may contribute to a pro-invasive/pro-invadopodia phenotype, the top 25 proteins with increased expression in GBM cells post- RT/TMZ treatment were examined (average log2-transformed LFQ ratio of 16.6 - 25.4). Functional enrichment analysis revealed that these proteins were significantly ($p<0.05$) associated with invadopodia-related cellular components (including 'filopodium tip' and 'focal adhesions') as well as exosomes, which was further reflected by their relevance to biological processes such as 'the MVB sorting pathway' and 'cytoskeletal anchoring at plasma membrane' (***Figure 6-1D***). Furthermore, high mRNA expression levels corresponding to these 25 increased proteins were found to significantly correlate with shorter GBM patient survival times (***Figure 6-1E***). As the upregulation of these transcripts may be of prognostic significance in GBM, this could indicate that the elevated protein expression levels detected in RT/TMZ treated GBM cells may also be of clinical importance, although further investigation is warranted. Considering this, 11 out of the top 25 proteins with increased abundance in RT/TMZ treated GBM cells are known to promote invasion, and therefore may contribute to a pro-invasive phenotype post-RT/TMZ treatment, however only 8 of these have been reported in the context of GBM (***Table 6-1***).

Figure 6-1: Analysis of DE proteins in RT/TMZ treated GBM cell lines

(**A.**) The number of DE proteins (LFQ ratio of >±2 and FDR ≤ 0.05) in each RT/TMZ treated GBM cell line relative to corresponding untreated GBM cells. Both ▲increased and ▼decreased proteins are shown. (**B.**) The increased proteins in RT/TMZ treated GBM cell lines were classified according to the PANTHER Protein Classification system, which identified 11 potential invasion-related categories/classes. The number of increased proteins within each invasion-related protein class is shown for each GBM cell line. (**C.**) The distribution of the top-50 DE proteins across all three GBM cell lines following RT/TMZ treatment (determined by the average log2-transformed LFQ ratios in untreated vs. RT/TMZ treated GBM cells) is shown as a heatmap, indicated by the normalised Z-score of each protein generated with the Perseus bioinformatics software platform. High relative expression is indicated in red and low relative expression is indicated in green. Proteins were divided into 2 clusters based on hierarchical clustering, as shown to the left of the heatmap: the pink and blue clusters represent the top 25 decreased and increased proteins following RT/TMZ treatment, respectively. (**D.**) Functional enrichment analysis of the top 25 increased proteins detected in RT/TMZ treated GBM cells was conducted using FunRich to identify significantly enriched GO annotations. (P values were calculated by two-sided hypergeometric test – the top 5 annotations with the most significant p values are shown). (**E.**) mRNA expression levels corresponding to the top 25 increased proteins were interrogated using the Glioblastoma Bio Discovery Portal (GBM-BioDP) web resource that utilises GBM patient expression and survival data from three TCGA microarray platforms (Affymetrix HGU133A, Agilent G4502A, and HuEx-1_0-st-v2), and one dataset generated by aggregating all three platforms (3-Platform Aggregates) [633]. A Cox proportional hazards model was constructed based on a prognostic index generated from the combined expression levels of the interrogated genes**,** and data was stratified according to the lowest quartile (QT) (blue- lowest expression) versus the highest quartile (QT) (red-highest expression). *P values below p=0.01 are listed as 'p-val=0.*

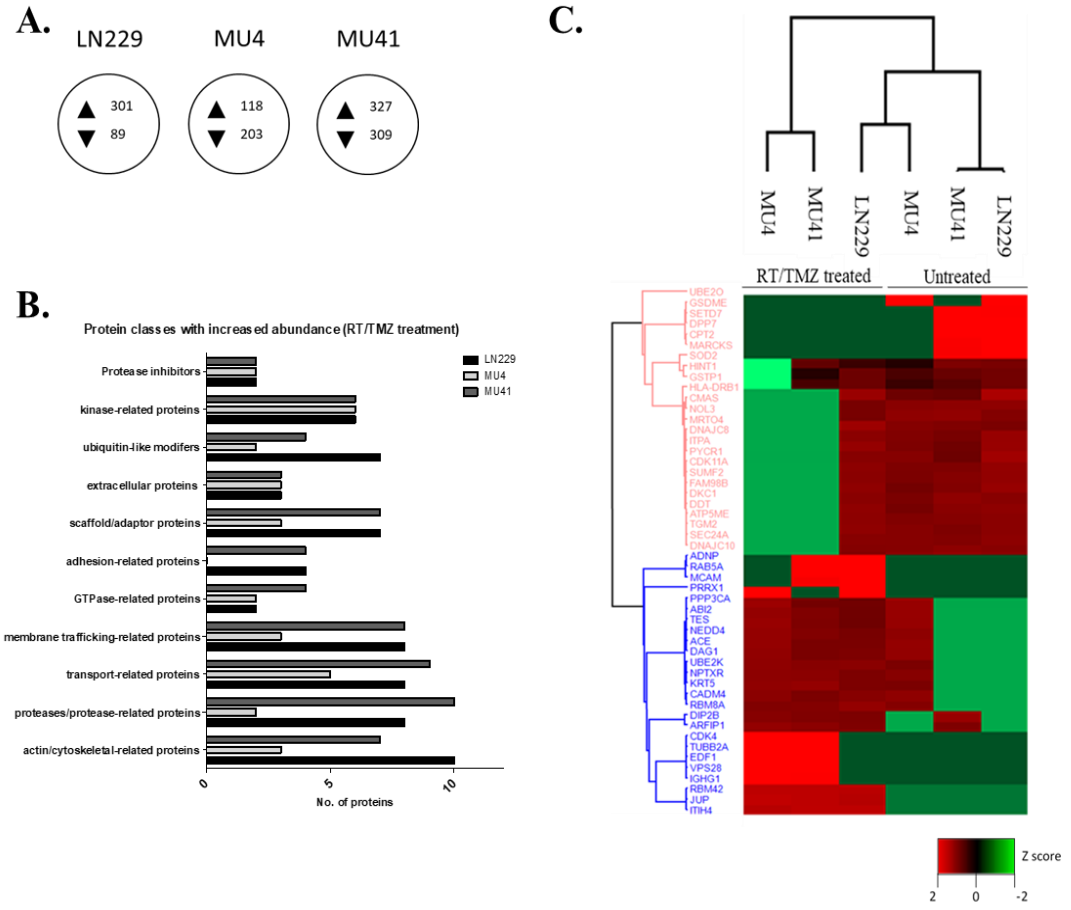
A.
LN229
MU4
MU41
301
89
118
203
327
309
B.
Protein classes with increased abundance (RT/TMZ treatment)
LN229
MU4
MU41
Protease inhibitors
kinase-related proteins
ubiquitin-like modifers
extracellular proteins
scaffold/adaptor proteins
adhesion-related proteins
GTPase-related proteins
membrane trafficking-related proteins
transport-related proteins
proteases/protease-related proteins
actin/cytoskeletal-related proteins
0
5
10
No. of proteins
C.
MU4
MU41
LN229
MU4
MU41
LN229
RT/TMZ treated
Untreated
UBE2O
GSDME
SETD7
DPP7
CPT2
MARCKS
SOD2
HINT1
GSTP1
HLA-DRB1
CMAS
NOL3
MRTO4
DNAJC8
ITPA
PYGR1
CDK11A
SUMF2
FAM98B
DKC1
DDT
ATP5ME
TGM2
SEC24A
DNAJC10
ADNP
RAB5A
MCAM
PRRX1
PPP3CA
ABI2
TES
NEDD4
ACE
DAG1
UBE2K
NPTXR
KRT5
CADM4
RBM8A
DIP2B
ARFIP1
CDK4
TUBB2A
EDF1
VPS28
IGHG1
RBM42
JUP
ITIH4
Z score
2
0
-2
D.
Top 25 proteins with increased abundance (RT/TMZ treatment)
Biological Process
regulation of neuron projection regeneration
positive regulation of cell-matrix adhesion
regulation of synapse organization
ub-dependent protein catabolic process via the MVB sortin
cytoskeletal anchoring at plasma membrane
Molecular Function
ubiquitin binding
vascular endothelial growth factor receptor 1 binding
metallodipeptidase activity
drug binding
protein-containing complex binding
Cellular Component
focal adhesion
apicolateral plasma membrane
filopodium tip
cytoplasm
extracellular exosome
0
1
2
3
4
5
-log10 (p value)
E.
HT_HG-U133A
24/25 proteins
AgilentG4502A_07
25/25 proteins
HuEx-1_0-st-v2
25/25 proteins
3-Platform Aggregates
24/25 proteins
Full cohort
Prognostic Index
1Qt
4Qt
Percentage survival
Survival in days
P=0
HR= 3.28
HR= 2.51
HR= 2.31
HR= 3.03

Table 6-1: Common invasion-related proteins that are increased in the three GBM cell lines post RT/TMZ treatment

Protein	Known role/s	Reported role in GBM
JUP	Junction plakoglobin was found to be overexpressed in OSC and promoted the proliferation, migration, and invasion of OSCC cells but inhibited apoptosis [634]	NA
DAG1	High expression of dystroglycan promoted prostate cancer cell invasion, but inhibited growth on soft agar [635]	Dystroglycan-receptor interactions promote a mesenchymal-like state and maintain GSCs in perivascular niches via anchoring to laminin and regulation of ERK signalling [636]
NEDD4	NEDD4 is significantly correlated with tumour metastasis and required for migration and invasion signalling of EGFR in gastric cancer cells [637]	NEDD4 promotes the invasion of malignant glioma cells *in vitro* via triggering ubiquitination of cyclic nucleotide Ras guanine nucleotide exchange factor (CNrasGEF) [638]
PRRX1	PRRX1-induces EMT (invasion/migration) but reduces cell proliferation and apoptosis of HNSCC [639]	Activation of Notch signalling by PRRX1 promotes GBM cell invasion and neurosphere formation *in vitro* [640]
RAB5A	Rab5a promotes the migration and invasion of hepatocellular carcinoma by up-regulating Cdc42 [641]	Overexpression of Rab5a was found to promote radio resistance and autophagy in glioma cells *in vitro* [642]
VPS28	VPS28 is a subunit of the ESCRT-I complex, required for the translocation of active Src from late endosomal/lysosomal compartment to focal adhesions, where Src functions to promote cell motility [643]	NA
ABI2	ABI2 is a regulator of actin cytoskeleton dynamics underlying cell motility and adhesion. It functions as a component of the WAVE2 complex, which activates actin nucleating machinery Arp2/3 to drive invadopodia formation [562, 563]	NA
ACE	ACE-inhibitors inhibit proliferation and invasion of cancer cells *in vitro* and tumour growth and metastasis *in vivo,* via the inhibition of MMP activity and VEGF expression [644]	ACE expression was detected via IHC staining on the endothelium of microvessels within GBM tissue samples [645]
MCAM	Silencing MCAM in SKOV-3 ovarian cancer cells reduced invasion, which correlated with decreased Rho GTPase (Cdc42 and RhoA) activation [646]	MCAM is upregulated in WHO grade III and IV gliomas, as determined by IHC staining. MCAM is also highly expressed in GSCs, and ectopic expression in differentiated GBM cells results in cell cycle arrest [647]

PPP3CA	PPP3CA is bound by C16orf74 to promote invasion in aggressive pancreatic cancers [648]	PPP3CA encodes calmodulin-binding catalytic subunit of calcineurin. Calcineurin expression was found to be elevated in areas of high infiltration/migration in GBM tissue [649]
NPTXR	NPTXR is a receptor for NPTX, which has been demonstrated to promote CRC metastasis through the activation of the Wnt/β-catenin signalling pathway [650]. It has also been correlated with Neuroblastoma tumour burden [651]	Ligands of NPTXR, NPTX1/2, are reported to cause dysfunction PI3K/AKT/mTOR signalling thereby affecting tumour progression in the U251 human glioma cell line [652]

NA: not applicable

6.2.1.3 DE analysis of invadopodia-related proteins in the GBM cell line proteome following RT/TMZ treatment

As functional experiments have revealed an increase in invadopodia formation and activity in GBM cells following RT/TMZ treatment (***Figure 3-4***), the DE invadopodia-related proteins in each GBM cell line post-RT/TMZ treatment were next examined (***Figure 6-2A, Supplementary Table 6***). A total of 19 previously reported invadopodia-related proteins were increased in the proteome of GBM cells following RT/TMZ treatment (***Figure 6-2B***). Interestingly, functional enrichment analysis of these 19 invadopodia-related proteins indicates their involvement in exocytosis and microtubule-mediated vesicle trafficking, with significant associations to 'microtubule plus-end binding', 'synaptic vesicle recycling' and 'positive regulation of exocytosis', suggesting a potential increase in the transport of vesicles to invadopodia post-RT/TMZ treatment ***(Figure 6-2C***).

Figure 6-2: Analysis of DE invadopodia-related proteins in GBM cells post-RT/TMZ treatment

(**A** The number of DE invadopodia-related proteins (LFQ ratio of >±2 and FDR ≤ 0.05) in each RT/TMZ treated GBM cell line relative to corresponding untreated GBM cells. Both ▲increased and ▼decreased proteins are shown. (**B**.) A Venn diagram comparing the increased invadopodia-related proteins in each GBM cell line post-RT/TMZ treatment, showing a total of 19 different proteins were identified in RT/TMZ treated GBM cell lines relative to untreated cells. (**C**.) Functional enrichment analysis of the 19 increased invadopodia-related proteins in RT/TMZ treated GBM cells showing the top 5 significantly enriched GO annotations for biological process and molecular function, as determined by FunRich. (*P values were calculated by two-sided hypergeometric test and are shown as -log10(P)*).

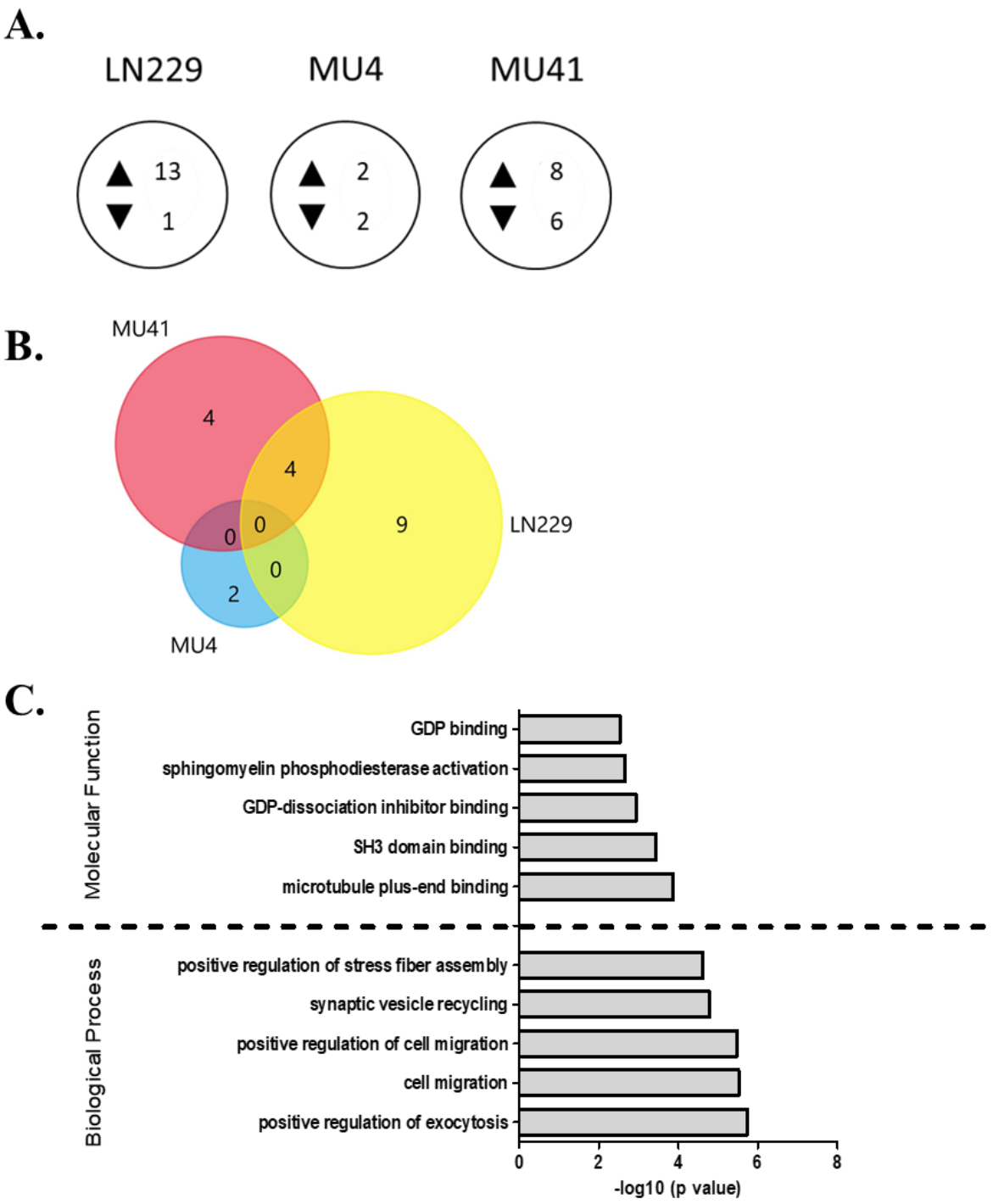
A.
LN229
MU4
MU41
13
1
2
2
8
6
B.
MU41
4
4
0
0
9
LN229
0
2
MU4
C.
Molecular Function
GDP binding
sphingomyelin phosphodiesterase activation
GDP-dissociation inhibitor binding
SH3 domain binding
microtubule plus-end binding
Biological Process
positive regulation of stress fiber assembly
synaptic vesicle recycling
positive regulation of cell migration
cell migration
positive regulation of exocytosis
0
2
4
6
8
-log10 (p value)

6.2.1.4 A distinct population of proteins is present in the proteome of sEVs enriched from RT/TMZ treated GBM cell lines.

Overall, a total 2248 proteins were detected in the GBM cell line sEV proteomes, with 429 proteins being uniquely identified in the proteome of sEVs enriched from RT/TMZ treated GBM cell lines (***Supplementary Figure 5***). Significantly enriched functional annotations for the 429 suggested an involvement in vesicle transport, membrane trafficking and viral budding, which both depend on ESCRT-machinery and MVBs within the cell prior to release, as well as endocytosis and protein folding (***Supplementary Figure 5B&D***).

6.2.1.5 DE analysis of sEV cargo proteins in response to RT/TMZ treatment

Differential expression (DE) analysis of the proteome of sEVs enriched from untreated and RT/TMZ treated GBM cells was next performed to determine changes in protein expression following RT/TMZ treatment. Significant DE proteins (log2-transformed LFQ ratio of $>\pm 2$ and FDR ≤ 0.05) detected in the proteome of sEVs from RT/TMZ donor treated cells relative to untreated donor cells were determined for each GBM cell line (***Figure 6-3A***) To investigate whether these significantly increased proteins may contribute to an increase in invasive capacity, the number of increased sEV cargo proteins corresponding to invasion-related protein classes identified using PANTHER was also investigated. Notably, the abundance levels of proteins associated with the cytoskeleton and intracellular transport, as well as protease-related activity and kinase activity were observed to increase in sEVs from RT/TMZ treated GBM cells compared to the corresponding donor GBM cells (***Figure 6-3B)***. The top-50 DE sEV cargo proteins across all three GBM cell lines following RT/TMZ treatment were next determined and visualised as a heatmap (***Figure 6-3C***). Functional enrichment analysis revealed that these sEV cargo proteins were significantly annotated as cell surface proteins with the potential for collagen-, enzyme- and receptor- binding capability, suggesting possible roles in mediating sEV interactions with ECM components or the activation of intracellular pathways in recipient cells via surface receptor binding (***Figure 6-3D***). Importantly, there was also an increase in the positive regulation of protein localization

to the plasma membrane which may be linked with enhanced invadopodia formation and activity. Furthermore, high mRNA expression levels corresponding to these 25 increased sEV cargo proteins were found to significantly correlate with shorter GBM patient survival times (***Figure 6-3E***). This could indicate potential prognostic significance of these sEV cargo proteins in GBM, however as mRNA expression levels may not directly correspond with protein abundance levels, further investigation of these 25 sEV proteins as potential biomarkers is warranted. Nevertheless, 14 of these proteins with increased abundance in sEVs from RT/TMZ treated GBM cells are known to promote invasion, and therefore may contribute to a pro-invasive phenotype post-RT/TMZ treatment, however only 11 of these have been reported in the context of GBM (***Table 6-2***).

Figure 6-3: Analysis of DE proteins in sEVs enriched from RT/TMZ treated GBM cell lines

(**A.**) The number of DE proteins (LFQ ratio of >±2 and FDR ≤ 0.05) detected in the sEVs enriched from each RT/TMZ treated GBM cell line relative to corresponding sEVs from untreated GBM cells. Both ▲increased and ▼decreased proteins are shown. (**B.**) Increased proteins in sEVs from RT/TMZ treated cells were classified according to the PANTHER Protein Classification system, which identified 11 potential invasion-related functional categories. The number of increased proteins within each invasion-related protein class is shown for sEVs from each GBM cell line. (**C.**) The distribution of the top-50 DE proteins detected in sEVs enriched from all three GBM cell lines following RT/TMZ treatment (determined by the average log2-transformed LFQ ratios in untreated vs. RT/TMZ treated GBM cells) is shown as a heatmap, indicated by the normalised Z-score of each protein generated with the Perseus bioinformatics software platform. High relative expression is indicated in red and low relative expression is indicated in green. Proteins were divided into 2 clusters based on hierarchical clustering, as shown to the left of the heatmap: the pink and blue clusters represent the top 25 decreased and increased sEV proteins following RT/TMZ treatment, respectively. (**D.**) Functional enrichment analysis of the top 25 increased proteins detected in sEVs from RT/TMZ treated GBM cells was conducted using FunRich to identify significantly enriched GO annotations. (P values were calculated by two-sided hypergeometric test – the top 5 annotations with the most significant p values are shown). (**E.**) mRNA expression levels corresponding to the top 25 increased proteins were interrogated using the Glioblastoma Bio Discovery Portal (GBM-BioDP) web resource that utilises GBM patient expression and survival data from three TCGA microarray platforms (Affymetrix HGU133A, Agilent G4502A, and HuEx-1_0-st-v2), and one dataset generated by aggregating all three platforms (3-Platform Aggregates) [633]. A Cox proportional hazards model was constructed based on a prognostic index generated from the combined expression levels of the interrogated genes**,** and data was stratified according to the lowest quartile (QT) (blue- lowest expression) versus the highest quartile (QT) (red-highest expression). *P values below p=0.01 are listed as 'p-val=0.*

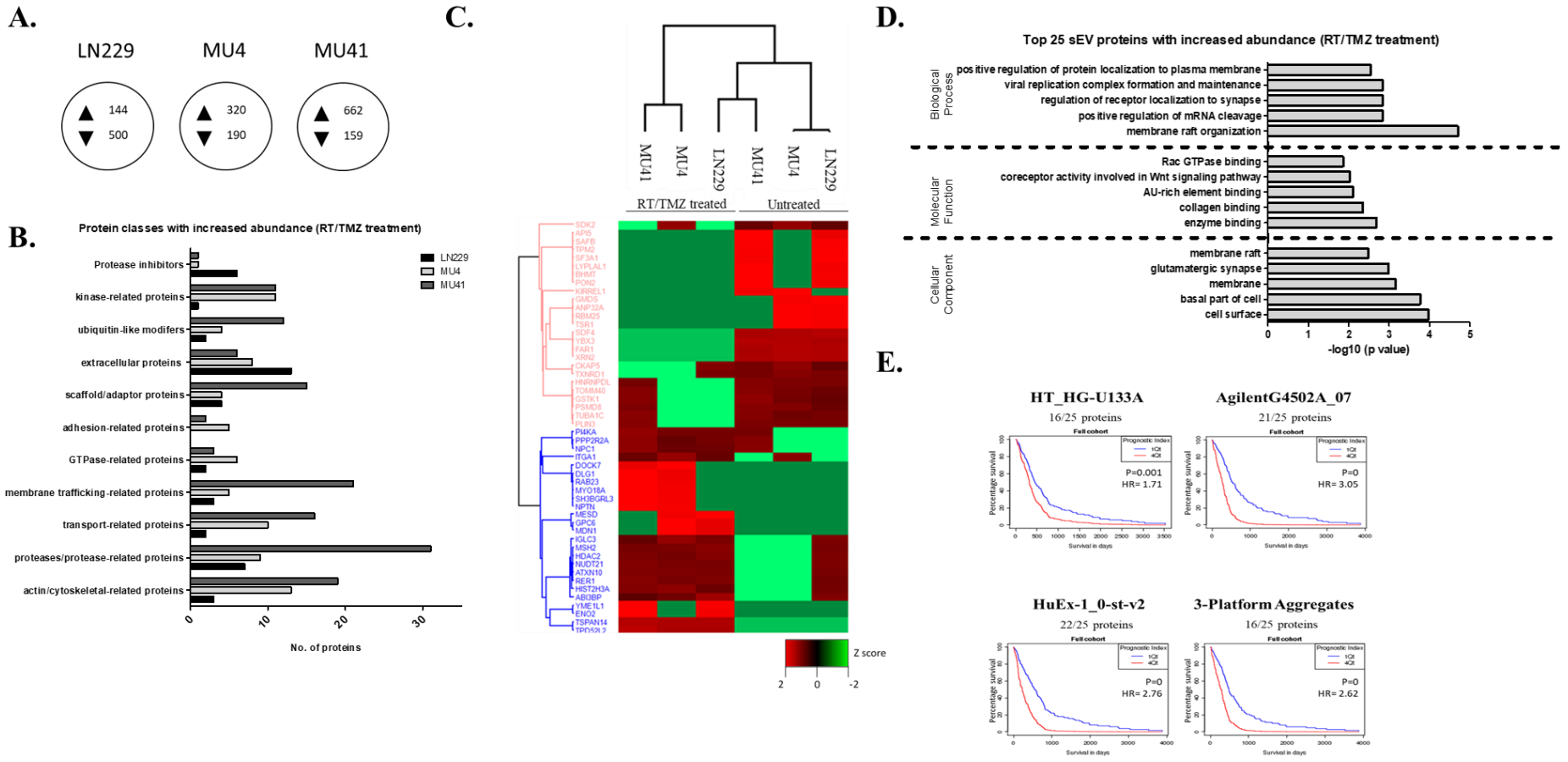
A.
LN229
MU4
MU41
144
500
320
190
662
159
B.
Protein classes with increased abundance (RT/TMZ treatment)
LN229
MU4
MU41
Protease inhibitors
kinase-related proteins
ubiquitin-like modifers
extracellular proteins
scaffold/adaptor proteins
adhesion-related proteins
GTPase-related proteins
membrane trafficking-related proteins
transport-related proteins
proteases/protease-related proteins
actin/cytoskeletal-related proteins
0
10
20
30
No. of proteins
C.
MU41
MU4
LN229
MU41
MU4
LN229
RT/TMZ treated
Untreated
Z score
2
0
-2
D.
Top 25 sEV proteins with increased abundance (RT/TMZ treatment)
Biological Process
positive regulation of protein localization to plasma membrane
viral replication complex formation and maintenance
regulation of receptor localization to synapse
positive regulation of mRNA cleavage
membrane raft organization
Molecular Function
Rac GTPase binding
coreceptor activity involved in Wnt signaling pathway
AU-rich element binding
collagen binding
enzyme binding
Cellular Component
membrane raft
glutamatergic synapse
membrane
basal part of cell
cell surface
0
1
2
3
4
5
-log10 (p value)
E.
HT_HG-U133A
16/25 proteins
P=0.001
HR= 1.71
AgilentG4502A_07
21/25 proteins
P=0
HR= 3.05
HuEx-1_0-st-v2
22/25 proteins
P=0
HR= 2.76
3-Platform Aggregates
16/25 proteins
P=0
HR= 2.62

Table 6-2: Common invasion-related proteins that are increased in sEVs enriched from GBM cells post RT/TMZ treatment

Protein	Known role/s	Reported role in GBM
DLG1	Interaction of Protein Kinase C-α with DLG1 promotes cellular invasion in non-small cell lung cancer lines [653]	DLG1, also known as synapse-associated protein 97 (SAP97), was found to contribute to the stability of sodium (Na_x) channels in the plasma membrane of C6 GBM cells [654]
RER1	RER1 enhances the progression of prostate cancer through promoting cell proliferation, migration and invasion [655]	NA
DOCK7	Inhibition of DOCK7 in ESCC cells expressing the oncoprotein SET reduced invasion through a 3D matrix and directional migration *in vitro* [656]	Acts as a GEF for Rac1 to promote HGF-dependent GBM cell invasion. Furthermore, depletion of Dock7 significantly decreased HGF-induced lamellipodia formation [657]
PI4KA	HCC patients who had been treated by surgical resection and had higher PI4KA mRNA concentrations in their tumour tissue exhibited a higher risk of tumour recurrence (median time: 20 months versus 49 months, P = 0.0012) [658]	Inhibition of PI4K IIIα using RNAi inhibited U251 cell migration and invasion *in vitro*, whilst its inhibition in U251 xenograft mice, using an agent known as simeprevir, also had a radiosensitizing effect [659]
HDAC2	Elevated expression of HDAC2 can promote the migration and invasion of non-small cell lung cancer cells via up regulation fibronectin through the activation of NF-κB signalling [660].	siRNA silencing of HDAC2 suppresses the *in vitro* proliferation, migration, and invasion of GBM U87MG and A172 cell lines, and increases the sensitivity of GBM cells to TMZ [661]
ITGA1	ITGA1 can promote CRC cell migration, invasion and tumorigenicity by activating the Ras/Erk signalling [662]	Overexpression of the long noncoding RNA 'HULC' increased GBM cell proliferation, invasion, and migration, which correlated with an upregulation of ITGA1 protein expression [663]
MYO18A	MYO18A is overexpressed in highly metastatic prostate cancer cell lines, and knockdown reduced the number of filopodia formed by these cells [664]. MYO18A colocalises with PAK2 in lamellipodia to promote epithelial cell migration [665]	MYO18A associates with GOLPH3 to promote Golgi extension and vesicle release, resulting in the secretion of growth factors and MMPs [4]. GOLPH3 promotes GBM cell migration and invasion via the mTOR signalling pathway [184]
GPC6	GPC6 promotes the migration, invasion, and proliferation of nasopharyngeal carcinoma cells in vitro [666]. Hedgehog signalling activation is also required for GPC6-mediated regulation of invasion, migration, and EMT in gastric cancer cells [667]	GPC6 was found to be expressed in the U251MG GBM cell line [668]

NPTN	NPTNβ can induce anchorage-independent growth, motility and invasiveness in lung cancer cells in response to extracellular S100A8/A9 [669]. Significantly higher NPTN immunoreactivity was detected in invasive breast tumour tissue compared to control breast tissue, suggesting that NPTN expression may promote tumour invasion [670]	NPTN is increased in EVs released from U373 GBM cells expressing EGFRvIII [228]
TSPAN14	Regulates ADAM10 trafficking and activity [671], which in turn can promote cell proliferation, migration, and invasion [672]	NA
TPD52L2	Knockdown of TPD52L2 suppressed PIK3CA/AKT signalling and suppressed the proliferation, migration and invasion of human pancreatic adenocarcinoma cells [673]	miR-485-5p downregulation of TPD52L2 reduced GBM cell proliferation, migration, and invasion *in vitro* [674]
ENO2	ENO2 is overexpressed in pancreatic ductal adenocarcinoma (PDAC) tissue and correlates with metastasis and poor prognosis in PDAC patients [675]	ENO2 is upregulated in hypoxic GBM cells and knockdown of ENO2 *in vivo* results in a survival benefit in mice [676]
RAB23	Rab23 promotes squamous cell carcinoma cells migration and invasion by regulating the Integrin β1/Rac1 pathway [677]	Rab23 is highly expressed in grade III and IV astrocytomas and promotes invasion via Rac1 activation in GBM cells [678]
SH3BGRL3	SH3BGRL3 promotes EMT, migration and proliferation of urothelial carcinoma *in vitro* via interaction with pEGFR through Grb2, which activates the Akt- signalling pathway [679]	Proteomic analysis identified that SH3BGRL3 is increased in GBM tissue compared to non-tumour brain tissue [680]

NA: not applicable

6.2.1.6 DE analysis of invadopodia-related proteins in the GBM cell derived sEV proteome following RT/TMZ treatment

As functional experiments have revealed an increase in invadopodia formation and activity in GBM cells following RT/TMZ treatment (***Figure 3-4***), the DE invadopodia-related proteins in the proteome of sEVs secreted from each GBM cell line post-RT/TMZ treatment were next examined (***Figure 6-4A, Supplementary Table 7***). A total of 20 previously reported invadopodia-related proteins (out of the 26 significantly DE proteins) were found to be increased in the cargo of sEVs post-RT/TMZ treatment (***Figure 6-4B***). These demonstrated significant ($p<0.05$) functional associations to signalling pathways known to drive actin polymerisation, as reflected by molecular functions such as 'integrin binding' and 'SH3 domain binding', suggesting that these proteins with increased abundance in sEVs post-RT/TMZ may possess roles in adhesion-related signalling pathways that drive actin polymerisation, and thus may promote invadopodia formation/initiation in recipient cells ***(Figure 6-4C***).

Figure 6-4: Analysis of DE invadopodia-related proteins in sEVs enriched from GBM cells post-RT/TMZ treatment

(**A** The number of DE invadopodia-related proteins (LFQ ratio of >±2 and FDR ≤ 0.05) in in the proteome of EVs enriched from each GBM cell line following RT/TMZ treatment. Both ▲increased and ▼decreased proteins are shown. (**B**.) A Venn diagram comparing the increased invadopodia-related proteins in sEVs from each GBM cell line post-RT/TMZ treatment, showing that a total of 20 different increased invadopodia-related proteins were identified in sEVs from RT/TMZ treated GBM cell lines relative to untreated cells. (**C**.) Functional enrichment analysis of the 20 increased invadopodia-related proteins in sEVs from RT/TMZ treated GBM cells showing the top 5 significantly enriched GO annotations for biological process and molecular function, as determined by FunRich. (*P values were calculated by two-sided hypergeometric test and are shown as -log10(P)*).

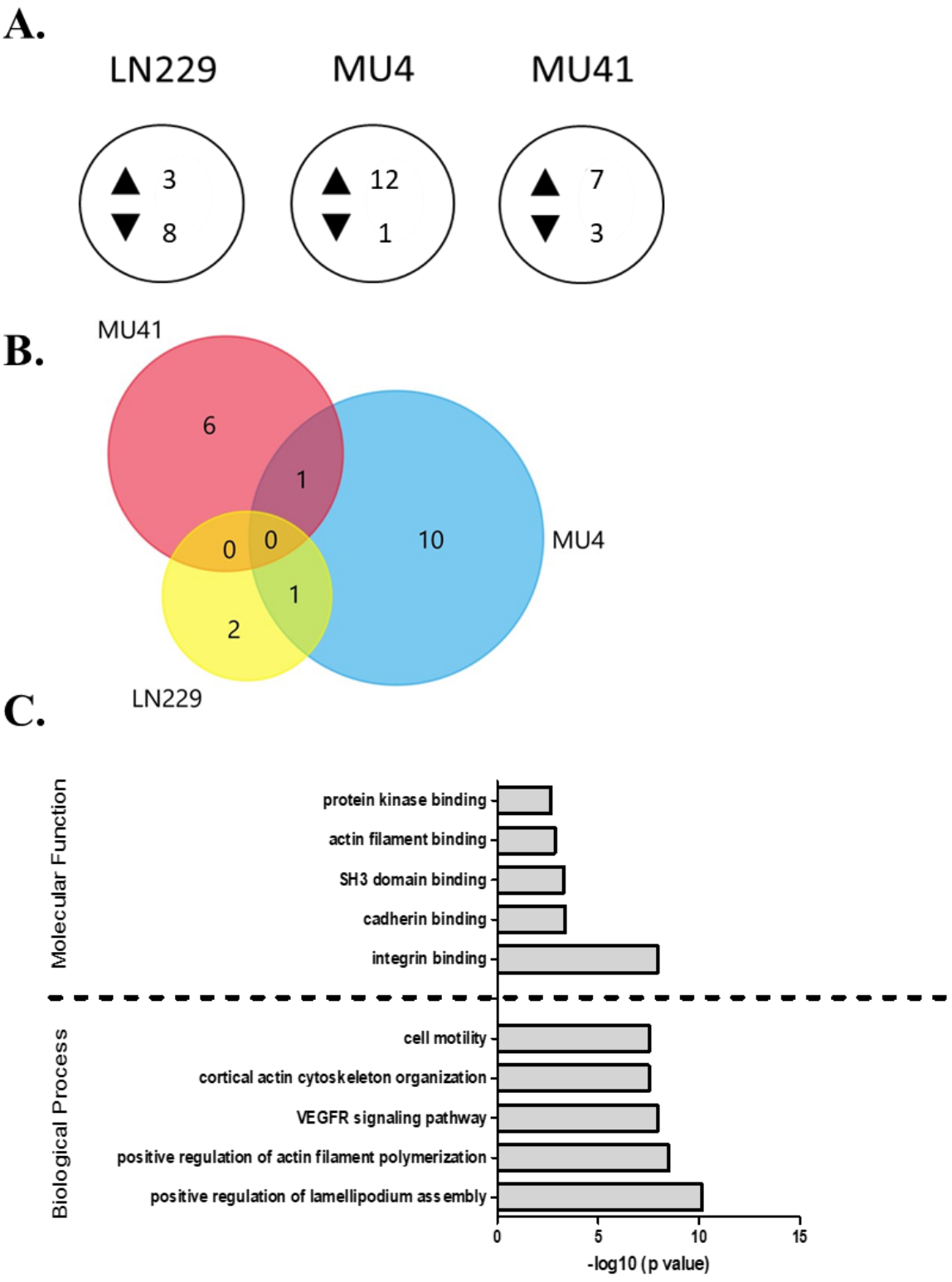
A.
LN229
MU4
MU41
3
8
12
1
7
3
B.
MU41
6
1
0
0
10
MU4
1
2
LN229
C.
Molecular Function
protein kinase binding
actin filament binding
SH3 domain binding
cadherin binding
integrin binding
Biological Process
cell motility
cortical actin cytoskeleton organization
VEGFR signaling pathway
positive regulation of actin filament polymerization
positive regulation of lamellipodium assembly
0
5
10
15
-log10 (p value)

6.2.2 Long-term (LT) treatment with RT/TMZ alters GBM cell line and sEV cargo protein expression

6.2.2.1 A distinct population of proteins is present in the proteome of LT RT/TMZ treated GBM cell lines

Overall, a total of 3230 proteins were detected in the proteomes of untreated and LT treated GBM cell lines, of which 199 proteins were uniquely detected in the proteome of LT RT/TMZ treated GBM cells. (***Supplementary Figure 6A***). Significantly enriched functional annotations for these 199 proteins suggested involvement in the intracellular transport of vesicles, membrane trafficking, and fatty acid metabolism (***Supplementary Figure 6B-D***). Additionally, significant annotations relating to 'Rho GTPase binding' and 'actin binding' (***Supplementary Figure 6C***) indicates an enrichment of proteins in LT RT/TMZ treated GBM cells that may be involved in invadopodia-related signalling pathways and actin dynamics which may facilitate invadopodia formation and activity.

6.2.2.2 DE analysis of GBM cell line proteins in response to LT RT/TMZ treatment

Differential expression (DE) analysis of the untreated and LT RT/TMZ treated GBM cell line proteomes was next performed to determine changes in protein expression following LT RT/TMZ treatment. Significant DE proteins (log2-transformed LFQ ratio of >±2 and FDR ≤ 0.05) detected in the LT RT/TMZ treated GBM cells relative to the untreated cells were determined for each GBM cell line (***Figure 6-5A***). It is worth noting that LT RT/TMZ treated LN229 cells displayed a reduction in the expression of a large number of proteins (1522 proteins) relative to untreated GBM cells and only a total of 143 proteins with increased expression post treatment. This difference between the number of increased and decreased proteins was not observed for the MU4 and MU41 GBM cell lines following LT RT/TMZ treatment. The number of increased proteins within each LT RT/TMZ treated GBM cell

line corresponding to invasion-related protein classes as determined in PANTHER was also investigated (***Figure 6-5B***). The greatest increases were observed for kinase-related and protease-related proteins in the MU41 and MU4 cell lines following LT RT/TMZ treatment, whereas considerably fewer proteins within each class were observed to increase for LT RT/TMZ treated LN229 cells. This is consistent with the reduction in invasive capacity previously observed for LT RT/TMZ treated LN229 cells (***Figure 3-8***).

Functional experiments in ***Chapter 3*** revealed that the MU4 and MU41 cell lines exhibit an augmented pro-invasive/pro-invadopodia phenotype following exposure to LT RT/TMZ treatment, whilst the LN229 cell line instead adopted a pro-proliferative and minimally invasive phenotype (outlined in ***Figure 3-24***). Therefore, DE proteins were next examined for each LT RT/TMZ treated cell line individually. The top-50 DE proteins in each LT RT/TMZ treated cell line relative to the corresponding untreated cell line were identified and annotated using FunRich. To determine which proteins may contribute to these distinct phenotypes, the top 25 proteins with increased expression in LT RT/TMZ treated GBM cells were examined (for annotations corresponding to decreased proteins, see ***Supplementary Figure 7***). Consistent with the enhanced invadopodia-mediated FITC-gelatin degrading activity observed in LT RT/TMZ treated MU4 and MU41 cells, functional annotations showed an enrichment of proteins with biological relevance to translation, membrane transport, and adhesion (***Figure 6-5D&E***). This suggests an upregulation of membrane trafficking processes which are crucial for the targeted delivery of specific cargoes to invadopodia, for example MT1-MMP that is transported to invadopodia in Golgi-derived vesicles along an actin/microtubule network [150]. Unlike the LT RT/TMZ treated MU4 and MU41 GBM cell lines, the functional annotations for LT treated LN229 cells suggest an upregulation of proteins involved in cellular metabolism, encompassing fatty acid oxidation (***Figure 6-5C***). Importantly, it can be observed that there is also an inhibition of translation ('negative regulation of biosynthetic process'), which may be reflected in the significant reduction in the expression of 1522 proteins in LN229 cells following LT RT/TMZ treatment.

Figure 6-5: Analysis of DE proteins in LT RT/TMZ treated GBM cell lines

(**A.**) The number of DE proteins (LFQ ratio of >±2 and FDR ≤ 0.05) in each LT RT/TMZ treated GBM cell line relative to the corresponding untreated GBM cell lines. Both ▲increased and ▼decreased proteins are shown. (**B.**) The increased proteins in LT RT/TMZ treated GBM cell lines were classified according to the PANTHER Protein Classification system, which identified 11 potential invasion-related classes. The number of increased proteins within each invasion-related protein class is shown for each GBM cell line. Functional enrichment analysis of the top 25 increased proteins detected in LT RT/TMZ treated GBM cells was conducted using FunRich to identify significantly enriched GO annotations. LT RT/TMZ treated cell lines were analysed separately as follows: (**C.**) LN229, (**D.**) MU4, (**E.**) MU41. (*P values were calculated by two-sided hypergeometric test – the top 5 annotations with the most significant p values are shown*).

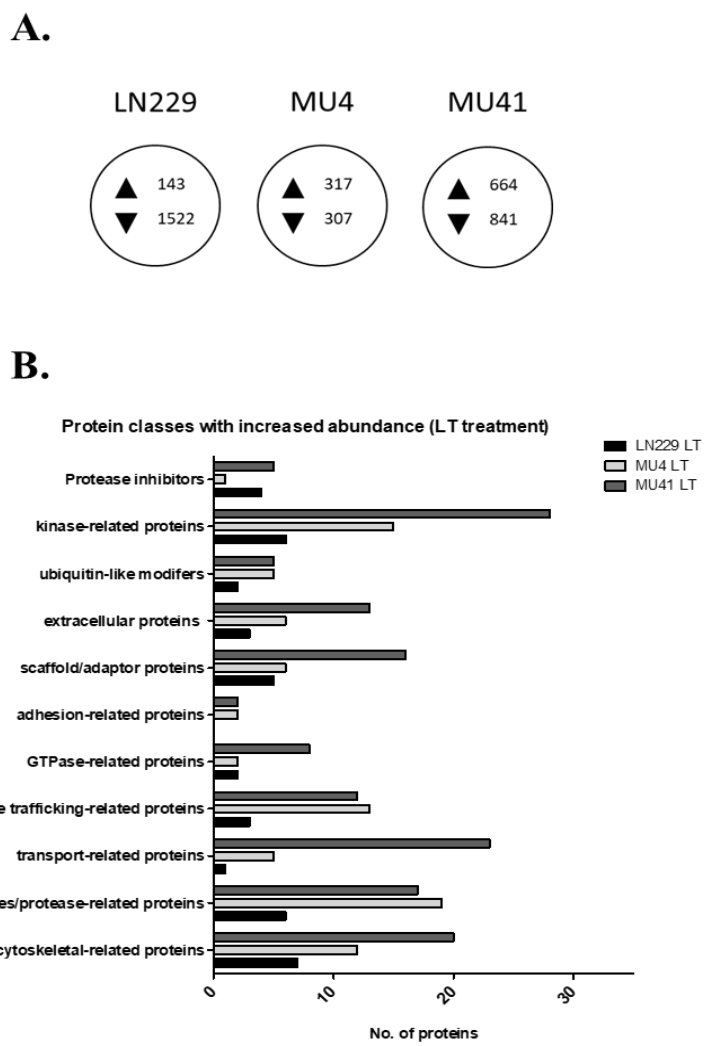
A.
LN229
MU4
MU41
143
1522
317
307
664
841
B.
Protein classes with increased abundance (LT treatment)
LN229 LT
MU4 LT
MU41 LT
Protease inhibitors
kinase-related proteins
ubiquitin-like modifers
extracellular proteins
scaffold/adaptor proteins
adhesion-related proteins
GTPase-related proteins
membrane trafficking-related proteins
transport-related proteins
proteases/protease-related proteins
actin/cytoskeletal-related proteins
0
10
20
30
No. of proteins
C.
Increased (LN229 LT)
Molecular Function
negative regulation of biosynthetic process
CDP-choline pathway
fatty acid beta-oxidation
dihydrobiopterin metabolic process
carnitine catabolic process
Biological Process
ethanolamine-phosphate cytidylyltransferase activity
6,7-dihydropteridine reductase activity
methylglutaconyl-CoA hydratase activity
itaconyl-CoA hydratase activity
farnesol dehydrogenase activity
2.2
2.4
2.6
2.8
3.0
-log10 (p value)
D.
Increased (MU4 LT)
Molecular Function
translation
nuclear-transcribed mRNA catabolic process
translational initiation
viral transcription
SRP-dependent cotranslational protein targeting to membrane
Biological Process
RNA binding
adenine binding
microfilament motor activity
actin-dependent ATPase activity
structural constituent of ribosome
0
2
4
6
8
-log10 (p value)
E.
Increased (MU41 LT)
Molecular Function
regulation of presynapse assembly
synaptic membrane adhesion
cell-cell junction organization
neurotransmitter receptor localization to postsynaptic membrane
regulation of cell junction assembly
Biological Process
neuregulin binding
myosin VI light chain binding
NADP-retinol dehydrogenase activity
alcohol dehydrogenase (NADP+) activity
allyl-alcohol dehydrogenase activity
0
2
4
6
-log10 (p value)

6.2.2.3 An altered metabolic proteome is detected in LT RT/TMZ treated LN229 GBM cells

6.2.2.3.1 Analysis of the LT RT/TMZ treated LN229 cell line proteome reveals a potential vulnerability to stress

Following LT RT/TMZ treatment, the LN229 GBM cell line exhibits a decrease in overall protein expression, with a significant reduction (LFQ ratio (FC) > -2) in the expression levels of 1522 proteins. Importantly, functional enrichment analysis highlighted a significant reduction in proteins that are involved in the elongation phase of translation, encompassing mitochondrial ribosomal proteins (25 proteins that form the large and small ribosomal subunits) and translation elongation factors (including TSFM) (***Table 6-3***). Liu *et al.* [681] has shown that during proteotoxic stress, malignant human kidney HEK293 cells reduce global protein synthesis by pausing ribosome activity on mRNA transcripts during the elongation phase, as the chaperones that are usually required to bind and process nascent peptides as they emerge from ribosomes are instead sequestrated by misfolded or damaged proteins. As decreased proteins in LT RT/TMZ treated LN229 cells are significantly associated with the molecular function of 'unfolded protein binding', this could indicate a reduction of chaperones in the LT RT/TMZ treated LN229 GBM cells, making this cell line more vulnerable to proteotoxic stress. Indeed, the LT RT/TMZ treated LN229 cells exhibit a reduction in the expression levels of 19 chaperone proteins compared to untreated cells, whilst the majority of these remained unchanged in the LT RT/TMZ treated MU4 and MU41 GBM cell lines (***Table 6-4***). As a validation of the loss in expression of these chaperones in the LT RT/TMZ treated LN229 GBM cell line, the chaperone protein with the greatest reduction in expression levels following LT RT/TMZ treatment, HSPB1 (also known as HSP27), was confirmed to be absent in the LT RT/TMZ treated LN229 GBM cells via western blot analysis (***Figure 6-6***). Taken together, this implies that the LN229 GBM cells may halt global protein synthesis to maintain protein homeostasis as a stress-induced response to LT RT/TMZ treatment.

Table 6-3: LT RT/TMZ treated LN229 GBM cells display a significant downregulation of proteins involved in mRNA translation and processing

Decreased Biological Processes		
Annotation	**No. proteins**	**P value**
mRNA splicing, via spliceosome	97	1.53E-40
mitochondrial translational elongation	39	5.06E-19
rRNA processing	48	2.18E-17
mitochondrial translational termination	36	4.13E-16
mitochondrial electron transport, NADH to ubiquinone	26	1.57E-15
mRNA export from nucleus	38	2.32E-15
RNA splicing	47	7.57E-15
mRNA 3'-end processing	27	5.15E-14
Decreased Molecular Functions		
Annotation	**No. proteins**	**P value**
RNA binding	385	1.87E-107
mRNA binding	45	3.29E-11
unfolded protein binding	33	8.84E-09
structural constituent of ribosome	36	2.07E-07

A FunRich functional enrichment analysis of 1522 proteins that decreased (FC>-2) in the LT RT/MZ treated LN229 GBM cells relative to untreated cells. (*P values were calculated by two-sided hypergeometric test – relevant annotations relating to translation and mRNA processing within the top 10 most significant biological processes and molecular functions are shown*).

Tables 6-4: Chaperone protein expression is reduced in LT RT/TMZ treated LN229 GBM cells

Gene Name	LN229 LT	MU4 LT	MU41 LT
DEAD-BOX Helicases			
DDX1	-2.276	NS	NS
DDX18	-28.16	NS	NS
DDX21	-3.688	NS	NS
DDX24	-25.52	NS	NS
DDX27	-25.6	NS	NS
DDX41	-24.86	NS	NS
DDX42	-2.364	NS	NS
DDX46	-3.393	24.07	NS
DDX54	-24.11	NS	NS
DDX56	-25.35	NS	NS
Heat shock Proteins			
HSP90AA1	NS	NS	-2.52
HSP90AB2P	-2.202	NS	NS
HSP90B2P	NS	NS	29.76
HSPA13	-24.85	NS	NS
HSPA14	-24.02	NS	25.46
HSPA1B	-6.889	NS	-5.183
HSPA8	-26.04	NS	-27.55
HSPB1	-31.11	NS	-33.33
HSPB11	-25.01	24.66	-25.55
HSPBP1	-25.87	-25.12	NS
HSPE1	-2.099	NS	NS
HSPG2	NS	NS	6.089

Numbers represent log2-FC in protein expression (LT RT/TMZ treated GBM cells relative to the corresponding untreated GBM cells). Significant changes above a threshold of FC > ±2 are listed. N*S: not significant.*

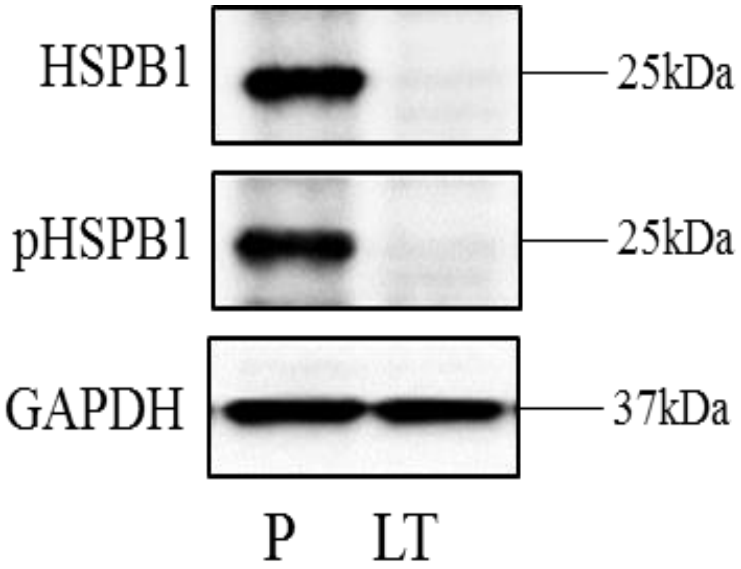

Figure 6-6: Western blot analysis of reduced HSPB1 expression levels in LT RT/TMZ treated LN229 cells

Western blot analysis of HSPB1 protein expression levels in untreated/parental (P) versus LT RT/TMZ treated (LT) LN229 cells. 20µg of protein was loaded per sample. *Data shown is representative of 3 independent experiments.*

6.2.2.3.2 Analysis of the LT RT/TMZ treated LN229 cell proteome indicates a metabolic switch to fatty acid oxidation

Energy maintenance in periods of metabolic stress requires cells to undergo a metabolic switch to increase ATP generation, as well as the availability of macromolecules (such as lipids and amino acids) and [682]. Interestingly, whilst LT RT/TMZ treated LN229 GBM cells displayed a significant reduction in a total of 1522 proteins, a functional enrichment analysis of the 143 proteins which were increased, revealed significant associations with metabolic processes involving fatty acid oxidation (FAO)/lipid metabolism (***Table 6-5***). Nine increased proteins with published links to FAO were identified in the proteome of the LT RT/TMZ treated LN229 cells (***Table 6-6)***. Importantly, five of these proteins have been implicated in aspects of cancer progression such as tumour cell proliferation and resistance to treatment: ACADL, AKR1B10, CAV1, DLAT and GPD1.

Table 6-5: The proteome of LN229 RT/TMZ LT treated GBM cells indicates a metabolic switch

Increased biological process	P-value (Hypergeometric test)
Cellular Lipid Catabolic Process	4.00E-04
Positive Regulation of Lipid Biosynthetic Process	7.60E-03
NADH Oxidation	1.60E-02
Cellular Protein Metabolic Process	2.50E-02
Acyl-CoA Metabolic Process	2.70E-02
Tricarboxylic Acid Cycle	3.20E-02
Fatty Acid Beta-Oxidation	4.40E-02

A functional enrichment analysis of the 143 increased proteins in LT RT/TMZ treated LN229 GBM cells was conducted with FunRich. There were seven significantly enriched GO annotations for biological process which were associated with fatty acid (lipid) metabolism. (*P values were calculated by a two-sided hypergeometric test and are shown as -log10(P)*).

Table 6-6: Increased FAO-related proteins detected in LT RT/TMZ treated GBM cells

Gene Name	Role in FAO	LN229 LT	MU4 LT	MU41 LT
ACSF2	ACSF2 is a fatty acyl CoA synthetase, involved in FAS.	25.56	ND	28.69
ACADL*	Acyl-CoA dehydrogenase long chain is a member of the acyl-CoA dehydrogenase family, is overexpressed in ESCC and associated with progression and poor prognosis [683]	26.42	28.5	ND
ACSL6	ACSL6 is critical for lipid metabolism in the central nervous system and serves a neuroprotective role [684]	24.82	-25.75	25.39
AKR1B15	Catalyses the reduction of androgens, estrogens and 3-keto-acyl-CoA conjugates and exhibits strong cofactor selectivity toward NADP(H). Shares 92% amino acid sequence identity with AKR1B10) [685]	6.888	2.239	30.94
AKR1B10*	AKR1B10 promotes metastasis of breast cancers and functions to support a metabolic switch to FAO during secondary site colonisation [686]	29.4	NS	29.35
AUH	Catalyzes the conversion of 3-methylglutaconyl-CoA to 3-hydroxy-3-methylglutaryl-CoA.	25.84	NS	NS
CAV1*	In cells overexpressing CAV1, CD36 is relocated to the plasma membrane, where it may play an increased role in fatty acid uptake [687]. CAV1 deficiency prevented a metabolic switch to FAO in CAV1-null mice [688]. Also involved in caveolin/raft-mediated endocytosis of EVs. High expression of CAV1 also correlates with shorter GBM patient survival [689].	2.766	NS	NS
DLAT*	Subunit of the pyruvate dehydrogenase complex catalyzes the overall conversion of pyruvate to acetyl-CoA. siRNA studies supported a role of DLAT in gastric cancer cell proliferation and carbohydrate metabolism [690]	2.875	-27.88	NS
GPD1*	Glycerol-3-phosphate dehydrogenase [NAD+] activity; found to be present in GBM stem cell populations, enriched at tumour borders and drives GBM tumour relapse after chemotherapy [691]	3.747	NS	2.043

Numbers represent log2-FC in protein expression (LT RT/TMZ treated GBM cells relative to corresponding untreated cells). Significant changes above a threshold of FC > ±2 are listed. N*S: not significant.*

** indicates proteins with published evidence linked to a potential role in tumour progression.*

6.2.2.4 DE analysis of invadopodia-related proteins in the GBM cell line proteomes following LT RT/TMZ treatment

As functional experiments revealed an increase in invadopodia formation and FITC-gelatin degrading activity in MU4 and MU41 cells following LT RT/TMZ treatment, whilst an inhibition of invadopodia-mediated FITC gelatin degrading activity was observed for LT RT/TMZ treated LN229 cells (***Figure 3-8***), the DE invadopodia-related proteins in the proteome of each GBM cell line following LT RT/TMZ treatment were next examined (***Figure 6-7A, Supplementary Table 8***). To identify proteins that may potentially contribute to the changes in invadopodia-mediated FITC-gelatin degrading activity observed for each LT RT/TMZ treated GBM cell line, the invadopodia-related proteins that increased for the MU4 (6 proteins) and MU41 (12 proteins) LT RT/TMZ treated GBM cells were compared to those that decreased in LN229 LT RT/TMZ treated GBM cells (23 proteins) (***Figure 6-7B***). These proteins were annotated for molecular function using FunRich (***Figure 6-7C***). Whilst the specific proteins identified varied between each LT RT/TMZ treated GBM cell line, with only three overlapping DE proteins between LN229 and MU4 and five overlapping DE proteins between LN229 and MU41, these proteins shared similar functional roles relating to cytoskeletal protein binding functions, as well as receptor or kinase activity. The elevated expression of proteins in the LT RT/TMZ treated MU4 and MU41 GBM cell lines could contribute to the enhanced invadopodia formation and FITC-gelatin degrading activity previously observed due to the increased availability of signalling proteins or cytoskeletal proteins. Conversely, the reduced expression of these proteins in the LT RT/TMZ treated LN229 GBM cells could also contribute to the loss of invadopodia FITC-gelatin degrading activity previously observed (***Figure 3-8***).

Figure 6-7: Analysis of DE invadopodia-related proteins in GBM cells post-LT RT/TMZ treatment

(**A**.) The number of DE invadopodia-related proteins (LFQ ratio of >±2 and FDR ≤ 0.05) in the proteome of each GBM cell line following LT RT/TMZ treatment. Both ▲increased and ▼decreased proteins are shown. (**B.**) A Venn diagram comparing increased invadopodia-related proteins in MU4 and MU41 LT RT/TMZ treated GBM cells, in addition to the decreased invadopodia-related proteins in the LN229 LT RT/TMZ treated GBM cell line. (**C**.) Functional enrichment annotations corresponding to invadopodia-related proteins in each cell line (***i***- 6 increased proteins- MU4, ***ii***- 12 increased proteins- MU41, ***iii***- 23 decreased proteins- LN229), showing the top 5 significantly enriched GO annotations for molecular function. (*P values were calculated by two-sided hypergeometric test and are shown as -log10(P)*).

A.

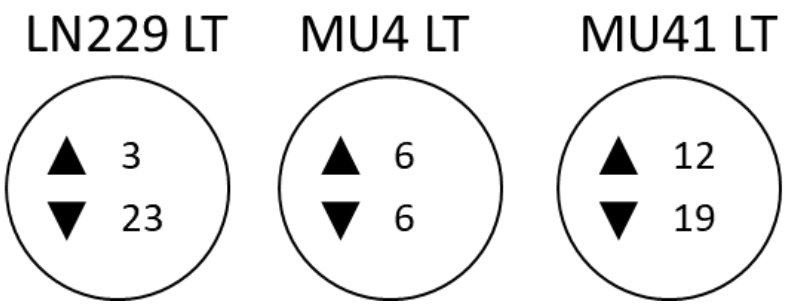
LN229 LT
MU4 LT
MU41 LT
▲ 3
▼ 23
▲ 6
▼ 6
▲ 12
▼ 19

B.

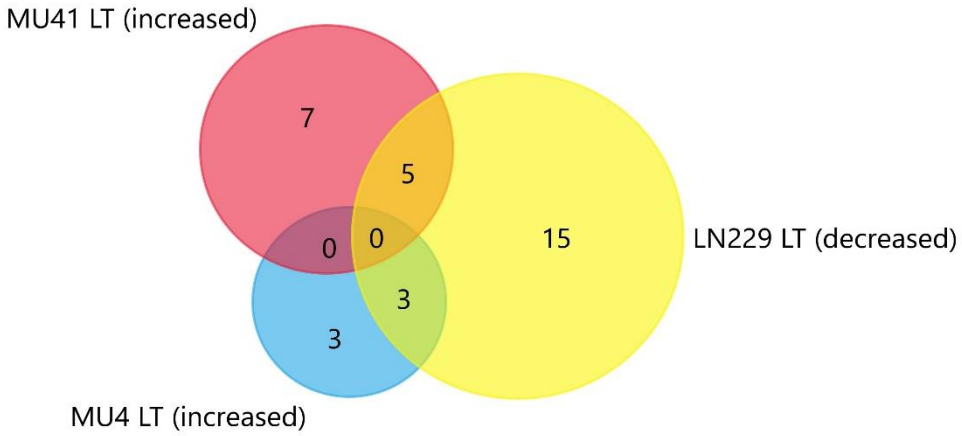
MU41 LT (increased)
7
5
0
0
15
LN229 LT (decreased)
3
3
MU4 LT (increased)

C. ***i.***

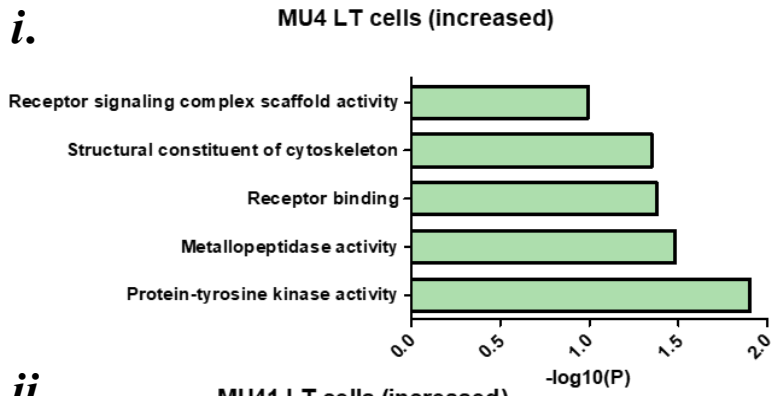
MU4 LT cells (increased)
Receptor signaling complex scaffold activity
Structural constituent of cytoskeleton
Receptor binding
Metallopeptidase activity
Protein-tyrosine kinase activity
0.0
0.5
1.0
1.5
2.0
-log10(P)

ii.

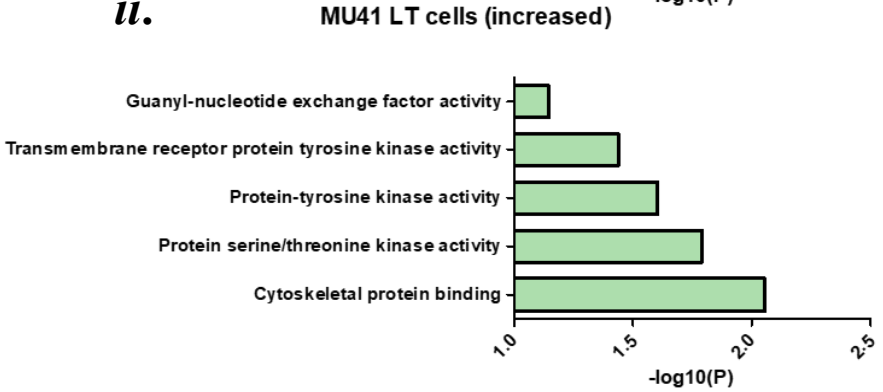
MU41 LT cells (increased)
Guanyl-nucleotide exchange factor activity
Transmembrane receptor protein tyrosine kinase activity
Protein-tyrosine kinase activity
Protein serine/threonine kinase activity
Cytoskeletal protein binding
1.0
1.5
2.0
2.5
-log10(P)

iii.

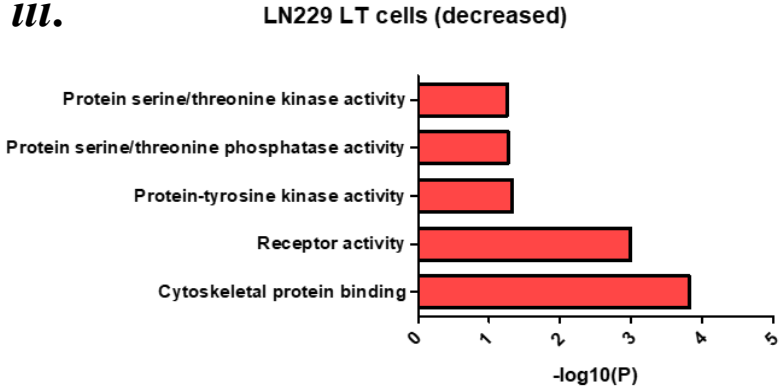
LN229 LT cells (decreased)
Protein serine/threonine kinase activity
Protein serine/threonine phosphatase activity
Protein-tyrosine kinase activity
Receptor activity
Cytoskeletal protein binding
0
1
2
3
4
5
-log10(P)

6.2.2.5 A distinct population of proteins is present in the proteome of sEVs enriched from LT treated GBM cell lines

Overall, 2697 proteins were detected in the proteomes of sEVs from untreated and LT treated GBM cell lines, with 424 proteins uniquely detected in sEVs from the LT RT/TMZ treated GBM cells. (***Supplementary Figure 8A***). Significantly enriched functional annotations for these 424 proteins indicated a potential involvement in intracellular vesicle transport, mRNA processing and protein phosphorylation/kinase activity (***Supplementary Figure 8B-D***). The biological processes and molecular functions were also reflected within the significantly enriched REACTOME pathways. These included the 'RHO GTPases Activate Formins' pathway which may be linked to increased invadopodia-mediated FITC-gelatin degrading activity in the LT RT/TMZ treated MU4 and MU41 GBM cell lines, as formins (such as FHOD1) are important for actin filament elongation during formation of the invadopodium core [385, 692]. Conversely, the enrichment of mitosis-related pathways could be associated with sEVs from LT treated LN229 cells, that may contain cargo to drive cellular pathways that promote cell proliferation.

6.2.2.6 DE analysis of LT RT/TMZ treated GBM cell line derived sEV cargo proteins

Differential expression (DE) analysis was next performed on the proteomes of sEVs enriched from untreated and LT RT/TMZ treated GBM cell lines to examine changes in protein expression following LT RT/TMZ treatment. Significant DE proteins (log2-transformed LFQ ratio of $>\pm 2$ and FDR ≤ 0.05) detected in sEVs from LT RT/TMZ treated GBM cells relative to the untreated cells were determined for each GBM cell line (***Figure 6-8A***). sEVs enriched from LT RT/TMZ treated LN229 GBM cells displayed a reduction in the expression of a large number of proteins (1411 proteins), as opposed to only 56 increased sEV proteins, which reflects the same trend observed in the LT RT/TMZ treated LN229 donor cell proteome. The number of increased proteins in sEVs enriched from each LT RT/TMZ treated GBM cell line corresponding to invasion-related protein classes using PANTHER was also

examined (***Figure 6-8B***). Emulating the trend observed with the corresponding donor GBM cells, the greatest number of increased proteins were seen for the kinase-related and protease-related classes in the MU4 and MU41 LT RT/TMZ treated GBM cell line derived sEVs, whereas considerably fewer proteins within each class were observed to increase for sEVs from LN229 LT RT/TMZ treated cells.

The top-50 DE proteins in sEVs from each LT RT/TMZ treated cell line relative to the corresponding untreated cell line were identified and annotated using FunRich. To determine which sEV proteins may contribute to the distinct phenotypic changes observed for each LT RT/TMZ treated GBM cell line (outlined in ***Figure 3-24***), the top 25 sEV proteins with increased expression were examined (for annotations corresponding to decreased proteins, see ***Supplementary Figure 9***). Reflecting the functional annotations for DE proteins in their relative donor cells, increased proteins in sEVs from MU4 and MU41 LT RT/TMZ treated GBM cells were significantly associated with translation, membrane transport, and adhesion (***Figure 6-8D&E***), whereas the functional annotations for LT RT/TMZ treated LN229 GBM cell derived sEVs indicated an upregulation of proteins with biological relevance to fibrin clot formation and plasminogen activation (***Figure 6-8C***).

As analysis of LT RT/TMZ treated LN229 GBM cells indicates that this pro-proliferative phenotype may be facilitated by a metabolic dependence on FAO, FAO-associated proteins in sEVs from LT RT/TMZ treated LN229 GBM cells was examined. As shown in ***Table 6-7***, six proteins involved in FAO and lipid metabolism were increased in sEVs from LT RT/TMZ treated LN229 GBM cells. This was not observed for all six proteins in the sEVs harvested from LT RT/TMZ treated MU4 and MU41 GBM cells, with only a few of these proteins observed to be increased >2-fold. This could indicate that sEVs secreted by LT RT/TMZ treated LN229 GBM cells facilitate the transport of proteins required for FAO/lipid metabolism, and therefore may support survival and proliferation via the promotion of a FAO-phenotype in recipient GBM cells.

Figure 6-8: DE analysis of the LT RT/TMZ treated GBM cell line derived sEV proteome

(**A.**) The number of DE proteins (LFQ ratio of >±2 and FDR ≤ 0.05) in the proteome of sEVs from each GBM cell line following LT RT/TMZ treatment. Both ▲increased and ▼decreased proteins are shown (**B.**) The increased proteins in sEVs from each LT RT/TMZ treated GBM cell line were classified according to the PANTHER Protein Classification system, which identified 11 potential invasion-related classes. The number of increased proteins within each invasion-related protein class is shown for each GBM cell line. Functional enrichment analysis of the top 25 increased proteins detected in sEVs from each LT RT/TMZ treated GBM cells was conducted using FunRich to identify significantly enriched GO annotations as follows: (**C.**) LN229, (**D.**) MU4, (**E.**) MU41. (*P values were calculated by two-sided hypergeometric test – the top 5 annotations with the most significant p values are shown*).

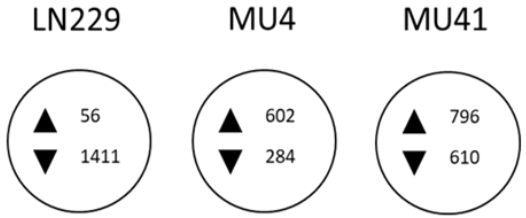
LN229
MU4
MU41
56
1411
602
284
796
610

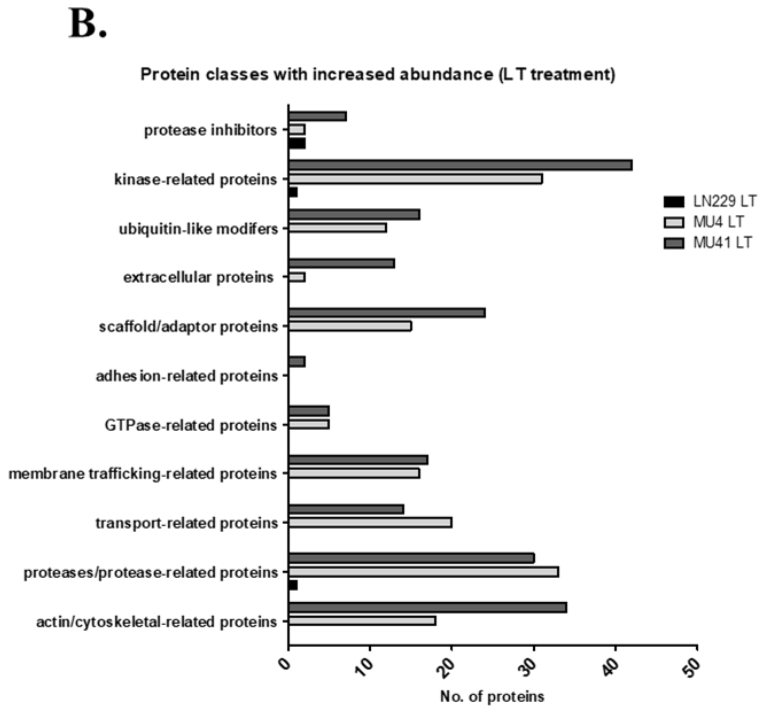
B.
Protein classes with increased abundance (LT treatment)
protease inhibitors
kinase-related proteins
ubiquitin-like modifers
extracellular proteins
scaffold/adaptor proteins
adhesion-related proteins
GTPase-related proteins
membrane trafficking-related proteins
transport-related proteins
proteases/protease-related proteins
actin/cytoskeletal-related proteins
LN229 LT
MU4 LT
MU41 LT
0
10
20
30
40
50
No. of proteins

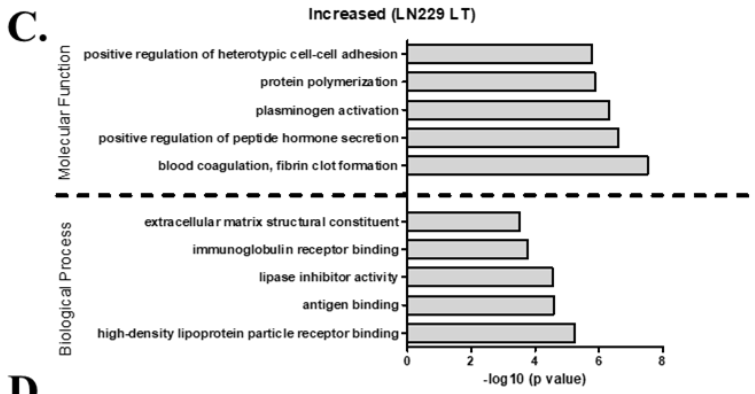
C.
Increased (LN229 LT)
Molecular Function
positive regulation of heterotypic cell-cell adhesion
protein polymerization
plasminogen activation
positive regulation of peptide hormone secretion
blood coagulation, fibrin clot formation
Biological Process
extracellular matrix structural constituent
immunoglobulin receptor binding
lipase inhibitor activity
antigen binding
high-density lipoprotein particle receptor binding
0
2
4
6
8
-log10 (p value)

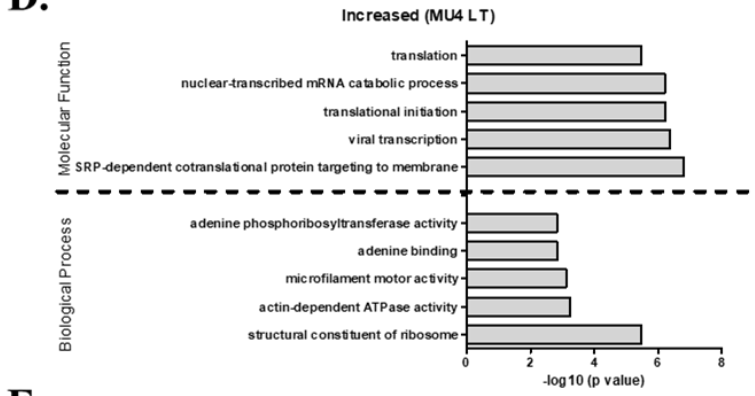
D.
Increased (MU4 LT)
Molecular Function
translation
nuclear-transcribed mRNA catabolic process
translational initiation
viral transcription
SRP-dependent cotranslational protein targeting to membrane
Biological Process
adenine phosphoribosyltransferase activity
adenine binding
microfilament motor activity
actin-dependent ATPase activity
structural constituent of ribosome
0
2
4
6
8
-log10 (p value)

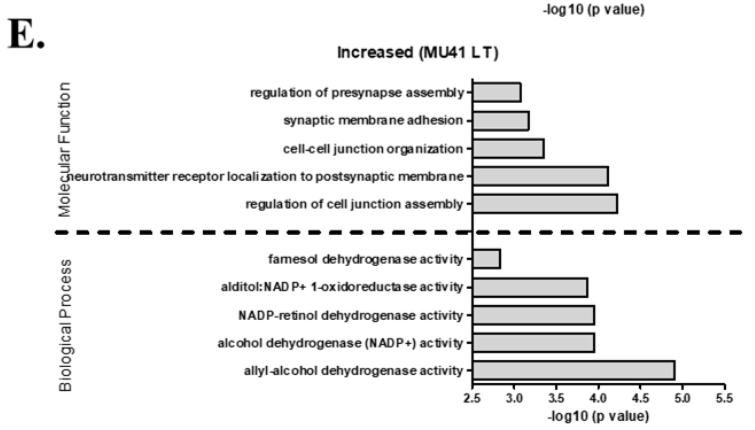
E.
Increased (MU41 LT)
Molecular Function
regulation of presynapse assembly
synaptic membrane adhesion
cell-cell junction organization
neurotransmitter receptor localization to postsynaptic membrane
regulation of cell junction assembly
Biological Process
farnesol dehydrogenase activity
alditol:NADP+ 1-oxidoreductase activity
NADP-retinol dehydrogenase activity
alcohol dehydrogenase (NADP+) activity
allyl-alcohol dehydrogenase activity
2.5
3.0
3.5
4.0
4.5
5.0
5.5
-log10 (p value)

Table 6-7: sEVs secreted by LT RT/TMZ treated LN229 GBM cells contain cargo proteins involved in fatty acid/lipid metabolism

Gene name	Role in FAO/lipid metabolism	LN229 LT	MU4 LT	MU41 LT
APOA1	APOA1 is a carrier of high-density lipoprotein (HDL) and cholesterol receptor, it also enhances HDL influx and cholesterol efflux.	5.461	NS	NS
APOA2	APOA2 stabilizes HDL structure by its association with lipids and is a regulator of HDL metabolism.	26.54	NS	NS
APOC3	Component of triglyceride-rich very low-density lipoproteins (VLDL) and HDLs in plasma and possesses a multifaceted role in triglyceride homeostasis.	27.15	NS	25.25
INS	Insulin inhibits the intracellular lipase that hydrolyses triglycerides to release fatty acids. This could stabilise triglycerides whilst in EVs, so that they may be metabolised when EV cargo is released into the recipient cell. It also increases cell permeability to monosaccharides, amino acids, and fatty acids.	2.018	3.928	NS
GPD1	Glycerol-3-phosphate dehydrogenase [NAD+] activity.	26.13	NS	28.15
AKR1B15	Catalyses the reduction of androgens, estrogens and 3-keto-acyl-CoA conjugates and exhibits strong cofactor selectivity toward NADP(H).	25.70	3.865	8.322

Numbers represent log2-FC in protein expression (sEVs from LT treated cells relative to corresponding untreated cells). Significant changes above a threshold of FC > ±2 are listed. A N*S: not significant.*

6.2.2.7 DE analysis of invadopodia-related proteins detected in sEVs from LT RT/TMZ treated GBM cells

The DE invadopodia-related proteins in the proteome of sEVs from each GBM cell line following LT RT/TMZ treatment were next examined (***Figure 6-9A, Supplementary Table 9***). To identify sEV proteins that may be involved in the altered invadopodia-mediated FITC-gelatin degrading activity observed for each LT RT/TMZ treated GBM cell line, invadopodia-related proteins that increased in sEVs from LT RT/TMZ treated MU4 (12 proteins) and MU41 (14 proteins) GBM cells were compared with those that decreased in the LN229 LT RT/TMZ treated GBM cells (26 proteins) (***Figure 6-9B***). These proteins were annotated for molecular function using FunRich (***Figure 6-9C***). Notably, unlike MU4 and MU41 derived sEVs, no invadopodia-related proteins displayed increased abundance in LN229 derived sEVs following LT RT/TMZ treatment, consistent with the lack of invadopodia activity exhibited by this LT treated cell line (***Figure 3-8***). The 26 invadopodia-related proteins that were decreased in sEVs from LT RT/TMZ treated LN229 GBM cells were primarily classified as possessing receptor binding, GTPase activity, kinase activity, and cytoskeletal binding functions (***Figure 6-9C-iii.***). These included key proteins which are involved in signalling cascades that facilitate actin polymerization and lead to invadopodia formation, such as Src, CD44, CD151, ITGA3 and ITGB1, suggesting that sEVs from LT RT/TMZ treated LN229 GBM cells may be deficient in many of the signalling proteins required for invadopodia initiation. Conversely, increased invadopodia-related proteins detected in sEVs from LT RT/TMZ treated MU4 and MU41 GBM cells were mostly associated with actin- and cytoskeletal- binding functions, including CTTN and FHOD1 that drive the formation of the invadopodium F-actin core, and therefore may play a role in promoting invadopodia assembly in recipient GBM cells (***Figure 6-9C-i&ii.***).

Figure 6-9: Analysis of DE invadopodia-related proteins in sEVs from GBM cells post-LT RT/TMZ treatment

(**A**.) The number of DE invadopodia-related proteins (LFQ ratio of >±2 and FDR ≤ 0.05) in the proteome of sEVs from each GBM cell line following LT RT/TMZ treatment. Both ▲increased and ▼decreased proteins are shown. (**B.**) A Venn diagram comparing increased invadopodia-related proteins in sEVs from the MU4 and MU41 LT RT/TMZ treated GBM cells, in addition to the decreased invadopodia-related proteins in sEVs from the LN229 LT RT/TMZ treated GBM cell line. (**C**.) Functional enrichment annotations corresponding to invadopodia-related proteins in each sEV proteome (***i***- 12 increased proteins- MU4, ***ii***- 14 increased proteins- MU41, ***iii***- 26 decreased proteins- LN229), showing the top 5 significantly enriched GO annotations for molecular function. (*P values were calculated by two-sided hypergeometric test and are shown as -log10(P)*).

A.

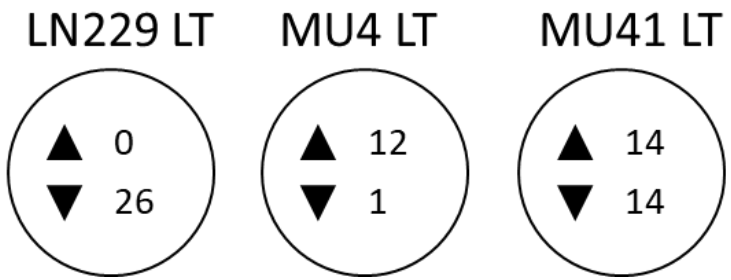
LN229 LT
MU4 LT
MU41 LT
▲ 0
▼ 26
▲ 12
▼ 1
▲ 14
▼ 14

B.

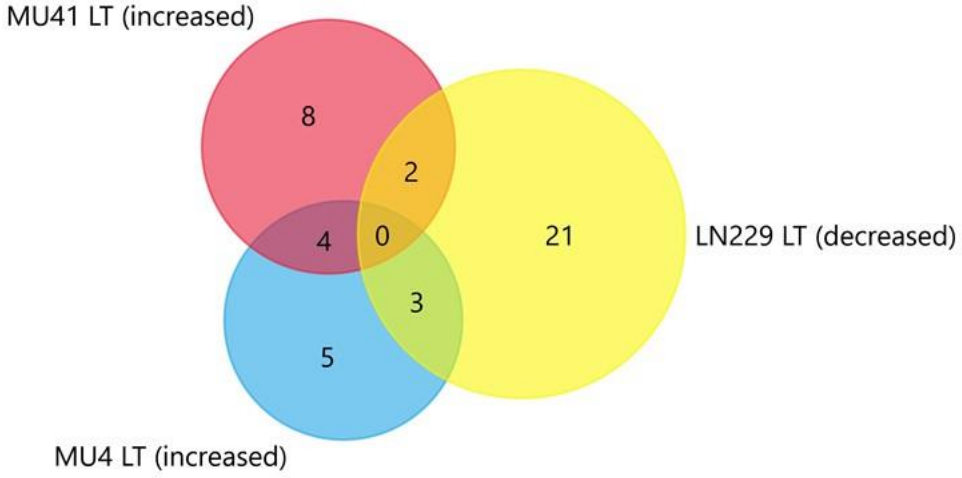
MU41 LT (increased)
8
2
4
0
21
LN229 LT (decreased)
3
5
MU4 LT (increased)

C. ***i.***

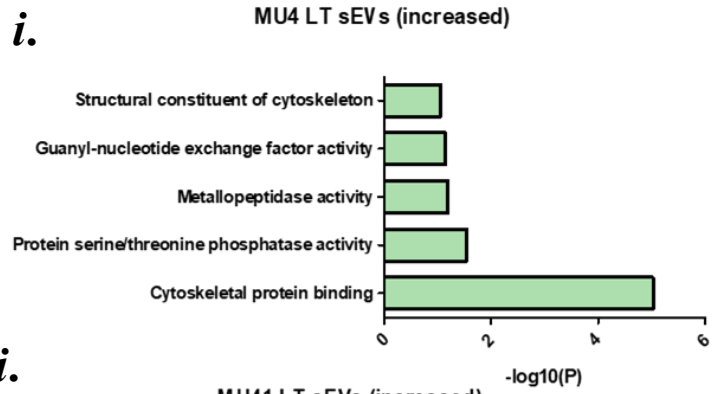
MU4 LT sEVs (increased)
Structural constituent of cytoskeleton
Guanyl-nucleotide exchange factor activity
Metallopeptidase activity
Protein serine/threonine phosphatase activity
Cytoskeletal protein binding
0
2
4
6
-log10(P)

ii.

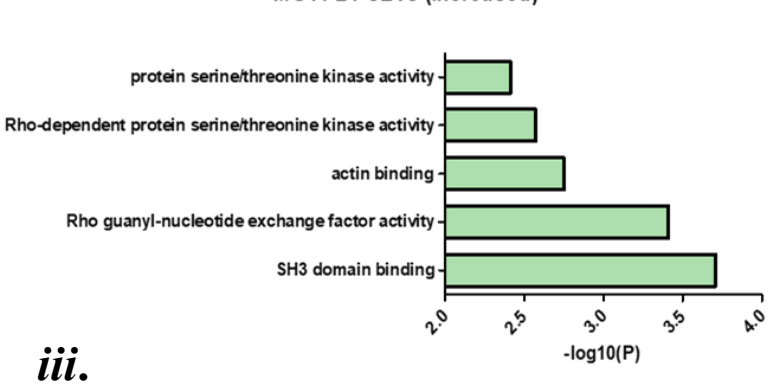
MU41 LT sEVs (increased)
protein serine/threonine kinase activity
Rho-dependent protein serine/threonine kinase activity
actin binding
Rho guanyl-nucleotide exchange factor activity
SH3 domain binding
2.0
2.5
3.0
3.5
4.0
-log10(P)

iii.

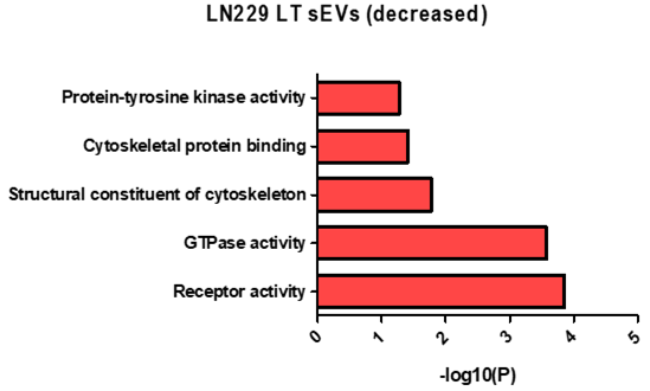
LN229 LT sEVs (decreased)
Protein-tyrosine kinase activity
Cytoskeletal protein binding
Structural constituent of cytoskeleton
GTPase activity
Receptor activity
0
1
2
3
4
5
-log10(P)

6.3 Discussion

Despite the introduction of temozolomide (TMZ) in 2005 to the standard therapeutic approach consisting of surgical resection and radiotherapy (RT), the prognosis for GBM patients remains dismal due to the inevitability of tumour recurrence [2, 18]. GBM tumours are highly invasive and heterogeneous, and often acquire resistance to therapy. In the previous chapters, it was demonstrated that augmented invadopodia FITC-gelatin degrading activity and enhanced sEV secretion may contribute to a pro-invasive phenotype following RT/TMZ treatment, implying that the current therapeutic approach for GBM may have a counterintuitive impact, however the molecular changes underlying this response to RT/TMZ remained to be elucidated. Therefore, in the present chapter, a proteomic approach was utilised to examine the potential changes that may occur within cells and the sEV-cargo for three GBM cell lines (LN229, MU4 and MU41) that may promote a pro-invadopodia/ pro-invasive phenotype following single and long-term (LT) RT/TMZ treatment.

Within the literature, the majority of proteomic studies in GBM have aimed to profile proteins in GBM cell lines, patient biopsies or EVs derived from patient serum/CSF or cultured cells to identify novel diagnostic biomarkers [500, 693-696], whereas few studies by comparison have analysed the GBM proteome in response to the current therapeutic approach. Whilst a small number of studies have investigated the impact of either RT or TMZ treatment on the proteome of GBM cells [399, 697-699] or EV cargo [488, 700], none of these studies addressed the impact of both RT and TMZ in combination. To our knowledge, this is the first report to identify the proteomic changes of multiple GBM cell lines and the corresponding cargo of sEVs following RT/TMZ treatment. These proteomic profiles offer a valuable insight into the altered proteomic landscape of GBM cells and sEV cargo following exposure to RT/TMZ treatment and how these changes may be targeted or utilized to facilitate the future development of novel therapeutic strategies to improve the clinical efficacy of RT and TMZ, and thus, GBM patient survival.

6.3.1. Increased proteins in single RT/TMZ treated GBM cells and sEVs indicate a pro-invasive/pro-invadopodia phenotype

Proteomic analysis highlighted an increase in the abundance of adhesion-related proteins, cytoskeletal regulators, and membrane trafficking proteins in GBM cells exposed to RT/TMZ treatment (***Figure 6-1***), with a pro-invadopodia and pro-invasive phenotype following RT/TMZ treatment [5, 6, 701]. Moreover, nineteen established invadopodia regulators were also increased in GBM cells exposed to RT/TMZ treatment that are predominantly associated with microtubule-mediated vesicle transport and exocytosis, indicating that GBM cells may respond to RT/TMZ treatment by increasing vesicle transport to- and potential release from- invadopodia (***Figure 6-2***). Supporting this possibility, recent studies have shown that vesicle-mediated membrane trafficking is crucial for delivery of MMPs to the maturing invadopodia in breast cancer cells [153, 154], and an important role has also been demonstrated for adhesion proteins in vesicle recruitment and capture at invadopodia [702]. Additionally, as invadopodia have been suggested as the docking sites of MVBs and subsequent sites of exosome release [229], this may result in a greater secretion of sEVs from RT/TMZ treated GBM cells, consistent with the increase in sEV and MMP-2 secretion previously observed (***Figure 3-2 and Figure 4-11***).

Furthermore, proteomic analysis of sEVs secreted from RT/TMZ treated GBM cells revealed increased expression levels of integrin-, actin- and kinase- related proteins that are associated with signalling cascades known to drive invadopodia initiation (***Figure 6-3 and Figure 6-4***). This may result in a positive feedback loop, with both increased invadopodia formation and sEV secretion driving one another in response to RT/TMZ treatment, ultimately contributing to tumour recurrence and ultimately, treatment failure [229]. It is also important to note that all GBM cell lines secrete a greater quantity of sEVs post-RT/TMZ treatment (***Figure 4-11***), and thus the effect of these DE sEV cargo proteins in recipient GBM cells may be further impacted by an increase sEV numbers. Therefore, novel therapeutic strategies adjuvant to RT/TMZ treatment that disrupt both invadopodia activity and sEV-mediated communication may impede GBM invasion and improve patient survival. Furthermore, whilst changes

in invadopodia activity post-RT/TMZ treatment may be driven by a different set of DE proteins in each GBM cell line, all RT/TMZ treated GBM cell lines exhibited an increase in the abundance of adhesion, cytoskeletal, and trafficking proteins, which may ultimately converge to promote invadopodia activity and sEV secretion through sustaining endocytic trafficking and oncogenic signalling. These are discussed in more detail in the following sections.

6.3.2.1. Adhesion proteins are increased in single RT/TMZ treated GBM cells and sEVs

Adhesion proteins represent a diverse group of cell surface molecules that, through their ability to interact with a variety of binding partners in the surrounding microenvironment, mediate a range of pro-tumorigenic functions, such as migration, invasion, proliferation and survival [703]. Several adhesion-related proteins were detected amongst the top 25 increased proteins in RT/TMZ treated GBM cells (JUP, DAG1, MCAM) and the corresponding sEVs (ITGA1, GPC6, NPTN, and TSPAN14) that are known to facilitate invasion (***Table 6-1 & 6-2***). Furthermore, invadopodia-related proteins increased in the cargo of sEVs secreted by RT/TMZ treated GBM cells were significantly associated with adhesion-related signalling mediated through integrins, encompassing proteins such as CD151, ICAM1, MT1-MMP, TGFBI (***Figure 6-4, Supplementary Table 8***). As integrins are widely reported to initiate intracellular signalling cascades responsible for invadopodia initiation and maturation, and are also involved in MT1-MMP trafficking and subsequent exocytosis from invadopodia [704], the elevated expression of integrin-binding proteins in sEVs released by RT/TMZ treated GBM cells may promote invadopodia activity in recipient GBM cells. Supporting this hypothesis, Brzozowski *et al.* has shown that sEVs containing elevated expression of the integrin-binding partners, CD151 and TGFBI, promoted recipient prostate cancer cell invasion through a basement membrane extract (BME) coated well of a Boyden-chamber [705]. Furthermore, Choi *et al*. has observed that sEVs derived from EGFRvIII-transformed U373 GBM cells contained elevated CD151 and TGFBI, and demonstrated enhanced uptake of these sEVs by recipient GBM cells expressing EGFRvIII compared to non-EGFRvIII expressing GBM cells [228]. This implies a potential role for integrins in facilitating sEV uptake by

GBM cells, and thus could indicate that sEVs with enhanced expression of integrin-binding proteins may be taken up more readily by recipient GBM cells post-RT/TMZ treatment. Importantly, Hoshino *et al.* has demonstrated that targeting sEV-recipient cell interactions with integrin-blocking decoy peptides can result in decreased pancreatic cell derived sEV uptake in the lung and liver using a metastatic mouse model [232]. Therefore, integrins and their binding partners may be promising targets to reduce sEV mediated transfer of pro-invadopodia/invasive cargo following RT/TMZ treatment, however, further studies are required.

Adhesion-mediated interactions between tumour cells and the surrounding ECM not only serve to promote cancer cell motility but can also contribute to treatment resistance via the promotion of anti-apoptotic signalling pathways or cell cycle arrest. For example, increased cell adhesion molecules such as CD44 and integrin subunits α2, β3 and β4 in radio- and chemo-resistant NSCLC cells results in constitutive activation of AKT and MAP kinase pathways that protects these cells from apoptosis [706], whilst integrin-mediated adhesion to fibronectin by myeloma cells promoted chemoresistance via the induction of G1/G0 cell cycle arrest [707]. In the context of GBM, recent proteomic analyses have revealed that adhesion molecules are increased in TMZ-resistant U87MG GBM cells [399] as well as in sEVs released by TMZ treated glioma stem cells (GSCs) [700]. Interestingly, increased adhesion proteins in GBM cells (such as DAG1 and MCAM) and sEVs (such as ITGA6 and CD151) following RT/TMZ treatment have been shown to promote a mesenchymal- and GSC- like phenotype [636, 647, 708-710]. The acquisition of GSC-like properties is similar to the transition to a mesenchymal phenotype in other cancers during the process of EMT and is associated with increased stemness, invasion and tumour aggression, as well as reported changes in EV secretion or composition [711], resulting in highly tumorigenic and invasive GBM cells that demonstrate increased resistance to treatment with radiation and chemotherapeutic drugs [712]. Collectively, this may indicate that the increased abundance of adhesion proteins in RT/TMZ treated GBM cells and their potential transfer via sEVs to recipient GBM cells may not only promote a pro-invasive/pro-invadopodia phenotype but may also increase the ability of GBM cells to overcome the impact of RT/TMZ treatment.

6.3.2.2. Actin regulatory proteins are increased in single RT/TMZ treated GBM cells and sEVs

The assembly of a branched actin network is essential for the formation of the invadopodium core, which is mediated by a variety of proteins and complexes that drive actin polymerisation. Several actin regulators that are involved in invadopodia-associated actin polymerization were increased in RT/TMZ treated GBM cells and sEVs relative to their untreated counterparts, including cortactin and fascin, as well as actin nucleating formins (such as FHOD1, DIAPH1), and components of the WAVE complex (such as NCKAP1, WASF2, ABI2) (***Supplementary Table 6 & 7***). The elevated expression levels of these proteins in GBM cells and sEVs following RT/TMZ treatment reflects a pro-invadopodia/pro-invasive phenotype that, in part, may be mediated through increased cytoskeletal modulation. Indeed, the overexpression of cortactin is associated with increased GBM cell invasion and poorer GBM patient prognosis [713], and has also been shown to inhibit the degradation of EGFR, leading to sustained EGFR signalling [714], which is a critical pathway known to drive invadopodia formation [123].

Emerging evidence also indicates that several of these actin regulators have reported roles in regulating therapeutic resistance. Eke *et al*. has demonstrated that knockdown of cortactin sensitises HNSCC cells to ionizing radiation downstream of FAK and β1 integrins, suggesting that cortactin may contribute to radioresistance in these cells [715]. As the expression levels of cortactin and integrin-associated proteins were increased in sEVs secreted by GBM cells following RT/TMZ treatment, these sEVs may also mediate resistance to RT/TMZ treatment in recipient GBM cells through a similar mechanism. Similarly, the invadopodia-related F-actin bundling protein, fascin, promotes chemoresistance to doxorubicin in hepatocellular carcinoma and breast cancer cells through the promotion of PI3K/Akt signalling and EMT [716, 717]. Interestingly, through their interactions with the cytoskeleton, both cortactin and fascin have also been implicated in endosomal trafficking to invadopodia in breast cancer cells, resulting in the release of sEVs that were enriched with invadopodial proteins such as MT1-MMP [470]. In our study, both proteins were increased in GBM cell derived sEVs following treatment of the cells with RT/TMZ, in addition to MT1-MMP and other cytoskeletal-associated invadopodial proteins such as PXN (paxillin), ROCK2. NCKAP1 and WASF2 (***Supplementary Table 7***). Ultimately, this

indicates that sEV-mediated cargo transfer between GBM cells post-treatment may facilitate not only a pro-invadopodia phenotype, but also a treatment-resistant phenotype in the recipient cells.

6.3.2.3. Membrane trafficking proteins are increased in single RT/TMZ treated GBM cells and sEVs

Invadopodia rely upon both the actin cytoskeleton and microtubules not only for the formation of the invadopodium core structure, but also for the targeted delivery of proteins, receptors, proteases, and vesicles to the cell membrane [454, 718]. Elevated expression levels of membrane trafficking proteins are often implicated in the increased invasive capacity of tumour cells [340, 551]. Notably, invadopodia-related proteins that increased in GBM cells following RT/TMZ treatment were significantly associated with microtubule-mediated transport and membrane trafficking (including ABI2, CLASP2, CLIP1, RAB3A, RAB5A, STX4) (***Figure 6-2C***). Furthermore, the top 25 proteins displaying the greatest increase in abundance in GBM cells and sEVs post-RT/TMZ treatment (***Figure 6-1C and Figure 6-3C***) were found to be associated with Rab GTPases, which are key mediators of the endocytic pathway. These proteins included Rab3a, Rab5a and Rab23, as well as MYO18A, DOCK7 and TPD52L2 that are known to interact with Rabs to regulate endocytic trafficking [719-721], indicating that Rab GTPase signalling pathways may be implicated in the observed increase of invadopodia-mediated FITC-gelatin degrading activity and sEV secretion in RT/TMZ treated GBM cells (as reported in ***Chapters 3 & 4***).

A key mechanism by which Rab GTPases may facilitate invadopodia activity is through their involvement in the dynamic recycling of MT1-MMP, thereby altering its availability at the cancer cell membrane [454, 551, 722]. Similarly, Rabs can also promote the endocytic uptake and recycling of membrane receptors such as integrins and RTKs. Liu *et al.* demonstrated that Rab5a expression was required for cervical cancer cell invasion via regulation of integrin recycling [723]. In addition to membrane trafficking, Rab GTPases can play a role in the activation and recruitment of other signalling

proteins required for invadopodium function. Liu *et al.* also showed that Rab5a is involved in the activation of Rac1, Cdc42, and RhoA and the subsequent formation of filopodia and lamellipodia in cervical cancer cells [723]. Furthermore, Zhang *et al.* demonstrated that the upregulation of Rab5a promoted the secretion of the key invadopodia-related protease, MMP-2, and subsequent invasion of HNSCC cell lines [724], thus supporting that the upregulation of Rab GTPase signalling pathways may potentially mediate the increase in GBM cell invadopodia formation and activity post RT/TMZ treatment. Further investigation is therefore warranted to determine the precise role of these Rab-related proteins in the regulation of enhanced invadopodia formation and activity following RT/TMZ treatment.

6.3.2. The expression of invadopodia-related proteins in long-term RT/TMZ treated GBM cells and EVs

The acquisition of mutations and molecular changes during RT/TMZ treatment is postulated to further amplify the impact of GBM molecular heterogeneity on treatment response [725]. Whilst our study identified the existence of a different set of DE proteins between single and LT RT/TMZ treated GBM cells and sEVs, the proteomes of LT RT/TMZ treated MU4 and MU41 cells and their corresponding sEVs indicate that enhanced adhesion-related signalling and membrane trafficking through the endosomal system is maintained (***Figure 6-5 & Figure 6-8***). As the process of invadopodia-mediated invasion is dynamic, requiring constant recycling of receptors and other proteins from the cell surface, these observations correlate with augmented invadopodia formation and FITC-gelatin degrading activity of the LT RT/TMZ treated MU4 and MU41 cell lines. Of interest, the MU4 GBM cell line demonstrated elevated expression of MT1-MMP in both cells and sEVs following LT RT/TMZ treatment, indicating that both increased cellular abundance as well as dynamic recycling of MT1-MMP may facilitate the observed enhanced invadopodia FITC gelatin-degrading activity of this cell line. Moreover, as Hakulinen *et al.* has shown that MT1-MMP on the surface of sEVs from cultured human

fibrosarcoma and melanoma cells is functionally active in the extracellular space [302], the increase of MT1-MMP in sEVs released by LT RT/TMZ treated MU4 GBM cells may also contribute to the invadopodia-mediated modification of the ECM to facilitate GBM cell invasion.

Furthermore, as invadopodia formation and activity are greatly reduced in the LN229 LT RT/TMZ treated GBM cells, the reduced expression of cytoskeletal and invadopodia-related signalling proteins in this cell line could serve to impede invadopodia assembly and elongation by reducing signalling cascades that drive invadopodia initiation, as well as limiting the availability of actin regulators that are necessary for the development of a cytoskeletal core of the invadopodium (***Figure 6-5***). For instance, the LT RT/TMZ treated LN229 GBM cell line proteome demonstrated a complete loss of detectable Src expression, which is required for the activation of numerous proteins involved in invadopodia maturation and matrix degradation activity [140]. Indeed, the inhibition of Src activity has been shown to suppress the secretion of MMP-2 in lung cancer cells [726], correlating with the loss of detectable MMP-2 secretion from LT treated LN229 cells (***Figure 3-8***). However, Src inhibition monotherapy has thus far proven to be unsuccessful in early clinical trials for a range of cancers, including GBM [175-178], potentially through the upregulation of compensatory pathways [123]. Accordingly, pre-clinical studies have demonstrated promising results when inhibitors of Src are combined with EGFR inhibitors in non-small cell lung, gastric and breast cancers [727-729]. Therefore, a more suitable approach to impede invadopodia formation and activity in GBM may involve a combination of inhibitors to target specific invadopodia-pathways. In this context, the invadopodia-related proteins that demonstrated a loss of expression in the LT RT/TMZ treated LN229 cell line proteome may provide insight into potential novel anti-invadopodia targets.

6.3.3. Proteomic analysis of LT RT/TMZ treated LN229 GBM cells indicates a link with fatty acid metabolism to sustain proliferation

Following LT RT/TMZ treatment, the LN229 GBM cell line exhibited a reduction in the expression of 1522 proteins that were significantly associated with translation elongation and mRNA processing

(***Figure 6-5 and Table 6-3***). Liu *et* al. reported that cells halt ribosome activity in the elongation phase of translation in order to overcome proteotoxic stress by reducing the accumulation of misfolded proteins [681]. It may be possible that the LT RT/TMZ treated LN229 GBM cells reduce global protein synthesis in response to proteotoxic stress induced by repeated RT/TMZ treatments, ultimately contributing to the reduced expression of many proteins in this cell line. Interestingly, however, the 143 proteins which were increased in this cell line following LT RT/TMZ treatment were significantly associated with metabolic processes involving lipids, known as fatty acid oxidation (FAO) (***Table 6-5***), and nine increased FAO-related proteins were identified in the LT RT/TMZ treated LN229 cell proteome (***Table 6-6***). Evidence indicates that many cancers become increasingly dependent on FAO during periods of metabolic stress, such as in nutrient- and oxygen-depleted conditions or as a result of treatment with anti-cancer agents [730, 731].

Interestingly, FAO has previously been shown to promote proliferation in GBM cells, consistent with the enhanced rate of proliferation in LT RT/TMZ treated LN229 cells (***Figure 3-7***). This may indicate that these cells switch their metabolic demands to favour a proliferative phenotype under therapeutically challenging conditions [49, 732]. As the LN229 GBM cell line also displays high basal level invadopodia activity, the upregulation of FAO following LT RT/TMZ treatment may allow for rapid and aggressive tumour growth at secondary sites in the brain, as is often seen for relapsing GBMs [725]. Indeed, FAO-related proteins that increased in LT RT/TMZ treated LN229 GBM cells are reported to promote tumour growth and survival during secondary site colonisation. For example, AKR1B10 supports breast cancer cells that have metastasized via promotion of a metabolic switch to FAO during secondary site colonisation [686], whereas CAV1 and GPD1 have both been shown to possess a tumorigenic role in GBM, with high expression levels correlating with poorer GBM patient survival [689] and promoting tumour relapse after chemotherapy [691], respectively. Specifically, elevated GPD1 expression in GBM cells is reported to be triggered during the misfolded protein response to stress and promoted resistance to TMZ [691], supporting the notion that these metabolic proteins are increased in LT RT/TMZ treated LN229 GBM cells in response to proteotoxic stress. Furthermore, the sEVs released by LT RT/TMZ treated LN229 GBM cells were enriched for fatty acid transporters

(***Table 6-7***), suggesting that the uptake of these EVs by recipient GBM cells may also facilitate FAO, as well as proteins involved in fibrin clotting and plasminogen activation (***Figure 6-8C***). Fibrin and clotted plasma are known to contribute to the GBM stem cell (GSC) niche microenvironment, which provides adhesive cues for GBM cells to promote growth and proliferation [733]. Upon activation, plasmin can degrade fibrin and activate latent collagenases to sustain these environmental cues [734]. Therefore, unlike MU4 and MU41, LT RT/TMZ treated LN229 GBM cells release sEVs containing proteins that may be implicated in the establishment of a tumour-permissive niche microenvironment that may further sustain a pro-proliferative phenotype.

Collectively, these results demonstrate that GBM cell lines exhibit different responses to prolonged RT/TMZ treatment. These functional differences between the GBM cell lines in response to LT RT/TMZ treatment may reflect the variation that is seen with GBM patient responses to the current treatment regime [735]. Whilst the response of LN229 GBM cells to LT RT/TMZ treatment may allow for rapid tumour growth post-treatment, but as these cells exhibit a reduction in invasive capacity, these tumours maybe more amenable to targeted treatments and repeat surgery adjacent to the original tumour bed. Ultimately, the variations in proteomic profiles observed between the different GBM cell lines following LT RT/TMZ treatment highlights the complexity and plasticity of GBM cellular responses to anti-cancer treatments such as RT/TMZ. Given the substantial heterogeneity present in GBM, it is likely that one tumour may harbour populations of tumour cells that adopt either a pro-proliferative or pro-invasive phenotype in response to treatment. Further elucidation of these processes in GBM cells may uncover novel adjuvant therapeutic strategies for improved management of GBM.

6.3.4. Conclusion

The proteomic analyses presented in this chapter indicate that that the current therapeutic approach of RT and TMZ promotes the increased expression of adhesion-related proteins, cytoskeletal regulators, and membrane trafficking proteins in GBM cells that may support a pro-invadopodia phenotype in surviving GBM cells, as well as potentially also aiding the ability of these cells to withstand cytotoxic

stress induced by RT/TMZ treatment. Furthermore, as GBM cells secrete a greater number of sEVs following RT/TMZ treatment with elevated expression levels of cargo proteins that are associated with signalling cascades known to drive invadopodia initiation, these sEVs may also invadopodia formation and activity in recipient GBM cells. Whilst these proteomic changes were generally maintained in LT RT/TMZ treated MU4 and MU41 cells, LT RT/TMZ treated LN229 cells instead demonstrated an increase in the abundance of proteins that serve to sustain cellular proliferation. This highlights that various GBM cell lines can exhibit vastly different responses to the same treatment regime and emphasises the limitations of studies that investigate a single cell line in response to the same treatment.

Nevertheless, the increased proteins and cellular processes presented here warrant further investigation as potential therapeutic targets to improve GBM patient response to RT/TMZ treatment, but also as potential biomarkers of GBM patient treatment response and enhanced tumour invasive capacity. The list of proteins that are involved in the regulation of invadopodia formation and activity in GBM and other cancers will continue to evolve over time, however, it is possible that many of the increased pro-invasive proteins in GBM cells and sEVs identified in this study may also contribute to the augmented invadopodia activity following RT/TMZ treatment. Although the therapeutic targeting of specific proteins involved in the GBM cell response to RT/TMZ treatment warrants further investigation, as sEV cargo proteins may be protected from certain treatments, as demonstrated by Hung *et al.* who showed that EV-encapsulated epidermal growth factor receptor (EGFR) is protected from inhibitors [736], strategies aimed at targeting the sEV-mediated transfer of cargo in GBM should also be explored. Ultimately, blocking sEV secretion or uptake in GBM cells may represent more effective methods to overcome RT/TMZ-induced invasion or treatment resistance.

CHAPTER 7:
Conclusion and Future Directions

7.1 Discussion, conclusions, and future directions

Glioblastoma (GBM) is the most prevalent and aggressive form of glioma, and is associated with an extremely poor prognosis, with a low median patient survival time of just 15 months post-diagnosis with the current therapeutic approach known as the Stupp protocol, consisting of surgical resection, followed by radiotherapy (RT) and concomitant chemotherapy with temozolomide (TMZ). A significant contributing factor that impacts the survival of GBM patients is the highly infiltrative nature of GBM cells, which prevents complete tumour resection and also limits the capacity of targeted therapies to effectively reach the infiltrating tumour cells [349]. Consequently, these tumours can exhibit high rates of recurrence, appearing within months following the completion of the first round of treatment and can also demonstrate minimal response to further rounds of RT/TMZ treatment [346]. Evidence suggests that the efficacy of current therapeutic approach may be compromised by an enhanced invasive phenotype that is displayed by the GBM cells that survive the current treatment protocol [3-7, 737]. The targeting of the enhanced invasive abilities exhibited by RT/TMZ treated GBM cells could provide a potential therapeutic approach for improving patient outcome, however, the mechanisms utilised by invasive GBM cells following treatment are not well understood. As GBM cells have been shown to form actin-rich membrane protrusions known as invadopodia that can facilitate invasion by degrading the surrounding ECM via highly localised proteolytic activity [121, 351, 352], it is possible that the enhanced invasive capabilities of GBM cells post- RT/TMZ treatment may be mediated by invadopodia.

In this thesis, we investigated the role of invadopodia in GBM cell invasion and response to RT/TMZ treatment. In ***Chapter 3***, using clinically relevant doses of RT (2Gy) and TMZ (50μM), it was demonstrated that the enhanced invasive capabilities of GBM cells post-RT/TMZ treatment may be attributed to an increase in invadopodia formation and activity. The role of intracellular communication between GBM cells via extracellular vesicles (EVs) was investigated in ***Chapter 4***, highlighting the ability of sEVs to transfer a pro-invadopodia phenotype to recipient GBM cells, as well as their potential to facilitate an enhanced pro-invadopodia phenotype following RT/TMZ treatment. Lastly, in ***Chapter 5 and*** 6, GBM cell lines and their corresponding secreted sEVs were subjected to comprehensive

proteomic profiling in order to identify proteins that may facilitate invadopodia formation and activity following exposure to RT/TMZ treatment, contributing to enhanced GBM invasion. Collectively, this project highlights the contributing role of invadopodia and sEVs to the pro-invasive abilities of GBM cells that survive RT/TMZ treatment, indicating that therapeutically targeting invadopodia formation and activity, as well as sEV secretion or uptake in GBM cells, represent promising strategies to overcome treatment induced GBM cell invasion, which may ultimately improve the clinical efficacy of RT and TMZ treatment. These key findings and suggestions for future studies are discussed in the following sections.

7.2 GBM cell line derived sEVs facilitate a pro-invadopodia phenotype

In ***Chapter 4***, sEVs (vesicles with a diameter less than 200nm) secreted from the high invadopodia-mediated FITC-gelatin degrading GBM cell line LN229 were found to promote invadopodia formation and invadopodia-mediated FITC-gelatin degradation in recipient GBM cell lines, highlighting a role for sEV-mediated cargo transfer in facilitating a pro-invadopodia phenotype in GBM cells. This finding supports the study by Hoshino *et al.* [229] that proposed a potential functional link between invadopodia and exosomes in HNSCC cell lines, whereby they demonstrated that exosomes were preferentially docked and secreted from mature invadopodia, stabilizing the invadopodial structure in both the donor cells and recipient HNSCC cells. However, the cargo that was present in the HNSCC cell line sEVs was not examined and therefore how the sEVs may facilitate invadopodia formation/activity was not determined. More recently, Beghein *et al*. [470] reported that a number of proteins present in the cargo of EVs derived from the MDA-MB-231 breast cancer cell line are classified as invadopodial related proteins including EGFR, Cdc42, fascin and MT1-MMP. The MDA-MB-231 donor cell line was observed to form gelatin-matrix degrading invadopodia, indicating the cell line and EV proteomes contain similar invadopodial related proteins, although the functional impact of these EVs on recipient cells was not assessed. Based on the observations from these studies, it is conceivable that the transfer of invadopodia-related sEV cargo proteins could enhance invadopodia formation and function in

recipient cancer cells. Importantly, as invadopodia have been observed to form in GBM cells, the transfer of invadopodial proteins as sEV cargo to recipient cells driving invadopodia formation and activity in the recipient cells is feasible [121, 351, 352].

Therefore, in our current study we examined both the protein cargo of the GBM cell line derived sEVs as well as the potential for these sEVs to promote a pro-invasive phenotype in recipient GBM cells. A comprehensive proteomic examination of the GBM cell line derived sEV cargo revealed 49 proteins with established roles in the biogenesis of invadopodia, including proteins involved in key invadopodia-related signalling cascades (such as adhesion-, GTPase-, and kinase- related proteins), as well as actin regulators and proteases. Furthermore, sEVs derived from GBM cell lines with high invadopodia-mediated FITC-gelatin degrading activity were enriched in many of these invadopodia-related proteins (***Figure 5-7***), and enhanced invadopodia formation and activity was observed in the recipient GBM cells following incubation with these sEVs (***Figure 4-6***). These results indicate that sEVs can potentially facilitate the transfer of a pro-invadopodia phenotype in GBM cells and suggest a potential role for the sEV-mediated delivery of these cargo proteins in the promotion of invadopodia formation/activity in recipient GBM cells. Therefore, the data presented here further substantiates a link between invadopodia and sEVs and provides a valuable insight into how GBM cells may utilize sEV-mediated communication to enhance invadopodia formation and activity in recipient GBM cells.

7.3 RT/TMZ treatment promotes a pro-invadopodia phenotype in GBM cell lines

Evidence within the literature indicates that surviving GBM cells following radiotherapy and/or TMZ treatment may exhibit enhanced migratory and invasive abilities [3-7, 737], implying that the current therapeutic approach for GBM may have a counterintuitive impact. However, the majority of these studies to date have only examined the effect of ionizing radiation on GBM cells [3, 4, 7, 737], and as such, have not determined the overall effect of the combined RT/TMZ treatment on GBM cells. Nevertheless, two studies by Trog *et al.* [5, 6] have investigated the impact of combined RT/TMZ treatment on GBM cell invasion, identifying an upregulation of MMP-2 and MT1-MMP protein

expression levels in U87MG GBM cells post-RT/TMZ treatment, as well as increased secreted levels of MMP-2. As MMP-2 is known to be secreted by invadopodia and degrade the ECM to facilitate invasion, we hypothesized that an enhanced invasive phenotype of GBM cell lines following RT/TMZ treatment is mediated through the action of invadopodia. Additionally, whilst Trog *et al*. [5, 6] treated U87MG cells with the clinically relevant dose of RT (2Gy), the dosage of TMZ utilized in these studies was 30μg/ml (equivalent to a concentration of 154μM). Pharmacokinetic studies have shown that TMZ levels in the cerebrospinal fluid (CSF) of GBM patients are within a concentration range of 1-10μg/ml (5.15 - 51.5μM) [353]. Therefore, in this project, the GBM cell lines were treated with clinically relevant doses of both RT (2Gy) and TMZ (50μM) for each relevant experiment utilizing RT and TMZ.

In ***Chapter 3***, GBM cell lines that survived RT/TMZ treatment were observed to exhibit augmented invadopodia formation and invadopodia-mediated FITC-gelatin-degrading activity, coupled with an upregulation of pro-invasive genes (including THBS1, VCAN and SERPINE1) and a downregulation of miRNAs with invadopodia-related targets (including hsa-let-7a-5p, hsa-let-7b-5p, hsa-let-125b-5p, hsa-miR-4454+hsa-miR-7975). In ***Chapter 4***, an increase in sEV secretion from RT/TMZ treated GBM cells was observed. As discussed previously, these sEVs can transfer cargo that can facilitate a pro-invadopodia phenotype in recipient GBM cells, indicating that sEV-mediated communication via cargo transfer between GBM cells may also contribute to the enhanced invadopodia activity observed following RT/TMZ treatment. Collectively, this data highlights the need to potentially target invadopodia and the sEV-mediated transfer of 'pro-invadopodia cargo' to recipient GBM cells for overcoming RT/TMZ-induced invasion in GBM cells that survive RT/TMZ which may improve the clinical efficacy of the current treatment regime.

Whilst GBM cells surviving RT/TMZ treatment may contain genetic aberrations, proteins ultimately drive functional changes. Consequently, proteins have primarily been the major targets for many therapeutic agents. Additionally, whilst radiotherapy or chemotherapy is known to enhance EV secretion from tumour cells, including GBM cells, comparably little is known about the impact of such treatment modalities on the proteomic composition and functional effect of these sEVs ono the recipient cells [257, 488, 489]. Furthermore, whilst several studies have addressed proteomic changes in GBM

cells or GBM cell line derived sEVs following TMZ treatment [697, 698, 700], no studies exist to date that have investigated the impact of RT in combination with TMZ on GBM cell or sEV proteomes. Therefore, in ***Chapter 6***, a comprehensive proteomic analysis was undertaken to identify potential changes at the protein level in GBM cell lines that survived RT/TMZ treatment and the corresponding secreted sEVs that may contribute to a pro-invadopodia phenotype. This proteomic profiling highlighted the differential expression of key invadopodia-related proteins detected in the GBM cell line and sEV proteomes in response to RT/TMZ treatment, and additionally revealed a significant upregulation of adhesion-related proteins, cytoskeletal regulators, and membrane trafficking proteins, which is consistent with an invasive phenotype post-RT/TMZ treatment. Indeed, recent studies have shown that vesicle-mediated membrane trafficking is crucial for delivery of MMPs to the maturing invadopodia in breast cancer cells [153, 154]. In addition, an important role has also been demonstrated for adhesion proteins in vesicle recruitment and capture at invadopodia [702]. Subsequently, this analysis highlighted potential 'anti-invasive' targets which can be further investigated to aid in the future development of new GBM treatments or biomarkers for the monitoring of GBM disease progression post-treatment.

Importantly, we demonstrated that augmented invadopodia FITC-gelatin degrading activity and sEV secretion was maintained in long-term (LT) RT/TMZ treated GBM cell lines, with the exception of LN229 cells which displayed a highly proliferative but minimally invasive phenotype following LT RT/TMZ treatment. Analysis of the proteome of LT RT/TMZ treated GBM cell lines and the secreted sEVs indicated that there are proteins that may contribute to an enhanced pro-invasive/pro-invadopodia phenotype in the LT RT/TMZ treated MU4 and MU41 GBM cell lines. In contrast, analysis of the proteome of LT RT/TMZ treated LN229 GBM cells and secreted sEVs demonstrated a reduction in global protein synthesis with a reduction in total proteins and a shift to metabolic pathway related proteins encompassing fatty acid oxidation/lipid metabolism. As fatty acid oxidation has been reported to promote GBM cell proliferation [49, 732], this shift may allow these surviving cells to sustain a pro-proliferative phenotype under therapeutically challenging conditions presented by repeated RT/TMZ treatments. This data demonstrates the varied responses that GBM cell lines can exhibit to prolonged

RT/TMZ treatment, which may also reflect the differences observed in GBM patient response to the current therapeutic approach of RT/TMZ treatment known as the Stupp protocol. This may have significant implications regarding the future development of treatments for GBM patients, for which, in this context, the altered proteomic profiles of RT/TMZ treated GBM cells and sEVs presented in ***Chapter 6*** could provide a 'pro-invasive' proteomic profile to compare with similar analyses carried out with patient biopsies.

7.4 Targeting RT/TMZ treatment-induced invadopodia activity in GBM cell lines

As GBM cell lines surviving RT/TMZ treatment adopt a pro-invadopodia phenotype, disruption of the formation or matrix-degrading activity of invadopodia could lead to the development of novel adjuvant therapeutic strategies that can be used in conjunction with the current therapeutic approach involving RT and TMZ. In accordance with previous data from our laboratory showing that the FDA-approved microtubule-destabilising agent Vinorelbine Tartrate (VT) reduces invadopodia-mediated FITC-gelatin degradation in GBM cells surviving RT/TMZ [12], the addition of VT to RT/TMZ treatment in our current study (***Figure 4-17***) reduced the enhanced levels of GBM cell line sEV secretion observed post RT/TMZ treatment, highlighting its potential as an adjuvant anti-invasive agent in GBM that can dualistically target invadopodia activity and EV-mediated intercellular cargo transfer. VT is reported to hinder microtubule dynamics by preventing the addition of tubulin subunits at the positive end of lengthening microtubules [25]. Supporting the relevance of this process in the pro-invadopodia response of GBM cells to RT/TMZ treatment, analysis of the proteome of RT/TMZ treated GBM cell lines in ***Chapter 6*** identified an upregulation of invadopodia-related proteins with microtubule plus-end binding functions (***Figure 6-1***). Invadopodia rely upon microtubules for the targeted delivery of secretory vesicles, such as those containing MMPs, to the cell membrane for subsequent secretion into the extracellular environment [137]. Therefore, this data indicates that FDA-approved agents such as microtubule-targeting agents may be repurposed as suitable candidates to impair invadopodia activity

and sEV secretion in GBM cells and should be considered in future as potential anti-invasive adjuvant agents for use alongside RT/TMZ treatment.

7.5 Future Directions

7.5.1 Determining whether sEVs secreted from GBM cell lines are capable of ECM degradation

As sEVs secreted from high invadopodia FITC-gelatin degrading activity GBM cell lines were observed to display higher levels of proteases (such as MT1-MMP, MMP-2, and the MMP-inducer, basigin) compared to sEVs enriched from low invadopodia FITC-gelatin degrading activity GBM cells (***Figure 5-7)***, this potentially demonstrates that these sEVs may possess two roles; as cargo carriers to recipient GBM cells and also to work synergistically with invadopodia to directly facilitate ECM degradation with their proteolytic cargo. This is supported by the work of Beghein *et al.* [470] which demonstrated that sEVs secreted from the invasive breast cancer cell line MDA-MB-231 contained MT1-MMP and possessed gelatinolytic activity. Additionally, Hakulinen *et al.* [302] has shown that fibrosarcoma and melanoma cell line derived EVs contained functionally active MT1-MMP which was able to activate pro-MMP-2 to degrade collagen and gelatin. However, the capacity of EVs to degrade the ECM is yet to be shown in the context of GBM. A strategy focussed on inhibiting sEV secretion from the surviving GBM cells may serve to reduce invadopodia-mediated ECM remodelling and the subsequent invasive capacity of the GBM cells.

In support of this hypothesis, we identified that a reduction in GBM cell line sEV secretion occurred with the calcium ion channel blocker, DMA, which in turn also impacted invadopodia-mediated FITC-gelatin degradation without significantly altering invadopodia formation (***Figure 4-10***). Several studies have reported that changes in intracellular calcium ion concentrations in GBM cells can contribute to enhanced MMP-2 and MMP-9 secretion and invadopodia-mediated focal ECM degradation [738-740]. Therefore the use of ion channel inhibitors has been proposed as a potential therapeutic avenue to inhibit

invadopodia-mediated MMP secretion in GBM cells [741]. However, these studies, including our own data do not discern whether the changes in extracellular MMP-2 activity upon treatment with the ion channel inhibitor is due to alterations in sEV secretion or the secretion of MMPs independent of what is present as sEV cargo. Consequently, future studies should further investigate the ability of GBM cell derived sEVs to degrade components of the ECM. This can initially be examined by adding an equal number of sEVs enriched from different GBM cell lines onto FITC-gelatin and correlating the amount of FITC-gelatin degradation observed and compared to the FITC-gelatin degrading invadopodia activity of each donor GBM cell line. This may also be extended to include a comparison of sEVs secreted from untreated and RT/TMZ treated GBM cell lines. If there exists a positive correlation between sEV-mediated and invadopodia-mediated FITC-gelatin degradation, it may be possible that sEVs not only act as cargo carriers to recipient cells, but also function to modify the surrounding ECM in combination with invadopodia. Consequently, therapeutic agents that may target invadopodia-associated sEV secretion (such as Vinorelbine Tartrate) could be investigated as a novel anti-invadopodia/anti-invasive therapy for the treatment of GBM.

7.5.2 Investigating the potential role of Thrombospondin-1 in the biogenesis of invadopodia in GBM cells

A greater understanding of the composition and dynamics of the protein networks and mechanisms that regulate invadopodia formation and activity is critical for the identification of novel invadopodia-related drug targets in the development of anti-invasive therapeutics. The adhesive glycoprotein, thrombospondin-1 (THBS1), was identified in ***Chapter 3*** as a potential pro-invasive/pro-invadopodia candidate gene from the Nanostring® Cancer gene panel array, as it was upregulated in the GBM cell lines that survived RT/TMZ treatment. THBS1 was initially described as an inhibitor of angiogenesis and THBS1 mimetics were trialled as anti-angiogenic therapeutic agents [742]. However, due to the complex interactome of THBS1, the use of these agents for cancer treatment has failed to significantly

display any significant impact on patient outcome in clinical trials, such as the THBS1-derived peptide ABT-510, utilized in phase II clinical trials for melanoma and sarcoma patients [743, 744]. Furthermore, anti-angiogenic therapies can result in a hypoxic tumour microenvironment, which has been shown to induce an aggressive, invasive phenotype in several cancers, including GBM [745-747]. In addition to its role as an angiogenesis inhibitor, it has more recently been reported that THBS1 may function in a facilitative role during GBM development [444, 447]. In a recent paper by Daubon *et al.* it was observed that THBS1 promoted GBM cell invasion following TGFβ1 stimulation [447], however the underlying mechanisms by which THBS1 is able to promote GBM invasion requires further elucidation.

We propose that the potential pro-invasive effect of THBS1 in GBM cells is mediated via the matrix-degrading activity of invadopodia. We utilized the STRING protein-protein interaction network database and determined that THBS1 is associated with several invadopodia regulators including Src, Cortactin, Tks5, MMP-2 and MMP-9. Furthermore, we demonstrated that the overexpression of THBS1 in GBM cell lines resulted in increased secretion of MMP-2 and an enhanced migration rate, whilst the localization of THBS1 within LN229 GBM cell invadopodia further supports a facilitative role of THBS1 in GBM cell invadopodia biogenesis (***Figure 3-19***). Whilst THBS1 has been reported to bind to a variety of invadopodia-related proteins, such as MMP-2 [448] and β1 integrins [453-455], to our knowledge this is the first report to demonstrate the localization of THBS1 within invadopodia. This could be further examined in future studies by seeding the transfected (THBS1 overexpression and knockdown) GBM cells on FITC-gelatin to determine whether these changes in MMP-2 secretion lead to altered invadopodia-mediated FITC-gelatin degrading activity.

Interestingly, the combination of bevacizumab and TAX2, a peptide that inhibits the interaction of THBS1 and CD47, impacted GBM cell invasion *in vivo* in an intracranial mouse GBM xenograft model, which resulted in an increase in survival [447]. However, as mentioned previously, despite demonstrating promising anti-invasive potential in preclinical models [447, 463, 748], targeting THBS1 in clinical trials has been largely ineffective due to pleiotropic nature of THBS1 with a variety of ligands which frequently leads to severe adverse effects [463]. Therefore, future studies should seek to further substantiate the role of THBS1 in invadopodia biogenesis and activity as well as how this is altered (in

addition to interacting proteins) post-RT/TMZ treatment, as this may allow for a better understanding of invadopodia response post-treatment and potentially aid in the identification of an invadopodia-associated regulator as a therapeutic target based on an interaction with THBS1.

7.5.3 Examining the role of invadopodia in GBM using patient-derived specimens

Whilst immortalised cell lines are routinely used to model GBM, they can lose various characteristics of the original tumour tissue from which they are derived and are not entirely representative of the GBM patient tumours. Therefore, employing the use of GBM patient derived tumour specimens is a crucial next step to further assess the clinical significance of the findings presented in this thesis. Various analytical approaches could be utilized to confirm the *in vitro* results obtained in this study including histological and immunohistochemical (IHC)/immunofluorescence (IF) based techniques to examine the localization and expression levels of various invadopodia-related proteins in the GBM tumour. IHC staining of GBM patient derived tumour sections from multiple areas of a tumour could be conducted to confirm the co-localization of the 61 putative invadopodia-related proteins identified via LC/MS-MS in ***Chapter 5*** with other known invadopodia proteins such as cortactin, Tks5, MMP-2, specifically at the invasive tumour periphery. This could be further expanded to include the four invadopodia-related proteins that were uniquely detected in sEVs compared to MVs (RCC2, PODXL, MYO10 and LPAR1) (***Figure 5-10***)**.** Furthermore, this could be extended to comparing the protein expression profile in tissue sections from the same patient with primary versus recurrent GBM tumours, which may then be cross-referenced with the proteomic profiles of the single and long-term RT/TMZ treated GBM cells (***Chapter 6***). The emergence of IHC/IF techniques such as OPAL^{TM} multiplexing which retains morphological and spatial characteristics is particularly promising in this context, as these techniques allow for the simultaneous detection of multiple proteins and would therefore reveal patterns of localization and expression, potentially revealing interactions that may be occurring between these invadopodial proteins.

Additionally, as immortalized GBM cell lines can fail to accurately model the true complexity of the heterogeneous disease from which they were initially derived, these limitations also apply to the EVs that are secreted from the GBM cell lines. Consequently, future studies should employ the use of GBM patient tissue derived sEVs to further validate the findings from this project, namely, the cargo present within the sEVs and also the sEV-mediated transfer of a pro-invadopodia phenotype to recipient GBM cells. Whilst circulating sEVs present in the blood of GBM patients offers a minimally invasive method of obtaining GBM patient sEVs, a major shortfall of this method is that due to the abundance of sEVs from other cell types, GBM tumour derived sEVs that may be present, will be at extremely low concentrations often require the use of immunoaffinity-based approaches for differentiation from other cell-derived sEVs and subsequent capture, meaning that only a specific subpopulation of sEVs may be enriched. More recent studies have highlighted the value of CUSA (cavitron ultrasonic surgical aspirator) fluid as a source of GBM tumour-derived sEVs [330, 472]. CUSA fluid consists of a mix of tumour cells, blood and CSF collected (usually for disposal) during brain tumour resection using an ultrasonic surgical aspirator. Although not exclusively GBM tumour cell derived sEVs, a benefit of this approach is that CUSA-obtained sEVs would provide a more relevant reflection of the sEVs present within the GBM patient tumour microenvironment. Additionally, Vella *et al.* [749] have developed an effective method for isolating sEVs from human brain tissue that maintains the integrity of the vesicles as well as their cargo. Using this method, in conjunction with GBM patient derived tissue specimens would provide for an enriched population of GBM cell derived EVs that could be compared alongside with the sEVs enriched from GBM cell lines, as outlined in this project. GBM patient derived sEVs obtained with either of these methods could be incubated with recipient GBM cells to investigate their ability to induce a pro-invadopodia phenotype, as observed in this project, which could subsequently be correlated with the sEV cargo and importantly, the clinical information of each GBM patient, including their progression free- or overall- survival. In addition, sEVs isolated from GBM patient CUSA fluids or tissue biopsies obtained at the time of initial surgery could be compared to later surgeries (upon tumour recurrence) to model the findings of our *in vitro* experiments investigating the effect of RT/TMZ treatment on sEV cargo and invadopodia formation/activity.

7.5.4 Investigating invadopodia activity *in vivo* using preclinical mouse models of GBM

Furthermore, the findings presented in this thesis could be further extended with the use of preclinical *in vivo* orthotopic mouse models of GBM to investigate the effect of single and LT RT/TMZ treatment on GBM cell invasion *in vivo*, as well as the effect of sEVs from high and low invadopodia FITC-gelatin degrading activity cell lines. One way in which this can be carried out is by pre-treating GBM cell lines with RT/TMZ or isolating sEVs from these cells and pre-incubating donor cells with the sEVs prior to intracranial implantation. Histological examination of the mouse brain sections would allow for the invasive capacity of the tumours to be examined under different conditions (untreated versus RT/TMZ treated cells; pre-incubation of GBM cells with enriched sEVs from different GBM donor cells). IHC staining for a variety of invadopodia-related proteins could also be conducted on these tissue sections to determine the expression levels and spatial distribution relative to the invasive edge of the tumour. The GBM *in vivo* mouse models could also be used to determine the efficacy of VT as an anti-invasive or anti-invadopodia agent for use in conjunction with the current clinical approach involving RT/TMZ treatment. As VT is already FDA-approved with a known pharmacokinetic and safety profile, if these pre-clinical mouse model studies yield positive outcomes, it could potentially be considered as an adjuvant therapy alongside the current therapeutic approach for GBM patients [750].

7.6 Overall Conclusions

The data presented in this thesis demonstrates that the enhanced invasive abilities of GBM cells that survive RT/TMZ treatment may be mediated through an increase in invadopodia formation and activity, which may be maintained after prolonged (long-term) RT/TMZ treatment. Therefore, disrupting the formation or activity of invadopodia represents a promising strategy for the development of novel adjuvant therapeutics for overcoming the invasive abilities of RT/TMZ treated GBM cells. As the biogenesis and matrix-degrading activity of invadopodia relies upon the coordination of a complex network of interacting proteins, it has been proposed that the efficient suppression of invadopodia

formation or activity will likely require the perturbation of a number of pathways involving multiple regulatory proteins [751]. We identified a number of invasion- and invadopodia- related adhesion, cytoskeletal and membrane trafficking proteins that were significantly increased in the proteome of GBM cells following RT/TMZ treatment, which was also reflected in the cargo of the sEVs secreted from these cells. This indicated that proteins involved in the invadopodia-specific vesicle transport machinery and components of cell adhesion may promote invadopodia activity and sEV secretion following RT/TMZ treatment. Therefore, targeting vesicle transport and protein trafficking to the plasma membrane of GBM cells may reduce the enhanced invadopodia activity and sEV secretion in GBM cells that survive RT/TMZ treatment, supported by our data with the microtubule destabilising agent, Vinorelbine Tartrate. Whilst further research is required for the clinical translation of these findings, the results presented in this thesis highlight the crucial role of invadopodia and sEVs as mediators of an enhanced invasive phenotype in GBM cells that survive RT/TMZ treatment, as well offering an additional insight into the potential underlying mechanisms that may promote this augmented invasive phenotype. Ultimately these findings could contribute future studies aimed at exploring new therapeutic avenues to abrogate treatment-induced invadopodia-mediated invasion in order to improve GBM patient outcome.

References

1. Hanahan, D. and R. Weinberg, *Hallmarks of Cancer: The Next Generation.* Cell, 2011. **144**(5): p. 646-674.
2. Stupp , R., et al., *Radiotherapy plus Concomitant and Adjuvant Temozolomide for Glioblastoma.* New England Journal of Medicine, 2005. **352**(10): p. 987-996.
3. Cordes, N., et al., *Irradiation differentially affects substratum-dependent survival, adhesion, and invasion of glioblastoma cell lines.* Br J Cancer, 2003. **89**(11): p. 2122-32.
4. Hegedus, B., et al., *Irradiation and Taxol treatment result in non-monotonous, dose-dependent changes in the motility of glioblastoma cells.* J Neurooncol, 2004. **67**(1-2): p. 147-57.
5. Trog, D., et al., *Is current therapy of malignant gliomas beneficial for patients? Proteomics evidence of shifts in glioma cells expression patterns under clinically relevant treatment conditions.* PROTEOMICS, 2006. **6**(9): p. 2924-2930.
6. Trog, D., et al., *Pro-invasive gene regulating effect of irradiation and combined temozolomide-radiation treatment on surviving human malignant glioma cells.* European Journal of Pharmacology, 2006. **542**(1): p. 8-15.
7. Wild-Bode, C., et al., *Sublethal Irradiation Promotes Migration and Invasiveness of Glioma Cells.* Implications for Radiotherapy of Human Glioblastoma, 2001. **61**(6): p. 2744-2750.
8. Dai, X., et al., *AHIF promotes glioblastoma progression and radioresistance via exosomes.* Int J Oncol, 2019. **54**(1): p. 261-270.
9. Godlewski, J., et al., *Belonging to a network—microRNAs, extracellular vesicles, and the glioblastoma microenvironment.* Neuro-oncology, 2015. **17**(5): p. 652-662.
10. Li, C.C.Y., et al., *Glioma microvesicles carry selectively packaged coding and non-coding RNAs which alter gene expression in recipient cells.* RNA biology, 2013. **10**(8): p. 1333-1344.
11. Skog, J., et al., *Glioblastoma microvesicles transport RNA and proteins that promote tumour growth and provide diagnostic biomarkers.* Nature Cell Biology, 2008. **10**(12): p. 1470-1476.
12. Whitehead, C.A., et al., *Inhibition of Radiation and Temozolomide-Induced Invadopodia Activity in Glioma Cells Using FDA-Approved Drugs.* Translational oncology, 2018. **11**(6): p. 1406-1418.
13. Ostrom, Q.T., et al., *CBTRUS statistical report: primary brain and other central nervous system tumors diagnosed in the United States in 2011–2015.* 2018. **20**(suppl_4): p. iv1-iv86.
14. Rosenthal, M., et al., *Management of glioma in Victoria (1998-2000): retrospective cohort study.* Medical Journal of Australia, 2006. **184**(6): p. 270-273.
15. Ostrom, Q.T., et al., *The epidemiology of glioma in adults: a "state of the science" review.* Neuro-Oncology, 2014. **16**(7): p. 896-913.
16. Louis, D.N., et al., *The 2016 World Health Organization Classification of Tumors of the Central Nervous System: a summary.* Acta Neuropathologica, 2016. **131**(6): p. 803-820.
17. Sahm, F. and D. Capper, *Addressing Diffuse Glioma as a Systemic Brain Disease With Single-Cell Analysis.* Archives of neurology, 2012. **69**(4): p. 523.
18. Thakkar, J.P., et al., *Epidemiologic and molecular prognostic review of glioblastoma.* Cancer Epidemiol Biomarkers Prev, 2014. **23**(10): p. 1985-96.
19. Schwartzbaum, J., et al., *Epidemiology and molecular pathology of glioma.* Nature clinical practice neurology, 2006. **2**(9): p. 494-503.
20. Yan, H., et al., *IDH1 and IDH2 mutations in gliomas.* N Engl J Med, 2009. **360**(8): p. 765-73.
21. Peng, S., et al., *Integrated genomic analysis of survival outliers in glioblastoma.* 2017. **19**(6): p. 833-844.
22. Omuro, A. and L.M. DeAngelis, *Glioblastoma and other malignant gliomas: a clinical review.* Jama, 2013. **310**(17): p. 1842-50.

23. Ohgaki, H. and P. Kleihues, *Genetic pathways to primary and secondary glioblastoma.* The American journal of pathology, 2007. **170**(5): p. 1445-1453.
24. Verhaak, R.G.W., et al., *Integrated Genomic Analysis Identifies Clinically Relevant Subtypes of Glioblastoma Characterized by Abnormalities in PDGFRA, IDH1, EGFR, and NF1.* Cancer Cell, 2010. **17**(1): p. 98-110.
25. Iser, I.C., et al., *The Epithelial-to-Mesenchymal Transition-Like Process in Glioblastoma: An Updated Systematic Review and In Silico Investigation.* Med Res Rev, 2017. **37**(2): p. 271-313.
26. Iwadate, Y., *Epithelial-mesenchymal transition in glioblastoma progression.* Oncology Letters, 2016. **11**(3): p. 1615.
27. Pietras, K. and A. Östman, *Hallmarks of cancer: Interactions with the tumor stroma.* Experimental cell research, 2010. **316**(8): p. 1324-1331.
28. Cancer Genome Atlas Research, N., *Comprehensive genomic characterization defines human glioblastoma genes and core pathways.* Nature, 2008. **455**(7216): p. 1061-1068.
29. Piper, K., et al., *Glioma Stem Cells as Immunotherapeutic Targets: Advancements and Challenges.* 2021. **11**(92).
30. Noroxe, D.S., H.S. Poulsen, and U. Lassen, *Hallmarks of glioblastoma: a systematic review.* ESMO Open, 2016. **1**(6): p. e000144.
31. Baxendine-Jones, J., I. Campbell, and D. Ellison, *p53 status has no prognostic significance in glioblastomas treated with radiotherapy.* Clinical neuropathology, 1997. **16**(6): p. 332-336.
32. Zhang, W., et al., *Significant Prognostic Features and Patterns of Somatic TP53 Mutations in Human Cancers.* Cancer Informatics, 2017. **16**: p. 1176935117691267.
33. Adams, J.M., *Ways of dying: multiple pathways to apoptosis.* Genes Dev, 2003. **17**(20): p. 2481-95.
34. Edinger, A. and C. Thompson, *Defective autophagy leads to cancer.* Cancer cell, 2003. **4**(6): p. 422-424.
35. Miracco, C., et al., *Protein and mRNA expression of autophagy gene Beclin 1 in human brain tumours.* 2007. **30**(2): p. 429-436.
36. Grivennikov, S., F. Greten, and M. Karin, *Immunity, Inflammation, and Cancer.* Cell, 2010. **140**(6): p. 883-899.
37. Brennan, C., et al., *The Somatic Genomic Landscape of Glioblastoma.* Cell, 2013. **155**(2): p. 462-477.
38. Dubois, L., et al., *Gliomas and the vascular fragility of the blood brain barrier.* Frontiers in Cellular Neuroscience, 2014. **8**: p. 418.
39. Ferrara, N., H.-P. Gerber, and J. LeCouter, *The biology of VEGF and its receptors.* Nature Medicine, 2003. **9**(6): p. 669-676.
40. Talmadge, J.E. and I.J. Fidler, *AACR centennial series: the biology of cancer metastasis: historical perspective.* Cancer Res, 2010. **70**(14): p. 5649-69.
41. Krakhmal, N.V., et al., *Cancer Invasion: Patterns and Mechanisms.* Acta Naturae, 2015. **7**(2): p. 17-28.
42. Friedl, P., Y. Hegerfeldt, and M.J.I.J.o.D.B. Tusch, *Collective cell migration in morphogenesis and cancer.* 2004. **48**(5-6): p. 441-449.
43. Yilmaz, M. and G. Christofori, *EMT, the cytoskeleton, and cancer cell invasion.* Cancer and Metastasis Reviews, 2009. **28**(1): p. 15-33.
44. Lo, H.W., et al., *Epidermal growth factor receptor cooperates with signal transducer and activator of transcription 3 to induce epithelial-mesenchymal transition in cancer cells via up-regulation of TWIST gene expression.* Cancer Res, 2007. **67**(19): p. 9066-76.
45. Zavadil, J. and E.P. Bottinger, *TGF-beta and epithelial-to-mesenchymal transitions.* Oncogene, 2005. **24**(37): p. 5764-74.
46. Pavlova, N.N. and C.B. Thompson, *The Emerging Hallmarks of Cancer Metabolism.* Cell Metab, 2016. **23**(1): p. 27-47.

47. Carracedo, A., L.C. Cantley, and P.P. Pandolfi, *Cancer metabolism: fatty acid oxidation in the limelight.* Nature reviews. Cancer, 2013. **13**(4): p. 227-232.
48. Guppy, M., et al., *Contribution by different fuels and metabolic pathways to the total ATP turnover of proliferating MCF-7 breast cancer cells.* 2002. **364**(1): p. 309-315.
49. Lin, H., et al., *Fatty acid oxidation is required for the respiration and proliferation of malignant glioma cells.* 2017. **19**(1): p. 43-54.
50. Strickland, M. and E.A. Stoll, *Metabolic Reprogramming in Glioma.* Frontiers in cell and developmental biology, 2017. **5**: p. 43-43.
51. Nduom, E.K., M. Weller, and A.B. Heimberger, *Immunosuppressive mechanisms in glioblastoma.* Neuro-Oncology, 2015. **17**(suppl_7): p. vii9-vii14.
52. Pyonteck, S.M., et al., *CSF-1R inhibition alters macrophage polarization and blocks glioma progression.* Nature medicine, 2013. **19**(10): p. 1264-1272.
53. Noy, R. and J.W. Pollard, *Tumor-associated macrophages: from mechanisms to therapy.* Immunity, 2014. **41**(1): p. 49-61.
54. Markovic, D.S., et al., *Gliomas induce and exploit microglial MT1-MMP expression for tumor expansion.* Proc Natl Acad Sci U S A, 2009. **106**(30): p. 12530-5.
55. Coniglio, S.J., et al., *Microglial stimulation of glioblastoma invasion involves epidermal growth factor receptor (EGFR) and colony stimulating factor 1 receptor (CSF-1R) signaling.* Mol Med, 2012. **18**(1): p. 519-27.
56. Greening, D.W., et al. *Exosomes and their roles in immune regulation and cancer*. in *Seminars in cell & developmental biology*. 2015. Elsevier.
57. Maas, S.L., et al., *Glioblastoma hijacks microglial gene expression to support tumor growth.* 2020. **17**: p. 1-18.
58. Burrell, R.A. and C.J.M.o. Swanton, *Tumour heterogeneity and the evolution of polyclonal drug resistance.* 2014. **8**(6): p. 1095-1111.
59. Garden, A., et al., *Outcome and patterns of failure following limited-volume irradiation for malignant astrocytomas.* Radiotherapy and oncology, 1991. **20**(2): p. 99-110.
60. Hess, C.F., et al., *Malignant glioma: patterns of failure following individually tailored limited volume irradiation.* Radiotherapy and Oncology, 1994. **30**(2): p. 146-149.
61. Stupp, R., et al., *Effects of radiotherapy with concomitant and adjuvant temozolomide versus radiotherapy alone on survival in glioblastoma in a randomised phase III study: 5-year analysis of the EORTC-NCIC trial.* Lancet Oncol, 2009. **10**(5): p. 459-66.
62. Nanegrungsunk, D., et al., *Current evidence of temozolomide and bevacizumab in treatment of gliomas.* Neurol Res, 2015. **37**(2): p. 167-83.
63. Ramos, P. and M. Bentires-Alj, *Mechanism-based cancer therapy: resistance to therapy, therapy for resistance.* Oncogene, 2015. **34**(28): p. 3617-26.
64. Franceschi, E., S. Minichillo, and A.A. Brandes, *Pharmacotherapy of Glioblastoma: Established Treatments and Emerging Concepts.* CNS Drugs, 2017. **31**(8): p. 675-684.
65. Hegi, M., et al., *MGMTGene Silencing and Benefit from Temozolomide in Glioblastoma.* The New England Journal of Medicine, 2005. **352**(10): p. 997-1003.
66. Chen, R., A. Cohen, and H. Colman, *Targeted Therapeutics in Patients With High-Grade Gliomas: Past, Present, and Future.* Current Treatment Options in Oncology, 2016. **17**(8): p. 1.
67. Cohen, A., S. Holmen, and H. Colman, *IDH1 and IDH2 Mutations in Gliomas.* Current Neurology and Neuroscience Reports, 2013. **13**(5): p. 345.
68. Chinot, O.L., et al., *Bevacizumab plus radiotherapy–temozolomide for newly diagnosed glioblastoma.* 2014. **370**(8): p. 709-722.
69. Herrlinger, U., et al., *Phase II Trial of Lomustine Plus Temozolomide Chemotherapy in Addition to Radiotherapy in Newly Diagnosed Glioblastoma: UKT-03.* Journal of clinical oncology, 2006. **24**(27): p. 4412-4417.

70. Nabors, L.B., et al., *Two cilengitide regimens in combination with standard treatment for patients with newly diagnosed glioblastoma and unmethylated MGMT gene promoter: results of the open-label, controlled, randomized phase II CORE study.* 2015. **17**(5): p. 708-717.
71. Taverna, P., et al., *Methoxyamine potentiates DNA single strand breaks and double strand breaks induced by temozolomide in colon cancer cells.* Mutation research - DNA repair, 2001. **485**(4): p. 269-281.
72. Narita, Y., *Bevacizumab for glioblastoma.* Therapeutics and Clinical Risk Management, 2015. **11**: p. 1759-1765.
73. Chinot, O., W. Wick, and T. Cloughesy, *Bevacizumab for newly diagnosed glioblastoma.* The New England Journal of Medicine, 2014. **370**(21): p. 2049-2049.
74. Chauffert, B., et al., *Randomized phase II trial of irinotecan and bevacizumab as neo-adjuvant and adjuvant to temozolomide-based chemoradiation compared with temozolomide-chemoradiation for unresectable glioblastoma: final results of the TEMAVIR study from ANOCEF†.* Ann Oncol, 2014. **25**(7): p. 1442-1447.
75. Sandmann, T., et al., *Patients With Proneural Glioblastoma May Derive Overall Survival Benefit From the Addition of Bevacizumab to First-Line Radiotherapy and Temozolomide: Retrospective Analysis of the AVAglio Trial.* Journal of clinical oncology, 2015. **33**(25): p. 2735-2744.
76. Piao, Y., et al., *Acquired resistance to anti-VEGF therapy in glioblastoma is associated with a mesenchymal transition.* Clinical cancer research, 2013. **19**(16): p. 4392-4403.
77. Sulman, E., et al., *Molecular predictors of outcome and response to bevacizumab (BEV) based on analysis of RTOG 0825, a phase III trial comparing chemoradiation (CRT) with and without BEV in patients with newly diagnosed glioblastoma (GBM).* Journal of clinical oncology, 2013. **31**(18_suppl): p. LBA2010-LBA2010.
78. de Groot, J.F., et al., *Tumor invasion after treatment of glioblastoma with bevacizumab: radiographic and pathologic correlation in humans and mice.* Neuro-oncology, 2010. **12**(3): p. 233-242.
79. Norden, A.D., et al., *Bevacizumab for recurrent malignant gliomas: efficacy, toxicity, and patterns of recurrence.* Neurology, 2008. **70**(10): p. 779-87.
80. Field, K.M., et al., *A randomized phase II study of carboplatin and bevacizumab in recurrent glioblastoma multiforme (CABARET).* Journal of Clinical Oncology, 2013. **31**(15_suppl): p. 2017-2017.
81. Heimberger, A.B., et al., *Prognostic effect of epidermal growth factor receptor and EGFRvIII in glioblastoma multiforme patients.* Clin Cancer Res, 2005. **11**(4): p. 1462-6.
82. Heimberger, A., et al., *Brain tumors in mice are susceptible to blockade of epidermal growth factor receptor (EGFR) with the oral, specific, EGFR-tyrosine kinase inhibitor ZD1839 (iressa).* Clinical cancer research, 2002. **8**(11): p. 3496-3502.
83. Learn, C., et al., *Resistance to tyrosine kinase inhibition by mutant epidermal growth factor receptor variant III contributes to the neoplastic phenotype of glioblastoma multiforme.* Clinical cancer research, 2004. **10**(9): p. 3216-3224.
84. Heimberger, A.B., et al., *Epidermal growth factor receptor VIII peptide vaccination is efficacious against established intracerebral tumors.* Clin Cancer Res, 2003. **9**(11): p. 4247-54.
85. Schuster, J., et al., *A phase II, multicenter trial of rindopepimut (CDX-110) in newly diagnosed glioblastoma: the ACT III study.* Neuro-Oncology, 2015. **17**(6): p. 854-861.
86. Patel, A., et al., *Single-cell RNA-seq highlights intratumoral heterogeneity in primary glioblastoma.* Science, 2014. **344**(6190): p. 1396-1401.
87. Snuderl, M., et al., *Mosaic Amplification of Multiple Receptor Tyrosine Kinase Genes in Glioblastoma.* Cancer cell, 2011. **20**(6): p. 810-817.

88. Szerlip, N., et al., *Intratumoral heterogeneity of receptor tyrosine kinases EGFR and PDGFRA amplification in glioblastoma defines subpopulations with distinct growth factor response.* Proceedings of the National Academy of Sciences of the United States of America, 2012. **109**(8): p. 3041-3046.
89. Lai, A., et al., *Evidence for Sequenced Molecular Evolution ofIDH1Mutant Glioblastoma From a Distinct Cell of Origin.* Journal of clinical oncology, 2011. **29**(34): p. 4482-4490.
90. Tateishi, K., et al., *Extreme Vulnerability of IDH1 Mutant Cancers to NAD+ Depletion.* Cancer Cell, 2015. **28**(6): p. 773-784.
91. Weller, M., et al., *Rindopepimut with temozolomide for patients with newly diagnosed, EGFRvIII-expressing glioblastoma (ACT IV): a randomised, double-blind, international phase 3 trial.* 2017. **18**(10): p. 1373-1385.
92. Reardon, D.A., et al., *Phase I/randomized phase II study of afatinib, an irreversible ErbB family blocker, with or without protracted temozolomide in adults with recurrent glioblastoma.* 2015. **17**(3): p. 430-439.
93. Sepúlveda-Sánchez, J.M., et al., *Phase II trial of dacomitinib, a pan–human EGFR tyrosine kinase inhibitor, in recurrent glioblastoma patients with EGFR amplification.* 2017. **19**(11): p. 1522-1531.
94. Neyns, B., et al., *Stratified phase II trial of cetuximab in patients with recurrent high-grade glioma.* 2009. **20**(9): p. 1596-1603.
95. Batchelor, T.T., et al., *Phase II study of cediranib, an oral pan–vascular endothelial growth factor receptor tyrosine kinase inhibitor, in patients with recurrent glioblastoma.* 2010. **28**(17): p. 2817.
96. Raizer, J., et al., *A phase II study of bevacizumab and erlotinib after radiation and temozolomide in MGMT unmethylated GBM patients.* 2016. **126**(1): p. 185-192.
97. Herrlinger, U., et al., *Bevacizumab plus irinotecan versus temozolomide in newly diagnosed O6-methylguanine–DNA methyltransferase nonmethylated glioblastoma: the randomized GLARIUS trial.* 2016. **34**(14): p. 1611-1619.
98. Field, K.M., et al., *Randomized phase 2 study of carboplatin and bevacizumab in recurrent glioblastoma.* Neuro-Oncology, 2015. **17**(11): p. 1504-1513.
99. Li, L., et al., *A phase II study of anti–epidermal growth factor receptor radioimmunotherapy in the treatment of glioblastoma multiforme.* 2010. **113**(2): p. 192-198.
100. Rich, J.N., et al., *Phase II trial of gefitinib in recurrent glioblastoma.* Journal of Clinical Oncology, 2004. **22**(1): p. 133-142.
101. Reardon, D.A., et al., *417PD - A Phase 2 Trial of the Multitargeted Kinase Inhibitor Lenvatinib (E7080) in Patients (PTS) with Recurrent Glioblastoma (GBM) And Disease Progression Following Prior Bevacizumab Treatment.* Annals of Oncology, 2012. **23**: p. ix146.
102. Kreisl, T., et al., *OT-12. A PHASE II TRIAL OF SUNITINIB IN THE TREATMENT OF RECURRENT GLIOBLASTOMA (GBM).* 2010. **12**(suppl_4).
103. Iwamoto, F.M., et al., *Phase II trial of pazopanib (GW786034), an oral multi-targeted angiogenesis inhibitor, for adults with recurrent glioblastoma (North American Brain Tumor Consortium Study 06-02).* 2010. **12**(8): p. 855-861.
104. Hatoum, A., R. Mohammed, and O. Zakieh, *The unique invasiveness of glioblastoma and possible drug targets on extracellular matrix.* Cancer Manag Res, 2019. **11**: p. 1843-1855.
105. Wang, M., et al., *The expression of matrix metalloproteinase-2 and -9 in human gliomas of different pathological grades.* Brain Tumor Pathol, 2003. **20**(2): p. 65-72.
106. Forsyth, P., et al., *Gelatinase-A (MMP-2), gelatinase-B (MMP-9) and membrane type matrix metalloproteinase-1 (MT1-MMP) are involved in different aspects of the pathophysiology of malignant gliomas.* 1999. **79**(11): p. 1828-1835.
107. Linder, S., C. Wiesner, and M. Himmel, *Degrading devices: invadosomes in proteolytic cell invasion.* Annu Rev Cell Dev Biol, 2011. **27**: p. 185-211.

108. Brandes, A.A., et al., *Recurrence pattern after temozolomide concomitant with and adjuvant to radiotherapy in newly diagnosed patients with glioblastoma: correlation with MGMT promoter methylation status.* 2009. **27**(8): p. 1275-1279.
109. Cuddapah, V.A., et al., *A neurocentric perspective on glioma invasion.* Nature reviews. Neuroscience, 2014. **15**(7): p. 455-465.
110. Glas, M., et al., *Residual tumor cells are unique cellular targets in glioblastoma.* Ann Neurol, 2010. **68**(2): p. 264-9.
111. Lim, Y.C., et al., *Increased sensitivity to ionizing radiation by targeting the homologous recombination pathway in glioma initiating cells.* Molecular oncology, 2014. **8**(8): p. 1603-1615.
112. Doan, P., et al., *Glioblastoma Multiforme Stem Cell Cycle Arrest by Alkylaminophenol Through the Modulation of EGFR and CSC Signaling Pathways.* Cells, 2020. **9**(3): p. 681.
113. Jung, J.-W., et al., *Ionising radiation induces changes associated with epithelial-mesenchymal transdifferentiation and increased cell motility of A549 lung epithelial cells.* European Journal of Cancer. **43**(7): p. 1214-1224.
114. Camphausen, K., et al., *Radiation therapy to a primary tumor accelerates metastatic growth in mice.* Cancer research, 2001. **61**(5): p. 2207-2211.
115. Araya, J., et al., *Ionizing radiation enhances matrix metalloproteinase-2 production in human lung epithelial cells.* American journal of physiology. Lung cellular and molecular physiology, 2001. **280**(1): p. L30-L38.
116. Qian, L.-W., et al., *Radiation-induced increase in invasive potential of human pancreatic cancer cells and its blockade by a matrix metalloproteinase inhibitor, CGS27023.* Clinical cancer research, 2002. **8**(4): p. 1223-1227.
117. Zhao, Y.O.M.S.W.M.E.C.R.W. and Y.O.M.S.W.M.E.C.W. Zhao, *Irradiation of rat tubule epithelial cells alters the expression of gene products associated with the synthesis and degradation of extracellular matrix.* International journal of radiation biology, 2000. **76**(3): p. 391-402.
118. Park, C.-M., et al., *Ionizing radiation enhances matrix metalloproteinase-2 secretion and invasion of glioma cells through Src/epidermal growth factor receptor-mediated p38/Akt and phosphatidylinositol 3-kinase/Akt signaling pathways.* Cancer research, 2006. **66**(17): p. 8511-8519.
119. Pei, J., et al., *Sublethal dose of irradiation enhances invasion of malignant glioma cells through p53-MMP 2 pathway in U87MG mouse brain tumor model.* Radiation oncology, 2015. **10**(1): p. 164.
120. Sawaya, R., et al., *Induction of tissue-type plasminogen activator and 72-kDa type-IV collagenase by ionizing radiation in rat astrocytes.* International journal of cancer, 1994. **56**(2): p. 214-218.
121. Stylli, S., A. Kaye, and P. Lock, *Invadopodia: At the cutting edge of tumour invasion.* Journal of clinical neuroscience, 2008. **15**(7): p. 725-737.
122. Kelly, T., et al., *Proteolysis of extracellular matrix by invadopodia facilitates human breast cancer cell invasion and is mediated by matrix metalloproteinases*. Vol. 16. 1998. 501-512.
123. Mader, C.C., et al., *An EGFR–Src–Arg–Cortactin Pathway Mediates Functional Maturation of Invadopodia and Breast Cancer Cell Invasion.* Cancer Research, 2011. **71**(5): p. 1730-1741.
124. Coopman, P.J., et al., *Phagocytosis of cross-linked gelatin matrix by human breast carcinoma cells correlates with their invasive capacity.* Clinical cancer research, 1998. **4**(2): p. 507-515.
125. Monsky, W.L., et al., *A potential marker protease of invasiveness, seprase, is localized on invadopodia of human malignant melanoma cells.* Cancer research, 1994. **54**(21): p. 5702-5710.
126. Clark, E.S., et al., *Cortactin is an essential regulator of matrix metalloproteinase secretion and extracellular matrix degradation in invadopodia.* Cancer Res, 2007. **67**(9): p. 4227-35.

127. Hayes, K.E., et al., *Ableson kinases negatively regulate invadopodia function and invasion in head and neck squamous cell carcinoma by inhibiting an HB-EGF autocrine loop.* Oncogene, 2013. **32**(40): p. 4766-4777.
128. Schoumacher, M., et al., *Actin, microtubules, and vimentin intermediate filaments cooperate for elongation of invadopodia.* The Journal of Cell Biology, 2010. **189**(3): p. 541-556.
129. Yamaguchi, H., *Pathological roles of invadopodia in cancer invasion and metastasis.* European Journal of Cell Biology, 2012. **91**(11-12): p. 902-907.
130. Gligorijevic, B., et al., *N-WASP-mediated invadopodium formation is involved in intravasation and lung metastasis of mammary tumors.* Journal of cell science, 2012. **125**(3): p. 724-734.
131. Sutoh, M., et al., *Invadopodia Formation by Bladder Tumor Cells.* Oncology Research Featuring Preclinical and Clinical Cancer Therapeutics, 2010. **19**(2): p. 85-92.
132. Yamamoto, H., et al., *Requirement for FBP17 in Invadopodia Formation by Invasive Bladder Tumor Cells.* The Journal of urology, 2011. **185**(5): p. 1930-1938.
133. Takkunen, M., et al., *Podosome-like structures of non-invasive carcinoma cells are replaced in epithelial-mesenchymal transition by actin comet-embedded invadopodia.* Journal of Cellular and Molecular Medicine, 2010. **14**(6b): p. 1569-1593.
134. Chen, W.T., *Proteolytic activity of specialized surface protrusions formed at rosette contact sites of transformed cells.* Journal of Experimental Zoology, 1989. **251**(2): p. 167-185.
135. Yamaguchi, H., et al., *Molecular mechanisms of invadopodium formation: the role of the N-WASP-Arp2/3 complex pathway and cofilin.* The Journal of cell biology, 2005. **168**(3): p. 441-452.
136. Linder, S., *The matrix corroded: podosomes and invadopodia in extracellular matrix degradation.* Trends Cell Biol, 2007. **17**(3): p. 107-17.
137. Murphy, D. and S. Courtneidge, *The 'ins' and 'outs' of podosomes and invadopodia: characteristics, formation and function.* Nature Reviews. Molecular Cell Biology, 2011. **12**(7): p. 413-426.
138. Jerrell, R.J. and A. Parekh, *Matrix rigidity differentially regulates invadopodia activity through ROCK1 and ROCK2.* Biomaterials, 2016. **84**: p. 119-129.
139. Artym, V.V., et al., *Dynamic Interactions of Cortactin and Membrane Type 1 Matrix Metalloproteinase at Invadopodia: Defining the Stages of Invadopodia Formation and Function.* Cancer Research, 2006. **66**(6): p. 3034-3043.
140. Beaty, B.T. and J. Condeelis, *Digging a little deeper: The stages of invadopodium formation and maturation.* European Journal of Cell Biology, 2014. **93**(10): p. 438-444.
141. Mandal, S., K.R. Johnson, and M.J. Wheelock, *TGF-β induces formation of F-actin cores and matrix degradation in human breast cancer cells via distinct signaling pathways.* Experimental Cell Research, 2008. **314**(19): p. 3478-3493.
142. Pignatelli, J., et al., *Hic-5 promotes invadopodia formation and invasion during TGF-β–induced epithelial–mesenchymal transition.* The Journal of Cell Biology, 2012. **197**(3): p. 421-437.
143. Rajadurai, C.V., et al., *Met receptor tyrosine kinase signals through a cortactin–Gab1 scaffold complex, to mediate invadopodia.* Journal of Cell Science, 2012. **125**(12): p. 2940-2953.
144. Díaz, B., et al., *Notch increases the shedding of HB-EGF by ADAM12 to potentiate invadopodia formation in hypoxia.* The Journal of Cell Biology, 2013. **201**(2): p. 279-292.
145. Tatin, F., et al., *A signalling cascade involving PKC, Src and Cdc42 regulates podosome assembly in cultured endothelial cells in response to phorbol ester.* J Cell Sci, 2006. **119**(Pt 4): p. 769-81.
146. Oikawa, T., et al., *Tks5-dependent formation of circumferential podosomes/invadopodia mediates cell-cell fusion.* The Journal of cell biology, 2012. **197**(4): p. 553-568.
147. Sharma, V., et al., *Tks5 and SHIP2 Regulate Invadopodium Maturation, but Not Initiation, in Breast Carcinoma Cells.* Current biology, 2013. **23**(21): p. 2079-2089.

148. Rysman, E., et al., *De novo lipogenesis protects cancer cells from free radicals and chemotherapeutics by promoting membrane lipid saturation.* 2010. **70**(20): p. 8117-8126.
149. Burger, K., et al., *Src-dependent Tks5 phosphorylation regulates invadopodia-associated invasion in prostate cancer cells.* The Prostate, 2014. **74**(2): p. 134-148.
150. Schoumacher, M., et al., *Actin, microtubules, and vimentin intermediate filaments cooperate for elongation of invadopodia.* The Journal of cell biology, 2010. **189**(3): p. 541-556.
151. Abram, C.L., et al., *The Adaptor Protein Fish Associates with Members of the ADAMs Family and Localizes to Podosomes of Src-transformed Cells.* Journal of Biological Chemistry, 2003. **278**(19): p. 16844-16851.
152. Ghersi, G., et al., *Regulation of Fibroblast Migration on Collagenous Matrix by a Cell Surface Peptidase Complex.* Journal of Biological Chemistry, 2002. **277**(32): p. 29231-29241.
153. Sakurai-Yageta, M., et al., *The interaction of IQGAP1 with the exocyst complex is required for tumor cell invasion downstream of Cdc42 and RhoA.* The Journal of Cell Biology, 2008. **181**(6): p. 985-998.
154. Steffen, A., et al., *MT1-MMP-Dependent Invasion Is Regulated by TI-VAMP/VAMP7.* Current Biology, 2008. **18**(12): p. 926-931.
155. Clark, E., et al., *Cortactin is an essential regulator of matrix metalloproteinase secretion and extracellular matrix degradation in invadopodia.* Cancer research, 2007. **67**(9): p. 4227-4235.
156. Leong, H., et al., *Invadopodia Are Required for Cancer Cell Extravasation and Are a Therapeutic Target for Metastasis.* Cell Reports, 2014. **8**(5): p. 1558-1570.
157. Stylli, S.S., A.H. Kaye, and P. Lock, *Invadopodia: at the cutting edge of tumour invasion.* J Clin Neurosci, 2008. **15**(7): p. 725-37.
158. Stylli, S.S., et al., *Prognostic significance of Tks5 expression in gliomas.* J Clin Neurosci, 2012. **19**(3): p. 436-42.
159. Stylli, S.S., *Expression of the adaptor protein Tks5 in human cancer: Prognostic potential.* Oncology Reports, 2014. **32**(3): p. 989.
160. Ni, Q.F., *Cortactin promotes colon cancer progression by regulating ERK pathway.* International journal of oncology, 2015. **47**(3): p. 1034.
161. Hwang, Y., K.-K. Park, and W.-Y. Chung, *Invadopodia formation in oral squamous cell carcinoma: The role of epidermal growth factor receptor signalling.* Archives of oral biology, 2012. **57**(4): p. 335-343.
162. Eckert, M., et al., *Twist1-Induced Invadopodia Formation Promotes Tumor Metastasis.* Cancer cell, 2011. **19**(3): p. 372-386.
163. Cemeus, C., et al., *Lovastatin enhances gefitinib activity in glioblastoma cells irrespective of EGFRvIII and PTEN status.* Journal of Neuro-Oncology, 2008. **90**(1): p. 9-17.
164. Learn, C.A., et al., *Resistance to tyrosine kinase inhibition by mutant epidermal growth factor receptor variant III contributes to the neoplastic phenotype of glioblastoma multiforme.* Clin Cancer Res, 2004. **10**(9): p. 3216-24.
165. Ma, H., et al., *The Efficacy of Erlotinib Versus Conventional Chemotherapy for Advanced Nonsmall-Cell Lung Cancer: A PRISMA-Compliant Systematic Review With Meta-Regression and Meta-Analysis.* Medicine, 2016. **95**(2): p. e2495-e2495.
166. Olson, J., et al., *The role of targeted therapies in the management of progressive glioblastoma.* Journal of Neuro-Oncology, 2014. **118**(3): p. 557-599.
167. Roy, R., J. Yang, and M. Moses, *Matrix Metalloproteinases As Novel Biomarker s and Potential Therapeutic Targets in Human Cancer.* Journal of clinical oncology, 2009. **27**(31): p. 5287-5297.
168. Betz, M., et al., *1.8-Å Crystal Structure of the Catalytic Domain of Human Neutrophil Collagenase (Matrix Metalloproteinase-8) Complexed with a Peptidomimetic Hydroxamate Primed-Side Inhibitor with a Distinct Selectivity Profile.* European Journal of Biochemistry, 1997. **247**(1): p. 356-363.

169. Winer, A., S. Adams, and P. Mignatti, *Matrix Metalloproteinase Inhibitors in Cancer Therapy: Turning Past Failures Into Future Successes.* Molecular cancer therapeutics, 2018. **17**(6): p. 1147-1155.
170. Gialeli, C., A.D. Theocharis, and N.K. Karamanos, *Roles of matrix metalloproteinases in cancer progression and their pharmacological targeting.* Febs j, 2011. **278**(1): p. 16-27.
171. Fleming, R.Y., et al., *Regulation of vascular endothelial growth factor expression in human colon carcinoma cells by activity of src kinase.* Surgery, 1997. **122**(2): p. 501-7.
172. Genda, T., et al., *Loss of cell-cell contact is induced by integrin-mediated cell-substratum adhesion in highly-motile and highly-metastatic hepatocellular carcinoma cells.* Lab Invest, 2000. **80**(3): p. 387-94.
173. Irby, R.B. and T.J. Yeatman, *Role of Src expression and activation in human cancer.* Oncogene, 2000. **19**: p. 5636.
174. Recchia, I., et al., *Pyrrolopyrimidine c-Src inhibitors reduce growth, adhesion, motility and invasion of prostate cancer cells in vitro.* 2003. **39**(13): p. 1927-1935.
175. Puls, L., M. Eadens, and W. Messersmith, *Current status of SRC inhibitors in solid tumor malignancies.* The oncologist, 2011. **16**(5): p. 566-578.
176. Kluger, H.M., *A phase II trial of dasatinib in advanced melanoma.* Journal of clinical oncology, 2009. **27**(15S): p. 9010.
177. Miller, A.A., et al., *A phase II study of dasatinib in patients with chemosensitive relapsed small cell lung cancer (Cancer and Leukemia Group B 30602).* J Thorac Oncol, 2010. **5**(3): p. 380-4.
178. Taylor, J., et al., *Phase 2 study of bosutinib, a Src inhibitor, in adults with recurrent glioblastoma.* Journal of Neuro-Oncology, 2015. **121**(3): p. 557-563.
179. Haura, E., et al., *Phase I/II Study of the Src Inhibitor Dasatinib in Combination With Erlotinib in Advanced Non–Small-Cell Lung Cancer.* Journal of clinical oncology, 2010. **28**(8): p. 1387-1394.
180. Mitchell, P., et al., *The exosome: a conserved eukaryotic RNA processing complex containing multiple 3'→ 5' exoribonucleases.* 1997. **91**(4): p. 457-466.
181. Emanueli, C., et al., *Exosomes and exosomal miRNAs in cardiovascular protection and repair.* 2015. **71**: p. 24-30.
182. Sahoo, S. and D.W.J.C.r. Losordo, *Exosomes and cardiac repair after myocardial infarction.* 2014. **114**(2): p. 333-344.
183. Azmi, A.S., et al., *Exosomes in cancer development, metastasis, and drug resistance: a comprehensive review.* 2013. **32**(3): p. 623-642.
184. Zhang, X., et al., *GOLPH3 promotes glioblastoma cell migration and invasion via the mTOR-YB1 pathway in vitro.* Mol Carcinog, 2015. **54**(11): p. 1252-63.
185. Valadi, H., et al., *Exosome-mediated transfer of mRNAs and microRNAs is a novel mechanism of genetic exchange between cells.* Nature Cell Biology, 2007. **9**(6): p. 654-659.
186. Josson, S., et al., *Stromal fibroblast-derived miR-409 promotes epithelial-to-mesenchymal transition and prostate tumorigenesis.* Oncogene, 2014. **34**: p. 2690.
187. Tadokoro, H., et al., *Exosomes Derived from Hypoxic Leukemia Cells Enhance Tube Formation in Endothelial Cells.* The Journal of Biological Chemistry, 2013. **288**(48): p. 34343-34351.
188. Chen, W.-x., et al., *Exosomes from Drug-Resistant Breast Cancer Cells Transmit Chemoresistance by a Horizontal Transfer of MicroRNAs.* PLoS ONE, 2014. **9**(4): p. e95240.
189. Corcoran, C., et al., *Docetaxel-resistance in prostate cancer: evaluating associated phenotypic changes and potential for resistance transfer via exosomes.* PLoS One, 2012. **7**(12): p. e50999.
190. Lv, M.-m., et al., *Exosomes mediate drug resistance transfer in MCF-7 breast cancer cells and a probable mechanism is delivery of P-glycoprotein.* Tumor Biology, 2014. **35**(11): p. 10773-10779.

191. Chiarugi, P. and P.J.C.l. Cirri, *Metabolic exchanges within tumor microenvironment.* 2016. **380**(1): p. 272-280.
192. Cocucci, E., G. Racchetti, and J. Meldolesi, *Shedding microvesicles: artefacts no more.* Trends Cell Biol, 2009. **19**(2): p. 43-51.
193. Bergsmedh, A., et al., *Horizontal transfer of oncogenes by uptake of apoptotic bodies.* Proceedings of the National Academy of Sciences of the United States of America, 2001. **98**(11): p. 6407-6411.
194. Kowal, J., et al., *Proteomic comparison defines novel markers to characterize heterogeneous populations of extracellular vesicle subtypes.* Proceedings of the National Academy of Sciences, 2016. **113**(8): p. E968-E977.
195. Zhang, H., et al., *Identification of distinct nanoparticles and subsets of extracellular vesicles by asymmetric flow field-flow fractionation.* Nature cell biology, 2018. **20**(3): p. 332.
196. Witwer, K.W., et al., *Minimal information for studies of extracellular vesicles 2018 (MISEV2018): a position statement of the International Society for Extracellular Vesicles and update of the MISEV2014 guidelines AU - Théry, Clotilde.* Journal of Extracellular Vesicles, 2018. **7**(1): p. 1535750.
197. Akers, J.C., et al., *Biogenesis of extracellular vesicles (EV): exosomes, microvesicles, retrovirus-like vesicles, and apoptotic bodies.* Journal of neuro-oncology, 2013. **113**(1): p. 1-11.
198. Hugel, B., et al., *Membrane Microparticles: Two Sides of the Coin.* Physiology, 2005. **20**(1): p. 22-27.
199. Muralidharan-Chari, V., et al., *ARF6-regulated shedding of tumor cell-derived plasma membrane microvesicles.* Current biology : CB, 2009. **19**(22): p. 1875-1885.
200. Li, B., et al., *RhoA triggers a specific signaling pathway that generates transforming microvesicles in cancer cells.* Oncogene, 2012. **31**: p. 4740.
201. Antonyak, M.A., et al., *Cancer cell-derived microvesicles induce transformation by transferring tissue transglutaminase and fibronectin to recipient cells.* Proceedings of the National Academy of Sciences, 2011. **108**(12): p. 4852-4857.
202. Colombo, M., et al., *Analysis of ESCRT functions in exosome biogenesis, composition and secretion highlights the heterogeneity of extracellular vesicles.* Journal of cell science, 2013. **126**(24): p. 5553-5565.
203. Hurley, J.H.J.T.E.j., *ESCRT s are everywhere.* 2015. **34**(19): p. 2398-2407.
204. Nabhan, J.F., et al., *Formation and release of arrestin domain-containing protein 1-mediated microvesicles (ARMMs) at plasma membrane by recruitment of TSG101 protein.* 2012. **109**(11): p. 4146-4151.
205. Wehman, Ann M., et al., *The P4-ATPase TAT-5 Inhibits the Budding of Extracellular Vesicles in C. elegans Embryos.* Current Biology, 2011. **21**(23): p. 1951-1959.
206. Stuffers, S., et al., *Multivesicular endosome biogenesis in the absence of ESCRTs.* 2009. **10**(7): p. 925-937.
207. Trajkovic, K., et al., *Ceramide triggers budding of exosome vesicles into multivesicular endosomes.* 2008. **319**(5867): p. 1244-1247.
208. Bianco, F., et al., *Acid sphingomyelinase activity triggers microparticle release from glial cells.* 2009. **28**(8): p. 1043-1054.
209. Antonucci, F., et al., *Microvesicles released from microglia stimulate synaptic activity via enhanced sphingolipid metabolism.* 2012. **31**(5): p. 1231-1240.
210. Ostrowski, M., et al., *Rab27a and Rab27b control different steps of the exosome secretion pathway.* Nat Cell Biol, 2010. **12**(1): p. 19-30; sup pp 1-13.
211. Desnos, C., et al., *Rab27A and its effector MyRIP link secretory granules to F-actin and control their motion towards release sites.* 2003. **163**(3): p. 559-570.
212. Mizuno, K., et al., *Rab27b regulates mast cell granule dynamics and secretion.* 2007. **8**(7): p. 883-892.

213. Savina, A., M. Vidal, and M.I.J.J.o.c.s. Colombo, *The exosome pathway in K562 cells is regulated by Rab11.* 2002. **115**(12): p. 2505-2515.
214. Korkut, C., et al., *Regulation of postsynaptic retrograde signaling by presynaptic exosome release.* 2013. **77**(6): p. 1039-1046.
215. Hsu, C., et al., *Regulation of exosome secretion by Rab35 and its GTPase-activating proteins TBC1D10A–C.* 2010. **189**(2): p. 223-232.
216. Sato, M., et al., *Regulation of endocytic recycling by C. elegans Rab35 and its regulator RME-4, a coated-pit protein.* 2008. **27**(8): p. 1183-1196.
217. Vadlamudi, R.K., et al., *Evidence of Rab3A expression, regulation of vesicle trafficking, and cellular secretion in response to heregulin in mammary epithelial cells.* 2000. **20**(23): p. 9092-9101.
218. Ng, E.L. and B.L.J.B.r.r. Tang, *Rab GTPases and their roles in brain neurons and glia.* 2008. **58**(1): p. 236-246.
219. Rao, S.K., et al., *Identification of SNAREs involved in synaptotagmin VII-regulated lysosomal exocytosis.* 2004. **279**(19): p. 20471-20479.
220. Gross, J., et al., *Active Wnt proteins are secreted on exosomes.* Nature Cell Biology, 2012. **14**(10): p. 1036-1045.
221. Pelham, H.R.J.T.i.c.b., *SNAREs and the specificity of membrane fusion.* 2001. **11**(3): p. 99-101.
222. Jahn, R. and D.J.N. Fasshauer, *Molecular machines governing exocytosis of synaptic vesicles.* 2012. **490**(7419): p. 201-207.
223. Koles, K. and V.J.C.l. Budnik, *Exosomes go with the Wnt.* 2012. **2**(3): p. 169-173.
224. Ulloa, F., et al., *Blockade of the SNARE protein syntaxin 1 inhibits glioblastoma tumor growth.* 2015. **10**(3): p. e0119707.
225. Sorkin, R., et al., *Nanomechanics of extracellular vesicles reveals vesiculation pathways.* 2018. **14**(39): p. 1801650.
226. Mittelbrunn, M., M. Vicente-Manzanares, and F.J.T. Sánchez-Madrid, *Organizing polarized delivery of exosomes at synapses.* 2015. **16**(4): p. 327-337.
227. Granger, E., et al. *The role of the cytoskeleton and molecular motors in endosomal dynamics*. in *Seminars in cell & developmental biology*. 2014. Elsevier.
228. Choi, D., et al., *The impact of oncogenic EGFRvIII on the proteome of extracellular vesicles released from glioblastoma cells.* Molecular & Cellular Proteomics, 2018. **17**(10): p. 1948-1964.
229. Hoshino, D., et al., *Exosome secretion is enhanced by invadopodia and drives invasive behavior.* Cell reports, 2013. **5**(5): p. 10.1016/j.celrep.2013.10.050.
230. Gangoda, L. and S. Mathivanan, *Cortactin enhances exosome secretion without altering cargo.* The Journal of Cell Biology, 2016. **214**(2): p. 129-131.
231. Mathivanan, S., H. Ji, and R.J.J.J.o.p. Simpson, *Exosomes: extracellular organelles important in intercellular communication.* 2010. **73**(10): p. 1907-1920.
232. Hoshino, A., et al., *Tumour exosome integrins determine organotropic metastasis.* Nature, 2015. **527**(7578): p. 329-335.
233. Christianson, H., et al., *Cancer cell exosomes depend on cell-surface heparan sulfate proteoglycans for their internalization and functional activity.* Proceedings of the National Academy of Sciences of the United States of America, 2013. **110**(43): p. 17380-17385.
234. Atai, N., et al., *Heparin blocks transfer of extracellular vesicles between donor and recipient cells.* Journal of Neuro-Oncology, 2013. **115**(3): p. 343-351.
235. Lawson, C., et al., *Microvesicles and exosomes: new players in metabolic and cardiovascular disease.* Journal of Endocrinology, 2016. **228**(2): p. R57-R71.
236. Bobrie, A., et al., *Diverse subpopulations of vesicles secreted by different intracellular mechanisms are present in exosome preparations obtained by differential ultracentrifugation.* Journal of Extracellular Vesicles, 2012. **1**(1): p. 18397.

237. Colombo, M., G. Raposo, and C. Théry, *Biogenesis, Secretion, and Intercellular Interactions of Exosomes and Other Extracellular Vesicles.* Annual Review of Cell and Developmental Biology, 2014. **30**(1): p. 255-289.
238. Dozio, V. and J.-C. Sanchez, *Characterisation of extracellular vesicle-subsets derived from brain endothelial cells and analysis of their protein cargo modulation after TNF exposure.* Journal of Extracellular Vesicles, 2017. **6**(1): p. 1302705.
239. Théry, C., *Exosomes: composition, biogenesis and function.* Nature Reviews. Immunology, 2002. **2**(8): p. 569.
240. Menck, K., et al., *Characterisation of tumour-derived microvesicles in cancer patients' blood and correlation with clinical outcome.* Journal of Extracellular Vesicles, 2017. **6**(1): p. 1340745.
241. Willms, E., et al., *Cells release subpopulations of exosomes with distinct molecular and biological properties.* Scientific Reports, 2016. **6**(1): p. 22519.
242. Yáñez-Mó, M., et al., *Biological properties of extracellular vesicles and their physiological functions.* Journal of extracellular vesicles, 2015. **4**(1): p. 27066.
243. Skliar, M., et al., *Membrane Proteins Significantly Restrict Exosome Mobility.* 2017: p. 196691.
244. Kim, D.-K., et al., *EVpedia: a community web portal for extracellular vesicles research.* 2015. **31**(6): p. 933-939.
245. Pathan, M., et al., *Vesiclepedia 2019: a compendium of RNA, proteins, lipids and metabolites in extracellular vesicles.* Nucleic Acids Research, 2018. **47**(D1): p. D516-D519.
246. Keerthikumar, S., et al., *ExoCarta: a web-based compendium of exosomal cargo.* 2016. **428**(4): p. 688-692.
247. Whitehead, C.A., et al., *Cancer exosomes in cerebrospinal fluid.* 2017. **6**(8): p. s1352-s1370.
248. Goldie, B., et al., *Activity-associated miRNA are packaged in Map1b-enriched exosomes released from depolarized neurons.* Nucleic acids research, 2014. **42**(14): p. 9195-9208.
249. Raiborg, C. and H.J.N. Stenmark, *The ESCRT machinery in endosomal sorting of ubiquitylated membrane proteins.* 2009. **458**(7237): p. 445-452.
250. Batagov, A.O. and I.V. Kurochkin, *Exosomes secreted by human cells transport largely mRNA fragments that are enriched in the 3'-untranslated regions.* Biol Direct, 2013. **8**: p. 12.
251. Koppers-Lalic, D., et al., *Nontemplated nucleotide additions distinguish the small RNA composition in cells from exosomes.* 2014. **8**(6): p. 1649-1658.
252. Zomer, A., et al., *Exosomes.* Communicative & integrative biology, 2010. **3**(5): p. 447-450.
253. Kalra, H., G.P.C. Drummen, and S. Mathivanan, *Focus on Extracellular Vesicles: Introducing the Next Small Big Thing.* International Journal of Molecular Sciences, 2016. **17**(2): p. 170.
254. D'Agostino, S., et al., *Membrane vesicles shed by oligodendroglioma cells induce neuronal apoptosis.* 2006. **29**(5): p. 1075-1085.
255. Al Nedawi, K., et al., *Intercellular transfer of the oncogenic receptor EGFRvIII by microvesicles derived from tumour cells.* Nature Cell Biology, 2008. **10**(5): p. 619-624.
256. Svensson, K.J., et al., *Hypoxia triggers a proangiogenic pathway involving cancer cell microvesicles and PAR-2–mediated heparin-binding EGF signaling in endothelial cells.* Proceedings of the National Academy of Sciences, 2011. **108**(32): p. 13147-13152.
257. Arscott, W.T., et al., *Ionizing radiation and glioblastoma exosomes: implications in tumor biology and cell migration.* Translational oncology, 2013. **6**(6): p. 638-648.
258. Kucharzewska, P., et al., *Exosomes reflect the hypoxic status of glioma cells and mediate hypoxia-dependent activation of vascular cells during tumor development.* Proceedings of the National Academy of Sciences, 2013. **110**(18): p. 7312-7317.
259. Sharghi-Namini, S., et al., *Dll4-containing exosomes induce capillary sprout retraction in a 3D microenvironment.* 2014. **4**(1): p. 1-8.
260. van der Vos, K.E., et al., *Directly visualized glioblastoma-derived extracellular vesicles transfer RNA to microglia/macrophages in the brain.* Neuro-oncology, 2015. **18**(1): p. 58-69.

261. Zhang, L., et al., *Microenvironment-induced PTEN loss by exosomal microRNA primes brain metastasis outgrowth.* 2015. **527**(7576): p. 100-104.
262. Setti, M., et al., *Extracellular vesicle-mediated transfer of CLIC1 protein is a novel mechanism for the regulation of glioblastoma growth.* 2015. **6**(31): p. 31413.
263. Ricklefs, F., et al., *Extracellular vesicles from high-grade glioma exchange diverse pro-oncogenic signals that maintain intratumoral heterogeneity.* 2016. **76**(10): p. 2876-2881.
264. Pinet, S., et al., *TrkB-containing exosomes promote the transfer of glioblastoma aggressiveness to YKL-40-inactivated glioblastoma cells.* Oncotarget, 2016. **7**(31): p. 50349.
265. Lang, H., et al., *Glioma cells promote angiogenesis through the release of exosomes containing long non-coding RNA POU3F3.* Eur Rev Med Pharmacol Sci, 2017. **21**(5): p. 959-72.
266. Lang, H.-L., et al., *Glioma cells enhance angiogenesis and inhibit endothelial cell apoptosis through the release of exosomes that contain long non-coding RNA CCAT2.* Oncology reports, 2017. **38**(2): p. 785-798.
267. Sun, X., et al., *Glioma stem cells-derived exosomes promote the angiogenic ability of endothelial cells through miR-21/VEGF signal.* Oncotarget, 2017. **8**(22): p. 36137.
268. Figueroa, J., et al., *Exosomes from glioma-associated mesenchymal stem cells increase the tumorigenicity of glioma stem-like cells via transfer of miR-1587.* Cancer research, 2017. **77**(21): p. 5808-5819.
269. Kore, R.A., et al., *Hypoxia-derived exosomes induce putative altered pathways in biosynthesis and ion regulatory channels in glioblastoma cells.* Biochemistry and biophysics reports, 2018. **14**: p. 104-113.
270. Hallal, S., et al., *Extracellular vesicles released by glioblastoma cells stimulate normal astrocytes to acquire a tumor-supportive phenotype via p53 and MYC signaling pathways.* 2019. **56**(6): p. 4566-4581.
271. Taheri, B., et al., *C6 glioma-derived microvesicles stimulate the proliferative and metastatic gene expression of normal astrocytes.* Neuroscience letters, 2018. **685**: p. 173-178.
272. Zhao, M., et al., *Expression profiles and potential functions of circular RNAs in extracellular vesicles isolated from radioresistant glioma cells.* 2019. **41**(3): p. 1893-1900.
273. Kreger, B.T., et al., *Microvesicle cargo and function changes upon induction of cellular transformation.* Journal of Biological Chemistry, 2016. **291**(38): p. 19774-19785.
274. Di Vizio, D., et al., *Oncosome formation in prostate cancer: association with a region of frequent chromosomal deletion in metastatic disease.* Cancer research, 2009. **69**(13): p. 5601-5609.
275. Graner, M.W., et al., *Proteomic and immunologic analyses of brain tumor exosomes.* The FASEB Journal, 2009. **23**(5): p. 1541-1557.
276. Jin, H., et al., *Exosomal zinc transporter ZIP4 promotes cancer growth and is a novel diagnostic biomarker for pancreatic cancer.* Cancer science, 2018. **109**(9): p. 2946.
277. Hosseini-Beheshti, E., et al., *Exosomes confer pro-survival signals to alter the phenotype of prostate cells in their surrounding environment.* Oncotarget, 2016. **7**(12): p. 14639-14658.
278. Takasugi, M., et al., *Small extracellular vesicles secreted from senescent cells promote cancer cell proliferation through EphA2.* Nature Communications, 2017. **8**: p. 15729.
279. Nabet, B.Y., et al., *Exosome RNA unshielding couples stromal activation to pattern recognition receptor signaling in cancer.* Cell, 2017. **170**(2): p. 352-366. e13.
280. Webber, J., et al., *Cancer exosomes trigger fibroblast to myofibroblast differentiation.* Cancer research, 2010. **70**(23): p. 9621-9630.
281. Hao, S., et al., *Epigenetic transfer of metastatic activity by uptake of highly metastatic B16 melanoma cell-released exosomes.* Exp Oncol, 2006. **28**(2): p. 126-131.
282. Chen, L., et al., *HCC-derived exosomes elicit HCC progression and recurrence by epithelial-mesenchymal transition through MAPK/ERK signalling pathway.* Cell death & disease, 2018. **9**(5): p. 513.

283. Costa-Silva, B., et al., *Pancreatic cancer exosomes initiate pre-metastatic niche formation in the liver.* Nature cell biology, 2015. **17**(6): p. 816.
284. Webber, J.P., et al., *Differentiation of tumour-promoting stromal myofibroblasts by cancer exosomes.* Oncogene, 2015. **34**(3): p. 290.
285. Gross, J.C., et al., *Active Wnt proteins are secreted on exosomes.* Nature cell biology, 2012. **14**(10): p. 1036.
286. Menck, K., et al., *Induction and transport of Wnt 5a during macrophage-induced malignant invasion is mediated by two types of extracellular vesicles.* Oncotarget, 2013. **4**(11): p. 2057.
287. Jeppesen, D.K., et al., *Quantitative proteomics of fractionated membrane and lumen exosome proteins from isogenic metastatic and nonmetastatic bladder cancer cells reveal differential expression of EMT factors.* Proteomics, 2014. **14**(6): p. 699-712.
288. Felicetti, F., et al., *Caveolin-1 tumor-promoting role in human melanoma.* International journal of cancer, 2009. **125**(7): p. 1514-1522.
289. Luga, V., et al., *Exosomes mediate stromal mobilization of autocrine Wnt-PCP signaling in breast cancer cell migration.* Cell, 2012. **151**(7): p. 1542-1556.
290. Raimondo, S., et al., *Chronic myeloid leukemia-derived exosomes promote tumor growth through an autocrine mechanism.* Cell Communication and Signaling, 2015. **13**(1): p. 8.
291. Yang, M., et al., *Microvesicles secreted by macrophages shuttle invasion-potentiating microRNAs into breast cancer cells.* Molecular Cancer, 2011. **10**: p. 117-117.
292. Singh, R., et al., *Exosome-mediated transfer of miR-10b promotes cell invasion in breast cancer.* Molecular cancer, 2014. **13**(1): p. 256.
293. Wang, M., et al., *Deregulated microRNAs in gastric cancer tissue-derived mesenchymal stem cells: novel biomarkers and a mechanism for gastric cancer.* British journal of cancer, 2014. **110**(5): p. 1199-1210.
294. Cheng, W.-C., et al., *RAB27B-activated secretion of stem-like tumor exosomes delivers the biomarker microRNA-146a-5p, which promotes tumorigenesis and associates with an immunosuppressive tumor microenvironment in colorectal cancer.* International Journal of Cancer. **0**(ja).
295. Mu, W., S. Rana, and M. Zöller, *Host matrix modulation by tumor exosomes promotes motility and invasiveness.* Neoplasia, 2013. **15**(8): p. 875-IN4.
296. Nawaz, M., et al., *Extracellular Vesicles and Matrix Remodeling Enzymes: The Emerging Roles in Extracellular Matrix Remodeling, Progression of Diseases and Tissue Repair*. Vol. 7. 2018.
297. Braundmeier, A.G., et al., *EMMPRIN is secreted by human uterine epithelial cells in microvesicles and stimulates metalloproteinase production by human uterine fibroblast cells.* Reproductive sciences (Thousand Oaks, Calif.), 2012. **19**(12): p. 1292-1301.
298. DOLO, V., et al., *Shed Membrane Vesicles and Selective Localization of Gelatinases and MMP-9/TIMP-1 Complexes.* Annals of the New York Academy of Sciences, 1999. **878**(1): p. 497-499.
299. Yokoi, A., et al., *Malignant extracellular vesicles carrying MMP1 mRNA facilitate peritoneal dissemination in ovarian cancer.* Nature communications, 2017. **8**: p. 14470.
300. Chu, H., et al., *Functional expression of CXC chemokine recepter-4 mediates the secretion of matrix metalloproteinases from mouse hepatocarcinoma cell lines with different lymphatic metastasis ability.* The international journal of biochemistry & cell biology, 2007. **39**(1): p. 197-205.
301. Li, M., et al., *Horizontal transfer of exosomal CXCR4 promotes murine hepatocarcinoma cell migration, invasion and lymphangiogenesis.* Gene, 2018. **676**: p. 101-109.
302. Hakulinen, J., et al., *Secretion of active membrane type 1 matrix metalloproteinase (MMP-14) into extracellular space in microvesicular exosomes.* Journal of Cellular Biochemistry, 2008. **105**(5): p. 1211-1218.

303. Park, J.E., et al., *Hypoxic tumor cell modulates its microenvironment to enhance angiogenic and metastatic potential by secretion of proteins and exosomes.* Molecular & cellular proteomics, 2010. **9**(6): p. 1085-1099.
304. Teng, X., et al., *Mesenchymal Stem Cell-Derived Exosomes Improve the Microenvironment of Infarcted Myocardium Contributing to Angiogenesis and Anti-Inflammation.* Cell Physiol Biochem, 2015. **37**(6): p. 2415-24.
305. King, H.W., M.Z. Michael, and J.M. Gleadle, *Hypoxic enhancement of exosome release by breast cancer cells.* BMC cancer, 2012. **12**(1): p. 421.
306. Wang, T., et al., *Hypoxia-inducible factors and RAB22A mediate formation of microvesicles that stimulate breast cancer invasion and metastasis.* Proceedings of the National Academy of Sciences of the United States of America, 2014. **111**(31): p. E3234-E3242.
307. Taraboletti, G., et al., *Shedding of the Matrix Metalloproteinases MMP-2, MMP-9, and MT1-MMP as Membrane Vesicle-Associated Components by Endothelial Cells.* The American Journal of Pathology, 2002. **160**(2): p. 673-680.
308. Al-Nedawi, K., et al., *Endothelial expression of autocrine VEGF upon the uptake of tumor-derived microvesicles containing oncogenic EGFR.* Proceedings of the National Academy of Sciences, 2009. **106**(10): p. 3794-3799.
309. Rabinovich, G.A., D. Gabrilovich, and E.M. Sotomayor, *Immunosuppressive strategies that are mediated by tumor cells.* Annual review of immunology, 2007. **25**: p. 267-296.
310. Sumida, T., et al., *Activated β-catenin in Foxp3+ regulatory T cells links inflammatory environments to autoimmunity.* Nature immunology, 2018. **19**(12): p. 1391.
311. Wang, Y., et al., *Regulation of PD-L1: Emerging Routes for Targeting Tumor Immune Evasion.* Frontiers in pharmacology, 2018. **9**: p. 536-536.
312. Chen, G., et al., *Exosomal PD-L1 contributes to immunosuppression and is associated with anti-PD-1 response.* Nature, 2018. **560**(7718): p. 382-386.
313. Ricklefs, F.L., et al., *Immune evasion mediated by PD-L1 on glioblastoma-derived extracellular vesicles.* Science Advances, 2018. **4**(3): p. eaar2766.
314. Theodoraki, M.-N., et al., *Clinical significance of PD-L1+ exosomes in plasma of head and neck cancer patients.* Clinical cancer research, 2018. **24**(4): p. 896-905.
315. Wieckowski, E.U., et al., *Tumor-derived microvesicles promote regulatory T cell expansion and induce apoptosis in tumor-reactive activated CD8+ T lymphocytes.* The Journal of Immunology, 2009. **183**(6): p. 3720-3730.
316. Fabbri, M., et al., *MicroRNAs bind to Toll-like receptors to induce prometastatic inflammatory response.* Proceedings of the National Academy of Sciences, 2012. **109**(31): p. E2110-E2116.
317. Ciravolo, V., et al., *Potential role of HER2-overexpressing exosomes in countering trastuzumab-based therapy.* Journal of cellular physiology, 2012. **227**(2): p. 658-667.
318. Nanayakkara, A.K., et al., *Targeted inhibitors of P-glycoprotein increase chemotherapeutic-induced mortality of multidrug resistant tumor cells.* Scientific reports, 2018. **8**(1): p. 967.
319. Gong, J., et al., *Microparticles and their emerging role in cancer multidrug resistance.* Cancer treatment reviews, 2012. **38**(3): p. 226-234.
320. Safaei, R., et al., *Abnormal lysosomal trafficking and enhanced exosomal export of cisplatin in drug-resistant human ovarian carcinoma cells.* 2005. **4**(10): p. 1595-1604.
321. Federici, C., et al., *Exosome release and low pH belong to a framework of resistance of human melanoma cells to cisplatin.* 2014. **9**(2): p. e88193.
322. Shedden, K., et al., *Expulsion of small molecules in vesicles shed by cancer cells: association with gene expression and chemosensitivity profiles.* Cancer research, 2003. **63**(15): p. 4331-4337.
323. Witwer, K.W., et al., *Standardization of sample collection, isolation and analysis methods in extracellular vesicle research.* 2013. **2**(1): p. 20360.

324. Lässer, C., et al., *Human saliva, plasma and breast milk exosomes contain RNA: uptake by macrophages.* 2011. **9**(1): p. 1-8.
325. Chiasserini, D., et al., *Proteomic analysis of cerebrospinal fluid extracellular vesicles: a comprehensive dataset.* 2014. **106**: p. 191-204.
326. Weber, M., et al., *Diagnostic performance of spectroscopic and perfusion MRI for distinction of brain tumors.* 2006. **66**(12): p. 1899-1906.
327. Ricklefs, F.L., et al., *Imaging flow cytometry facilitates multiparametric characterization of extracellular vesicles in malignant brain tumours.* Journal of extracellular vesicles, 2019. **8**(1): p. 1588555-1588555.
328. Osti, D., et al., *Clinical significance of extracellular vesicles in plasma from glioblastoma patients.* Clinical Cancer Research, 2019. **25**(1): p. 266-276.
329. Morishita, M., et al., *Quantitative Analysis of Tissue Distribution of the B16BL6-Derived Exosomes Using a Streptavidin-Lactadherin Fusion Protein and Iodine-125-Labeled Biotin Derivative After Intravenous Injection in Mice.* Journal of pharmaceutical sciences, 2015. **104**(2): p. 705-713.
330. Hallal, S., et al., *Extracellular Vesicles from Neurosurgical Aspirates Identifies Chaperonin Containing TCP1 Subunit 6A as a Potential Glioblastoma Biomarker with Prognostic Significance.* Proteomics, 2019. **19**(1-2): p. 1800157.
331. Chandran, V.I., et al., *Ultrasensitive immunoprofiling of plasma extracellular vesicles identifies syndecan-1 as a potential tool for minimally invasive diagnosis of glioma.* Clinical Cancer Research, 2019: p. clincanres. 2946.2018.
332. Chen, W.W., et al., *BEAMing and droplet digital PCR analysis of mutant IDH1 mRNA in glioma patient serum and cerebrospinal fluid extracellular vesicles.* Molecular Therapy-Nucleic Acids, 2013. **2**: p. e109.
333. Akers, J.C., et al., *A cerebrospinal fluid microRNA signature as biomarker for glioblastoma.* Oncotarget, 2017. **8**(40): p. 68769.
334. Zeng, A., et al., *Exosomal transfer of miR-151a enhances chemosensitivity to temozolomide in drug-resistant glioblastoma.* Cancer letters, 2018. **436**: p. 10-21.
335. Barretina, J., et al., *The Cancer Cell Line Encyclopedia enables predictive modelling of anticancer drug sensitivity.* Nature, 2012. **483**(7391): p. 603-7.
336. Patil, V., J. Pal, and K. Somasundaram, *Elucidating the cancer-specific genetic alteration spectrum of glioblastoma derived cell lines from whole exome and RNA sequencing*. Oncotarget, 2015. **6**(41): p. 43452-43471.
337. Filipe, V., A. Hawe, and W.J.P.r. Jiskoot, *Critical evaluation of Nanoparticle Tracking Analysis (NTA) by NanoSight for the measurement of nanoparticles and protein aggregates.* 2010. **27**(5): p. 796-810.
338. Cox, J., et al., *Andromeda: a peptide search engine integrated into the MaxQuant environment.* J Proteome Res, 2011. **10**(4): p. 1794-805.
339. Tyanova, S., et al., *The Perseus computational platform for comprehensive analysis of (prote) omics data.* 2016. **13**(9): p. 731.
340. Pathan, M., et al., *FunRich: An open access standalone functional enrichment and interaction network analysis tool.* Proteomics, 2015. **15**(15): p. 2597-601.
341. Mi, H., et al., *Large-scale gene function analysis with the PANTHER classification system.* Nature protocols, 2013. **8**(8): p. 1551-1566.
342. Szklarczyk, D., et al., *STRING v11: protein-protein association networks with increased coverage, supporting functional discovery in genome-wide experimental datasets.* Nucleic acids research, 2019. **47**(D1): p. D607-D613.
343. Velásquez, C., et al., *Molecular and Clinical Insights into the Invasive Capacity of Glioblastoma Cells.* Journal of oncology, 2019. **2019**: p. 1740763-1740763.
344. Sellers, W., *A Blueprint for Advancing Genetics-Based Cancer Therapy.* Cell, 2011. **147**(1): p. 26-31.

345. Vilalta, M., M. Rafat, and E.E. Graves, *Effects of radiation on metastasis and tumor cell migration.* Cellular and molecular life sciences : CMLS, 2016. **73**(16): p. 2999-3007.
346. Johnson, B.E., et al., *Mutational analysis reveals the origin and therapy-driven evolution of recurrent glioma.* Science (New York, N.Y.), 2014. **343**(6167): p. 189-193.
347. Vanderbeek, A.M., et al., *The clinical trials landscape for glioblastoma: is it adequate to develop new treatments?* 2018. **20**(8): p. 1034-1043.
348. Zanders, E.D., F. Svensson, and D.S. Bailey, *Therapy for glioblastoma: is it working?* Drug Discovery Today, 2019. **24**(5): p. 1193-1201.
349. Bianco, J., et al., *On glioblastoma and the search for a cure: where do we stand?* Cellular and Molecular Life Sciences, 2017: p. 1-16.
350. Demuth, T. and M. Berens, *Molecular Mechanisms of Glioma Cell Migration and Invasion.* Journal of Neuro-Oncology, 2004. **70**(2): p. 217-228.
351. Petropoulos, C., et al. *Functional invadopodia formed in glioblastoma stem cells are important regulators of tumor angiogenesis*. Oncotarget, 2018. **9**, 20640-20657 DOI: 10.18632/oncotarget.25045.
352. Mao, L., et al., *Enhancement of invadopodia activity in glioma cells by sublethal doses of irradiation and temozolomide.* J Neurosurg, 2017: p. 1-13.
353. Ostermann, S., et al., *Plasma and Cerebrospinal Fluid Population Pharmacokinetics of Temozolomide in Malignant Glioma Patients.* Clinical Cancer Research, 2004. **10**(11): p. 3728-3736.
354. Rhodes, D.R., et al., *Oncomine 3.0: genes, pathways, and networks in a collection of 18,000 cancer gene expression profiles.* Neoplasia (New York, NY), 2007. **9**(2): p. 166.
355. Imperato, J., N. Paleologos, and N. Vick, *Effects of treatment on long-term survivors with malignant astrocytomas.* Annals of neurology, 1990. **28**(6): p. 818-822.
356. Kowalski, J.R., et al., *Cortactin regulates cell migration through activation of N-WASP.* 2005. **118**(1): p. 79-87.
357. Kohrman, A.Q. and D.Q. Matus, *Divide or conquer: cell cycle regulation of invasive behavior.* Trends in cell biology, 2017. **27**(1): p. 12-25.
358. Ren, Z., J. Chen, and R.A. Khalil, *Zymography as a Research Tool in the Study of Matrix Metalloproteinase Inhibitors.* Methods in molecular biology (Clifton, N.J.), 2017. **1626**: p. 79-102.
359. Löffek, S., O. Schilling, and C.-W. Franzke, *Biological role of matrix metalloproteinases: a critical balance.* 2011. **38**(1): p. 191-208.
360. Wu, X., S. Chen, and C. Lu, *Amyloid precursor protein promotes the migration and invasion of breast cancer cells by regulating the MAPK signaling pathway.* Int J Mol Med, 2020. **45**(1): p. 162-174.
361. Culicchia, F., et al., *Upregulation of beta-amyloid precursor protein expression in glioblastoma multiforme.* Neuroreport, 2008. **19**(9): p. 981-5.
362. Grass, G.D., et al., *CD147, CD44, and the epidermal growth factor receptor (EGFR) signaling pathway cooperate to regulate breast epithelial cell invasiveness.* J Biol Chem, 2013. **288**(36): p. 26089-104.
363. Grass, G.D., M. Bratoeva, and B.P. Toole, *Regulation of invadopodia formation and activity by CD147.* J Cell Sci, 2012. **125**(Pt 3): p. 777-88.
364. Yang, M., et al., *Prognostic significance of CD147 in patients with glioblastoma.* J Neurooncol, 2013. **115**(1): p. 19-26.
365. Liang, Q., et al., *Inhibition of basigin expression in glioblastoma cell line via antisense RNA reduces tumor cell invasion and angiogenesis.* Cancer Biol Ther, 2005. **4**(7): p. 759-62.
366. Jung, S.H., et al., *The serum protein fetuin-B is involved in the development of acute myocardial infarction.* Clin Sci (Lond), 2015. **129**(1): p. 27-38.
367. Zhang, X., et al., *Lipocalin-1 Expression as a Prognosticator Marker of Survival in Breast Cancer Patients.* 2019: p. 1-9.

368. Hirahata, M., et al., *PAI-1, a target gene of miR-143, regulates invasion and metastasis by upregulating MMP-13 expression of human osteosarcoma.* Cancer Med, 2016. **5**(5): p. 892-902.
369. Hjortland, G.O., et al., *Plasminogen activator inhibitor-1 increases the expression of VEGF in human glioma cells.* Exp Cell Res, 2004. **294**(1): p. 130-9.
370. Xi, X., et al., *ACT001, a novel PAI-1 inhibitor, exerts synergistic effects in combination with cisplatin by inhibiting PI3K/AKT pathway in glioma.* Cell Death Dis, 2019. **10**(10): p. 757.
371. Colin, C., et al., *High expression of cathepsin B and plasminogen activator inhibitor type-1 are strong predictors of survival in glioblastomas.* Acta Neuropathol, 2009. **118**(6): p. 745-54.
372. Bigelow, R.L.H., et al., *TIMP-1 overexpression promotes tumorigenesis of MDA-MB-231 breast cancer cells and alters expression of a subset of cancer promoting genes in vivo distinct from those observed in vitro.* Breast cancer research and treatment, 2009. **117**(1): p. 31-44.
373. Schelter, F., et al., *Tumor cell-derived Timp-1 is necessary for maintaining metastasis-promoting Met-signaling via inhibition of Adam-10.* Clin Exp Metastasis, 2011. **28**(8): p. 793-802.
374. Aaberg-Jessen, C., et al., *Low expression of tissue inhibitor of metalloproteinases-1 (TIMP-1) in glioblastoma predicts longer patient survival.* Journal of Neuro-Oncology, 2009. **95**(1): p. 117-128.
375. Overall, C.M. and C. López-Otín, *Strategies for MMP inhibition in cancer: innovations for the post-trial era.* Nat Rev Cancer, 2002. **2**(9): p. 657-72.
376. Lu, K.V., et al., *Upregulation of tissue inhibitor of metalloproteinases (TIMP)-2 promotes matrix metalloproteinase (MMP)-2 activation and cell invasion in a human glioblastoma cell line.* Lab Invest, 2004. **84**(1): p. 8-20.
377. Ceccarelli, M., et al., *Molecular Profiling Reveals Biologically Discrete Subsets and Pathways of Progression in Diffuse Glioma.* Cell, 2016. **164**(3): p. 550-63.
378. Gravendeel, L.A., et al., *Intrinsic gene expression profiles of gliomas are a better predictor of survival than histology.* Cancer Res, 2009. **69**(23): p. 9065-72.
379. Madhavan, S., et al., *Rembrandt: helping personalized medicine become a reality through integrative translational research.* Mol Cancer Res, 2009. **7**(2): p. 157-67.
380. Freije, W.A., et al., *Gene expression profiling of gliomas strongly predicts survival.* Cancer Res, 2004. **64**(18): p. 6503-10.
381. Ndishabandi, D., et al., *Thrombospondin-1 Modulates Actin Filament Remodeling and Cell Motility in Mouse Mammary Tumor cells in Vitro.* Discoveries (Craiova, Romania), 2014. **2**(4): p. e31.
382. Pal, S.K., et al., *THBS1 is induced by TGFB1 in the cancer stroma and promotes invasion of oral squamous cell carcinoma.* Journal of Oral Pathology & Medicine, 2016. **45**(10): p. 730-739.
383. Joseph, J.V., et al., *TGF-β is an inducer of ZEB1-dependent mesenchymal transdifferentiation in glioblastoma that is associated with tumor invasion.* Cell Death & Disease, 2014. **5**(10): p. e1443-e1443.
384. Karamanou, K., et al., *Epithelial-to-mesenchymal transition and invadopodia markers in breast cancer: Lumican a key regulator.* Semin Cancer Biol, 2020. **62**: p. 125-133.
385. Gardberg, M., et al., *FHOD1, a Formin Upregulated in Epithelial-Mesenchymal Transition, Participates in Cancer Cell Migration and Invasion.* PLOS ONE, 2013. **8**(9): p. e74923.
386. Szklarczyk, D., et al., *The STRING database in 2017: quality-controlled protein–protein association networks, made broadly accessible.* 2016: p. gkw937.
387. Aguirre-Gamboa, R., et al., *SurvExpress: an online biomarker validation tool and database for cancer gene expression data using survival analysis.* PloS one, 2013. **8**(9): p. e74250-e74250.
388. Bao, Z.S., et al., *RNA-seq of 272 gliomas revealed a novel, recurrent PTPRZ1-MET fusion transcript in secondary glioblastomas.* Genome Res, 2014. **24**(11): p. 1765-73.

389. Joo, K.M., et al., *Patient-specific orthotopic glioblastoma xenograft models recapitulate the histopathology and biology of human glioblastomas in situ.* Cell Rep, 2013. **3**(1): p. 260-73.
390. Li, J., et al., *Epigenetic suppression of EGFR signaling in G-CIMP+ glioblastomas.* Oncotarget, 2014. **5**(17): p. 7342-56.
391. Murat, A., et al., *Stem cell-related "self-renewal" signature and high epidermal growth factor receptor expression associated with resistance to concomitant chemoradiotherapy in glioblastoma.* J Clin Oncol, 2008. **26**(18): p. 3015-24.
392. Nutt, C.L., et al., *Gene expression-based classification of malignant gliomas correlates better with survival than histological classification.* Cancer Res, 2003. **63**(7): p. 1602-7.
393. Schoumacher, M., et al., *Actin, microtubules, and vimentin intermediate filaments cooperate for elongation of invadopodia.* 2010. **189**(3): p. 541-556.
394. Mentlein, R., K. Hattermann, and J. Held-Feindt, *Lost in disruption: role of proteases in glioma invasion and progression.* Biochimica et Biophysica Acta (BBA)-Reviews on Cancer, 2012. **1825**(2): p. 178-185.
395. Oser, M., et al., *Cortactin regulates cofilin and N-WASp activities to control the stages of invadopodium assembly and maturation.* J Cell Biol, 2009. **186**(4): p. 571-87.
396. Revach, O.-Y. and B. Geiger, *The interplay between the proteolytic, invasive, and adhesive domains of invadopodia and their roles in cancer invasion.* Cell adhesion & migration, 2014. **8**(3): p. 215-225.
397. Yano, S., et al., *Invading cancer cells are predominantly in G0/G1 resulting in chemoresistance demonstrated by real-time FUCCI imaging.* Cell Cycle, 2014. **13**(6): p. 953-960.
398. Bayarmagnai, B., et al., *Invadopodia-mediated ECM degradation is enhanced in the G1 phase of the cell cycle.* 2019. **132**(20): p. jcs227116.
399. Sun, S., et al., *Protein alterations associated with temozolomide resistance in subclones of human glioblastoma cell lines.* Journal of Neuro-Oncology, 2012. **107**(1): p. 89-100.
400. Talkenberger, K., et al., *Amoeboid-mesenchymal migration plasticity promotes invasion only in complex heterogeneous microenvironments.* Scientific reports, 2017. **7**(1): p. 9237-9237.
401. Kathagen, A., et al., *Hypoxia and oxygenation induce a metabolic switch between pentose phosphate pathway and glycolysis in glioma stem-like cells.* 2013. **126**(5): p. 763-780.
402. Gerlee, P. and S. Nelander, *The impact of phenotypic switching on glioblastoma growth and invasion.* PLoS computational biology, 2012. **8**(6): p. e1002556.
403. Pourfarhangi, K.E., et al., *Contact guidance is cell cycle-dependent.* 2018. **2**(3): p. 031904.
404. Walmod, P.S., et al., *Cell-cycle-dependent regulation of cell motility and determination of the role of Rac1.* Experimental Cell Research, 2004. **295**(2): p. 407-420.
405. Vega, S., et al., *Snail blocks the cell cycle and confers resistance to cell death.* Genes & development, 2004. **18**(10): p. 1131-1143.
406. Buettner, R., et al., *Inhibition of Src family kinases with dasatinib blocks migration and invasion of human melanoma cells.* Molecular Cancer Research, 2008. **6**(11): p. 1766-1774.
407. Cheung, Kevin J., et al., *Collective Invasion in Breast Cancer Requires a Conserved Basal Epithelial Program.* Cell, 2013. **155**(7): p. 1639-1651.
408. Gao, C.-F., et al., *Proliferation and invasion: Plasticity in tumor cells.* Proceedings of the National Academy of Sciences of the United States of America, 2005. **102**(30): p. 10528-10533.
409. Tiek, D.M., et al., *Alterations in cell motility, proliferation, and metabolism in novel models of acquired temozolomide resistant glioblastoma.* Scientific reports, 2018. **8**(1): p. 7222.
410. Zhang, X., et al., *Expression and significance of urokinase type plasminogen activator gene in human brain gliomas.* Journal of surgical oncology, 2000. **74**(2): p. 90-94.
411. Verbovšek, U., et al., *Expression analysis of all protease genes reveals cathepsin K to be overexpressed in glioblastoma.* PloS one, 2014. **9**(10): p. e111819.

412. Drucker, K.L., et al., *Prognostic significance of multiple kallikreins in high-grade astrocytoma.* BMC cancer, 2015. **15**(1): p. 565.
413. Kachra, Z., et al., *Expression of matrix metalloproteinases and their inhibitors in human brain tumors.* Clinical & Experimental Metastasis, 1999. **17**(7): p. 555-566.
414. Wick, W., et al., *BCL-2-induced glioma cell invasiveness depends on furin-like proteases.* 2004. **91**(6): p. 1275-1283.
415. Santamaría, I., et al., *Cathepsin L2, a novel human cysteine proteinase produced by breast and colorectal carcinomas.* Cancer Res, 1998. **58**(8): p. 1624-30.
416. Sivaparvathi, M., et al., *Expression of cysteine protease inhibitors in human gliomas and meningiomas.* Clin Exp Metastasis, 1996. **14**(4): p. 344-50.
417. Liu, Y., Y. Zhou, and K.J.P.o. Zhu, *Inhibition of glioma cell lysosome exocytosis inhibits glioma invasion.* 2012. **7**(9): p. e45910.
418. Zheng, W., et al., *Inhibition of Cathepsin D (CTSD) enhances radiosensitivity of glioblastoma cells by attenuating autophagy.* 2020. **59**(6): p. 651-660.
419. Iizuka, S., et al., *Crosstalk between invadopodia and the extracellular matrix.* 2020: p. 2020.02.26.966762.
420. Lee, J., et al., *Anti-invasive and Anti-tumor Effects of Dryopteris crassirhizoma Extract by Disturbing Actin Polymerization.* Integrative cancer therapies, 2019. **18**: p. 1534735419851197-1534735419851197.
421. Kleiner, D.E. and W.G. Stetler-Stevenson, *Quantitative zymography: detection of picogram quantities of gelatinases.* Anal Biochem, 1994. **218**(2): p. 325-9.
422. Mason, S.D. and J.A. Joyce, *Proteolytic networks in cancer.* Trends in cell biology, 2011. **21**(4): p. 228-237.
423. Butler, G.S., et al., *The TIMP2 membrane type 1 metalloproteinase "receptor" regulates the concentration and efficient activation of progelatinase A. A kinetic study.* J Biol Chem, 1998. **273**(2): p. 871-80.
424. Arslan, F., et al., *The role of versican isoforms V0/V1 in glioma migration mediated by transforming growth factor-β 2.* 2007. **96**(10): p. 1560-1568.
425. Seker, F., et al., *Identification of SERPINE1 as a regulator of glioblastoma cell dispersal with transcriptome profiling.* 2019. **11**(11): p. 1651.
426. Behnan, J., G. Finocchiaro, and G.J.B. Hanna, *The landscape of the mesenchymal signature in brain tumours.* 2019. **142**(4): p. 847-866.
427. Duan, S., et al., *Exogenous Let-7a-5p Induces A549 Lung Cancer Cell Death Through BCL2L1-Mediated PI3Kγ Signaling Pathway.* 2019. **9**(808).
428. Wang, X.-R., et al., *Overexpressed let-7a inhibits glioma cell malignancy by directly targeting K-ras, independently of PTEN.* Neuro-oncology, 2013. **15**(11): p. 1491-1501.
429. Al-Harbi, B., et al., *Let-7b inhibits cancer-promoting effects of breast cancer-associated fibroblasts through IL-8 repression.* 2018. **9**(25): p. 17825.
430. Yang, Q., et al., *MiR-125b regulates epithelial-mesenchymal transition via targeting Sema4C in paclitaxel-resistant breast cancer cells.* 2015. **6**(5): p. 3268.
431. Xi, X., et al., *Joint bioinformatics analysis of underlying potential functions of hsa-let-7b-5p and core genes in human glioma.* Journal of Translational Medicine, 2019. **17**(1): p. 129.
432. Guo, Y., et al., *Let-7b expression determines response to chemotherapy through the regulation of Cyclin D1 in Glioblastoma.* Journal of Experimental & Clinical Cancer Research, 2013. **32**(1): p. 41.
433. Zhang, W., et al., *Decreased let-7b is associated with poor prognosis in glioma.* 2019. **98**(22).
434. Luo, W., et al., *Integrative analyses of miRNA-mRNA interactions reveal let-7b, miR-128 and MAPK pathway involvement in muscle mass loss in sex-linked dwarf chickens.* 2016. **17**(3): p. 276.
435. Zhang, Y., et al., *Identification of miR-125b targets involved in acute promyelocytic leukemia cell proliferation.* 2016. **478**(4): p. 1758-1763.

436. Yamaguchi, H., et al., *Phosphatidylinositol 4,5-bisphosphate and PIP5-kinase Iα are required for invadopodia formation in human breast cancer cells.* 2010. **101**(7): p. 1632-1638.
437. Tague, S.E., V. Muralidharan, and C. D'Souza-Schorey, *ADP-ribosylation factor 6 regulates tumor cell invasion through the activation of the MEK/ERK signaling pathway.* Proc Natl Acad Sci U S A, 2004. **101**(26): p. 9671-6.
438. Jacob, A., et al., *The role and regulation of Rab40b–Tks5 complex during invadopodia formation and cancer cell invasion.* 2016. **129**(23): p. 4341-4353.
439. Li, Y., et al., *miR-182 suppresses invadopodia formation and metastasis in non-small cell lung cancer by targeting cortactin gene.* Journal of experimental & clinical cancer research : CR, 2018. **37**(1): p. 141-141.
440. Iruela-Arispe, M.L., *Regulation of thrombospondin1 by extracellular proteases.* Current drug targets, 2008. **9**(10): p. 863-868.
441. Albo, D., et al., *Thrombospondin-1 and transforming growth factor beta-1 upregulate plasminogen activator inhibitor type 1 in pancreatic cancer.* Journal of Gastrointestinal Surgery, 1999. **3**(4): p. 411-417.
442. Naganuma, H., et al., *Quantification of thrombospondin-1 secretion and expression of αvβ3 and α3β1 integrins and syndecan-1 as cell-surface receptors for thrombospondin-1 in malignant glioma cells.* 2004. **70**(3): p. 309-317.
443. Wang, T.N., et al., *Thrombospondin-1 (TSP-1) Promotes the Invasive Properties of Human Breast Cancer.* Journal of Surgical Research, 1996. **63**(1): p. 39-43.
444. Qi, C., et al., *Thrombospondin -1 is a prognostic biomarker and is correlated with tumor immune microenvironment in glioblastoma.* Oncol Lett, 2021. **21**(1): p. 22.
445. Taraboletti, G., et al., *The heparin binding 25 kDa fragment of thrombospondin-1 promotes angiogenesis and modulates gelatinase and TIMP-2 production in endothelial cells.* 2000. **14**(12): p. 1674-1676.
446. Wang, S., et al., *Internalization but not binding of thrombospondin-1 to low density lipoprotein receptor-related protein-1 requires heparan sulfate proteoglycans.* J Cell Biochem, 2004. **91**(4): p. 766-76.
447. Daubon, T., et al., *Deciphering the complex role of thrombospondin-1 in glioblastoma development.* Nature Communications, 2019. **10**(1): p. 1146.
448. Bein, K. and M. Simons, *Thrombospondin Type 1 Repeats Interact with Matrix Metalloproteinase 2 REGULATION OF METALLOPROTEINASE ACTIVITY.* Journal of Biological Chemistry, 2000. **275**(41): p. 32167-32173.
449. Yang, Z., D.K. Strickland, and P.J.J.o.B.C. Bornstein, *Extracellular matrix metalloproteinase 2 levels are regulated by the low density lipoprotein-related scavenger receptor and thrombospondin 2.* 2001. **276**(11): p. 8403-8408.
450. Crombie, R. and R. Silverstein, *Lysosomal integral membrane protein II binds thrombospondin-1. Structure-function homology with the cell adhesion molecule CD36 defines a conserved recognition motif.* J Biol Chem, 1998. **273**(9): p. 4855-63.
451. Duquette, M., et al., *Members of the thrombospondin gene family bind stromal interaction molecule 1 and regulate calcium channel activity.* Matrix biology : journal of the International Society for Matrix Biology, 2014. **37**: p. 15-24.
452. Ndishabandi, D., et al., *Thrombospondin-1 Modulates Actin Filament Remodeling and Cell Motility in Mouse Mammary Tumor cells in Vitro.* Discoveries (Craiova), 2014. **2**(4).
453. Hastie, E.L. and D.R. Sherwood, *A new front in cell invasion: The invadopodial membrane.* European journal of cell biology, 2016. **95**(11): p. 441-448.
454. Jacob, A. and R. Prekeris, *The regulation of MMP targeting to invadopodia during cancer metastasis.* Frontiers in cell and developmental biology, 2015. **3**: p. 4-4.
455. Calzada, M.J., et al., *Identification of novel beta1 integrin binding sites in the type 1 and type 2 repeats of thrombospondin-1.* J Biol Chem, 2004. **279**(40): p. 41734-43.

456. Cen, J., et al., *Exosomal Thrombospondin-1 Disrupts the Integrity of Endothelial Intercellular Junctions to Facilitate Breast Cancer Cell Metastasis.* Cancers, 2019. **11**(12): p. 1946.
457. Lai, Y.-H., et al., *Thrombospondin 1-induced exosomal proteins attenuate hypoxia-induced paraptosis in corneal epithelial cells and promote wound healing.* 2021. **35**(1): p. e21200.
458. Goicoechea, S., et al., *Thrombospondin mediates focal adhesion disassembly through interactions with cell surface calreticulin.* J Biol Chem, 2000. **275**(46): p. 36358-68.
459. Lillis, A.P., et al., *LDL receptor-related protein 1: unique tissue-specific functions revealed by selective gene knockout studies.* Physiological reviews, 2008. **88**(3): p. 887-918.
460. Orr, A.W., et al., *Thrombospondin signaling through the calreticulin/LDL receptor-related protein co-complex stimulates random and directed cell migration.* 2003. **116**(14): p. 2917-2927.
461. Iizuka, S., et al., *Serine-threonine kinase TAO3-mediated trafficking of endosomes containing the invadopodia scaffold TKS5α promotes cancer invasion and tumor growth.*
462. Liu, J., et al., *The Role of the Exocyst in Matrix Metalloproteinase Secretion and Actin Dynamics during Tumor Cell Invadopodia Formation.* Molecular Biology of the Cell, 2009. **20**(16): p. 3763-3771.
463. Jeanne, A., et al., *Original insights on thrombospondin-1-related antireceptor strategies in cancer.* Frontiers in pharmacology, 2015. **6**: p. 252-252.
464. Good, D.J., et al., *A tumor suppressor-dependent inhibitor of angiogenesis is immunologically and functionally indistinguishable from a fragment of thrombospondin.* 1990. **87**(17): p. 6624-6628.
465. Chen, H., M.E. Herndon, and J. Lawler, *The cell biology of thrombospondin-1.* Matrix Biology, 2000. **19**(7): p. 597-614.
466. Anilkumar, N., et al., *Trimeric assembly of the C-terminal region of thrombospondin-1 or thrombospondin-2 is necessary for cell spreading and fascin spike organisation.* J Cell Sci, 2002. **115**(Pt 11): p. 2357-66.
467. Huang, T., et al., *Thrombospondin-1 is a multifaceted player in tumor progression.* 2017. **8**(48): p. 84546.
468. Raposo, G. and W. Stoorvogel, *Extracellular vesicles: Exosomes, microvesicles, and friends.* The Journal of Cell Biology, 2013. **200**(4): p. 373-383.
469. D'Asti, E., et al., *Oncogenic extracellular vesicles in brain tumor progression.* Frontiers in physiology, 2012. **3**: p. 294-294.
470. Beghein, E., et al., *Cortactin and fascin-1 regulate extracellular vesicle release by controlling endosomal trafficking or invadopodia formation and function.* Scientific Reports, 2018. **8**(1): p. 15606.
471. Havrylov, S. and M. Park, *MS/MS-based strategies for proteomic profiling of invasive cell structures.* Proteomics, 2015. **15**(2-3): p. 272-86.
472. Mallawaaratchy, D.M., et al., *Comprehensive proteome profiling of glioblastoma-derived extracellular vesicles identifies markers for more aggressive disease.* Journal of Neuro-Oncology, 2017. **131**(2): p. 233-244.
473. Schlienger, S., S. Campbell, and A. Claing, *ARF1 regulates the Rho/MLC pathway to control EGF-dependent breast cancer cell invasion.* Molecular biology of the cell, 2014. **25**(1): p. 17-29.
474. Lee, Y.S. and A. Dutta, *MicroRNAs in cancer.* Annual review of pathology, 2009. **4**: p. 199-227.
475. Savina, A., et al., *Exosome release is regulated by a calcium-dependent mechanism in K562 cells.* Journal of biological chemistry, 2003. **278**(22): p. 20083-20090.
476. Sreekumar, P.G., et al., *αB Crystallin Is Apically Secreted within Exosomes by Polarized Human Retinal Pigment Epithelium and Provides Neuroprotection to Adjacent Cells.* PLOS ONE, 2010. **5**(10): p. e12578.

477. Chalmin, F., et al., *Membrane-associated Hsp72 from tumor-derived exosomes mediates STAT3-dependent immunosuppressive function of mouse and human myeloid-derived suppressor cells.* Journal of Clinical Investigation, 2010. **120**(2): p. 457-471.
478. Giusti, I., M. Di Francesco, and V. Dolo, *Extracellular Vesicles in Glioblastoma: Role in Biological Processes and in Therapeutic Applications.* Current Cancer Drug Targets, 2017. **17**(3): p. 221-235.
479. Mulcahy, L.A., R.C. Pink, and D.R.F.J.J.o.e.v. Carter, *Routes and mechanisms of extracellular vesicle uptake.* 2014. **3**(1): p. 24641.
480. Shimoda, M. and R. Khokha, *Proteolytic factors in exosomes.* Proteomics, 2013. **13**(10-11): p. 1624-36.
481. Shimoda, M. and R. Khokha, *Metalloproteinases in extracellular vesicles.* Biochimica et Biophysica Acta (BBA) - Molecular Cell Research, 2017. **1864**(11, Part A): p. 1989-2000.
482. Gould, C.M. and S.A. Courtneidge, *Regulation of invadopodia by the tumor microenvironment.* Cell adhesion & migration, 2014. **8**(3): p. 226-235.
483. Demory Beckler, M., et al., *Proteomic analysis of exosomes from mutant KRAS colon cancer cells identifies intercellular transfer of mutant KRAS.* Mol Cell Proteomics, 2013. **12**(2): p. 343-55.
484. Singh, A., et al., *Exosome-mediated Transfer of αvβ3 Integrin from Tumorigenic to Nontumorigenic Cells Promotes a Migratory Phenotype.* Molecular cancer research : MCR, 2016. **14**(11): p. 1136-1146.
485. Yue, J., K. Zhang, and J. Chen, *Role of integrins in regulating proteases to mediate extracellular matrix remodeling.* Cancer microenvironment : official journal of the International Cancer Microenvironment Society, 2012. **5**(3): p. 275-283.
486. Lu, J., et al., *Exosomal tetraspanins mediate cancer metastasis by altering host microenvironment.* Oncotarget, 2017. **8**(37): p. 62803-62815.
487. Sun, Z., et al., *Effect of exosomal miRNA on cancer biology and clinical applications.* Molecular Cancer, 2018. **17**(1): p. 147.
488. Mrowczynski, O.D., et al., *Exosomes impact survival to radiation exposure in cell line models of nervous system cancer.* Oncotarget, 2018. **9**(90): p. 36083-36101.
489. Bandari, S.K., et al., *Therapy-induced chemoexosomes: Sinister small extracellular vesicles that support tumor survival and progression.* 2020.
490. Tabak, S., S. Schreiber-Avissar, and E. Beit-Yannai, *Extracellular vesicles have variable dose-dependent effects on cultured draining cells in the eye.* Journal of cellular and molecular medicine, 2018. **22**(3): p. 1992-2000.
491. Keklikoglou, I., et al., *Chemotherapy elicits pro-metastatic extracellular vesicles in breast cancer models.* Nature cell biology, 2019. **21**(2): p. 190-202.
492. Ngan, V.K., et al., *Novel actions of the antitumor drugs vinflunine and vinorelbine on microtubules.* 2000. **60**(18): p. 5045-5051.
493. Biassoni, V., et al., *A case of relapsing glioblastoma multiforme responding to vinorelbine.* J Neurooncol, 2006. **80**(2): p. 195-201.
494. Massimino, M., et al., *Results of nimotuzumab and vinorelbine, radiation and re-irradiation for diffuse pontine glioma in childhood.* 2014. **118**(2): p. 305-312.
495. Kuttesch Jr, J.F., et al., *Phase II evaluation of intravenous vinorelbine (Navelbine) in recurrent or refractory pediatric malignancies: a Children's Oncology Group study.* 2009. **53**(4): p. 590-593.
496. Cappellano, A.M., et al., *Single agent vinorelbine in pediatric patients with progressive optic pathway glioma.* 2015. **121**(2): p. 405-412.
497. Samala, R., et al., *Vinorelbine Delivery and Efficacy in the MDA-MB-231BR Preclinical Model of Brain Metastases of Breast Cancer.* Pharm Res, 2016. **33**(12): p. 2904-2919.
498. Toso, C. and C. Lindley, *Vinorelbine: A novel vinca alkaloid.* American Journal of Health-System Pharmacy, 1995. **52**(12): p. 1287-1304.

499. Cho, W.C.J.G., proteomics and bioinformatics, *Proteomics technologies and challenges.* 2007. **5**(2): p. 77-85.
500. Kalinina, J., et al., *Proteomics of gliomas: initial biomarker discovery and evolution of technology.* Neuro Oncol, 2011. **13**(9): p. 926-42.
501. Pitt, J.J.J.T.C.B.R., *Principles and applications of liquid chromatography-mass spectrometry in clinical biochemistry.* 2009. **30**(1): p. 19.
502. Tabb, D.L., et al., *Repeatability and reproducibility in proteomic identifications by liquid chromatography-tandem mass spectrometry.* J Proteome Res, 2010. **9**(2): p. 761-76.
503. Artym, V., et al., *Dynamic interactions of cortactin and membrane type 1 matrix metalloproteinase at invadopodia: defining the stages of invadopodia formation and function.* Cancer research, 2006. **66**(6): p. 3034-3043.
504. McNiven, M.A., *Breaking away: matrix remodeling from the leading edge.* Trends in cell biology, 2013. **23**(1): p. 16-21.
505. Beaty, B.T., et al., *β1 integrin regulates Arg to promote invadopodial maturation and matrix degradation.* Molecular Biology of the Cell, 2013. **24**(11): p. 1661-1675.
506. Destaing, O., et al., *1A Integrin Is a Master Regulator of Invadosome Organization and Function*. Vol. 21. 2010. 4108-19.
507. Tehrani, S., et al., *Src phosphorylation of cortactin enhances actin assembly.* Proceedings of the National Academy of Sciences of the United States of America, 2007. **104**(29): p. 11933-11938.
508. Weaver, A., et al., *Cortactin promotes and stabilizes Arp2/3-induced actin filament network formation.* Current biology, 2001. **11**(5): p. 370-374.
509. Stylli, S.S., et al., *Nck adaptor proteins link Tks5 to invadopodia actin regulation and ECM degradation.* Journal of Cell Science, 2009. **122**(15): p. 2727-2740.
510. Courtneidge, S.A., et al., *The SRC substrate Tks5, podosomes (invadopodia), and cancer cell invasion.* Cold Spring Harb Symp Quant Biol, 2005. **70**: p. 167-71.
511. Crimaldi, L., S.A. Courtneidge, and M. Gimona, *Tks5 recruits AFAP-110, p190RhoGAP, and cortactin for podosome formation.* Exp Cell Res, 2009. **315**(15): p. 2581-92.
512. Frame, M., et al., *v-SRC'S hold over actin and cell adhesions.* Nature Reviews. Molecular Cell Biology, 2002. **3**(4): p. 233-245.
513. Mueller, S.C., Y. Yeh, and W.T. Chen, *Tyrosine phosphorylation of membrane proteins mediates cellular invasion by transformed cells.* The Journal of cell biology, 1992. **119**(5): p. 1309-1325.
514. Ayala, I., et al., *Multiple regulatory inputs converge on cortactin to control invadopodia biogenesis and extracellular matrix degradation.* Journal of Cell Science, 2008. **121**(3): p. 369-378.
515. Nakahara, H., et al., *Involvement of Cdc42 and Rac small G proteins in invadopodia formation of RPMI7951 cells.* Genes Cells, 2003. **8**(12): p. 1019-27.
516. Rohatgi, R., et al., *The interaction between N-WASP and the Arp2/3 complex links Cdc42-dependent signals to actin assembly.* Cell, 1999. **97**(2): p. 221-31.
517. Hoshino, D., K.M. Branch, and A.M. Weaver, *Signaling inputs to invadopodia and podosomes.* Journal of cell science, 2013. **126**(Pt 14): p. 2979-2989.
518. Indira Chandran, V., et al., *Global extracellular vesicle proteomic signature defines U87-MG glioma cell hypoxic status with potential implications for non-invasive diagnostics.* Journal of Neuro-Oncology, 2019. **144**(3): p. 477-488.
519. Chun, S., et al., *Exosome Proteome of U-87MG Glioblastoma Cells.* Biology, 2016. **5**(4): p. 50.
520. Haraszti, R.A., et al., *High-resolution proteomic and lipidomic analysis of exosomes and microvesicles from different cell sources.* Journal of extracellular vesicles, 2016. **5**(1): p. 32570.

521. Pei, J., et al., *Proteomic Analysis between U87MG and U343MG-A Cell Lines: Searching for Candidate Proteins for Glioma Invasion.* Brain tumor research and treatment, 2014. **2**(1): p. 22-28.
522. Fukuda, M.E., et al., *Cathepsin D is a potential serum marker for poor prognosis in glioma patients.* Cancer Res, 2005. **65**(12): p. 5190-4.
523. Hurst, I.R., et al., *Actin-related protein 2/3 complex is required for actin ring formation.* J Bone Miner Res, 2004. **19**(3): p. 499-506.
524. Helgeson, L.A., et al., *Interactions with actin monomers, actin filaments, and Arp2/3 complex define the roles of WASP family proteins and cortactin in coordinately regulating branched actin networks.* J Biol Chem, 2014. **289**(42): p. 28856-69.
525. Marchesin, V., G. Montagnac, and P. Chavrier, *ARF6 promotes the formation of Rac1 and WAVE-dependent ventral F-actin rosettes in breast cancer cells in response to epidermal growth factor.* PLoS One, 2015. **10**(3): p. e0121747.
526. Yang, H., et al., *Mechanosensitive caveolin-1 activation-induced PI3K/Akt/mTOR signaling pathway promotes breast cancer motility, invadopodia formation and metastasis in vivo.* Oncotarget, 2016. **7**(13): p. 16227-47.
527. Hong, I.K., et al., *Homophilic interactions of Tetraspanin CD151 up-regulate motility and matrix metalloproteinase-9 expression of human melanoma cells through adhesion-dependent c-Jun activation signaling pathways.* J Biol Chem, 2006. **281**(34): p. 24279-92.
528. Zhao, P., et al., *The CD44s splice isoform is a central mediator for invadopodia activity.* J Cell Sci, 2016. **129**(7): p. 1355-65.
529. Zhu, B., et al., *CLASP2 is involved in the EMT and early progression after transurethral resection of the bladder tumor.* BMC cancer, 2017. **17**(1): p. 105-105.
530. Fukata, M., et al., *Rac1 and Cdc42 capture microtubules through IQGAP1 and CLIP-170.* Cell, 2002. **109**(7): p. 873-85.
531. Suzuki, K. and K. Takahashi, *Regulation of lamellipodia formation and cell invasion by CLIP-170 in invasive human breast cancer cells.* Biochem Biophys Res Commun, 2008. **368**(2): p. 199-204.
532. Markwell, S.M., et al., *Cortactin Phosphorylation by Casein Kinase 2 Regulates Actin-Related Protein 2/3 Complex Activity, Invadopodia Function, and Tumor Cell Invasion.* Mol Cancer Res, 2019. **17**(4): p. 987-1001.
533. Uruno, T., et al., *Sequential interaction of actin-related proteins 2 and 3 (Arp2/3) complex with neural Wiscott-Aldrich syndrome protein (N-WASP) and cortactin during branched actin filament network formation.* The Journal of biological chemistry, 2003. **278**(28): p. 26086-26093.
534. Li, Z., et al., *Mammalian diaphanous-related formin 1 is required for motility and invadopodia formation in human U87 glioblastoma cells.* Int J Mol Med, 2014. **33**(2): p. 383-91.
535. Zhang, Y., et al., *Dynamin2 GTPase contributes to invadopodia formation in invasive bladder cancer cells.* Biochem Biophys Res Commun, 2016. **480**(3): p. 409-414.
536. Goicoechea, S.M., et al., *A RhoG-mediated signaling pathway that modulates invadopodia dynamics in breast cancer cells.* Journal of cell science, 2017. **130**(6): p. 1064-1077.
537. Rajadurai, C.V., et al., *5'-Inositol phosphatase SHIP2 recruits Mena to stabilize invadopodia for cancer cell invasion.* J Cell Biol, 2016. **214**(6): p. 719-34.
538. Hirano, T., et al., *FARP1 boosts CDC42 activity from integrin αvβ5 signaling and correlates with poor prognosis of advanced gastric cancer.* Oncogenesis, 2020. **9**(2): p. 13.
539. Gulvady, A.C., I.J. Forsythe, and C.E. Turner, *Hic-5 regulates Src-induced invadopodia rosette formation and organization.* Mol Biol Cell, 2019. **30**(11): p. 1298-1313.
540. Peláez, R., et al., *Integrins: Moonlighting Proteins in Invadosome Formation.* Cancers, 2019. **11**(5): p. 615.

541. Peláez, R., et al., *β3 integrin expression is required for invadopodia-mediated ECM degradation in lung carcinoma cells.* PLoS One, 2017. **12**(8): p. e0181579.
542. Williams, K.C. and M.G. Coppolino, *SNARE-dependent interaction of Src, EGFR and β1 integrin regulates invadopodia formation and tumor cell invasion.* J Cell Sci, 2014. **127**(Pt 8): p. 1712-25.
543. Ngan, E., et al., *LPP is a Src substrate required for invadopodia formation and efficient breast cancer lung metastasis.* Nat Commun, 2017. **8**: p. 15059.
544. Nakahara, H., et al., *Transmembrane/cytoplasmic domain-mediated membrane type 1-matrix metalloprotease docking to invadopodia is required for cell invasion.* Proc Natl Acad Sci U S A, 1997. **94**(15): p. 7959-64.
545. Lomakina, M.E., et al., *Arpin downregulation in breast cancer is associated with poor prognosis.* Br J Cancer, 2016. **114**(5): p. 545-53.
546. Lin, C.W., et al., *Podocalyxin-like 1 promotes invadopodia formation and metastasis through activation of Rac1/Cdc42/cortactin signaling in breast cancer cells.* Carcinogenesis, 2014. **35**(11): p. 2425-35.
547. Li, X., et al., *High expression of protein phosphatase 4 is associated with the aggressive malignant behavior of colorectal carcinoma.* Mol Cancer, 2015. **14**: p. 95.
548. Genna, A., et al., *Pyk2 and FAK differentially regulate invadopodia formation and function in breast cancer cells.* J Cell Biol, 2018. **217**(1): p. 375-395.
549. Ueno, H., et al., *Augmentation of invadopodia formation in temozolomide-resistant or adopted glioma is regulated by c-Jun terminal kinase-paxillin axis.* Biochem Biophys Res Commun, 2015. **468**(1-2): p. 240-7.
550. Frittoli, E., et al., *A RAB5/RAB4 recycling circuitry induces a proteolytic invasive program and promotes tumor dissemination.* 2014. **206**(2): p. 307-328.
551. Wiesner, C., K. El Azzouzi, and S. Linder, *A specific subset of RabGTPases controls cell surface exposure of MT1-MMP, extracellular matrix degradation and three-dimensional invasion of macrophages.* J Cell Sci, 2013. **126**(Pt 13): p. 2820-33.
552. Humphries, J.D., et al., *Proteomic analysis of integrin-associated complexes identifies RCC2 as a dual regulator of Rac1 and Arf6.* Sci Signal, 2009. **2**(87): p. ra51.
553. Bravo-Cordero, J.J., et al., *A novel spatiotemporal RhoC activation pathway locally regulates cofilin activity at invadopodia.* Curr Biol, 2011. **21**(8): p. 635-44.
554. Burger, K.L., et al., *Src-dependent Tks5 phosphorylation regulates invadopodia-associated invasion in prostate cancer cells.* Prostate, 2014. **74**(2): p. 134-48.
555. Brasher, M.I., et al., *Interaction of Munc18c and syntaxin4 facilitates invadopodium formation and extracellular matrix invasion of tumor cells.* J Biol Chem, 2017. **292**(39): p. 16199-16210.
556. Dekky, B., et al., *Proteomic screening identifies the zonula occludens protein ZO-1 as a new partner for ADAM12 in invadopodia-like structures.* Oncotarget, 2018. **9**(30): p. 21366-21382.
557. Thuault, S., et al., *A proximity-labeling proteomic approach to investigate invadopodia molecular landscape in breast cancer cells.* 2019: p. 869545.
558. Meng, D.F., et al., *CDC42-interacting protein 4 promotes metastasis of nasopharyngeal carcinoma by mediating invadopodia formation and activating EGFR signaling.* J Exp Clin Cancer Res, 2017. **36**(1): p. 21.
559. Carmona, G., et al., *Lamellipodin promotes invasive 3D cancer cell migration via regulated interactions with Ena/VASP and SCAR/WAVE.* Oncogene, 2016. **35**(39): p. 5155-69.
560. Zuzga, D.S., et al., *Phosphorylation of vasodilator-stimulated phosphoprotein Ser239 suppresses filopodia and invadopodia in colon cancer.* Int J Cancer, 2012. **130**(11): p. 2539-48.

561. Abou-Kheir, W., et al., *Membrane targeting of WAVE2 is not sufficient for WAVE2-dependent actin polymerization: a role for IRSp53 in mediating the interaction between Rac and WAVE2.* J Cell Sci, 2008. **121**(Pt 3): p. 379-90.
562. Kikuchi, K. and K. Takahashi, *WAVE2- and microtubule-dependent formation of long protrusions and invasion of cancer cells cultured on three-dimensional extracellular matrices.* Cancer Sci, 2008. **99**(11): p. 2252-9.
563. Chen, Z., et al., *Structure and control of the actin regulatory WAVE complex.* Nature, 2010. **468**(7323): p. 533-8.
564. Chakraborty, S., et al., *An oncogenic role of Agrin in regulating focal adhesion integrity in hepatocellular carcinoma.* Nat Commun, 2015. **6**: p. 6184.
565. Revach, O.Y., et al., *Cross-Talk between Receptor Tyrosine Kinases AXL and ERBB3 Regulates Invadopodia Formation in Melanoma Cells.* Cancer Res, 2019. **79**(10): p. 2634-2648.
566. Harper, K., et al., *Autotaxin promotes cancer invasion via the lysophosphatidic acid receptor 4: participation of the cyclic AMP/EPAC/Rac1 signaling pathway in invadopodia formation.* Cancer Res, 2010. **70**(11): p. 4634-43.
567. Ren, X.L., et al., *Cortactin recruits FMNL2 to promote actin polymerization and endosome motility in invadopodia formation.* Cancer Lett, 2018. **419**: p. 245-256.
568. Harper, K., et al., *The Hypoxic Tumor Microenvironment Promotes Invadopodia Formation and Metastasis through LPA1 Receptor and EGFR Cooperation.* Mol Cancer Res, 2018. **16**(10): p. 1601-1613.
569. Kerber, M.L. and R.E. Cheney, *Myosin-X: a MyTH-FERM myosin at the tips of filopodia.* J Cell Sci, 2011. **124**(Pt 22): p. 3733-41.
570. Nicholas, N.S., et al., *Differential role for PAK1 and PAK4 during the invadopodia lifecycle.* Small GTPases, 2019. **10**(4): p. 289-295.
571. Jacquemet, G., et al., *RCP-driven α5β1 recycling suppresses Rac and promotes RhoA activity via the RacGAP1-IQGAP1 complex.* J Cell Biol, 2013. **202**(6): p. 917-35.
572. Ma, J., et al., *Human U87 astrocytoma cell invasion induced by interaction of βig-h3 with integrin α5β1 involves calpain-2.* PLoS One, 2012. **7**(5): p. e37297.
573. Guo, Y.S., et al., *βig-h3 promotes human osteosarcoma cells metastasis by interacting with integrin α2β1 and activating PI3K signaling pathway.* PLoS One, 2014. **9**(3): p. e90220.
574. Kim, Y.H., H.J. Kwon, and D.S. Kim, *Matrix metalloproteinase 9 (MMP-9)-dependent processing of βig-h3 protein regulates cell migration, invasion, and adhesion.* J Biol Chem, 2012. **287**(46): p. 38957-69.
575. Furnari, F.B., et al., *Malignant astrocytic glioma: genetics, biology, and paths to treatment.* 2007. **21**(21): p. 2683-2710.
576. Mężyk-Kopeć, R., et al., *ADAM17 Promotes Motility, Invasion, and Sprouting of Lymphatic Endothelial Cells.* PLoS One, 2015. **10**(7): p. e0132661.
577. Zheng, X., et al., *ADAM17 promotes glioma cell malignant phenotype.* Molecular carcinogenesis, 2012. **51**(2): p. 150-164.
578. Chakraborty, S., et al., *An oncogenic role of Agrin in regulating focal adhesion integrity in hepatocellular carcinoma.* Nature communications, 2015. **6**: p. 6184-6184.
579. Wolburg, H., et al., *The disturbed blood–brain barrier in human glioblastoma.* 2012. **33**(5-6): p. 579-589.
580. Wu, X., S. Chen, and C.J.I.j.o.m.m. Lu, *Amyloid precursor protein promotes the migration and invasion of breast cancer cells by regulating the MAPK signaling pathway.* 2020. **45**(1): p. 162-174.
581. Riihilä, P., et al., *Complement Factor I Promotes Progression of Cutaneous Squamous Cell Carcinoma.* Journal of Investigative Dermatology, 2015. **135**(2): p. 579-588.
582. Gasque, P., et al., *Expression of complement components of the alternative pathway by glioma cell lines.* J Immunol, 1992. **149**(4): p. 1381-7.

583. Cholia, R.P., et al., *Oxidative stress stimulates invasive potential in rat C6 and human U-87 MG glioblastoma cells via activation and cross-talk between PKM2, ENPP2 and APE1 enzymes.* Metab Brain Dis, 2018. **33**(4): p. 1307-1326.
584. Monzo, P., et al., *Mechanical confinement triggers glioma linear migration dependent on formin FHOD3.* 2016. **27**(8): p. 1246-1261.
585. Haas, T.L., et al., *Integrin α7 Is a Functional Marker and Potential Therapeutic Target in Glioblastoma.* Cell Stem Cell, 2017. **21**(1): p. 35-50.e9.
586. Li, X., et al., *PI3K/Akt/mTOR signaling pathway and targeted therapy for glioblastoma.* Oncotarget, 2016. **7**(22): p. 33440-50.
587. Yu, Z.H., et al., *NID2 can serve as a potential prognosis prediction biomarker and promotes the invasion and migration of gastric cancer.* Pathol Res Pract, 2019. **215**(10): p. 152553.
588. Okawa, S., et al., *Proteome and Secretome Characterization of Glioblastoma-Derived Neural Stem Cells.* Stem cells (Dayton, Ohio), 2017. **35**(4): p. 967-980.
589. Qu, J., et al., *Notch2 signaling contributes to cell growth, invasion, and migration in salivary adenoid cystic carcinoma.* Mol Cell Biochem, 2016. **411**(1-2): p. 135-41.
590. Bazzoni, R. and A. Bentivegna, *Role of Notch Signaling Pathway in Glioblastoma Pathogenesis.* Cancers, 2019. **11**(3): p. 292.
591. Daubon, T., et al., *The invasive proteome of glioblastoma revealed by laser-capture microdissection.* Neuro-Oncology Advances, 2019. **1**(1).
592. Xia, Z., et al., *Decreased Expression of MiRNA-204-5p Contributes to Glioma Progression and Promotes Glioma Cell Growth, Migration and Invasion.* PloS one, 2015. **10**(7): p. e0132399-e0132399.
593. Zhou, L., et al., *Bioinformatics analyses of significant genes, related pathways and candidate prognostic biomarkers in glioblastoma.* Molecular medicine reports, 2018. **18**(5): p. 4185-4196.
594. Wu, J.X., et al., *Rap2a is a novel target gene of p53 and regulates cancer cell migration and invasion.* Cell Signal, 2015. **27**(6): p. 1198-207.
595. Wang, L., et al., *Regulation of glioma migration and invasion via modification of Rap2a activity by the ubiquitin ligase Nedd4-1.* Oncology reports, 2017. **37**(5): p. 2565-2574.
596. Pan, Y.B., et al., *Transforming growth factor beta induced (TGFBI) is a potential signature gene for mesenchymal subtype high-grade glioma.* J Neurooncol, 2018. **137**(2): p. 395-407.
597. Spinelli, C., et al., *Molecular subtypes and differentiation programmes of glioma stem cells as determinants of extracellular vesicle profiles and endothelial cell-stimulating activities.* 2018. **7**(1): p. 1490144.
598. Li, D., et al., *Glioma-associated human endothelial cell-derived extracellular vesicles specifically promote the tumourigenicity of glioma stem cells via CD9.* Oncogene, 2019. **38**(43): p. 6898-6912.
599. Guan, X., et al., *Rho GTPases and related signaling complexes in cell migration and invasion.* Experimental Cell Research, 2020. **388**(1): p. 111824.
600. Keerthikumar, S., et al., *Proteogenomic analysis reveals exosomes are more oncogenic than ectosomes.* Oncotarget, 2015. **6**(17): p. 15375-96.
601. Williams, K.C., et al., *Invadopodia are chemosensing protrusions that guide cancer cell extravasation to promote brain tropism in metastasis.* Oncogene, 2019. **38**(19): p. 3598-3615.
602. Juin, A., et al., *N-WASP Control of LPAR1 Trafficking Establishes Response to Self-Generated LPA Gradients to Promote Pancreatic Cancer Cell Metastasis.* Developmental cell, 2019. **51**(4): p. 431-445.e7.
603. Yu, H., et al., *RCC2 promotes proliferation and radio-resistance in glioblastoma via activating transcription of DNMT1.* Biochem Biophys Res Commun, 2019. **516**(3): p. 999-1006.
604. Binder, Z.A., et al., *Podocalyxin-like protein is expressed in glioblastoma multiforme stem-like cells and is associated with poor outcome.* PloS one, 2013. **8**(10): p. e75945-e75945.

605. Amaral, R.F., et al., *Microglial lysophosphatidic acid promotes glioblastoma proliferation and migration via LPA1 receptor.* 2021. **156**(4): p. 499-512.
606. Loskutov, Y.V., et al., *LPA signaling is regulated through the primary cilium: a novel target in glioblastoma.* Oncogene, 2018. **37**(11): p. 1457-1471.
607. Chen, Q., et al., *RCC2 contributes to tumor invasion and chemoresistance to cisplatin in hepatocellular carcinoma.* Human Cell, 2020. **33**(3): p. 709-720.
608. Snyder, K.A., et al., *Podocalyxin enhances breast tumor growth and metastasis and is a target for monoclonal antibody therapy.* Breast Cancer Research, 2015. **17**(1): p. 46.
609. Xu, Y., et al., *Podocalyxin-like, targeted by miR-138, promotes colorectal cancer cell proliferation, migration, invasion and EMT.* Eur Rev Med Pharmacol Sci, 2018. **22**(24): p. 8664-8674.
610. Nightingale, T.D., D.F. Cutler, and L.P.J.T.i.c.b. Cramer, *Actin coats and rings promote regulated exocytosis.* 2012. **22**(6): p. 329-337.
611. Zhang, Y., et al., *Dynamin2 GTPase contributes to invadopodia formation in invasive bladder cancer cells.* 2016. **480**(3): p. 409-414.
612. Chanda, D., et al., *Fibronectin on the Surface of Extracellular Vesicles Mediates Fibroblast Invasion.* Am J Respir Cell Mol Biol, 2019. **60**(3): p. 279-288.
613. Fedele, C., et al., *The αvβ6 integrin is transferred intercellularly via exosomes.* The Journal of biological chemistry, 2015. **290**(8): p. 4545-4551.
614. Zhang, H., et al., *Exosome-delivered EGFR regulates liver microenvironment to promote gastric cancer liver metastasis.* Nat Commun, 2017. **8**: p. 15016.
615. Gabison, E.E., et al., *EMMPRIN/CD147, an MMP modulator in cancer, development and tissue repair.* Biochimie, 2005. **87**(3): p. 361-368.
616. Sameshima, T., et al., *Expression of emmprin (CD147), a cell surface inducer of matrix metalloproteinases, in normal human brain and gliomas.* 2000. **88**(1): p. 21-27.
617. Tang, Y., et al., *Tumor-stroma interaction: positive feedback regulation of extracellular matrix metalloproteinase inducer (EMMPRIN) expression and matrix metalloproteinase-dependent generation of soluble EMMPRIN.* 2004. **2**(2): p. 73-80.
618. Hikita, T., et al., *Src in endosomal membranes promotes exosome secretion and tumor progression.* Scientific Reports, 2019. **9**(1): p. 3265.
619. Lane, R., et al., *Cell-derived extracellular vesicles can be used as a biomarker reservoir for glioblastoma tumor subtyping.* 2019. **2**(1): p. 1-12.
620. Bravo-Cordero, J.J., et al., *A novel spatiotemporal RhoC activation pathway locally regulates cofilin activity at invadopodia.* 2011. **21**(8): p. 635-644.
621. Malacombe, M., et al., *Intersectin-1L nucleotide exchange factor regulates secretory granule exocytosis by activating Cdc42.* The EMBO journal, 2006. **25**(15): p. 3494-3503.
622. Holliday, L.S., L.P.d. Faria, and W.J.J.I.J.o.M.S. Rody, *Actin and actin-associated proteins in extracellular vesicles shed by osteoclasts.* 2020. **21**(1): p. 158.
623. Das, A., et al., *Exosomes as a storehouse of tissue remodeling proteases and mediators of cancer progression.* Cancer Metastasis Rev, 2019. **38**(3): p. 455-468.
624. Ginestra, A., et al., *The amount and proteolytic content of vesicles shed by human cancer cell lines correlates with their in vitro invasiveness.* Anticancer Res, 1998. **18**(5a): p. 3433-7.
625. Costa-Silva, B., et al., *Pancreatic cancer exosomes initiate pre-metastatic niche formation in the liver.* Nature cell biology, 2015. **17**(6): p. 816-826.
626. Fouad, Y.A. and C.J.A.j.o.c.r. Aanei, *Revisiting the hallmarks of cancer.* 2017. **7**(5): p. 1016.
627. Meads, M., R. Gatenby, and W. Dalton, *Environment-mediated drug resistance: a major contributor to minimal residual disease.* Nature Reviews. Cancer, 2009. **9**(9): p. 665-674.
628. Szerlip, N.J., et al., *Intratumoral heterogeneity of receptor tyrosine kinases EGFR and PDGFRA amplification in glioblastoma defines subpopulations with distinct growth factor response.* Proc Natl Acad Sci U S A, 2012. **109**(8): p. 3041-6.

629. Hatzikirou, H., et al., *'Go or grow': the key to the emergence of invasion in tumour progression?* Mathematical medicine and biology: a journal of the IMA, 2012. **29**(1): p. 49-65.
630. Ichikawa, T., et al., *Phenotypic Transition as a Survival Strategy of Glioma.* Neurol Med Chir (Tokyo), 2016. **56**(7): p. 387-95.
631. Blanc, L. and M. Vidal, *New insights into the function of Rab GTPases in the context of exosomal secretion.* Small GTPases, 2018. **9**(1-2): p. 95-106.
632. Bergink, S., et al., *DNA damage triggers nucleotide excision repair-dependent monoubiquitylation of histone H2A.* 2006. **20**(10): p. 1343-1352.
633. Celiku, O., et al., *Visualizing molecular profiles of glioblastoma with GBM-BioDP.* 2014. **9**(7): p. e101239.
634. Fang, J., et al., *Junction plakoglobin, a potential prognostic marker of oral squamous cell carcinoma, promotes proliferation, migration and invasion.* J Oral Pathol Med, 2020. **49**(1): p. 30-38.
635. Mitchell, A., et al., *Dystroglycan function is a novel determinant of tumor growth and behavior in prostate cancer.* Prostate, 2013. **73**(4): p. 398-408.
636. Day, B.W., et al., *The dystroglycan receptor maintains glioma stem cells in the vascular niche.* Acta Neuropathologica, 2019. **138**(6): p. 1033-1052.
637. Shao, G., et al., *The E3 ubiquitin ligase NEDD4 mediates cell migration signaling of EGFR in lung cancer cells.* Mol Cancer, 2018. **17**(1): p. 24.
638. Zhang, H., et al., *NEDD4-1 regulates migration and invasion of glioma cells through CNrasGEF ubiquitination in vitro.* PloS one, 2013. **8**(12): p. e82789-e82789.
639. Jiang, J., et al., *PRRX1 Regulates Cellular Phenotype Plasticity and Dormancy of Head and Neck Squamous Cell Carcinoma Through miR-642b-3p.* Neoplasia, 2019. **21**(2): p. 216-229.
640. Sugiyama, M., et al., *Paired related homeobox 1 is associated with the invasive properties of glioblastoma cells.* Oncol Rep, 2015. **33**(3): p. 1123-1130.
641. Yang, X., et al., *Rab5a promotes the migration and invasion of hepatocellular carcinoma by up-regulating Cdc42.* Int J Clin Exp Pathol, 2018. **11**(1): p. 224-231.
642. Gao, W., M. Qiao, and K. Luo, *Long Noncoding RNA TP53TG1 Contributes to Radioresistance of Glioma Cells Via miR-524-5p/RAB5A Axis.* Cancer Biother Radiopharm, 2020.
643. Tu, C., et al., *Endosomal-sorting complexes required for transport (ESCRT) pathway-dependent endosomal traffic regulates the localization of active Src at focal adhesions.* Proc Natl Acad Sci U S A, 2010. **107**(37): p. 16107-12.
644. Lindberg, H., et al., *Angiotensin converting enzyme inhibitors for cancer treatment?* Acta Oncol, 2004. **43**(2): p. 142-52.
645. Bradshaw, A.R., et al., *Glioblastoma Multiforme Cancer Stem Cells Express Components of the Renin-Angiotensin System.* Front Surg, 2016. **3**: p. 51.
646. Wu, Z., et al., *MCAM is a novel metastasis marker and regulates spreading, apoptosis and invasion of ovarian cancer cells.* Tumour Biol, 2012. **33**(5): p. 1619-28.
647. Yawata, T., et al., *CD146 is highly expressed in glioma stem cells and acts as a cell cycle regulator.* J Neurooncol, 2019. **144**(1): p. 21-32.
648. Nakamura, T., et al., *Overexpression of C16orf74 is involved in aggressive pancreatic cancers.* Oncotarget, 2017. **8**(31): p. 50460-50475.
649. Brun, M., et al., *Calcineurin regulates nuclear factor I dephosphorylation and activity in malignant glioma cell lines.* 2013. **288**(33): p. 24104-24115.
650. Xu, C., et al., *NPTX2 promotes colorectal cancer growth and liver metastasis by the activation of the canonical Wnt/β-catenin pathway via FZD6.* Cell Death & Disease, 2019. **10**(3): p. 217.
651. Bartolini, A., et al., *The Neuronal Pentraxin-2 Pathway Is an Unrecognized Target in Human Neuroblastoma, Which Also Offers Prognostic Value in Patients.* Cancer Res, 2015. **75**(20): p. 4265-71.

652. Huo, L., et al., *miR-128-3p inhibits glioma cell proliferation and differentiation by targeting NPTX1 through IRS-1/PI3K/AKT signaling pathway.* Exp Ther Med, 2019. **17**(4): p. 2921-2930.
653. O'Neill, A.K., et al., *Protein kinase Cα promotes cell migration through a PDZ-dependent interaction with its novel substrate discs large homolog 1 (DLG1).* J Biol Chem, 2011. **286**(50): p. 43559-68.
654. Matsumoto, M., et al., *SAP97 promotes the stability of Nax channels at the plasma membrane.* 2012. **586**(21): p. 3805-3812.
655. Chen, S., et al., *RER1 enhances carcinogenesis and stemness of pancreatic cancer under hypoxic environment.* J Exp Clin Cancer Res, 2019. **38**(1): p. 15.
656. Yuan, X., et al., *Directional Migration in Esophageal Squamous Cell Carcinoma (ESCC) is Epigenetically Regulated by SET Nuclear Oncogene, a Member of the Inhibitor of Histone Acetyltransferase Complex.* Neoplasia (New York, N.Y.), 2017. **19**(11): p. 868-884.
657. Murray, D.W., et al., *Guanine nucleotide exchange factor Dock7 mediates HGF-induced glioblastoma cell invasion via Rac activation.* British journal of cancer, 2014. **110**(5): p. 1307-1315.
658. Ilboudo, A., et al., *Overexpression of phosphatidylinositol 4-kinase type IIIα is associated with undifferentiated status and poor prognosis of human hepatocellular carcinoma.* BMC Cancer, 2014. **14**(1): p. 7.
659. Park, Y., et al., *Inhibition of PI4K IIIα radiosensitizes in human tumor xenograft and immune-competent syngeneic murine tumor model.* 2017. **8**(66): p. 110392.
660. Li, Z., et al., *USP4 inhibits p53 and NF-κB through deubiquitinating and stabilizing HDAC2.* 2016. **35**(22): p. 2902-2912.
661. Zhang, Z., et al., *Silencing of histone deacetylase 2 suppresses malignancy for proliferation, migration, and invasion of glioblastoma cells and enhances temozolomide sensitivity.* Cancer Chemother Pharmacol, 2016. **78**(6): p. 1289-1296.
662. Li, H., et al., *Integrin α1 promotes tumorigenicity and progressive capacity of colorectal cancer.* Int J Biol Sci, 2020. **16**(5): p. 815-826.
663. Hu, Y., et al., *Quantitative Proteomics Analysis Indicates That Upregulation of lncRNA HULC Promotes Pathogenesis of Glioblastoma Cells.* OncoTargets and therapy, 2020. **13**: p. 5927-5938.
664. Makowska, K.A., et al., *Specific Myosins Control Actin Organization, Cell Morphology, and Migration in Prostate Cancer Cells.* Cell reports, 2015. **13**(10): p. 2118-2125.
665. Hsu, R.-M., et al., *Identification of MYO18A as a novel interacting partner of the PAK2/betaPIX/GIT1 complex and its potential function in modulating epithelial cell migration.* Molecular biology of the cell, 2010. **21**(2): p. 287-301.
666. Fan, C., et al., *GPC6 Promotes Cell Proliferation, Migration, and Invasion in Nasopharyngeal Carcinoma.* J Cancer, 2019. **10**(17): p. 3926-3932.
667. Zeng, C., et al., *Hedgehog signaling activation required for glypican-6-mediated regulation of invasion, migration, and epithelial-mesenchymal transition of gastric cancer cells.* Biosci Rep, 2020. **40**(6).
668. Listik, E. and L. Toma, *Glypican-1 in human glioblastoma: implications in tumorigenesis and chemotherapy.* Oncotarget, 2020. **11**(9): p. 828-845.
669. Sumardika, I.W., et al., *Neuroplastin-β mediates S100A8/A9-induced lung cancer disseminative progression.* Mol Carcinog, 2019. **58**(6): p. 980-995.
670. Rodriguez-Pinto, D., et al., *Identification of novel tumor antigens with patient-derived immune-selected antibodies.* Cancer Immunol Immunother, 2009. **58**(2): p. 221-34.
671. Dornier, E., et al., *TspanC8 tetraspanins regulate ADAM10/Kuzbanian trafficking and promote Notch activation in flies and mammals.* J Cell Biol, 2012. **199**(3): p. 481-96.
672. Fu, L., et al., *ADAM10 regulates proliferation, invasion, and chemoresistance of bladder cancer cells.* Tumour Biol, 2014. **35**(9): p. 9263-8.

673. Chen, Q., et al., *MicroRNA-217 inhibits cell proliferation, invasion and migration by targeting Tpd52l2 in human pancreatic adenocarcinoma.* Oncol Rep, 2017. **38**(6): p. 3567-3573.
674. Yu, J., S.-W. Wu, and W.-P. Wu, *A tumor-suppressive microRNA, miRNA-485-5p, inhibits glioma cell proliferation and invasion by down-regulating TPD52L2.* American journal of translational research, 2017. **9**(7): p. 3336-3344.
675. Zheng, Y., et al., *Insulin-like growth factor 1-induced enolase 2 deacetylation by HDAC3 promotes metastasis of pancreatic cancer.* Signal Transduction and Targeted Therapy, 2020. **5**(1): p. 53.
676. Sanzey, M., et al., *Comprehensive analysis of glycolytic enzymes as therapeutic targets in the treatment of glioblastoma.* PloS one, 2015. **10**(5): p. e0123544-e0123544.
677. Jian, Q., et al., *Rab23 promotes squamous cell carcinoma cell migration and invasion via integrin β1/Rac1 pathway.* Oncotarget, 2016. **7**(5): p. 5342-52.
678. Wang, M., Q. Dong, and Y. Wang, *Rab23 is overexpressed in human astrocytoma and promotes cell migration and invasion through regulation of Rac1.* Tumour Biol, 2016. **37**(8): p. 11049-55.
679. Chiang, C.Y., et al., *SH3BGRL3 Protein as a Potential Prognostic Biomarker for Urothelial Carcinoma: A Novel Binding Partner of Epidermal Growth Factor Receptor.* Clin Cancer Res, 2015. **21**(24): p. 5601-11.
680. Khalil, A.A., *Biomarker discovery: A proteomic approach for brain cancer profiling.* 2007. **98**(2): p. 201-213.
681. Liu, B., Y. Han, and S.-B.J.M.c. Qian, *Cotranslational response to proteotoxic stress by elongation pausing of ribosomes.* 2013. **49**(3): p. 453-463.
682. Munir, R., et al., *Lipid metabolism in cancer cells under metabolic stress.* British journal of cancer, 2019. **120**(12): p. 1090-1098.
683. Yu, D.-L., et al., *Acyl-CoA dehydrogenase long chain expression is associated with esophageal squamous cell carcinoma progression and poor prognosis.* OncoTargets and therapy, 2018. **11**: p. 7643-7653.
684. Fernandez, R.F., et al., *Acyl-CoA synthetase 6 enriches the neuroprotective omega-3 fatty acid DHA in the brain.* 2018. **115**(49): p. 12525-12530.
685. Weber, S., et al., *Aldo-keto Reductase 1B15 (AKR1B15): a mitochondrial human aldo-keto reductase with activity toward steroids and 3-keto-acyl-CoA conjugates.* The Journal of biological chemistry, 2015. **290**(10): p. 6531-6545.
686. van Weverwijk, A., et al., *Metabolic adaptability in metastatic breast cancer by AKR1B10-dependent balancing of glycolysis and fatty acid oxidation.* Nature communications, 2019. **10**(1): p. 2698-2698.
687. Mattern, H.M., L.S. Raikar, and C.D. Hardin, *The effect of caveolin-1 (Cav-1) on fatty acid uptake and CD36 localization and lipotoxicity in vascular smooth muscle (VSM) cells.* International journal of physiology, pathophysiology and pharmacology, 2009. **1**(1): p. 1-14.
688. Asterholm, I.W., et al., *Altered mitochondrial function and metabolic inflexibility associated with loss of caveolin-1.* Cell Metab, 2012. **15**(2): p. 171-85.
689. Pu, W., et al., *Correlation of the invasive potential of glioblastoma and expression of caveola-forming proteins caveolin-1 and CAVIN1.* J Neurooncol, 2019. **143**(2): p. 207-220.
690. Goh, W.Q., et al., *DLAT subunit of the pyruvate dehydrogenase complex is upregulated in gastric cancer-implications in cancer therapy.* Am J Transl Res, 2015. **7**(6): p. 1140-51.
691. Rusu, P., et al., *GPD1 Specifically Marks Dormant Glioma Stem Cells with a Distinct Metabolic Profile.* Cell Stem Cell, 2019. **25**(2): p. 241-257.e8.
692. Paul, N.R., et al., *α5β1 integrin recycling promotes Arp2/3-independent cancer cell invasion via the formin FHOD3.* 2015. **210**(6): p. 1013-1031.
693. Vogel, T.W., et al., *Proteins and protein pattern differences between glioma cell lines and glioblastoma multiforme.* 2005. **11**(10): p. 3624-3632.

694. Furuta, M., et al., *Protein patterns and proteins that identify subtypes of glioblastoma multiforme.* 2004. **23**(40): p. 6806-6814.
695. Polisetty, R.V., et al., *LC-MS/MS analysis of differentially expressed glioblastoma membrane proteome reveals altered calcium signaling and other protein groups of regulatory functions.* 2012. **11**(6): p. M111. 013565.
696. Collet, B., et al., *Differential analysis of glioblastoma multiforme proteome by a 2D-DIGE approach.* 2011. **9**(1): p. 1-14.
697. Kumar, D.M., et al., *Temozolomide-modulated glioma proteome: role of interleukin-1 receptor-associated kinase-4 (IRAK4) in chemosensitivity.* Proteomics, 2013. **13**(14): p. 2113-24.
698. Yi, G.-Z., et al., *Identification of Key Candidate Proteins and Pathways Associated with Temozolomide Resistance in Glioblastoma Based on Subcellular Proteomics and Bioinformatical Analysis.* BioMed research international, 2018. **2018**: p. 5238760-5238760.
699. Li, M., et al., *Integrated proteomic and metabolomic profiling the global response of rat glioma model by temozolomide treatment.* 2020. **211**: p. 103578.
700. André-Grégoire, G., N. Bidère, and J. Gavard, *Temozolomide affects extracellular vesicles released by glioblastoma cells.* Biochimie, 2018. **155**: p. 11-15.
701. Friedl, P. and S.J.C. Alexander, *Cancer invasion and the microenvironment: plasticity and reciprocity.* 2011. **147**(5): p. 992-1009.
702. Branch, K.M., D. Hoshino, and A.M. Weaver, *Adhesion rings surround invadopodia and promote maturation.* Biol Open, 2012. **1**(8): p. 711-22.
703. Turaga, S.M. and J.D. Lathia, *Adhering towards tumorigenicity: altered adhesion mechanisms in glioblastoma cancer stem cells.* CNS oncology, 2016. **5**(4): p. 251-259.
704. Bravo-Cordero, J.J., et al., *MT1-MMP proinvasive activity is regulated by a novel Rab8-dependent exocytic pathway.* Embo j, 2007. **26**(6): p. 1499-510.
705. Brzozowski, J.S., et al., *Extracellular vesicles with altered tetraspanin CD9 and CD151 levels confer increased prostate cell motility and invasion.* 2018. **8**(1): p. 1-13.
706. Kraus, A.C., et al., *In vitro chemo-and radio-resistance in small cell lung cancer correlates with cell adhesion and constitutive activation of AKT and MAP kinase pathways.* 2002. **21**(57): p. 8683-8695.
707. Hazlehurst, L., et al., *Adhesion to fibronectin via β1 integrins regulates p27 kip1 levels and contributes to cell adhesion mediated drug resistance (CAM-DR).* 2000. **19**(38): p. 4319-4327.
708. Liang, Y.-K., et al., *STEM-11. CD146/MCAM REGULATES MESENCHYMAL PROPERTIES, STEMNESS, RADIO-RESISTANCE AND YAP ACTIVITY IN GLIOBLASTOMA.* Neuro-Oncology, 2019. **21**(Supplement_6): p. vi236-vi236.
709. Lathia, J.D., et al., *Integrin alpha 6 regulates glioblastoma stem cells.* 2010. **6**(5): p. 421-432.
710. Tilghman, J., et al., *Regulation of Glioblastoma Tumor-Propagating Cells by the Integrin Partner Tetraspanin CD151.* Neoplasia (New York, N.Y.), 2016. **18**(3): p. 185-198.
711. Garnier, D., et al., *Divergent evolution of temozolomide resistance in glioblastoma stem cells is reflected in extracellular vesicles and coupled with radiosensitization.* 2018. **20**(2): p. 236-248.
712. Singh, S.K., et al., *Cancer stem cells in nervous system tumors.* 2004. **23**(43): p. 7267-7273.
713. Wang, L., et al., *Expression of cortactin in human gliomas and its effect on migration and invasion of glioma cells.* 2015. **34**(4): p. 1815-1824.
714. Timpson, P., et al., *Cortactin overexpression inhibits ligand-induced down-regulation of the epidermal growth factor receptor.* 2005. **65**(8): p. 3273-3280.
715. Eke, I., et al., *β 1 Integrin/FAK/cortactin signaling is essential for human head and neck cancer resistance to radiotherapy.* 2012. **122**(4): p. 1529-1540.
716. Ghebeh, H., et al., *Fascin is involved in the chemotherapeutic resistance of breast cancer cells predominantly via the PI3K/Akt pathway.* 2014. **111**(8): p. 1552-1561.

717. Zhang, Y., et al., *FSCN-1 increases doxorubicin resistance in hepatocellular carcinoma through promotion of epithelial-mesenchymal transition.* International journal of oncology, 2018. **52**(5): p. 1455-1464.
718. Schnaeker, E.-M., et al., *Microtubule-dependent matrix metalloproteinase-2/matrix metalloproteinase-9 exocytosis: prerequisite in human melanoma cell invasion.* 2004. **64**(24): p. 8924-8931.
719. Buschman, M.D. and S.J. Field, *MYO18A: An unusual myosin.* Advances in biological regulation, 2018. **67**: p. 84-92.
720. Larocque, G., et al., *Tumor protein D54 defines a new class of intracellular transport vesiclesNew small transport vesicles defined by TPD54.* 2020. **219**(1).
721. Toma-Fukai, S. and T.J.M. Shimizu, *Structural Insights into the Regulation Mechanism of Small GTPases by GEFs.* 2019. **24**(18): p. 3308.
722. Lagal, V., et al., *Spire-1 contributes to the invadosome and its associated invasive properties.* 2014. **127**(2): p. 328-340.
723. Liu, S.-s., et al., *Knockdown of Rab5a expression decreases cancer cell motility and invasion through integrin-mediated signaling pathway.* Journal of biomedical science, 2011. **18**(1): p. 58-58.
724. Zhang, D., C. Lu, and H. Ai, *Rab5a is overexpressed in oral cancer and promotes invasion through ERK/MMP signaling.* Molecular medicine reports, 2017. **16**(4): p. 4569-4576.
725. Kamiya-Matsuoka, C. and M.R.J.C.o. Gilbert, *Treating recurrent glioblastoma: an update.* 2015. **4**(2): p. 91-104.
726. Zheng, R., et al., *[Effect of Src tyrosine kinase inhibition on secretion of MMP-2 and MMP-9 by non-small cell lung cancer cells].* Zhongguo Fei Ai Za Zhi, 2011. **14**(1): p. 13-7.
727. Yoshida, T., et al., *Tyrosine phosphoproteomics identifies both codrivers and cotargeting strategies for T790M-related EGFR-TKI resistance in non–small cell lung cancer.* 2014. **20**(15): p. 4059-4074.
728. Jin, M.H., et al., *Resistance Mechanism against Trastuzumab in HER2-Positive Cancer Cells and Its Negation by Src Inhibition.* Mol Cancer Ther, 2017. **16**(6): p. 1145-1154.
729. Formisano, L., et al., *Epidermal growth factor-receptor activation modulates Src-dependent resistance to lapatinib in breast cancer models.* Breast Cancer Res, 2014. **16**(3): p. R45.
730. Liu, Y., L.S. Zuckier, and N.V. Ghesani, *Dominant uptake of fatty acid over glucose by prostate cells: a potential new diagnostic and therapeutic approach.* Anticancer Res, 2010. **30**(2): p. 369-74.
731. Beloribi-Djefaflia, S., S. Vasseur, and F. Guillaumond, *Lipid metabolic reprogramming in cancer cells.* Oncogenesis, 2016. **5**(1): p. e189-e189.
732. Duman, C., et al., *Acyl-CoA-binding protein drives glioblastoma tumorigenesis by sustaining fatty acid oxidation.* 2019. **30**(2): p. 274-289. e5.
733. Knowles, L.M., et al., *Fibrin As a Target for Glioblastoma Detection and Treatment.* Blood, 2019. **134**(Supplement_1): p. 3630-3630.
734. Stoppelli, M.P., *The plasminogen activation system in cell invasion*, in *Madame Curie Bioscience Database [Internet]*. 2013, Landes Bioscience.
735. Bi, W.L. and R. Beroukhim, *Beating the odds: extreme long-term survival with glioblastoma.* Neuro Oncol, 2014. **16**(9): p. 1159-60.
736. Hung, Y., et al., *The exosomal compartment protects epidermal growth factor receptor from small molecule inhibitors.* Biochemical and Biophysical Research Communications, 2019. **510**(1): p. 42-47.
737. Steinle, M., et al., *Ionizing radiation induces migration of glioblastoma cells by activating BK K(+) channels.* Radiotherapy and oncology, 2011. **101**(1): p. 122-126.
738. Jang, H.S., S. Lal, and J.A. Greenwood, *Calpain 2 is required for glioblastoma cell invasion: regulation of matrix metalloproteinase 2.* Neurochem Res, 2010. **35**(11): p. 1796-804.

739. Sun, J., et al., *STIM1- and Orai1-mediated Ca(2+) oscillation orchestrates invadopodium formation and melanoma invasion.* J Cell Biol, 2014. **207**(4): p. 535-48.
740. Kato, Y., et al., *Acidic extracellular pH increases calcium influx-triggered phospholipase D activity along with acidic sphingomyelinase activation to induce matrix metalloproteinase-9 expression in mouse metastatic melanoma.* Febs j, 2007. **274**(12): p. 3171-83.
741. Dinevska, M., et al., *Inhibition of Radiation and Temozolomide-Induced Glioblastoma Invadopodia Activity Using Ion Channel Drugs.* Cancers, 2020. **12**(10): p. 2888.
742. Taraboletti, G., et al., *Targeting tumor angiogenesis with TSP-1-based compounds: rational design of antiangiogenic mimetics of endogenous inhibitors.* 2010. **1**(7): p. 662.
743. Baker, L.H., et al., *Randomized, phase II study of the thrombospondin-1-mimetic angiogenesis inhibitor ABT-510 in patients with advanced soft tissue sarcoma.* 2008. **26**(34): p. 5583-5588.
744. Markovic, S.N., et al., *A phase II study of ABT-510 (thrombospondin-1 analog) for the treatment of metastatic melanoma.* 2007. **30**(3): p. 303-309.
745. Almendros, I., et al., *Intermittent hypoxia increases melanoma metastasis to the lung in a mouse model of sleep apnea.* Respir Physiol Neurobiol, 2013. **186**(3): p. 303-7.
746. Widmer, D.S., et al., *Hypoxia contributes to melanoma heterogeneity by triggering HIF1α-dependent phenotype switching.* J Invest Dermatol, 2013. **133**(10): p. 2436-2443.
747. Monteiro, A.R., et al., *The Role of Hypoxia in Glioblastoma Invasion.* Cells, 2017. **6**(4): p. 45.
748. Amagasaki, K., et al., *Antisense-mediated reduction in thrombospondin-1 expression reduces cell motility in malignant glioma cells.* Int J Cancer, 2001. **94**(4): p. 508-12.
749. Vella, L.J., et al., *A rigorous method to enrich for exosomes from brain tissue.* J Extracell Vesicles, 2017. **6**(1): p. 1348885.
750. Chong, C.R. and D.J. Sullivan, Jr., *New uses for old drugs.* Nature, 2007. **448**(7154): p. 645-6.
751. Stoletov, K. and J.D. Lewis, *Invadopodia: a new therapeutic target to block cancer metastasis.* Expert Rev Anticancer Ther, 2015. **15**(7): p. 733-5.
752. Iizuka, S., et al., *The role of Tks adaptor proteins in invadopodia formation, growth and metastasis of melanoma.* Oncotarget, 2016. **7**(48): p. 78473-78486.
753. Lagoutte, E., et al., *LIMK Regulates Tumor-Cell Invasion and Matrix Degradation Through Tyrosine Phosphorylation of MT1-MMP.* Sci Rep, 2016. **6**: p. 24925.
754. Crowley, J.L., et al., *Supervillin reorganizes the actin cytoskeleton and increases invadopodial efficiency.* Mol Biol Cell, 2009. **20**(3): p. 948-62.

Supplementary Figures

Supplementary Figure 1: Profiling of secreted proteases/inhibitors in GBM Cell Lines

To determine the effect of RT/TMZ on the secretion of a variety of proteases and their inhibitors, conditioned serum-free OptiMEM® medium from untreated, single treated (2Gy RT and 50μM TMZ) and LT treated U87MG, LN229, MU4 and MU41 cells was collected after a 24h incubation and screened using human protease and inhibitor antibody arrays (Proteome Profiler TM Array, R&D Systems) (Chemiluminescent Readout). Media sample volumes were normalized to a 300μg threshold of corresponding protein cell lysate. A profile map for the **(A.)** protease array and for the **(B.)** inhibitor array is provided. Protease array membranes are shown for each GBM cell line. Outlined on the protease arrays are the two key invadopodia-associated proteases MMP-2 (green) and MMP-9 (red).

A.

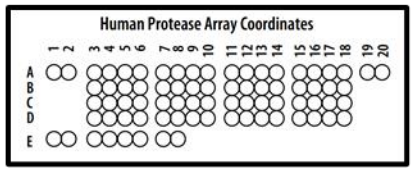

Spot Coordinate	Protease/Control	Isoform
C7, C8	Kallikrein 10	Proform & Active
C9, C10	Kallikrein 11	Proform & Active
C11, C12	Kallikrein 13	Proform & Active
C13, C14	MMP-1	Proform & Active
C15, C16	MMP-2	Proform & Active
C17, C18	MMP-3	Proform & Active
D3, D4	MMP-7	Proform & Active
D5, D6	MMP-8	Proform & Active
D7, D8	MMP-9	Proform & Active
D9, D10	MMP-10	Proform & Active
D11, D12	MMP-12	Proform & Active
D13, D14	MMP-13	Proform
D15, D16	Neprilysin/CD10	Ectodomain
D17, D18	Presenilin	N-terminal fragment
E1, E2	Reference Spots	-
E3, E4	Proprotein Convertase 9	Active
E5, E6	Proteinase 3	Active
E7, E8	uPA/Urokinase	Proform & Active
E9, E10	Negative Control	-

Spot Coordinate	Protease/Control	Isoform
A1, A2	Reference Spots	-
A3, A4	ADAM8	Ectodomain
A5, A6	ADAM9	Ectodomain
A7, A8	ADAMTS1	Proform
A9, A10	ADAMTS13	Active
A11, A12	Cathepsin A	Proform & Active
A13, A14	Cathepsin B	Proform
A15, A16	Cathepsin C	Proform & Active
A17, A18	Cathepsin D	Proform & Active
A19, A20	Reference Spots	-
B3, B4	Cathepsin E	Proform & Active
B5, B6	Cathepsin L	Proform & Active
B7, B8	Cathepsin S	Proform & Active
B9, B10	Cathepsin V	Proform & Active
B11, B12	Cathepsin X/Z/P	Proform & Active
B13, B14	DPPIV/CD26	Ectodomain
B15, B16	Kallikrein 3/PSA	Proform & Active
B17, B18	Kallikrein 5	Proform & Active
C3, C4	Kallikrein 6	Proform & Active
C5, C6	Kallikrein 7	Proform & Active

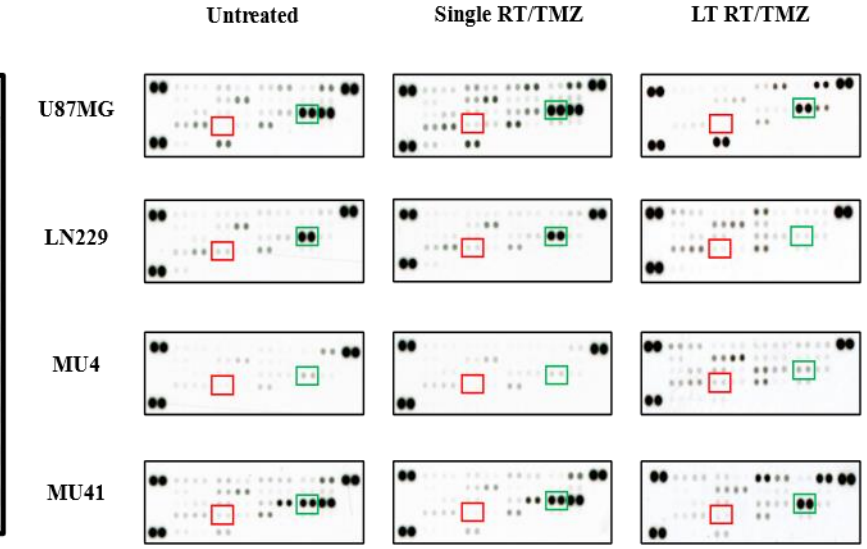

B.

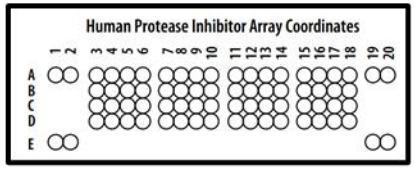

Spot Coordinate	Inhibitor/Control
A1, A2	Reference Spots
A3, A4	APP/Protease Nexin II (pan)
A5, A6	Cystatin A
A7, A8	Cystatin B
A9, A10	Cystatin C
A11, A12	Cystatin E/M
A13, A14	EMMPRIN/CD147
A15, A16	Fetuin B
A17, A18	HAI-1
A19, A20	Reference Spots
B3, B4	HAI-2
B5, B6	HE4/WFDC2
B7, B8	Latexin
B9, B10	Lipocalin-1
B11, B12	Lipocalin-2/NGAL
B13, B14	RECK
B15, B16	Serpin A5/Protein C Inhibitor
B17, B18	Serpin A8/Angiotensinogen

Spot Coordinate	Inhibitor/Control
C3, C4	Serpin A9/Centerin
C5, C6	Serpin A12
C7, C8	Serpin B5/Maspin
C9, C10	Serpin B6
C11, C12	Serpin B8/Proteinase Inhibitor 8
C13, C14	Serpin E1/PAI-1
C15, C16	Serpin F1/PEDF
C17, C18	Testican 1/SPOCK1
D3, D4	Testican 2/SPOCK2
D5, D6	TFPI
D7, D8	TFPI-2
D9, D10	TIMP-1
D11, D12	TIMP-2
D13, D14	TIMP-3
D15, D16	TIMP-4
D17, D18	Trappin-2/Elafin
E1, E2	Reference Spots
E19, E20	Negative Control

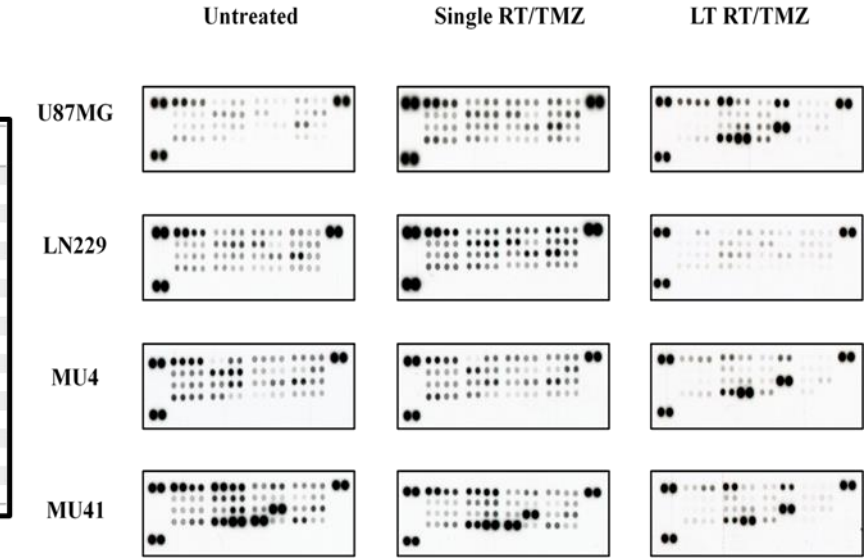

Supplementary Figure 2: Differential expression analysis of genes in GBM cell lines following RT/TMZ treatment

(**A.**) Differential expression heatmaps for genes within each biological process (angiogenesis, cancer metabolism, ECM layers, ECM remodelling, EMT, hypoxia, metastasis, transcription factor, tumour growth, tumour invasion). Unsupervised hierarchical clustering of gene expression fold changes was performed using the Perseus Bioinformatics platform (version 1.5.5.0) [339]. Normalised Z-scores are indicated by colour, whereby red indicates upregulated gene expression and green indicates downregulated gene expression in RT/TMZ treated GBM cells relative to the corresponding untreated cells. Genes were divided into 4 clusters based on hierarchical clustering, as shown to the left of the heatmap, revealing a different set of upregulated genes in each GBM cell line. (**B.**) Unsupervised hierarchical clustering was also performed on the top 100 DE genes in each cell line following RT/TMZ treatment. Gene expression was first normalised, and genes below a minimum threshold of 100 transcript counts were removed. The log2-FC difference in expression following RT/TMZ treatment was then calculated, and the top 100 DE genes for each cell line were identified. These were combined across the four GBM cell lines to give 390 DE genes that were included in the analysis, which was performed using the Perseus Bioinformatics platform (version 1.5.5.0) [339]. The log2-FC expression data was transformed to a standardized z scale, indicated by colour, whereby red indicates upregulated gene expression and green indicates downregulated gene expression in RT/TMZ treated GBM cells relative to the corresponding untreated cells.

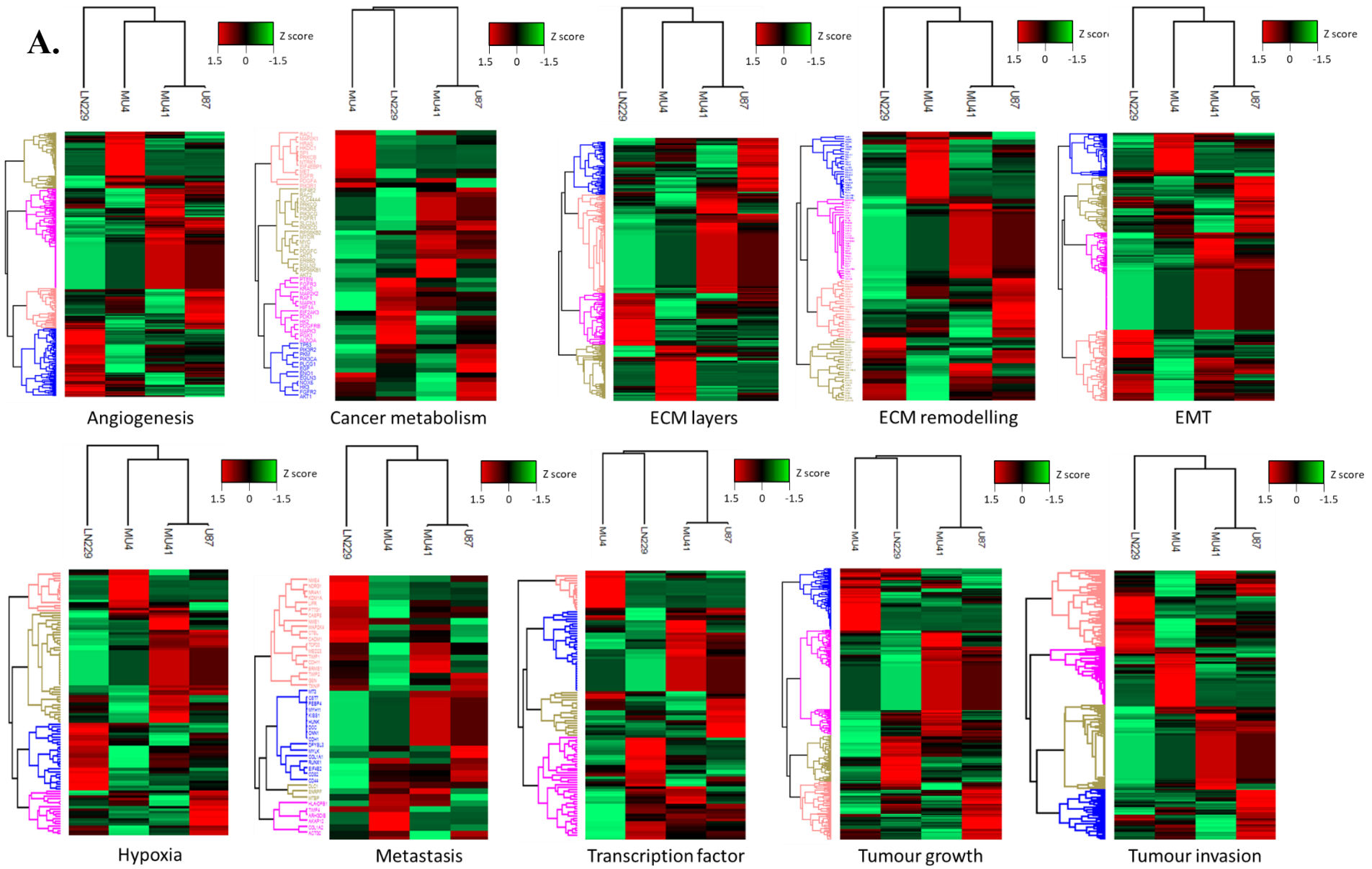
A.
Z score
1.5
0
-1.5
LN229
MU4
MU41
U87
Angiogenesis
Cancer metabolism
ECM layers
ECM remodelling
EMT
Hypoxia
Metastasis
Transcription factor
Tumour growth
Tumour invasion

B.

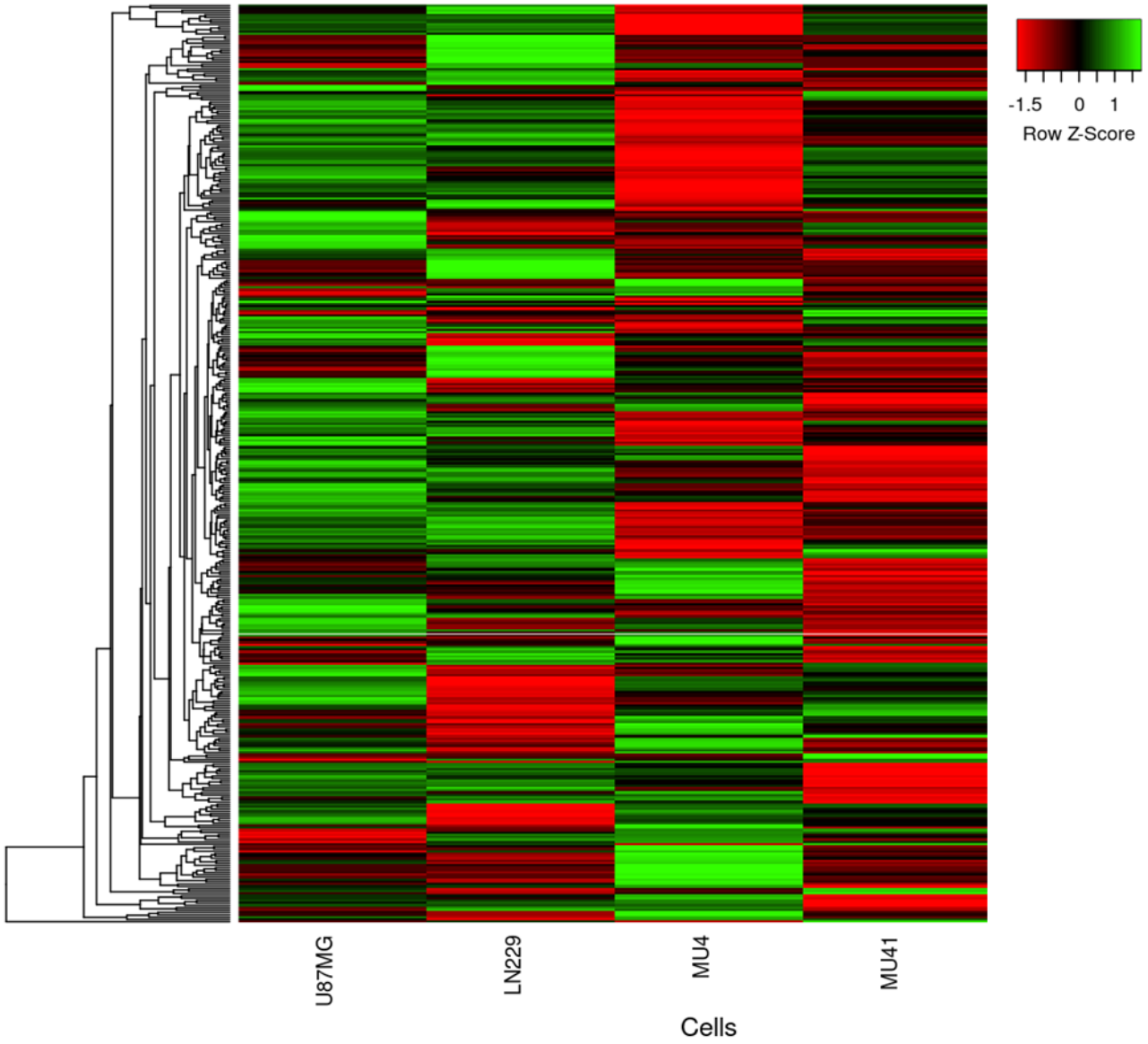

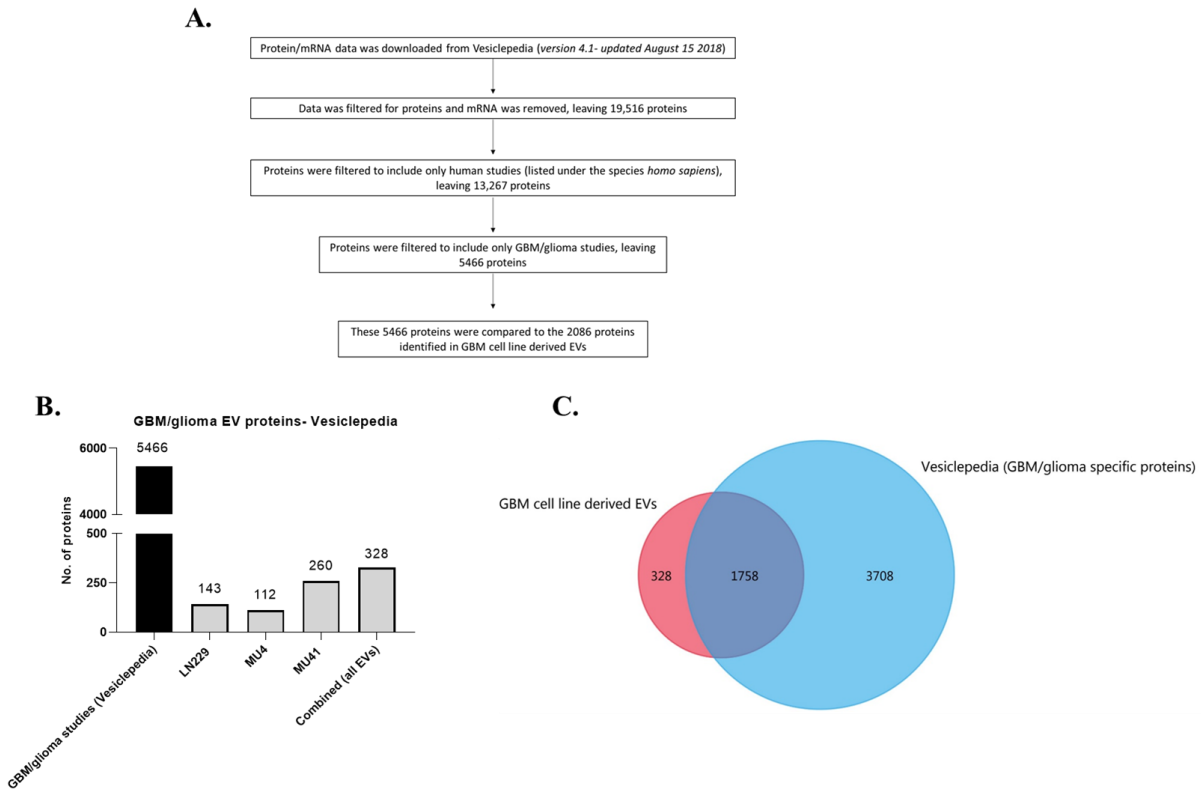

Supplementary Figure 3: Functional enrichment analysis of proteins uniquely expressed in RT/TMZ treated GBM cell lines

(**A.**) A schematic representing the workflow utilised to identify proteins present in the GBM cell line derived EV proteome that are not included in GBM and/or glioma datasets in Vesiclepedia (version 4.1) [245]. (**B.**) Comparison of the proteins identified in GBM cell line derived EVs from each cell line with proteins identified in GBM and/or glioma EV datasets (5468 proteins) as compiled in Vesiclepedia. (**G.**) Venn diagram showing overlap between proteins identified in EVs isolated from GBM cell lines (red-2086 proteins) and EV proteins listed in GBM and/or glioma datasets recorded in Vesiclepedia (blue-5468 proteins). (*Proteins matched by gene name; restricted to proteins annotated as originating from 'homo sapiens')*

Supplementary Figure 4: Functional enrichment analysis of proteins uniquely expressed in RT/TMZ treated GBM cell lines

(**A.**) A Venn diagram comparing the proteins detected in the proteomes of untreated and RT/TMZ treated GBM cell lines (LN229, MU4 and MU41 cell lines: untreated- 2323 total proteins, treated- 2432 total proteins). FunRich analysis of the 263 proteins uniquely detected in RT/TMZ treated GBM cells revealing the top 10 significantly enriched annotations for - (**B.**) biological processes, - (**C.**) molecular functions, and - (**D.**) REACTOME pathways. Only 9 significantly enriched REACTOME pathways were identified. (*P values were calculated by two-sided hypergeometric test and are shown as -log10(P)*)

A.

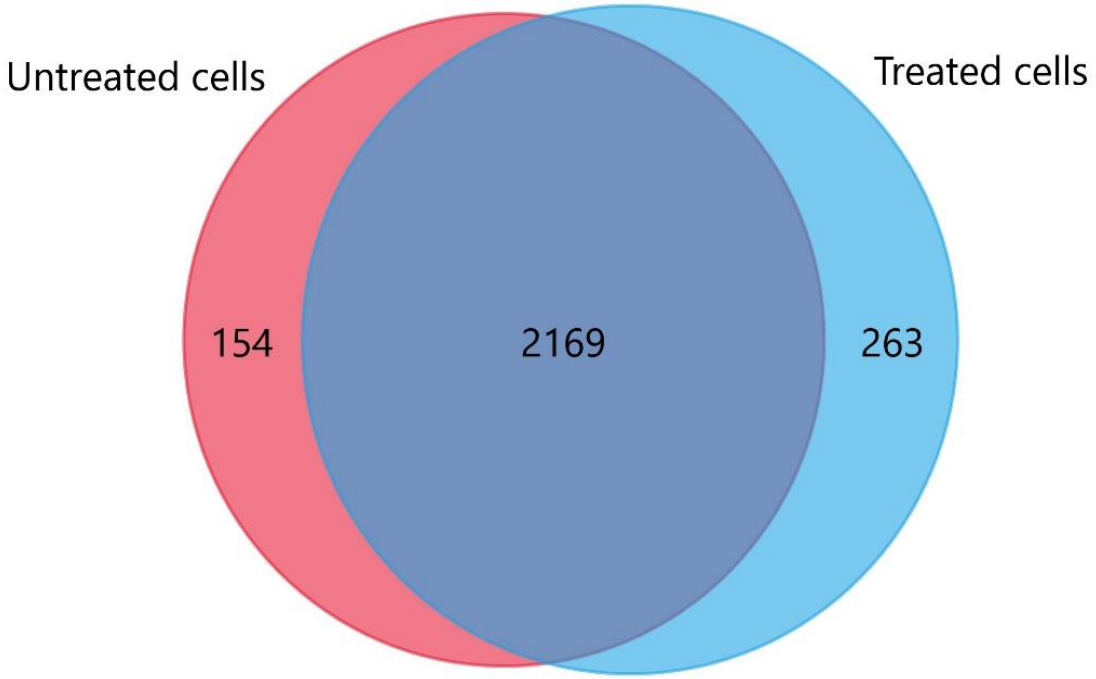

B.

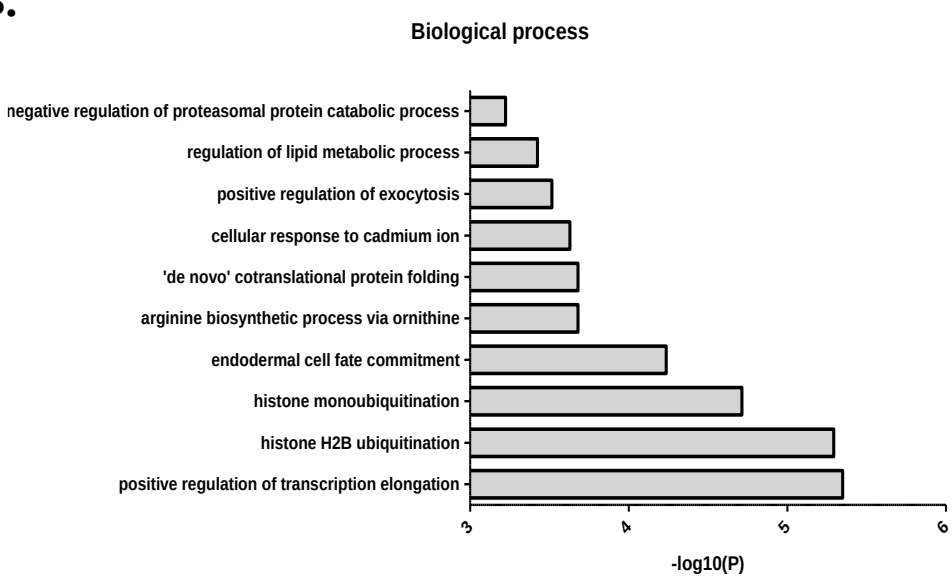
Biological process
negative regulation of proteasomal protein catabolic process
regulation of lipid metabolic process
positive regulation of exocytosis
cellular response to cadmium ion
'de novo' cotranslational protein folding
arginine biosynthetic process via ornithine
endodermal cell fate commitment
histone monoubiquitination
histone H2B ubiquitination
positive regulation of transcription elongation
3
4
5
6
-log10(P)

C.

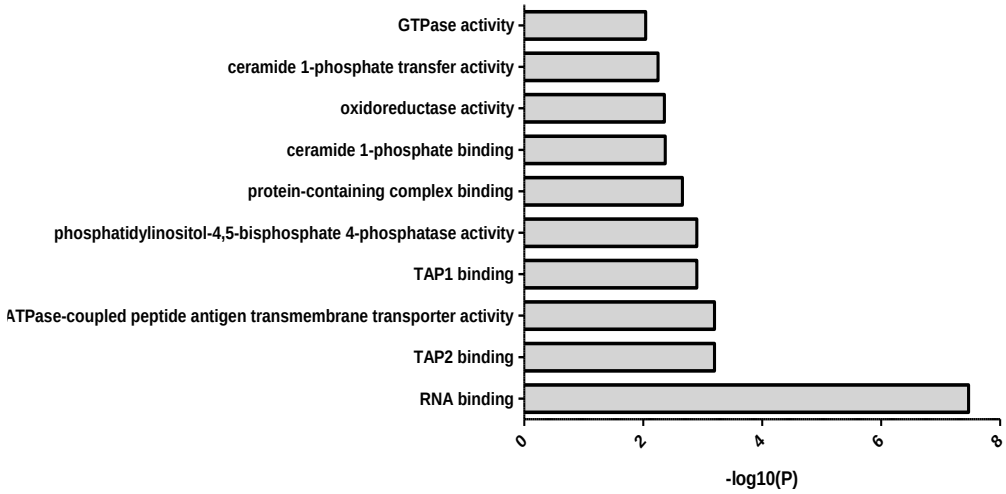
Molecular function
GTPase activity
ceramide 1-phosphate transfer activity
oxidoreductase activity
ceramide 1-phosphate binding
protein-containing complex binding
phosphatidylinositol-4,5-bisphosphate 4-phosphatase activity
TAP1 binding
ATPase-coupled peptide antigen transmembrane transporter activity
TAP2 binding
RNA binding
0
2
4
6
8
-log10(P)

D.

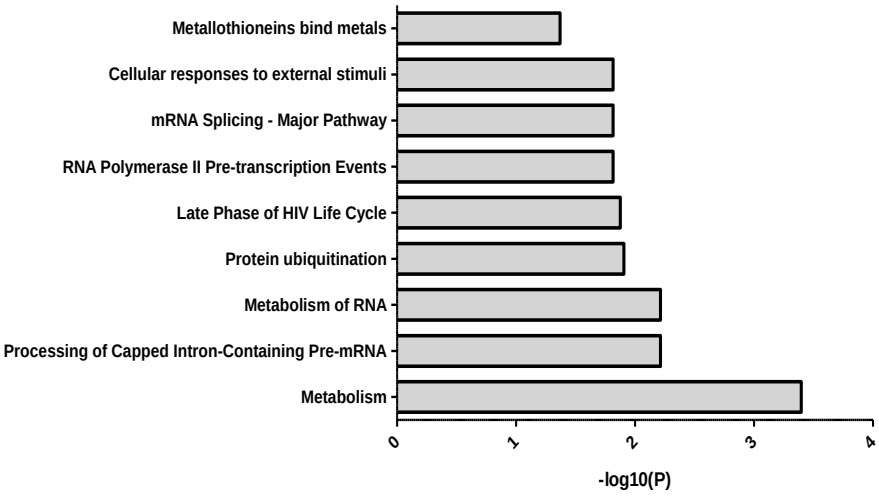
REACTOME pathways
Metallothioneins bind metals
Cellular responses to external stimuli
mRNA Splicing - Major Pathway
RNA Polymerase II Pre-transcription Events
Late Phase of HIV Life Cycle
Protein ubiquitination
Metabolism of RNA
Processing of Capped Intron-Containing Pre-mRNA
Metabolism
0
1
2
3
4
-log10(P)

Supplementary Figure 5: Functional enrichment analysis of proteins uniquely detected in EVs isolated from RT/TMZ treated GBM cell lines

(**A.**) A Venn diagram comparing the proteins detected in the proteomes of EVs isolated from untreated and RT/TMZ treated GBM cell lines (LN229, MU4 and MU41 cell lines: EVs (untreated cells)- 1819 proteins, EVs (treated cells)- 1971 proteins). 429 proteins were uniquely detected in the proteome of EVs from RT/TMZ treated cells. FunRich analysis of the 429 proteins uniquely detected in EVs isolated from RT/TMZ treated GBM cells revealing the top 10 significantly enriched annotations for - (**B.**) biological processes, - (**C.**) molecular functions, and - (**D.**) REACTOME pathways. (*P values were calculated by two-sided hypergeometric test and are shown as -log10(P)*).

A.

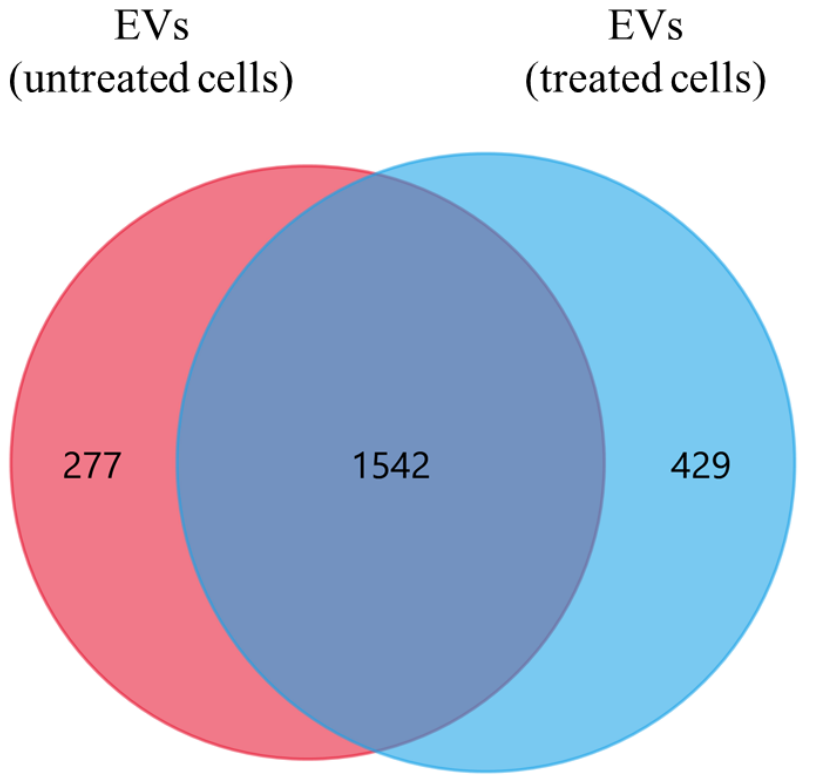

B.

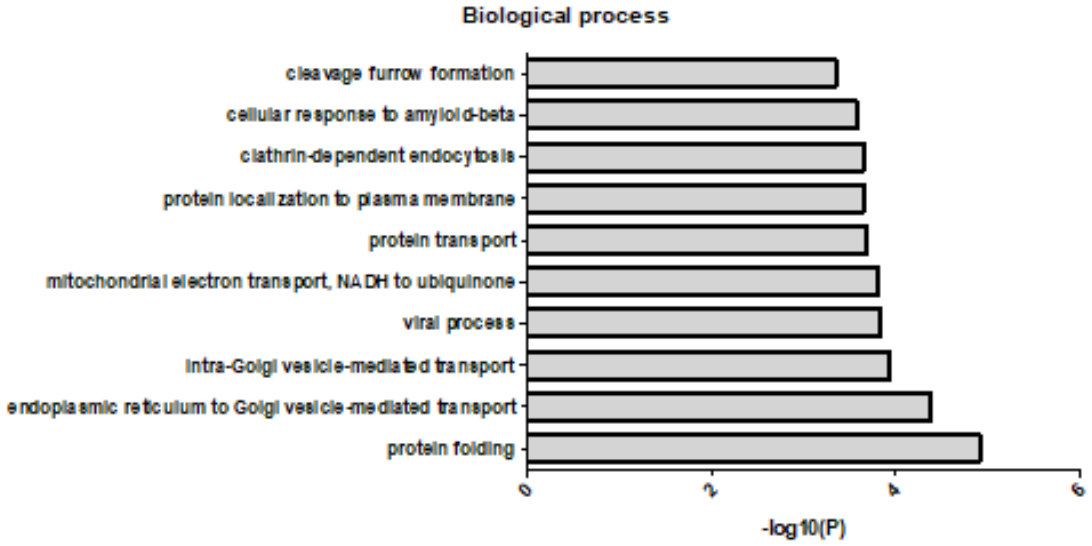
Biological process
cleavage furrow formation
cellular response to amyloid-beta
clathrin-dependent endocytosis
protein localization to plasma membrane
protein transport
mitochondrial electron transport, NADH to ubiquinone
viral process
intra-Golgi vesicle-mediated transport
endoplasmic reticulum to Golgi vesicle-mediated transport
protein folding
0
2
4
6
-log10(P)

C.

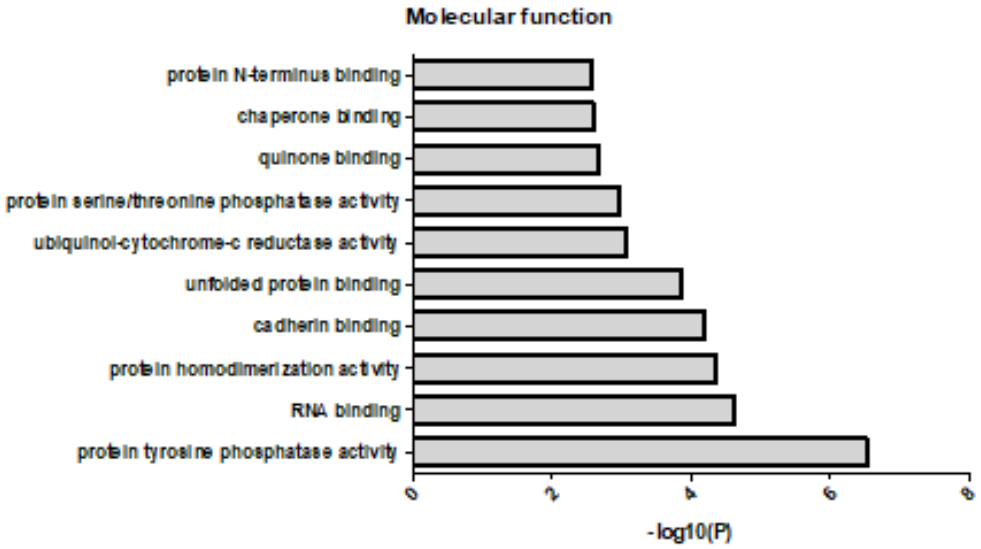
Molecular function
protein N-terminus binding
chaperone binding
quinone binding
protein serine/threonine phosphatase activity
ubiquinol-cytochrome-c reductase activity
unfolded protein binding
cadherin binding
protein homodimerization activity
RNA binding
protein tyrosine phosphatase activity
0
2
4
6
8
-log10(P)

D.

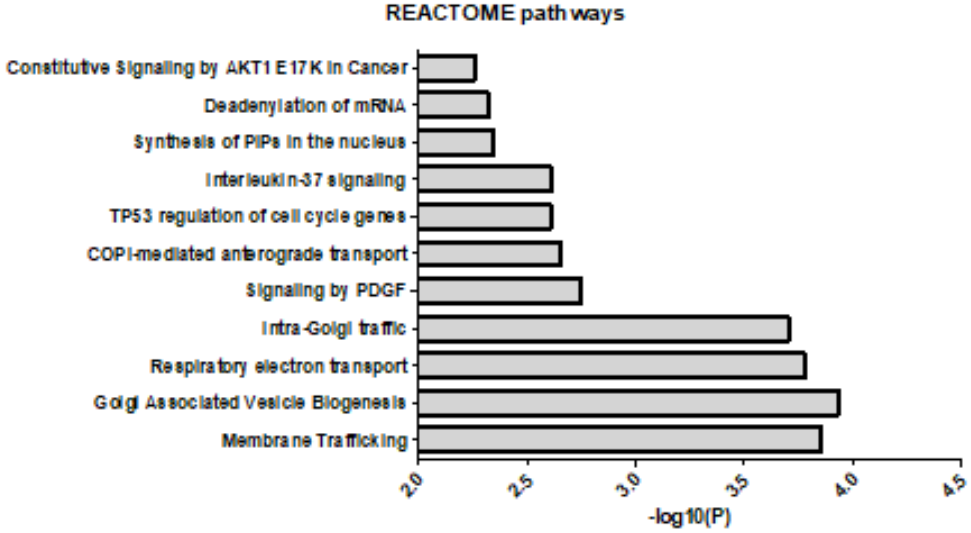
REACTOME pathways
Constitutive Signaling by AKT1 E17K in Cancer
Deadenylation of mRNA
Synthesis of PIPs in the nucleus
Interleukin-37 signaling
TP53 regulation of cell cycle genes
COPI-mediated anterograde transport
Signaling by PDGF
Intra-Golgi traffic
Respiratory electron transport
Golgi Associated Vesicle Biogenesis
Membrane Trafficking
2.0
2.5
3.0
3.5
4.0
4.5
-log10(P)

Supplementary Figure 6: Functional enrichment analysis of proteins uniquely expressed in LT treated GBM cell lines

(**A.**) A Venn diagram comparing the proteins detected in the proteomes of untreated and LT treated GBM cell lines (LN229, MU4 and MU41 cell lines: untreated- 3031 total proteins, treated- 2355 total proteins). FunRich analysis of the 199 proteins uniquely detected in LT treated GBM cells revealing the top 10 significantly enriched annotations for - (**B.**) biological processes, - (**C.**) molecular functions, and - (**D.**) REACTOME pathways. Only 8 significantly enriched REACTOME pathways were identified. (*P values were calculated by two-sided hypergeometric test and are shown as -log10(P)*).

A.

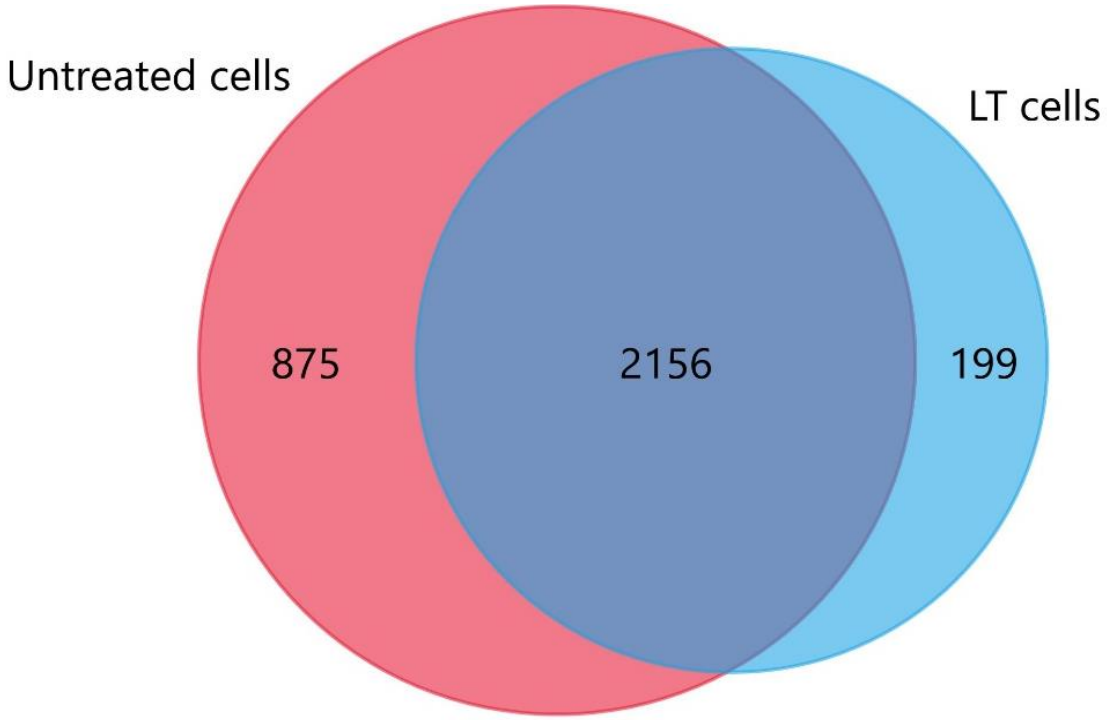

B.

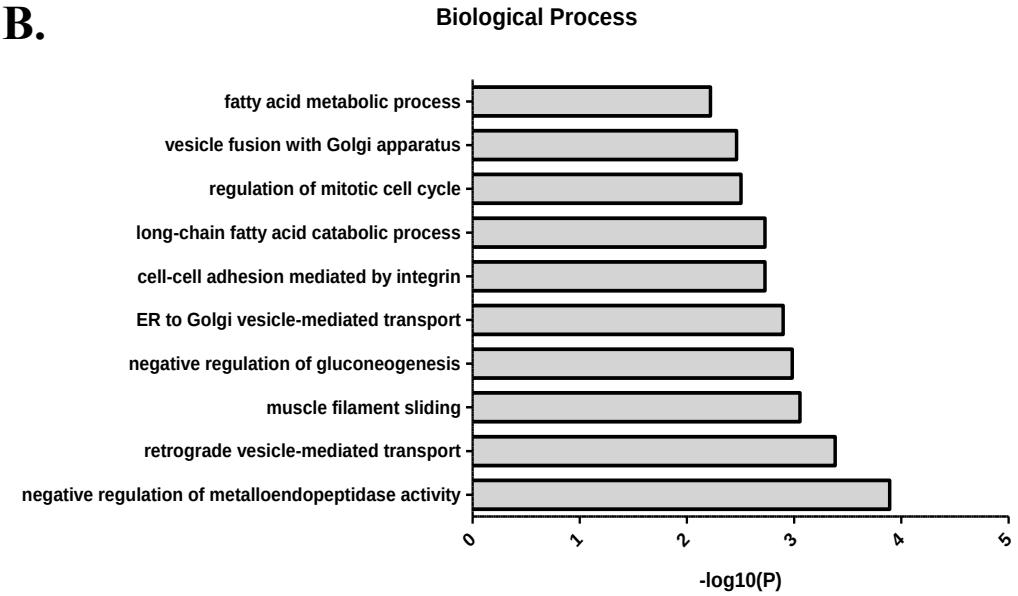
Biological Process
fatty acid metabolic process
vesicle fusion with Golgi apparatus
regulation of mitotic cell cycle
long-chain fatty acid catabolic process
cell-cell adhesion mediated by integrin
ER to Golgi vesicle-mediated transport
negative regulation of gluconeogenesis
muscle filament sliding
retrograde vesicle-mediated transport
negative regulation of metalloendopeptidase activity
0
1
2
3
4
5
-log10(P)

C.

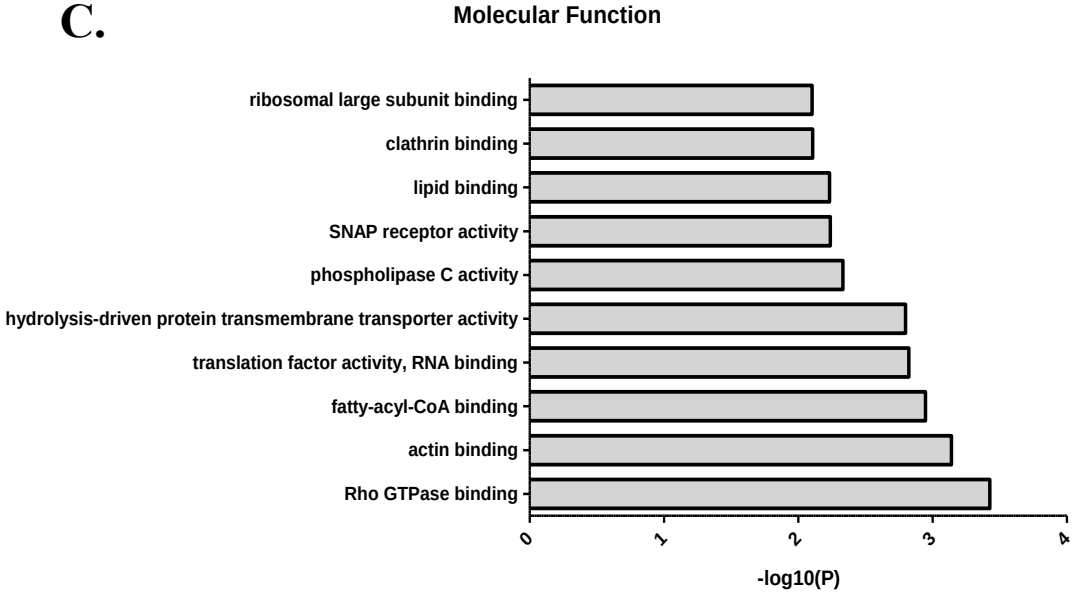
Molecular Function
ribosomal large subunit binding
clathrin binding
lipid binding
SNAP receptor activity
phospholipase C activity
hydrolysis-driven protein transmembrane transporter activity
translation factor activity, RNA binding
fatty-acyl-CoA binding
actin binding
Rho GTPase binding
0
1
2
3
4
-log10(P)

D.

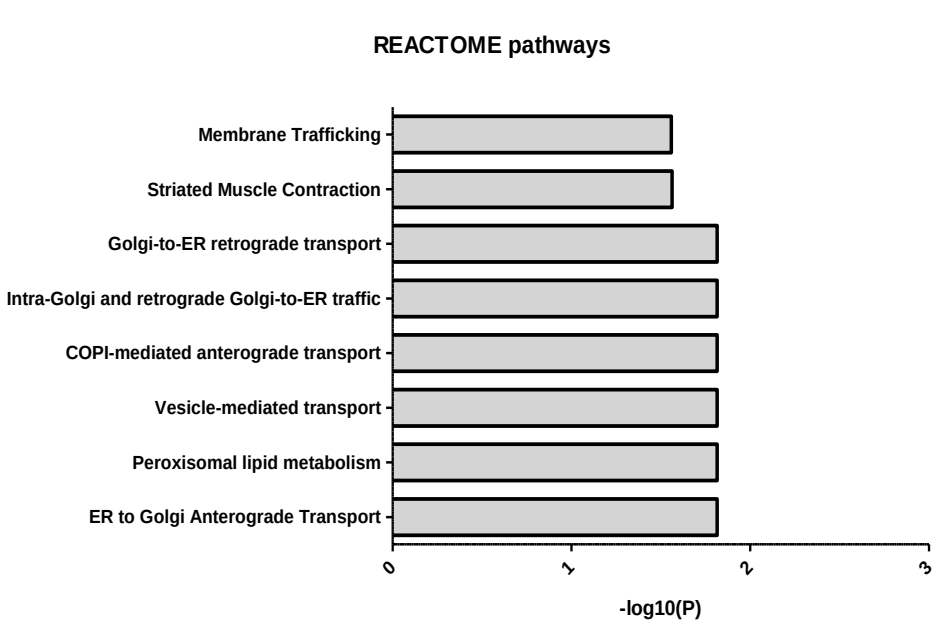
REACTOME pathways
Membrane Trafficking
Striated Muscle Contraction
Golgi-to-ER retrograde transport
Intra-Golgi and retrograde Golgi-to-ER traffic
COPI-mediated anterograde transport
Vesicle-mediated transport
Peroxisomal lipid metabolism
ER to Golgi Anterograde Transport
0
1
2
3
-log10(P)

Supplementary Figure 7: Analysis of the top 25 decreased proteins in GBM cell lines post-LT treatment

FunRich analysis was performed on the top 25 decreased proteins for each LT treated GBM cell line relative to the corresponding untreated cell line. The top 5 significantly enriched GO annotations are displayed, highlighting the functional associations to biological processes and molecular functions for LT treated (**A.**) LN229, (**B.**) MU4 and (**C.**) MU41 cell lines. (*P values were calculated by two-sided hypergeometric test – the top 5 annotations with the most significant p values are shown*).

A.

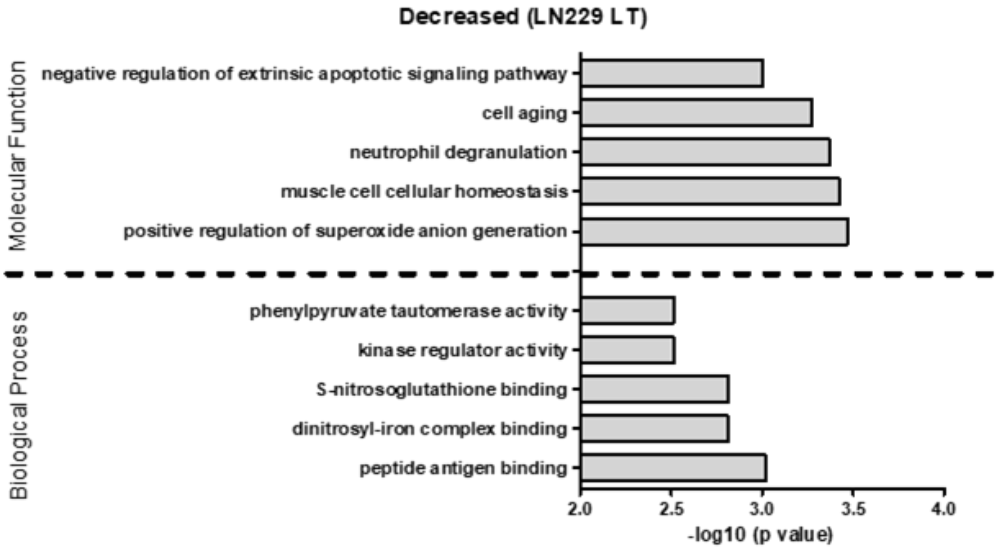
Decreased (LN229 LT)
Molecular Function
negative regulation of extrinsic apoptotic signaling pathway
cell aging
neutrophil degranulation
muscle cell cellular homeostasis
positive regulation of superoxide anion generation
Biological Process
phenylpyruvate tautomerase activity
kinase regulator activity
S-nitrosoglutathione binding
dinitrosyl-iron complex binding
peptide antigen binding
2.0
2.5
3.0
3.5
4.0
-log10 (p value)

B.

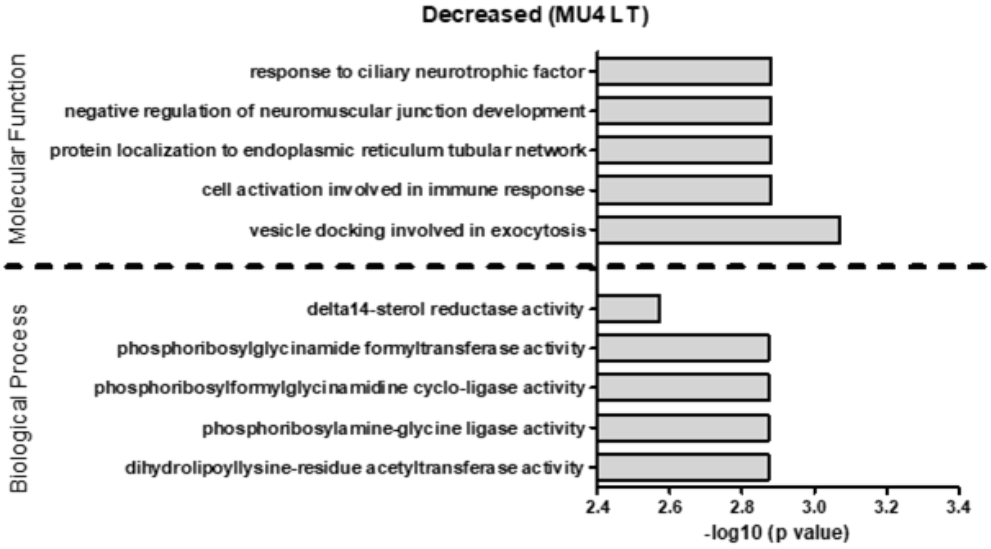
Decreased (MU4 LT)
Molecular Function
response to ciliary neurotrophic factor
negative regulation of neuromuscular junction development
protein localization to endoplasmic reticulum tubular network
cell activation involved in immune response
vesicle docking involved in exocytosis
Biological Process
delta14-sterol reductase activity
phosphoribosylglycinamide formyltransferase activity
phosphoribosylformylglycinamidine cyclo-ligase activity
phosphoribosylamine-glycine ligase activity
dihydrolipoyllysine-residue acetyltransferase activity
2.4
2.6
2.8
3.0
3.2
3.4
-log10 (p value)

C.

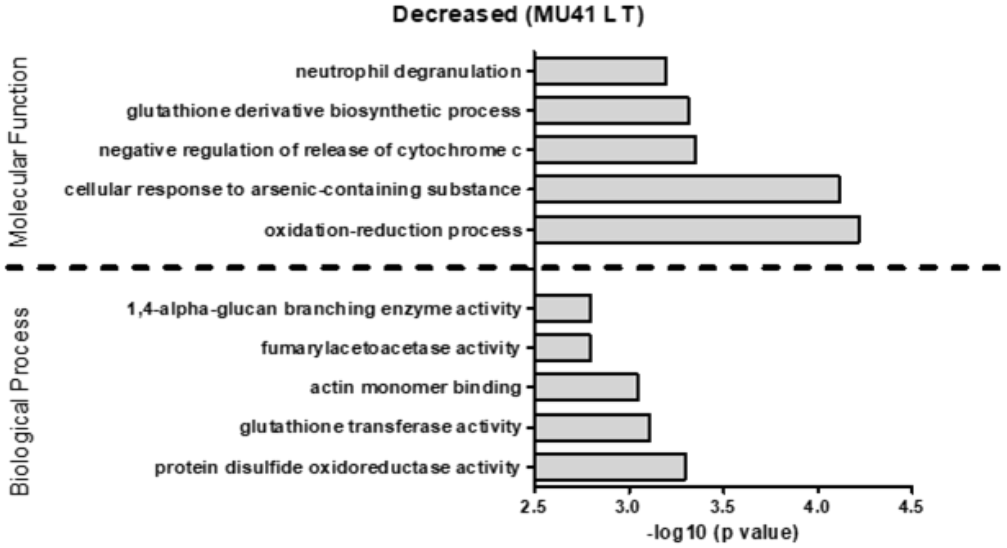
Decreased (MU41 LT)
Molecular Function
neutrophil degranulation
glutathione derivative biosynthetic process
negative regulation of release of cytochrome c
cellular response to arsenic-containing substance
oxidation-reduction process
Biological Process
1,4-alpha-glucan branching enzyme activity
fumarylacetoacetase activity
actin monomer binding
glutathione transferase activity
protein disulfide oxidoreductase activity
2.5
3.0
3.5
4.0
4.5
-log10 (p value)

Supplementary Figure 8: Functional enrichment analysis of proteins uniquely detected in sEVs from LT RT/TMZ treated GBM cell lines

(**A.**) A Venn diagram comparing the proteins detected in the proteomes of sEVs harvested from untreated and LT treated GBM cell lines (LN229, MU4 and MU41 cell lines: sEVs (untreated cells)- 2273 proteins, sEVs (LT treated cells)- 2195 proteins). 424 proteins were uniquely detected in the proteome of sEVs from LT treated cells. FunRich analysis of the 424 proteins uniquely detected in sEVs isolated from LT treated GBM cells revealing the top 10 significantly enriched annotations for - (**B.**) biological processes, - (**C.**) molecular functions, and - (**D.**) REACTOME pathways. (*P values were calculated by two-sided hypergeometric test and are shown as -log10(P)*).

A.

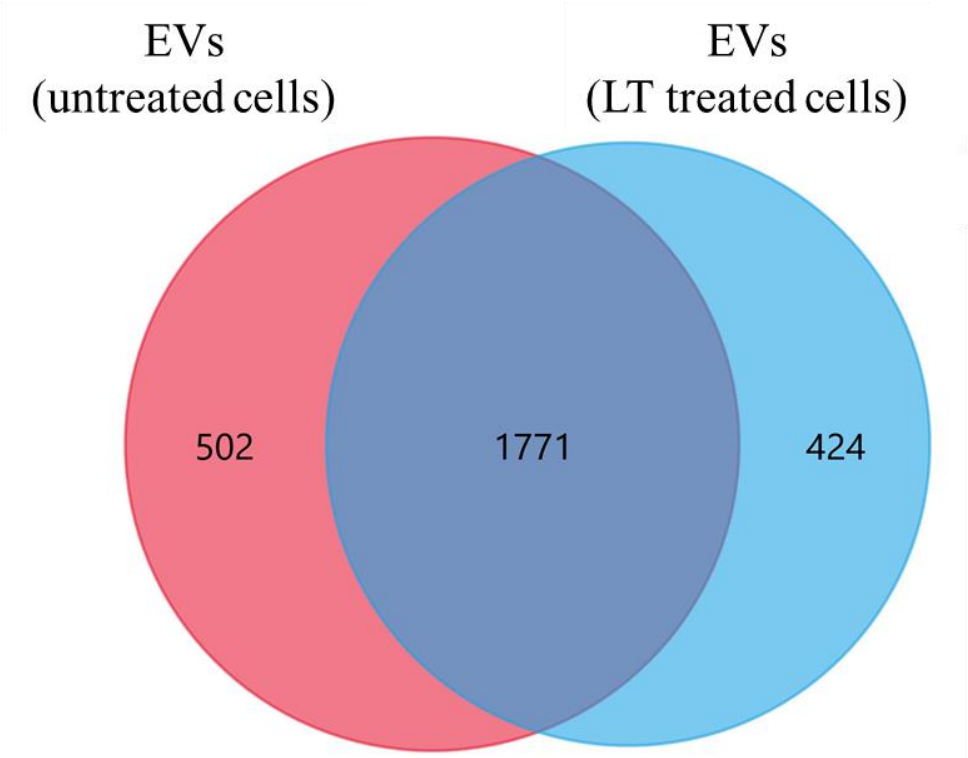

B.

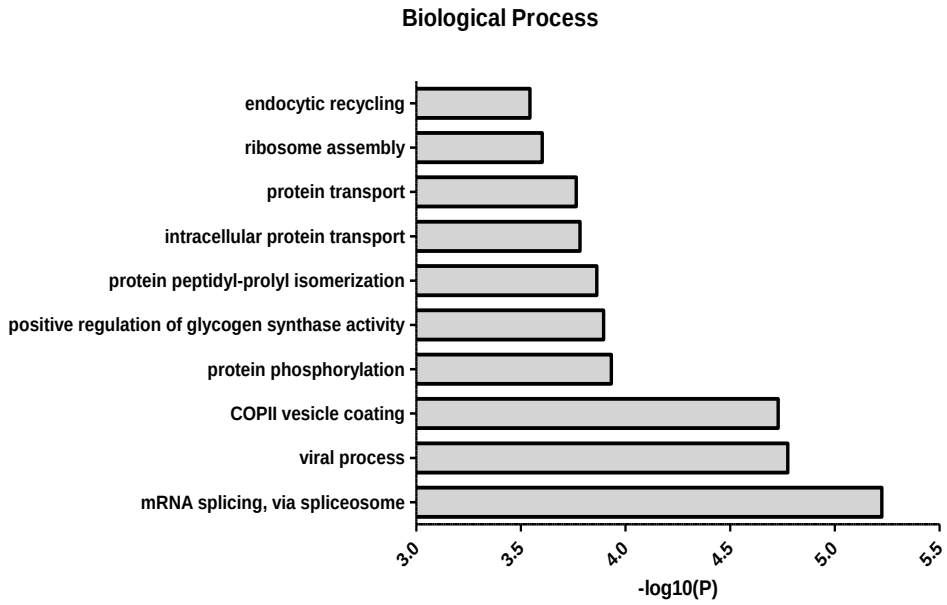
Biological Process
endocytic recycling
ribosome assembly
protein transport
intracellular protein transport
protein peptidyl-prolyl isomerization
positive regulation of glycogen synthase activity
protein phosphorylation
COPII vesicle coating
viral process
mRNA splicing, via spliceosome
3.0
3.5
4.0
4.5
5.0
5.5
-log10(P)

C.

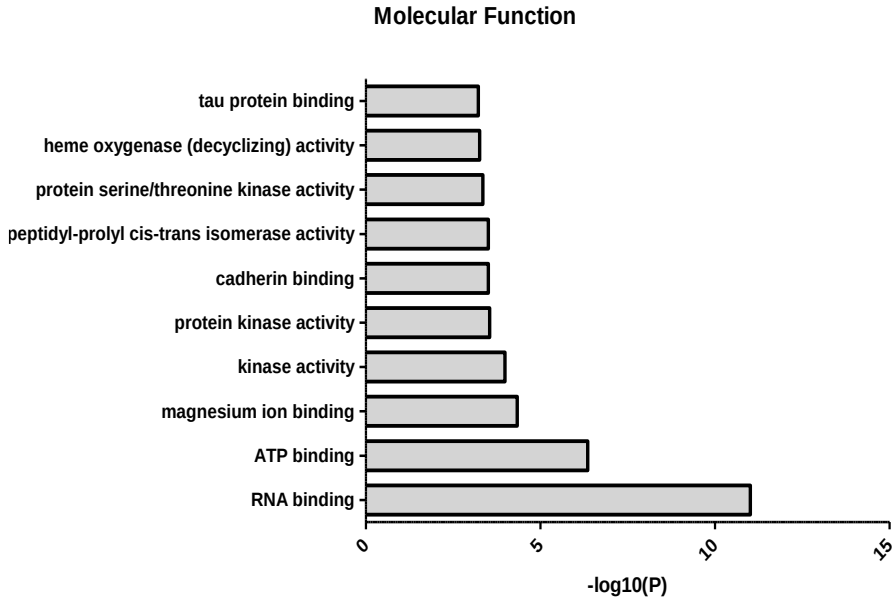
Molecular Function
tau protein binding
heme oxygenase (decyclizing) activity
protein serine/threonine kinase activity
peptidyl-prolyl cis-trans isomerase activity
cadherin binding
protein kinase activity
kinase activity
magnesium ion binding
ATP binding
RNA binding
0
5
10
15
-log10(P)

D.

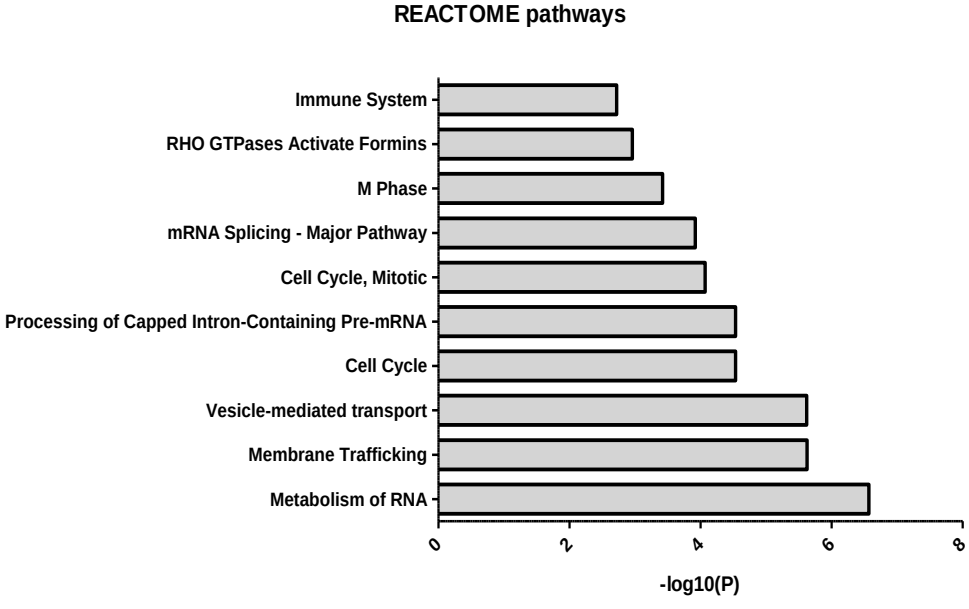
REACTOME pathways
Immune System
RHO GTPases Activate Formins
M Phase
mRNA Splicing - Major Pathway
Cell Cycle, Mitotic
Processing of Capped Intron-Containing Pre-mRNA
Cell Cycle
Vesicle-mediated transport
Membrane Trafficking
Metabolism of RNA
0
2
4
6
8
-log10(P)

Supplementary Figure 9: Analysis of the top 25 decreased proteins in sEVs from GBM cell lines post-LT RT/TMZ treatment

FunRich analysis was performed on the top 25 decreased proteins for sEVs from each LT treated GBM cell line relative to sEVs from the corresponding untreated cell line. The top 5 significantly enriched GO annotations are displayed, highlighting the functional associations to biological processes and molecular functions for LT treated (**A.**) LN229, (**B.**) MU4 and (**C.**) MU41 cell lines. (*P values were calculated by two-sided hypergeometric test – the top 5 annotations with the most significant p values are shown*).

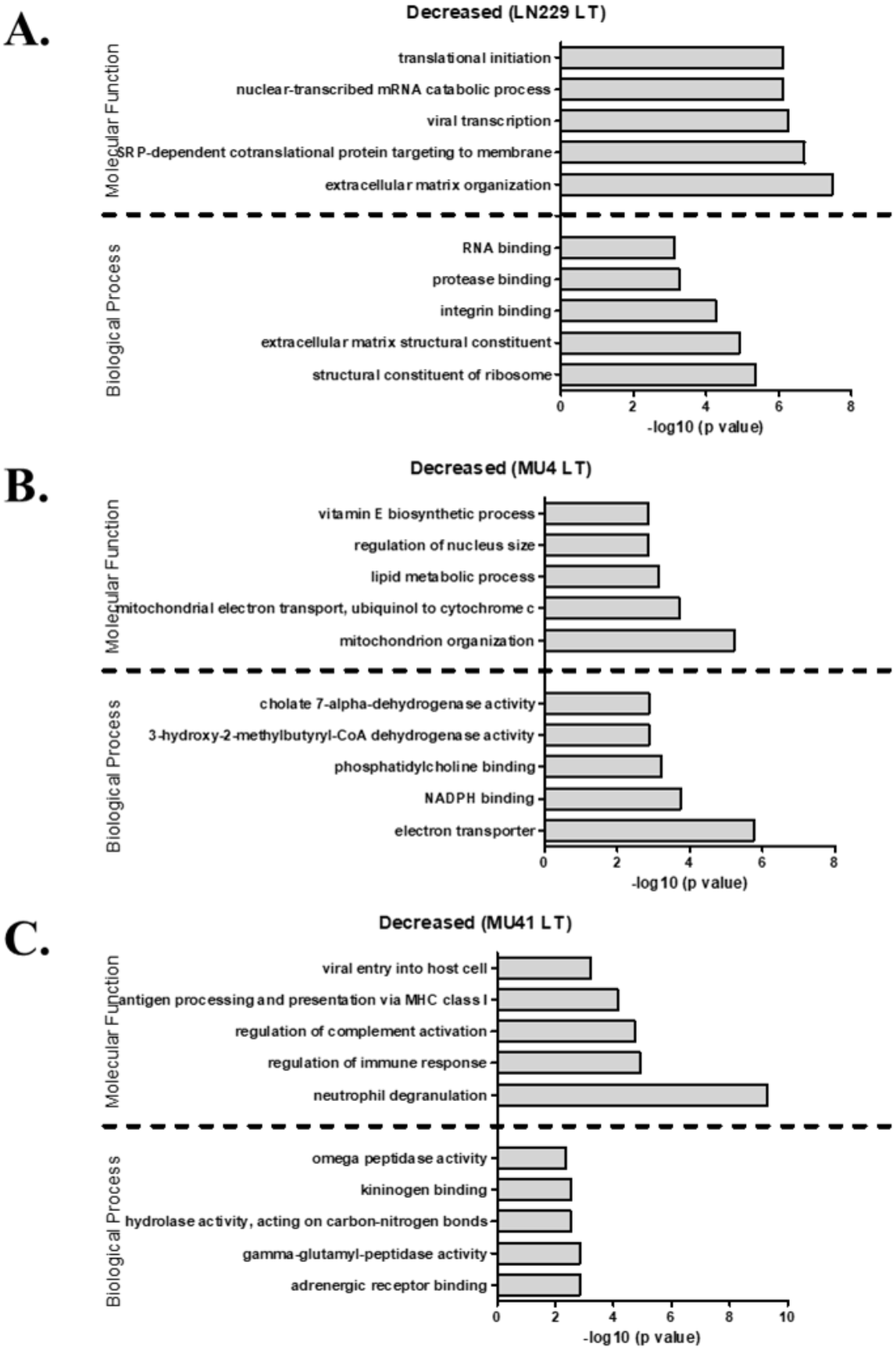
A.
Decreased (LN229 LT)
Molecular Function
translational initiation
nuclear-transcribed mRNA catabolic process
viral transcription
SRP-dependent cotranslational protein targeting to membrane
extracellular matrix organization
Biological Process
RNA binding
protease binding
integrin binding
extracellular matrix structural constituent
structural constituent of ribosome
0
2
4
6
8
-log10 (p value)
B.
Decreased (MU4 LT)
Molecular Function
vitamin E biosynthetic process
regulation of nucleus size
lipid metabolic process
mitochondrial electron transport, ubiquinol to cytochrome c
mitochondrion organization
Biological Process
cholate 7-alpha-dehydrogenase activity
3-hydroxy-2-methylbutyryl-CoA dehydrogenase activity
phosphatidylcholine binding
NADPH binding
electron transporter
0
2
4
6
8
-log10 (p value)
C.
Decreased (MU41 LT)
Molecular Function
viral entry into host cell
antigen processing and presentation via MHC class I
regulation of complement activation
regulation of immune response
neutrophil degranulation
Biological Process
omega peptidase activity
kininogen binding
hydrolase activity, acting on carbon-nitrogen bonds
gamma-glutamyl-peptidase activity
adrenergic receptor binding
0
2
4
6
8
10
-log10 (p value)

Supplementary Tables

Supplementary Table 1: Overexpression of invadopodia regulators correlates with poorer GBM patient survival

Dataset	Gene 1	Gene 2	Gene 3	Gene 4	Concordance Index (CI)	P-value	Sample size
Freije-2	CTTN	TKS4			65.44	1.89E-05	85
Nutt	CTTN				65.39	9.32E-05	50
Nutt	MMP9	CTTN			65.39	9.32E-05	50
Freije-2	TKS5	TKS4	CTTN		66.8	1.55E-04	85
Freije-2	CTTN				59.16	1.62E-04	85
TCGA	TKS5	SRC			55.58	5.58E-04	538
Joo Kim	TKS5	SRC			62.47	6.09E-04	55
Freije	MMP2				59.74	7.06E-04	85
Nutt	MMP2	CTTN			63.73	7.30E-04	50
Freije	MMP2	CTTN			63.01	1.35E-03	85
Nutt	CTTN	TKS5			64.46	1.97E-03	50
Joo Kim	TKS5	TKS4	CTTN		61.04	2.53E-03	55
Freije	MMP9				59.38	2.82E-03	85
Gravendeed	CTTN	SRC			55.9	3.03E-03	270
Gravendeed	TKS5	TKS4	CTTN	SRC	58.14	4.20E-03	270
Freije	MMP9	CTTN			63.01	4.36E-03	85
TCGA	SRC				54.65	5.98E-03	538
Nutt	CTTN	SRC			64.04	6.31E-03	50
Joo Kim	MMP2	TKS4			64.05	6.77E-03	55
Nutt	SRC				56.48	1.38E-02	50
Joo Kim	MMP2	TKS5			62.85	1.44E-02	55
Freije-2	CTTN	TKS5			61.39	1.62E-02	85
Freije-2	TKS4				58.77	1.63E-02	85
Lee-2	TKS5	TKS4	CTTN		62.93	1.69E-02	27
TCGA	CTTN	SRC			54.72	2.35E-02	538
Gravendeed	MMP2	TKS5			56.06	2.50E-02	270
Freije	MMP9	TKS5			59.77	2.53E-02	85

Gravendeed	TKS5	TKS4	CTTN	57.74	2.54E-02	270
TCGA -2016	MMP9	CTTN		55.95	2.61E-02	148
Gravendeed	TKS5	TKS4		56.39	2.67E-02	270
Nutt	MMP9	TKS5		59.9	2.87E-02	50
Joo Kim	TKS5	TKS4		60.81	3.20E-02	55
Gravendeed	MMP9	TKS4		56.1	3.30E-02	270
Lee-2	CTTN	TKS5		60.34	3.32E-02	27
Yamanaka	TKS5	SRC		85.26	3.44E-02	29
TCGA -2016	MMP2			54.78	3.57E-02	148
Joo Kim	MMP2	CTTN		60.51	3.77E-02	55
Freije	MMP2	TKS5		61.26	4.00E-02	85
Joo Kim	TKS4	SRC		60.81	4.10E-02	55
Lee-2	TKS4	SRC		62.93	4.34E-02	27
Lee-2	SRC			62.36	4.34E-02	27
Gravendeed	TKS5	SRC		55.78	4.40E-02	270

Overexpression of various invadopodia regulators (including CTTN, MMP2, MMP9, TKS4, TKS5 and SRC) correlates with poorer patient outcome as determined by analysis of GBM-derived gene expression datasets deposited within the SurvExpress database. A Cox proportional hazards models was used to generate a prognostic index and subsequent risk groups for each gene combination displayed. Concordance indexes, which estimate the probability that subjects with a higher survival risk (longer survival) will experience the event after subjects with a lower survival risk (shorter survival), are displayed for each gene combination. The data presented was obtained from the analysis of nine independent studies and is ordered by log-rank p-value, with the most significant correlation at the top and decreasing p-values following below. All p-values in the table at $p<0.05$.

Supplementary Table 2: mRNA levels of upregulated genes are overexpressed in GBM tissue

Study	Gene	P Value	Fold Change
Bredel 2	MFAP4	0.002	2.052
Lee	MFAP4	1.77E-05	5.37
Liang	MFAP4	NS	NS
Murat	MFAP4	7.52E-07	1.562
Sun	MFAP4	5.48E-13	3.325
TCGA	MFAP4	1.95E-05	1.699
Bredel 2	GDF15	0.008	1.919
Lee	GDF15	NS	NS
Liang	GDF15	NS	NS
Murat	GDF15	4.36E-07	2.143
Sun	GDF15	3.13E-13	4.732
TCGA	GDF15	1.33E-09	3.962
Bredel 2	COL7A1	NS	NS
Lee	COL7A1	NS	NS
Liang	COL7A1	NS	NS
Murat	COL7A1	0.049	1.114
Sun	COL7A1	0.026	1.304
TCGA	COL7A1	NS	NS
Bredel 2	HMOX1	1.12E-09	15.039
Lee	HMOX1	NS	NS
Liang	HMOX1	NS	NS
Murat	HMOX1	NS	NS
Sun	HMOX1	2.28E-10	2.831
TCGA	HMOX1	1.19E-05	5.392
Bredel 2	THBS1	0.014	1.997
Lee	THBS1	1.58E-09	17.825
Liang	THBS1	0.002	3.821
Murat	THBS1	3.19E-06	1.579
Sun	THBS1	0.000467	1.17
TCGA	THBS1	1.18E-08	4.277
Bredel 2	VCAN	1.35E-11	3.563
Lee	VCAN	9.84E-06	1.688
Liang	VCAN	0.013	3.535
Murat	VCAN	3.38E-09	2.69
Sun	VCAN	1.79E-15	3.395
TCGA	VCAN	1.36E-12	4.703
Bredel 2	SERPINE1	1.73E-06	2.877
Lee	SERPINE1	7.50E-11	7.899

Liang	SERPINE1	0.015	4.923
Murat	SERPINE1	8.55E-05	1.913
Sun	SERPINE1	5.35E-10	6.875
TCGA	SERPINE1	3.91E-06	3.45
Bredel 2	VEGFB	NS	NS
Lee	VEGFB	NS	NS
Liang	VEGFB	NS	NS
Murat	VEGFB	0.007	1.271
Sun	VEGFB	4.43E-05	1.317
TCGA	VEGFB	NS	NS
Bredel 2	SRGN	NS	NS
Lee	SRGN	NS	NS
Liang	SRGN	NS	NS
Murat	SRGN	0.007	1.271
Sun	SRGN	4.43E-05	1.317
TCGA	SRGN	NS	NS
Bredel 2	ENPP2	NS	NS
Lee	ENPP2	0.00018	4.298
Liang	ENPP2	NS	NS
Murat	ENPP2	NS	NS
Sun	ENPP2	NS	NS
TCGA	ENPP2	NS	NS
Bredel 2	GPR56	1.18E-08	2.552
Lee	GPR56	NS	NS
Liang	GPR56	ND	ND
Murat	GPR56	0.019	1.877
Sun	GPR56	2.01E-12	1.924
TCGA	GPR56	7.13E-10	2.033
Bredel 2	WNT5B	NS	NS
Lee	WNT5B	NS	NS
Liang	WNT5B	NS	NS
Murat	WNT5B	NS	NS
Sun	WNT5B	0.032	1.356
TCGA	WNT5B	NS	NS

mRNA expression levels of shortlisted genes (based on upregulation in the GBM cell lines following RT/TMZ treatment) were examined in GBM tissue using the Oncomine database. Displayed are the mean fold changes of each gene in GBM tissue versus normal brain tissue, using six independent datasets (Bredel 2, Lee, Liang, Murat, Sun, and TCGA). Tissue samples largely consisted of primary GBMs; however, the Murat study and the Liang study also contain 10 and 4 recurrent GBM specimens, respectively. Gene expression data shown is log-transformed and normalized (*$p<0.05$ displayed, NS: not significant*).

Supplementary Table 3: Overexpression of EV markers correlates with poorer GBM patient survival

Dataset	Gene 1	Gene 2	Gene 3	Gene 4	Gene 5	Concordance Index (CI)	P-value	Sample size
Freije	CD151	CD63	CD81	CD9		62.3	1.51E-04	85
Freije	ALIX	TSG101	CD9	CD63	CD81	63.69	4.14E-04	85
Gravendeed	CD9	CD63				59.47	5.83E-04	270
Freije -2	ALIX					63.46	7.73E-04	85
Nutt	CD9	CD63	CD81			65.08	8.84E-04	50
Nutt	CD9	CD81				66.11	8.84E-04	50
Nutt	CD151	CD9	CD81			66.11	8.84E-04	50
Freije	CD151	CD63	CD81			62.17	1.04E-03	85
TCGA	CD151	CD9	CD81			54.63	1.08E-03	538
TCGA-2016	CD151	CD9	CD81			61.62	1.10E-03	148
TCGA	CD9	CD63	CD81			55.03	1.28E-03	538
Freije	CD9	CD63				59.9	2.19E-03	85
Freije	CD151	CD63				60.97	2.91E-03	85
TCGA	CD63	CD81				55.03	2.92E-03	538
Gravendeed	CD63					57.52	3.00E-03	270
Nutt	CD81					60.73	3.07E-03	50
TCGA	CD151	CD63	CD81	CD9		55.17	3.30E-03	538
TCGA-2016	CD63	CD81				61.63	3.31E-03	148
TCGA-2016	CD9	CD81				60.46	3.41E-03	148
Lee-2	ALIX	TSG101	CD9	CD63	CD81	75.29	3.51E-03	27
TCGA	CD151	CD63				54.77	3.80E-03	538

TCGA-2016	CD81				59.94	3.84E-03	148
Freije	CD151	CD9	CD63		61.1	4.25E-03	85
Gravendeed	ALIX				56.34	4.93E-03	270
Freije	CD63	CD81			62.3	5.36E-03	85
Gravendeed	ALIX	TSG101			56.92	6.18E-03	270
Freije	CD9	CD63	CD81		62.27	6.47E-03	85
TCGA	CD151	CD81			54.51	6.97E-03	538
TCGA-2016	CD151	CD63	CD81		61.72	7.03E-03	148
TCGA-2016	CD151	CD81			61.75	7.03E-03	148
Freije	CD63				59.9	1.06E-02	85
TCGA	CD151	CD63	CD81		55.2	1.16E-02	538
TCGA-2016	CD151	CD63	CD81	CD9	61.52	1.26E-02	148
Lee-2	CD151	CD63	CD81	CD9	66.09	1.28E-02	27
TCGA	CD151	CD9	CD63		54.65	1.31E-02	538
Murat	CD9	CD63	CD81		58.68	1.63E-02	80
Murat	CD9	CD63			59.22	1.63E-02	80
Murat	CD151	CD9	CD63		59.08	1.63E-02	80
TCGA	ALIX				53.04	1.68E-02	538
TCGA	CD151				53.72	1.92E-02	538
TCGA	CD63				53.79	2.35E-02	538
TCGA-2016	CD9	CD63	CD81		61.3	2.49E-02	148
TCGA	ALIX	TSG101			53.12	2.70E-02	538
Murat	CD151	CD63	CD81	CD9	58.78	3.27E-02	80
Murat	CD151	CD63	CD81	CD9	58.78	3.27E-02	80
TCGA	CD151	CD9			53.83	3.33E-02	538

Murat	CD151	CD9	58.61	3.35E-02	80
Nutt	TSG101		56.79	3.44E-02	50
Lee-2	ALIX		69.25	3.53E-02	27
Murat	CD9	CD81	58.34	3.70E-02	80
Freije-2	CD9		55.95	3.76E-02	85
Murat	CD9		58.51	3.95E-02	80
Gravendeed	CD9		55.64	4.16E-02	270
TCGA	CD9	CD81	54.03	4.20E-02	538
Freije	CD151	CD9	55.99	4.56E-02	85

Overexpression of EV markers (including CD9, CD63, CD81, CD151, Alix and TSG101) correlates with poorer patient outcome as determined by analysis of GBM gene expression datasets deposited within the SurvExpress database. The data presented was obtained from the analysis of 8 independent studies and is ordered by log-rank p-value, with the most significant correlation at the top and decreasing p-values following below. All p-values in the table at $p<0.05$.

Supplementary Table 4: Proteins detected in the GBM cell line derived sEV proteome that are not listed in Vesiclepedia

111 proteins in GBM cell line derived sEVs not listed in EV datasets recorded on Vesiclepedia	328 proteins in GBM cell line derived sEVs not listed in GBM/glioma EV datasets recorded on Vesiclepedia
AAR2	A1BG
ADGRL2	AAR2
ADGRL3	ABCF2
ADSS2	ABR
AFDN	ACTL6A
ANKRA2	ACTR5
APMAP	ADGRL2
ATP5F1A	ADGRL3
ATP5F1B	ADK
ATP5F1C	ADSS2
ATP5MD	AFDN
ATP5ME	AGT
ATP5MF	AHSA1
ATP5MG	AK1
ATP5PB	AKR1B10
ATP5PD	AKR1B15
ATP5PF	ANKRA2
ATP5PO	ANP32E
CALHM5	AP3D1
CAVIN1	APCS
CAVIN3	APMAP
CCAR2	APOA2
CEMIP2	APOA4
CIP2A	ARAF
CLUH	ATG4B
COLGALT1	ATL3
CORO2B	ATP5F1A
DIPK2A	ATP5F1B
DNAAF5	ATP5F1C
ECPAS	ATP5MD
EFL1	ATP5ME
ELOB	ATP5MF
ELOC	ATP5MG
ELP1	ATP5PB
ERBIN	ATP5PD
ERO1A	ATP5PF
EVA1B	ATP5PO
FBH1	ATP9A
FRMD8P1	BDH2

GARNL3	BGN
GARS1	BLK
GCN1	BTN3A3
GID8	CALHM5
GSDME	CAPS2
H1-0	CARS2
H1-2	CASP8
H1-5	CAVIN1
H2BC13	CAVIN3
H3-2	CBFB
H3-3A	CC2D1B
H4C1	CCAR2
HNRNPLL	CCDC171
IGHD	CD74
IGHV3-53	CDC42BPA
IGHV3-72	CEMIP2
IGKV1-12	CFB
IGKV1-33	CIP2A
IGLV1-47	CLPX
JMJD6	CLUH
KARS1	COG2
KIAA1549L	COLGALT1
KIFBP	COPB2
KIRREL1	COPE
L3HYPDH	CORO2B
LIMS4	CPB2
MAP3K20	CPEB4
MEAK7	CPT1A
MMUT	CTBP1
MPP2	CTPS1
MRPL58	DAG1
MT-CO2	DDX1
MVB12A	DDX39A
MVB12B	DIPK2A
MYDGF	DNAAF5
NARS1	DNAH8
NDUFA3	DRG2
NECTIN2	ECPAS
NIBAN1	EFL1
NIBAN2	EFNB1
NIFK	EFR3B
NTRK2	EGFLAM
OGA	EIF4H
P3H1	ELOB
PLPP3	ELOC
PRXL2A	ELP1

PTPA	ENG
RACK1	ENPP2
RIPOR1	EPHX1
RPL39P5	ERBIN
RTCB	ERO1A
RTRAF	ERP44
SEPTIN10	ESD
SEPTIN11	EVA1B
SEPTIN2	F9
SEPTIN7	FAM114A1
SEPTIN8	FAM98A
SEPTIN9	FAR1
SESN2	FBH1
SF3B6	FHOD1
SNX21	FIS1
SQOR	FKBP10
SRPRA	FRMD8P1
STK26	FTL
TARS1	FUBP3
TCAF1	GARNL3
TENM3	GARS1
TMEM258	GCN1
TOMM70	GEMIN5
VPS35L	GFPT2
WASHC5	GGT1
ZP4	GID8
	GLCE
	GNG10
	GREM1
	GSDMB
	GSDME
	GSPT1
	GTPBP2
	GYG1
	H1-0
	H1-2
	H1-5
	H2BC13
	H3-2
	H3-3A
	H4C1
	HADH
	HEATR1
	HEG1
	HM13
	HNRNPF

	HNRNPH2
	HNRNPLL
	HRG
	HSP90AB2P
	HUWE1
	IDH3G
	IGF2BP3
	IGHA1
	IGHA2
	IGHD
	IGHG1
	IGHG2
	IGHG3
	IGHG4
	IGHM
	IGHV3-53
	IGHV3-72
	IGKC
	IGKV1-12
	IGKV1-33
	IGLC1
	IGLC3
	IGLV1-47
	INF2
	INS
	JMJD6
	KARS1
	KIAA1549L
	KIFBP
	KIRREL1
	KNG1
	KPNA6
	L3HYPDH
	LAS1L
	LCN1
	LHFPL2
	LIMS4
	LMAN2
	LRRC8A
	LRRCC1
	LUC7L2
	MANF
	MAP1A
	MAP3K20
	MATR3
	MCM4

	ME2
	MEAK7
	METAP1
	MMUT
	MOB1B
	MPP2
	MRPL58
	MT2A
	MT-CO2
	MTHFD1L
	MTX2
	MUC5B
	MVB12A
	MVB12B
	MYDGF
	MYO5A
	NACA
	NANS
	NARS1
	NCEH1
	NDUFA3
	NECTIN2
	NIBAN1
	NIBAN2
	NIFK
	NIT2
	NOL9
	NOTCH1
	NPTXR
	NTRK2
	NUMB
	OCIAD2
	OGA
	ORM1
	ORM2
	OSBPL6
	P3H1
	PCDH7
	PDCD11
	PDPR
	PDXDC1
	PGLYRP2
	PGRMC2
	PI4K2A
	PLPP3
	PMVK

	POLR2A
	POLR2H
	PON1
	POR
	PPM1G
	PRDX5
	PRKCI
	PRPF19
	PRPH
	PRPS2
	PRXL2A
	PTGES2
	PTPA
	PTPN1
	RAB3GAP1
	RACK1
	RANBP2
	RBM14
	RBP4
	RELN
	RFC2
	RIPOR1
	RIT1
	RNF114
	RPL23
	RPL39P5
	RPS6KA3
	RTCB
	RTRAF
	S100A9
	SDF4
	SDK2
	SEC13
	SEC23A
	SEC62
	SEC63
	SEMA7A
	SEPTIN10
	SEPTIN11
	SEPTIN2
	SEPTIN7
	SEPTIN8
	SEPTIN9
	SERPING1
	SESN2
	SF3B6

	SFPQ
	SHISA4
	SLC24A1
	SLC25A1
	SLC25A11
	SLC27A1
	SLC2A3
	SLC43A3
	SLC5A3
	SMARCA5
	SNRPD2
	SNRPN
	SNX1
	SNX21
	SQOR
	SRP14
	SRPRA
	SRPRB
	SRSF9
	SSRP1
	STAT1
	STAT6
	STEAP2
	STEAP4
	STK26
	STOML2
	STON2
	STRN3
	STT3A
	STT3B
	SYNE1
	SYNM
	TARS1
	TCAF1
	TENM3
	TIAL1
	TM9SF3
	TM9SF4
	TMED2
	TMED7
	TMEM258
	TOMM70
	TPR
	TRIM47
	TRIP12
	TRIP13

	TSN
	TSPAN7
	TXNL1
	UBE2V1
	UBE3C
	UBXN4
	UNC45A
	UQCRC1
	VPS13D
	VPS35L
	WASHC5
	WDR82
	ZP4

Proteins are listed via the corresponding gene name. Vesiclepedia Version 4.1 - updated 15/08/2018

Supplementary Table 5: Proteins that were uniquely detected in the proteome of sEVs from each GBM cell line compared to the corresponding donor cell

Unique in LN229 sEVs compared to donor cells	Unique in MU4 sEVs compared to donor cells	Unique in MU41 sEVs compared to donor cells	Unique in all 3 sEVs compared to donor cells
A1BG	ACTG1	AACS	ADAM17
ABCG2	ADAM17	AAR2	AGRN
ABI1	ADAMTSL3	ABCF3	APP
ACACA	ADGRL2	ABCG2	AXL
ACTG1	AGPS	ABHD10	CFB
ADAM10	AGRN	ABI2	CFI
ADAM17	ALCAM	ACACA	CIT
ADAM9	APOA1	ACTR5	EFR3A
ADGRL3	APOC3	ACVR1	ENPP2
AGRN	APP	ADAM17	FMNL2
AGT	ARL3	ADAM9	IGHA1
AHSG	ARRDC1	ADGRL2	IGHG2
ALCAM	ASAH1	ADGRL3	IGHV3-72
ALDH1L1	ATP1A3	AFDN	IGKC
AMBP	ATRN	AGRN	IGLC1
ANGPTL2	AXL	AIDA	INS
ANLN	BID	AIFM2	IST1
AP1B1	BLVRA	ALDH1L2	ITGA7
APCS	C3	ALDH3B1	ITIH4
APOA1	CAPN5	ANKFY1	MTOR
APOA2	CBR3	ANKRA2	NEDD4L
APOA4	CCDC50	ANO6	NID2
APOB	CCT6B	ANTXR2	NOTCH2
APOC3	CD81	APOB	NPTN
APOH	CDH13	APP	PLP1
APP	CFB	ARAF	PLXNB2
ARRDC1	CFI	ARFGEF2	PTPRM
ATRN	CHMP6	ARFRP1	RAB22A
AXL	CHRDL1	ARL15	RACGAP1
B2M	CIT	ARMC9	RAP2A
BASP1	COL1A1	ATG4B	RELN
BGN	COL1A2	ATP5MF	SLC5A3
C1R	COL3A1	ATP6V0D2	TGFBI
C1S	COL4A2	ATP9A	TOM1
C4A	COL5A1	AURKB	TSPAN14
CASK	COL5A2	AXL	VPS28
CBFB	COL6A1	BCAT1	
CCDC171	COL6A3	BDH2	
CD276	COPS8	BLK	

CD47	CORO1B	BOP1	
CD55	CP	BPIFA1	
CD58	CSNK1A1	BTN3A3	
CD63	DAGLB	C1R	
CD82	DIP2A	C3	
CD9	DMD	CA9	
CDC42BPA	ECPAS	CAB39	
CDH2	EFEMP2	CACNA2D1	
CEMIP2	EFNB1	CADM4	
CEP55	EFR3A	CALHM5	
CFB	EGFLAM	CAMK2G	
CFH	ENPP2	CAPN5	
CFI	EPB41L2	CASK	
CHMP2A	EPHB3	CASP8	
CHMP4B	EVA1B	CC2D1A	
CIT	EXOC5	CC2D1B	
CLDND1	F10	CCM2	
CLPX	F9	CCNY	
CLSTN1	FBN1	CCNYL1	
CLTA	FGG	CD46	
CLU	FMNL2	CD55	
COL18A1	FREM2	CD58	
COL1A2	FSTL1	CD74	
COL4A2	GALK1	CD9	
COL6A2	GID8	CD99L2	
CP	GJA1	CDC42BPA	
CPNE2	GOLGA7	CDC42BPB	
CPNE8	GPC6	CDC42SE2	
DHCR7	GPM6B	CDK9	
DIP2B	GPRC5B	CEP55	
DIP2C	GSR	CFB	
DLG1	GULP1	CFI	
DNAJC5	H1-0	CHMP6	
DPP9	HAPLN1	CIP2A	
EBF2	HBB	CIT	
ECM1	HLA-DRA	CLDN12	
EFEMP2	HLA-DRB1	CLDND1	
EFNB1	HSD17B12	CLU	
EFR3A	HTRA1	CLUH	
EHD2	HTRA2	CNIH4	
ELOB	IGHA1	CNRIP1	
EMC2	IGHD	COG2	
ENPP2	IGHG2	COG3	
EPHA2	IGHG4	COG4	
EPHB2	IGHV3-72	CPB2	
EPHB3	IGKC	CPEB4	

ERGIC1	IGLC1	CPNE8	
EXOC3	IGSF3	CPSF2	
EXOC7	IGSF8	CSK	
F2	INS	CTBP2	
FARP1	IST1	DAG1	
FAT1	ITGA7	DAGLB	
FERMT3	ITGB5	DCBLD2	
FGA	ITIH4	DCUN1D3	
FGB	KIAA1549L	DDAH2	
FGG	KIF23	DDR2	
FHL2	KRT17	DDX27	
FLNC	LAMA4	DERL1	
FMNL2	LAPTM4A	DHCR7	
FREM2	LOXL2	DHX29	
FST	LPAR1	DIP2B	
FSTL1	LTBP1	DIP2C	
FTH1	LTBP3	DIPK2A	
GARNL3	LTBP4	DMBT1	
GC	MASP1	DNAAF5	
GEMIN2	MMP19	DNAH8	
GIPC1	MMP2	DNAJC5	
GNA11	MOB4	DOCK1	
GNAI1	MRPL53	DOCK10	
GNAO1	MTOR	DOCK5	
GNG12	MVB12B	DTNA	
HAPLN3	NCSTN	ECPAS	
HBB	NECTIN2	EFL1	
HMCN1	NEDD4L	EFR3A	
HRG	NID1	EFR3B	
HTRA1	NID2	EHBP1L1	
IGHA1	NINJ1	EHD3	
IGHA2	NOTCH1	EIF2B4	
IGHD	NOTCH2	EIF4E	
IGHG1	NPTN	ELP1	
IGHG2	NRP2	ELP3	
IGHG3	NTN1	EMC2	
IGHG4	NTRK2	EMILIN1	
IGHM	OLFML3	EMP3	
IGHV3-53	PCDH7	ENG	
IGHV3-72	PCDHGC3	ENPP2	
IGKC	PCSK6	EPB41	
IGKV1-33	PDPR	EPB41L1	
IGKV3-20	PGLYRP2	EPHA2	
IGLC1	PI4KA	EPHB2	
IGLC3	PIP4K2A	ERBIN	
IGLV1-47	PKP4	EVI2B	

IGSF3	PLAUR	EXOC1	
INS	PLP1	EXOC2	
IQGAP3	PLPP3	EXOC3	
IST1	PLTP	EXOC5	
ITGA1	PLXNB2	EXOC6B	
ITGA7	PNPT1	EXOC7	
ITGB8	PRELP	EXOC8	
ITIH1	PTGES2	F10	
ITIH2	PTPRG	F11R	
ITIH4	PTPRM	F3	
JAK1	PTPRS	FABP5	
JAM3	PXDNL	FAM126A	
KATNAL2	RAB22A	FAP	
KIF14	RAB32	FAR1	
KNG1	RAB9A	FARP1	
KPRP	RACGAP1	FARP2	
KRT14	RAP2A	FAS	
KRT5	RBP4	FAT1	
LAS1L	RELN	FBH1	
LDLR	RGN	FBLL1	
LRRC57	RNF130	FERMT1	
MAP2K1	ROBO2	FLG2	
MASP1	RPL34	FMNL2	
MET	RTN4RL2	FRMD8P1	
MIA	SDC4	FTL	
MPP6	SDF4	FUCA2	
MPZL1	SEMA3A	FYN	
MTOR	SEMA3C	GAK	
MVB12A	SERPINF1	GCSH	
MYO10	SLC12A4	GEMIN5	
MYO1E	SLC27A1	GFM2	
MYO5A	SLC2A1	GGT1	
NCAM1	SLC2A3	GLO1	
NDUFA3	SLC5A3	GLRX5	
NEDD4L	SLIT2	GMPPB	
NIBAN1	SNAP23	GNA11	
NID2	SRC	GNAI1	
NME1	SRPX2	GNB4	
NOTCH2	SSC5D	GNG10	
NPTN	TGFB1	GNL3	
NRP1	TGFBI	GOLGA7	
NRP2	THBS1	GPC6	
NUP85	THBS4	GPNMB	
OLFML3	TNIK	GREM1	
ORM1	TOLLIP	GSDMB	
ORM2	TOM1	GSK3A	

PCOLCE	TSPAN14	GSK3B	
PFDN1	TSPAN7	GSS	
PFDN5	TSPAN9	GSTM2	
PGLYRP2	TTYH2	GSTZ1	
PI4KA	UBA6	GTPBP2	
PIP4K2A	UQCRC2	HBA2	
PKN2	UXS1	HEATR1	
PLAT	VANGL1	HECTD1	
PLAU	VAT1	HEG1	
PLCB3	VCAN	HERC2	
PLG	VPS28	HERC4	
PLP1		HGS	
PLP2		HINT3	
PLTP		HLA-C	
PLXNB2		HMGCL	
PON1		HRAS	
PRSS23		HSDL2	
PTMA		HSPA4L	
PTPRM		IGHA1	
PXDN		IGHG1	
QSOX1		IGHG2	
RAB22A		IGHV3-72	
RAB23		IGKC	
RAB27B		IGKV1-12	
RAB35		IGLC1	
RACGAP1		IKBKB	
RAP2A		IKBKG	
RAP2B		IL1RAP	
RAP2C		INS	
RELN		IQGAP3	
RFTN1		IST1	
RHOA		ITCH	
RIC8A		ITGA2	
RIN1		ITGA6	
RPL34		ITGA7	
SCARB1		ITGB5	
SDK2		ITIH4	
SEC61A1		JAK1	
SERPINA1		JAM2	
SERPINC1		JMJD6	
SERPING1		KANK2	
SHISA4		KIF14	
SHMT1		KIFBP	
SLC12A2		KIRREL1	
SLC16A1		KPNA1	
SLC1A4		KPRP	

SLC24A1		KRIT1	
SLC30A1		KRT5	
SLC38A2		LAS1L	
SLC4A7		LCN1	
SLC5A3		LCP1	
SLC5A6		LDLR	
SLC7A5		LGALS8	
SLC9A3R1		LHFPL2	
SRC		LOXL2	
SRGAP2		LRRC15	
SRPX		LRRC57	
SRSF6		LRRC8A	
SRSF9		LRRCC1	
STEAP3		LTF	
STEAP4		LYPLAL1	
STK26		LYZ	
STOM		M6PR	
STON2		MAP1S	
STRA6		MAP3K20	
SYNE1		MAPKAP1	
SYNE2		MARCKS	
SYPL1		MET	
TAOK3		METAP1	
TENM3		MINK1	
TGFBI		MITD1	
THBS1		MMGT1	
THBS2		MMP1	
TIMP1		MMS19	
TIMP2		MPP1	
TIMP3		MPP2	
TINAGL1		MPP6	
TMEM109		MPZL1	
TMEM258		MRPL58	
TNC		MSH2	
TOLLIP		MT2A	
TOM1		MTHFD2	
TOM1L2		MTOR	
TRIM23		MTR	
TRIM47		MTX1	
TRPV2		MTX2	
TSG101		MUC5B	
TSPAN14		MYADM	
TSPAN6		MYH14	
TTYH3		MYO9B	
UBE2C		NAGK	
UNC45A		NAPG	

VCAN		NCAPD2	
VPS13D		NECTIN2	
VPS28		NEDD4L	
VPS37B		NID1	
VTI1B		NID2	
VTN		NIFK	
XPOT		NOL9	
YES1		NOLC1	
ZP4		NOP2	
		NOTCH2	
		NPM3	
		NPTN	
		NRP1	
		NTMT1	
		NUMB	
		NUP107	
		NUP43	
		NXF1	
		OGA	
		OSBPL6	
		PAG1	
		PAK4	
		PANK4	
		PANX1	
		PARP12	
		PCK2	
		PCOLCE2	
		PCYT2	
		PDCD11	
		PDXDC1	
		PEF1	
		PELO	
		PFAS	
		PHACTR4	
		PHKB	
		PHLDA2	
		PIGR	
		PIK3R4	
		PIP4K2C	
		PIP5K1A	
		PIPSL	
		PKP4	
		PLAU	
		PLCB3	
		PLCG1	
		PLD1	

		PLEKHB2	
		PLEKHO2	
		PLGRKT	
		PLP1	
		PLPP3	
		PLSCR1	
		PLSCR3	
		PLXNA1	
		PLXNB2	
		PMVK	
		POLR2A	
		PPAT	
		PPIL3	
		PPP1R7	
		PRKCI	
		PRPS2	
		PRSS23	
		PRXL2A	
		PSEN1	
		PTP4A2	
		PTPRA	
		PTPRG	
		PTPRJ	
		PTPRK	
		PTPRM	
		PTX3	
		PVR	
		PXDN	
		QSOX1	
		QTRT1	
		RAB11FIP5	
		RAB22A	
		RAB23	
		RAB27B	
		RAB3B	
		RAB3GAP1	
		RAB8B	
		RAB9A	
		RACGAP1	
		RAI14	
		RAP2A	
		RAPH1	
		RASA1	
		RASA3	
		RELL1	
		RELN	

		RER1	
		RFC2	
		RFTN1	
		RGS17	
		RHOA	
		RHOQ	
		RIC8A	
		RIPOR1	
		RIT1	
		RND3	
		RNF114	
		RNF213	
		RP2	
		RPL28	
		RPL39P5	
		RRAGC	
		RRAS2	
		RRM2	
		RSPRY1	
		S100A16	
		S100A8	
		S100A9	
		SAR1B	
		SCAMP3	
		SCAMP4	
		SCRIB	
		SCRN1	
		SDC1	
		SEC16A	
		SEC62	
		SEMA7A	
		SERINC3	
		SERPINA1	
		SERPINA3	
		SESN2	
		SH3BP4	
		SHOC2	
		SLC12A4	
		SLC16A3	
		SLC1A4	
		SLC20A1	
		SLC29A1	
		SLC2A3	
		SLC30A1	
		SLC38A1	
		SLC38A2	

		SLC43A3	
		SLC44A1	
		SLC4A7	
		SLC5A3	
		SLC5A6	
		SLC6A8	
		SLC7A1	
		SLC9A3R1	
		SLFN5	
		SNAP23	
		SNAP25	
		SNTB1	
		SNX17	
		SNX21	
		SPTLC1	
		SRGAP2	
		SRPX	
		SRPX2	
		SSC5D	
		STAT2	
		STAT6	
		STC1	
		STEAP2	
		STK10	
		STK26	
		STX16	
		STX3	
		SYNGR2	
		SYNM	
		SYPL1	
		TAOK1	
		TAOK3	
		TBC1D10A	
		TBC1D10B	
		TBK1	
		TBL3	
		TCAF1	
		TGFBI	
		THBS2	
		TLN2	
		TMEM237	
		TNFRSF10B	
		TOM1	
		TPBG	
		TRADD	
		TRIM16	

		TRIO	
		TSFM	
		TSPAN14	
		TSTA3	
		TTC7A	
		TTC7B	
		TTN	
		TUBGCP2	
		TYK2	
		UAP1L1	
		UBE3C	
		UBTD1	
		UBXN6	
		UFL1	
		USP10	
		UXS1	
		VAC14	
		VAMP5	
		VANGL1	
		VBP1	
		VKORC1	
		VPS28	
		VPS35L	
		VPS45	
		VPS4B	
		WASHC5	
		WDR11	
		WDR36	
		WDR77	
		WDR82	
		WLS	
		WNT5A	
		XPO7	
		YES1	
		ZDHHC20	
		ZDHHC5	

Proteins are listed via the corresponding gene name.

Supplementary Table 6: DE invadopodia-related proteins in GBM cells post-RT/TMZ treatment

Gene	Protein	Invadopodia related evidence	LFQ ratio (RT/TMZ treated/untreated cells)		
			LN229	MU4	MU41
ABI2	Abl interactor 2	Regulator of actin cytoskeleton dynamics underlying cell motility and adhesion. Functions as a component of the WAVE2 complex, which activates actin nucleating machinery Arp2/3 to drive invadopodia formation. [562, 563]	24.44	NS	25.51
AGRN	Agrin	Secreted and cell surface Agrin binds the Lrp4 receptor and promotes the formation of a Agrin–Lrp4–MuSK signalling complex, which activates FAK and Arp2/3 associated invadopodia formation [564]	22.76	NS	NS
CD151	CD151 antigen	CD151, together with integrin α3β1 located at invadopodia, was found to regulate expression and activity of MMPs [527]	25.15	NS	NS
CLASP2	CLIP-associating protein 2	Microtubule stabilising protein involved in the regulation of cell protrusions such as podosomes and invadopodia [529]	24.09	NS	25.29
CLIP1	CAP-Gly domain-containing linker protein 2	Also known as CLIP-170. Microtubule binding protein that forms a complex with RAC1/Cdc42/IQGAP1 and is involved in the regulation of invadopodia formation and invasion in human breast cancer cells [530, 531]	26.37	NS	NS
DIAPH1	Protein diaphanous homolog 1	Actin nucleation and elongation factor required for the assembly of F-actin structures. DIAPH1 was found to be critical for invadopodia formation in U87MG cells [534]	NS	24.14	NS
DOCK1	Dedicator of cytokinesis protein 1	Rac1 exchange factor that is localised to invadopodia, involved in modulating invadopodia dynamics in breast cancer cells [536]	NS	NS	25.63
FHOD1	FH1/FH2 domain-containing protein 1	Superresolution microscopy revealed the presence of formin FHOD1 and unbranched radial F-actin fibers emanating from invadopodia [539]	24.45	NS	NS
GRB2	Growth factor receptor-bound protein 2	Upstream activator of N-WASP in invadopodia formation [135]	NS	NS	23.18
LPP	Lipoma-preferred partner	Src-mediated LPP phosphorylation at specific tyrosine residues (Y245/301/302) is critical for invadopodia formation in breast cancer cells [543]	24.76	NS	NS
MMP14	Matrix metalloproteinase-14	MT1-MMP: transmembrane protease located within invadopodia [544]	NS	-26.17	NS
MMP2	72 kDa type IV collagenase	Metalloprotease that is widely associated with invadopodia [136]	NS	-23.69	NS
PODXL	Podocalyxin	Podocalyxin-like 1 promotes invadopodia formation and metastasis through activation of Rac1/Cdc42/cortactin signalling in breast cancer cells [546]	26.38	NS	NS
PPP4C	Serine/threonine-protein phosphatase 4 catalytic subunit	Protein phosphatase that upregulates MMP-2 and MMP-9 via pAKT [547]	24.94	NS	NS
RAB3A	Ras-related protein Rab-3A	Rab3A GTPase is a key player in regulating exocytosis of vesicles containing MMPs at invadopodia [722]	NS	23.88	NS

RAB5A	Ras-related protein Rab-5A	Rab5a GTPase is a major regulator of MT1-MMP trafficking and invadopodia formation [550]. MT1-MMP vesicles that are positive for Rab5a localise to invadopodia [551]	25.09	NS	25.44
RHOA	Transforming protein RhoA	RhoA–ROCK signalling promotes invadopodia formation and activity [140]	-2.68	NS	2.66
SH3PXD2B	SH3 and PX domain-containing protein 2B	Adaptor protein also known as Tks4 that is required for functional invadopodia formation [752]	23.77	NS	NS
STX4	Syntaxin-4	SNARE protein syntaxin4: mediates trafficking of MT1-MMP and EGFR for invadopodia activity [555]	24.23	NS	NS
TGFBI	Transforming growth factor-beta-induced protein ig-h3	A transforming growth factor beta (TGFβ) inducible secreted extracellular matrix (ECM) protein. It has been shown to promote MMP secretion at invadopodia by interacting with integrin α2β1 and activating PI3K/AKT signalling. Processing of TGFBI by MMP-2 induces adhesion-related FAK/Src signalling in glioma cells and promotes invasion [572-574]	NS	NS	25.74
TJP1	Tight junction protein ZO-1	Tight Junction Protein is a scaffolding protein that plays a role in the regulation of cell migration by targeting CDC42BPB to the leading edge of migrating cells. Plays a role as a partner for ADAM-12 in invadopodia [556, 557]	24.3	NS	2.03
TRIP10	Cdc42-interacting protein 4	CDC42-interacting protein 4: promotes metastasis of nasopharyngeal carcinoma by mediating invadopodia formation and activating EGFR signalling. Also promotes CDC42-induced actin polymerization by recruiting WASL/N-WASP which in turn activates the Arp2/3 complex [558]	NS	NS	-24.64
VASP	Vasodilator-stimulated phosphoprotein	Actin-associated protein that stimulates actin filament elongation by promoting the transfer of profilin-bound actin monomers onto the barbed end of growing actin filaments. In colon cancer cells, VASP is found within invadopodia, where it colocalizes with cortactin and actin [559, 560]	NS	NS	-25.41
WASF2	Wiskott-Aldrich syndrome protein family member 2	Promotes formation of actin filaments. Part of the WAVE complex that activates actin nucleating machinery Arp2/3 to drive invadopodia formation [561, 562]	NS	NS	-25.25

Significantly changed DE proteins above a threshold of FC >2 (averaged log2-transformed protein intensity identified in RT/TMZ treated cells relative to the corresponding untreated cell line) (*NS: not significant)*

Supplementary Table 7: DE invadopodia-related proteins in sEVs harvested from GBM cells post-RT/TMZ treatment

Gene	Protein	Invadopodia related evidence	LFQ ratio (sEVs from RT/TMZ treated/untreated cells)		
			LN229	MU4	MU41
AGRN	Agrin	Secreted and cell surface Agrin binds the Lrp4 receptor and promotes the formation of a Agrin–Lrp4–MuSK signalling complex, which activates FAK and Arp2/3 associated invadopodia formation [564]	NS	NS	-25.16
ARF6	ADP-ribosylation factor 6	ARF6 has an established role in invadopodia. It promotes the formation of Rac1 and WAVE dependent ventral F-actin rosettes in breast cancer cells in response to epidermal growth factor. ARF6 also localizes to invadopodia in melanoma cells, where it regulates invadopodia activity through the activation of the MEK/ERK signalling pathway [437, 525]	NS	NS	2.45
CD151	CD151 antigen	CD151, together with integrin α3β1 located at invadopodia, was found to regulate expression and activity of MMPs [527]	NS	24.88	NS
CLIP1	CAP-Gly domain-containing linker protein 2	Also known as CLIP-170. Microtubule binding protein that forms a complex with RAC1/Cdc42/IQGAP1 and is involved in the regulation of invadopodia formation and invasion in human breast cancer cells [530, 531]	-25.43	NS	NS
CSNK2A1	Casein kinase II subunit alpha	Subunit of Casein Kinase 2. Casein Kinase 2 phosphorylates cortactin and regulates Arp2/3 activity and subsequent invadopodia function [532]	-2.50	NS	-2.36
CSNK2A2	Casein kinase II subunit alpha	Subunit of Casein Kinase 2. Casein Kinase 2 phosphorylates cortactin and regulates Arp2/3 activity and subsequent invadopodia function [532]	NS	24.67	25.44
CTTN	Src substrate cortactin	Cortactin is a critical regulator of actin nucleation in the development of invadopodia [533]	-24.78	NS	25.54
DNM2	Dynamin-2	Dynamin2 GTPase is a microtubule-associated force-producing protein that contributes to invadopodia formation in invasive bladder cancer cells via its proline/arginine-rich domain (PRD) [535]	-27.25	25.12	NS
DOCK1	Dedicator of cytokinesis protein 1	Rac1 exchange factor that is localised to invadopodia, involved in modulating invadopodia dynamics in breast cancer cells [536].	NS	25.83	NS
ENPP2	Ectonucleotide pyrophosphatase/phosphodiesterase family member 2	Can induce invadopodia formation in the fibrosarcoma cell line HT1080 through activation of the LPA4 receptor [566]	2.21	25.46	NS
FAP	Prolyl endopeptidase FAP	Also known as Seprase, a gelatin-degrading membrane-protease complex that is expressed at the invasive front of malignant melanoma cells on invadopodia [125]	NS	NS	2.19
FMNL2	Formin-like protein 2	Cortactin directly binds to FMNL2 to promote actin polymerization and recycling endosome motility. FMNL2 was necessary for invadopodia formation and function in CRC cells [567]	NS	NS	25.76

FSCN1	Fascin	Actin bundling protein that stabilises actin filaments in invadopodia [470]	NS	23.80	NS
ICAM1	Intercellular adhesion molecule 1	A cell adhesion molecule in the ICAM superfamily, known for their ability to bind integrins to activate signalling. Often expressed at the cell surface where it may play a role in invadopodia maturation via interactions with integrins [540]	2.22	NS	NS
ITGA3	Integrin alpha-3	Integrin alpha-3/beta-3 provides a docking site for FAP (seprase) at invadopodia plasma membranes in a collagen-dependent manner and hence may participate in the adhesion, formation of invadopodia and matrix degradation processes [541]	NS	-2.70	NS
LPP	Lipoma-preferred partner	Src-mediated LPP phosphorylation at specific tyrosine residues (Y245/301/302) is critical for invadopodia formation in breast cancer cells [543]	NS	24.63	NS
MMP14	Matrix metalloproteinase-14	MT1-MMP: transmembrane protease located within invadopodia [544]	-25.74	25.6	NS
MTOR	Serine/threonine-protein kinase mTOR	Cav-1 activation-induces PI3K/Akt/mTOR signalling to promote invadopodia formation in breast carcinoma MDA-MB-231 cells [526]	NS	NS	24.16
NCKAP1	Nck-associated protein 1	A subunit of the Arp2/3-WAVE complex involved in actin organisation during invadopodia formation [545]	25.38	NS	NS
PXN	Paxillin	A cytoskeletal protein involved in actin-membrane attachment at sites of cell adhesion to the ECM. JNK-paxillin signalling can promote invadopodia activity [549]	-24.49	24.43	25.01
RAB5A	Ras-related protein Rab-5A	Rab5a GTPase is a major regulator of MT1-MMP trafficking and invadopodia formation [550]. MT1-MMP vesicles that are positive for Rab5a localise to invadopodia [551]	NS	NS	-25.46
RCC2	Protein RCC2	Acts as a regulator of Rac1 and Arf6, as well as binding to cortactin, linking RCC2 to number of key invadopodia proteins [552]	-26.18	25.06	NS
ROCK2	Rho-associated protein kinase 2	Protein kinase which is a key regulator of actin cytoskeleton. Matrix rigidity can drive ROCK signalling to enhance invadopodia function [138]	NS	25.38	NS
TGFBI	Transforming growth factor-beta-induced protein ig-h3	A transforming growth factor beta (TGFβ) inducible secreted extracellular matrix (ECM) protein. It has been shown to promote MMP secretion at invadopodia by interacting with integrin α2β1 and activating PI3K/AKT signalling. Processing of TGFBI by MMP-2 induces adhesion-related FAK/Src signalling in glioma cells and promotes invasion [572-574]	NS	25.52	NS
TJP1	Tight junction protein ZO-1	Tight Junction Protein is a scaffolding protein that plays a role in the regulation of cell migration by targeting CDC42BPB to the leading edge of migrating cells. Plays a role as a partner for ADAM-12 in invadopodia [556, 557]	-24.89	NS	NS
WASF2	Wiskott-Aldrich syndrome protein family member 2	Promotes formation of actin filaments. Part of the WAVE complex that activates actin nucleating machinery Arp2/3 to drive invadopodia formation [561, 562]	NS	NS	24.81

Significantly changed DE proteins above a threshold of FC >2 (log2-transformed averaged protein intensity identified in sEVs from RT/TMZ treated cells relative to sEVs from the corresponding untreated cell line) (*NS: not significant)*

Supplementary Table 8: DE invadopodia-related proteins in GBM cells following LT RT/TMZ treatment

Gene	Protein	Invadopodia related evidence	LFQ ratio (LT treated/untreated)		
			LN229	MU4	MU41
ARF6	ADP-ribosylation factor 6	ARF6 has an established role in invadopodia. It promotes the formation of Rac1 and WAVE dependent ventral F-actin rosettes in breast cancer cells in response to epidermal growth factor. ARF6 also localizes to invadopodia in melanoma cells, where it regulates invadopodia activity through the activation of the MEK/ERK signaling pathway [437, 525]	NS	NS	2.84
AXL	Tyrosine-protein kinase receptor UFO	Cross-talk between Receptor Tyrosine Kinases AXL and ERBB3 regulates invadopodia formation in melanoma cells [565]	-23.7	-24.17	24.16
BSG	Basigin	Basigin/CD147: upregulation induced MT1-MMP-dependent invadopodia activity in breast epithelial cells. Also promotes epidermal growth factor receptor (EGFR)-Ras-ERK signalling via interactions with CD44 [362, 363]	-3.83	NS	-4.11
CAV1	Caveolin-1	Mechanosensitive caveolin-1 activation-induced PI3K/Akt/mTOR signaling pathway promotes breast cancer motility, invadopodia formation and metastasis *in vivo* [526]	2.76	NS	NS
CD151	CD151 antigen	CD151, together with integrin α3β1 located at invadopodia, was found to regulate expression and activity of MMPs [527]	-24.74	NS	NS
CD44	CD44 antigen	Splice isoform CD44s promotes cortactin phosphorylation and recruits MT1-MMP to invadopodia [528]	-2.74	NS	NS
CFL1	Cofilin-1	Cofilin is necessary for the stabilization and maturation of invadopodia [135]	NS	NS	-3.13
CLASP2	CLIP-associating protein 2	Microtubule stabilising protein involved in the regulation of cell protrusions such as podosomes and invadopodia [529]	NS	-2.92	26.87
CLIP1	CAP-Gly domain-containing linker protein 2	Also known as CLIP-170. Microtubule binding protein that forms a complex with RAC1/Cdc42/IQGAP1 and is involved in the regulation of invadopodia formation and invasion in human breast cancer cells [530, 531]	NS	-24.66	-25.14
CSNK2A1	Casein kinase II subunit alpha	Subunit of Casein Kinase 2. Casein Kinase 2 phosphorylates cortactin and regulates Arp2/3 activity and subsequent invadopodia function [532]	-2.05	NS	2.45
CSNK2A2	Casein kinase II subunit alpha	Subunit of Casein Kinase 2. Casein Kinase 2 phosphorylates cortactin and regulates Arp2/3 activity and subsequent invadopodia function [532]	-26.01	NS	NS
CTTN	Src substrate cortactin	Cortactin is a critical regulator of actin nucleation in the development of invadopodia [533]	NS	NS	-30.51
DIAPH1	Protein diaphanous homolog 1	Actin nucleation and elongation factor required for the assembly of F-actin structures. DIAPH1 was found to be critical for invadopodia formation in U87MG cells [534]	-25.74	NS	-25.09

DOCK1	Dedicator of cytokinesis protein 1	Rac1 exchange factor that is localised to invadopodia, involved in modulating invadopodia dynamics in breast cancer cells [536].	2.952	NS	NS
EGFR	Epidermal growth factor receptor	Established receptor involved in invadopodia maturation, via an EGFR-Src-Arg-cortactin signalling pathway [123]	NS	NS	-11.38
ENAH	Protein enabled homolog	Also known as 'Mena'. Involved in regulating the assembly of actin filaments. It is recruited to stabilise invadopodia via SHIP2 [537]	NS	25.15	NS
FAP	Prolyl endopeptidase FAP	Also known as Seprase, a gelatin-degrading membrane-protease complex that is expressed at the invasive front of malignant melanoma cells on invadopodia [125]	-24.83	NS	-2.38
FARP1	FERM, ARHGEF and pleckstrin domain-containing protein 1	FARP1 overexpression promotes cell motility and filopodium formation via CDC42 activation [538]	NS	NS	28.46
FHOD1	FH1/FH2 domain-containing protein 1	Superresolution microscopy revealed the presence of formin FHOD1 and unbranched radial F-actin fibers emanating from invadopodia [539]	-24.65	-25.81	NS
FSCN1	Fascin	Actin bundling protein that stabilises actin filaments in invadopodia [470]	-6.53	NS	-4.6
GRB2	Growth factor receptor-bound protein 2	Upstream activator of N-WASP in invadopodia formation [135]	NS	24.97	NS
ICAM1	Intercellular adhesion molecule 1	A cell adhesion molecule in the ICAM superfamily, known for their ability to bind integrins to activate signalling. Often expressed at the cell surface where it may play a role in invadopodia maturation via interactions with integrins [540]	-3.33	-25.13	-23.94
ITGA3	Integrin alpha-3	Integrin alpha-3/beta-3 provides a docking site for FAP (seprase) at invadopodia plasma membranes in a collagen-dependent manner and hence may participate in the adhesion, formation of invadopodia and matrix degradation processes [541]	NS	NS	-5.21
ITGB3	Integrin beta-3	Integrin alpha-3/beta-3 provides a docking site for FAP (seprase) at invadopodia plasma membranes in a collagen-dependent manner and hence may participate in the adhesion, formation of invadopodia and matrix degradation processes [541]	-3.1	NS	-4.30
LIMK1	LIM domain kinase 1	Kinase that phosphorylates cofilin and MT1-MMP, promoting binding to cortactin. LIMK1 is also required for endosomal accumulation of cortactin, and is required for invadopodia formation in breast carcinoma cells [753]	NS	NS	26.56
LPP	Lipoma-preferred partner	Src-mediated LPP phosphorylation at specific tyrosine residues (Y245/301/302) is critical for invadopodia formation in breast cancer cells [543]	-24.82	24.92	-26.78
MMP14	Matrix metalloproteinase-14	MT1-MMP: transmembrane protease located within invadopodia [544]	NS	25.72	-2.00
MMP2	72 kDa type IV collagenase	Metalloprotease that is widely associated with invadopodia [136]	NS	NS	-3.01

PODXL	Podocalyxin	Podocalyxin-like 1 promotes invadopodia formation and metastasis through activation of Rac1/Cdc42/cortactin signalling in breast cancer cells [546]	-27.97	NS	NS
PPP4C	Serine/threonine-protein phosphatase 4 catalytic subunit	Protein phosphatase that upregulates MMP-2 and MMP-9 via pAKT [547]	NS	-24.32	-24.2
PTK2	Focal adhesion kinase 1	PTK2 is a focal adhesion-associated protein kinase involved in focal adhesion-mediated motility and has been implicated in invadopodia regulation [548]	NS	NS	26.21
PXN	Paxillin	A cytoskeletal protein involved in actin-membrane attachment at sites of cell adhesion to the ECM. JNK-paxillin signalling can promote invadopodia activity [549]	-25.53	NS	NS
RAB3A	Ras-related protein Rab-3A	Rab3A GTPase is a key player in regulating exocytosis of vesicles containing MMPs at invadopodia [722]	-25.3	-25.99	26.04
RAB5A	Ras-related protein Rab-5A	Rab5a GTPase is a major regulator of MT1-MMP trafficking and invadopodia formation [550]. MT1-MMP vesicles that are positive for Rab5a localise to invadopodia [551]	NS	NS	-25.32
RACGAP1	Rac GTPase-activating protein 1	Binds to IQGAP1 to mediate Rac1 deactivation. Phosphorylation of RacGAP1 promotes its recruitment to IQGAP1 at the tips of invadopodia [571]	NS	NS	-24.25
RCC2	Protein RCC2	Acts as a regulator of Rac1 and Arf6, as well as binding to cortactin, linking RCC2 to number of key invadopodia proteins [552]	-2.62	NS	3.23
RHOG	Rho-related GTP-binding protein RhoG	RhoG and SGEF modulate the phosphorylation of paxillin, which plays a key role during invadopodia disassembly [536]	2.26	NS	NS
SH3PXD2B	SH3 and PX domain-containing protein 2B	Adaptor protein also known as Tks4 that is required for functional invadopodia formation [752]	NS	NS	24.95
SRC	Proto-oncogene tyrosine-protein kinase Src	Src tyrosine kinase activates numerous proteins in invadopodia-related signalling pathways, including adaptor proteins such as Tks5 [554]	-24.61	24.62	NS
STX4	Syntaxin-4	SNARE protein syntaxin4: mediates trafficking of MT1-MMP and EGFR for invadopodia activity [555]	-25.03	NS	NS
SVIL	Supervillin	Supervillin is a peripheral membrane protein that binds F-actin and myosin II and reorganizes the actin cytoskeleton to potentiate invadopodia function. Overexpressed SVIL induces redistribution of lamellipodial cortactin and lamellipodin/RAPH1/PREL1 away from the cell periphery to internal sites and concomitantly increases the numbers of F-actin punctae [754]	-23.64	NS	25.22
TGFBI	Transforming growth factor-beta-induced protein ig-h3	A transforming growth factor beta (TGFβ) inducible secreted extracellular matrix (ECM) protein. It has been shown to promote MMP secretion at invadopodia by interacting with integrin α2β1 and activating PI3K/AKT signalling. Processing of TGFBI by MMP-2 induces adhesion-related FAK/Src signalling in glioma cells and promotes invasion [572-574]	-24.50	2.95	NS

TJP1	Tight junction protein ZO-1	Tight Junction Protein is a scaffolding protein that plays a role in the regulation of cell migration by targeting CDC42BPB to the leading edge of migrating cells. Plays a role as a partner for ADAM-12 in invadopodia [556, 557]	NS	NS	28.72
TRIP10	Cdc42-interacting protein 4	CDC42-interacting protein 4: promotes metastasis of nasopharyngeal carcinoma by mediating invadopodia formation and activating EGFR signalling. Also promotes CDC42-induced actin polymerization by recruiting WASL/N-WASP which in turn activates the Arp2/3 complex [558]	NS	NS	-26.05
VASP	Vasodilator-stimulated phosphor-protein	Actin-associated protein that stimulates actin filament elongation by promoting the transfer of profilin-bound actin monomers onto the barbed end of growing actin filaments. In colon cancer cells, VASP is found within invadopodia, where it colocalizes with cortactin and actin [559, 560]	-24.86	NS	-26.21

Significantly changed DE proteins above a threshold of FC >±2 (log2-transformed averaged protein intensity identified in LT RT/TMZ treated cells relative to the corresponding untreated cell line) (*NS: not significant)*

Supplementary Table 9: DE invadopodia-related proteins in sEVs harvested from GBM cells following LT RT/TMZ treatment

Gene	Protein	Invadopodia related evidence	LFQ ratio (LT treated/untreated)		
			LN229	MU4	MU41
ABI2	Abl interactor 2	Regulator of actin cytoskeleton dynamics underlying cell motility and adhesion. Functions as a component of the WAVE2 complex, which activates actin nucleating machinery Arp2/3 to drive invadopodia formation. [562, 563]	NS	NS	25.43
ACTR2	Actin-related protein 2	Actin-related protein 2 is a major constituent of the ARP2/3 complex, an essential component involved in invadopodia precursor core formation. Arp2/3 promotes actin polymerization to form branched F-actin networks [523, 524]	-3.187	2.521	NS
ACTR3	Actin-related protein 3	Actin-related protein 3 is a major constituent of the ARP2/3 complex, an essential component involved in invadopodia precursor core formation. Arp2/3 promotes actin polymerization to form branched F-actin networks [523, 524]	-3.735	NS	NS
ARF6	ADP-ribosylation factor 6	ARF6 has an established role in invadopodia. It promotes the formation of Rac1 and WAVE dependent ventral F-actin rosettes in breast cancer cells in response to epidermal growth factor. ARF6 also localizes to invadopodia in melanoma cells, where it regulates invadopodia activity through the activation of the MEK/ERK signalling pathway [437, 525]	-3.096	3.421	NS
BSG	Basigin	Basigin/CD147: upregulation induced MT1-MMP-dependent invadopodia activity in breast epithelial cells. Also promotes epidermal growth factor receptor (EGFR)-Ras-ERK signalling via interactions with CD44 [362, 363]	-4.623	-2.343	-5.866
CAV1	Caveolin-1	Mechanosensitive caveolin-1 activation-induced PI3K/Akt/mTOR signaling pathway promotes breast cancer motility, invadopodia formation and metastasis *in vivo* [526]	-27.5	NS	NS
CD151	CD151 antigen	CD151, together with integrin α3β1 located at invadopodia, was found to regulate expression and activity of MMPs [527]	-25.5	NS	-28.05
CD44	CD44 antigen	Splice isoform CD44s promotes cortactin phosphorylation and recruits MT1-MMP to invadopodia [528]	-3.642	NS	NS
CDC42	Cell division control protein 42 homolog	N-WASP and Arp2/3 form an active complex through CDC42 which promotes invadopodia assembly [135]	-2.337	NS	NS
CFL1	Cofilin-1	Cofilin is necessary for the stabilization and maturation of invadopodia [135]	-3.281	NS	NS
CLASP2	CLIP-associating protein 2	Microtubule stabilising protein involved in the regulation of cell protrusions such as podosomes and invadopodia [529]	NS	NS	25.42
CSNK2A1	Casein kinase II subunit alpha	Subunit of Casein Kinase 2. Casein Kinase 2 phosphorylates cortactin and regulates Arp2/3 activity and subsequent invadopodia function [532]	NS	NS	2.198
CSNK2A2	Casein kinase II subunit alpha	Subunit of Casein Kinase 2. Casein Kinase 2 phosphorylates cortactin and regulates Arp2/3 activity and subsequent invadopodia function [532]	NS	25.58	NS
CTTN	Src substrate cortactin	Cortactin is a critical regulator of actin nucleation in the development of invadopodia [533]	-25.06	24.23	NS

DIAPH1	Protein diaphanous homolog 1	Actin nucleation and elongation factor required for the assembly of F-actin structures. DIAPH1 was found to be critical for invadopodia formation in U87MG cells [534]	NS	24.42	NS
DNM2	Dynamin-2	Dynamin2 GTPase is a microtubule-associated force-producing protein that contributes to invadopodia formation in invasive bladder cancer cells via its proline/arginine-rich domain (PRD) [535]	-2.701	NS	NS
DOCK1	Dedicator of cytokinesis protein 1	Rac1 exchange factor that is localised to invadopodia, involved in modulating invadopodia dynamics in breast cancer cells [536].	NS	2.42	5.582
ENAH	Protein enabled homolog	Also known as 'Mena'. Involved in regulating the assembly of actin filaments. It is recruited to stabilise invadopodia via SHIP2 [537]	NS	NS	25.92
FAP	Prolyl endopeptidase FAP	Also known as Seprase, a gelatin-degrading membrane-protease complex that is expressed at the invasive front of malignant melanoma cells on invadopodia [125]	-25.06	NS	-26.81
FARP1	FERM, ARHGEF and pleckstrin domain-containing protein 1	FARP1 overexpression promotes cell motility and filopodium formation via CDC42 activation [538]	NS	NS	28
FHOD1	FH1/FH2 domain-containing protein 1	Superresolution microscopy revealed the presence of formin FHOD1 and unbranched radial F-actin fibers emanating from invadopodia [539]	NS	25.72	25.5
FSCN1	Fascin	Actin bundling protein that stabilises actin filaments in invadopodia [470]	-28.82	NS	-4.3141
ICAM1	Intercellular adhesion molecule 1	A cell adhesion molecule in the ICAM superfamily, known for their ability to bind integrins to activate signalling. Often expressed at the cell surface where it may play a role in invadopodia maturation via interactions with integrins [540]	-31.4	NS	-24.71
ITGA3	Integrin alpha-3	Integrin alpha-3/beta-3 provides a docking site for FAP (seprase) at invadopodia plasma membranes in a collagen-dependent manner and hence may participate in the adhesion, formation of invadopodia and matrix degradation processes [541]	-5.371	NS	-6.338
ITGB3	Integrin beta-3	Integrin alpha-3/beta-3 provides a docking site for FAP (seprase) at invadopodia plasma membranes in a collagen-dependent manner and hence may participate in the adhesion, formation of invadopodia and matrix degradation processes [541]	-30.77	NS	-4.786
LIMK1	LIM domain kinase 1	Kinase that phosphorylates cofilin and MT1-MMP, promoting binding to cortactin. LIMK1 is also required for endosomal accumulation of cortactin, and is required for invadopodia formation in breast carcinoma cells [753]	NS	NS	24.58
LPAR1	Lysophosphatidic acid receptor 1	A common and major receptor used for hypoxia-induced invadopodia production [568]	NS	24.63	NS
MMP14	Matrix metalloproteinase-14	MT1-MMP: transmembrane protease located within invadopodia [544]	NS	27.45	-2.529
MMP2	72 kDa type IV collagenase	Metalloprotease that is widely associated with invadopodia [136]	-9.43	NS	-8.841

NCKAP1	Nck-associated protein 1	A subunit of the Arp2/3-WAVE complex involved in actin organisation during invadopodia formation [545]	-26.92	NS	NS
PODXL	Podocalyxin	Podocalyxin-like 1 promotes invadopodia formation and metastasis through activation of Rac1/Cdc42/cortactin signalling in breast cancer cells [546]	-26.69	NS	NS
PPP4C	Serine/threonine-protein phosphatase 4 catalytic subunit	Protein phosphatase that upregulates MMP-2 and MMP-9 via pAKT [547]	NS	24.21	24.15
PTK2	Focal adhesion kinase 1	PTK2 is a focal adhesion-associated protein kinase involved in focal adhesion-mediated motility and has been implicated in invadopodia regulation [548]	NS	NS	24.57
RACGAP1	Rac GTPase-activating protein 1	Binds to IQGAP1 to mediate Rac1 deactivation. Phosphorylation of RacGAP1 promotes its recruitment to IQGAP1 at the tips of invadopodia [571]	-29.16	NS	-25.08
RCC2	Protein RCC2	Acts as a regulator of Rac1 and Arf6, as well as binding to cortactin, linking RCC2 to number of key invadopodia proteins [552]	NS	4.043	4.962
RHOA	Transforming protein RhoA	RhoA–ROCK signalling promotes invadopodia formation and activity [140]	-3.985	NS	NS
RHOG	Rho-related GTP-binding protein RhoG	RhoG and SGEF modulate the phosphorylation of paxillin, which plays a key role during invadopodia disassembly [536]	-27.62	NS	NS
ROCK2	Rho-associated protein kinase 2	Protein kinase which is a key regulator of actin cytoskeleton. Matrix rigidity can drive ROCK signaling to enhance invadopodia function [138]	NS	NS	3.352
SRC	Proto-oncogene tyrosine-protein kinase Src	Src tyrosine kinase activates numerous proteins in invadopodia-related signalling pathways, including adaptor proteins such as Tks5 [554]	-25.66	NS	-26.98
STX4	Syntaxin-4	SNARE protein syntaxin4: mediates trafficking of MT1-MMP and EGFR for invadopodia activity [555]	-26.85	NS	-3.837
TGFBI	Transforming growth factor-beta-induced protein ig-h3	A transforming growth factor beta (TGFβ) inducible secreted extracellular matrix (ECM) protein. It has been shown to promote MMP secretion at invadopodia by interacting with integrin α2β1 and activating PI3K/AKT signalling. Processing of TGFBI by MMP-2 induces adhesion-related FAK/Src signalling in glioma cells and promotes invasion [572-574]	-3.045	NS	-4.257
TJP1	Tight junction protein ZO-1	Tight Junction Protein is a scaffolding protein that plays a role in the regulation of cell migration by targeting CDC42BPB to the leading edge of migrating cells. Plays a role as a partner for ADAM-12 in invadopodia [556, 557]	-25.4	NS	2.082
WASF2	Wiskott-Aldrich syndrome protein family member 2	Promotes formation of actin filaments. Part of the WAVE complex that activates actin nucleating machinery Arp2/3 to drive invadopodia formation [561, 562]	NS	25.45	NS

Significantly changed DE proteins above a threshold of FC >±2 (log2-transformed averaged protein intensity identified in sEVs isolated from LT RT/TMZ treated cells relative to sEVs isolated from the corresponding untreated cell line) (*NS: not significant)*